



**HAL**  
open science

# Hydrogen-bonded supramolecular polymers as dynamic scaffolds for catalysis

Xavier Caumes

► **To cite this version:**

Xavier Caumes. Hydrogen-bonded supramolecular polymers as dynamic scaffolds for catalysis. Material chemistry. Université Pierre et Marie Curie - Paris VI, 2016. English. NNT : 2016PA066554 . tel-01534681

**HAL Id: tel-01534681**

**<https://theses.hal.science/tel-01534681>**

Submitted on 8 Jun 2017

**HAL** is a multi-disciplinary open access archive for the deposit and dissemination of scientific research documents, whether they are published or not. The documents may come from teaching and research institutions in France or abroad, or from public or private research centers.

L'archive ouverte pluridisciplinaire **HAL**, est destinée au dépôt et à la diffusion de documents scientifiques de niveau recherche, publiés ou non, émanant des établissements d'enseignement et de recherche français ou étrangers, des laboratoires publics ou privés.

# Université Pierre et Marie Curie

Ecole doctorale physique et chimie des matériaux (ED 397)

*Institut Parisien de Chimie Moléculaire / Laboratoire de Chimie des Polymères (UMR 8232)*

## **Hydrogen-bonded supramolecular polymers as dynamic scaffolds for catalysis**

Par Xavier Caumes

Thèse de doctorat de Chimie

Dirigée par Laurent Bouteiller

Présentée et soutenue publiquement le 6 décembre 2016

Devant un jury composé de :

M. Voituriez Arnaud	Chargé de recherche Institut de chimie des substance naturelle	Rapporteur
M. Giuseppone Nicolas	Professeur Institut Charles Sadron	Rapporteur
M. Vidal-Ferran Anton	Professeur Institut Català d'Investigació Química	Examineur
Mme. Aubert Corinne	Directeur de recherche Université Pierre et Marie Curie	Examinatrice
M. Bouteiller Laurent	Directeur de recherche Université Pierre et Marie Curie	Directeur de thèse
M. Raynal Matthieu	Chargé de recherche Université Pierre et Marie Curie	Co-encadrant



Except where otherwise noted, this work is licensed under  
<http://creativecommons.org/licenses/by-nc-nd/3.0/>

*“On a light-year scale, our galaxy system is also chiral.”*

Minghua Liu



## Remerciements

Je souhaiterais d'abord remercier Arnaud Voituriez et Nicolas Giuseppone d'avoir accepté d'être les rapporteurs de cette thèse. J'espère que cette dernière sera suffisamment digeste. I also would like to thank Anton Vidal-Ferran for his agreement to be part of my thesis jury. Ensuite mes remerciements vont également à l'endroit des membres de l'IPCM de mon jury : Corinne Aubert qui en est la présidente, Laurent Bouteiller, mon directeur de thèse, et Matthieu Raynal mon superviseur durant ces trois années.

Je souhaite remercier plus amplement Laurent pour avoir eu deux thèses encore disponibles en juillet sur projet ANR et dans un labo à moins de quinze minutes de chez moi. Plus sérieusement, ces trois années m'ont permis d'apprendre beaucoup sur un domaine de la chimie qui m'était relativement inconnu (les polymères). Mais elles furent aussi l'opportunité de travailler avec un grand esprit scientifique dont les échanges nous ont toujours fait avancer dans la bonne direction.

Mes plus amples remerciements vont aussi à Matthieu qui aura subi ma prose durant la rédaction et m'aura donné l'impression d'être Dr. Frankenstein devant les morceaux éparpillés de mon introduction. J'ai découvert pendant cette thèse un bourreau de la bibliographie avec la même tendance aux méthodes de synthèse bourrines (des clips et des bouchons s'en souviennent).

Je remercie aussi les membres du projet ANR, Jérémy Zimbron, Christophe Thomas et notamment Piet van Leeuwen pour leurs conseils et participation à cette thèse. Je remercie aussi Virginie Mouries-Mansuy, Louis Fensterbank et Fabien Gagosz pour leur aide concernant la catalyse à l'or. Un mot aussi pour les stagiaires qui sont passés au labo et que j'ai eu le bonheur d'encadrer : Assia Nouar, Arianna Baldi, Julien Smith et Jesse Gordon qui auront tous apporté leurs contributions à cette thèse.

Viennent ensuite les membres de l'équipe, en premier Virgile avec qui j'ai partagé un bureau pendant quasiment deux ans et demi. De ces moments je retiens forcément les trois mois passés à rédiger nos thèses mais aussi les cours de contrôle de la colère, notre intérêt commun pour le whisky (écossais de préférence), les soirées jeux de plateaux et un amour insensé de la ville de Lyon. Puis Alaric avec qui j'ai eu de la chance de travailler sur le projet ANR et qui a fait que notre bureau foisonnait d'idées plus ou moins réalisables. Le reste de l'équipe n'est pas oublié bien sur, je pense à Thomas, Emilie, Léo, Benjamin et Sandrine. Je souhaite aussi remercier tout les membres du groupe polymère, notamment Morgan avec qui j'ai pris plaisir à discuter synthèse organique et mode op. C'est avec bonheur que j'ai passé ces trois ans (et un peu de rab) dans ce labo. J'ai aussi une pensée pour les membres des services d'analyse que ce soit la RMN (Claire Troufflard) ou les GC/HPLC chirales (Omar Khaled).

Je suis aussi reconnaissant à mes amis en dehors du labo que ce soit ceux du lycée et avant (la liste est un peu longue), aux pièces rapportées de l'école Centrale (étonnamment là aussi la liste est longue) et ceux qui ont subis comme moi l'épreuve de la thèse (la liste est moins longue mais pas de jaloux).

Pour finir ma famille qui m'a soutenu et supporté pendant 28 ans et permis d'arriver jusqu'en thèse. Je remercie donc mes parents, mes sœurs (et leur maris), mes nièces mais aussi mes oncles, tantes et cousins, cousines.

# Table of contents

Abbreviations .....	10
General Introduction.....	11
I. Emerging strategies towards tunable and dynamic homogeneous catalysts .....	13
A. Introduction .....	14
1. Catalyst design in molecular catalysts.....	15
B. Discrete supramolecular species as a scaffold for catalysis .....	17
1. Catalyst modularity: ligand libraries .....	18
2. Improved catalyst selectivity .....	20
3. Chirality induction.....	25
C. Dynamic covalent and supramolecular polymer structures as scaffold for catalysis .....	29
1. Recyclable stereoselective catalysts .....	29
2. Stimulus-induced modification of the catalytic performance.....	31
3. Chirality transfer.....	44
D. Conclusion.....	55
E. References .....	56
II. Supramolecular polymers as scaffolds in catalysis: definition, presentation and objectives of the PhD project.....	59
A. Definition and properties of supramolecular polymers .....	60
B. Interest of the use of supramolecular polymers as scaffolds for catalysis.....	61
C. Choice of the assembly units.....	64
1. Benzene-1,3,5-tricarboxamide (BTA) scaffold .....	64
2. Bis-urea scaffold.....	72
D. Comparison of the BTA and bis-urea scaffolds .....	77
E. Examples of catalysts built on BTA and urea supramolecular scaffold.....	78
1. BTA as polymers scaffolds for catalysis .....	78
2. Metal catalysts with a single urea function .....	79
F. Objectives of the project.....	82

1.	General consideration.....	82
2.	Strategies .....	83
G.	References .....	86
III.	Synthesis and self-assembly properties of new bis-urea monomers .....	89
A.	Elements of design for the new bis-urea monomers.....	90
B.	Synthesis and characterisation.....	91
1.	Synthesis and characterisation of bis-urea co-monomers.....	91
2.	Synthesis and characterisation of bis-urea ligands .....	91
C.	Self-association properties.....	94
1.	Gelation tests .....	94
2.	FT-IR analyses .....	96
3.	SANS analyses .....	97
4.	CD analyses.....	101
D.	Concluding remarks .....	102
E.	Experimental part: .....	103
F.	References .....	132
IV.	Asymmetric rhodium-catalysed hydrogenation of dimethylitaconate.....	133
A.	Introduction .....	134
B.	Results and discussion.....	135
1.	Catalytic experiments.....	136
2.	Characterisation of the assemblies. ....	139
3.	Rationalisation of the selectivity outcome .....	142
C.	Conclusions .....	144
D.	Experimental section .....	144
E.	References .....	172
V.	Asymmetric copper-catalysed hydrosilylation of acetophenone derivatives .....	175
A.	Introduction .....	176
B.	Design rules and choice of the catalytic reaction .....	177



C.	Chirality induction and solubility .....	178
1.	Screening of ligands and co-monomers .....	178
2.	Optimisation of the reaction conditions for method A .....	180
3.	Influence of the method of preparation of the catalyst .....	182
D.	Chirality amplification: diluted majority rule experiments .....	184
E.	Characterisation of the Cu supramolecular catalyst .....	187
1.	FT-IR analyses: .....	187
2.	SANS analyses: .....	188
3.	$^{31}\text{P}\{^1\text{H}\}$ NMR analyses.....	190
4.	CD analyses .....	191
F.	Conclusion.....	192
G.	Experimental part: .....	193
1.	Supplementary Figures:.....	193
2.	Synthesis.....	193
3.	Catalytic experiments (screening) .....	195
4.	Catalytic procedures for the chirality amplification experiments: .....	196
5.	GC analyses.....	197
H.	References .....	203
VI.	Gold(I) complexes supported on supramolecular scaffolds: characterisation and use in catalysis .....	205
A.	Introduction .....	206
1.	Gold(I) catalysis .....	206
2.	Emerging strategies to control the selectivity of gold catalysis .....	208
3.	Interest of gold catalysts supported by supramolecular scaffolds .....	212
B.	Synthesis, characterisation and self-assembly properties of neutral gold chloride complexes containing a bis-urea or a BTA moiety .....	212
1.	Synthesis and characterisation.....	212
2.	SANS analyses .....	213
3.	FT-IR analyses .....	215

4. CD analyses.....	216
C. Synthesis, characterisation and self-assembly properties of NTf <sub>2</sub> gold complexes containing a bis-urea or a BTA moiety.....	217
D. Gold-catalysed reactions.....	219
1. Generation of catalytically-active phosphine gold species under mild conditions.....	219
2. Gold-catalysed reactions with gold complexes containing a BTA or bis-urea moiety.....	222
E. Conclusion.....	224
F. Experimental Part.....	225
1. Complementary figures.....	225
2. Synthesis of the gold complexes:.....	227
3. Catalysis:.....	231
G. References.....	235
VII. Use of salts additives to tune the structures of urea-based supramolecular polymers: <i>towards switchable hydrogen-bonded organocatalysts</i> .....	237
A. Introduction.....	238
B. Salt influence on the structure of ( <i>rac</i> )-EHUT self-assemblies.....	240
1. FT-IR analyses.....	240
2. SANS analysis.....	242
C. Salt influence on the structure of thiourea assemblies.....	243
1. Synthesis of the monomers.....	243
2. Characterisation of the self-assemblies.....	244
D. Organocatalytic reactions.....	246
1. Michael addition.....	246
2. Friedel-Craft reactions.....	249
E. Conclusion.....	251
F. Experimental part.....	251
1. Supplementary figures.....	252
2. Synthesis of the thiourea monomers.....	253
3. Catalytic experiments.....	254

G. References .....	257
General conclusion .....	259
Appendix: Asymmetric catalysts supported on hydrogen-bonded scaffolds: other potential systems and reactions .....	262
A. Introduction .....	262
B. Copper-catalyzed hydrosilylation of 4'-NO <sub>2</sub> acetophenone .....	262
1. Chirality induction.....	262
2. Chirality switch .....	263
3. Experimental section .....	264
C. Rhodium-catalysed hydroboration of styrene.....	265
1. Introduction .....	265
2. Catalytic results .....	266
3. Experimental part .....	268
D. Palladium-catalysed hydrosilylation of styrene.....	269
1. Introduction .....	269
2. Catalytic results .....	270
3. Experimental part .....	270
E. Phosphine-catalysed 3+2 cycloaddition reactions.....	271
1. Introduction .....	271
2. Catalytic results.....	272
3. Experimental part .....	274
F. Conclusion.....	274
G. References .....	275

## Abbreviations

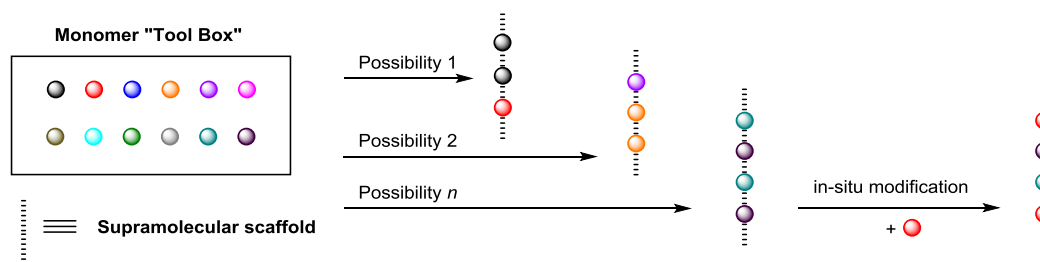
acac: acetylacetone	NMR: nuclear magnetic resonance
AHF: asymmetric hydroformylation	NPs: nanoparticles
BArF: tetrakis(3,5-bistrifluoromethylphenyl)borate	NTf <sub>2</sub> : bis-(trifluoromethanesulfonyl)imide
BArF <sub>20</sub> : tetrakis(pentafluorophenyl)borate	PEGMA: poly-ethyleneglycol-methylmethacrylate
BP: benzophenone	PMHS: polymethylhydrosiloxane
BTA: benzene-1,3,5- tricarboxamide	PNIPAM: poly(N-isopropylacrylamide)
BTAMA: benzene-1,3,5 tricarboxamide-methylacrylate	SANS: small angle neutron scattering
CD: circular dichroism	s.e.: screw-sense excess
Cha: cyclohexylalanine	T <sub>cl</sub> : clearance temperature
COD: 1,5-cyclooctadiene	TMS: trimethylsilyl
Col <sub>ho</sub> : columnar discotic phase	TON: turn-over number
DABCO: 1,4-diazabicyclo[2.2.2]octane	
DCM: dichloromethane	
d.e.: diastereomeric excess	
DFT: density functional theory	
DIPEA: N,N'-diisopropylethylamine	
DME: dimethoxyethane	
D <sub>p</sub> : degrees of polymerisation	
EDG: electron donating group	
e.e.: enantiomeric excess	
ESI: electrospray ionisation	
EWG: electron withdrawing group	
FT-IR: Fourier transform Infrared	
hse: helix screw-sense excess	
ITC: isothermal titration calorimetry	
LMWG: low-molecular weight gelator	
MCH: methylcyclohexane	
MEK: methylethylketone	
Mes: 1,3,5-trimethylbenzene	
MM/MD: molecular mechanics/ molecular dynamics	

# General Introduction

Catalysis is a central discipline of chemical science that refers to the ability of a catalyst to provide a more efficient pathway for a reaction.<sup>[1]</sup> It is very attractive as it allows faster reaction, milder conditions, atom-economy and higher selectivity compared to non-catalysed reactions. These main features of catalysis are of primary importance in order to reduce waste and costs. Optimisation of the catalyst properties and more particularly its selectivity (*i.e.* chemo, regio, enantio and diastereoselectivity) are often made by tailoring the immediate surroundings of the catalytic site (*i.e.* changing its chemical structure) which usually requires painstaking synthetic procedures.

Recently a new approach for catalyst design has emerged based on non-covalent and reversible interactions, namely supramolecular catalysis.<sup>[2,3]</sup> This new field appeared as an ideal solution to overcome the painstaking steps of ligand design by introducing tunability. In this case, the supramolecular catalytic species is formed in-situ by self-assembly of small building blocks. On top of tunability, supramolecular catalysts can also display better performances than classical covalent catalysts and so are of utmost interest.

Another approach in the field of catalysis is the use of macromolecular structures in order to induce recyclability, stimuli-responsiveness or chirality induction. Stimuli-responsiveness implies that the structure and thus the reactivity of the catalyst is modified upon exposure to an external stimulus whereas the chirality induction means that the chirality of the catalytic centre do not arise from neighbouring groups but from the macromolecular structure.



Scheme 1: Representation of the monomer “tool box” and its potential self-assembly into dynamic supramacromolecular scaffolds. Each monomer possesses different properties and the size and distribution of the resulting supramacromolecular structure in this scheme is only represented as example.

In the frame of this thesis our aim was to combine the tunability of the supramolecular approach with the properties of a macromolecular structure. In order to simplify the development of such homogeneous catalysts, we sought to divide the catalyst into small blocks (monomers) that could be picked-up from a “tool box” of monomers according to the needs of the reaction and then be self-assembled to give an active catalyst. The resulting self-assembled macrostructure should possess the targeted properties such as stimuli-responsiveness, chirality induction and higher selectivity. Moreover, as the scaffolds are based on supramolecular interactions, dynamic behaviour of the

resulting catalyst is anticipated. Thus in-situ modification of the structure of the catalyst could be envisaged which is of particular interest for engineering chemical processes.

The first chapter of this manuscript will cover the emerging strategies proposed in the literature towards dynamic and tunable homogeneous catalysts. The second chapter will focus on the interesting properties of two types of hydrogen-bonded supramolecular polymers selected as scaffolds for catalysis in the frame of this thesis. The several strategies envisioned will also be explained.

Synthesis and characterisation of bis-urea co-monomers and ligands as new scaffolds for catalysis will be described in the third chapter. Their self-association properties will be probed by FT-IR, CD spectroscopy and SANS.

Catalytic Applications of the supramolecular scaffolds will be reported in the chapter IV to VII according to the strategies employed and the type of reaction (rhodium-catalysed hydrogenation of dimethyl itaconate, copper-catalysed hydrosilylation of acetophenones derivatives, gold-catalysed cycloisomerisation of enyne and Conia-ene reaction, thiourea-catalysed Michael addition and Friedel-Craft reaction). Correlation between the catalytic properties and the structure of the supramolecular scaffolds will also be investigated.

## References

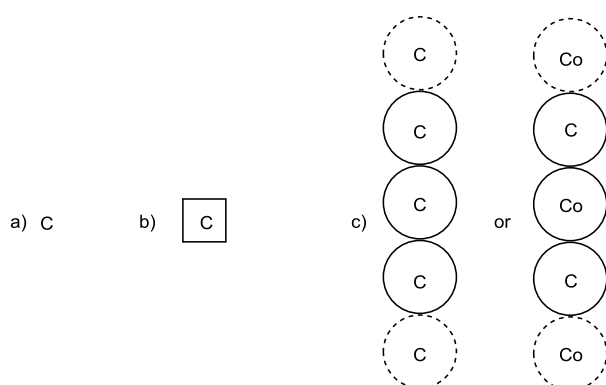
- [1] P. W. N. M. van Leeuwen, *Homogeneous Catalysis*, Springer Netherlands, Dordrecht, **2004**.
- [2] M. Raynal, P. Ballester, A. Vidal-Ferran, P. W. N. M. van Leeuwen, *Chem. Soc. Rev.* **2014**, *43*, 1660–1733.
- [3] M. Raynal, P. Ballester, A. Vidal-Ferran, P. W. N. M. van Leeuwen, *Chem. Soc. Rev.* **2014**, *43*, 1734–1787.

# **I. Emerging strategies towards tunable and dynamic homogeneous catalysts**

*Abstract:* After a brief review on the influence of the catalyst design on its selectivity, this chapter will describe emerging strategies towards tunable and dynamic catalysts. Firstly, recent examples of tunable discrete supramolecular catalysts will be reported, which show improved regio- and enantioselectivities compared to covalent catalysts. Secondly, the importance of a macromolecular structure for imparting the catalysts with recyclability, reactivity and chirality induction properties will be discussed. Particular emphasis will be placed on the importance of designing catalysts supported on both a tunable and dynamic scaffold.

## A. Introduction

A large number of industrial processes for fine chemical production and petrochemical conversion rely on homogeneous catalysis. Also tremendous advances have been done for a better understanding and a better control of the mechanisms underlying homogeneous catalysis. The importance of transition-metal catalysis in chemical sciences has been recognised as several Nobel prizes rewarding scientists in this domain have been awarded in the last 20 years. In parallel, (small)organic molecules as catalysts (organocatalysts) have emerged as a very valuable complementary approach for the development of homogeneous catalytic processes. Currently, main interests in homogeneous catalysis research concern the discovery of new catalytic reactions for the elaboration of sophisticated molecules or the improvement of the properties of existing catalysts in terms of their scope, reactivity and selectivity. Most of the catalysts developed to date are molecular in the sense that their structure consists in covalent bonds or in strong metal-ligand bonds. Many efforts have been done in order to correlate the performance of such molecular catalysts with their properties (electronic, steric, chiral nature). A good relationship between the structure and properties of molecular catalysts has been established and elements of design exist which enable to control and predict their performance to a certain extent. However, as these catalysts are based on a hardly tunable structure, tuning their properties is a laborious task necessitating the whole molecular backbone to be adapted.



Scheme I-1: Representation of a) molecular catalyst (C), b) discrete supramolecular catalyst and c) covalent or supramolecular polymeric catalyst (Co = not catalytically active co-monomer)

After a brief overview on the influence of the structure in the performance of molecular catalysts (Scheme I-1a), we will discuss on emerging strategies towards dynamic and tunable homogeneous catalysts. Firstly, we will describe strategies in which non-covalent interactions have been used to construct “discrete” supramolecular catalysts, *i.e.* catalysts based on small self-assemblies with a defined size and structure. (Scheme I-1b) The properties of those catalysts (selectivity, modularity) arise directly from the presence of these non-covalent interactions. Then, we will show how polymeric species, either covalent or supramolecular, can be used as scaffolds to design highly dynamic and tunable catalysts (Scheme I-1c). The catalysts are dynamic in the sense that their performance can be altered using different stimuli (*e.g.* temperature, concentration, solvent, degree of aggregation). Moreover, we will show that catalysts based on a dynamic polymeric backbone possess additional



properties (recyclability, structural change, chirality switch and amplification) which are inherent to their macromolecular structure. These new properties must be further exploited for the design of catalysts for innovative applications.

### 1. Catalyst design in molecular catalysts

Metal-catalysed chemical processes like hydroformylation of olefins, cross-coupling reactions (for which the 2010 Nobel Prize was awarded to Heck, Suzuki and Negishi) and asymmetric hydrogenation reactions (2001 Nobel Prize of Noyori and Sharpless) require a finely matched combination between one or several ligands and a metal in order to achieve high reaction rates, selectivities and stabilities. Another interesting and well-illustrating example of the influence of the ligand on the selectivity of a chemical reaction is the polymerisation of 1,3-butadiene. According to the valence state of the Ni centre and the ligand, the reaction outcome can be shifted towards one of the products shown in Figure I-1.<sup>[1]</sup>

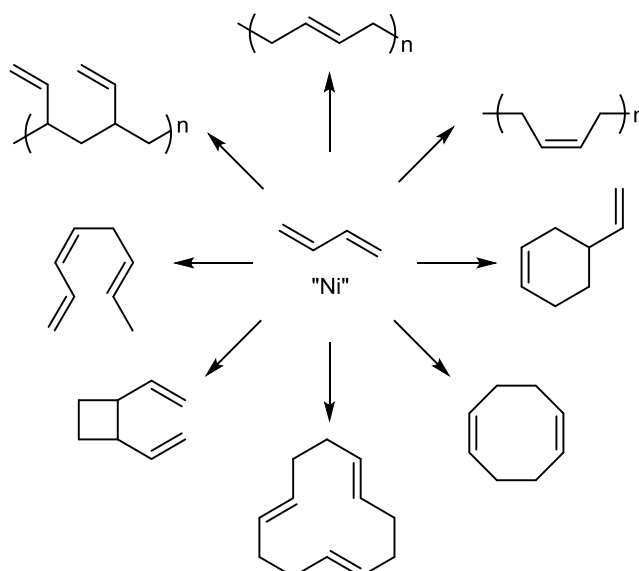


Figure I-1: Polymerisation outcome of 1,3-butadiene using various nickel catalysts

Such differences in selectivity arise from the intrinsic properties of the metal (electronic configuration, oxidation state) and the ligand. Phosphorus-derived ligands are ubiquitous in homogeneous catalysis as their properties can be modulated by changing the nature of the groups connected to the phosphorus atom. The most commonly used are phosphine, phosphite, phosphinite, and phosphoramidite ligands as they span a wide range of electronic, steric and geometrical properties (Figure I-2).

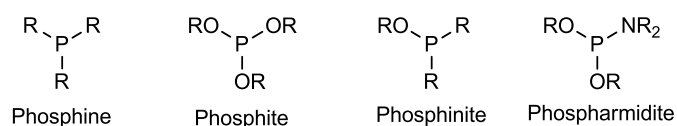


Figure I-2: Example of commonly used phosphorus-derived ligands

Electronic properties of phosphine ligands rely on: i) the  $\sigma$ -donation from the lone-pair of the phosphorus atom to the d orbital of the metal centre, ii) the  $\pi$ -back donation which reflects the capacity of the  $\sigma^*$  orbital of the ligand to receive electronic density from filled d orbitals of the metal. Both

effects are strongly influenced by the groups connected to the phosphorus atom, *e.g.* strong electron donating substituents will increase the  $\sigma$ -donating power of the phosphorus-derived ligand. Those two electronic properties are reflected by the redox potential of the ligands: strong  $\sigma$ -donor and good  $\pi$ -acceptor ligands exhibit a low and a high oxidation potential respectively. Alternatively, those properties can be determined by measuring the C $\equiv$ O stretching frequency of nickel complexes of formula  $[\text{Ni}(\text{C}\equiv\text{O})_x(\text{PR}_3)_{4-x}]$  by means of Fourier-Transform Infrared (FT-IR) spectroscopy: the stronger the  $\sigma$ -donating power the lower the C $\equiv$ O frequency (Figure I-3). This value corresponds to the Tolman electronic parameter ( $\chi$ ).

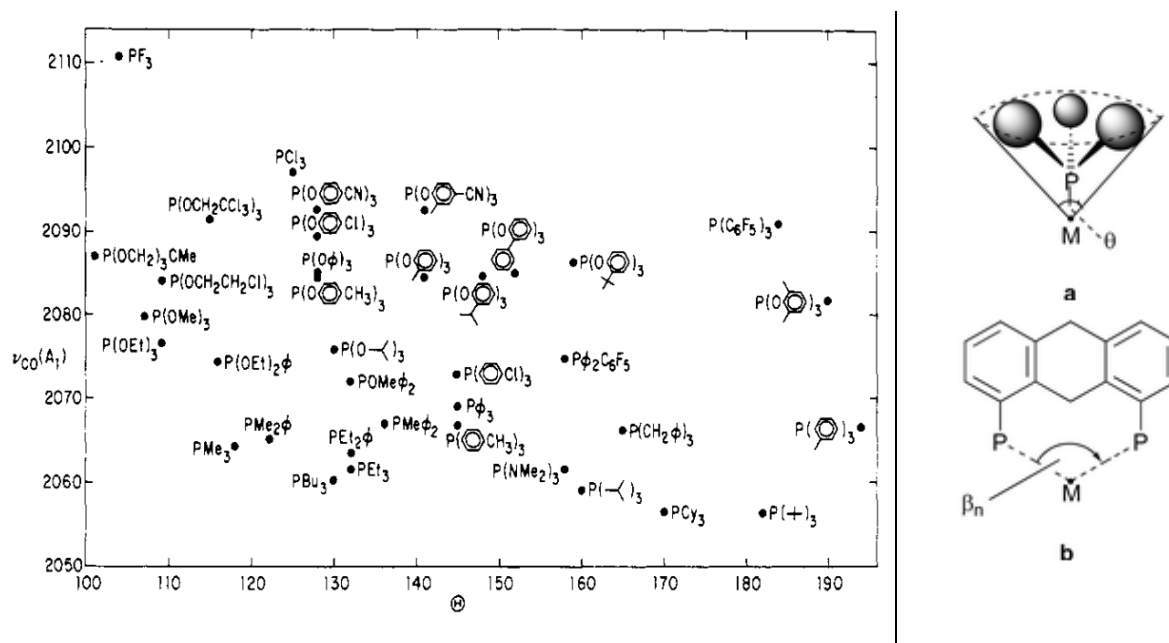


Figure I-3: Left: Electronic and steric properties diagram of commonly-used phosphine and phosphite ligands. C $\equiv$ O frequencies and cone angle ( $\Theta$ ) measured for the Ni complexes of formula  $[\text{Ni}(\text{C}\equiv\text{O})_x(\text{PR}_3)_{4-x}]$ . Right: Description of the cone angle ( $\Theta$ , **a**) and of the bite angle ( $\beta_n$ , **b**) adapted from reference<sup>[2,4]</sup>

Steric properties of phosphine-derived ligands are usually discussed using the cone angle ( $\Theta$ ) as defined by Tolman.<sup>[2]</sup> Determined from space-filling CPK models, the cone angle is defined as the apex angle of a cylindrical cone centred 2.28 Å from the centre of the phosphorus atom and just touching the van der Waals radii of the outermost atoms of the molecule. This simple descriptor is still widely used to compare steric properties of phosphine ligands even though more elaborated descriptors have been developed.<sup>[3]</sup> High cone angle values represent an important steric hindrance near the metal and can explain why some ligands do not behave as expected while considering only their electronic properties. The steric properties of a phosphorus-derived ligand have a strong influence on the geometry of the metal complex and thus on its reactivity in homogeneous catalysis (Figure I-3,**a**). Determination of the steric properties of bidentate ligands requires the calculation of the phosphorus-metal-phosphorus angle (Figure I-3,**b**). The latter is then preferentially used to describe the steric properties of bidentate ligands.<sup>[5]</sup> The bite-angle ( $\beta_n$ ) has a strong influence on the geometry of the metal complexes, thus on their reactivity, since the coordination of the two phosphorus atoms to the metal is fixed within a certain flexibility range (Figure I-4).

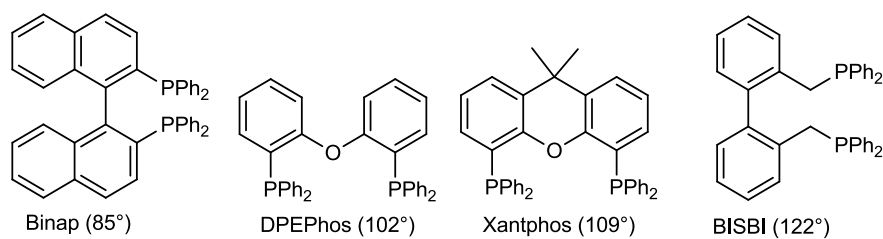


Figure I-4: Example of bidentate ligands with their natural bite angle between brackets

All these descriptors of the properties of the phosphine ligands allow for a fine control of the first coordination sphere of the metal centre and are thus of prime importance for improving the performance of the resulting homogeneous catalysts. Main strategies towards the discovery of a catalytic hit rely on: i) combinatorial approaches, ii) privileged ligands and iii) modular ligands.<sup>[6,7]</sup> Privileged ligands are ligands which have been optimised for a catalytic reaction and a given substrate but also, prove to be efficient for a broader scope of catalytic processes. Modular ligands are constructed on a covalent backbone which can be easily modified.<sup>[8]</sup> It is important to note that in all cases, any modification of the electronic and steric properties of such covalent catalysts will require the painstaking synthesis of a new set of (phosphine) ligands.

Finding an “universal” catalyst, *i.e.* a catalyst that will be efficient for a wide range of catalytic processes, is therefore an ongoing quest in homogeneous catalysis. One can ask what would be the properties of such an ideal catalyst. It should possess high selectivity and reactivity in order to limit wastes associated with low-conversion chemical processes and side reactions. It is particularly important in the case of late-transition metal catalysts due to the high cost of the metal (Pd, Rh, Ru for example) and the synthetic ligand. Recyclability is also sought as the catalyst cost is generally high compared to the feedstock of reactants and transition-metals cannot be considered as renewable resources. An ideal catalyst must also possess a dynamic and tunable architecture which will be easily constructed, modified and will accommodate to different modes of action and selectivity. In this thesis, a dynamic architecture is defined as a structure which is not fixed in time and can be modified during the catalytic reaction. It constitutes a class of catalysts for which the three-dimensional structure can be switched upon activation by a stimulus. Tunable stands for the ease of modification of the structural backbone of those catalysts. A possibility to design dynamic and tunable catalysts is to use non-covalent interactions or dynamic covalent interactions for the construction of their backbone.

## B. Discrete supramolecular species as a scaffold for catalysis

Supramolecular catalysis has prospered during the last decades as it merged two important fields of chemistry: supramolecular chemistry and homogeneous catalysis. As introduced previously, homogeneous catalysis has seen a lot of discoveries and improvements at the fundamental level which led to important applications in industrial processes. Supramolecular chemistry has followed the same trend with an outstanding growth thereafter the Nobel Prize attributed to Cram, Lehn and Pedersen in 1987 “for their development and use of molecules with structure-specific interactions and high

selectivity” and this year to Sauvage, Stoddart and Feringa “for the design and synthesis of molecular machines”.

Supramolecular catalysis can be defined as reactions that involve non-covalent interactions that do not form a part of the basic catalytic reaction.<sup>[9–12]</sup> An important number of supramolecular catalysts have been investigated that differs by the nature of the non-covalent interactions (hydrogen-bond, metal coordination, ion pair, hydrophobic) and of the reaction partners (substrate, ligand, additives, ions and metal) involved in these interactions. In the following part, we will present several selected examples of catalysts constructed by means of non-covalent interactions. These non-covalent interactions occur between the ligands or between a ligand and an additive and the final catalyst is a well-defined discrete species. We will show that these catalysts possess properties that can be hardly achieved by covalent catalysts and that these properties are the result of the presence of non-covalent interactions maintained during the catalytic process. These properties are divided as followed: i) catalyst modularity: ligand libraries, ii) improved catalyst selectivity and iii) chirality induction.

### 1. Catalyst modularity: ligand libraries

Monodentate ligands assembled by means of non-covalent interactions offer an easy way to screen bidentate ligand libraries.<sup>[13]</sup> Indeed, by preparing two groups of *m* and *n* and hetero-complementary monodentate ligands, which combine as 1 : 1 complexes, an *m* x *n* library of bidentate ligands is obtained which enables a rapid screening of various ligand combinations. For example, Breit *et al.* designed ligands containing the recognition motifs of the natural A-T (adenosine and thymine) complementary nucleobase pair.<sup>[14]</sup> Use of phosphine ligands appended with aminopyridine and isoquinolone complementary units led to the formation of the rhodium hetero-complex as the sole metal species (Figure I-5). In that example, the chirality was located on the ligands (BINOL, TADDOL or BIPHEP-derived phosphonates and phosphines).

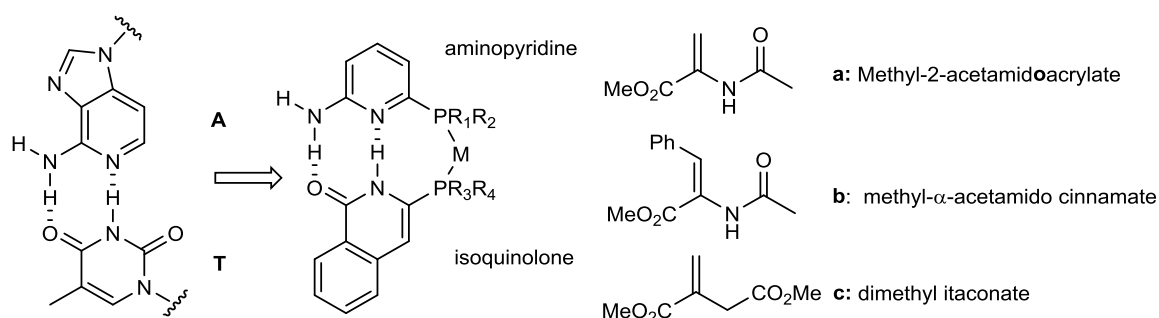


Figure I-5: Heterocomplex containing the phosphine ligands appended with aminopyridine and isoquinolone complementary units. These complexes have been used in the rhodium-catalysed asymmetric hydrogenation of methyl-2-acetamidoacrylate (a), methyl- $\alpha$ -acetamido cinnamate (b) and dimethyl itaconate (c). Adapted from reference<sup>[14]</sup>

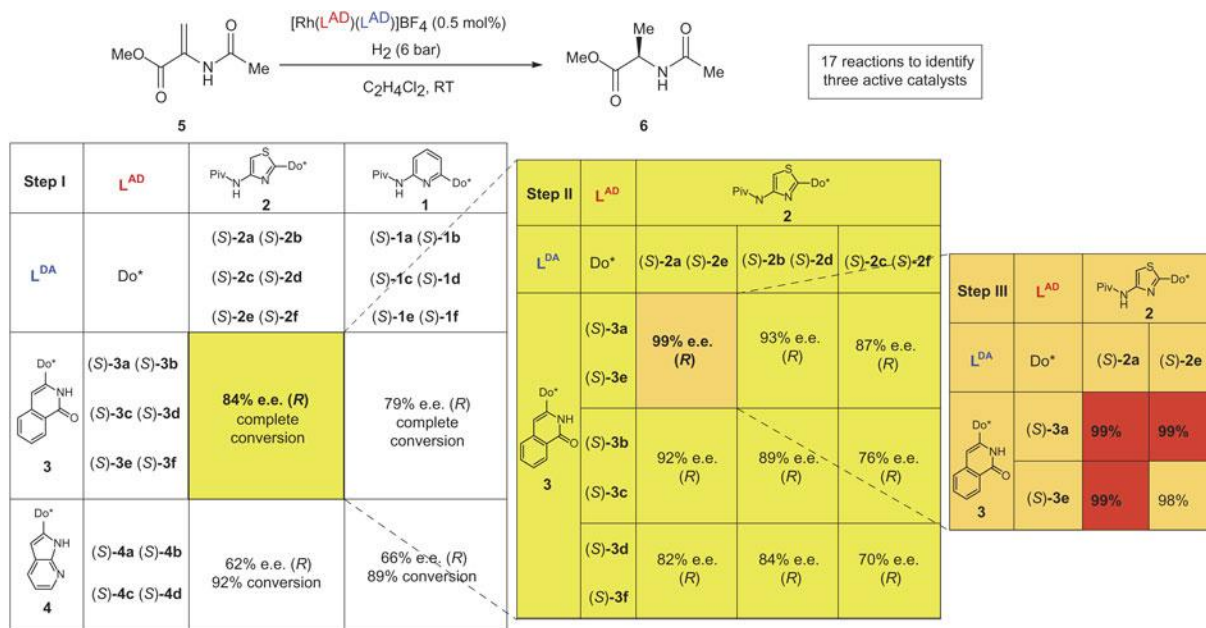


Figure I-6: Combinatorial approach developed by Breit. Do\* = chiral P-donor substituent, RT = room temperature. From reference<sup>[14]</sup>

The formation of the heterocomplexes has been proved using mass spectroscopy (MS) and <sup>1</sup>H nuclear magnetic resonance (NMR). A 10x4 library composed of 10 monophosphine ligands derived from aminopyridine and 4 monophosphine ligands derived from isoquinolone was tested in the hydrogenation of methyl-2-acetamidoacrylate (substrate **a**, Figure I-6). Lower activity and enantioselectivity was observed for the homo-combination of ligands. A mismatch effect for the hetero-complex containing ligands of opposite chirality was also observed. The best pair of ligands in the hydrogenation of methyl-2-acetamidoacrylate (99% e.e.) yielded lower enantioselectivity in the case of the methyl- $\alpha$ -acetamido cinnamate (substrate **b**, 90% e.e.) and dimethyl itaconate (substrate **c**, 94% e.e.) substrates. Further optimisation was needed to obtain a ligand hetero combination providing the highest enantioselectivity in the rhodium hydrogenation of the three substrates. In that aim, a larger library of ligands was screened. In order to decrease the number of experiments needed to determine the best ligand hetero combinations, a combined combinatorial/deconvolution approach was implemented.<sup>[15]</sup> Based on a 12x10 ligand library (monodentate ligands derived from isoquinolone/7-azaindole (L<sup>DA</sup>) and from thiazole/aminopyridine (L<sup>AD</sup>), (Figure I-6), the best ligand combinations for the asymmetric hydrogenation of methyl- $\alpha$ -acetamido cinnamate were identified in only 17 catalytic experiments and analyses instead of the 120 experiments required for the individual screening of each ligand combinations. To limit the number of reactions the library of ligands was divided into 4 subgroups according to the recognition units attached to the monodentate ligand and mixtures of complexes contained in these 4 subgroups were evaluated (Figure I-6 left). The assumption was that even in the case of complex mixtures, a high conversion and enantiomeric excess at the end of the reaction meant that at least one pair of ligands in the mixture was able to achieve high reactivity and selectivity. Repeating this methodology in an iterative fashion led to fast discovery of the best ligand hetero combination. The success of the combinatorial approach was confirmed by analyzing the 120

possible pairs of ligands individually which led to 6 combinations with enantiomeric excess over 99%. On those 6 combinations, the best three which combined high enantioselectivity and high activity were the ones discovered by means of the combinatorial/deconvolution approach.

This examples illustrates how self-assembly facilitates the construction of catalysts in order to modulate their catalytic performance. This is a general property of catalysts built on a supramolecular scaffold.

## **2. Improved catalyst selectivity**

As noted previously tuning the selectivity of a catalytic system is of prime importance. In the following part, we will see how supramolecular interactions can be used as an element of design in order to achieve a significant enhancement of the selectivity of a catalyst. Such supramolecular catalysts reach similar reactivity and selectivity than classical covalent ones and may even provide higher or unusual selectivity in some examples. Such interesting cases have notably been reported in rhodium-catalysed hydroformylation and hydrogenation reactions.

Hydroformylation, also called oxo-reaction, is a reaction intensely used in industry for the massive production of aldehydes from alkenes since aldehydes are precursors for alcohol or can be directly used in perfumes. This reaction is a textbook example of the correlation between the nature/structure of the ligands and the catalytic performance of the resulting rhodium catalyst.<sup>[1]</sup> Indeed, two aldehyde regioisomers, the linear and the branched, can be formed during the reaction depending on the ratio and reactivity of the two isomeric complexes which are key catalytic intermediates in the catalytic process (denoted as **ae** and **ee** complexes in Figure I-7). The ratio and reactivity of the two isomeric complexes depend on the electronic, steric and bite-angle properties of the ligands. In the case of rhodium-catalysed hydroformylation, several bidentate ligands was designed that display excellent regioselectivity towards one regioisomer. One limitation of this class of ligands is that usually a large number of synthetic steps are required for their preparation.

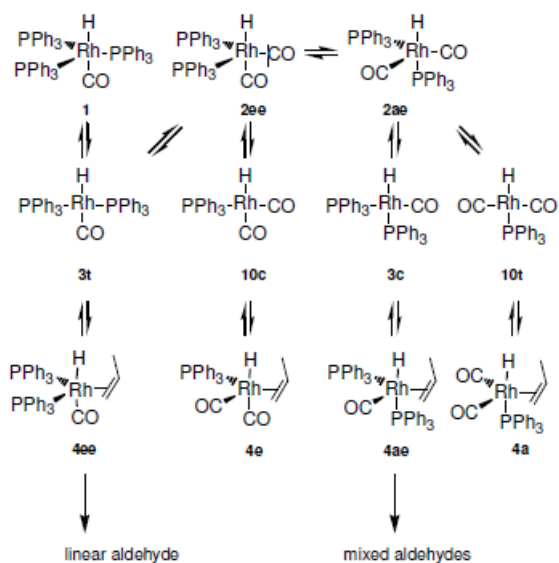


Figure I-7: Simplified mechanism for hydroformylation of 1-propene (the letters **a** and **e** in the complex name are the respective position axial or equatorial of the phosphine ligands) from reference<sup>[1]</sup>

Recent approaches have been reported to prepare supramolecular bidentate ligands in which two monodentate ligands are linked together by means of metal-ligand or hydrogen bond interactions. In 2003, Reek *et al.* described a tris-(zinc-porphyrin)phosphite ligand (**1**, Figure I-8) that acted as a bidentate ligand upon coordination of the porphyrin units with 1,4-diazabicyclo[2.2.2]octane (**a**, DABCO).<sup>[16]</sup> Addition of 1.5 equivalent of DABCO relatively to the ligand led to the formation of the structure **2** (Figure I-8, a) as titrated using <sup>1</sup>H NMR and UV/vis spectroscopy.

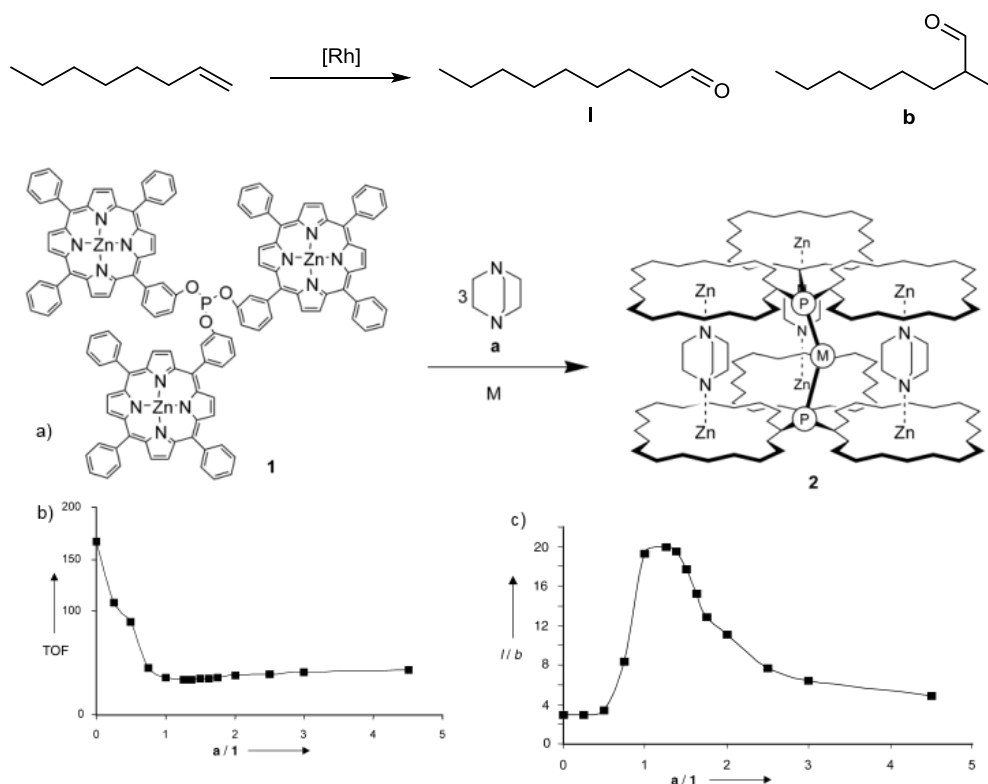


Figure I-8: a) Formation of the supramolecular bidentate ligand used in the rhodium-catalysed hydroformylation of 1-octene; b) Plot of the TOF versus the ratio between DABCO and **a/1**; c) Plot of linear/branched ratio. TOF= Turnover frequency. From reference<sup>[16]</sup>

The activity and selectivity displayed by the ligand in the rhodium-catalysed hydroformylation of 1-octene were strongly influenced by the number of equivalents of DABCO added in solution (Figure I-8b and c). An optimum **a/1** ratio (around 1.5) led to a selectivity (l/b ratio of 20) which is close to the one obtained with covalent bidentate phosphites. The decrease of the activity with increasing equivalents of DABCO was consistent with the successive formation of a bulkier monodentate ligand and then of a bidentate ligand (above 1.5 equivalents of DABCO added). The plot of the linear/branched aldehyde ratio versus **a/1** ratio indicated that introducing more DABCO molecules than that required for the formation of **2** led to the destabilisation of the supramolecular structure. This example illustrates how non-covalent interactions can be used to change the first coordination sphere of a metal catalyst and thus the reactivity and selectivity of the catalytic reaction. Use of supramolecular chemistry by the means of reversible metal ligand interactions offers a novel approach towards the preparation of active catalysts with tunable selectivity.

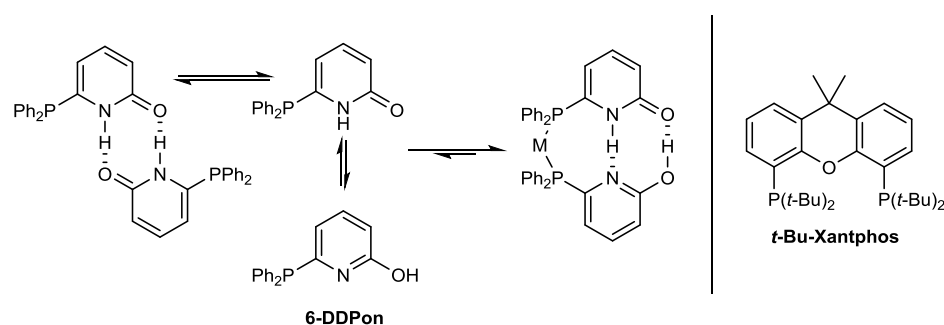


Figure I-9: Left: Tautomeric equilibrium between 2-pyridone and 2-hydroxypyridine phosphine (**6-DDPon**) in absence and in presence of a metal atom coordinated to the phosphorus atom. Right: structure of *t*-Bu-Xantphos. Adapted from reference<sup>[17]</sup>

Moreover, supramolecular catalysts can exhibit catalytic performances hardly achieved with covalent catalysts as exposed in the following example. Breit *et al.* published in 2003 the preparation of a bidentate ligand consisting of two tautomeric forms linked by hydrogen bonds (**6-DDPon**, Figure I-9).<sup>[17]</sup> This supramolecular bidentate ligand exhibited very high activity and selectivity (l:b ratio) in the hydroformylation of 1-octene. Importantly, its catalytic performances exceeded those of covalent monodentate (**PPh<sub>3</sub>**) and bidentate (*t*-Bu-Xantphos) ligands (Table I-1). The **6-DDPon** supramolecular ligand remained assembled until a temperature of 110 °C in a low polarity solvent (toluene), and alkenes with a wide variety of functional groups (such as ester, phenol, alcohol and carbamate) was converted into aldehydes with high selectivity. As expected the disruption of the hydrogen bond interactions, by using methanol as solvent or by adding 0.5 equivalent of acetic acid, led to a significant drop in the l/b ratio for the hydroformylation of 10-undecen-1-ol. Characterisation of the supramolecular rhodium complex was made by means of FT-IR, UV-vis, NMR and X-Ray analyses.<sup>[18]</sup> Density functional theory (DFT) calculations indicated that the O-H...O hydrogen bond remained unaffected during the catalysis and allowed the supramolecular ligand to remain bidentate whereas the N-H...N hydrogen bond was sufficiently flexible to induce subtle modifications of the bite angle. This flexibility in the conformation adopted by the supramolecular bidentate ligand is



presumably at the origin of the high activity and selectivity displayed by the **6-DDPon** catalytic system in the hydroformylation reaction.

Table I-1: Hydroformylation of 1-octene

Entry	ligand	conv. (%)	isom. (%)	l:b
1	<b>PPh<sub>3</sub></b>	22	0.3	2.7
2	<b><i>t</i>-Bu-Xantphos</b>	6	1	49
3	<b>6-DDPon</b>	56	3	32

Reaction parameters: Rh:ligand:1-octene (1:20:7000), *c* (1-octene) 1.4 M, 4h, toluene, 10 bar CO/H<sub>2</sub> (1:1). From reference<sup>[17]</sup>

These two examples are a good illustration of the ability of supramolecular catalysts to reach equal or higher selectivity than molecular catalysts. In the case of the hydroformylation reaction, for which wide bite-angle ligands usually provide high l/b ratios,<sup>[1]</sup> the use of non-covalent interactions allow to tune the ligand bite-angle in a way that cannot be obtained with classical covalent catalysts.

Supramolecular catalysts also allow a fine tuning of the selectivity notably in regards of the rhodium-catalysed asymmetric hydrogenation of prochiral substrates. A large variety of covalent ligands were developed for this reaction.<sup>[19]</sup> Historically, bidentate ligands were considered more effective than monodentate ones but recently monodentate phosphoramidite ligands provided high enantioselectivity for many hydrogenation reactions.<sup>[20]</sup> Supramolecular catalysts were also designed for asymmetric hydrogenation reactions using metal-ligand or hydrogen bond interactions but only the latter case will be discussed thereafter.

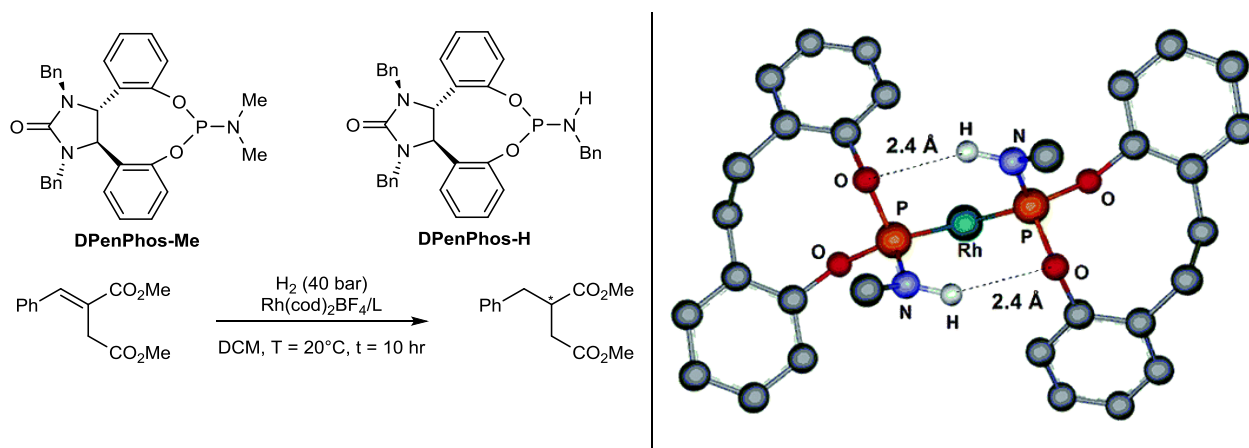


Figure I-10: Left: DPenPhos-Me and DPenPhos-H ligands tested in the rhodium-catalysed hydrogenation of (*E*)-β-aryl itaconate derivatives. Right: B3LYP/6-31G(d) optimised structure of the Rh/DPenPhos-H complex. All C-H hydrogen atoms, and 1,5-cyclooctadiene (COD) are omitted for clarity. Adapted from reference<sup>[21]</sup>

In a similar fashion than previously described for the hydroformylation reaction, formation of a bidentate ligand by means of hydrogen bond interactions can lead to an increase in the catalyst selectivity. Ding *et al.* investigated a series of ligands related to the phosphoramidites **DPenPhos** (Figure I-10 left).<sup>[21]</sup> Hydrogenation of (*E*)-β-aryl itaconate derivatives proved to be challenging as notably no monodentate ligand provided high enantioselectivity. Indeed, several binol-derived phosphoramidite ligands but also **DPenPhos** ligands with a fully substituted nitrogen atom (like **DPenPhos-Me** in Figure I-10, left) are inactive. Replacement of one substituent on the nitrogen atom

by a hydrogen (**DPenPhos-H** in Figure I-10, left) led to full conversion and enantioselectivity up to 98% e.e. Hydrogen-bond interactions between the two **DPenPhos-H** ligands after complexation with cationic rhodium were revealed by  $^1\text{H}$  NMR analyses (see the energy-minimised structure of the complex in Figure I-10, right). This intermolecular hydrogen bonding between the two **DPenPhos-H** monodentate ligands in the catalyst was believed to be crucial for optimal catalyst performance.

Another strategy to modulate the selectivity of ligands by means of non-covalent interactions is the introduction of a regulatory site at a distinct site from the catalytic centre. Vidal-Ferran *et al.* developed several diphosphite ligands in which the two phosphite groups were connected by a covalent ether chain. The ether chain binded alkali metal cations and ammoniums serving as regulatory agents.<sup>[22]</sup> Cation binding brings the two phosphite moiety closer to each other which facilitated the binding of the rhodium catalytic centre in a bidentate fashion (Figure I-11).<sup>[23]</sup> Faster coordination to the rhodium is thus observed leading to no induction period for the hydroformylation reaction. The branched/linear ratio and the stereoselectivity of the hydroformylation of vinyl-acetate were also strongly dependent on the regulatory agent used.

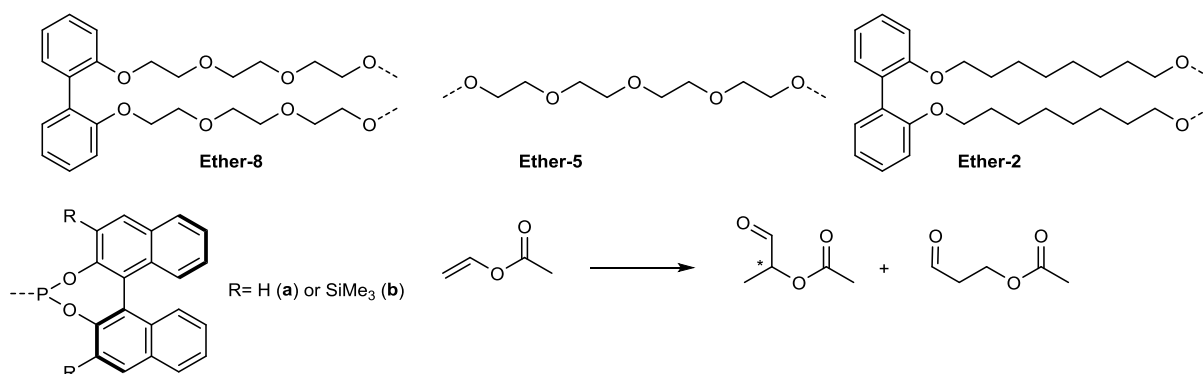


Figure I-11: Bidentate ligand with regulatory agent binding sites and their use in the asymmetric hydroformylation (AHF) of vinyl acetate. Reaction conditions: Vinyl acetate, RA, Ligand,  $[\text{Rh}(\text{acac})(\text{CO})_2]$  with the following ratio (100/1.56/1.2/0.5),  $\text{P}(\text{H}_2/\text{CO} \text{ 1/1}) = 10$  bar, toluene/THF (97/3 v/v). Adapted from reference<sup>[23]</sup>

The selectivity was correlated to the bite-angle of the supramolecular bidentate ligand, as evaluated by DFT calculations (Figure I-12). Indeed, complexation of sodium increased the bite angle as well as the enantioselectivity compared to the ligand alone (from 35% e.e. to 72% e.e.) and use of larger cations ( $\text{K}^+$ ,  $\text{Cs}^+$  and  $\text{Rb}^+$ ) gave higher bite angles and enantioselectivities (up to 96% e.e.).

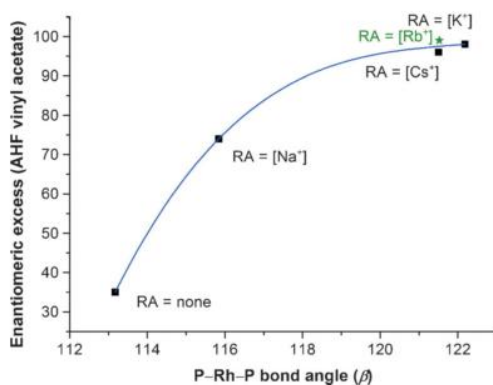


Figure I-12: Plot of the enantiomeric excess obtained in the AHF of vinyl acetate with **Ether-5-b** versus the bite angle of this ligand with different regulatory agents. The bite angles were calculated by DFT calculations. From reference<sup>[23]</sup>

These examples provide a perfect illustration of the influence of supramolecular interactions in the selectivity of a catalyst. Various weak interactions were used to finely tune the properties of the supramolecular catalyst. Importantly, these interactions increased the selectivity and led to unusual selectivities compared to molecular catalysts.

### 3. Chirality induction

Usual strategies for the design of asymmetric catalysts rely on a short distance between the coordinating atom and the stereogenic centre embedded in the same molecular structure. However, recent advances in supramolecular chemistry allowed the development of different strategies for chiral induction using either a chiral group at a remote distance of the coordinating atom or chiral counterions. The latter has been extensively studied and reviewed<sup>[24–26]</sup> during the last years including ion pairs formed between an intrinsically achiral cationic metal catalyst and an enantiopure anion. Next, examples will focus on chirality induction from remote chiral groups to achiral metal centres embedded within the same discrete chiral supramolecular structure.

A seminal example for implementation of remote chirality induction in catalysis was described by Breit *et al.* They investigated supramolecular analogues of the **PhanePhos** ligand named **SupraPhanePhos** (Figure I-13).<sup>[27]</sup> It was designed to mimic the planar chirality of the **PhanePhos** ligand by means H-bonds between amino-acid derivatives located in a remote position of the phosphorus atoms. Without chirality in the vicinity of the phosphorus atom (Do = PPh<sub>2</sub>), a modest enantiomeric excess was achieved (51% e.e. for the hydrogenation of methyl-2-acetamidoacrylate). Not surprisingly, replacement of the phenyl groups on the phosphorus atom by enantiopure Binol led to higher enantiomeric excesses (99%).

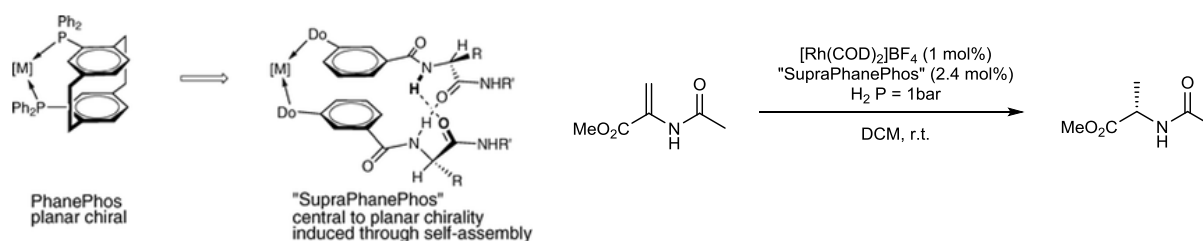


Figure I-13: Comparison of **PhanePhos** ligand and **SupraPhanePhos** ligand with planar chirality induced by remote chiral groups, adapted from reference<sup>[27]</sup>

This example of remote chiral induction was further developed by Kirin *et al.* under the name of backdoor induction.<sup>[28]</sup> They synthesised a large library of monodentate ligands with peptidic chains of various lengths and different position of the phosphorus atom relatively to the aromatic ring. Higher enantioselectivities were obtained (up to 84% e.e.) and rationalisation of the stereoselectivity of the reaction was made using an analogy with the Herrick helical conformation adopted by disubstituted ferrocene peptides (Figure I-14).

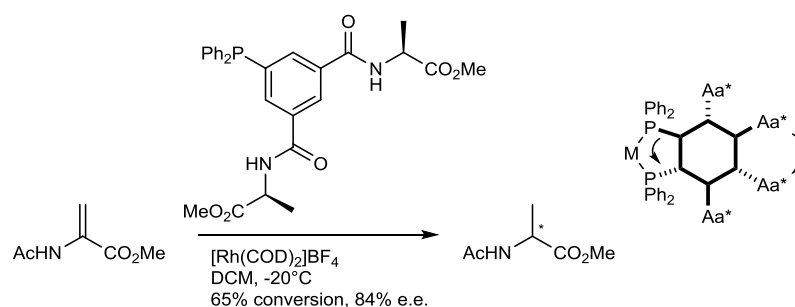


Figure I-14: Left: Monodentate ligand with “backdoor” chiral induction. Reaction conditions: Right: model of the chirality induction. Adapted from reference<sup>[28]</sup>

Chiral ions were used to remotely induce chirality to a metal complex. Reek *et al.* designed a bidentate ligand possessing a remote anion binding pocket.<sup>[29]</sup> The anion binding site was constituted of two 7-aminoindole moieties connected by a methyne bridge (Figure I-15). The X-ray structure of the ligand after coordination with  $[\text{Rh}(\text{nbd})_2]\text{BF}_4$  highlighted the presence of the  $\text{BF}_4^-$  anion in the anion binding site. Rhodium-catalysed hydrogenation of alkene was attempted using anions derivatives of  $\alpha$ -amino-acid as chiral inducers. Substituents on the nitrogen atom of the amino-acids were required to get enantioselectivity. Carbamate and urea derivatives of *L*-Valine provided modest e.e. (23 and 29% respectively). On the other hand, replacement of the urea group by a thiourea strikingly increased the enantiomeric excess (99%). This influence of the nitrogen substituent on the selectivity of the catalytic reaction was probed by DFT calculations. Hydrogen bonding between the amino-acid anion and the amide of the substrate was observed and was in accordance with the lower enantioselectivity obtained for substrates lacking an amide function.

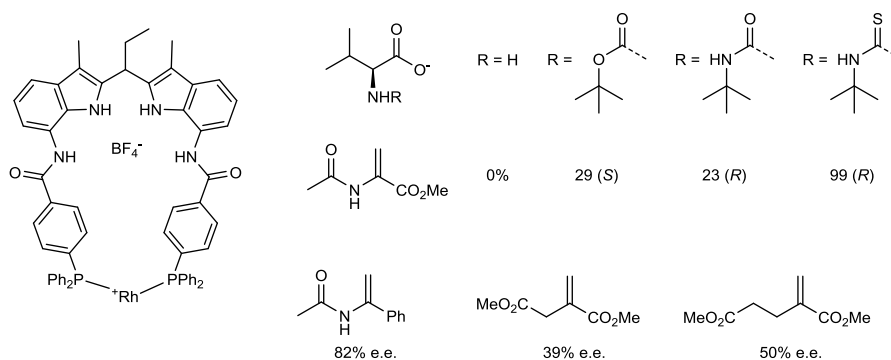


Figure I-15: Design of a ligand with an anion binding pocket. Structures and selectivity of the chiral inducers tested in the rhodium-catalysed hydrogenation of various alkenes. Adapted from reference<sup>[29]</sup>

In the previous examples, the chiral inducers remained present bound to the ligand during the course of the reaction. In the following example, the chirality is brought by the ligand to the helical structure and then the handedness of the helical structure is maintained after removal of the stereogenic centre (chiral memory). Yashima *et al.* developed a double helical molecule based on two alkynyl-platinum complexes (Figure I-16a) appended with complementary amidine/carboxylic groups.<sup>[30]</sup> Formation of ionic hydrogen bond interactions between the two Pt complexes led to formation of the double strand helical structure in which the Pt atoms were in close proximity (Figure I-16a). Enantiopure monophosphine (MOP) ligands introduced in the Pt complex **1a** induced a preferred handedness to the double helix. Interestingly the complex **1a** only displayed a small CD signal in  $\text{CDCl}_3$  whereas upon formation of the helical structure with achiral Pt complex **2** a strong CD signal was observed (**1a.2** assembly). The chirality of the double helix **1a.2** was tuned by the temperature and switched by the solvent (inverse diastereoisomers are observed in toluene and in  $\text{CDCl}_3$ ). Replacement of the MOP and  $\text{PPh}_3$  ligands in the double helical molecule **1a.2** by **dppm** locked the inherent chirality of the complex **3a**. No more stereogenic centres were present in the molecular structure of **3a** but its chirality was retained to a certain extent as demonstrated by CD analyses (chiral memory). Its helicity was directly related to the temperature of preparation and decreasing the temperature from  $25^\circ\text{C}$  to  $-60^\circ\text{C}$  increased the helix screw sense excess (% of maintained helicity of **1a.2**) from 25% to 81%.

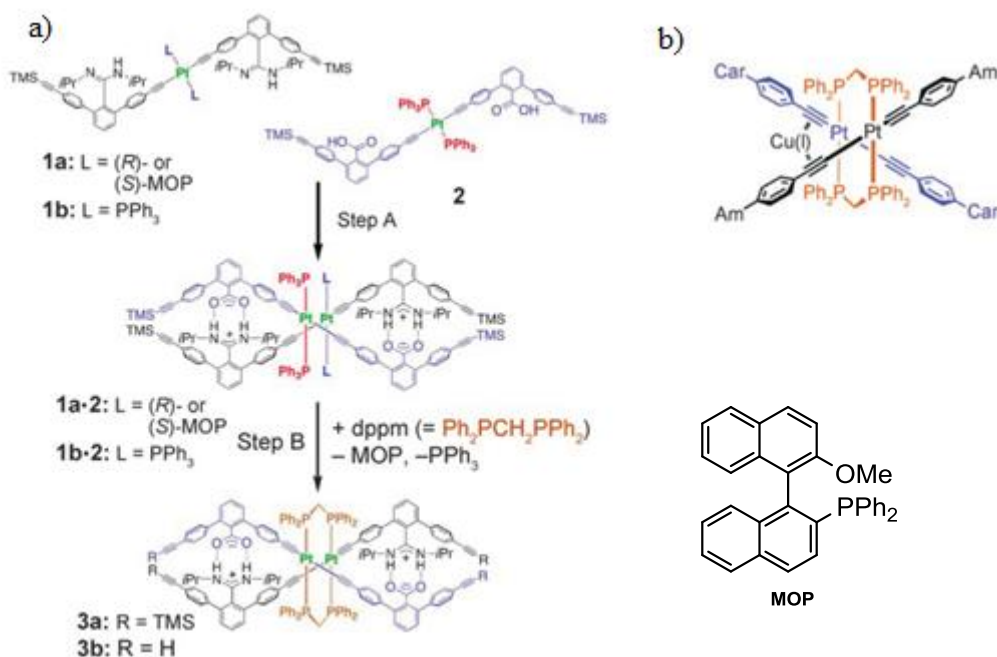


Figure I-16: a) Double helical structure designed by Yashima *et al.* with chiral memory of the handedness upon removal of the MOP ligands. b) Tweezers-like coordination of copper(I) atoms by the alkynes groups in complex **3**. From reference<sup>[30]</sup>

The alkyne groups in **3a** were well positioned for the formation of tweezers-like complexes with copper(I) salts (Figure I-16b). The combination of complex **3a** (with retention of chirality) and  $[(\text{MeCN})_4\text{Cu}]\text{PF}_6$  was tested in the cyclopropanation of styrene (Figure I-17). Enantioselectivity was obtained which increased linearly as a function of the helix screw sense excess of complex **3a**. Up to 85% e.e. was obtained for the *trans* diastereoisomer (main product) albeit the reactivity of the complex was quite low (50 mol% of catalyst loading required to reach 95% yield).

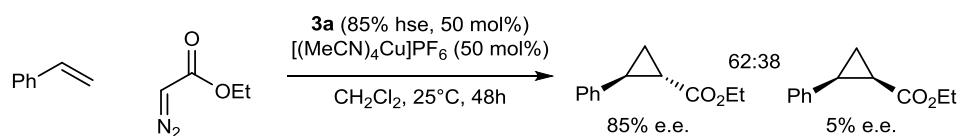


Figure I-17: Cyclopropanation of styrene (2 equivalents) with diazoacetate (1 equivalent) catalysed by a combination of complex **3a** and  $[(\text{MeCN})_4\text{Cu}]\text{PF}_6$ . hse = helix screw sense. Adapted from reference<sup>[30]</sup>

These examples show that chirality induction from remote stereogenic centres to achiral metal centres embedded in the same discrete supramolecular structure may allow efficient enantioselective catalysis. The first two examples allow the modular synthesis of chiral ligands by introduction of chiral inducers at remote positions of the metal centres. In the last example, a different strategy was developed in which the chirality was brought to the catalytic structure during the synthesis and then memorised after removal of the chiral inducer. In that case, one can envision to recycle the chiral inducer in order to perform a truly absolute asymmetric synthesis, *i.e.* a synthesis with no help of a chiral species.

## C. Dynamic covalent and supramolecular polymer structures as scaffold for catalysis

Catalysts mentioned in the previous part are constructed on a discrete and well-defined supramolecular scaffold. Interesting features of these catalysts are their ease of preparation and the possibility of modulating their performance by just changing the nature of one of their building blocks. Important properties arise from the supramolecular interactions present in these catalysts which enable higher selectivity or induction of chirality. One limitation of these catalysts is that they are composed of a limited number of building blocks which implies that their macroscopic properties (solubility, overall structure, three-dimensional conformation) will be modestly affected by changes of their local environment or by activation with a stimulus. In the following part, we will see that catalysts built on a dynamic macromolecular scaffold possess the same features as those mentioned above for the discrete supramolecular catalysts but also additional ones such as the possibility to recycle them, to change their structure by means of a stimulus and the possibility to efficiently induce, switch and amplify supramolecular chirality towards intrinsically achiral metal centres.

### 1. Recyclable stereoselective catalysts

Recyclability of catalytic systems containing expensive transition-metals has been largely studied during the past decades. Homogeneous catalysts covalently immobilised on polymers or adsorbed on silica have notably been intensively studied but often led to poorly active catalysts and the recyclability was limited by the stability of the catalytic resting state. In overall, immobilisation strategies of homogenous catalysts have been scarcely used in industrial processes.<sup>[31]</sup> Supramolecular approaches have also been developed in which the catalysts were connected to an insoluble structure by means of non-covalent interactions<sup>[32,33]</sup> or embedded in a coordination polymer (self-supported catalysts).<sup>[34-36]</sup>

A particularly interesting case has also been developed recently in which the catalyst was reversibly switched between a soluble and an insoluble state by means of non-covalent interactions. Jun *et al.* developed a strategy for which the catalyst was embedded in a hydrogen bond network albeit in a reversible way.<sup>[37]</sup> At high temperature, the hydrogen bond network is disrupted and the catalyst is soluble or miscible with the reactant phase and thus active. At room temperature, the hydrogen bond network was restored and the catalyst was immiscible or insoluble and thus inactive. The first example was a biphasic system consisting of a non polar phase (neat alkene reactant) and a polar phase (containing the Rh catalyst, the ligand, 2-aminopyridine (necessary for the hydroacylation steps) and a mixture of 4,4'-bipyridyl and phenol (Figure I-18)).<sup>[38]</sup> The ligand (P-4-CO<sub>2</sub>HPh(Ph)<sub>2</sub>) had a carboxylic acid moiety that can participate in the hydrogen-bond network. At room temperature the catalyst was embedded in the hydrogen bond network formed by 4,4'-bipyridyl and phenol and was thus inactive. At reaction temperature (150°C) the hydrogen bond network was disrupted, the alcohol reactant was

added and the reaction is monophasic. Once the reaction was completed, the reaction mixture was cooled to room temperature, the hydrogen bond network was thus restored; the catalyst and the products being immiscible the catalyst was recovered by simple decantation.

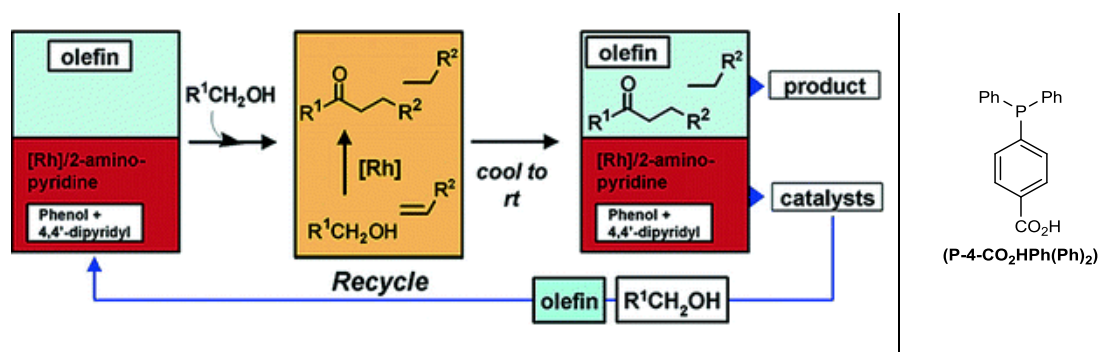


Figure I-18: Left: schematised representation of the biphasic system developed by Jun *et al.* In blue the apolar phase containing the olefin and the final products and in red the polar phase containing the catalyst and a mixture of phenol and 4,4'-dipyridyl. Right: (P-4-CO<sub>2</sub>HPh(Ph)<sub>2</sub>) ligand. From reference<sup>[38]</sup>

The same authors developed a different recyclable catalytic system in which the rhodium complex was covalently attached to a barbiturate unit and put in presence of two metal-free monomers: a tri-aminopyrimidine derived monomer and a barbiturate derived monomer (see formula in Figure I-19).<sup>[39]</sup> The recyclability relied on the strong complementarities between the barbiturate and the tri-aminopyrimidine moieties. At reaction temperature (150 °C) the hydrogen-bond network was disrupted and the reaction occurred in an isotropic liquid phase. Once the reaction was complete, the temperature was cooled to room temperature leading to the restoration of the hydrogen bond network between the barbiturate and the tri-aminopyrimidine moieties. The formed supramolecular polymer was insoluble and was recovered by simple filtration.

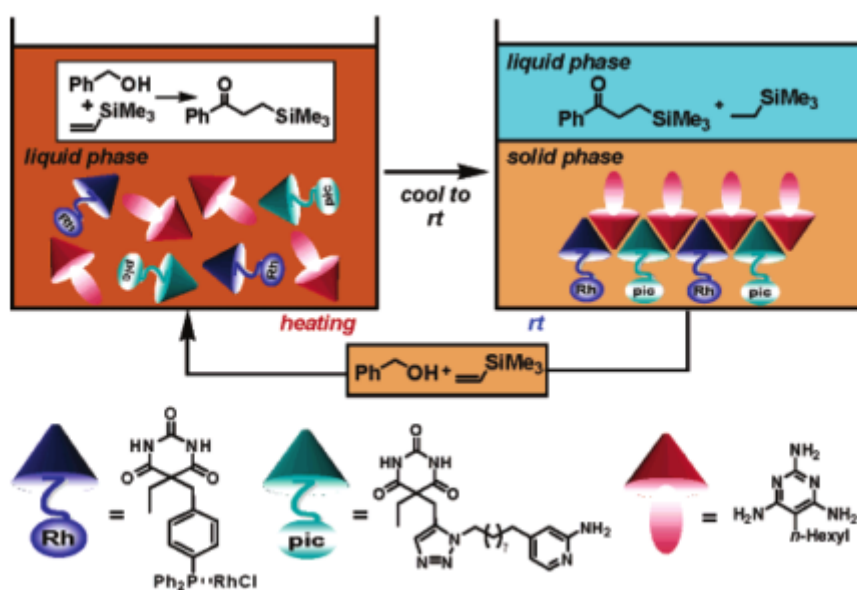


Figure I-19 : Top: Schematised representation of the recyclable system developed by Jun *et al.* for the rhodium-catalysed coupling between benzylic alcohol and trimethyl(vinyl)silane. Bottom: Hydrogen-bond network formed by the self-assembly between the catalyst, barbiturate-derived monomer and tri-aminopyrimidine-derived monomer. From reference<sup>[39]</sup>



Both systems showed high recyclability over at least 8 runs even though for the phenol/4,4'-bipyridyl system rhodium leaching was found (0.005% and 0.01% of the initial Rh for the first two runs). However for both systems, recycling needed to be carried out under argon to avoid degradation of the catalyst which is a major drawback for their potential use in industrial processes.

Supramolecular interactions allowed for the formation of self-supported catalysts which were recovered by filtration or decantation. In these examples, the non-covalent interactions were disrupted in order to process the catalytic reaction and restored in order to recycle the catalytic system. However, the structural changes induced by the self-assembly has not been used to alter the performance of the catalysts. In the following sections, we will show how modification of the three-dimensional organisation of the structure supporting the catalyst will directly influence its catalytic properties.

## 2. Stimulus-induced modification of the catalytic performance

Enzymes have always been a source of inspiration for the design of homogenous catalysts since they display astonishing properties: i) high kinetics (up to diffusion control of the substrate), ii) high selectivity and iii) high substrate selectivity as they are able to discriminate between very similar substrates. Their high selectivity arises from the three-dimensional organisation of the enzyme as the folding leads to the creation of a hydrophobic pocket or a highly polar region (*e.g.* oxyanion hole) which may stabilise a transition state, destabilise the ground state of a substrate or strongly bind substrates. Enzymes are strongly dynamic and switchable catalysts. Indeed, they change their tertiary and quaternary structure under various stimuli, which in turn affects the kinetic and/or the selectivity (allosteric control). Allosteric effects occur when a regulatory ion or a molecule binds to a specific allosteric site distinct from the active site and eventually triggers a change in the conformation of the protein.<sup>[40]</sup> In the case of enzymes, allosteric effects lead to an increase (positive allosterism) or a decrease (negative allosterism) of the enzyme kinetics, to an on/off switch of the enzyme activity or to a change in the selectivity.

Many efforts for the design of artificial catalysts have been deployed in order to mimic the selectivity and dynamic properties of enzymes over the last decades.<sup>[12]</sup> Notably, it has been demonstrated that catalysts based on a polymeric scaffold can adapt their structure upon activation with a stimulus. These structural changes lead to a significant enhancement of their catalytic performance in a way which is reminiscent of the mode of action of allosterically-regulated enzymatic processes.

### a) Solvent and temperature-responsive polymers

#### (1) Thermoresponsive polymers

Most of the thermoresponsive polymers are derived from poly-N-isopropylacrylamide (**p-NIPAM**) since aqueous solutions of **p-NIPAM** show inversed solubility upon heating.<sup>[41]</sup> This transition

between a hydrophilic and a hydrophobic polymer occurs in most cases at a temperature between 30 and 35°C. This is related to the shrinkage of the polymer chains into globules (Figure I-20). This transition can also occur by changing the composition of binary solvent systems as **p-NIPAM** is soluble in water or methanol but shrinks in a mixture of both liquids.

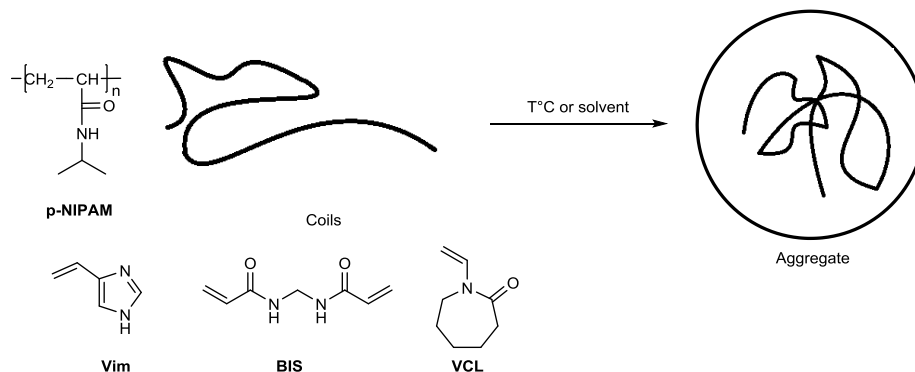


Figure I-20: Schematic view of the effect of temperature or solvent on the structure of p-NIPAM polymer and the chemical structure of the various monomers mentioned in this chapter.

The seminal report of a **p-NIPAM** polymer used as a switchable support for catalysis was published by Tanaka *et al.* using a copolymer between N-isopropylacrylamide and vinylimidazole (**Vim**) monomers, cross-linked by means of N,N'-methylenebisacrylamide (**BIS**) monomers. The ability of the imidazole units to accelerate the reaction rate of hydrolytic reactions was investigated using *para*-nitrophenylacetate (**NPA**) as the model substrate.<sup>[42]</sup> This polymer NIPAM-co-pVim-co-BIS formed a gel in aqueous and ethanol solutions. In aqueous-ethanol binary solvent mixtures, the diameter of the gel decreased as a result of the shrinking of the polymer chains (Figure I-21a). Clearly, the reaction rate of the hydrolysis was enhanced upon gel shrinking (Figure I-21b, open circles). As a control experiment, the authors showed that the catalytic activity of the vinylimidazole monomer was not affected by the composition of the binary solvent system (Figure I-21b, filled circles). Similar example without the cross-linker was also described.<sup>[43]</sup>

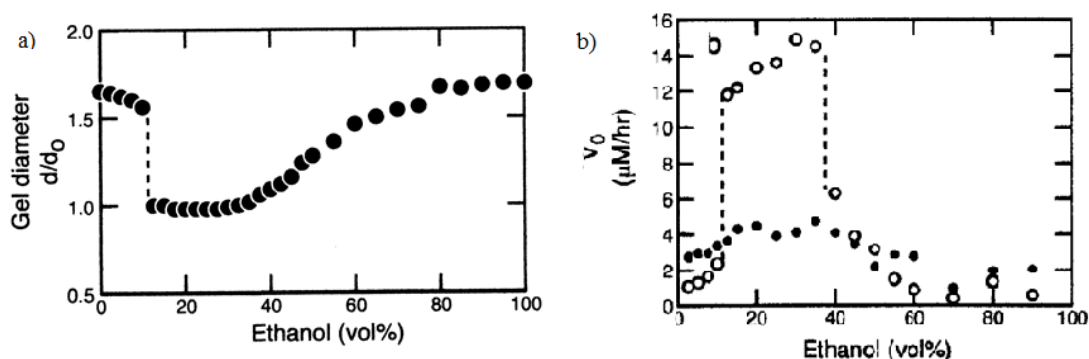


Figure I-21: a) Gel diameter,  $d$ , as a function of vol% of ethanol in ethanol: aqueous buffer mixtures (pH 8.0). b) The initial reaction rate,  $V_0$ , of the hydrolysis of **NPA** as a function of vol% of ethanol in ethanol-buffer mixtures. Catalysis performed by the polymer gel (open circles) and by vinylimidazole monomers (filled circles). In relation with the swelling and shrinking of the gel, the catalytic activity undergoes a discontinuous but reversible change. From reference<sup>[42]</sup>

The thermoresponsiveness of **NIPAM-Vim** or **VCL-Vim** co-polymers for the hydrolysis of **NPA** was studied by Khokhlov *et al.* a few years later.<sup>[44]</sup> Careful interpretation of the data is required in such

cases since the temperature has a direct influence on the reaction rate (Arrhenius law). However, a non-linear behaviour of the semi-logarithmic plot of the reaction rate as function of temperature was observed indicating a change in the catalyst structure as a function of the temperature (Figure I-22). It was likely related to the hydrodynamic radius of the co-polymer and the formation of aggregates upon raising the temperature. The authors postulated that the aggregation lead to an enhanced adsorption of the substrate (**NPA**) on the surface of the aggregates, a region where the local concentration of imidazole moieties is high. However at temperatures above the transition, the activity of the co-polymers gradually decreases.

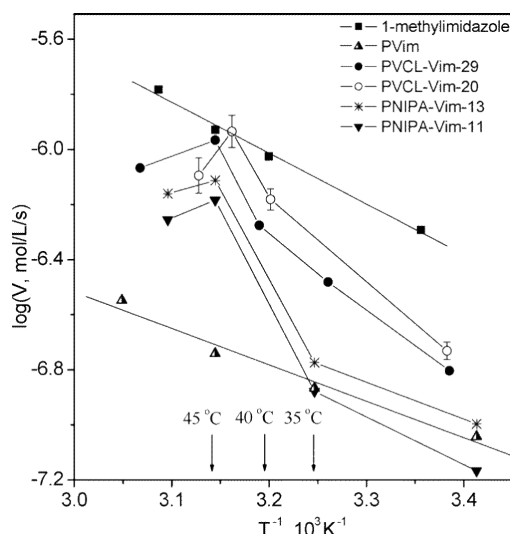


Figure I-22: Semi-logarithmic plot of the reaction rate of the hydrolysis of **NPA** as function of  $T^{-1}$ . The composition of the co-polymer is indicated as follows: PVCL-Vim-29 means 29% of Vim monomer in the co-polymer with VCL. From reference<sup>[44]</sup>

A Similar behaviour was observed for the epoxidation of cyclohexene using a random core-shell co-polymer.<sup>[45]</sup> The core is composed of poly(styrene-co-NIPAM) as scaffold and the shell of poly(NIPAM-co-vinyl pyridine) as schematised in Figure I-23. The epoxidation reaction is catalysed by the iron-porphyrin anchored to the shell by means of metal-ligand interactions with the pyridine moieties of the shell. Thermal responsive behaviour was also studied for the oxidation of phenol into quinone mediated by light with a random p-benzophenone-co-NIPAM catalyst (Figure I-23, right).<sup>[46]</sup> In both cases (as well as for **NIPAM-Vim** or **VCL-Vim** copolymers mentioned above), the catalytic activity was optimal at a temperature close to the transition temperature. The authors hypothesised that the shrinking of the coiled polymers into globules first increases the reaction rate but further aggregation of the polymer chains limits the accessibility of the substrate to the catalytic sites leading to a gradual decrease of the reaction rates at higher temperatures.

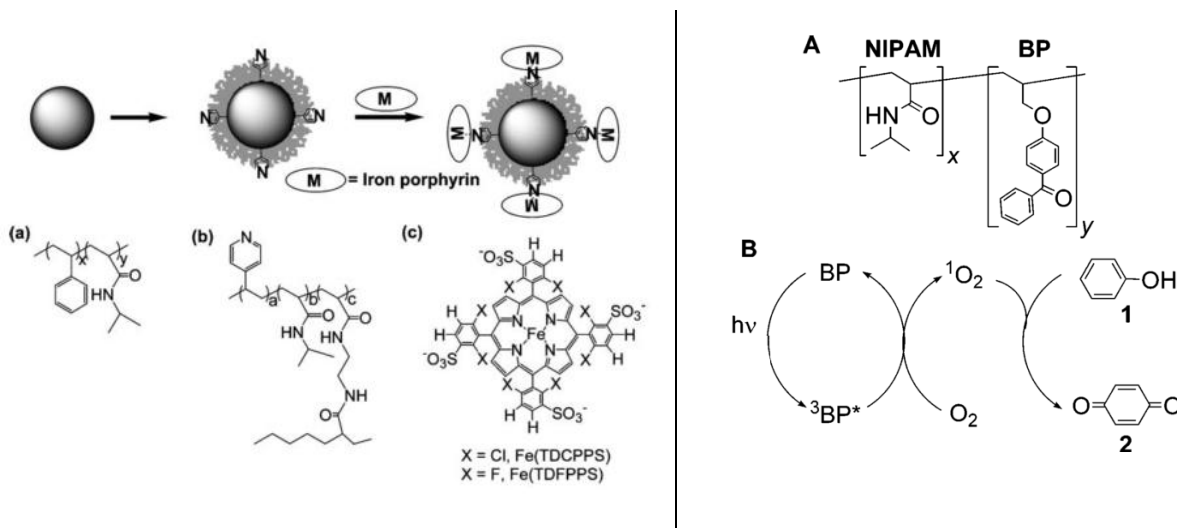


Figure I-23: Left: Thermoresponsive polymers used for epoxidation of cyclohexene. Right: light-induced oxidation of phenol to *p*-quinone by *p*-benzophenone-co-NIPAM catalyst. From references<sup>[45,46]</sup>

Polymers based on NIPAM or VCL monomers were able to change their structures upon thermal treatment or upon changing the solvent composition. The activity of catalysts supported by these polymers was related to these structural changes. In all cases, higher kinetics, were observed around the transition temperature which was reminiscent of the optimal temperature range usually observed in enzymatic catalysis.

## (2) Aggregation-induced structural changes

In the following examples, non-covalent interactions were used to reversibly control the structure of a catalyst supported on a covalent or a non-covalent polymer scaffold.

The concept was notably very well illustrated by the control of the folding/unfolding of polymeric nanoparticles embedding various types of catalysts. Meijer *et al.* designed a random copolymer containing three types of monomers.<sup>[47]</sup> The main monomer was poly(ethyleneglycol)methacrylate (**PEGMA**) which allows the solubility of the polymer in water. The second one was a methylmethacrylate monomer connected to a 1,3,5-benzene tricarboxamide (BTA) unit (**BTAMA**), the BTA moiety serving as a reversible assembly unit. The third one was 4-diphenylphosphinostyrene which enabled the incorporation of a metal catalyst in the polymer upon coordination to the PPh<sub>2</sub> units. Similarly to an enzyme, the resulting amphiphilic copolymer contained a highly hydrophilic part (**PEGMA**) and a hydrophobic part (**BTAMA**, Figure I-24). Folding of the polymer chain arised upon intramolecular self-assembly of the BTA moieties by means of hydrogen bond and  $\pi$ - $\pi$  stacking interactions (more details in part II.C.1). The resulting single chain nanoparticles have a smaller radius of gyration ( $\approx 6.8$  nm) in water than poly(**PEGMA**) confirming the presence of interactions between the BTA moieties within the random copolymer. CD and FT-IR analyses confirmed the association of the BTA moieties. At high temperature the single chain nanoparticles unfolded as a result of the breaking of the hydrogen bond interactions. However, the process was reversible as the polymer folds

again at room temperature. This folding led to the formation of a hydrophobic cavity protecting the coordinated metal from water.

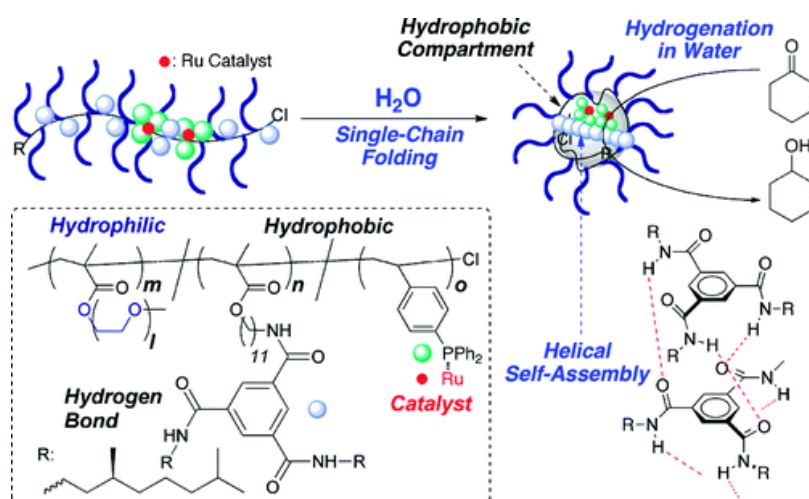


Figure I-24: Schematic representation of the folding of the random copolymer containing PEGMA, BTAMA and 4-diphenylphosphinostyrene monomers. The hydrogen-bond pattern of helical BTA assemblies is also shown. From reference<sup>[47]</sup>

The phosphine Ru catalyst embedded in the polymer nanoparticles was active in the transfer hydrogenation of cyclohexanone into cyclohexanol in water (TON of 980 and TOF 10-20 h<sup>-1</sup>) whereas the corresponding monomeric ruthenium catalysts ([RuCl<sub>2</sub>(PPh<sub>3</sub>)<sub>3</sub>] or [RuCl<sub>2</sub>(P(3-C<sub>6</sub>H<sub>4</sub>SO<sub>3</sub>Na)Ph<sub>2</sub>)<sub>2</sub>]) were inactive. BTA monomers have lateral chiral chains which allow the probing of the self-assembly process by CD spectroscopy. However, even though the BTA monomers assemble under the form of one-handed helices, no enantioselectivity has been observed for the reduction of cyclohexanone by the copolymer. This indicates that the supramolecular chirality of the BTA helices is not transmitted to the catalytic site in the polymer nanoparticles.

The same strategy was used for the construction of an organocatalyst whose reactive site is embedded in the folded copolymer. In that case, 4-diphenylphosphinostyrene was replaced by a proline-derived methacrylate monomer in the random copolymer.<sup>[48]</sup> These copolymers proved to be selective (94% d.e., 74% e.e.) for the aldol reaction between 4-nitrobenzaldehyde and cyclohexanone (Figure I-25). Proline alone is active in micellar systems but poorly active when used alone in water.<sup>[49]</sup> It infers that the good activity and selectivity observed for the copolymer is related to the confinement of the proline units in the hydrophobic part of the co-polymer.

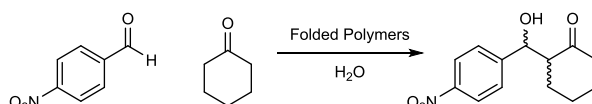


Figure I-25: Aldol condensation between 4-nitrobenzaldehyde and cyclohexanone from reference<sup>[48]</sup>

As a control experiment, a copolymer was prepared in which the amide functions have been alkylated precluding the self-association of BTAs through hydrogen bonds. As expected, the absence of hydrogen bonds between the BTA units prevents the folding of the polymers and thus no activity is detected. Influence of the chemical structure of the copolymer on the stereochemical outcome of the

reaction was probed and most of the modifications (length of the polymer chain, % of proline monomers and addition of propargyl monomers as hydrophobic groups) led to a strong erosion of the stereoselectivity of the catalyst. Interestingly, using achiral instead of chiral BTA monomers led to a decrease of the diastereoselectivity but not of the enantioselectivity.

Higher enantioselectivity for these folded copolymers can be achieved using a supramolecular approach: the random copolymers were combined with a monomeric BTA.<sup>[50]</sup> The aim of the approach was to incorporate any type of catalysts in the copolymers by means of hydrogen-bond interactions between a catalyst-appended BTA monomer (*e.g.* **(S)-BTA-L-Pro**) and the BTA units covalently attached to the folded copolymers (*e.g.* **p[oEGMA-co-BTAMA]**, Figure I-26).

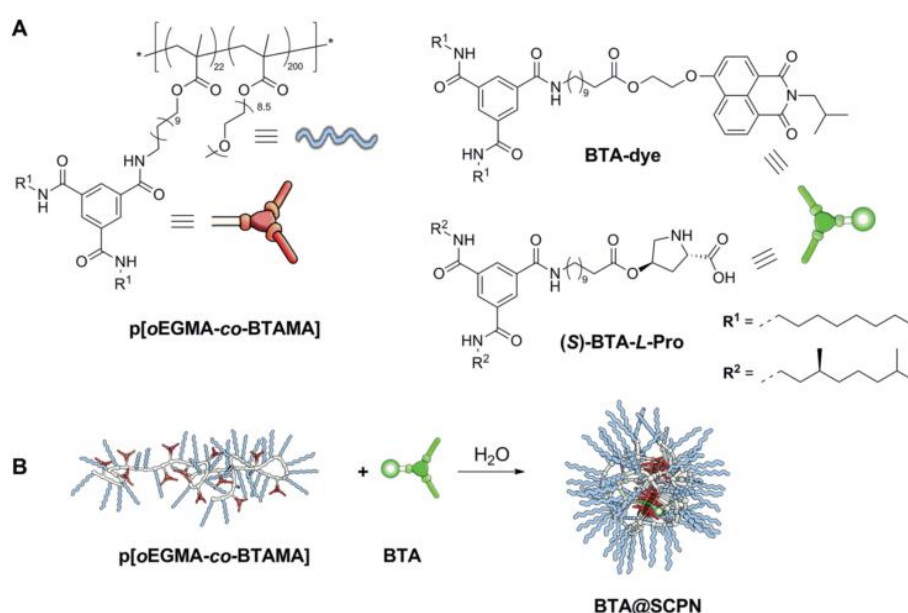


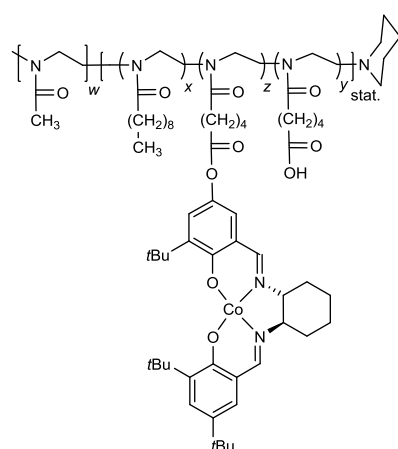
Figure I-26: A): structure of the co-polymer **p[oEGMA-co-BTAMA]**, **BTA-dye** and **(S)-BTA-L-Pro** B): schematic representation of the folding the **p[oEGMA-co-BTAMA]** in water in presence of a BTA monomer. From reference<sup>[50]</sup>

A BTA appended with a fluorescent moiety (**BTA-dye**) was prepared and its incorporation into the polymer was probed by UV and fluorescence analyses. A shift in the main absorbance band of the UV spectrum of the **BTA-dye** when mixed with the copolymer unambiguously ascertains the incorporation of **BTA-dye** within the BTA stacks of the co-polymer. Catalytic experiments were performed by mixing a BTA monomer connected to a proline moiety (**(S)-BTA-L-Pro**) with the copolymer **p[oEGMA-co-BTAMA]**. A significant increase of both the diastereoselectivity (91% d.e.) and enantioselectivity (98% e.e.) was found comparatively to the copolymer with covalently attached proline units. Interestingly, the authors found out that **(S)-BTA-L-Pro** alone is also selective yet significantly less active for the same reaction (see Figure I-28 for more details on this catalytic system).

A similar strategy was described previously by Weberskirch *et al.* using a random copolymer containing a catalytically-active cobalt salen complex (Figure I-27a). As a result of its amphiphilic character, this copolymer is able to form vesicles in water (Figure I-27b, ≈14.3 nm).<sup>[51]</sup> Cobalt salen

complexes are commonly used as catalysts for the hydrolytic kinetic resolution (HKR) of epoxides which leads to enantiopure epoxides and diols of opposite configurations.<sup>[52]</sup> In these reactions controlling the amount of water is crucial in order to limit the conversion and ensure high enantioselectivity. On the contrary, the co-polymer in Figure I-27 is active and selective in pure water. The aggregation behaviour of the polymer into vesicles induces the formation of a hydrophobic pocket around the cobalt-salen complex that limits the access of water molecules to the Co centre. It led to controlled conversion (around 50 %) and high selectivity (from 91 to >99% e.e. for the epoxide and from 87 to 95% e.e. for the diol depending on the nature of starting epoxides).

a)



b)

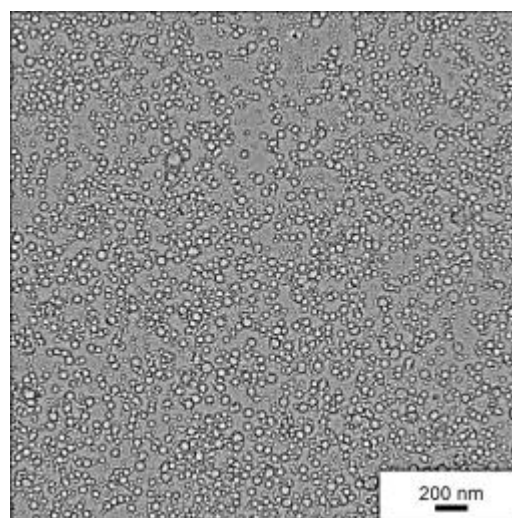


Figure I-27: a) Random copolymer used for the HKR of epoxides. b) TEM micrograph of the vesicles formed by the polymer in water (concentration in polymer = 2 mg.mL<sup>-1</sup>, 0.31 mmol). From reference<sup>[51]</sup>

### (3) Supramolecular assembly

In the preceding examples, the catalyst is supported by a covalent backbone whose conformation can be altered upon aggregation. Not surprisingly, catalysts supported by non-covalent backbones have also been investigated since such backbones will be particularly responsive to small variations of the experimental conditions. Two classes of non-covalent backbones are described below: supramolecular polymers and low-molecular weight gelators (LMWGs). The main differences between those two types of supramolecular assemblies are their structures and stabilities. LMWGs form a 3D fibrillar networks resulting from dense cross-linking between long 1D assemblies. These gels constitute a metastable state between solution and precipitate. Supramolecular polymers form well-defined, predictable, thermodynamically stable one-dimensional assemblies. A precise definition of supramolecular polymers and their potential properties as supramolecular scaffolds for catalysis will be discussed more precisely in Chapter II. Herein, examples of their recent application as dynamic supramacromolecular scaffolds for catalysis will be discussed followed by application of LMWGs in catalysis.

Palmans *et al.* investigated the aggregation properties in water of BTA monomers bearing a peripheral proline unit group able to catalyse the aldol reaction. **(S)-BTA-L-Pro** (Figure I-28) was found to form long helical supramolecular polymers when dispersed in water as indicated by its CD spectra which displayed characteristic signals for long helical rods. The proline unit was used as the catalytic site for a model aldol reaction (between cyclohexanone and *para*-nitrobenzaldehyde, Figure I-25). When the supramolecular polymer was dispersed in water, it provided 10% conversion and 60% d.e. and no e.e. for the reaction. However, temperature treatment of the supramolecular polymer, prior to catalysis, increased the conversion and diastereoselectivity of the reaction (90% conversion, 90% de and 97% e.e.).<sup>[53]</sup> Running the reaction with a soluble catalyst (either in 5% methanol in water or in pure methanol) strongly decreased the activity. The enhanced activity likely arised from a reorganisation of the proline groups along the supramolecular polymer. The appearance of a different CD signal after the temperature treatment seemed to corroborate this hypothesis as well as the appearance of a CD signal for **BTA-Pro** which lack stereogenic centres on the alkyl side chains. Replacement of the alkyl chain of the BTA by poly(ethyleneglycol) (**BTA-PEG-L-Pro** Figure I-28) allowed to avoid the temperature treatment, but resulted in a slightly lower reactivity and selectivity(5% loss).<sup>[54]</sup> Diluting the proline groups along the supramolecular polymer was made by using **BTA-PEG** as co-monomer. However, it had minimal effect on the reaction outcome (maximum variation of the selectivity = 6%). These results pointed out a completely different catalytic behaviour for **BTA-L-Pro** and **BTA-PEG-L-Pro** self-assemblies.

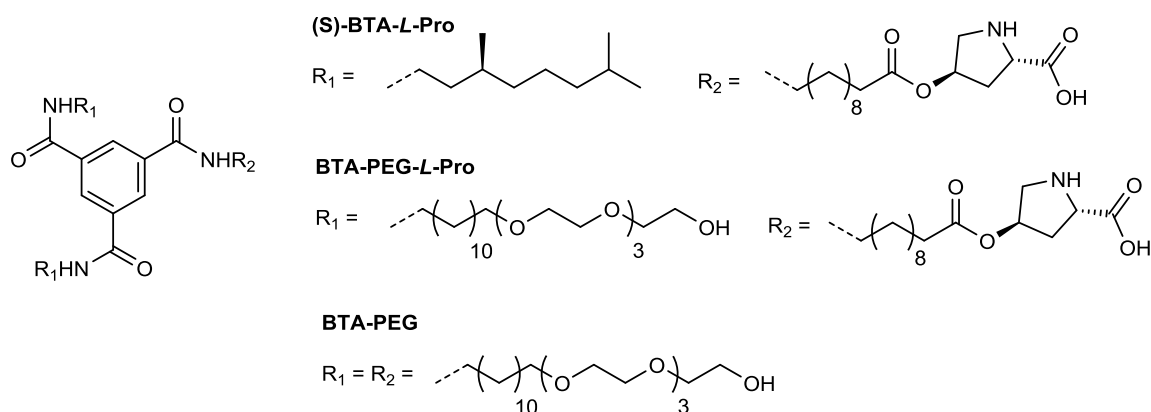


Figure I-28: Chemical structures of **BTA-L-Pro** and **BTA-PEG-L-Pro** used as catalysts for aldol reactions in water. Adapted from references<sup>[53,54]</sup>

These examples show the influence of the substituents of the BTAs on their assembly behaviour. On one hand, **(S)-BTA-L-Pro** is not or poorly soluble in water and requires reorganisation of its proline groups upon heating to be catalytically active and selective. On the other hand, **BTA-PEG-L-Pro**, is soluble in water, and is directly organised to perform the catalysis upon dissolution. The catalytic properties of those BTA-based supramolecular polymers arise from the macromolecular organisation of their catalytic centres along the macrostructure. In the following example, similar effects are also observed through the inclusion of additives inside the macrostructure.



Elemans *et al.* recently reported the self-assembly properties of tris-porphyrin-substituted BTAs in organic solvents and on surfaces.<sup>[55]</sup> In solution, these BTAs assembled into long columnar stacks with the classical three-fold hydrogen bond and aromatic interactions of the BTA core but also with  $\pi$ - $\pi$  interactions involving the peripheral porphyrin moieties. Coordination of manganese by the porphyrins did not alter the self-assembly of tris-porphyrin-substituted BTA monomers (**Mn-TAP**, Figure I-29a). Manganese porphyrins were known to catalyse the photo-oxidation of *cis*-stilbene to epoxide (Figure I-29b) with usually poor stereoselectivity (*trans/cis* ratio around 1.3) and the solvent was found to have little influence on this ratio. Use of **Mn-TAP** as photocatalyst took advantage of the formation of a supra-macromolecular structure to modulate the stereoselectivity of the epoxidation of *cis*-stilbene.<sup>[56]</sup> A modest selectivity in favour of the *trans* isomer (*trans/cis* ratio=2.4) was observed in DCM. Running the reaction in cyclohexane in which the catalyst is self-assembled led to a significantly higher *trans/cis* ratio (up to 7.3). This enhanced selectivity in favour of the *trans* isomer may arise from the little space left around the porphyrins within the stacks. The influence of the number of equivalents of DABCO with respect to the Mn-porphyrin ( $r_{\text{DABCO}}$ ) on the selectivity of the reaction was also investigated. In both DCM and cyclohexane solvents the conversion decreased upon increasing  $r_{\text{DABCO}}$ . However, the influence of  $r_{\text{DABCO}}$  on the selectivity was only observed when the reaction was run in cyclohexane with an optimal selectivity for  $r_{\text{DABCO}} = 2$ . A possible rationale for the selectivity was given: an aromatic interaction between the aryl groups of *cis*-stilbene and the porphyrins favours the formation of the *trans*-epoxide (Figure I-29c).

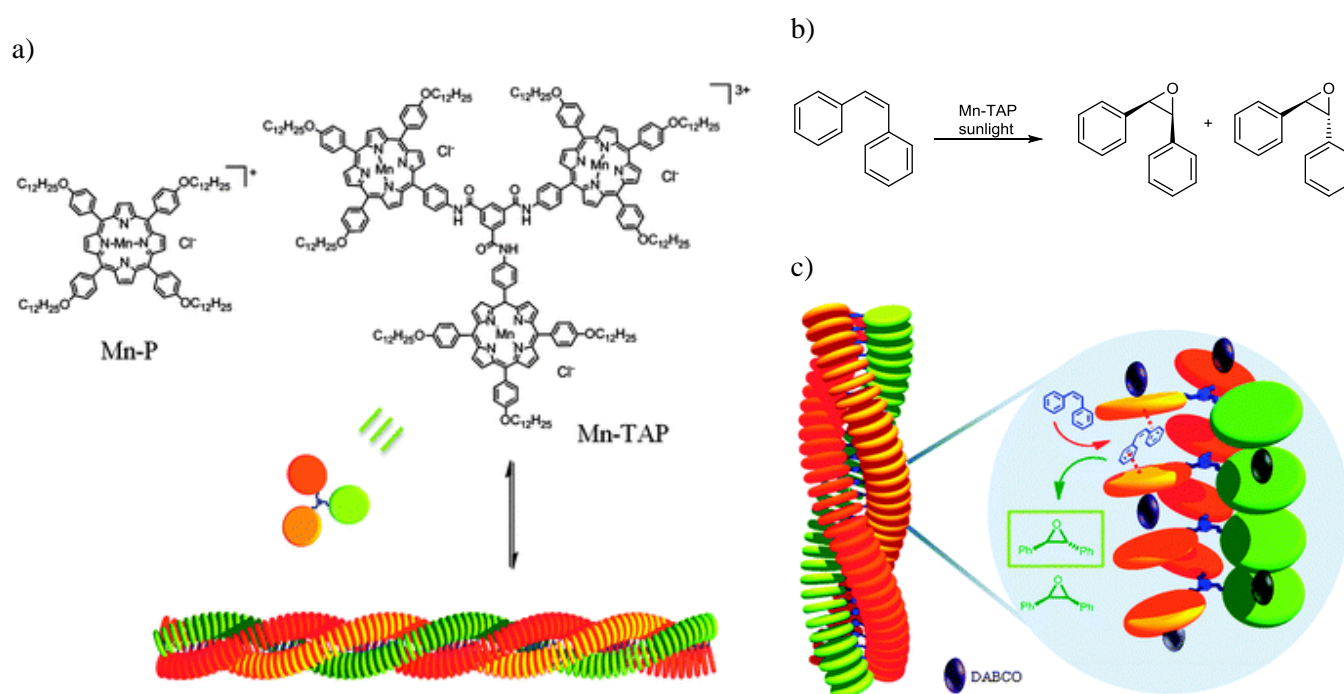


Figure I-29: a) Chemical structures of monomers Mn-P and Mn-TAP and a schematic representation of the columnar stacks formed by Mn-TAP. b) Photo-catalytic epoxidation of *cis*-stilbene c) Proposed schematic model of part of a catalytic stack of Mn-TAP, including DABCO axial porphyrin ligands, showing the way *cis*-stilbene enters the stacks to react in the restricted space imposed by the porphyrin units. From reference<sup>[56]</sup>

Similar organisation effects on the catalytic outcome were found by means of LMWGs as scaffolds and examples will be discussed below. LMWGs usually gel the solvent upon cooling from their isotropic state (solution).<sup>[57]</sup> Examples of physical gels used as reaction vessel are limited compared to their use in a multitude of other applications. One may ask if the diffusion of the reactive species is not limited by the viscosity of the medium. On the one hand, several groups have studied diffusion phenomena in gels and no significant influence of the viscosity of the reaction medium on the diffusion was found.<sup>[58-60]</sup> On the other hand, a strong decrease in the reaction rate is observed when compared gel and stirred solution (10-20 fold) whilst this difference decreases in an unstirred medium (1-3 fold).<sup>[61]</sup>

The seminal paper on the use of a LMWG gel for catalysis was published by Inoue *et al.* They described the catalytic addition of hydrogen cyanide on aromatic aldehydes catalysed by a dipeptide (Figure I-30).<sup>[62]</sup> The cyclic dipeptide forms a gel under the reaction conditions and they observed higher enantiomeric excess for the reaction of benzaldehyde in the gel state (97 % e.e.) than in solution (up to 82 % e.e. with some racemisation issues). However, rationalisation of the results appeared quite difficult at that time as the enantiomeric excess strongly depended on the purification method of the catalyst.

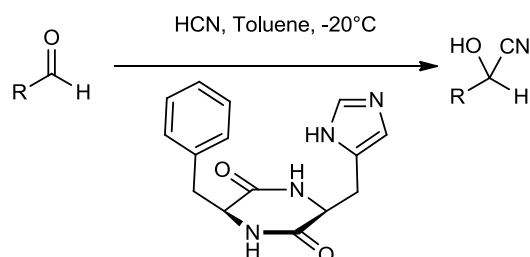
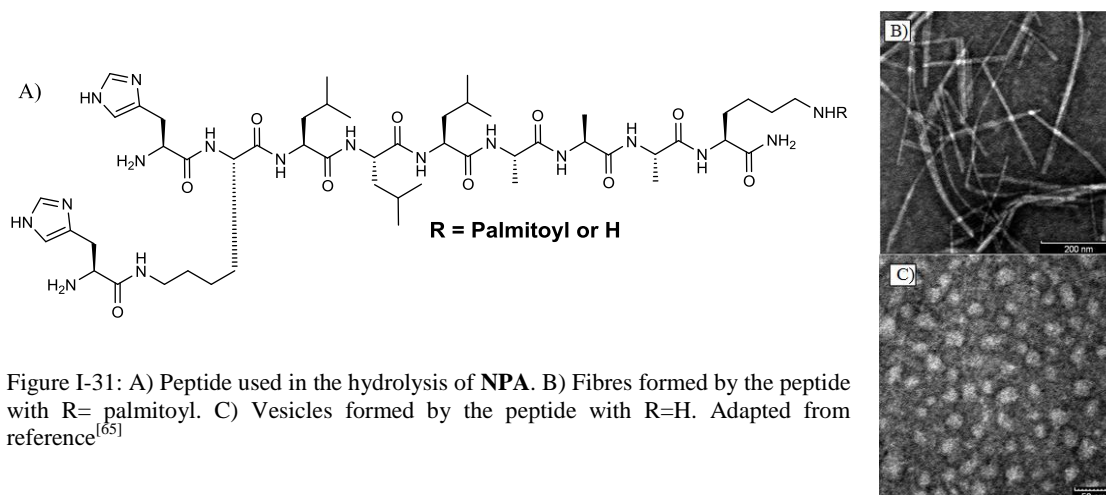


Figure I-30: Dipeptide-catalysed addition of hydrogen cyanide on aromatic aldehydes. Adapted from references<sup>[62,63,64]</sup>

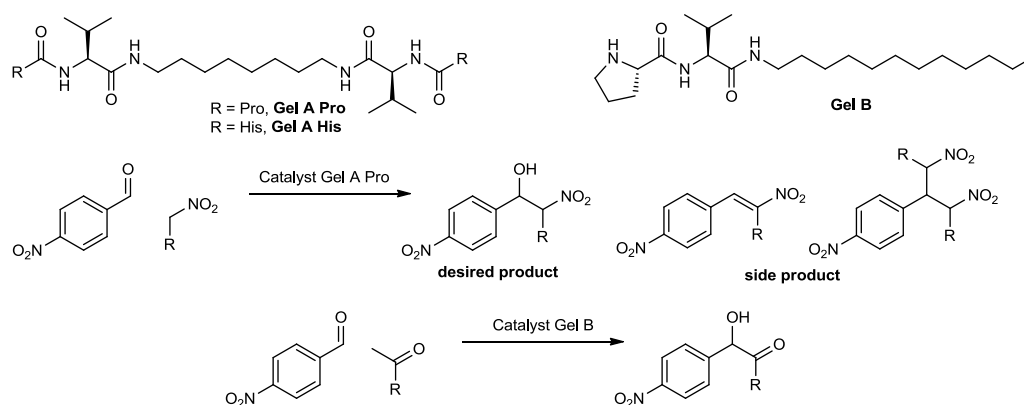
Danda *et al.* further investigated the intriguing properties of this catalytic system and discovered that the preparation of the catalyst itself was less important than its morphology in the solid-state. Indeed, the gel made from the amorphous solid induces higher enantiomeric excesses than that prepared from the crystalline solid.<sup>[63]</sup> The enantiomeric excess was also found to be influenced by the stirring rate as the gel was thixotropic (*i.e.* the viscosity of the medium decreased with the age of the stirred gel). Additionally, this catalytic system constitutes a rare example of an asymmetric auto-catalyst.<sup>[64]</sup> Indeed, the enantiomeric excess of the product was found to increase with the conversion and only a small enantiomeric excess of the dipeptide catalyst was required to obtain the highest enantioselectivities. The active catalyst was supposed to be a chiral aggregate between the dipeptide and the product leading to the auto-catalytic pathway and thus amplification of chirality. This example illustrates the impact of the dynamic structure of the gel on the stereoselectivity of the reaction as the incorporation of the product into the gel led to an autocatalytic pathway.

Further investigations on the relation between a gel macrostructure and its reactivity were done more recently. The hydrolysis of *para*-nitrophenylacetate (**NPA**) was surveyed using several polypeptides

with or without long peripheral alkyl chains (R group, Figure I-31).<sup>[65]</sup> Polypeptides with palmitoyl alkyl chains formed long fibres while those lacking the palmitoyl group formed vesicles. The catalytic rate strongly depends on the morphology of the aggregates: long fibres are four times more active than vesicles. The superior reactivity of the fibres over the vesicles likely arose from the formation of clusters of reactive sites (the imidazole moieties) at the surface of the fibres.



The influence of the gel macrostructures formed by assembly of small molecules on the reactivity was described by Miravet *et al.* They designed polypeptidic LMWGs containing peripheral proline units and tested them as catalysts in the Henry reaction (**Gel A Pro**, Figure I-32)<sup>[66]</sup>. At 5°C (gel), the reaction between 4-nitrobenzaldehyde and nitroethane reached full conversion whereas at 25°C (solution) the reaction only reached 20% conversion with consequent amounts of side products (see formulas in Figure I-32). This difference in reactivity between the gel and the solution was explained by the increased basicity of the proline residues due to their alignment in the gel phase. However, this peculiar reactivity was dependent on the substrate used: other aromatic aldehydes mostly led to side products meaning that the selectivity depended on the substrate. A significant increase of the conversion in the gelled state compared to the solution was also observed in the case of the hydrolysis of **NPA** using **Gel A His** (Figure I-32).<sup>[67]</sup>



Dipeptides containing proline and valine residues were also investigated in aldol reactions (**Gel B**, Figure I-32). The conversion increases with the hydrophobic character of the substrate.<sup>[69]</sup> This effect was attributed to the formation of a bilayer by the catalyst that buried the proline residues into a hydrophobic pocket. Unfortunately, the enantiomeric excesses remained modest for all the substrates tested (up to 40% e.e.). They could also observe up to four polymorphs according to the preparation method of the gel from **Gel B** (sonication, heating, temperature and pH). A strong dependence was found between the polymorphism of the gel and their reactivity: polymorph **A** prepared by sonication of the solution after heating gave the highest enantioselectivity (70% e.e.) and shortest reaction time (2, 4 and 24 h for polymorphs **A**, **B** and **C** respectively).<sup>[68]</sup>

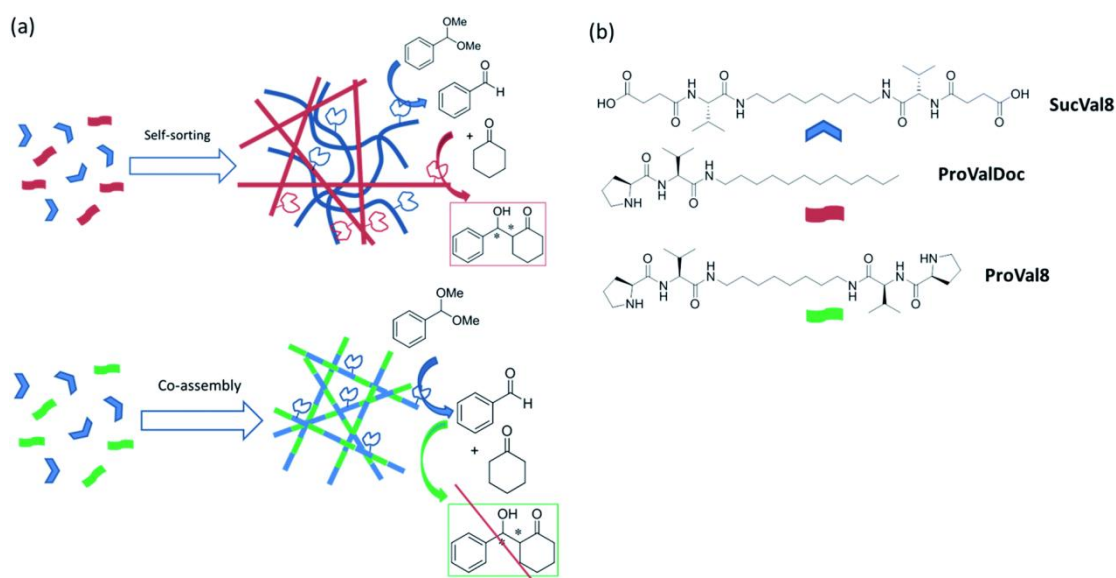


Figure I-33: Dual catalysis system based on space separation of incompatible catalytic reactive sites. From reference<sup>[70]</sup>

Based on their previous examples, Miravet *et al.* developed a gel system for the one-pot conversion of acetal into cross-aldol products.<sup>[70]</sup> This two-step reaction requires a Brønsted acid (acetal hydrolysis) and base (cross-aldol reaction) that will immediately be deactivated through acid-base reaction if mixed together in solution. To tackle this challenge, the two catalytic species should self-sort into two different compartments in order to maintain their inherent reactivities. It was achieved by supporting the two catalysts on two distinct supramolecular structures (Figure I-33). Hydrogelators **SucVal8** and **ProValDoc** self-sort into two different structures and thus catalyse the tandem catalytic process. On the contrary, **SucVal8** and **ProVal8** co-assemble in the same fibers, leading to a quenching of the catalysts. It provides an interesting example in which compartmentalisation of the two catalytic sites (acidic and basic) is achieved through the self-sorting and yield an efficient tandem catalyst.

Catalyst organisation in the previous examples led to an increased reactivity and/or selectivity but has also permitted two incompatible reactions to be pursued in the same flask. This space separation of several reactive sites in order to avoid non-desired reactions and catalyst degradation is also found in enzymes and these examples underlined the importance of supramolecular chemistry for the design of dynamic catalysts.

Substrate pre-organisation is a prerequisite to obtain high reaction rates in enzymes. It was also envisaged as a solution to increase the rates of photocatalytic reactions conducted in ionic gels. Shinkai *et al.* studied two-component gels between gallic acid derivatives and 2-anthracene-carboxylic acid (Figure I-34a). The photodimerisation of the latter was investigated in both the gel and solution states. The formation of the gel has a beneficial effect on the selectivity of the reaction as only head-to-head products were obtained (**C** and **D**) in gel instead of a mixture of head-to-head and head-to-tail (**A** and **B**) dimers in solution.<sup>[71]</sup> In both cases, the enantioselectivity remained low (10% ee at the maximum for **B** and **C**) and modification of the chemical structures of gallic acid derivatives was not sufficient to improve significantly the enantioselectivity.<sup>[72]</sup> In a similar fashion, [2+2] photodimerisation of olefins in the gel state was observed by Biradha *et al.*<sup>[73]</sup> In that case, the two-component gel was composed of pyridyl-benzimidazole (Figure I-34b) and a silver salt. In the gel, only head-to-tail dimers of pyridyl-benzimidazole were observed, the same reactivity was also observed in the xerogel (obtained after removal of the solvent) thus indicating that efficient pre-organisation of the substrate occurred in the gel phase.

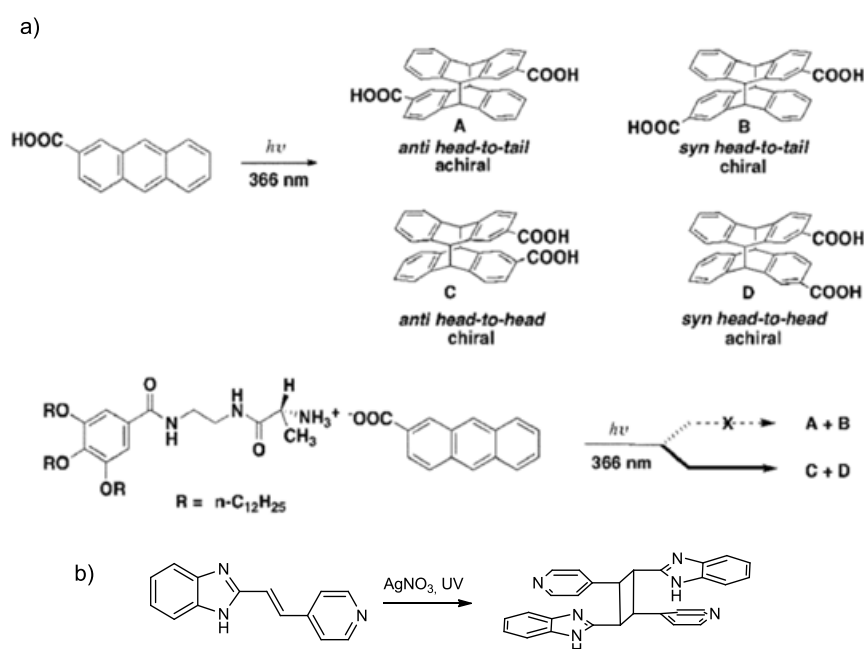


Figure I-34: Gelators used for photodimerisation reactions and the products obtained. From references<sup>[71-73]</sup>

The examples mentioned in this section clearly demonstrate how catalytic sites can be affected upon a structural change of their dynamic covalent or supramolecular polymer scaffold. This spatial reorganisation of the catalytic sites often led to a significant modification of their catalytic performance (activity, selectivity) compared to their pristine state. Enhanced activity and selectivity in the reorganised state is likely the result of a compartmentalisation of the catalytic sites which may limit side reactions and favour cooperative effects. The influence of the structural change (*e.g.* folding/unfolding of the polymeric backbone) on the catalytic outcome of the reaction has been compared for two *independent reactions*. Future investigations must focus on dynamic systems for

which structural changes, and their influence on the catalytic reaction, can be triggered reversibly during the course of the catalytic reaction.

### 3. Chirality transfer

In section B.3, we have seen examples of chirality transfer between an intrinsically achiral catalyst and a chiral inducer located in the same discrete supramolecular structure. We will show here that dynamic covalent and supramolecular polymers can also be used to induce, switch and amplify chirality to catalytic sites located at their peripheries.

#### a) Chirality induction

Recently, dynamic polymers were used as scaffolds in catalysis in order to modulate reactivity or to induce chirality. The modulation of reactivity mainly concerns thermoresponsive polymers (see C.2.a)) whereas chirality inducing strategies are based on polymers with a dynamic helical conformation.<sup>[74–76]</sup> Chirality induction and amplification are well known phenomena in synthetic helical polymers such as polyisocyanates.<sup>[77]</sup> Two major effects were observed in these polymers: sergeants-and-soldiers (S&S) and majority rule (MR) effects. S&S principle is the ability of a small amount of chiral monomers, copolymerised with achiral monomers, to transfer their chirality to the macromolecules. On the other hand, MR principle describes the preference for one handedness for a helical polymer composed of a scalemic mixture of enantiopure monomers. Several static helical macromolecules have been investigated as scaffolds for catalysis but their catalytic results in asymmetric reactions were modest.<sup>[78–82]</sup> Major advances in this domain were made recently by Suginome *et al.* with the use of dynamic helical polymers as efficient scaffolds for asymmetric catalysis (Figure I-35).

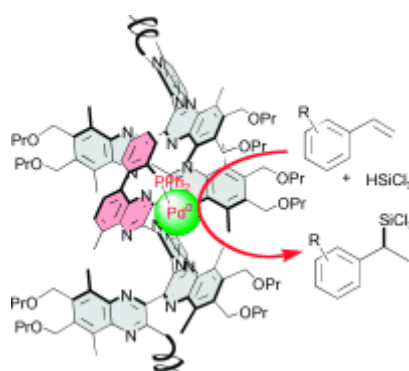


Figure I-35: Chemical structure of the PQQ ligands used in palladium-catalysed asymmetric hydrosilylation reactions. From reference<sup>[83]</sup>

Suginome *et al.* first developed the helix-sense selective living polymerisation of *o*-diisocyanobenzenes for the preparation of enantio-enriched poly(quinoxaline-2,3-diyil)s (PQQ). These polymers exhibit a dynamic and robust helical structure in solution.<sup>[75]</sup> The polymers obtained by mixing a chiral initiator and two different achiral monomers (one that will act as a spacer, the other as ligand) exhibited a high screw-sense excess and were soluble in a large variety of organic solvents.<sup>[83]</sup>

Low-molecular weight polymeric ligands (20-40 quinoxaline units, Figure I-36) were tested in the palladium-catalysed hydrosilylation of styrene with low catalyst loading (0.05 mol%). The influence of the ratio and of the relative position of the different monomeric units on the selectivity of the reaction was precisely probed (Table I-2).

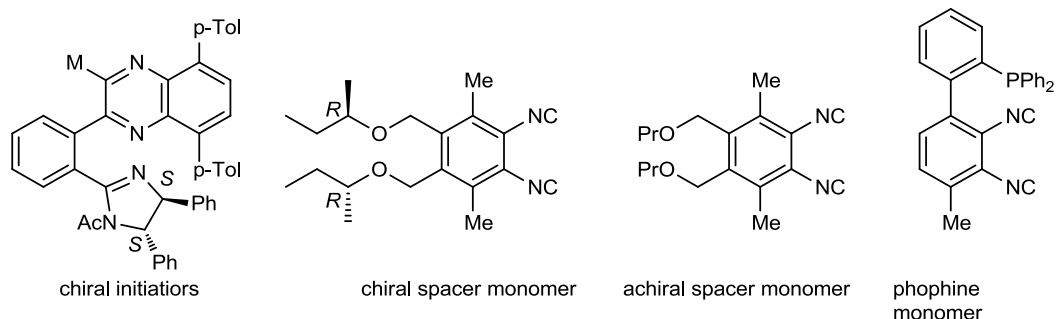
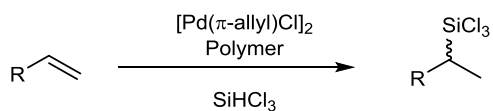


Figure I-36: Monomers used for the preparation of random copolymers by Suginome *et al.* For the chiral initiator, M= [PdI(PMe<sub>2</sub>Ph)] or [NiCl(PMe<sub>3</sub>)]. The phosphine monomer is incorporated during the polymerisation under the oxidised form and reduced thereafter in order to obtain the functional catalyst. Adapted from references<sup>[83]</sup>

Polymers with phosphine units are needed to obtain reactivity (entries 1 and 2). Also, helices with inversed handedness gave the opposite enantiomer for the hydrosilylation product with the same selectivity (85% e.e., entry 3). The distance between the chiral initiator and the phosphine units as well as the number of monomers after the phosphine unit in the polymer did not influence the enantioselectivity (entries 2,4 and 5). In contrast, the presence of several contiguous phosphine units led to an erosion of the enantioselectivity (entries 2,7-9). The absence of spacer at the end of the polymer dramatically lowered the selectivity of the catalytic reaction as well (from 85% e.e. to 5% e.e. compared entries 2 and 6). Longer polymers with multiple phosphine groups separated by blocks of approximately 10 spacer units provide the same e.e. (83%) than shorter polymers with similar monomer composition.

Table I-2: Catalytic experiments with different PQX ligands used in the palladium-catalysed hydrosilylation of styrene. From reference<sup>[83]</sup>



Entry	Ligand	yield (%)	e.e. (%) <sup>(a)</sup>
1	( <i>P</i> )-poly-2*	0	-
2	( <i>P</i> )-P(10-1-10)	97	85 ( <i>S</i> )
3	( <i>M</i> )-P(10-1-10)	98	85 ( <i>R</i> )
4	( <i>P</i> )-P(30-1-10)	88	84 ( <i>S</i> )
5	( <i>P</i> )-P(10-1-30)	89	84 ( <i>S</i> )
6	( <i>P</i> )-P(10-1-0)	94	5 ( <i>S</i> )
7	( <i>P</i> )-P(10-2-10)	86	80 ( <i>S</i> )
8	( <i>P</i> )-P(10-3-10)	92	76 ( <i>S</i> )
9	( <i>P</i> )-P(10-5-10)	91	70 ( <i>S</i> )

Composition of the polymer: (M)-P(x-y-x) where (M) or (P) indicates the handedness of the polymer *i.e.* right or left handed respectively, x the number of achiral spacer monomer and y the number of achiral phosphine monomer. \* Poly-2 corresponds to the polymer lacking the phosphine monomers (a) Determined by chiral HPLC

PQX polymers were then prepared without chiral initiators by random living copolymerisation between chiral and achiral *o*-diisocyanobenzene monomers (random polymer of 950 chiral spacer monomers and 50 phosphine monomers Figure I-36). These copolymers were easier to prepare and provided better catalytic results than those synthesised by block polymerisation with chiral initiators. Also, higher molar masses were accessible which allowed catalyst recycling.<sup>[84]</sup> Variation of the nature of the phosphine moieties on the polymers led to high enantioselectivity for asymmetric silaborative cleavage of *meso*-methylene cyclopropane<sup>[85]</sup>, Suzuki-Miyaura coupling<sup>[86]</sup> and ring opening arylation reactions.<sup>[87]</sup> It is worth mentioning that in these cases the chiral monomers were used in excess compared to the achiral ones.

Example of chirality transfer between chiral supramolecular polymeric structures and catalytic centres located at their periphery was rarely reported. Liu *et al.* found that the chiral nanotubular structure formed by *N,N'*-hexadecanedioyl-di-*L*-glutamic (**L-HDGA**) acid in water is maintained upon addition of a copper salt. This two-component system was investigated in the asymmetric Diels-Alder reaction between cyclopentadiene and azachalcone (Figure I-37).<sup>[88]</sup> The nanotubular structure of the active catalyst was required to get selectivity as the addition of EtOH led to a complete loss of selectivity. Also, the chirality of the nanotubes dictated the nature of the major enantiomer obtained for the catalytic reaction. However, even in the optimised conditions the enantiomeric excess remained modest (up to 55% ee).

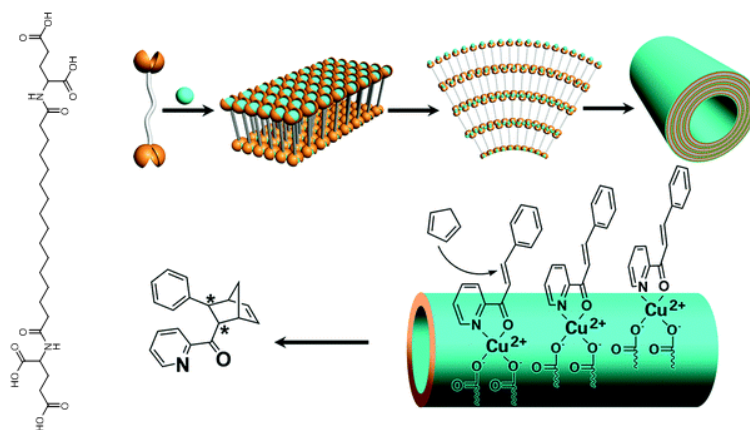


Figure I-37: Left: chemical structure of the amphiphilic monomer **L-HDGA**. Top: schematic representation of co-assembly process between **L-HDGA** and  $\text{Cu}^{2+}$  leading to the formation of the nanotubular structure. Below: schematic representation of the Diels-Alder reaction occurring at the surface of the nanotubes. From reference<sup>[88]</sup>

Recently in our group, BTA supramolecular polymers have been used as chiral scaffold for the rhodium-catalysed asymmetric hydrogenation of dimethyl itaconate.<sup>[89]</sup> The aim was to transfer chirality from the helical supramolecular polymer formed by the BTA (see chapter II for more details) to the catalytic rhodium centre. For this purpose, BTA ligand monomers were prepared as well as ligand-free chiral BTA co-monomers (Figure I-38).



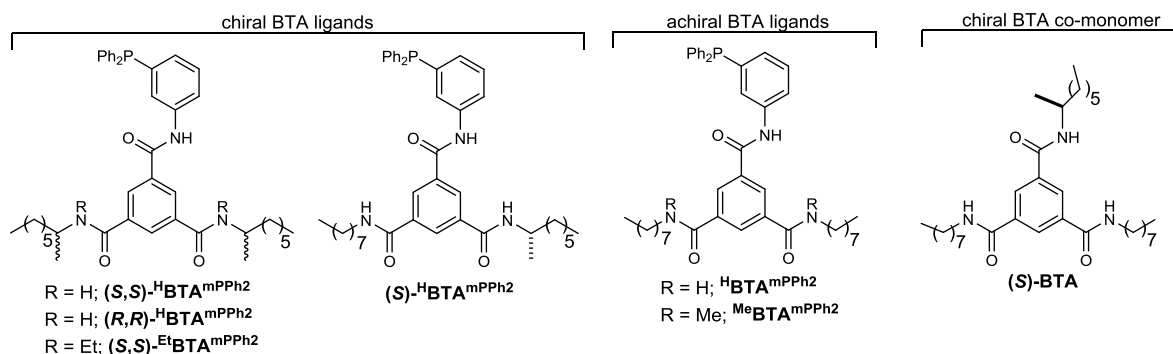


Figure I-38: Chiral and achiral BTA ligands and BTA co-monomers investigated in the rhodium-catalysed asymmetric hydrogenation of dimethyl itaconate. From reference<sup>[89]</sup>

The catalytic species were prepared by simply mixing the BTA ligand and the rhodium precursor with or without BTA additives in DCM in which all BTA monomers were free. Evaporation of the DCM and suspension in hexane of the yellow solid gave the pre-catalyst used for the hydrogenation of dimethyl itaconate for which the results were listed in the table below.

Table I-3: BTAs as chiral supramolecular scaffolds for the rhodium-catalysed hydrogenation of dimethyl itaconate From reference<sup>[89]</sup>

Entry	BTA ligand	BTA co-monomer	Rh precursor	e.e. (%)
1	<b>(S,S)-<sup>H</sup>BTA<sup>mPPh2</sup></b>	-	[Rh(cod) <sub>2</sub> ]BAr <sub>F</sub>	82 ( <i>R</i> )
2	<b>(S)-<sup>H</sup>BTA<sup>mPPh2</sup></b>	-	[Rh(cod) <sub>2</sub> ]BAr <sub>F</sub>	67 ( <i>R</i> )
3	<b>(R,R)-<sup>H</sup>BTA<sup>mPPh2</sup></b>	-	[Rh(cod) <sub>2</sub> ]BAr <sub>F</sub>	-81 ( <i>S</i> )
4	<b>(S,S)-<sup>H</sup>BTA<sup>mPPh2</sup></b>	-	[Rh(cod) <sub>2</sub> ]BF <sub>4</sub>	15 <sup>b</sup> ( <i>R</i> )
5	<b>(S,S)-<sup>Et</sup>BTA<sup>mPPh2</sup></b>	-	[Rh(cod) <sub>2</sub> ]BAr <sub>F</sub>	0
6	<b>(S,S)-<sup>Et</sup>BTA<sup>mPPh2</sup></b>	<b>(S)-BTA<sup>(c)</sup></b>	[Rh(cod) <sub>2</sub> ]BAr <sub>F</sub>	0
7	<b>(S,S)-<sup>H</sup>BTA<sup>mPPh2</sup></b>	<b>(S)-BTA<sup>(c)</sup></b>	[Rh(cod) <sub>2</sub> ]BAr <sub>F</sub>	<b>88</b> ( <i>R</i> )
8	<b>(S)-<sup>H</sup>BTA<sup>mPPh2</sup></b>	<b>(S)-BTA<sup>(c)</sup></b>	[Rh(cod) <sub>2</sub> ]BAr <sub>F</sub>	86 ( <i>R</i> )
9	<b><sup>H</sup>BTA<sup>mPPh2</sup></b>	-	[Rh(cod) <sub>2</sub> ]BAr <sub>F</sub>	0
10	<b><sup>H</sup>BTA<sup>mPPh2</sup></b>	<b>(S)-BTA<sup>(c)</sup></b>	[Rh(cod) <sub>2</sub> ]BAr <sub>F</sub>	31 ( <i>R</i> )
11	<b>MeBTA<sup>mPPh2</sup></b>	<b>(S)-BTA<sup>(c)</sup></b>	[Rh(cod) <sub>2</sub> ]BAr <sub>F</sub>	0

Conversion 100%, the experiments were performed at least in triplicate (except for control experiments 4,5,6, 9,11). Standard deviation for the e.e. < 2% (entries 1,3,7,8), =5% (entry 10), =8% (entry 2). Conversion 90%. (c) BTA co-monomer (2.5 mol%).

With **(S,S)-<sup>H</sup>BTA<sup>mPPh2</sup>** (*S,S*), good selectivity was obtained (82% e.e., entry 1) even though the chiral centres are located 12 atoms away from the metal centre. Opposite selectivity was obtained with the enantiomer of this BTA ligand (**(S,S)-<sup>H</sup>BTA<sup>mPPh2</sup>**), -81% e.e., entry 3). Using a chiral ligand with only one chiral centre (**(S)-<sup>H</sup>BTA<sup>mPPh2</sup>**) only slightly affects the selectivity (entries 1 and 2) while replacing the BAr<sub>F</sub> anion by a BF<sub>4</sub> led to a strong erosion of the enantioselectivity (entry 4). In order to check if the formation of chiral self-assembly was at the origin of the enantioselectivity of the catalytic reaction, two control experiments were performed: i) the use of an ethylated ligand **(S,S)-<sup>Et</sup>BTA<sup>mPPh2</sup>** (*i.e.* not able to assemble into long aggregates) and ii) the use of more polar solvents. In the first case (i), no selectivity was observed (entry 6). In the second case, the enantioselectivity drastically decreases with the polarity of the solvent (hexane/toluene: 46% e.e., toluene: 28% e.e. and no selectivity in DCM). These results highlighted the role of the self-assembly in the transmission of the

chiral information from the remote chiral alkyl chain(s) to the rhodium catalytic centre. Interestingly, the selectivity was increased by combining the chiral ligand with a chiral BTA co-monomer (entries 7 and 8). As the catalytic species was not soluble in hexane, only the self-assembly behaviour of the chiral ligand was investigated using FT-IR, SANS and CD analyses. All these analytical data indicate that  $(S,S)$ - $\text{H}^{\text{BTA}}{}^{\text{mPPh}_2}$  is self-assembled into long helical stacks with a preferred handedness in solution which allowed to propose a probable structure for the selective catalyst (Figure I-39).

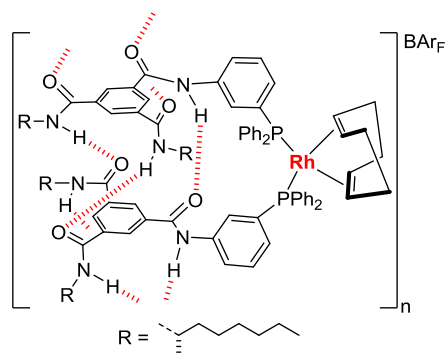


Figure I-39: Proposed structure for the pre-catalyst derived from  $(S,S)$ - $\text{H}^{\text{BTA}}{}^{\text{PPh}_2}$ .  $n$ , the degree of polymerisation, depends on the reaction conditions; it is probably high in hexane, giving rise to a selective catalyst and low in DCM (non-selective catalyst). From reference<sup>[89]</sup>

Inducing chirality to an intrinsically achiral metal centre was also tried. The achiral ligand  $\text{H}^{\text{BTA}}{}^{\text{mPPh}_2}$  was mixed with  $\text{H}^{\text{BTA}}(\text{S})$  providing a modest but encouraging enantiomeric excess (31% e.e., entry 10). Experiments performed with the methylated ligand ( $\text{Me}^{\text{BTA}}{}^{\text{mPPh}_2}$ ) demonstrated that the enantiomeric excess arose from the co-assembly of the ligand and the chiral additive (entry 11). In contrast to the above-mentioned studies in which the selectivity was mainly imposed by an intrinsically chiral catalyst, the selectivity in these BTA supramolecular catalysts was dictated by the supramolecular chirality of the assemblies.

These examples by Liu and Raynal demonstrate that supramolecular assemblies are able to transfer their chirality to catalytic centres in a similar way than covalent polymers developed by Suginome. For both examples, reaction conditions and especially the nature of the solvent have a huge influence on the structure of the polymers and thus on their catalytic performance.

## b) Chirality switch

Switching the chirality of an enantiopure catalyst by means of a stimulus (additives, solvent, light among others possible stimuli) is of particular interest in enantioselective catalysis as it would allow the synthesis of both product enantiomers with a single chiral catalyst. Controlling the enantioselective outcome of a catalyst by fine tuning of the reaction conditions is a very attractive goal. Most existing examples concern discrete molecular catalysts.<sup>[90–98]</sup> Recently, examples have emerged of chirality-switchable catalysts based on an inherently chiral macromolecular scaffold. It mainly concerns catalysts constructed on G-quadruplexes or on the previously described PQX synthetic polymers.

Use of homochiral natural polymers such as peptides<sup>[99–104]</sup> or DNA<sup>[81,105–107]</sup> as scaffolds for catalysis has drawn particular attention in the last two decades. Such natural polymeric scaffolds are used as chirality inducers to intrinsically achiral or racemic catalysts. The biomacromolecule and the catalyst can be anchored by means of several methods. The non-covalent anchoring constitutes a privileged strategy as demonstrated by the efficiency of the biotin/avidin<sup>[108]</sup> and the DNA<sup>[81,109,110]</sup> supramolecular hybrid catalysts. Thereafter, we will focus on examples in which the chirality-switchable properties of the inherent chirality of a biomacromolecular scaffold have been particularly investigated. Recently, examples of dynamic catalytic systems based on G-quadruplexes have been published. G-quadruplexes are composed of a single DNA strand with intramolecular bonding of four guanines in a same plane (guanine tetrads). The guanine tetrads are stabilised by eight Hoogsteen hydrogen-bonds, an octa-coordinated monovalent or divalent cation and by  $\pi$ - $\pi$  interaction between stacked tetrads in the G-quadruplex.<sup>[111]</sup> The cation has notably a strong influence on the stability and the structure of the G-quadruplexes. In the following examples, the tetrads will be represented as coloured rectangles.

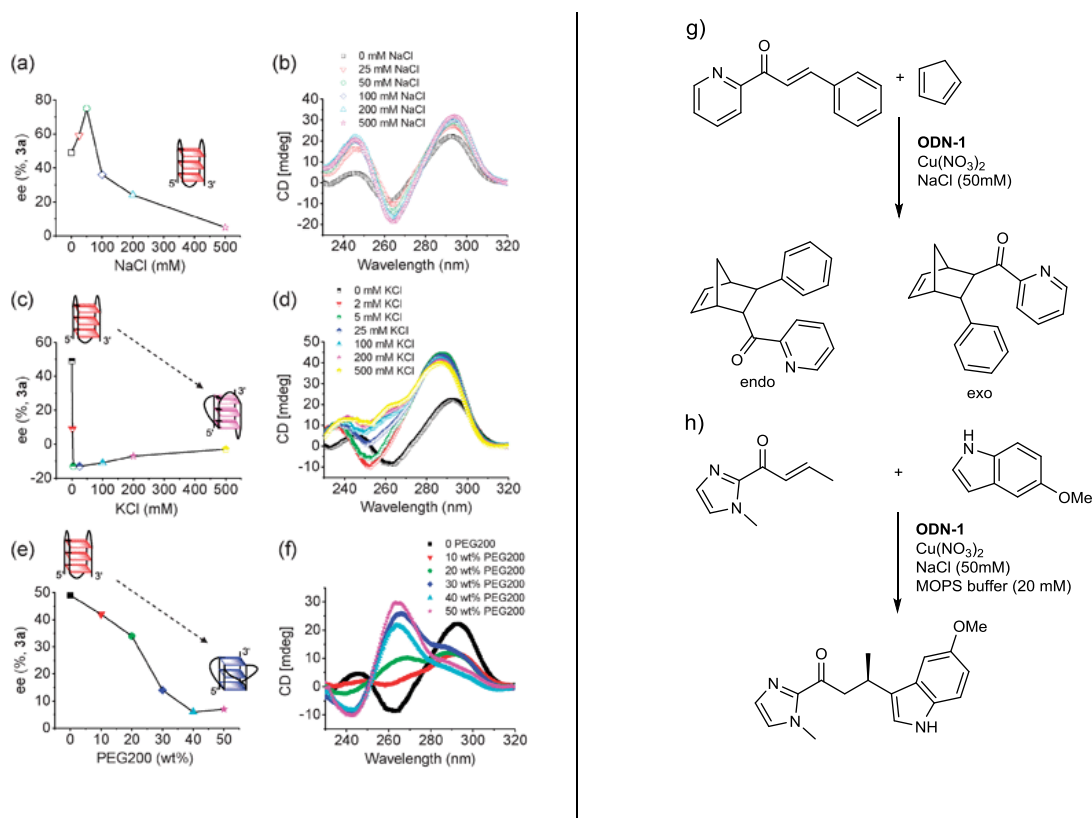


Figure I-40: e.e. values obtained for the product 3a for the F–C reaction catalyzed by G-quadruplex–Cu<sup>2+</sup> as a function of the concentration of various additives: (a) Na<sup>+</sup> ions, (c) K<sup>+</sup> ions, and (e) PEG200. The corresponding CD spectra of G-quadruplex–Cu<sup>2+</sup> hybrid catalysts obtained for different concentrations of additives: (b) Na<sup>+</sup> ions, (d) K<sup>+</sup> ions, and (f) PEG200. (g) Diels-Alder reaction. MOPS = 3-(N-(morpholino)propanesulfonic acid). From references<sup>[112,113]</sup>

Li *et al.* observed a dynamic behaviour for the G-quadruplexes from human telomeric DNA (**ODN-1**) employed as scaffolds for metal-catalysed Diels-Alder<sup>[112]</sup> and the Friedel-Craft<sup>[113]</sup> reactions. The G-quadruplexes were mixed with various metal salts and the mixtures were directly investigated in these

asymmetric catalytic reactions. Copper proved to be the metal of choice since the use of other metals (Ni, Zn, Co) only results in very low enantioselectivity in the Diels-Alder reaction. The influence on the selectivity of the proportion of NaCl, KCl or PEG200 added to the **ODN-1**- Cu<sup>2+</sup> hybrid catalytic systems was also precisely probed (Figure I-40).

For the Friedel-Craft reaction, a concentration of 50 mM in NaCl induced a stabilisation of the G-quadruplex tertiary structure as demonstrated by CD spectroscopy. This stabilisation might explain the higher selectivity of the catalytic reaction at this concentration (*ca.* 80% ee) compared to the sodium-free catalytic system (*ca.* 50% ee). The decrease of the enantioselectivity at higher concentration of NaCl was presumably related to the competition between the copper and the sodium cations to stabilise the G-quadruplex tetrads. Adding potassium instead of sodium to the catalytic systems induced a different G-quadruplex tertiary structure as indicated by first a strong erosion of the enantiomeric excess and then an inversion in the stereochemical outcome of the reaction. In these systems, the enantioselectivity was affected by any change in the loop sequence suggesting a strong relationship between the structural organisation of the G-quadruplex and the stereochemical outcome of the catalytic reaction. PEG-200 is referred to as a molecular crowding in the sense that it simulates the high macromolecules concentration present in the cell. Addition of PEG-200 to the G-quadruplex-hybrid catalyst led to a change of the G-quadruplex structure as stated by CD spectroscopy. However, this structural change only resulted in a decrease of the enantiomeric excess for the catalytic reaction. Structural changes in the ternary structures of the G-quadruplex according to the nature of the cation used were further investigated.

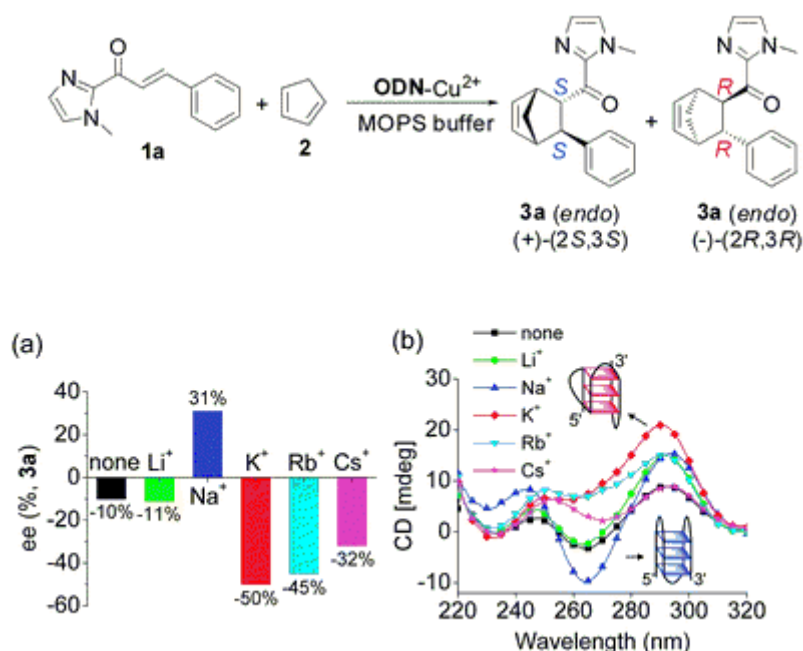


Figure I-41: (a) Enantiomeric excesses of **3a** (*endo*) for the Diels-Alder reaction catalyzed by ODN-Cu<sup>2+</sup> as a function of metal ion additives (50 mM). Conversions are within 5–20% (b) CD spectra of ODN-Cu<sup>2+</sup> recorded in the presence of alkali metal ions (50 mM) From reference<sup>[114]</sup>

The selectivity of the Diels-Alder catalytic reaction drawn in Figure I-41 is strongly influenced by the nature of the cation.  $\text{Li}^+$ ,  $\text{K}^+$ ,  $\text{Rb}^+$  and  $\text{Cs}^+$  cations provide the same enantiomer than the cation-free system but with higher selectivities in the last three cases.<sup>[114]</sup> On contrary,  $\text{Na}^+$  led to an inversion in the stereochemical outcome of the catalytic reaction since the (*S,S*) enantiomer is obtained as the main product. A good correlation was found between the selectivity of the catalytic reaction and the handedness and the net helicity of the tertiary structure of the G-quadruplex  $\text{Cu}^{2+}$  hybrid catalyst (CD analyses, (Figure I-41a and b). These examples show that controlling the tertiary structure of G-quadruplexes  $\text{Cu}^{2+}$  hybrid catalysts with additives is of particular interest as it offers the possibility of tuning the stereochemical outcome of the reaction using only a single homochiral natural molecule. However selectivities and conversion remain low for the all the G-quadruplex  $\text{Cu}^{2+}$  hybrid catalytic systems investigated so far.

PQX polymers mentioned in section C.3.a) exhibited chirality switch according to the solvent in which the polymer was dissolved.<sup>[84]</sup> For example, polymer (*R*)-**P(950\*/0/50)**, a random copolymer of 950 chiral spacer monomers and 50 phosphine monomers (Figure I-36), forms a *P*-helix in chloroform and a *M*-helix in a trichloroethane/toluene (3/1) solvent mixture (Figure I-42). These two chiral helical polymers gave opposite enantiomers as products of the palladium-catalysed hydrosilylation of styrene with comparable e.e.s (97% for *P*-helix and 93% for the *M*-helix).

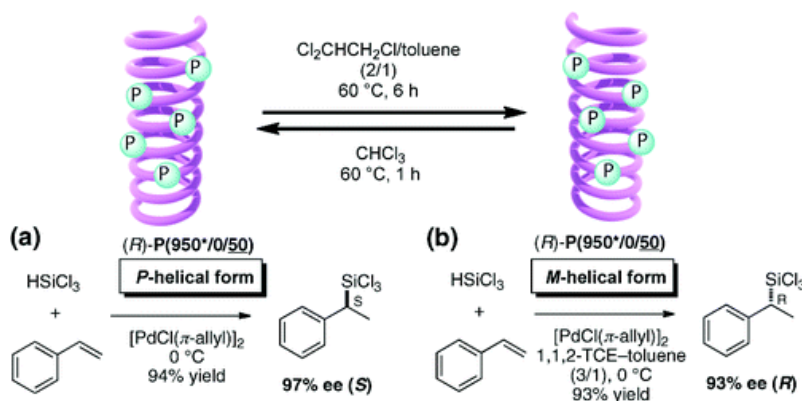


Figure I-42: Asymmetric hydrosilylation using chirality-switchable (*R*)-**P(950\*/0/50)** helical polymer adopting (a) *P*-helical form or (b) *M*-helical form depending on the nature of the solvent. From reference<sup>[84]</sup>

The capacity of the PQX to switch from *P*-helix to *M*-helix in different solvents is quite remarkable and has also been observed in the case of solvents having similar polarity. Indeed, a switch in the helical sense has been observed by changing the solvent from cyclohexane to *n*-hexane<sup>[115]</sup> or between ethereal solvents<sup>[116]</sup> however no catalytic applications of the latter PQX polymers was reported.

The chirality switches presented here allow preparation of both enantiomers of a reaction using the same enantiopure catalyst after preparation with the right cation for the G-quadruplex or the selection of the right solvent for the PQX polymers. Unfortunately for both types of catalysts, a chirality switch of the catalyst during the reaction course has not been documented despite the great interest in developing such types of catalysts.

### c) Chirality amplification

The previous results are interesting although they all require a large amount of enantiopure monomers with respect to the catalytic centre (phosphine or metal) in order to obtain good enantioselectivities. To overcome the use of large amounts of enantiopure starting material, chirality amplification properties of macromolecules must be developed in the context of catalytic applications. As previously stated in this chapter, two chirality amplification phenomena exist in supramolecular assemblies: sergeants-and-soldiers and majority rule effects. Both have been used for construction of PQX ligands exhibiting high chirality amplification properties.

S&S effect in PQX polymers was probed using a large variety of chiral monomers and two achiral monomers, one structurally-related to the chiral monomers and the other one more different.<sup>[117]</sup> Among the chiral monomers tested all gave chirality amplification but some gave opposite helicity according to the achiral monomer in the co-polymer.

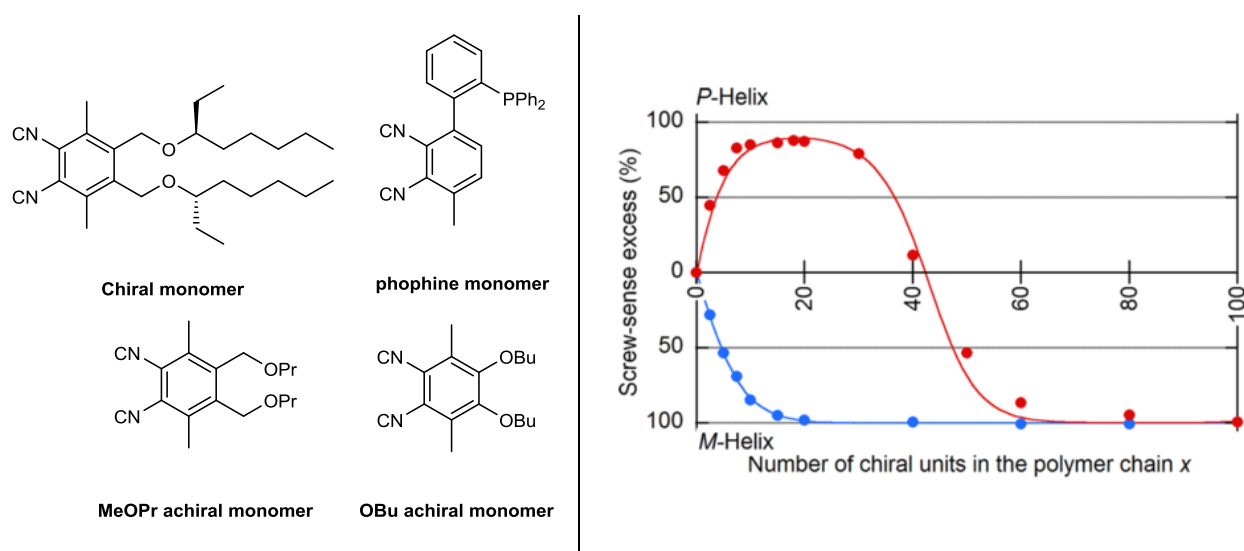


Figure I-43: Left: Chiral monomers and achiral monomers used for the S&S effect in PQX-catalysed reactions. Right: Correlation between the number of chiral monomers  $x$  and the se of copolymers MeOPr( $x/y$ ) (blue filled circle) and OBu( $x/y$ ) (red filled circle) ( $x + y = 100$ ) in  $\text{CHCl}_3$ . se = screw sense Adapted from reference<sup>[117]</sup>

Further S&S studies using random copolymers of revealed different behaviours. Indeed classical S&S effect was observed with the random copolymer of chiral monomer with MeOPr achiral monomer, and the maximum screw-sense excess was obtained with 20% chiral sergeants (Figure I-43 right, blue filled circle). In contrast, an abnormal S&S effect was observed for the random polymer of chiral monomer and OBu monomer (Figure I-43 right, red filled circle). At first *P*-helix is obtained for low content of chiral monomers ( $0\% < \text{chiral monomer} < 40\%$ ) whereas above 40% of chiral monomers in the random copolymer *M*-helix is obtained. Rationalisation of this abnormal S&S effect was made using Sato modified Ising model in which the preference of screw-sense induction of a monomer unit depends on the monomer units in its immediate vicinity.<sup>[118]</sup> They were able to take advantage of this difference in the screw-sense induction between the chiral-chiral pair and chiral-achiral pairs by making random copolymers and block copolymers with the same composition but opposite helicity. In

the random copolymer (Figure I-44, purple helix) the chiral monomer is mixed with the achiral monomer and thus the polymer adopted *P*-helicity like in the S&S experiment (Figure I-43). On the other hand, in the block copolymer, all the chiral monomers are regrouped and then their influence on the vicinal achiral monomers is null. This led for the block copolymer to keep the preferred *M*-helicity of the chiral monomer (Figure I-44, blue helix). Both polymer only contain 18% of enantiopure monomers but adopt homochiral helices (se >99%) indicating that the polymers displayed strong chirality amplification. Using this change in the preferred helicity according to the method of preparation of the copolymer they made a ter-polymer with a phosphine monomer and they obtained also *M*-helix for the random polymer and *P*-helix for the block polymer (Figure I-44 right). Application of these polymers in the palladium-catalysed hydrosilylation of  $\beta$ -methylstyrene gave both enantiomers with high e.e. (94%) according to the polymer used. This example points out the strong dynamic and chirality amplification properties of the PQW polymers.

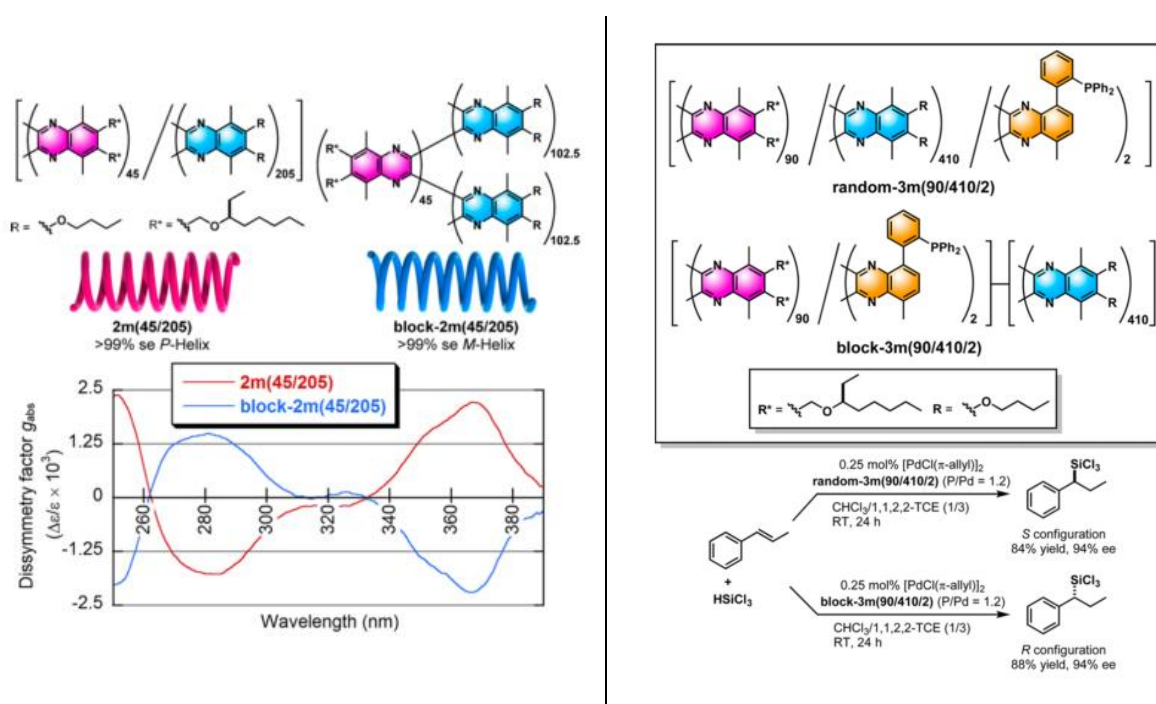


Figure I-44: Left: structures and CD spectra of random OBU(45\*/205) polymer (purple) and block-OBU(45\*/205) polymer (blue) in  $CHCl_3$  where 45\* is the number of chiral monomer. Right random and block co-polymer of OBU monomer, chiral monomer and phosphine monomer and their application in palladium-catalysed hydrosilylation of  $\beta$ -methylstyrene. From reference<sup>[117]</sup>

Investigation of the MR properties of PQX polymers was made by mixing scalemic mixtures of enantiopure monomers and measuring the screw sense excess of the resulting copolymers.

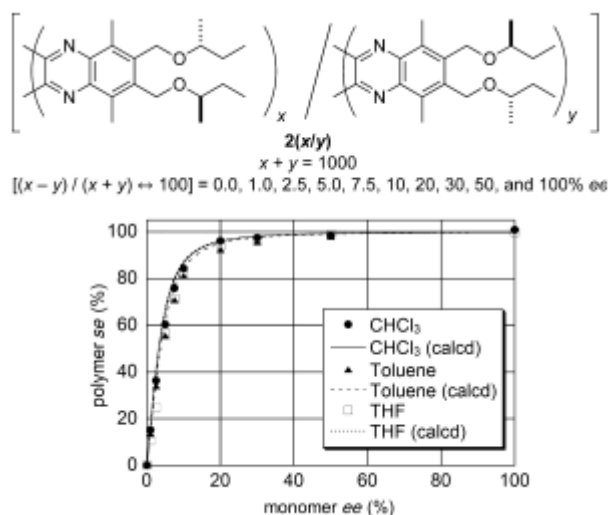


Figure I-45: Majority rule experiments with PQX polymers. Correlation between value screw-sense excess (*se*) value of the polymer and the ee of the monomer. Co-polymer: 2(*x*/*y*), DP: 1000, in CHCl<sub>3</sub>, THF or toluene. From reference<sup>[119]</sup>

For monomers with butan-2-ol side chains, strong majority rule effects were observed since only 30% of enantiomeric excess in one of the monomers led to polymer with the higher screw-sense excess value. (Figure I-45).<sup>[119]</sup> With the aim of applying this property for the construction of a chirally-amplified catalyst, they prepared a random ter-polymer composed of scalemic mixture (30% e.e.) of the chiral monomers (*R,R*)-**2**, (*S,S*)-**2** and the achiral phosphine monomer. This polymer is able to perform the palladium-catalysed hydrosilylation of  $\beta$ -methylstyrene with high performance (90% yield, 94% e.e.). This result is quite remarkable but still requires the enantiopure synthesis of the chiral monomers before their mixing.

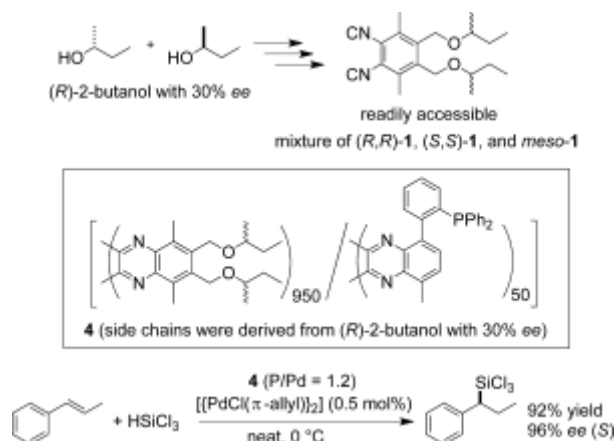


Figure I-46: Asymmetric hydrosilylation of  $\beta$ -methylstyrene in the presence of PQX ligand **4** derived from (*R*)-2-butanol with 30% ee. From reference<sup>[119]</sup>

To render the application of MR in their system more attractive, Suginome and co-workers were able to go further. They obtained butan-2-ol with low enantiomeric excess (30%) from a poorly selective catalytic reaction and they prepared PQX monomers with this scalemic mixture of butan-2-ol enantiomers (Figure I-46). This led to a mixture of (*R,R*), (*S,S*) and *meso* monomers with a ratio of 43.3 :13.3 :43.4 respectively. The PQX resulting from the random polymerisation of this mixture of monomers and a phosphine monomer (formula in Figure I-46) was able to catalyse the hydrosilylation



of  $\beta$ -methylstyrene in high yield and enantioselectivity. This PQX polymer was also successfully used in the enantioselective palladium-catalysed hydrosilylation of  $\beta$ -methylstyrene and in Suzuki-Miyaura coupling of biaryl compounds. This high enantioselectivity arose from the majority rule effect between the two enantiomers and a sergeants-and-soldiers effect between the major enantiomer and achiral monomers (*meso* monomer and phosphine monomers) leading to high enantio-induction. The chirality switch properties were still present in these PQX polymers leading to an inversion of the stereoselectivity with a change in the nature of the solvent.

PQX showed interesting properties in enantioselective catalysis namely: chirality induction, amplification and switching. A limitation of PQX is that any modification of their chemical structure will require the whole synthesis of a new PQX.

## **D. Conclusion**

The importance of the fine tuning the structure of homogenous molecular catalysts to direct their reactivity and their selectivity outcome was briefly reviewed as well as new types of catalysts. Higher performance in tunability or selectivity can be obtained using discrete supramolecular catalysts. Nevertheless, these discrete supramolecular catalysts do not display the following properties: recyclability, dynamic behaviour and chirality amplification. The catalysts supported by a dynamic macromolecular scaffold possess one or severe of these properties described in part C of this chapter, Gel-based catalysts have interesting dynamic behaviour that lead to modulation of the catalyst and selectivity however neither recyclability nor chirality amplification properties was developed. PQX polymers display the recyclability and chirality amplification however at the cost of the tunability as they relied on a covalent polymer.

Use of a supramolecular polymer instead of a covalent one seems for us the solution towards the development of catalysts with such properties. The BTAs developed by Meijer display a dynamic structural change based on the temperature treatment prior to catalysis. BTAs have also demonstrated their ability, as chiral supramacromolecules, to induce chirality from the helical macromolecule to the metallic centre. However for the moment no supramolecular polymer scaffolds possess all the required properties and some are not developed yet such as recyclability and chirality amplification and chirality switch.

In the following chapter we will discuss the interest of supramolecular polymers as dynamic scaffold for catalysis before introducing the different strategies envisaged for this implementation of these scaffolds in catalysis.

## E. References

- [1] P. W. N. M. van Leeuwen, *Homogeneous Catalysis*, Springer Netherlands, Dordrecht, **2004**.
- [2] C. A. Tolman, *Chem. Rev.* **1977**, *77*, 313–348.
- [3] H. Clavier, S. P. Nolan, *Chem. Commun.* **2010**, *46*, 841–861.
- [4] J. A. Gillespie, D. L. Dodds, P. C. J. Kamer, *Dalt. Trans.* **2010**, *39*, 2751–2764.
- [5] C. P. Casey, G. T. Whiteker, *Isr. J. Chem.* **1990**, *30*, 299–304.
- [6] C. Gennari, U. Piarulli, *Chem. Rev.* **2003**, *103*, 3071–3100.
- [7] C. Jäkel, R. Paciello, *Chem. Rev.* **2006**, *106*, 2912–2942.
- [8] H. Fernández-Pérez, P. Etayo, A. Panossian, A. Vidal-Ferran, *Chem. Rev.* **2011**, *111*, 2119–2176.
- [9] C. J. Brown, F. D. Toste, R. G. Bergman, K. N. Raymond, *Chem. Rev.* **2015**, *115*, 3012–3035.
- [10] K. Ohmatsu, T. Ooi, *Tetrahedron Lett.* **2015**, *56*, 2043–2048.
- [11] M. Raynal, P. Ballester, A. Vidal-Ferran, P. W. N. M. van Leeuwen, *Chem. Soc. Rev.* **2014**, *43*, 1660–1733.
- [12] M. Raynal, P. Ballester, A. Vidal-Ferran, P. W. N. M. van Leeuwen, *Chem. Soc. Rev.* **2014**, *43*, 1734–1787.
- [13] B. Breit, *Angew. Chem. Int. Ed.* **2005**, *44*, 6816–6825.
- [14] M. Weis, C. Waloch, W. Seiche, B. Breit, *J. Am. Chem. Soc.* **2006**, *128*, 4188–4189.
- [15] J. Wieland, B. Breit, *Nat. Chem.* **2010**, *2*, 832–837.
- [16] V. F. Slagt, P. W. N. M. van Leeuwen, J. N. H. Reek, *Angew. Chem. Int. Ed.* **2003**, *42*, 5619–5623.
- [17] B. Breit, W. Seiche, *J. Am. Chem. Soc.* **2003**, *125*, 6608–6609.
- [18] U. Gellrich, W. Seiche, M. Keller, B. Breit, *Angew. Chem. Int. Ed.* **2012**, *51*, 11033–11038.
- [19] P. Etayo, A. Vidal-Ferran, *Chem. Soc. Rev.* **2013**, *42*, 728–754.
- [20] J. F. Teichert, B. L. Feringa, *Angew. Chem. Int. Ed.* **2010**, *49*, 2486–2528.
- [21] Y. Liu, C. A. Sandoval, Y. Yamaguchi, X. Zhang, Z. Wang, K. Kato, K. Ding, *J. Am. Chem. Soc.* **2006**, *128*, 14212–14213.
- [22] M. Vaquero, L. Rovira, A. Vidal-Ferran, *Chem. Commun.* **2016**, *52*, 11038–11051.
- [23] A. Vidal-Ferran, I. Mon, A. Bauzá, A. Frontera, L. Rovira, *Chem. Eur. J.* **2015**, *21*, 11417–11426.
- [24] R. J. Phipps, G. L. Hamilton, F. D. Toste, *Nat. Chem.* **2012**, *4*, 603–614.
- [25] M. Mahlau, B. List, *Angew. Chem. Int. Ed.* **2013**, *52*, 518–533.
- [26] K. Brak, E. N. Jacobsen, *Angew. Chem. Int. Ed.* **2013**, *52*, 534–561.
- [27] A. C. Laungani, B. Breit, *Chem. Commun.* **2008**, 844–846.
- [28] Z. Kokan, S. I. Kirin, *Eur. J. Org. Chem.* **2013**, *2013*, 8154–8161.
- [29] P. Dydio, C. Rubay, T. Gadzikwa, M. Lutz, J. N. H. Reek, *J. Am. Chem. Soc.* **2011**, *133*, 17176–17179.
- [30] T. Hasegawa, Y. Furusho, H. Katagiri, E. Yashima, *Angew. Chem. Int. Ed.* **2007**, *46*, 5885–5888.
- [31] S. Hübner, J. G. de Vries, V. Farina, *Adv. Synth. Catal.* **2016**, *358*, 3–25.
- [32] L. Shi, X. Wang, C. A. Sandoval, M. Li, Q. Qi, Z. Li, K. Ding, *Angew. Chem. Int. Ed.* **2006**, *45*, 4108–4112.
- [33] D. de Groot, B. F. M. de Waal, J. N. H. Reek, A. P. H. J. Schenning, P. C. J. Kamer, E. W. Meijer, P. W. N. M. van Leeuwen, *J. Am. Chem. Soc.* **2001**, *123*, 8453–8458.
- [34] S. Takizawa, H. Somei, D. Jayaprakash, H. Sasai, *Angew. Chem. Int. Ed.* **2003**, *42*, 5711–5714.
- [35] X. Wang, K. Ding, *J. Am. Chem. Soc.* **2004**, *126*, 10524–10525.
- [36] X. Wang, L. Shi, M. Li, K. Ding, *Angew. Chem. Int. Ed.* **2005**, *44*, 6362–6366.
- [37] Y. J. Park, J. Park, C. Jun, *Acc. Chem. Res.* **2008**, *41*, 222–234.
- [38] D.-H. Chang, D.-Y. Lee, B.-S. Hong, J.-H. Choi, C.-H. Jun, *J. Am. Chem. Soc.* **2004**, *126*, 424–425.
- [39] D.-W. Kim, S.-G. Lim, C.-H. Jun, *Org. Lett.* **2006**, *8*, 2937–2940.
- [40] L. Kovbasyuk, R. Krämer, *Chem. Rev.* **2004**, *104*, 3161–3188.
- [41] H. G. Schild, *Prog. Polym. Sci.* **1992**, *17*, 163–249.
- [42] G. Wang, K. Kuroda, T. Enoki, A. Grosberg, S. Masamune, T. Oya, Y. Takeoka, T. Tanaka, *Proc. Natl. Acad. Sci.* **2000**, *97*, 9861–9864.
- [43] Z. Ge, D. Xie, D. Chen, X. Jiang, Y. Zhang, H. Liu, S. Liu, *Macromolecules* **2007**, *40*, 3538–3546.
- [44] I. M. Okhapkin, L. M. Bronstein, E. E. Makhaeva, V. G. Matveeva, E. M. Sulman, M. G. Sulman, A. R. Khokhlov, *Macromolecules* **2004**, *37*, 7879–7883.
- [45] B. G. Choi, R. Song, W. Nam, B. Jeong, *Chem. Commun.* **2005**, 2960–2962.
- [46] H. Koizumi, Y. Shiraishi, S. Tojo, M. Fujitsuka, T. Majima, T. Hirai, *J. Am. Chem. Soc.* **2006**, *128*, 8751–8753.
- [47] T. Terashima, T. Mes, T. F. A. De Greef, M. A. J. Gillissen, P. Besenius, A. R. A. Palmans, E. W. Meijer, *J. Am. Chem. Soc.* **2011**, *133*, 4742–4745.
- [48] E. Huerta, P. J. M. Stals, E. W. Meijer, A. R. A. Palmans, *Angew. Chem. Int. Ed.* **2013**, *52*, 2906–2910.
- [49] A. Córdova, W. Notz, C. F. Barbas III, *Chem. Commun.* **2002**, 3024–3025.

- [50] E. Huerta, B. van Genabeek, P. J. M. Stals, E. W. Meijer, A. R. A. Palmans, *Macromol. Rapid Commun.* **2014**, *35*, 1320–1325.
- [51] B. M. Rossbach, K. Leopold, R. Weberskirch, *Angew. Chem. Int. Ed.* **2006**, *45*, 1309–1312.
- [52] M. Tokunaga, J. F. Larrow, F. Kakiuchi, E. N. Jacobsen, *Science* **1997**, *277*, 936–938.
- [53] E. Huerta, B. van Genabeek, B. A. G. Lamers, M. M. E. Koenigs, E. W. Meijer, A. R. A. Palmans, *Chem. Eur. J.* **2015**, *21*, 3682–3690.
- [54] L. N. Neumann, M. B. Baker, C. M. A. Leenders, I. K. Voets, R. P. M. Lafleur, A. R. A. Palmans, E. W. Meijer, *Org. Biomol. Chem.* **2015**, *13*, 7711–7719.
- [55] R. van Hameren, P. Schon, A. M. van Buul, J. Hoogboom, S. V. Lazarenko, J. W. Gerritsen, H. Engelkamp, P. C. M. Christianen, H. A. Heus, J. C. Maan, *et al.*, *Science* **2006**, *314*, 1433–1436.
- [56] M. de Torres, R. van Hameren, R. J. M. Nolte, A. E. Rowan, J. A. A. W. Elemans, *Chem. Commun.* **2013**, *49*, 10787–10789.
- [57] P. Terech, R. G. Weiss, *Chem. Rev.* **1997**, *97*, 3133–3160.
- [58] A. Masuda, K. Ushida, H. Koshino, K. Yamashita, T. Kluge, *J. Am. Chem. Soc.* **2001**, *123*, 11468–11471.
- [59] F. Galindo, M. Isabel Burguete, R. Gavara, S. V. Luis, *J. Photochem. Photobiol. A Chem.* **2006**, *178*, 57–61.
- [60] M. Yemloul, E. Steiner, A. Robert, S. Bouguet-Bonnet, F. Allix, B. Jamart-Grégoire, D. Canet, *J. Phys. Chem. B* **2011**, *115*, 2511–2517.
- [61] J. Bachl, A. Hohenleutner, B. B. Dhar, C. Cativiela, U. Maitra, B. König, D. D. Díaz, *J. Mater. Chem. A* **2013**, *1*, 4577.
- [62] K. Tanaka, A. Mori, S. Inoue, *J. Org. Chem.* **1990**, *55*, 181–185.
- [63] H. Danda, *Synlett* **1991**, *1991*, 263–264.
- [64] H. Danda, H. Nishikawa, K. Otaka, *J. Org. Chem.* **1991**, *56*, 6740–6741.
- [65] M. O. Guler, S. I. Stupp, *J. Am. Chem. Soc.* **2007**, *129*, 12082–12083.
- [66] F. Rodríguez-Llansola, B. Escuder, J. F. Miravet, *J. Am. Chem. Soc.* **2009**, *131*, 11478–11484.
- [67] N. Singh, M. P. Conte, R. V. Ulijn, J. F. Miravet, B. Escuder, *Chem. Commun.* **2015**, *51*, 13213–13216.
- [68] S. Díaz-Oltra, C. Berdugo, J. F. Miravet, B. Escuder, *New J. Chem.* **2015**, *39*, 3785–3791.
- [69] C. Berdugo, J. F. Miravet, B. Escuder, *Chem. Commun.* **2013**, *49*, 10608–10610.
- [70] N. Singh, K. Zhang, C. A. Angulo-Pachón, E. Mendes, J. H. van Esch, B. Escuder, *Chem. Sci.* **2016**, *7*, 5568–5572.
- [71] A. Dawn, N. Fujita, S. Haraguchi, K. Sada, S. Shinkai, *Chem. Commun.* **2009**, 2100–2102.
- [72] A. Dawn, N. Fujita, S. Haraguchi, K. Sada, S. Tamaru, S. Shinkai, *Org. Biomol. Chem.* **2009**, *7*, 4378.
- [73] S. Samai, P. Ghosh, K. Biradha, *Chem. Commun.* **2013**, *49*, 4181–4183.
- [74] Y. Nagata, T. Yamada, T. Adachi, Y. Akai, T. Yamamoto, M. Suginome, *J. Am. Chem. Soc.* **2013**, *135*, 10104–10113.
- [75] Y. Ito, T. Miyake, S. Hatano, R. Shima, T. Ohara, M. Suginome, *J. Am. Chem. Soc.* **1998**, *120*, 11880–11893.
- [76] E. Yashima, K. Maeda, H. Iida, Y. Furusho, K. Nagai, *Chem. Rev.* **2009**, *109*, 6102–6211.
- [77] M. M. Green, J.-W. Park, T. Sato, A. Teramoto, S. Lifson, R. L. B. Selinger, J. V. Selinger, *Angew. Chem. Int. Ed.* **1999**, *38*, 3138–3154.
- [78] M. Reggelin, M. Schultz, M. Holbach, *Angew. Chem. Int. Ed.* **2002**, *41*, 1614–1617.
- [79] M. Reggelin, S. Doerr, M. Klussmann, M. Schultz, M. Holbach, *Proc. Natl. Acad. Sci.* **2004**, *101*, 5461–5466.
- [80] C. A. Müller, T. Hoffart, M. Holbach, M. Reggelin, *Macromolecules* **2005**, *38*, 5375–5380.
- [81] G. Roelfes, B. L. Feringa, *Angew. Chem. Int. Ed.* **2005**, *44*, 3230–3232.
- [82] A. J. Boersma, R. P. Megens, B. L. Feringa, G. Roelfes, *Chem. Soc. Rev.* **2010**, *39*, 2083–2092.
- [83] T. Yamamoto, M. Suginome, *Angew. Chem. Int. Ed.* **2009**, *48*, 539–542.
- [84] T. Yamamoto, T. Yamada, Y. Nagata, M. Suginome, *J. Am. Chem. Soc.* **2010**, *132*, 7899–7901.
- [85] Y. Akai, T. Yamamoto, Y. Nagata, T. Ohmura, M. Suginome, *J. Am. Chem. Soc.* **2012**, *134*, 11092–11095.
- [86] T. Yamamoto, Y. Akai, Y. Nagata, M. Suginome, *Angew. Chem. Int. Ed.* **2011**, *50*, 8844–8847.
- [87] T. Yamamoto, Y. Akai, M. Suginome, *Angew. Chem. Int. Ed.* **2014**, *53*, 12785–12788.
- [88] Q. Jin, L. Zhang, H. Cao, T. Wang, X. Zhu, J. Jiang, M. Liu, *Langmuir* **2011**, *27*, 13847–13853.
- [89] M. Raynal, F. Portier, P. W. N. M. van Leeuwen, L. Bouteiller, *J. Am. Chem. Soc.* **2013**, *135*, 17687–17690.
- [90] Y. Sohtome, S. Tanaka, K. Takada, T. Yamaguchi, K. Nagasawa, *Angew. Chem. Int. Ed.* **2010**, *49*, 9254–9257.
- [91] M. Messerer, H. Wennemers, *Synlett* **2011**, *2011*, 499–502.
- [92] X. Tian, C. Cassani, Y. Liu, A. Moran, A. Urakawa, P. Galzerano, E. Arceo, P. Melchiorre, *J. Am.*

- Chem. Soc.* **2011**, *133*, 17934–17941.
- [93] P. Oczipka, D. Müller, W. Leitner, G. Franciò, *Chem. Sci.* **2016**, *7*, 678–683.
- [94] S. Mortezaei, N. R. Catarineu, X. Duan, C. Hu, J. W. Canary, *Chem. Sci.* **2015**, *6*, 5904–5912.
- [95] G. Storch, O. Trapp, *Angew. Chem. Int. Ed.* **2015**, *54*, 3580–3586.
- [96] S. Mortezaei, N. R. Catarineu, J. W. Canary, *J. Am. Chem. Soc.* **2012**, *134*, 8054–8057.
- [97] J. Wang, B. L. Feringa, *Science* **2011**, *331*, 1429–1432.
- [98] S. Schoumacker, O. Hamelin, J. Pécaut, M. Fontecave, *Inorg. Chem.* **2003**, *42*, 8110–8116.
- [99] S. R. Gilbertson, X. Wang, *Tetrahedron Lett.* **1996**, *37*, 6475–6478.
- [100] S. R. Gilbertson, S. E. Collibee, A. Agarkov, *J. Am. Chem. Soc.* **2000**, *122*, 6522–6523.
- [101] A. Agarkov, S. Greenfield, D. Xie, R. Pawlick, G. Starkey, S. R. Gilbertson, *Biopolymers* **2006**, *84*, 48–73.
- [102] R. Sambasivan, Z. T. Ball, *J. Am. Chem. Soc.* **2010**, *132*, 9289–9291.
- [103] G. Guisado-Barrios, B. K. Muñoz, P. C. J. Kamer, B. Lastdrager, G. van der Marel, M. Overhand, M. Vega-Vázquez, M. Martin-Pastor, *Dalt. Trans.* **2013**, *42*, 1973–1978.
- [104] L. Zheng, A. Marcozzi, J. Y. Gerasimov, A. Herrmann, *Angew. Chem. Int. Ed.* **2014**, *53*, 7599–7603.
- [105] M. Wilking, U. Hennecke, *Org. Biomol. Chem.* **2013**, *11*, 6940.
- [106] S. Dey, A. Jäschke, *Angew. Chem. Int. Ed.* **2015**, *54*, 11279–11282.
- [107] S. Roe, D. J. Ritson, T. Garner, M. Searle, J. E. Moses, *Chem. Commun.* **2010**, *46*, 4309–4311.
- [108] T. R. Ward, *Acc. Chem. Res.* **2011**, *44*, 47–57.
- [109] G. Roelfes, A. J. Boersma, B. L. Feringa, *Chem. Commun.* **2006**, 635–637.
- [110] A. J. Boersma, J. E. Klijn, B. L. Feringa, G. Roelfes, *J. Am. Chem. Soc.* **2008**, *130*, 11783–11790.
- [111] E. Largy, A. Marchand, S. Amrane, V. Gabelica, J.-L. Mergny, *J. Am. Chem. Soc.* **2016**, *138*, 2780–2792.
- [112] C. Wang, G. Jia, J. Zhou, Y. Li, Y. Liu, S. Lu, C. Li, *Angew. Chem. Int. Ed.* **2012**, *51*, 9352–9355.
- [113] C. Wang, Y. Li, G. Jia, Y. Liu, S. Lu, C. Li, *Chem. Commun.* **2012**, *48*, 6232–6234.
- [114] C. Wang, G. Jia, Y. Li, S. Zhang, C. Li, *Chem. Commun.* **2013**, *49*, 11161.
- [115] Y. Nagata, T. Nishikawa, M. Sugimoto, *J. Am. Chem. Soc.* **2014**, *136*, 15901–15904.
- [116] Y. Nagata, T. Kuroda, K. Takagi, M. Sugimoto, *Chem. Sci.* **2014**, *5*, 4953–4956.
- [117] Y. Nagata, T. Nishikawa, M. Sugimoto, *J. Am. Chem. Soc.* **2015**, *137*, 4070–4073.
- [118] T. Sato, K. Terao, A. Teramoto, M. Fujiki, *Macromolecules* **2002**, *35*, 5355–5357.
- [119] Y.-Z. Ke, Y. Nagata, T. Yamada, M. Sugimoto, *Angew. Chem. Int. Ed.* **2015**, *54*, 9333–9337.

# **II. Supramolecular polymers as scaffolds in catalysis: definition, presentation and objectives of the PhD project**

*Abstract:* Catalyst based on supramolecular polymers will combine properties related to their non covalent and macromolecular scaffold: tunability, dynamic, stimuli responsiveness and chirality amplification. The common properties of supramolecular polymers will be presented before focussing on two particular scaffolds: BTAs and bis-ureas. These scaffolds have been selected given their unique properties: simplicity, predictable 1D architecture, tunability and chirality amplification. For the BTA scaffold recent applications in catalysis will be briefly reminded. Literature examples of transition metal complexes containing urea moiety will be mentioned. Finally, different strategies will be presented for the implementation of hydrogen-bonded supramolecular polymers as scaffolds in catalysis.

## A. Definition and properties of supramolecular polymers

Supramolecular polymers are at the crossroad between polymer sciences and supramolecular chemistry. Meijer defined supramolecular polymers “(...) as polymeric arrays of monomeric units that are brought together by reversible and highly directional secondary interactions, resulting in polymeric properties in dilute and concentrated solutions, as well as in the bulk. The monomeric units of the supramolecular polymers themselves do not possess a repetition of chemical fragments. The directionality and strength of the supramolecular bonding are important features of systems that can be regarded as polymers and that behave according to well-established theories of polymer physics.”.<sup>[1]</sup> Due to their dynamic and reversible properties supramolecular polymers have been studied and used in material sciences and more specifically as opto-electronic, self-healing (see *e.g.* Figure II-1) and biomedical materials.<sup>[2]</sup>

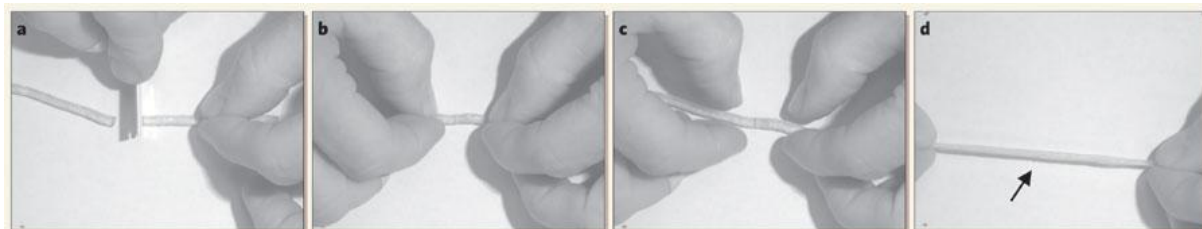


Figure II-1: Example of self-healing material based on supramolecular polymer: a–d) cut, join, mend, stretch. From reference<sup>[3]</sup>

Highly directional interactions are used in order to design supramolecular polymers with well-defined and predictable structures in solution. Commonly used directional interactions are aromatic interactions, metal coordination and hydrogen bonds either alone or in combination. These interactions have a strong influence on the polymerisation/depolymerisation processes according to their strength, number and position (central or peripheral) in the monomeric unit. Polymerisation/depolymerisation equilibria of supramolecular polymers are under thermodynamic control and thus influenced by the temperature, the concentration in monomer and the pressure. Formation of supramolecular polymers with high degrees of polymerisation ( $D_p$ , the number of monomer units in a supramolecular polymer) can lead to increased viscosity and thus formation of gels. In contrast to most physical gels formed by low molecular weight organogelators, supramolecular polymers are thermodynamically stable nanostructures and thus their respective gels remain stable over time. Three main mechanisms of polymerisation have been described: isodesmic, ring-chain equilibrium and cooperative growth (Figure II-2). In isodesmic and cooperative modes of self-assembly, the growing polymer chains are directly in equilibrium with monomers whilst in the ring-chain polymerisation process the cyclic monomers first aggregate into larger rings which further form polymer chains. Isodesmic and cooperative self-assembly processes differ by the amplitude of the association constants between the monomers and the growing polymer chains. When the association constants are equal for each monomer adding to the polymer chain, the process is said isodesmic. In contrast, when the association constant is higher for a monomer adding to the polymer chain than to another monomer the process is

said cooperative. Consequently, supramolecular polymers formed via a cooperative growth mechanism will have higher  $D_p$  than those form via an isodesmic mechanism. Clearly, establishing the mechanism of assembly of a given monomer is of importance to tune the properties of the resulting supramolecular polymers.

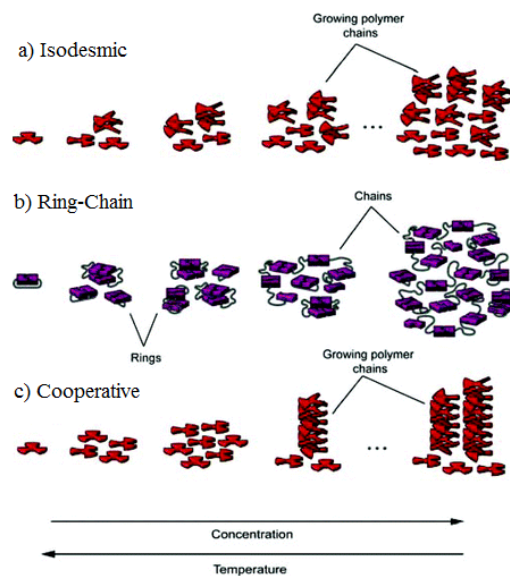


Figure II-2: The self-association mechanisms for supramolecular polymers from reference<sup>[4]</sup>.

Supramolecular copolymers can be obtained by mixing monomers having complementary units; however, in most existing cases only statistical supramolecular copolymerisation is achieved. Also, the precise control of the  $D_p$  of supramolecular polymers remains challenging. Recent examples of controlled polymerisation (living supramolecular polymerisation) have been reported with a fine tuning of the structure, length and composition of supramolecular polymers in solution.<sup>[5,6]</sup> Living supramolecular polymerisation allows the formation of supramolecular polymers with dispersity around 1.1 (a value of 1 indicates that all the chains possess exactly the same length). Up to now, control of the polymerisation has only been achieved in the case of very strongly associated monomers which are poorly dynamic (reshuffling of the monomers among these supramolecular polymers have been estimated for reference<sup>[5]</sup> at several hours or day). To conclude, living supramolecular polymerisation offers controlled of the  $D_p$  albeit at the price of a slowed dynamic behaviour of the supramolecular polymers.

## B. Interest of the use of supramolecular polymers as scaffolds for catalysis

In Chapter I, we described emerging strategies for the development of tunable and dynamic homogeneous catalysts. Supramolecular polymers clearly appear as promising scaffolds in that prospect. The aim of the thesis will be to support catalysts on hydrogen-bonded polymer scaffolds and to correlate the outcome of the catalytic reaction with the polymeric structure adopted by the

assemblies. With this goal in mind, supramolecular polymers appear to be scaffolds of choice for several reasons:

**Their tunability:** the composition of supramolecular polymers can be easily changed by simply mixing complementary monomers. Indeed, monomers with similar complementary units usually co-polymerise allowing their statistical distribution along the polymer chain. It allows a rapid screening of the best monomer mixtures compared to the important synthetic effort required by the preparation of covalent catalysts, *e.g.* those based on a covalent polymer backbone.

**Their chiral properties:** Chirality induction from chiral building blocks to a discrete supramolecular structure is well known and has been applied for the construction of efficient asymmetric catalysts.<sup>[7]</sup> Chirality amplification phenomena are only observed in sufficiently long macromolecules since it requires the transfer of chirality from a chiral monomer to many achiral co-monomers. Chirality amplification phenomena are thus common in covalent<sup>[8]</sup> and in supramolecular polymers.<sup>[9]</sup> Applying such chirality amplification effects in catalysis is particularly appealing: a small number of chiral molecules can be sufficient to induce chirality to a large number of catalytic centres. Chirality amplification phenomena have been divided into two principles: sergeants and soldiers (S&S) and majority rule (MR) effects, that are illustrated in Figure II-3.<sup>[10]</sup> The S&S effect represents the ability of a minimum of chiral monomers (the “sergeants”) to impose their chirality to a large number of achiral monomers (the “soldiers”). This kind of effect is monitored by circular dichroism (CD) spectroscopy by plotting the CD effect observed against the fraction of chiral sergeants (Figure II-3b). Such effect can also be plotted using the net helicity (CD effect of the mixture of sergeants and soldier normalised by the CD effect of the pure chiral sergeant). On the other hand, the MR effect is defined by the ability of the major enantiomer to impose its preferred handedness to the whole supramolecular assembly composed of a scalemic (*i.e.* non-racemic) mixture of enantiomers. A plot of the net helicity of the supramolecular polymer against the enantiomeric excess of the monomers can be used to monitor this effect (Figure II-3c).<sup>[11]</sup> Thus the MR effect allows to decrease the amount of chiral monomer in excess to reverse the handedness of a supramacromolecule. For example, in the case of molecule **32**, a 3:1 ratio in the two enantiomeric monomers (e.e. = 50%) is enough to fully impose the handedness of the enantiomer present in excess (Figure II-3c). Therefore, chirality amplification in supramolecular polymers by those two principles is potentially interesting in catalysis with the aim of reducing the amount of chiral units (S&S) or enabling the design of chirality-switchable catalysts (MR).



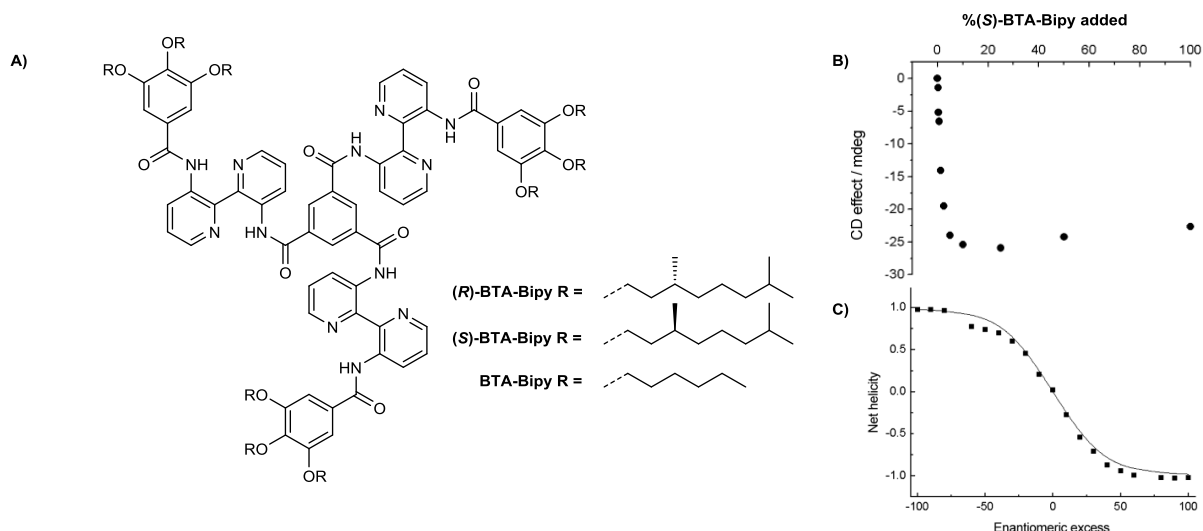


Figure II-3: (a) Disc-shaped monomers with bipyridine units (**BTA-bipy**) that form helical stacks. (b) Chirality amplification (S&S effect) is observed upon mixing solutions of (*S*)-**BTA-bipy** and **BTA-bipy** in hexane as shown by a nonlinear relationship between the CD effect and the amount of chiral (*S*)-**BTA-bipy** added to achiral **BTA-bipy**. (c) Net helicity as a function of enantiomeric excess measured by CD spectroscopy of mixtures of (*S*)-**BTA-bipy** and (*R*)-**BTA-bipy** in *n*-octane. The non-linearity of the data is also characteristic of chirality amplification (MR effect). Net helicity = CD effect / CD effect for the homochiral assemblies. Adapted from reference<sup>[10,11]</sup>

**Their dynamic properties:** supramolecular polymers are dynamic and thus their size and structure can be tuned by fine control of the concentration in monomer, temperature and mixture composition but also by means of various other stimuli (such as solvent polarity). Consequently, if a catalyst is constructed on a supramolecular polymer backbone, the nature of the assembly can be modulated as a function of simple experimental parameters. Of particular interest are systems which may form supramolecular polymers having different morphologies (filament, helices, tapes...) in solution. Structural modification of the supramolecular scaffold is hoped to have a strong influence on the environment of the catalyst supported on the supramolecular polymer and thus should modulate its properties. In case of significant morphology changes, a modification of the second coordination sphere is expected and thus important variation of the selectivity. In that case not only the enantioselectivity is hoped to be influenced but also the regioselectivity. Such dynamic and tunable properties of supramolecular polymers could not only be used to tune the catalytic features prior to the catalytic experiment but also during the course of the catalytic reaction. Indeed, if the kinetics of the reaction is slow enough, the tunability of a supramolecular polymer scaffold can in principle be used to prepare the catalytic species for a first reaction before adjusting the polymeric scaffold for a second reaction.

For all these reasons supramolecular polymers are appealing scaffolds for the development of innovative catalysts. The next part of the chapter will describe the two scaffolds chosen in the frame of our project and their properties and interests.

## C. Choice of the assembly units

In this thesis, we will focus on two types of scaffold, benzene-1,3,5-tricarboxamide (BTA) and bis-urea, which have been selected according to their inherent properties: facility of preparation and predictability of their self-assembly behaviour (structure, stability, chiroptical and chirality amplification properties). Both types of supramolecular polymers have been extensively studied over the last decade and their self-assembly properties are detailed thereafter.

### 1. Benzene-1,3,5-tricarboxamide (BTA) scaffold

#### a) Alkyl BTAs

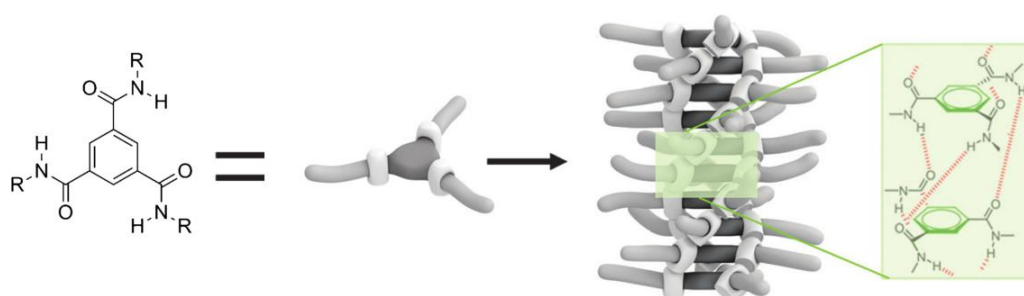


Figure II-4: Schematic representation of benzene-1,3,5-tricarboxamide self-assembly into helical one-dimensional aggregates, which are stabilised by threefold intermolecular H-bonding and aromatic interactions. Adapted from reference.<sup>[12]</sup>

Benzene-1,3,5-tricarboxamide monomers are based on aryl spacer with three carboxamide groups. Those with alkyl chains connected to the amide functions (alkyl BTAs) are easy to prepare and form helical rods (also called stacks) with a predictable structure in low polarity organic solvents (alkanes and toluene mostly). One-dimensional helical rods are formed by means of a threefold hydrogen-bond and aromatic interactions between consecutive monomers in the stacks (Figure II-4).<sup>[12]</sup> Herein, only the properties of C=O centred BTAs will be discussed. N-centered BTAs supramolecular polymers, formed from BTA monomers with inverted amide groups, proved to be less stable and exhibit poorer chirality amplification properties.<sup>[13]</sup>

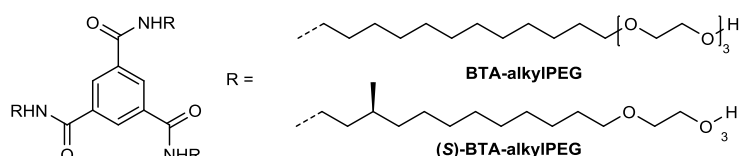


Figure II-5: Water-soluble BTA monomers developed by Meijer *et al.*: **BTA-alkylPEG** from 0 to 3 PEG substituents. Adapted from references<sup>[14]</sup>

Water solubility can be achieved for BTAs by introducing polyethylene glycol chains at the periphery of BTAs (**BTA-alkyl-PEG**, Figure II-5).<sup>[14]</sup> A hydrophobic moiety between the PEG chains and the amide functions is required in order to maintain assembly in water. The exact structure of such assemblies in water is still under investigation. On the other hand, **BTA-Bipy** (Figure II-3a) with peripheral alkyl chains forms rod-like polymers in chloroform but the hydrogen bond network differs from that indicated in Figure II-4. Indeed, the hydrogen bonds occur intramolecularly within each monomer between the N-H of the amide and the pyridine moieties. As a probably consequence of the

non-involvement of the H-bonds in the stacking of BTA-Bipy monomers, the polymerisation mechanism is isodesmic thus making this scaffold less interesting in the frame of this project.<sup>[15]</sup>

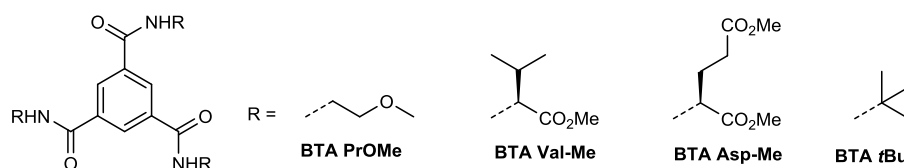


Figure II-6: Chemical structures of BTAs for which the rod-like assembly (Figure II-4) has been characterised by X-ray diffraction analysis.<sup>[16–18]</sup>

With those conclusions in mind, we decided to focus on structurally-simple BTAs: alkyl BTAs and ester BTAs, the latter being BTAs derived from  $\alpha$ -amino esters. Extensive studies have been done aiming at correlating the structure of these BTA monomers (*e.g.* nature of the lateral chain bound to the amide groups and substituents on the benzene ring) and their self-assembly properties. The molecular arrangement in the stacks depicted in Figure II-4 corresponds to the one found in the X-ray crystal structures of **BTA PrOMe**<sup>[18]</sup> and other BTA derivatives (Figure II-6).<sup>[16–18]</sup> These BTAs are poorly soluble in apolar solvents in contrast to those having long alkyl side chains (such as **BTA C8**, see Figure II-7). The self-association behaviour of **BTA C8**, and related alkyl BTAs, in apolar solvents have been assessed by many experimental techniques and computational analyses. Notably, **BTA C8** in apolar solvents forms the same type of rod-like structures than **BTA PrOMe** in the crystalline state as shown by their similar spectroscopic signatures. **BTA C8** forms a rod-like structure in the solid-state and in alkanes as revealed by Fourier-transform infrared (FT-IR) spectroscopy as this structure exhibits characteristic vibrations for the N-H ( $3240\text{ cm}^{-1}$ ) and the amide C=O ( $1640\text{ cm}^{-1}$  and  $1560\text{ cm}^{-1}$ ). In general, FT-IR spectroscopy allows for an easy monitoring of the self-association of BTAs in solution as the N-H stretching frequency for the free monomers has also a characteristic value ( $3450\text{ cm}^{-1}$ ). SANS analyses of BTAs in alkanes are consistent with the formation of long rods in solution (usually  $> 250\text{ \AA}$ ).

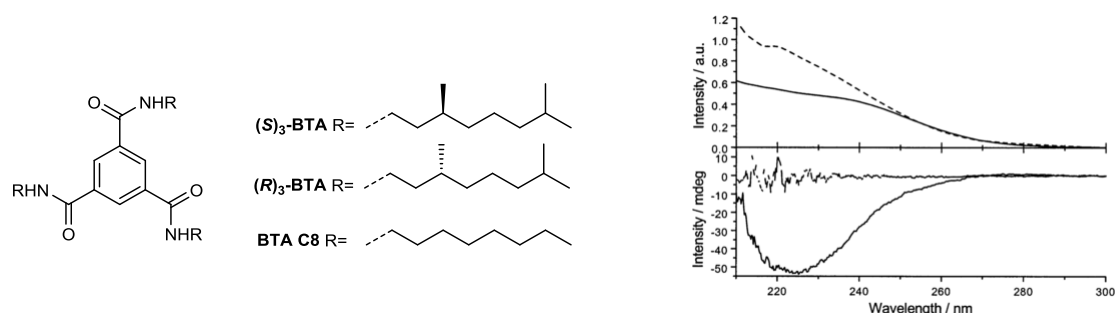


Figure II-7: Left: Chemical structures of  $(S)_3$ -BTA,  $(R)_3$ -BTA and **BTA C8**. Right: Absorption (top) and CD (bottom) spectra of **BTA (S)<sub>3</sub>** in heptane ( $65\text{ }\mu\text{M}$ ) at  $10^\circ\text{C}$  (plain line) and at  $90^\circ\text{C}$  (dashed line). From reference<sup>[19]</sup>

Enantiopure BTAs can be obtained by placing a chiral substituent on the amide alkyl chain (Figure II-7). Enantiopure **BTA (S)<sub>3</sub>** self-assembles into long helical rods in apolar solvents (heptane or  $\text{CCl}_4$ ) whereas it is not associated in  $\text{CHCl}_3$ .<sup>[19]</sup> Introducing chirality in supramolecular BTA assemblies

allows the probing of their self-association mechanism and their chirality amplification properties by circular dichroism (CD) spectroscopy. Chirality amplification properties exhibited by supramolecular BTA helices are particularly interesting for our project and are described in detail below.

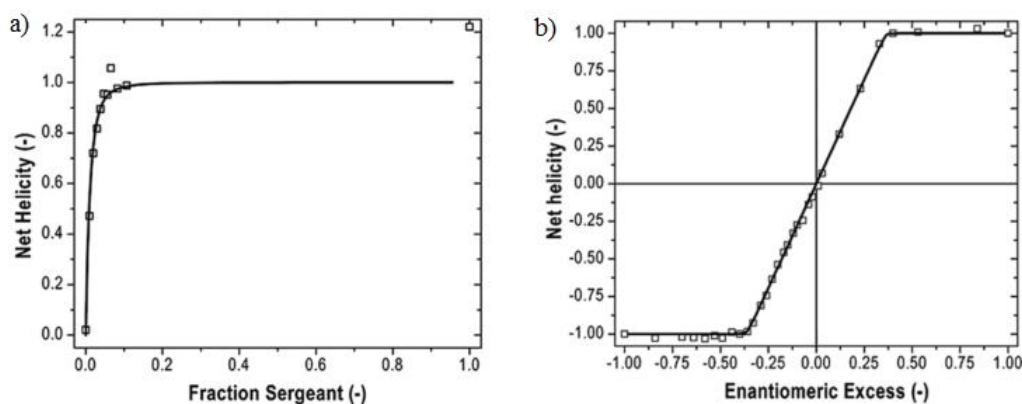


Figure II-8: a) Net helicity as a function of the fraction of “sergeant” ( $(S)_3$ -BTA) for  $(S)_3$ -BTA-BTA **C8** mixtures with the corresponding fit. Concentration= 20  $\mu$ M in methylcyclohexane (MCH) b) Net helicity as a function of the e.e. for  $(S)_3$ -BTA- $(R)_3$ -BTA mixtures with the corresponding fit. Concentration= 20  $\mu$ M in MCH. From reference<sup>[19]</sup>

The overall helicity of the supramolecular polymers of **BTA C8**, an achiral BTA monomer, is null. It is due to the formation of an equimolar mixture of right and left handed helices or of helices with both right-handed and left-handed blocks connected through helix reversals. However for BTAs with at least one chiral centre on the alkyl chain (*e.g.*  $(S)_3$ -BTA, Figure II-7), the long helical stacks formed in hexane exhibit a strong CD signal in the region corresponding to the amide and aromatic chromophores. This signal is absent in the monomer (Figure II-7 right) demonstrating that this signal arises from the formation of supramolecular chiral assemblies. Helices formed by  $(S)_3$ -BTA are left-handed as confirmed by combined experimental/computational studies.<sup>[20]</sup> Most of the BTA supramolecular polymers investigated to date also followed the sergeant-and-soldiers and majority rule principles. The CD signal exhibited by a mixture composed of 5% of the enantiopure  $(S)_3$ -BTA monomers (the sergeants) and 95% of the achiral **BTA C8** monomers (the soldiers) has the same intensity as that of a solution of pure  $(S)_3$ -BTA.<sup>[21]</sup> It implies that both supramolecular polymers carry the same net helicity (Figure II-8a) and that one sergeant ( $(S)_3$ -BTA) transmits its chirality to 20 molecules of soldier (**BTA C8**). Majority rule effect, which describes a non-linear relationship between the enantiomeric excess of the mixture of BTA and the resulting helicity of the supramolecular polymer, was also observed for those BTAs.<sup>[21]</sup> Indeed, a mixture of  $(S)_3$ -BTA and  $(R)_3$ -BTA with 40% enantiomeric excess of  $(S)_3$ -BTA contains fully homochiral helices with a handedness dictated by  $(S)_3$ -BTA (Figure II-8b).

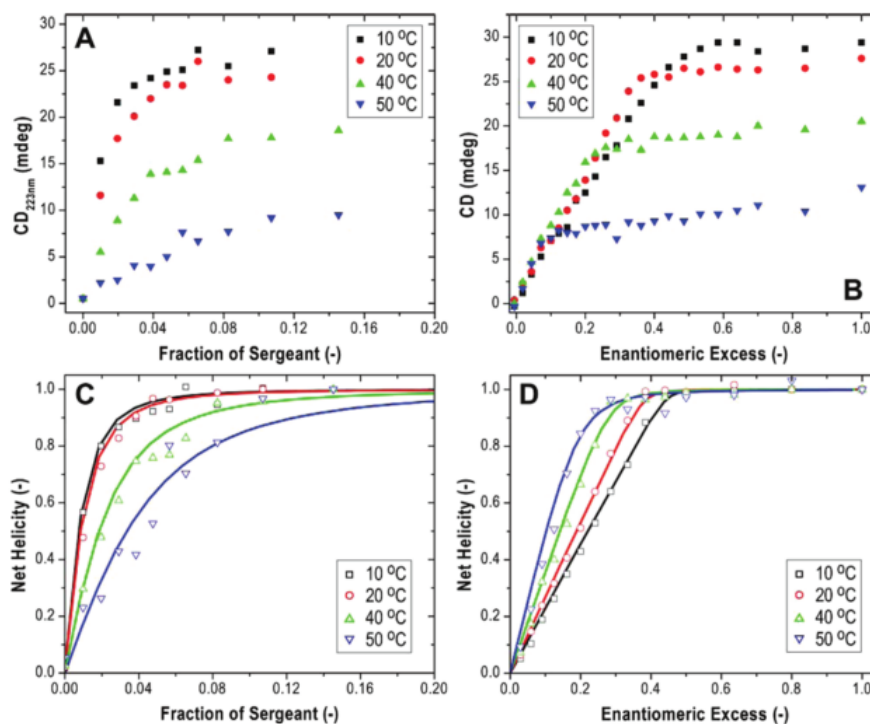


Figure II-9: CD intensity at 223 nm versus the fraction of  $(S)_3$ -BTA “sergeant” for  $(S)_3$ -BTA:BTA C8 mixtures (A) or versus e.e. for  $(S)_3$ -BTA:  $(R)_3$ -BTA mixtures (B). Net helicity versus fraction of “sergeant” for  $(S)_3$ -BTA:BTA C8 mixtures (C) or versus e.e. for  $(S)_3$ -BTA:  $(R)_3$ -BTA mixtures (D). Experiments recorded at four different temperatures: 10 (black), 20 (red), 40 (green), and 50 °C (blue). In (C) and (D) the corresponding fit is also shown. Concentration, 20  $\mu$ M in MCH. From reference<sup>[21]</sup>

Importantly for our objective, the influence of several parameters such as the temperature and the nature of the monomers on the chirality amplification properties of BTA supramolecular polymers have been investigated in details. Influence of the temperature on chirality amplification exhibited by BTA helices was probed for both S&S and MR effects.<sup>[21]</sup> For all mixtures, the maximum intensity of the CD signal at  $\lambda=223$  nm decreased with the temperature which is due to shorter stacks and increased monomer concentration (Figure II-9A and B). In the case of S&S experiments, an increase of the temperature leads to an increase of the minimal amount of chiral sergeants required to get fully homochiral assemblies meaning weaker chirality amplification (e.g. more than 20% of sergeants is needed at 50 °C, Figure II-9C). In contrast, for MR experiments, a lower enantiomeric excess is needed to reach the maximum helicity at 50 °C ( $\approx 30\%$  ee) compared to lower temperatures ( $\approx 50\%$  ee, Figure II-9D).

Investigation of both effects (S&S and MR) at the same time was made by mixing the three monomers  $(S)_3$ -BTA,  $(R)_3$ -BTA and BTA C8 in different proportions and at different temperatures (a so-called diluted majority rule experiment). Firstly, at a given temperature, the lower the enantiomeric excess the higher is the amount of enantiopure monomers required to get fully homochiral assemblies. The effect of temperature is less important than for the S&S and MR separate experiments mentioned above probably since both effects compensate to some extent in the diluted majority rule experiment.

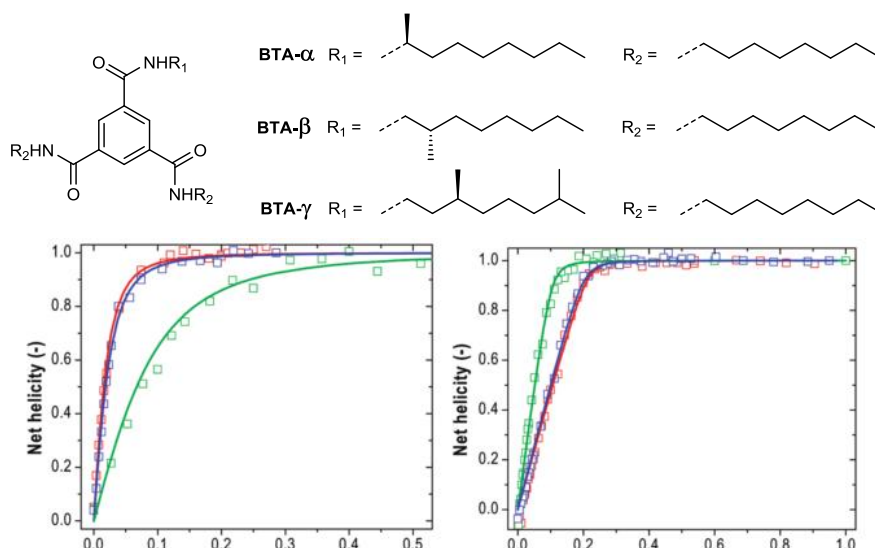


Figure II-10: Top: Chemical structures of BTAs which have been used to probe the influence of the asymmetric carbon position and number on chirality amplification in BTA supramolecular polymers. Bottom left: Net helicity versus the fraction of sergeant for **BTA-α**:**BTA C8**, **BTA-β**:**BTA C8** and **BTA-γ**:**BTA C8** mixtures. Bottom right: Net helicity versus e.e. for scalemic mixtures of **BTA-α** (red square), **BTA-β** (green square) and **BTA-γ** (blue square). Adapted from references<sup>[21,22]</sup>

Meijer *et al.* also investigated the influence of the nature of the BTA monomers on chirality amplification phenomena.<sup>[22]</sup> Concerning S&S experiments, polymers of BTAs with chirality at  $\alpha$  or  $\gamma$  positions (Figure II-10) respectively exhibited similar chirality amplification properties as only 15% of sergeants are needed to get single-handed helices (Figure II-10, bottom left). On the contrary, a larger amount of sergeants **BTA-β** (30%) was required to get homochiral assemblies. Similarly to previous observations on the influence of the temperature, S&S and MR experiments display opposite effects: polymers of **BTA-β** displayed stronger chirality amplification effects in MR experiments than those formed by **BTA-α** and **BTA-γ** (Figure II-10, bottom right).

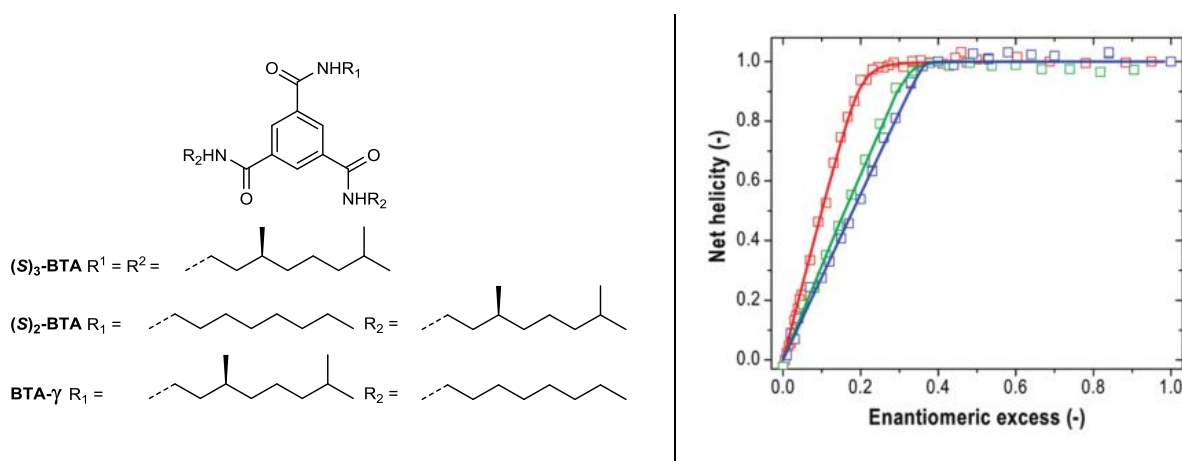


Figure II-11: Left structure of **(S)<sub>3</sub>-BTA**, **(S)<sub>2</sub>-BTA**, **BTA-γ**. Left: Net helicity versus e.e. for scalemic mixtures of **BTA-γ** (red square), **(S)<sub>2</sub>-BTA** (green square) and **(S)<sub>3</sub>-BTA** (blue square) from reference<sup>[22]</sup>

The influence of the number of stereogenic centres on the chirality amplification properties of BTA supramolecular polymers was also probed. MR experiments were performed using **BTA-α**, **(S)<sub>2</sub>-BTA** and **(S)<sub>3</sub>-BTA** which only differ by the number of stereogenic centre in their chemical structure (Figure II-11). Higher chirality amplification was observed with **BTA-α**, *i.e.* the BTA with only one

stereogenic centre. The result was quite expected considering that it was easier to impose a chirality sense to a monomer which had the lower inherent chirality preference. No experiments for the effect of the number of stereogenic centres were made for the S&S principle. However, an opposite trend is expected, *i.e.* that increasing the number of stereogenic centres should increase the extent of chirality amplification. These studies clearly establish the strong chirality transfer and amplification properties of BTA supramolecular polymers. These properties can be modulated by several parameters including the temperature and the nature of the BTA monomers.

## b) Ester BTAs

In the context of catalytic experiments, it is important to access a range of enantiopure BTAs of different chemical structures which can potentially exhibit different chiroptical properties. For these reasons the self-assembly behaviour of chiral ester BTAs derived from the dodecyl-ester of natural and non-natural amino-acids was investigated in our group (Figure II-12) as they possess  $C_3$  symmetry and chirality in  $\alpha$  position of the amide group.<sup>[23]</sup> Choice of  $\alpha$ -amino-acid as source of chirality was driven by their accessibility and their structural and functional diversity. Indeed, a large library of ester BTAs could be synthesised rapidly with important variation of the nature of the substituents attached to the  $\alpha$ -carbon and the ester moiety.

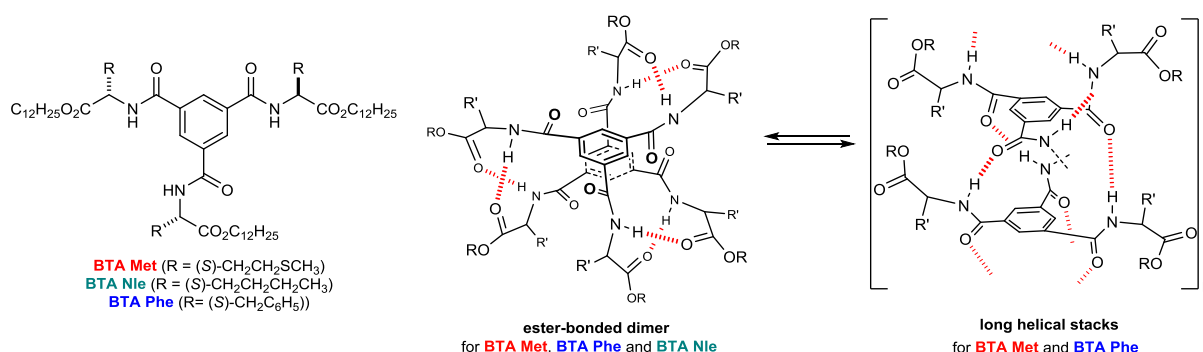


Figure II-12: Ester BTAs derived from amino-acid developed by Raynal *et al.* and their self-assembly behaviour. From reference<sup>[23]</sup>

A first set of ester BTAs, **BTA Met**, **BTA Nle** and **BTA Phe**, have been prepared in two steps, a dodecyl chain was chosen to ensure solubility. Their self-assembly properties were studied in cyclohexane. Based on previous investigation of octyl esters of leucine, phenylalanine and glycine it was expected that these BTAs would display poor association properties.<sup>[24,25]</sup> However, in our group studies revealed that **BTA Phe** and **BTA Met** did form long stacks at mM concentration in solution. **BTA Nle** on the contrary only forms discrete small assemblies in cyclohexane. This structure was determined to be a BTA dimer by means of several analytical techniques (FT-IR, NMR, SANS and CD). FT-IR analyses revealed that the dimers possess signals that strongly differ from those of stacks and indicated that hydrogen-bonds occur between the N-H of the amide group and the carbonyl group of the ester (not of the amide) functions. SANS data, fitted with a form factor for a spherical object gave a radius of 13.5 Å and a molar mass being 1.9 that of the monomer which is consistent with a

dimer. CD spectra of the dimers of the BTA NLe gave an intense signal very different in shape of that displayed by stacks. Unfortunately, none of these ester BTAs formed stacks in the solid state which prevented the exact structure determination of the dimers by X-Ray diffraction. Further screening of amino-acids led us to discover that the ester BTA derived from cyclohexylalanine (Cha) forms dimers in the solid state. Replacement of the dodecyl chain of the ester by smaller groups (*t*Bu and *i*Pr to favor crystallisation) did not affect its self-assembly and thus crystals suitable for X-Ray diffraction were obtained. We were pleased to observe that these crystals displayed virtually identical FT-IR spectra in solution and solid-state. The structure of the dimer was thus determined by X-ray diffraction (Figure II-13).<sup>[26]</sup>

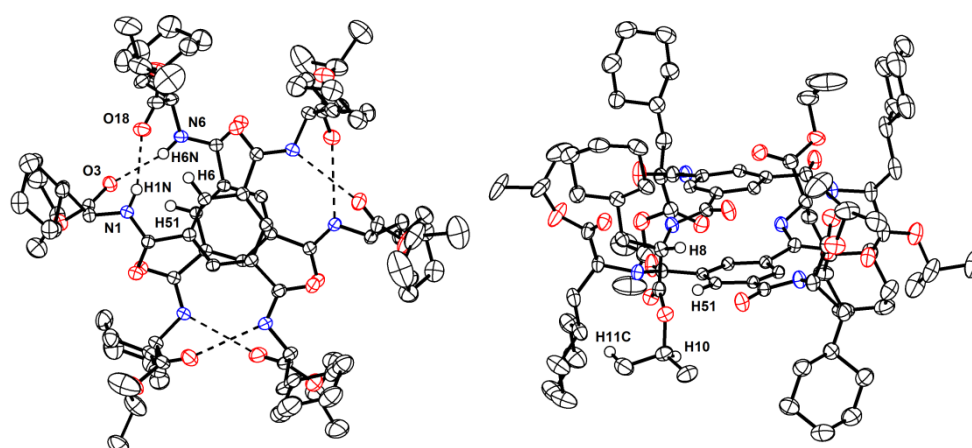


Figure II-13: X-ray crystal structure of BTA (S)-Cha-*i*Pr-0.25CH<sub>3</sub>CN-0.5H<sub>2</sub>O in top view (left) and side view (right). Hydrogen atoms (except H1N, H6N, H6, H51, H8, H10, H11C) and solvent molecules are omitted for clarity. Ellipsoids are represented at 30% probability level. Selected distances (Å): H1N-O18: 2.159(3); H6N-O3: 2.204(3); H6-O18: 2.482(2); H51-O3: 2.352(3); H51-H8: 4.337(4); H51-H10: 3.489(4); H51-H11C: 4.674(4).

The dimeric structure possesses a D<sub>3</sub> symmetry with a) crossed hydrogen bond between the hydrogen of the amide group and the carbonyl of the ester between the two monomers (average length=2.2 Å) b) a  $\pi$ - $\pi$  interaction between the two aromatic rings (distance of 3.47 Å) c) a (*P*) planar chiral arrangement of the aromatic rings induced by the (*S*) chirality of the peripheral amino ester groups d) alternating cyclohexyl and ester groups from the upper and lower monomer, respectively.

A larger set of ester BTAs was synthesised to assess the influence of the substituent present on the  $\alpha$ -carbon on the supramolecular structure (Figure II-14).<sup>[27]</sup> The library can be divided into several groups according to the substituents: a) influence of the ester (BTA Gly and C15); b) absence of chirality (BTA Gly and Aib); c) influence of the length (BTA Ala, Abu, Nle) and the ramification (BTA Abu, Val, Leu and Ile) of the alkyl chain d) influence of the steric hindrance (BTA Ala, *t*Leu and Phg); e) influence of the aromaticity (BTA Phe and Cha).



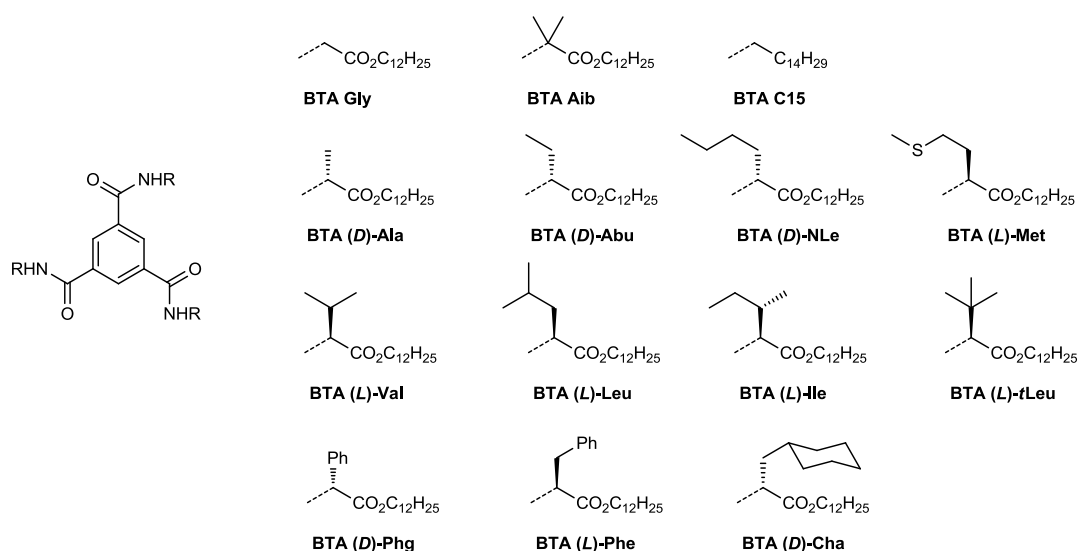


Figure II-14: Library of ester BTAs synthesised in our group from reference<sup>[27]</sup>

The influence of the amino-acid substituent on the self-assembly of the ester BTAs were probed in bulk and solution data (Table II-1). All ester BTAs except two (BTA Gly and BTA Cha) formed stacks in the bulk as determined by solid state CD and FT-IR analyses. Among them, these with the highest clearing temperature ( $T_{cl}$ ) were also those that form stacks in solution (BTA Abu, BTA Phe, BTA Met and BTA Aib) at the notable exception of BTA Ala. The  $T_{cl}$  corresponds to the transition between stacks and dimmers in the bulk. The critical concentration in cyclohexane obeyed the same trend as the  $T_{cl}$ . The ester moiety disfavored the formation of long stacks (BTA C15 vs BTA Gly) and most bulky substituents (BTA Leu, BTA Nle, BTA tLeu, BTA Cha) likely destabilised the stacks in solution. However, this effect was counterbalanced by the presence of some substituents which allowed the formation of stacks in bulk and in solution, possibly because they introduced secondary interactions among the lateral chain (*e.g.* BTA Phe and BTA Met).

Table II-1 Assembly properties of ester BTAs From reference<sup>[27]</sup>  
Assemblies in bulk<sup>(a)</sup>

	structure (20°C)	$T_{cl}$ (°C)	mesophase	structure	$c^*$ at 20°C (M)
<b>BTA Gly</b>	unidentified	-( <sup>b</sup> )	-( <sup>b</sup> )	dimers+“short stacks”	-( <sup>b</sup> )
<b>BTA (R)-Cha</b>	dimers	-( <sup>b</sup> )	-( <sup>b</sup> )	dimers	-( <sup>b</sup> )
<b>BTA Phg</b>	stacks	74	Col <sub>ho</sub>	dimers	-( <sup>b</sup> )
<b>BTA Ile</b>	stacks	131	Col <sub>ho</sub>	dimers	-( <sup>b</sup> )
<b>BTA (R)-Ala</b>	stacks	132	Col <sub>ho</sub>	dimers+“short stacks”+stacks	$8 \times 10^{-2}$
<b>BTA tert-Leu</b>	stacks	134	Col <sub>ho</sub>	dimers	-( <sup>b</sup> )
<b>BTA Nle</b>	stacks	136	Col <sub>ho</sub>	dimers	-( <sup>b</sup> )
<b>BTA Leu</b>	stacks	138	Col <sub>ho</sub>	dimers	-( <sup>b</sup> )
<b>BTA Val</b>	stacks	158	Col <sub>ho</sub>	dimers	-( <sup>b</sup> )
<b>BTA (R)-Abu</b>	stacks	165	Col <sub>ho</sub>	dimers+stacks	$8 \times 10^{-2}$
<b>BTA Phe</b>	stacks	168	Col <sub>ho</sub>	dimers+stacks	$4.4 \times 10^{-4}$
<b>BTA Met</b>	stacks	189	Col <sub>ho</sub>	dimers+stacks	$2.8 \times 10^{-4}$
<b>BTA Aib</b>	stacks	213	Col <sub>ho</sub>	dimers+stacks	$3.0 \times 10^{-5}$
<b>BTA-C15</b>	stacks	214	Col <sub>ho</sub>	stacks	

(a) All DSC data are derived from the second heating run (20°C.min<sup>-1</sup>), (b) no transition, (c)  $C^*$  measured by ITC experiments at 20°C Col<sub>ho</sub> = columnar discotic phase

Chirality amplification properties of these ester BTAs were probed using **BTA (D)-Met** or **BTA (L)-Phe** as sergeants and **BTA C8** as soldier. CD spectra of sergeant and soldier mixtures were recorded at different ratios but fixed total BTA concentration and both ester BTAs gave high chirality amplification (Figure II-15, left). Indeed, only 5% of sergeants was needed in order to reach the maximum net helicity (Figure II-15, right). This result is very important in the context of exploiting ester BTA monomers as chiral inducers in asymmetric catalysis.

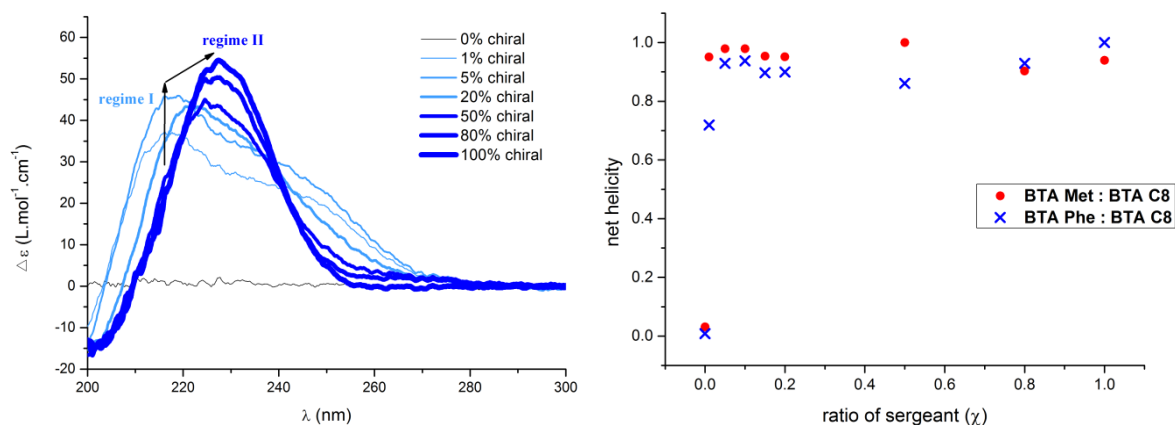


Figure II-15: Left: CD spectra of mixtures of **BTA-Phe:BTA-C8**. Right: Net helicity versus fraction of “sergeant” for mixtures of **BTA Met:BTA-C8** and for mixtures of **BTA Phe:BTA-C8**.  $c = 2.0$ . From reference<sup>[23]</sup>

## 2. Bis-urea scaffold

### a) Structure/Property relationship of bis-ureas

Urea is a ubiquitous group in supramolecular chemistry due to its well known ability to bind anions<sup>[28]</sup> and it is also used as a highly predictable self-assembly group for supramolecular polymers or gelators.<sup>[2,29]</sup> The bis-urea molecule **EHUT** (Figure II-16a) self-assembles into supramolecular polymers in apolar solvents (alkanes and toluene)<sup>[30,31]</sup> and these polymers show interesting rheological properties.<sup>[32]</sup> **EHUT** displays characteristic FT-IR signals in solution depending on its degree of association: stretching frequencies of free N-H appear at 3444 cm<sup>-1</sup> for the aliphatic N-H and 3429 cm<sup>-1</sup> for the aromatic N-H whilst the stretching frequencies for bound N-H are found at 3340 cm<sup>-1</sup> for the aliphatic N-H and 3280 cm<sup>-1</sup> for the aromatic N-H. FT-IR spectra recorded at different concentrations enable the determination of the self-association mechanism of **EHUT**: its polymerisation obeys a cooperative mechanism.<sup>[33]</sup>

This cooperativity means that it is easier for an **EHUT** monomer to bind to a growing supramolecular polymer than to another monomer. Also, **EHUT** assembles into two distinct supramolecular structures in competition in solution as revealed by spectroscopic and scattering analyses. The hydrogen bond pattern is distinct in these two structures as shown by the different shapes and intensities of the stretching frequencies associated with the bound N-H. SANS analyses performed at various temperatures reveal a transition between a tubular structure with 3 molecules in the cross section and a filament structure with a single molecule of **EHUT** in the cross-section. A pseudo-phase diagram<sup>[34,35]</sup>

was drawn for **EHUT** in toluene using FT-IR, viscosimetry and calorimetric analyses (Figure II-16b). The exact molecular arrangement of **EHUT** molecules in the filament form remains unclear as three morphologies (straight, zig-zag or helical) could exist which display similar energies as revealed by extensive experimental and MM/MD (molecular mechanics/molecular dynamics) computational studies.<sup>[36]</sup> The tubular nature of the second supramolecular polymer structure of **EHUT** was confirmed by several experiments.<sup>[37,38]</sup> A molecular representation of this tubular structure that is in agreement with these experimental data was proposed based on MM/MD calculations.<sup>[38]</sup>

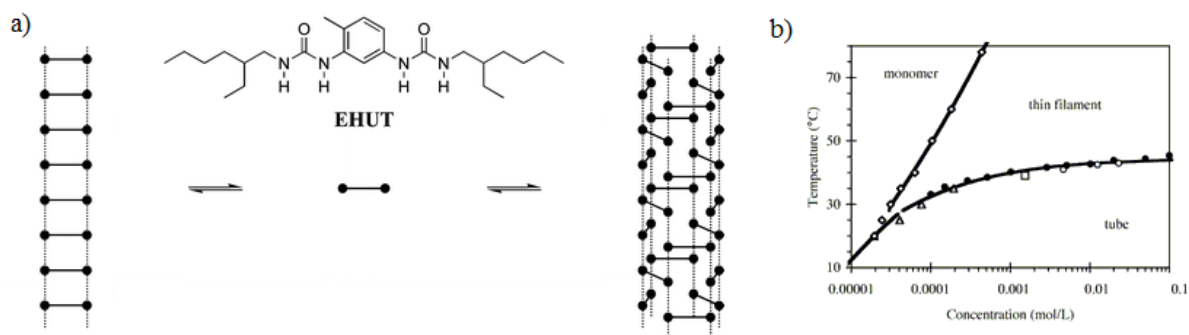


Figure II-16: a) Schematic view of the filament and tube structures of **EHUT** b) Pseudo-phase diagram for **EHUT** solutions in toluene. Transition between monomers and supramolecular polymers determined by ITC ( $\diamond$ ). Transition between filaments and tubes determined by ITC ( $\Delta$ ), viscosimetry ( $\square$ ), FTIR ( $\circ$ ), or DSC ( $\bullet$ ). From references<sup>[34,35]</sup>

Extensive studies have been performed in order to correlate the molecular structure of the bis-urea monomers with the structure of the resulting supramolecular polymers (morphology, stability).<sup>[39]</sup> These studies reveal crucial structure/property relationships that can be used to tune the properties of bis-urea supramolecular polymers. Some of these results, particularly important in the context of our project, are detailed here. Firstly, the influence of the side chain on the solubility of the bis-urea supramolecular polymers was probed. Branched alkyl chains were found to be absolutely necessary for the solubility of the corresponding bis-ureas in apolar solvent.<sup>[33]</sup> Solubility in more polar solvent such as DCM was obtained by replacing 2-ethylhexyl side chain in **EHUT** by an ether alkyl side chain (**EAUT**, Figure II-17, left) however without gelation.<sup>[40]</sup> Introduction of an ester function on the lateral chain (Figure II-17, right) has a strong influence on the structure of the supramolecular polymer. Surprisingly, even though the ester function is not involved in the hydrogen bond network, these bis-ureas exhibit a double filament/filament transition instead of a tube/filament transition.<sup>[41]</sup> The molecular arrangement of the ester bis-urea monomers in this double filament structure is still under investigation.

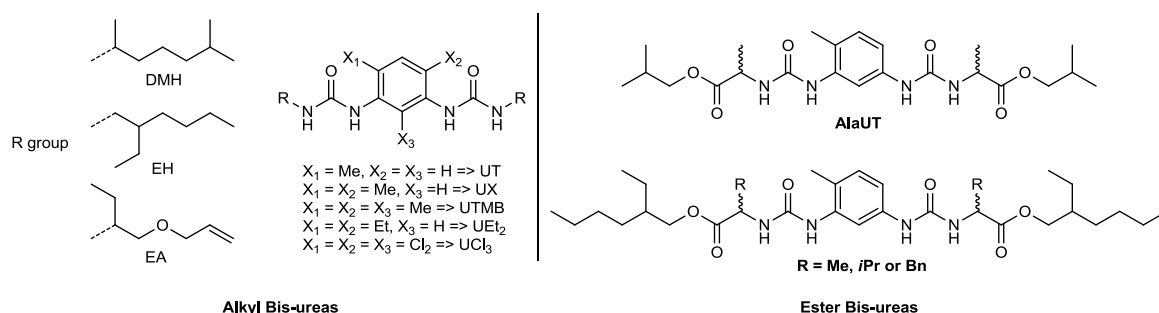


Figure II-17: Left: Various alkyl bis-ureas previously investigated and their nomenclature by addition of the R group prefix to the spacer name. Right: Structure of recently investigated ester bis-ureas. Adapted from references<sup>[28,40]</sup>

Substituents on the benzene ring were found to influence strongly the self-association properties of bis-urea monomers. It was related to a conformational effect as these substituents push the urea groups out of the plane of the benzene ring and thus pre-organise the monomer for the supramolecular polymerisation.<sup>[42]</sup> The stability of the tubular structure is strongly enhanced by replacing the tolyl spacer by a xylyl spacer. It results that the viscosity of **EHUX** is higher than that of **EHUT** in toluene at the same concentration. However, others substituents may lead to the destabilisation of the tubular form. For example, **EHUTMB** has a methyl group that points inwards the cavity and thus destabilises the tube form.<sup>[43]</sup> Halogen substituents on the aromatic ring (*e.g.* **EHUCl<sub>3</sub>**) increase the stability of the filament form.<sup>[44]</sup> **EAUX** combines a xylyl spacer that enhances the association and an ether allyl group which provide solubility in polar solvents. This bis-urea is able to form long aggregates in tetrahydrofuran (THF) or methylethylketone (MEK) that are potential solvents for catalytic applications.<sup>[40]</sup> All these results demonstrate that the structure and stability of bis-urea supramolecular polymers can be finely tuned by careful design of the nature of the bis-urea monomer.

Moreover, a synergetic behaviour was observed for mixtures of bis-ureas having different aromatic spacers. For example, a higher tube/filament transition temperature ( $T^{**}$ ) was observed for a 1/1 **EHUT/EHUTMB** mixture ( $T^{**}=73^{\circ}\text{C}$ ) in toluene comparatively to those of the individual components ( $T^{**}=40^{\circ}\text{C}$  for **EHUT** and  $T^{**}=-5^{\circ}\text{C}$  for **EHUTMB**). For the same reason, gelation was observed for the 1/1 **EHUT/EHUTMB** mixture in  $\text{CHCl}_3$ , a solvent in which both bis-ureas form fluid solutions.<sup>[43]</sup> Since mixing two different monomers may lead to a better stability or a different structure of the resulting copolymer, such synergy effects are very important in the context of our project in order to tune the properties of the supported catalysts.

## b) Chiral properties of bis-urea supramolecular polymers

Compared to BTAs, the chirality transfer and chirality amplification properties of bis-urea monomers have been less studied. However, influence of the chirality on the self-assembly properties of bis-urea monomers was precisely probed in the case of **EHUT** (*(S,S)*-**EHUT** and *(R,R)*-**EHUT**).<sup>[45]</sup> Both enantiomers of **EHUT** form tubular and filament structures. The nanotubes formed by *(S,S)*-**EHUT** and *(R,R)*-**EHUT** are slightly more stable than those of *rac*-**EHUT** as determined by calorimetric analyses.<sup>[46]</sup> CD spectra reveal that the tubular form of *(S,S)*-**EHUT** exhibits a positive Cotton effect

with maxima at  $\lambda=236$  and 224 nm and as expected the CD signal exhibited by (*R,R*)-EHUT (in the same condition) is the mirror image of that of (*S,S*)-EHUT (Figure II-18, bold lines). This signal is absent in the monomeric form (dotted line) demonstrating that within the tubular form the local chirality of the monomer is transferred to the supramolecular level. In contrast, the filament structure exhibits no supramolecular chirality (thin line).

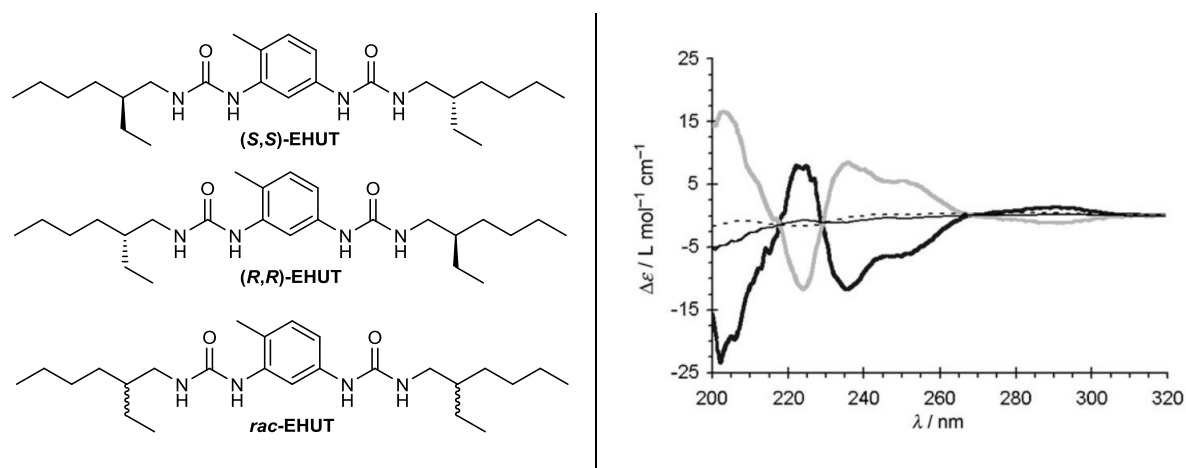


Figure II-18: Left: Structure of (*S,S*)-EHUT and (*R,R*)-EHUT. CD spectra of 1 mM solutions in cyclohexane of: (*S,S*)-EHUT at 20°C (bold black line), (*R,R*)-EHUT at 20°C, (bold grey line), (*S,S*)-EHUT at 60°C (black line) and *rac*-EHUT at 20°C (dashed black line). From reference<sup>[45]</sup>

A strong majority rule effect was observed for the tubular form of EHUT as demonstrated by CD analyses of scalemic mixtures of (*S,S*)-EHUT and (*R,R*)-EHUT. Indeed only 10% of enantiomeric excess was sufficient to reach the same helicity as enantiomerically pure EHUT. The influence of a chiral solvent was also investigated using naturally occurring apolar limonene (both enantiomers being commercially available). A solution of (*rac*)-EHUT in enantiopure limonene gave a CD signal similar in shape to that obtained with enantiopure EHUT. From the intensity of the signal, a value of 33% was determined for the chiral induction to EHUT by the chiral solvent. Although full chirality induction by the solvent alone is not reached, this value is quite significant.

Chirality transfer was also probed using a mixture composed of a chiral bis-urea and a bis-urea functionalised with an intrinsically achiral gold complex (Figure II-19, left). Transferring chirality to gold is not a trivial task due to the linear geometry adopted by gold(I) complexes<sup>[47]</sup> which imposes ligands to be at remote positions of the gold centre. Two bis-urea acetylide gold complexes were investigated which differ by the nature of the peripheral phosphine groups ( $\text{PPh}_3$  vs  $\text{PCy}_3$ ). Both bis-ureas self-assembled in chloroform and in  $\text{CH}_2\text{Cl}_2:\text{THF}$  9:1 as shown by FT-IR spectroscopy and SANS analyses.<sup>[48]</sup>

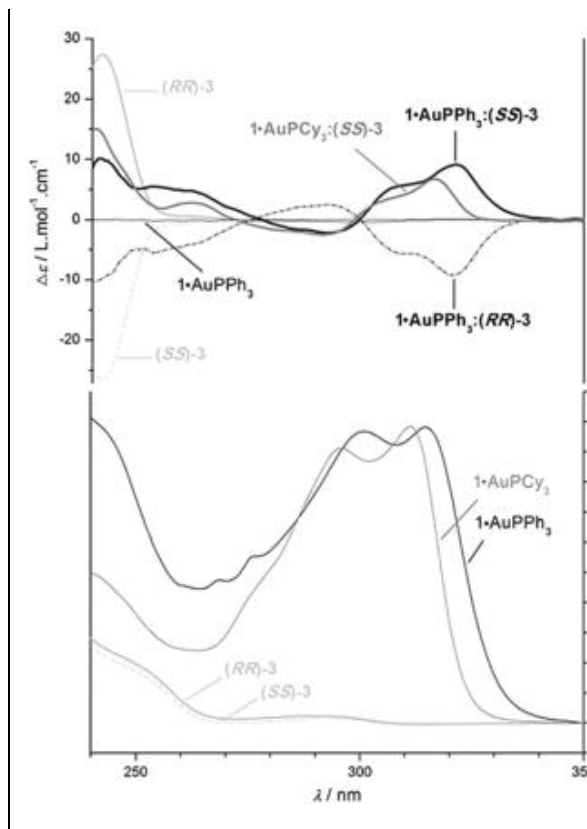
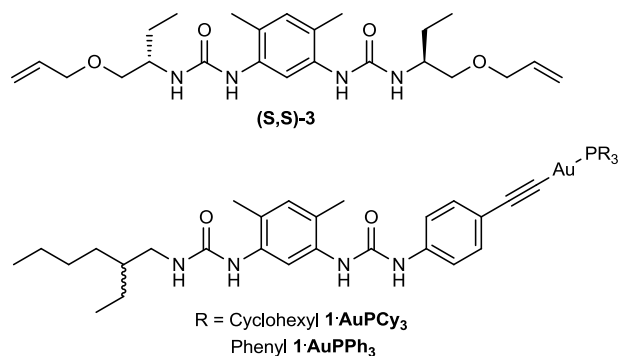


Figure II-19: Left: Chemical structures of chiral additive **(S,S)-3** (sergeant) and of gold complexes **1-AuPCy<sub>3</sub>** and **1-AuPPh<sub>3</sub>** (soldiers). Right: Top: CD spectra of **(S,S)-3**, **(R,R)-3**, **1-AuPPh<sub>3</sub>** and their 1:1 mixtures (1 mM, CH<sub>2</sub>Cl<sub>2</sub>/THF 9:1, -11°C). Bottom: UV absorption spectra of gold complexes and of sergeants. From reference<sup>[47]</sup>

Upon mixing of **1-AuPPh<sub>3</sub>** and **(S,S)-3** a strong modification of the CD signal appeared, the large band at  $\lambda=244$  nm belonging to pure **(S,S)-3** disappeared and was replaced by a less intense signal with opposite sign at the same wavelength (Figure II-19, right). The fact that the CD spectrum of the mixture was completely different from the spectra of the pure samples implied that co-assembly occurred. More interestingly, a CD signal appeared in the 270-340 nm region, a region in which the gold complex absorbed but not the chiral inducer. This induced CD signal denoted a chirality transfer between the chiral bis-urea and the gold complex within the co-assembly. Importantly, the gold complex was in a chiral environment that can be tuned: chirality was inverted with **(R,R)-3** and switched “on” and “off” reversibly with the temperature.

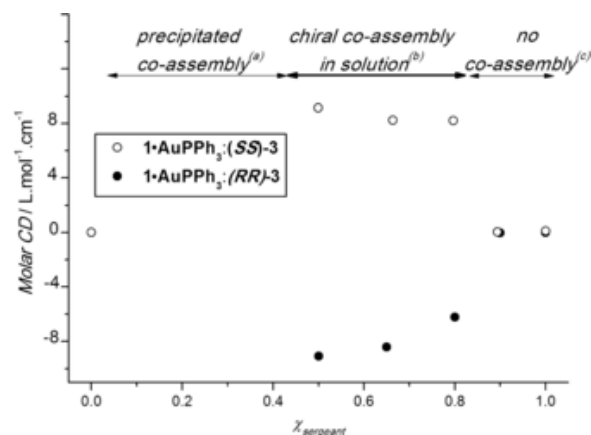


Figure II-20: Net helicity (319 nm) versus fraction of sergeants in **1·AuPPh<sub>3</sub>** / (*S,S*)-**3** or **1·AuPPh<sub>3</sub>** / (*R,R*)-**3** mixtures (1 mM, CH<sub>2</sub>Cl<sub>2</sub>/THF 9:1, -11°C) (a) Social self-sorting between **1·AuPPh<sub>3</sub>** and the sergeant occurs but determination of the molar CD is precluded by the heterogeneous nature of the mixtures. (b) Social self-sorting between **1·AuPPh<sub>3</sub>** and the sergeant in solution. (c) Narcissistic self-sorting *i.e.* the individual assemblies formed by **1·AuPPh<sub>3</sub>** and the sergeant do not co-assemble.  $\chi_{\text{sergeant}} = n_{\text{sergeants}} / (n_{\text{bis-ureas total}})$ . From references<sup>[47]</sup>

The chirality induction is strongly dependent on the proportion of the two monomers and three regimes are observed (Figure II-20). In the first one ( $0 < \chi_{\text{sergeant}} < 0.5$ ), the two monomers co-assemble into a non-soluble supramolecular polymer. In the second one ( $0.5 < \chi_{\text{sergeant}} < 0.8$ ), the co-assembly is soluble and exhibits chirality transfer whilst in the last regime ( $\chi_{\text{sergeant}} > 0.8$ ) the monomers do not co-assemble. These results indicate that complex co-assembly behaviour might arise when two structurally-different bis-urea monomers are mixed in solution. This example of chirality transfer from a ligand-free chiral bis-urea monomer to an intrinsically-achiral metal complex is particularly appealing in the context of our project.

## D. Comparison of the BTA and bis-urea scaffolds

Self-assembly properties of both supramolecular scaffolds have been discussed in the previous paragraphs but a point by point comparison is summed up in the following table.

Table II-2: Comparison of the structural, solubility and chirality properties of the two supramolecular polymer scaffolds

Properties	BTA	Bis-urea
Structure prediction	+++	-
Chirality transfer	+++	++
Chirality amplification	yes	yes
Association in apolar solvent	++	+++
Association in THF & DCM	-	+++
Structure tunability	Monomer/Dimer/Stacks	Monomer/Filament/Tube or double Filament

Both scaffolds are of interest in catalysis as they feature different properties. Even though both types of monomers assemble in alkanes and toluene, bis-urea monomers also assemble in more polar solvents such as DCM, CHCl<sub>3</sub> and even moderately polar solvents (THF). This property of bis-urea supramolecular polymers can be exploited to perform catalytic experiments in solvents that are usually considered as hydrogen-bond competitors.

The rod-like helical and the dimeric structures formed by BTAs are characterised at the molecular level. On the contrary, the exact molecular arrangement of bis-urea assemblies is less established. The morphology of bis-urea supramolecular polymers is also highly affected by subtle changes in the molecular structure of the bis-urea monomers. It has been well-established for ester bis-ureas which form a double filament structure whereas the corresponding alkyl bis-urea monomers form a tubular structure. Such tunability in the structures adopted by bis-urea supramolecular polymers is quite interesting in the frame of our project since one can expect drastic modification of the catalyst environment by changing the macromolecular structure.

Chirality amplification has been demonstrated for both scaffolds however there are more examples in the literature for BTAs especially concerning the sergeants-and-soldiers experiments. Parameters (temperature, concentration, monomers) which influence the extent of chirality amplification in BTA supramolecular polymers have also been investigated and chirality amplification phenomena have been rationalised. Bis-urea supramolecular polymers show strong chirality amplification properties (majority rule) and chirality can be induced to the tubular structure by a chiral solvent.

## **E. Examples of catalysts built on BTA and urea supramolecular scaffold**

This part of the chapter focuses on published examples of supramolecular catalysts constructed on 1D supramolecular BTA scaffold and of metal catalysts containing an urea function.

### **1. BTA as polymers scaffolds for catalysis**

Since the beginning of this Ph. D. project (2013), a few examples appeared in the literature for the use of supramolecular BTA polymers as scaffolds for catalysis. These recent applications of BTA polymers in catalysis have been reviewed in the introduction of this thesis (**I.C.2.a**)(3) and **I.C.3.a**) and we will just sum up the main results herein (see structures in Figure II-21). Palmans *et al.* investigated the influence of the modification of the supramolecular structure on the reactivity of the catalyst. BTA self-assemblies appended with proline moieties efficiently catalyse the aldol reaction in water and that structural organisation of the proline units at the surface of the BTA polymer is of prime importance to control the rate of this reaction.<sup>[49]</sup> However, the selectivity of the reaction is little affected by modification of the supramolecular polymer structure.<sup>[50]</sup> Elemans *et al.* demonstrated that the BTA polymer structure can organise Mn porphyrin catalysts located at its periphery in order to achieve the stereoselective epoxidation of *cis*-stilbene.<sup>[51]</sup>



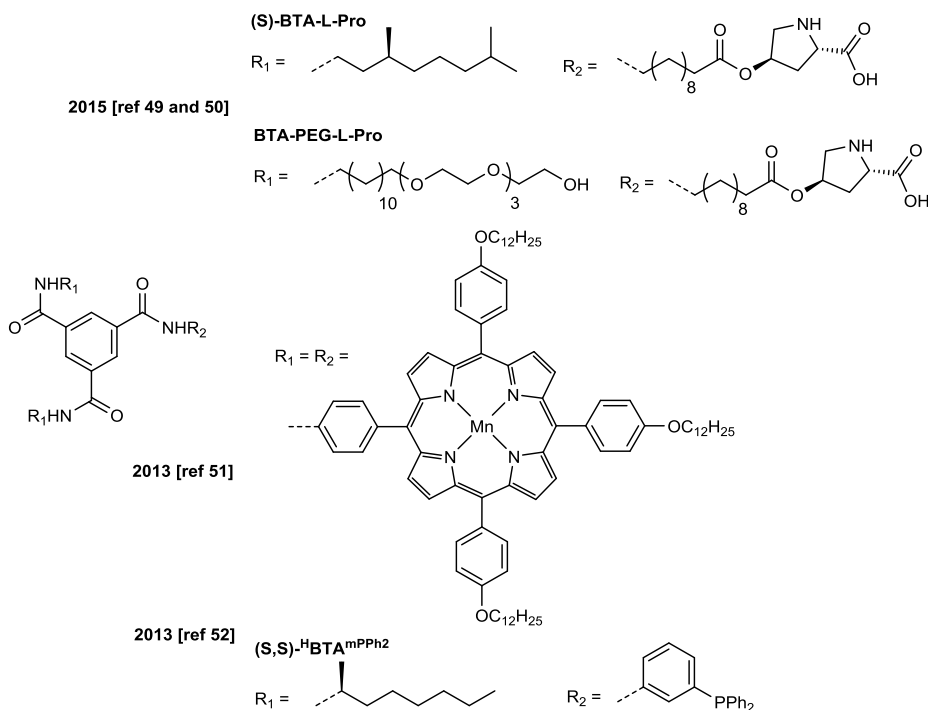


Figure II-21: Previously described catalysts based on a BTA supramolecular polymer scaffold and their years of publication adapted from references<sup>[49-51]</sup>

In our group, we sought to take advantage of the supramolecular chirality of the polymer helices in order to perform asymmetric catalysis.<sup>[52]</sup> Induction of the helical chirality of the BTA to a metal centre was demonstrated in rhodium-catalysed hydrogenation of dimethyl itaconate. The importance of the self-assembly on the chirality induction was also shown. The BTA ligands and additives prepared for this proof-of-concept served as a first BTA set for this PhD project. Other BTA ligands and additives (see formulas in loose sheet) have been prepared by co-workers and myself along the course of this project. The synthesis and characterisation of these new BTAs will be mentioned in the experimental parts of the chapters mentioning the use of these BTA monomers in catalysis.

## 2. Metal catalysts with a single urea function

The urea motif occurrence in catalysis design is somehow less frequent than the amide motif but literature examples exist in both fields of organic and transition-metal catalysis.<sup>[53-58]</sup> Notably, molecules with urea and thiourea functions acting as strong hydrogen bond donors constitute an ubiquitous family of organocatalysts.<sup>[59]</sup> Also, single urea units have been used as association units for the construction of supramolecular bidentate ligands<sup>[60-64]</sup> or to control the reactivity of a substrate<sup>[65]</sup> To the best of our knowledge, the association moiety consisting of two urea functions connected by an aromatic ring as described in (II.C.2) has not been studied in catalysis. However, examples of metal catalysts with a single urea function will be mentioned since information on the reactivity of a urea function in presence of a metal centre can be useful when using bis-urea supramolecular polymers as scaffolds for catalysis.

Of particular interest is the use of the mono-urea moiety as an association unit with the aim of constructing supramolecular bidentate ligands. It was first attempted by Love and co-workers in 2005 who studied the coordination chemistry properties of the ureaphosphine ligand **ureaPPh<sub>3</sub>** into details (Figure II-22). **ureaPPh<sub>3</sub>** reacted with [PdCl<sub>2</sub>(PhCN)<sub>2</sub>] to yield first the soluble *cis* bis-(ureaphosphine) palladium dichloride complex which quickly evolved into the insoluble mixture of *cis/trans* isomer. The insolubility of the *trans* isomer was thought to be related to the formation of a polymeric species in which metal complexes were linked by intermolecular hydrogen-bonded ureas acting as a bridge.<sup>[60]</sup> However addition of tetrabutylammonium chloride (TBACl) led to the formation of a discrete *trans*-palladium complex with a chloride anion bridging the two urea groups both in the solid state and in solution (Figure II-22). Upon reacting **ureaPPh<sub>3</sub>** with [{RhCl(CO)<sub>2</sub>]<sub>2</sub>] the *trans* complexes *trans*-[RhCl(CO)(ureaPPh<sub>3</sub>)<sub>2</sub>] (**UreaRh**) and *trans*-[nBu<sub>4</sub>N][RhCl(CO)(ureaPPh<sub>3</sub>)<sub>2</sub>.Cl] (**UreaRhTBACl**) were isolated in absence and presence of TBACl respectively. **UreaRh** and **UreaRhTBACl** were investigated as precatalysts in rhodium-catalysed hydroformylation of 1-octene. Both complexes provide the same selectivity for the reaction (1:b ratio of ≈ 3) but **UreaRh** reacted faster than **UreaRhTBACl**. It suggested that the abstraction of the chloride anion required in these rhodium chloride precatalysts for the formation of the Rh hydride resting state was faster for **UreaRh** than for **UreaRhTBACl**. This was probably due to the presence of a chloride anion in the urea binding pocket of **UreaRhTBACl** which prevented the urea functions to facilitate the chloride abstraction step.

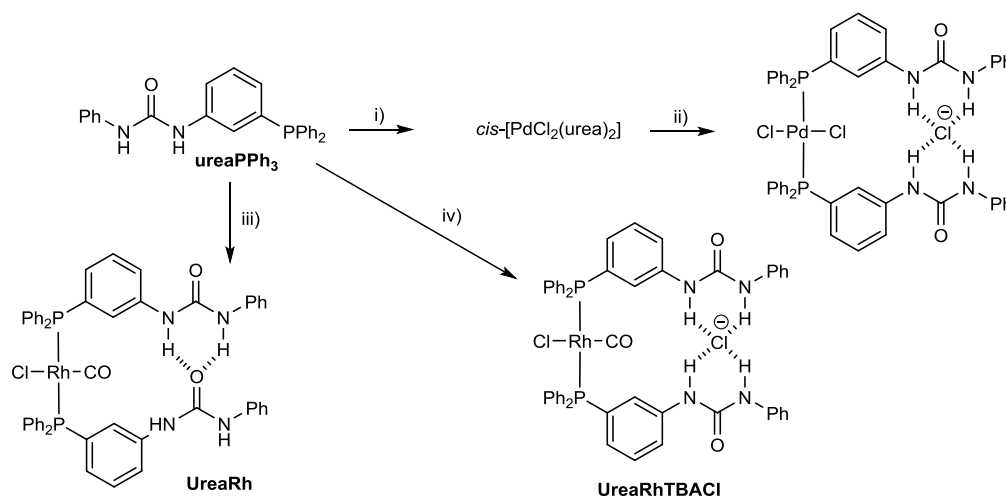


Figure II-22: Reagents and conditions: (i) [PdCl<sub>2</sub>(PhCN)<sub>2</sub>], DCM, 5 min; (ii) nBu<sub>4</sub>NCl, DCM (iii) [Rh(μ-Cl)(CO)<sub>2</sub>]<sub>2</sub>, DCM; (iv) [Rh(CO)<sub>2</sub>Cl]<sub>2</sub>, nBu<sub>4</sub>NCl, DCM. Adapted from reference<sup>[60]</sup>

As structurally-related mono-urea phosphine (**Gly-Urea-PPh<sub>3</sub>**, Figure II-23) was developed by Reek *et al.* and its coordination behaviour was probed.<sup>[61]</sup> Upon complexation with [PdClMe(COD)], the *trans* bis(ureaphosphine) palladium complex was obtained suggesting that the presence of an anion was not compulsory to bind the urea functions intramolecularly. This *trans* complex did not form intermolecular aggregates up to 42 mM (highest concentration investigated). Addition of CO at low temperature displaced the coordinated chloride anion from the rhodium atom to the urea functions

(Figure II-23). The hydrogen bonds between the ureas were restored after heating the complex to room temperature as the result of the migratory insertion of the CO into the methyl palladium bond and the migration of the chloride anion from the urea functions to the palladium centre.

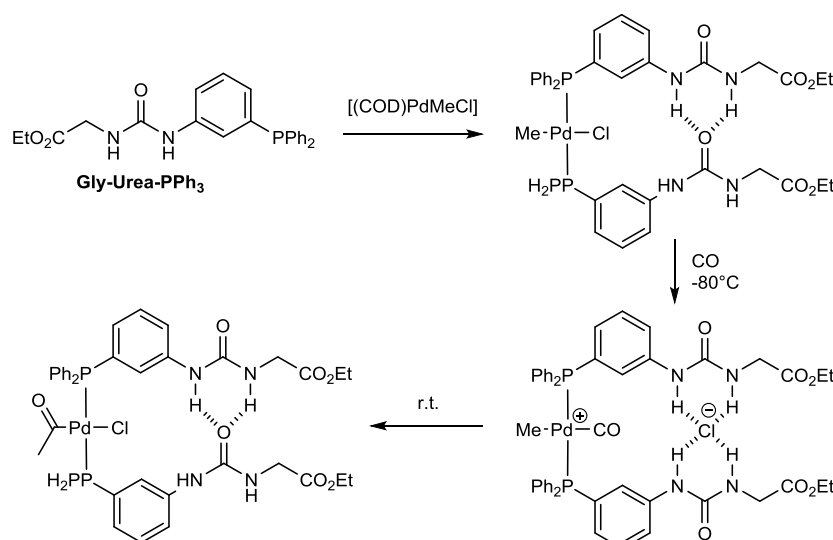


Figure II-23: Coordination studies of **Gly-Urea-PPh<sub>3</sub>** ligands with Pd. Adapted from reference<sup>[61]</sup>

For both examples, it is important to keep in mind that presence of halide ions as salts are often present in catalysis and may lead to modification of the hydrogen bonding of urea groups. This could interfere with our supramolecular scaffold and thus special attention should be paid to the presence of halide anions in the reaction mixture.

Also, the structure of metal complexes incorporating ureaphosphine ligands changed with the nature of the metal precursor and with the experimental conditions.<sup>[63]</sup> It was particularly investigated in the case of the flexible ureaphosphine ligand **UreaPPh<sub>2</sub>** (Figure II-24). Upon mixing 2 equivalents of **UreaPPh<sub>2</sub>** with [Rh(nbd)<sub>2</sub>]BF<sub>4</sub> the *cis* bis(ureaphosphine) cationic rhodium complex was obtained in which the two urea groups are bound to each other. This example showed that ureaphosphine ligand can bind to each other in *cis*-coordinated complexes. However, no hint on the aggregation properties of this complex was provided. If only one equivalent of **UreaPPh<sub>2</sub>** was used, coordination of the rhodium by the carbonyl of the urea occurred. Use of neutral rhodium precursors gave different coordination modes. Starting from [Rh(COD)Cl]<sub>2</sub> hydrogen bond between the chloride and the urea was observed whereas from [Rh(acac)(CO)<sub>2</sub>] deprotonation of the urea group led to the formation of a P,N bidentate ligand. These examples pointed out that urea hydrogen-bond network was maintained in the presence of transition metals; however, metal precursors containing relatively basic coordinated ligands or anionic ligands should be avoided since their use can lead to a disruption of the hydrogen bond network. Also the molar ratio of phosphine ligand and metal precursors is of importance to control the nature of the metal complex.

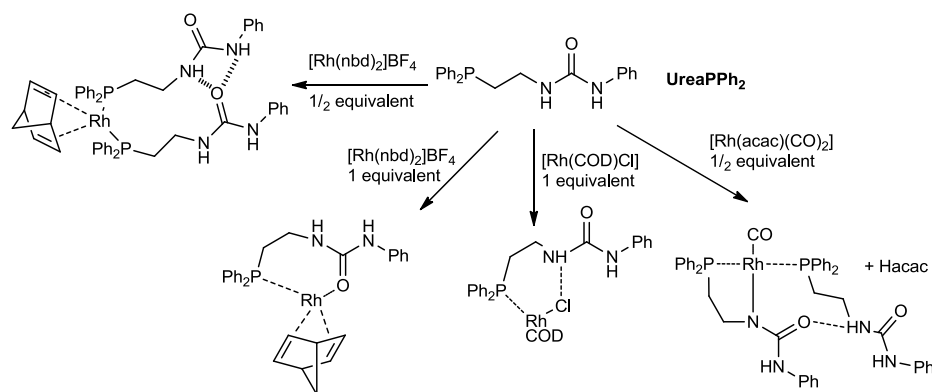


Figure II-24: Coordination and binding mode of **UreaPPh<sub>2</sub>** according to the metal source. Adapted from reference<sup>[63]</sup>

Libraries of bidentate ligands formed by hydrogen bonding between two monourea groups; (such as in complex **Rh-urea-phosphite** in (Figure II-25) have been screened in rhodium-catalysed asymmetric hydrogenation reactions.<sup>[62,63,66]</sup> The chirality was located on the phosphorus atoms and the rhodium complexes of these supramolecular bidentate ligands did not assemble in solution. It is thus of high interest to probe bis-ureaphosphine ligands in catalysis since bis-urea moieties tend to aggregate far more easily in solution than mono-ureas.

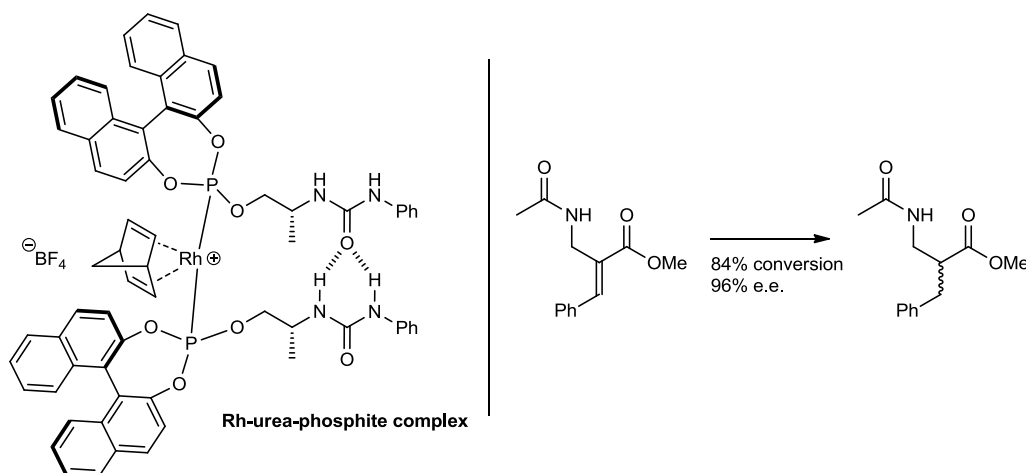


Figure II-25: Hydrogenation of 2-[(acetylamino)methyl]-3-phenyl-2-propenoic methyl ester by Rh-urea-phosphite complex. Adapted from reference<sup>[65]</sup>

## F. Objectives of the project

### 1. General consideration

The aim of the thesis is to support catalysts on hydrogen-bonded polymer scaffolds and to correlate the outcome of the catalytic reaction with the polymeric structure adopted by the assemblies. The chirality induction and chirality amplification properties of BTA and bis-urea supramolecular polymers have been established as well as the possibility to tune the structure and stability of bis-urea supramolecular polymers. Applying such properties of the supramolecular polymers in view of tuning the catalytic properties of peripheral catalytic groups is appealing. However under the light of the literature a

challenge appears: preserving the supramolecular scaffold during the reaction course. In order to succeed some crucial points have to be examined: a) the competition of salts and solvents with the self-assembly, b) the reactivity of urea and amide groups and c) the solubility of the supramolecular scaffolds with embedded catalysts functions.

For the first point, ureas are known to bind anions through hydrogen-bonds and the literature examples in part (II.E.2) provide perfect illustrations. Nevertheless halogen anions are not the only problem as amide and urea groups can also bind cations through their carbonyl group. Competition for hydrogen-bonding could also arise from the solvent of the reaction and hydrogen-bond competing solvents are commonly used in catalysis (*e.g.* dioxane, THF). Secondly, the use of mild reagents and reaction intermediates during the reaction should also be considered as aromatic ureas<sup>[67]</sup> can be deprotonated by, for example an acac anion.

The last important parameter is the solubility of the supramolecular catalyst. Indeed the previous experience in our group showed that we can take advantage of the tunability and of the chirality induction properties of the supramolecular polymers even if the active catalyst is not soluble.<sup>[52]</sup> However, the dynamic behaviour of the supramolecular catalyst is lost. Special attention will be brought on the choice of the catalytic reaction and experimental conditions that should be compatible with the use of supramolecular scaffolds.

## 2. Strategies

Several strategies have been applied in the framework of this PhD project. Those strategies can be divided in two groups: those dealing with a change in the chiral nature of the catalytic centre (Figure II-26) and those aiming at changing the reactivity of the catalytic groups (Figure II-27).

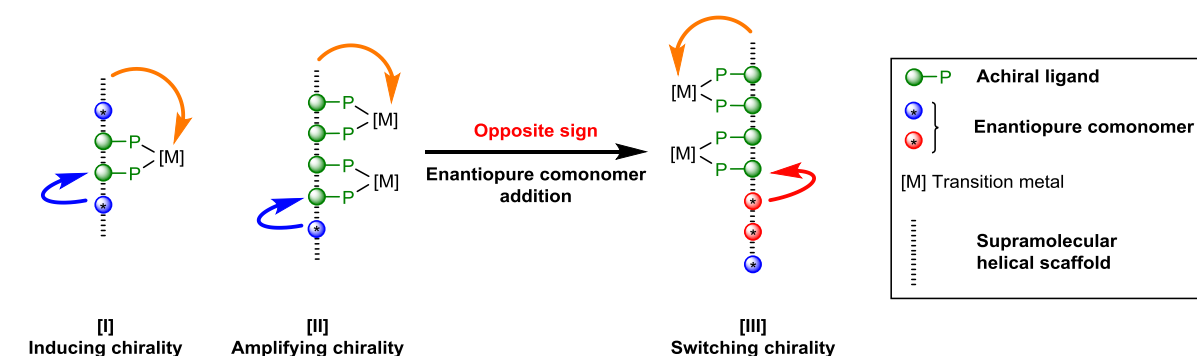


Figure II-26: Chirality based-strategies with catalysts supported by supramolecular polymers envisaged during this PhD thesis

Strategies based on *controlling the chirality* are the following: I) inducing chirality, II) amplifying chirality (S&S) and III) switching chirality (MR) to the intrinsically achiral metal centres located at the periphery of the supramolecular assemblies (represented as [M] in Figure II-26). The first step is to be able to induce chirality from the chiral monomer to the catalytic sites and thus to obtain significant selectivities in asymmetric metal-catalysed reactions. In this regard, the proof-of-concept obtained

with BTA ligands in the rhodium-catalysed hydrogenation of dimethyl itaconate<sup>[52]</sup> constitutes an important starting point to further develop these strategies. In this thesis, the same and structurally-related BTA ligands and BTA co-monomers will be used to implement strategies [II] and [III]. In these strategies, the aim is to take advantage of the chirality amplification properties of the supramolecular polymer to (for strategy [II]) amplify the chirality of a few chiral co-monomers to the supramolecular polymer mainly composed of intrinsically achiral metal centres using the S&S principle. For strategy [III] the objective is the inversion of the handedness of the supramolecular polymer by addition of a chiral co-monomer of opposite sign using the MR principle. Use of the MR is necessary to impose the chirality to the whole supramolecular polymer with only a small chiral bias from an enantiopure co-monomers.

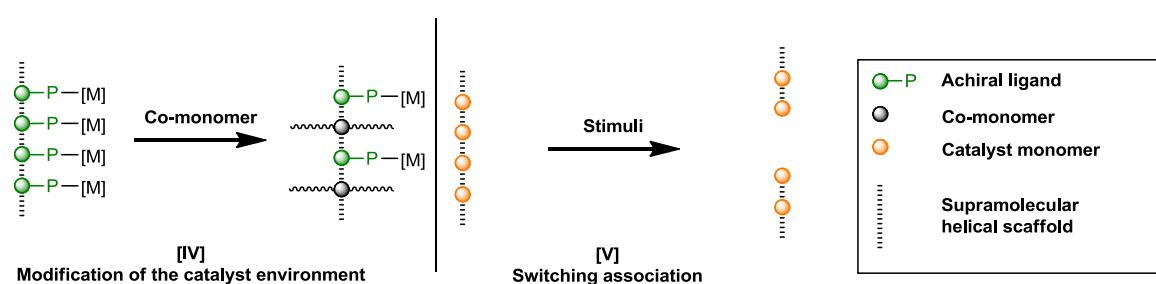


Figure II-27: Reactivity based-strategies with catalysts supported by supramolecular polymers envisioned during this PhD thesis. Catalyst monomer= a molecule in which the association unit is also the catalytic unit

*Reactivity-based strategies* focus on the dynamic behaviour of supramolecular polymer scaffolds by tuning the structure of the supramolecular polymer either to modulate reactivity (strategy [IV]) or to induce it (strategy [V]) using various stimuli (temperature, concentration or additives).

Strategy [IV] is based on the modulation of the environment of the metal centre in order to modify its reactivity. Modification of the coordination modes/coordination sphere or of the electronic/steric environment of the metal centres have important effects on its catalytic performance as often observed in the rhodium-catalysed hydroformylation of alkenes. Another possibility is to increase the bulkiness of the ligands in order to trigger the folding of a substrate in a suitable conformation for reaction. Such effects are particularly important in order to enhance the reaction rates of metal-catalysed cyclisation reactions.

In the case of strategy [V], the assembly unit located in the monomer is also the catalytic unit. The aim of this strategy is to control the degree of association of the catalytic units by various stimuli. Reversibility of this process should allow the “on and off” switching of the activity of the supramolecular catalyst. This control of the activity is particularly interesting in the context of living polymerisation reactions since it could allow a fine control of the polymerisation kinetics but also easy formation of block co-polymers.<sup>[68]</sup>

These strategies will be tested with old and new BTA and bis-urea ligands and co-monomers in several transition-metal catalysed reactions: the rhodium-catalysed hydrogenation of alkenes, the

copper-catalysed hydrosilylation of ketones, the palladium-catalysed hydrosilylation of styrene, the rhodium-catalysed hydroboration of styrene and gold-catalysed cycloisomerisation of 1,6-enyne among others. The aim will be to identify catalytic reactions with mild conditions that will not interfere with the hydrogen-bond network of our supramolecular scaffolds.

This PhD thesis contains the following chapters:

In chapter III will be reported the synthesis and characterisation of bis-urea co-monomer and ligands. Their self-association properties will be probed by FT-IR, CD spectroscopy and SANS.

In the chapter IV will be discussed the use of BTAs for the rhodium-catalysed hydrogenation of dimethyl itaconate. The use of ester BTA (co-monomers) and achiral BTA ligand mixture in catalysis and implementation of strategies [I] and [II] as well as the characterisation of the pre-catalytic species will be reported.

Chapter V will describe the application of strategy [I] and [III] in the frame of copper-catalysed hydrosilylation of acetophenone derivatives using enantiopure BTA co-monomers and achiral BTA ligand. Formation of a chirality-switchable catalyst and characterisation of the pre-catalytic species will be reported.

Chapter VI will describe the synthesis and characterisation of BTA and bis-urea gold complexes and their use in various catalytic reactions. For gold catalysis, strategy [I] and [IV] was envisioned with both supramolecular scaffolds.

In chapter VII, investigation of the influence of salts on the self-assemblies formed by bis-urea and of a urea-thiourea monomer will be reported and as well as the application of the latter monomer in organocatalysis in the frame of strategy [V].

Use of bis-urea scaffolds for copper-catalysed hydrosilylation of acetophenone derivatives will be reported in the annex as well as the investigation of other catalyses in the frame of strategy [I] (rhodium-catalysed hydroboration, palladium hydrosilylation of styrene and phosphine organocatalysis).

## G. References

- [1] L. Brunsveld, B. J. B. Folmer, E. W. Meijer, R. P. Sijbesma, *Chem. Rev.* **2001**, *101*, 4071–4098.
- [2] L. Yang, X. Tan, Z. Wang, X. Zhang, *Chem. Rev.* **2015**, *115*, 7196–7239.
- [3] P. Cordier, F. Tournilhac, C. Soulié-Ziakovic, L. Leibler, *Nature* **2008**, *451*, 977–980.
- [4] T. F. A. De Greef, M. M. J. Smulders, M. Wolffs, A. P. H. J. Schenning, R. P. Sijbesma, E. W. Meijer, *Chem. Rev.* **2009**, *109*, 5687–5754.
- [5] S. Ogi, K. Sugiyasu, S. Manna, S. Samitsu, M. Takeuchi, *Nat. Chem.* **2014**, *6*, 188–195.
- [6] J. Kang, D. Miyajima, T. Mori, Y. Inoue, Y. Itoh, T. Aida, *Science* **2015**, *347*, 646–651.
- [7] M. Liu, L. Zhang, T. Wang, *Chem. Rev.* **2015**, *115*, 7304–7397.
- [8] E. Yashima, K. Maeda, H. Iida, Y. Furusho, K. Nagai, *Chem. Rev.* **2009**, *109*, 6102–6211.
- [9] A. R. A. Palmans, E. W. Meijer, *Angew. Chem. Int. Ed.* **2007**, *46*, 8948–8968.
- [10] J. J. van Gorp, J. A. J. M. Vekemans, E. W. Meijer, *J. Am. Chem. Soc.* **2002**, *124*, 14759–14769.
- [11] J. van Gestel, A. R. A. Palmans, B. Titulaer, J. A. J. M. Vekemans, E. W. Meijer, *J. Am. Chem. Soc.* **2005**, *127*, 5490–5494.
- [12] S. Cantekin, T. F. A. de Greef, A. R. A. Palmans, *Chem. Soc. Rev.* **2012**, *41*, 6125–6137.
- [13] P. J. M. Stals, J. C. Everts, R. De Bruijn, I. A. W. Filot, M. M. J. Smulders, R. Martín-Rapún, E. A. Pidko, T. F. A. De Greef, A. R. A. Palmans, E. W. Meijer, *Chem. Eur. J.* **2010**, *16*, 810–821.
- [14] P. J. M. Stals, J. F. Haveman, R. Martín-Rapún, C. F. C. Fitié, A. R. A. Palmans, E. W. Meijer, *J. Mater. Chem.* **2009**, *19*, 124–130.
- [15] T. Metzroth, A. Hoffmann, R. Martín-Rapún, M. M. J. Smulders, K. Pieterse, A. R. A. Palmans, J. A. J. M. Vekemans, E. W. Meijer, H. W. Spiess, J. Gauss, *Chem. Sci.* **2011**, *2*, 69–76.
- [16] P. P. Bose, M. G. B. Drew, A. K. Das, A. Banerjee, *Chem. Commun.* **2006**, *300*, 3196–3918.
- [17] M. Kristiansen, P. Smith, H. Chanzy, C. Baerlocher, V. Gramlich, L. McCusker, T. Weber, P. Pattison, M. Blomenhofer, H.-W. Schmidt, *Cryst. Growth Des.* **2009**, *9*, 2556–2558.
- [18] M. P. Lightfoot, F. S. Mair, R. G. Pritchard, J. E. Warren, *Chem. Commun.* **1999**, *34*, 1945–1946.
- [19] L. Brunsveld, A. P. H. J. Schenning, M. A. C. Broeren, H. M. Janssen, J. A. J. M. Vekemans, E. W. Meijer, *Chem. Lett.* **2000**, *29*, 292–293.
- [20] Y. Nakano, T. Hirose, P. J. M. Stals, E. W. Meijer, A. R. A. Palmans, *Chem. Sci.* **2012**, *3*, 148–155.
- [21] M. M. J. Smulders, I. A. W. Filot, J. M. A. Leenders, P. van der Schoot, A. R. A. Palmans, A. P. H. J. Schenning, E. W. Meijer, *J. Am. Chem. Soc.* **2010**, *132*, 611–619.
- [22] M. M. J. Smulders, P. J. M. Stals, T. Mes, T. F. E. Paffen, A. P. H. J. Schenning, A. R. A. Palmans, E. W. Meijer, *J. Am. Chem. Soc.* **2010**, *132*, 620–626.
- [23] A. Desmarchelier, M. Raynal, P. Brocorens, N. Vanthuyne, L. Bouteiller, *Chem. Commun.* **2015**, *51*, 7397–7400.
- [24] M. A. J. Veld, D. Haveman, A. R. A. Palmans, E. W. Meijer, *Soft Matter* **2011**, *7*, 524–531.
- [25] M. de Loos, J. H. van Esch, R. M. Kellogg, B. L. Feringa, *Tetrahedron* **2007**, *63*, 7285–7301.
- [26] X. Caumes, A. Baldi, G. Gontard, P. Brocorens, R. Lazzaroni, N. Vanthuyne, C. Troufflard, M. Raynal, L. Bouteiller, *Chem. Commun.* **2016**, DOI 10.1039/C6CC07325E.
- [27] A. Desmarchelier, B. G. Alvarenga, X. Caumes, L. Dubreucq, C. Troufflard, M. Tessier, N. Vanthuyne, J. Idé, T. Maistriaux, D. Beljonne, *et al.*, *Soft Matter* **2016**, *12*, 7824–7838.
- [28] J. W. Steed, *Chem. Soc. Rev.* **2010**, *39*, 3686–3699.
- [29] L. Bouteiller, in *Adv. Phys. Sci.* (Ed.: Springer), **2007**, pp. 79–112.
- [30] F. Lortie, S. Boileau, L. Bouteiller, C. Chassenieux, B. Demé, G. Ducouret, M. Jalabert, F. Lauprêtre, P. Terech, *Langmuir* **2002**, *18*, 7218–7222.
- [31] S. Boileau, L. Bouteiller, F. Lauprêtre, F. Lortie, *New J. Chem.* **2000**, *24*, 845–848.
- [32] E. Sbadini, K. R. Francisco, L. Bouteiller, *Langmuir* **2010**, *26*, 1482–1486.
- [33] V. Simic, L. Bouteiller, M. Jalabert, *J. Am. Chem. Soc.* **2003**, *125*, 13148–13154.



- [34] L. Bouteiller, O. Colombani, F. Lortie, P. Terech, *J. Am. Chem. Soc.* **2005**, *127*, 8893–8898.
- [35] M. Bellot, L. Bouteiller, *Langmuir* **2008**, *24*, 14176–14182.
- [36] P. Brocorens, M. Linares, C. Guyard-Duhayon, R. Guillot, B. Andrioletti, D. Suhr, B. Isare, R. Lazzaroni, L. Bouteiller, *J. Phys. Chem. B* **2013**, *117*, 5379–5386.
- [37] T. Pinault, B. Isare, L. Bouteiller, *ChemPhysChem* **2006**, *7*, 816–819.
- [38] T. Shikata, T. Nishida, B. Isare, M. Linares, R. Lazzaroni, L. Bouteiller, *J. Phys. Chem. B* **2008**, *112*, 8459–8465.
- [39] B. Isare, S. Pensec, M. Raynal, L. Bouteiller, *C. R. Chimie* **2016**, *19*, 148–156.
- [40] F. Ouhib, M. Raynal, B. Jouvelet, B. Isare, L. Bouteiller, *Chem. Commun.* **2011**, *47*, 10683–10685.
- [41] M. Dirany, V. Ayzac, B. Isare, M. Raynal, L. Bouteiller, *Langmuir* **2015**, *31*, 11443–11451.
- [42] B. Isare, G. Pembouong, F. Boué, L. Bouteiller, *Langmuir* **2012**, *28*, 7535–7541.
- [43] B. Isare, M. Linares, R. Lazzaroni, L. Bouteiller, *J. Phys. Chem. B* **2009**, *113*, 3360–3364.
- [44] I. Giannicchi, B. Jouvelet, B. Isare, M. Linares, A. Dalla Cort, L. Bouteiller, *Chem. Commun.* **2014**, *50*, 611–613.
- [45] B. Isare, M. Linares, L. Zargarian, S. Femandjian, M. Miura, S. Motohashi, N. Vanthuyne, R. Lazzaroni, L. Bouteiller, *Chem. Eur. J.* **2010**, *16*, 173–177.
- [46] B. Jouvelet, B. Isare, L. Bouteiller, P. van der Schoot, *Langmuir* **2014**, *30*, 4570–4575.
- [47] P. Pyykkö, *Angew. Chem. Int. Ed.* **2004**, *43*, 4412–4456.
- [48] J. Dubarle-Offner, J. Moussa, H. Amouri, B. Jouvelet, L. Bouteiller, M. Raynal, *Chem. Eur. J.* **2016**, *22*, 3985–3990.
- [49] E. Huerta, B. van Genabeek, B. A. G. Lamers, M. M. E. Koenigs, E. W. Meijer, A. R. A. Palmans, *Chem. Eur. J.* **2015**, *21*, 3682–3690.
- [50] L. N. Neumann, M. B. Baker, C. M. A. Leenders, I. K. Voets, R. P. M. Lafleur, A. R. A. Palmans, E. W. Meijer, *Org. Biomol. Chem.* **2015**, *13*, 7711–7719.
- [51] M. de Torres, R. van Hameren, R. J. M. Nolte, A. E. Rowan, J. A. A. W. Elemans, *Chem. Commun.* **2013**, *49*, 10787–10789.
- [52] M. Raynal, F. Portier, P. W. N. M. van Leeuwen, L. Bouteiller, *J. Am. Chem. Soc.* **2013**, *135*, 17687–17690.
- [53] A. J. Neuvonen, P. M. Pihko, *Org. Lett.* **2014**, *16*, 5152–5155.
- [54] F. Sladojevich, Á. L. Fuentes de Arriba, I. Ortín, T. Yang, A. Ferrali, R. S. Paton, D. J. Dixon, *Chem. Eur. J.* **2013**, *19*, 14286–14295.
- [55] T. Yang, A. Ferrali, F. Sladojevich, L. Campbell, D. J. Dixon, *J. Am. Chem. Soc.* **2009**, *131*, 9140–9141.
- [56] P. Vachal, E. N. Jacobsen, *Org. Lett.* **2000**, *2*, 867–870.
- [57] M. J. Campbell, F. D. Toste, *Chem. Sci.* **2011**, *2*, 1369.
- [58] X. Cui, Y. Zhou, N. Wang, L. Liu, Q.-X. Guo, *Tetrahedron Lett.* **2007**, *48*, 163–167.
- [59] S. J. Connon, *Chem. Eur. J.* **2006**, *12*, 5418–5427.
- [60] P. A. Duckmanton, A. J. Blake, J. B. Love, *Inorg. Chem.* **2005**, *44*, 7708–7710.
- [61] L. K. Knight, Z. Freixa, P. W. N. M. van Leeuwen, J. N. H. Reek, *Organometallics* **2006**, *25*, 954–960.
- [62] A. J. Sandee, A. M. van der Burg, J. N. H. Reek, *Chem. Commun.* **2007**, *2*, 864–866.
- [63] J. Meeuwissen, R. Detz, A. J. Sandee, B. de Bruin, M. A. Siegler, A. L. Spek, J. N. H. Reek, *Eur. J. Inorg. Chem.* **2010**, *2010*, 2992–2997.
- [64] J. Meeuwissen, A. J. Sandee, B. de Bruin, M. A. Siegler, A. L. Spek, J. N. H. Reek, *Organometallics* **2010**, *29*, 2413–2421.
- [65] K. Lang, J. Park, S. Hong, *Angew. Chem. Int. Ed.* **2012**, *51*, 1620–1624.
- [66] J. Meeuwissen, M. Kuil, A. M. van der Burg, A. J. Sandee, J. N. H. Reek, *Chem. Eur. J.* **2009**, *15*, 10272–10279.
- [67] G. Jakab, C. Tancon, Z. Zhang, K. M. Lippert, P. R. Schreiner, *Org. Lett.* **2012**, *14*, 1724–1727.
- [68] X. Wang, A. Thevenon, J. L. Brosmer, I. Yu, S. I. Khan, P. Mehrkhodavandi, P. L. Diaconescu, *J. Am. Chem. Soc.* **2014**, *136*, 11264–11267.



# III. Synthesis and self-assembly properties of new bis-urea monomers

*The chemical structures of the bis-urea ligands, the bis-urea co-monomers and the bis-ureas of reference used in the framework of this project are drawn in the loose sheet accompanying this PhD report.*

*Abstract:* In this chapter, the synthesis and characterisation of new bis-urea monomers are described: co-monomers and ligands. For the synthesis, the main steps towards the preparation of the monomers will be presented and issues met during the synthesis will be stressed out. The complete synthetic procedure is detailed in the experimental part of this chapter. Concerning the characterisation, emphasis will be placed on the self-assembly properties of the new bis-urea monomers in common solvents (*i.e.* toluene, CHCl<sub>3</sub>, DCM and THF) using several techniques: SANS, FT-IR and CD spectroscopy. The nature of the self-assemblies formed by these bis-ureas will be compared with those formed by *(rac)*-EHUT<sup>[1]</sup>, *(rac)*-EHUCl<sub>2</sub><sup>[2]</sup> and *(rac)*-EHUX<sup>[3]</sup>, three previously investigated bis-urea monomers. The new bis-urea monomers are fully assembled at mM in toluene, CHCl<sub>3</sub> and DCM either under the form of a “thick structure” with two molecules in the cross-section or under the filament form with one molecule in the cross-section. Only the bis-ureas with a xylyl spacer are assembled in THF. Self-assemblies formed by *(R)*-*m*-PPh3PBEUX are chiral at the supramolecular level in DCM and CHCl<sub>3</sub>

## A. Elements of design for the new bis-urea monomers

**Bis-urea ligands:** At the exception of the bis-urea acetylide gold complexes mentioned in Chapter II, no example of bis-urea monomers with a peripheral metal complex has been published. One important element of design is the selection of a class of ligands which should be able to coordinate a large range of metal centres. Phosphines are known to coordinate a large variety of metals which in turn form catalytic species used in a huge number of reactions. Among the phosphine ligands, triphenylphosphine ones are particularly appealing since they are quite stable to air and moisture. Accordingly, we decided to prepare 11 bis-urea ligands composed of a central bis-urea association unit and one or two peripheral triphenylphosphine moieties. Several other elements of design were implemented for the chemical structures of these bis-urea ligands. Bis-ureas (8 ligands), with two different side chains, were preferred over those having two identical side chains (2 ligands) since they were expected to be more soluble. Also, bis-urea ligands with three different types of aryl groups between the urea functions (tolyl, 1,3-xylyl, 1,3-dichlorobenzene spacers) were synthesised since the nature of the spacer was known to strongly influence the self-association properties of bis-urea monomers. Variation of the lateral chain had also been used in order to modulate the solubility, the association properties and the chirality of the bis-urea monomers. Finally, bis-urea ligand isomers were prepared which only differ by the position of the  $\text{PPh}_2$  group relatively to the bis-urea association unit. The position of the  $\text{PPh}_2$  group was expected to strongly affect their coordination ability towards the metal catalyst located at the periphery of the assemblies. The final library is composed of 2 achiral ( $(m\text{-PPh}_3)_2\text{UT}$  and  $(m\text{-PPh}_3)_2\text{UCl}_2$ ), 8 racemic ( $(rac)\text{-}m\text{-PPh}_3\text{EHUT}$ ,  $(rac)\text{-}m\text{-PPh}_3\text{EHUCl}_2$ ,  $(rac)\text{-}m\text{-PPh}_3\text{EHUX}$ ,  $(rac)\text{-}m\text{-PPh}_3\text{DMHUCl}_2$ ,  $(rac)\text{-}p\text{-PPh}_3\text{EHUCl}_2$ ,  $(rac)\text{-}p\text{-PPh}_3\text{EHUX}$ ,  $(rac)\text{-}m\text{-PPh}_3\text{PBEUX}$  and  $(rac)\text{-}p\text{-PPh}_3\text{PBEUX}$ ) and 1 enantiopure ( $(R)\text{-}m\text{-PPh}_3\text{PBEUX}$ ) bis-urea ligand.

**Bis-urea co-monomers:** The self-association properties of a variety of ligand-free bis-urea monomers were characterised in the group prior to this project. These bis-urea monomers can be used as co-monomers of the bis-urea ligands in the context of this project either to induce/amplify chirality or to modulate the reactivity. However, new bis-urea co-monomers were also synthesised for the following reasons: i) only a few number of chiral monomers has been developed which limits the possibility of tuning the chiral nature of the resulting supramolecular bis-urea polymers, ii) only a limited number of monomers assemble into DCM and THF which were relevant solvents for catalytic reactions. Hence, we prepared 4 enantiopure symmetrical bis-ureas,  $(R,R)\text{-PBEUT}$ ,  $(R,R)\text{-PBEUCl}_2$ ,  $(R,R)\text{-PBEUX}$  and  $(S,S)\text{-PPheUT}$  which were derived from amino-alcohols. Also,  $(rac)\text{-EHUCl}_2$  and  $(rac)\text{-DMHUCl}_2$  were synthesised since these bis-urea monomers were expected to form strong assemblies in moderately polar solvents.

## B. Synthesis and characterisation

### 1. Synthesis and characterisation of bis-urea co-monomers

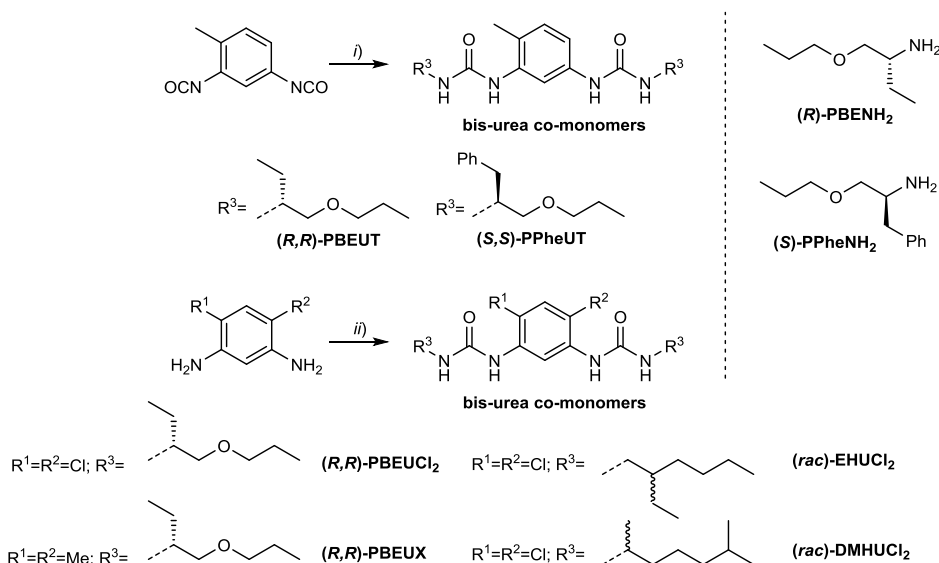


Figure III-1: Synthesis of bis-urea co-monomers i)  $(R)$ -PBENH<sub>2</sub> or  $(S)$ -PPheNH<sub>2</sub>, 46% and 52% yield for  $(R,R)$ -PBEUT and  $(S,S)$ -PPheUT respectively ii) R<sup>3</sup>NH<sub>2</sub>, triphosgene, DIEA (18%<yield<53%).

Bis-urea co-monomers were synthesised following classical procedures (Figure III-1).  $(R,R)$ -PBEUT and  $(S,S)$ -PPheUT were obtained by reacting toluene 2,4-diisocyanate with two equivalents of  $(R)$ -PBENH<sub>2</sub> and  $(S)$ -PPheNH<sub>2</sub> respectively. The 1,3-xylyl and 1,3-dichlorobenzene analogues of  $(R,R)$ -PBEUT were synthesised from the corresponding aromatic amine by first in-situ formation of the corresponding diisocyanatobenzene using triphosgene before addition of  $(R)$ -PBENH<sub>2</sub>.  $(rac)$ -EHUCl<sub>2</sub> and  $(rac)$ -DMHUCl<sub>2</sub> were prepared by adapting existing procedures.<sup>[2]</sup> The yields, enantiopurity and representative analytical data for these new bis-urea co-monomers are compiled in Table III-1.

Table III-1: Yield, e.e. and representative analytical data for the bis-urea co-monomers

Entry	Bis-urea co-monomer	Yield	e.e. <sup>(a)</sup>	d.e. <sup>(a)</sup>	Representative chemical shift <sup>(b)</sup>	
					N-H aromatic	N-H aliphatic
1	$(rac)$ -EHUCl <sub>2</sub>	49%	-	-	8.9	6.9
2	$(rac)$ -DMHUCl <sub>2</sub>	31%	-	-	8.9	6.8
3	$(R,R)$ -PBEUT	46%	>99%	80%	8.3, 7.6	6.4, 5.9
4	$(R,R)$ -PBEUCl <sub>2</sub>	18%	>99%	95%	9.0	6.9
5	$(R,R)$ -PBEUX	37%	>99%	95%	8.0	6.2,
6	$(S,S)$ -PPheUT	52%	nd	nd	8.4, 7.6	6.6, 6.0

(a) e.e. and d.e. determined by chiral HPLC (see experimental part for details). (b) <sup>1</sup>H NMR in DMSO-*d*<sub>6</sub>. nd: not determined

### 2. Synthesis and characterisation of bis-urea ligands

Bis-urea ligand  $(m$ -PPh<sub>3</sub>)<sub>2</sub>UT with two phosphine units was prepared by reacting 3-(diphenylphosphino)aniline and toluene-2,4-diisocyanate.  $(m$ -PPh<sub>3</sub>)<sub>2</sub>UCl<sub>2</sub> was also obtained by a one-pot procedure involving 3-(diphenylphosphino)aniline and 1,5-dichloro-2,4-diisocyanatobenzene, the latter being formed *in situ* by reacting 1,5-diamino-2,4-dichlorobenzene with triphosgene. These two bis-ureas were easily isolated in a pure form either by precipitation from DCM or by column

chromatography on silica gel. Purity was checked by NMR analyses. Notably, in  $^{31}\text{P}\{^1\text{H}\}$  NMR, a single signal is observed at -5.8 ppm for both symmetrical bis-ureas.

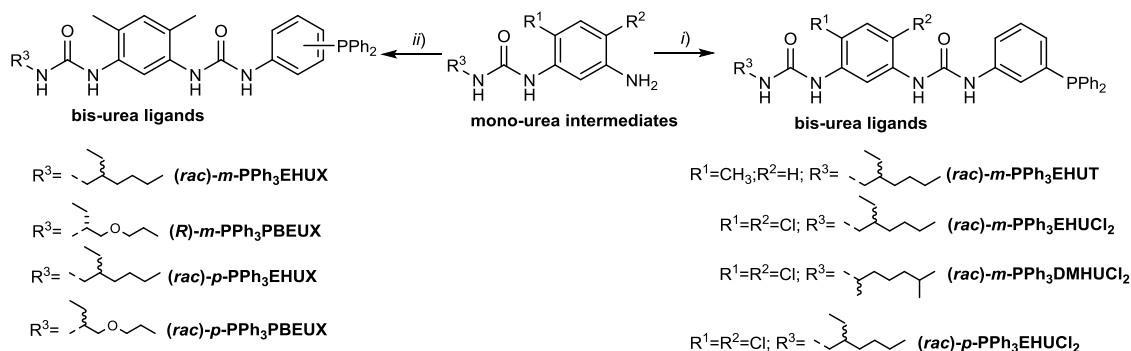


Figure III-2: Synthesis of non-symmetrical bis-urea ligands: i) mono-urea intermediate, triphosgene, DIEA and then 3- or 4-(diphenylphosphino)aniline, ii) 3- or 4-(diphenylphosphino)aniline, 1,1'-Carbonyldiimidazole (CDI) and then mono-urea intermediate.

Bis-urea ligands with a single phosphine unit were prepared by coupling 3- or 4-(diphenylphosphino)aniline with various mono-urea intermediates (Figure III-2). These intermediates were isolated in two or three steps from the respective 1,5-diaminobenzene derivatives following classical synthetic procedures (see the experimental part for more details).

One difficulty in the last step of the preparation of the bis-urea ligands arose from the inherent low nucleophilicity of the anilines which have to be coupled. Low kinetics in the formation of the intermediates will favour the formation of side products, e.g. formation of symmetrical ureas instead of the desired non-symmetrical ones. Another difficulty came from the purification of the bis-urea ligands due to the presence of two strong hydrogen bond donors and a basic  $\text{PPh}_2$  moiety.

Table III-2: Yield, e.e. and representative analytical data for the bis-urea ligands

Entry	Bis-urea ligands	Yield	Representative chemical shift <sup>(a)</sup> (ppm)			$^{31}\text{P}\{^1\text{H}\}$
			N-H Arom.	N-H Alkyl	Me Arom.	
1	( <i>m</i> -PPh <sub>3</sub> ) <sub>2</sub> UT	25%	9.08, 7.86	-	-	-5.8
2	( <i>m</i> -PPh <sub>3</sub> ) <sub>2</sub> UCl <sub>2</sub>	32%	9.44, 8.27	-	-	-5.8
3	( <i>rac</i> )- <i>m</i> -PPh <sub>3</sub> EHUT	25%	8.51, 7.83	6.50	2.10	-6.3
4	( <i>rac</i> )- <i>m</i> -PPh <sub>3</sub> EHUCI <sub>2</sub>	50% <sup>(b)</sup>	9.37, 8.19, 8.01	6.94	-	-5.9
5	( <i>rac</i> )- <i>m</i> -PPh <sub>3</sub> DMHUCI <sub>2</sub>	55%	9.39, 8.20, 7.90	6.87	-	-5.8
6	( <i>rac</i> )- <i>p</i> -PPh <sub>3</sub> EHUCI <sub>2</sub>	30% <sup>(b)</sup>	9.52, 8.30, 8.02	6.95	-	-8.5
7	( <i>rac</i> )- <i>m</i> -PPh <sub>3</sub> EHUX	51%	8.87, 8.03, 7.74	6.31	2.09 <sup>(c)</sup>	-5.7
8	( <i>R</i> )- <i>m</i> -PPh <sub>3</sub> PBEUX	40% (99% e.e.) <sup>(d)</sup>	8.87, 8.05, 7.74	6.28	2.08 <sup>(c)</sup>	-6.2
9	( <i>rac</i> )- <i>m</i> -PPh <sub>3</sub> PBEUX	16%	"	"	"	-6.0
10	( <i>rac</i> )- <i>p</i> -PPh <sub>3</sub> EHUX	33% <sup>(b)</sup>	9.02, 8.07, 7.87	6.30	2.12, 2.10	-8.0
11	( <i>rac</i> )- <i>p</i> -PPh <sub>3</sub> PBEUX	44% <sup>(b)</sup>	9.01, 8.09, 7.85	6.30	2.12, 2.10	-8.0

(a)  $^1\text{H}$  NMR in  $\text{DMSO-}d_6$ , (b) presence of impurity <5% for (*rac*)-*p*-PPh<sub>3</sub>EHUX and (*rac*)-*p*-PPh<sub>3</sub>PBEUX, 7% for (*rac*)-*m*-PPh<sub>3</sub>EHUCI<sub>2</sub> and 9% for (*rac*)-*p*-PPh<sub>3</sub>EHUCI<sub>2</sub> (c) the two methyl aromatic signals have the same chemical shift (d) e.e. determined by chiral HPLC (see experimental part)

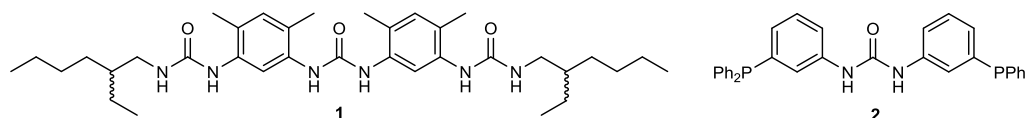
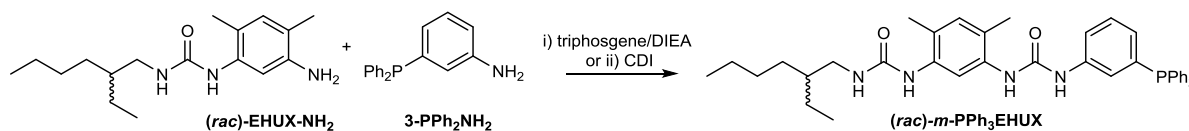
Two different methods were followed for the synthesis of the bis-urea ligands depending on the nature of the spacer. For tolyl and 1,3-dichloroaryl spacer, the 3- or 4-(diphenylphosphino)aniline was added to the isocyanate of the mono-urea intermediate generated *in situ* by slow addition of triphosgene. (*rac*)-*m*-PPh<sub>3</sub>EHUCI<sub>2</sub>, (*rac*)-*p*-PPh<sub>3</sub>EHUCI<sub>2</sub> and (*rac*)-*m*-PPh<sub>3</sub>DMHUCI<sub>2</sub> was purified by

recrystallisation from acetonitrile and thus obtained with modest (30%) to good yields (55%). **(rac)-m-PPh<sub>3</sub>EHUCl<sub>2</sub>** and **(rac)-p-PPh<sub>3</sub>EHUCl<sub>2</sub>** were obtained with impurity (less than 10%) in the aromatic region but none visible in <sup>31</sup>P NMR. In all cases, spectroscopic analyses were in agreement with the chemical structures of these bis-urea ligands. Notably, a single signal was observed in their <sup>31</sup>P{<sup>1</sup>H} spectra at *ca.* -6 ppm for ligands with the PPh<sub>2</sub> group located in meta position and at *ca.* -8 ppm for those with the PPh<sub>2</sub> in para position.

The preparation of the bis-urea ligands with a xylyl spacer proved to be trickier and required the screening of various experimental conditions. The conditions were optimised for the isolation of **(rac)-m-PPh<sub>3</sub>EHUX** obtained by coupling **(rac)-EHUX-NH<sub>2</sub>** and 3-diphenylphosphinoaniline (Table III-3). Indeed, in the conditions mentioned above, *i.e.* by slow addition of **(rac)-EHUX-NH<sub>2</sub>** on triphosgene, **(rac)-m-PPh<sub>3</sub>EHUX** was formed together with the large proportion of symmetrical tris-urea **1** (entry 1). Inversing the order of addition of the reactants, *i.e.* by slowly adding the 3-(diphenylphosphino)aniline to triphosgene, only gave a mixture of intractable and non-identified products. It infers that the formation of the intermediate isocyanates was very slow and could not be achieved cleanly in a convenient way. Also, the symmetrical ureas **1** and **2** proved to be quite difficult to separate from **(rac)-m-PPh<sub>3</sub>EHUX** by both recrystallisation and chromatography techniques. However, identification of tris-urea **1**, in the final mixtures proved to be easy given the characteristic shifts for its methyl aromatic protons ( $\delta = 2.13$  and 2.09 ppm in dms<sub>o</sub>-d<sub>6</sub>)

Accordingly, we looked for an alternative reactant to triphosgene for the activation of the aniline derivatives. We turned our attention to the protocole described by Padiya *et al.* for the preparation of non-symmetrical ureas in high yields by means of CDI in polar solvents.<sup>[4]</sup> In this publication, the reaction was conducted in acetonitrile a solvent in which 3-(diphenylphosphino)aniline was soluble but not **(rac)-EHUX-NH<sub>2</sub>**. We thus screened different conditions (order of addition, solvent, equivalents of CDI) for the preparation of **(rac)-m-PPh<sub>3</sub>EHUX**.

Table III-3: Reaction conditions screened for the formation of **(rac)-m-PPh<sub>3</sub>EHUX** and the side products **1** and **2**



Entry	Method	1 <sup>st</sup> aniline added	Equiv. CDI	<b>(rac)-m-PPh<sub>3</sub>EHUX : 1 : 2</b>
1	triphosgene	<b>(rac)-EHUX-NH<sub>2</sub></b>	1	1 : 0.6 : 0
2	CDI	3-PPh <sub>2</sub> NH <sub>2</sub>	1	1 : 0.3 : 0.2
3	CDI	3-PPh <sub>2</sub> NH <sub>2</sub>	2	1 : 0.16 : 0
4	CDI	3-PPh <sub>2</sub> NH <sub>2</sub>	2.5 <sup>(a)</sup>	1 : 0 : 0

(a) addition of 1 mL of water to hydrolyze the excess of CDI

The optimised conditions were a slow addition 3-(diphenylphosphino)aniline on an excess of CDI to form the intermediate 3-(diphenylphosphino)aniline-carbamoylimidazole. The excess of CDI was required to prevent the formation of the ureaphosphine **2** and was hydrolysed before the addition of (*rac*)-**EHUX-NH<sub>2</sub>** in order to avoid the formation of the tris-urea **1**. It led to the clean formation of (*rac*)-***m*-PPh<sub>3</sub>EHUX** in 51% yield after recrystallisation from acetonitrile. The same methodology was applied for the preparation of the other bis-urea ligands with a xylyl spacer: (*R*)-***m*-PPh<sub>3</sub>PBEUX** (40% yield), (*rac*)-***m*-PPh<sub>3</sub>PBEUX** (16% yield), (*rac*)-***p*-PPh<sub>3</sub>EHUX** (33% yield) and (*rac*)-***p*-PPh<sub>3</sub>PBEUX** (44% yield). All the analytical data were in agreement with the clean formation of the bis-urea ligands except for (*rac*)-***p*-PPh<sub>3</sub>PBEUX** and (*rac*)-***p*-PPh<sub>3</sub>EHUX**. Indeed impurity from the starting 4-(diphenylphosphino)aniline gave side-products with similar solubility and migration on TLC (thin layer chromatography). Application of this methodology to (*rac*)-**EHUCl<sub>2</sub>-NH<sub>2</sub>** was investigated but did not yield the corresponding bis-urea. This might arise from the lower nucleophilicity of the 1,3-dichlorophenyl compared to the xylyl spacer. (*R*)-***m*-PPh<sub>3</sub>PBEUX** was obtained in its enantiopure form (99% e.e.) as determined by chiral HPLC (see the experimental part).

## C. Self-association properties

### 1. Gelation tests

Table III-4: Solubility and gelation tests of the bis-urea monomers at 10 mM

	Name	C <sub>6</sub> H <sub>12</sub>	Et <sub>2</sub> O	Toluene	CHCl <sub>3</sub>	DCM	DCE	THF	AcOEt
ref <sup>[1]</sup>	<b>EHUT</b>	G	G	G	S	NS	nd	S	NS
co-monomer	( <i>S,S</i> )- <b>PPheUT</b>	G	NS	G	S	S	P	S	S
co-monomer	( <i>R,R</i> )- <b>PBEUT</b>	G*	NS	G	S	NS	nd	S	P
ligand	( <i>m</i> -PPh <sub>3</sub> ) <sub>2</sub> <b>UT</b>	NS	NS	NS	NS	NS	NS	S	NS
ligand	( <i>rac</i> )- <b><i>m</i>-PPh<sub>3</sub>EHUT</b>	NS	NS	S*	S*	S*	NS	S	NS
ref <sup>[2]</sup>	<b>EHUCl<sub>2</sub></b>	G	G	G	V	NS	NS	S	NS
ligand	( <i>m</i> -PPh <sub>3</sub> ) <sub>2</sub> <b>UCl<sub>2</sub></b>	NS	NS	NS	V	NS	NS	S	NS
ligand	( <i>rac</i> )- <b><i>p</i>-PPh<sub>3</sub>EHUCl<sub>2</sub></b> <sup>(a)</sup>	NS	NS	V	V	S	S*	S	NS
ligand	( <i>rac</i> )- <b><i>m</i>-PPh<sub>3</sub>EHUCl<sub>2</sub></b> <sup>(a)</sup>	NS	NS	G	S	V	NS	S	S*
co-monomer	<b>DMHUCl<sub>2</sub></b>	V	S	V	S	P	Go*	S	P
ligand	( <i>rac</i> )- <b><i>m</i>-PPh<sub>3</sub>DMHUCl<sub>2</sub></b>	NS	NS	G	V	V	S	S	S
co-monomer	( <i>R,R</i> )- <b>PBEUCl<sub>2</sub></b>	G	S	G	S	NS	S	S	P
ref <sup>[3]</sup>	<b>EHUX</b>	nd	nd	G	G	nd	nd	S	P
co-monomer	( <i>R,R</i> )- <b>PBEUX</b>	nd	G	G	G	NS	ND	G	nd
ligand	( <i>rac</i> )- <b><i>m</i>-PPh<sub>3</sub>EHUX</b>	NS	NS	G	G	G	nd	S	nd
ligand	( <i>R</i> )- <b><i>m</i>-PPh<sub>3</sub>PBEUX</b>	NS	NS	G*	G	G	G*	S	NS
ligand	( <i>rac</i> )- <b><i>m</i>-PPh<sub>3</sub>PBEUX</b>	NS	NS	G*	G	G	G*	S	NS
ligand	( <i>rac</i> )- <b><i>p</i>-PPh<sub>3</sub>EHUX</b> <sup>(a)</sup>	nd	nd	G	G	G	nd	S	nd
ligand	( <i>rac</i> )- <b><i>p</i>-PPh<sub>3</sub>PBEUX</b> <sup>(a)</sup>	nd	nd	G	G	G	nd	S	nd

DCE = 1,2-dichloroethane, NS = non soluble even after heating, S = fluid solution, V = viscous solution, G = transparent gel, Go = opaque gel, P = precipitation after heating and nd = not determined. \*heating required to get an homogeneous gel, (a) these bis-urea contained an impurity

The gelation ability of the 11 bis-urea ligands and the 6 co-monomers was probed at a concentration of 10 mM in solvents of various polarities. The samples were heated only if dissolution did not occur after shaking the samples overnight on the shaking table (250 rpm). Gelation tests provided a first hint of the solubility and the self-association properties of bis-urea monomers. A homogenous transparent



gel usually indicates the presence of long one-dimensional assemblies. The solution and gelation properties of the newly synthesised bis-ureas were compared with that of bis-ureas of reference: **EHUT**, **EHUCl<sub>2</sub>** and **EHUX** (Table III-4).

As anticipated, bis-urea with two phosphine units (*m*-**PPh<sub>3</sub>**)<sub>2</sub>**UT** and (*m*-**PPh<sub>3</sub>**)<sub>2</sub>**UCl<sub>2</sub>** proved to be poorly soluble. This was consistent with the poor solubility of a previously described symmetrical bis-urea having terminating aryl groups.<sup>[1]</sup> However, (*m*-**PPh<sub>3</sub>**)<sub>2</sub>**UCl<sub>2</sub>** formed a viscous solution in chloroform which inferred the formation of long assemblies for this bis-urea in this solvent. In contrast to bis-urea co-monomers and reference bis-ureas, the bis-urea ligands with a single phosphine unit were not soluble in cyclohexane and diethyl ether. This was apparently due to the relatively polar PPh<sub>2</sub> groups. However, most of the bis-urea ligands synthesised were soluble in toluene, DCM, CHCl<sub>3</sub> and THF and thus their self-association properties will be compared in these solvents.

At the exception of (*rac*)-*m*-**PPh<sub>3</sub>****EHUT**, all bis-urea ligands were strongly associated in toluene as suggested by the fact that they formed gel or viscous solutions in this solvent. (*rac*)-*m*-**PPh<sub>3</sub>****EHUT** was in fact the only bis-urea ligand that did not form a gel in any of the investigated solvents. This might be a first indication of the poorer aggregation ability of this ligand compared to the other bis-urea ligands. When compared to **EHUT**, the lower aggregation ability of (*rac*)-*m*-**PPh<sub>3</sub>****EHUT** was likely related to the presence of the polar PPh<sub>2</sub> group which act as a hydrogen-bond competitor. However, this decrease in the stability of the hydrogen-bonded network was compensated by changing the nature of the spacer.

Indeed gelation tests in Table III-4 also suggested that the trend in the strength of the self-assemblies formed by the bis-ureas of reference (*i.e.* **EHUX**>**EHUCl<sub>2</sub>**>**EHUT**) was the same for the bis-urea ligands. Indeed, bis-urea ligands with a 1,3-xylyl spacer formed gels in DCM, CHCl<sub>3</sub> and THF while bis-urea ligands with a 1,3-dichlorobenzene or a tolyl spacer only formed viscous or fluid solutions in the same solvents. Bis-urea ligands with 1,3-dichlorobenzene spacer were, in turn, more associated than those with a tolyl spacer as evidenced by their ability to gel toluene and formed viscous solutions in DCM and CHCl<sub>3</sub>. The ability of the bis-urea ligands with a 1,3-xylyl and 1,3-dichlorobenzene spacer to form long assemblies in moderately polar solvents such as DCM, CHCl<sub>3</sub> which were commonly-used solvents in homogenous catalysis, was of particular interest for our project. In contrast to the spacer, the nature of the lateral chain seemed to marginally affect the solubility and self-association properties of bis-urea monomers.

If gelation test was an easy and quick visual method to assess both solubility and strong association ability of supramolecular polymers, it did not allow a clear distinction between bis-urea that are monomeric and those which form filaments. Indeed, bis-urea that self-assembles into long filaments in solution form non-viscous solutions.<sup>[1]</sup> However a rapid and clear determination of the self-assembly formed by these bis-ureas could be obtained by FT-IR spectroscopy. A more precise determination of

the nature of the self-assemblies formed by the bis-urea ligands in toluene will be made by means of SANS analyses (vide infra).

## 2. FT-IR analyses

For the co-monomers, this was particularly interesting in the case of chloroform solutions which were mostly non viscous. In chloroform, the bonded N-H of (*rac*)-EHUT are at 3340 and 3280  $\text{cm}^{-1}$  whereas the free N-H are at *ca.* 3450  $\text{cm}^{-1}$ .<sup>[1]</sup>

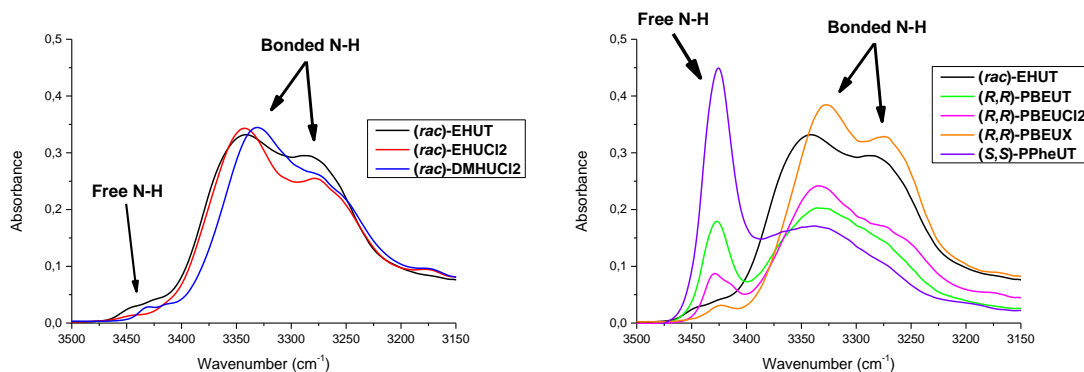


Figure III-3: FT-IR spectra at 10 mM in chloroform of the bis-urea co-monomers

Comparison with (*rac*)-EHUT allowed us to probe the self-association behaviour of the newly synthesised co-monomers (Figure III-3). In the cases of (*rac*)-EHUCl<sub>2</sub> and (*rac*)-DMHUCl<sub>2</sub> the two bonded N-H frequencies were observed as well as a weak free N-H peak *ca.* 3430  $\text{cm}^{-1}$  (Figure III-3, left). Those results pointed out the formation of a supramolecular polymer in CHCl<sub>3</sub> for these bis-ureas even though no viscosity was observed. (*rac*)-EHUCl<sub>2</sub> and (*rac*)-DMHUCl<sub>2</sub> likely formed a “thick structure” in CHCl<sub>3</sub> as shown by the combined FT-IR and SANS data (vide infra). Similarly the same comparison was made for the bis-urea co-monomers with the PBE and PPhe side chains (Figure III-3, right). Interestingly almost no free N-H was observed for (*R,R*)-PBEUX whereas for the other bis-ureas, the amount of free N-H stretch steadily increased in the following order (*R,R*)-PBEUCl<sub>2</sub> < (*R,R*)-PBEUT < (*S,S*)-PPheUT. This confirmed the trend in the self-association of the spacer. It also indicated that a phenyl group destabilised the self-assemblies to a greater extent than an ethyl group since (*R,R*)-PBEUT formed longer assemblies than (*S,S*)-PPheUT. The conclusion of this FT-IR study is that only (*rac*)-EHUCl<sub>2</sub>, (*rac*)-DMHUCl<sub>2</sub> and (*R,R*)-PBEUX formed long assemblies (likely filaments) in CHCl<sub>3</sub>.

FT-IR analyses also allowed us to investigate the self-assembly of the bis-urea ligands in THF, a potential solvent for catalysis.

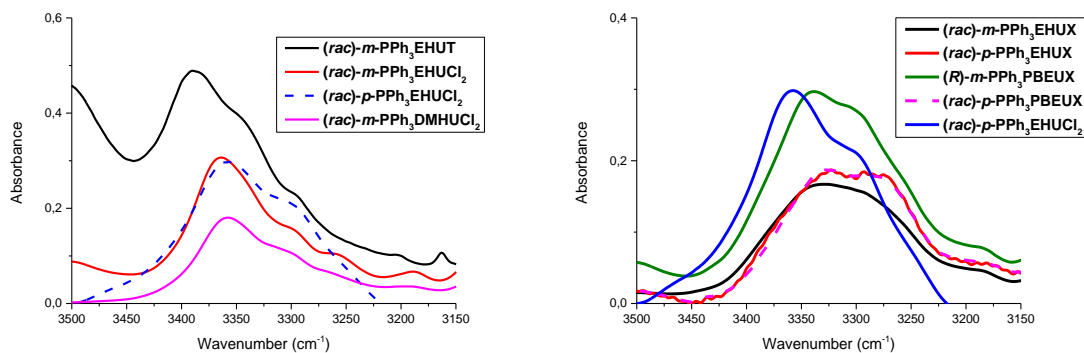


Figure III-4: FT-IR spectra in THF of the bis-urea ligands at 10 mM. Left: tolyl and 1,3-dichlorobenzene spacer. Right: xylyl spacer with *(rac)*-**p-PPh<sub>3</sub>EHUCl<sub>2</sub>** for comparison.

All bis-urea ligands with tolyl or 1,3-dichloro spacer were very poorly associated in THF as indicated by main stretching frequency at  $3375\text{ cm}^{-1}$  which corresponded to a N-H bonded to THF (Figure III-4, left). On the other hand, self-assemblies were formed in THF for all the ligands with a 1,3-xylyl spacer. Indeed no (or few) N-H bonded to THF were observed for these four bis-ureas (Figure III-4, right). Combined FT-IR and SANS data (vide infra) indicate that these bis-urea form long filaments in THF. These results were highly encouraging considering our aim of maintain the supramolecular scaffolds during catalysis in this competing solvent.

### 3. SANS analyses

In order to determine the structure of the self-assemblies SANS analyses were firstly performed in toluene- $d_8$  (0.6% wt *ca.* 10 mM) in order to compare the geometrical features of the assemblies formed by the bis-urea ligands and co-monoers in this solvent. Representative SANS analyses with the corresponding fits are shown in Figure III-5 (for all the SANS analysis, see the experimental part).

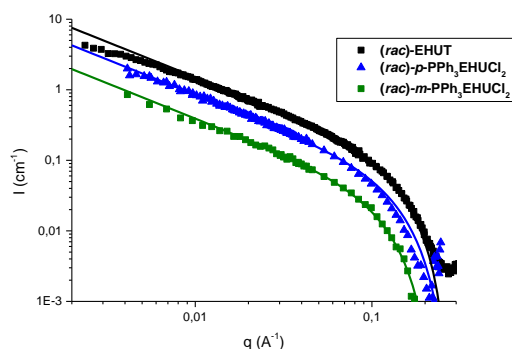


Figure III-5: Representative SANS data for *(rac)*-EHUT, *(rac)*-**p-PPh<sub>3</sub>EHUCl<sub>2</sub>** and *(rac)*-**m-PPh<sub>3</sub>EHUCl<sub>2</sub>** (0.6 wt% in toluene- $d_8$  at  $20^\circ\text{C}$ ). The data are fitted with the form factor for infinitely long rigid rods of circular cross-section. According to these fits, the number of molecules present in the cross-section of the rods is 2.6, 1.8 and 0.8 for *(rac)*-EHUT, *(rac)*-**p-PPh<sub>3</sub>EHUCl<sub>2</sub>** and *(rac)*-**m-PPh<sub>3</sub>EHUCl<sub>2</sub>** respectively.

For all bis-urea ligands, the shape of the scattering intensity was representative of the presence of isolated cylindrical objects in solution ( $q^{-1}$  dependence of the intensity). In all cases, the  $q^{-1}$  dependence was maintained down to the lowest  $q$  values measured, meaning that a significant fraction

of the bis-urea assemblies were longer than 200 Å (*i.e.* more than 40 bis-ureas). The curves were fitted according to the form factor for rigid rods with a circular cross section and a uniform scattering length density. The results of the fits are given in Table III-5.

Table III-5: geometrical radius ( $r$ ), linear density ( $n_L$ ) and number of bisurea molecules ( $n$ ) in the cross-section of the cylindrical objects deduced from the fits of the SANS data at 20°C and in toluene- $d_8$ .

	Sample	$C^{\text{ion}}$ (mM)	$r$ (Å)	$n_L$	$n$	Sample aspect	Structure name
ref	<b>EHUT</b>	16.0	13.9	0.55	2.6	gel	tube
co-monomer	<b>(R,R)-PBEUT</b>	15.9	-	-	-	gel (opaque)	fibre <sup>(a)</sup>
co-monomer	<b>(S,S)-PPheUT</b>	12.4	15.4	0.45	2.1	gel	“thick structure”
ligand	<b>(rac)-m-PPh<sub>3</sub>EHUT</b>	12.0	12.4	0.15	0.7	fluide	filament
ref	<b>EHUCI<sub>2</sub></b>	14.3	13.8	0.52	2.4	viscous	“thick structure” or tube
ligand	<b>(rac)-m-PPh<sub>3</sub>EHUCI<sub>2</sub>*</b>	10.9	16.9	0.17	0.8	viscous	filament
ligand	<b>(rac)-p-PPh<sub>3</sub>EHUCI<sub>2</sub>*</b>	10.9	17.1	0.39	1.8	viscous	“thick structure”
co-monomer	<b>DMHUCI<sub>2</sub></b>	14.3	14.5	0.44	2.1	viscous (opaque)	“thick structure”
ligand	<b>(rac)-m-PPh<sub>3</sub>DMHUCI<sub>2</sub></b>	10.8	14.1	0.37	1.8	fluid	“thick structure”
co-monomer	<b>(R,R)-PBEUCI<sub>2</sub></b>	13.2	12.3	0.45	2.1	fluid	“thick structure”
ref	<b>EHUX</b>	16.4	12.1	0.68	3.2	gel	tube
ligand	<b>(rac)-m-PPh<sub>3</sub>EHUX</b>	11.6	15.9	0.35	1.7	gel	“thick structure”
ligand	<b>(rac)-p-PPh<sub>3</sub>EHUX*</b>	12.4	14.2	0.24	1.1	gel <sup>*(b)</sup>	filament or “thick structure”
co-monomer	<b>(R,R)-PBEUX</b>	14.3	13.4	0.41	1.9	gel	“thick structure”
ligand	<b>(R)-m-PPh<sub>3</sub>PBEUX</b>	10.9	15.2	0.36	1.7	gel	“thick structure”
ligand	<b>(rac)-p-PPh<sub>3</sub>PBEUX*</b>	12.7	15.8	0.23	1.4	gel <sup>*(b)</sup>	filament or “thick structure”

$n$  = the number of bis-urea molecules in the cross-section, assuming a repeat distance of 4.6 Å. The length of the cylindrical objects is superior to 200 Å in all cases. \* these bis-ureas contain an impurity (a) The sample precipitated prior to SANS analysis (b) The results of the fits are not in agreement with the “thick structure” expected for the bis-ureas given their macroscopic aspect and the FT-IR data that might arise from gel syneresis.

From these results some general observations can be made, firstly all the bis-ureas (co-monomers or ligands) were self-assembled into long objects in toluene at about 10 mM. This was in clear agreement with the previous observation (gelation tests and FT-IR analyses). Secondly only four bis-ureas out of the thirteen (**(rac)-m-PPh<sub>3</sub>EHUT**, **(rac)-m-PPh<sub>3</sub>EHUCI<sub>2</sub>**, **(rac)-p-PPh<sub>3</sub>EHUX** and **(rac)-p-PPh<sub>3</sub>PBEUX**) self-assembled into “filament” that contained a single molecule in the cross-section. For **(rac)-m-PPh<sub>3</sub>EHUT** this observation was coherent with the non gelation observed and might result from the hydrogen-bond competitor ability of the phosphine compared to **(rac)-EHUT**. For **(rac)-m-PPh<sub>3</sub>EHUCI<sub>2</sub>** it also pointed out an influence of the phosphine on the self-assembly properties. However the presence of an impurity in the batch of **(rac)-m-PPh<sub>3</sub>EHUCI<sub>2</sub>** can also alter the result of the FT-IR. Indeed for this bis-urea the results of the fit were not in agreement with the macroscopic aspect of the sample. All other bis-ureas formed assemblies with about two molecules in the cross-section. However, the number of molecules in the cross-section actually had to be taken with some precaution as it was proportionally affected by any experimental error on the concentration of the samples. In the case of **(R,R)-PBEUT**, the formation of fibre in the SANS solution could be explained by a low solubility of the bis-urea.

The thermal stability of the supramolecular polymers formed by three of the bis-urea ligands was also probed by SANS (Table III-6 and figures in experimental part). For two ligands (**(rac)-p-**

**PPh<sub>3</sub>EHUCl<sub>2</sub>** and **(R)-m-PPh<sub>3</sub>PBEUX**) the “thick structure” present at 20°C, transformed into the filament upon heating to 70°C and 97°C, respectively. On the other hand, for **(rac)-m-PPh<sub>3</sub>EHUCl<sub>2</sub>**, the filament structure observed at 20°C disassembled into monomers upon heating to 70°C as indicated by the low value of the scattering intensity.

Table III-6: number of bis-urea molecules (*n*) in the cross-section of the cylindrical objects deduced from the fit of the SANS data (see figure in experimental section)

Sample	n at 20°C	structure	n at 70°C	structure
<b>(rac)-m-PPh<sub>3</sub>EHUCl<sub>2</sub></b>	0.8	filament	0.4	monomer
<b>(rac)-p-PPh<sub>3</sub>EHUCl<sub>2</sub></b>	1.8	“thick structure”	1.3	filament
<b>(R)-m-PPh<sub>3</sub>PBEUX</b>	1.7	“thick structure”	0.9*	filament*

\* sample heated to 97°C

Concerning the chiral ligand **(R)-m-PPh<sub>3</sub>PBEUX**, determining the structure in other solvents than toluene was important since it was previously shown that in the case of **(R,R)-EHUT** (Chapitre II.C.2.b), the filament form did not possess supramolecular chirality.<sup>[5]</sup> Combined SANS and the FT-IR spectra analyses provide insight into the structure adopted by **(R)-m-PPh<sub>3</sub>PBEUX** in different solvent.

Fitting of the SANS data (Table III-7) showed that **(R)-m-PPh<sub>3</sub>PBEUX** was associated in a “thick structure” in three out of the four typical catalysis solvents (toluene, CHCl<sub>3</sub> and DCM). Formation of a thick structure in these solvents is important since these structure are expected to be chiral at the supramolecular level. On the other hand, only the filament structure was observed in THF indicating shorter self-assembly in this competing solvent and thus possible absence of supramolecular chiral objects in this solvent.

Table III-7: Investigation of the structure of **(R)-m-PPh<sub>3</sub>PBEUX** in different solvents by SANS at 20°C

solvent	Cion (mM)	r	<i>n<sub>L</sub></i>	n	Structure
toluene-d <sub>8</sub>	10.9	15.2	0.36	1.7	“thick structure”
CDCl <sub>3</sub>	5.3	17	0.46	2	“thick structure”
DCM-d <sub>2</sub>	8.9	13.2	0.39	1.8	“thick structure”
THF-d <sub>8</sub>	11.1	12.4	0.15	0.7	filament

Geometrical radius (*r*), linear density (*n<sub>L</sub>*) and number of bis-urea molecules (*n*) in the cross-section of the cylindrical objects deduced from the fit of the SANS data.

Combination of SANS and FT-IR data was thus used to estimate the structure of the supramolecular polymers in various solvents. The shape and relative intensity of the NH bands are related to the conformation and environment of the urea functions within the hydrogen bond network.<sup>[6]</sup> Thus bis-urea ligands that display spectra with virtually similar N-H bands in two different solvents can be considered to possess closely related structures. In the Figure III-6 is represented two FT-IR spectra of **(R)-m-PPh<sub>3</sub>PBEUX** and **(rac)-m-PPh<sub>3</sub>EHUCl<sub>2</sub>** in toluene and DCM. For **(R)-m-PPh<sub>3</sub>PBEUX** both spectra were virtually identical and SANS data (Table III-7) confirmed for both solvent the self-assembly in “thick structure”. On the other hand, the SANS of **(rac)-m-PPh<sub>3</sub>EHUCl<sub>2</sub>** data in toluene revealed the formation of filament structure and as the FT-IR spectra were virtually identical in toluene and DCM, the same structure (*i.e.* filament) can be hypothesised in DCM.

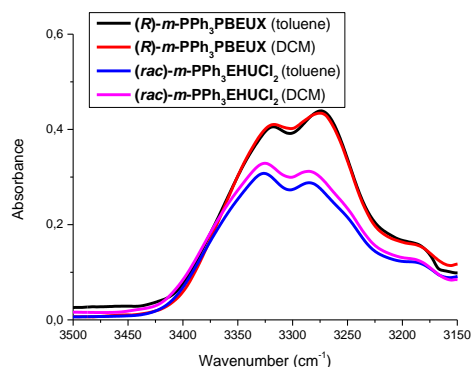


Figure III-6: FT-IR spectra of **(R)-m-PPh<sub>3</sub>PBEUX** and **(rac)-m-PPh<sub>3</sub>EHUCl<sub>2</sub>** in toluene and DCM at 10 mM

Thus analysis of the shape of FT-IR spectra of the bis-urea ligands and comparison with the FT-IR spectra in toluene for which the structure have been determined by SANS gave the following results (Table III-8).

Table III-8: determination of the structure of the bis-urea ligands in various solvents by combined SANS and FT-IR<sup>(a)</sup> analyses at 20°C

Bis-urea	C <sup>ion</sup> (mM)	SANS	Toluene	CHCl <sub>3</sub>	DCM	DCE	THF
<b>(S,S)-PPheUT</b>	12.4		<b>T<sup>(b)</sup></b>	F/M	NS	nd	M
<b>(rac)-m-PPh<sub>3</sub>EHUT</b>	12.0		<b>F<sup>(b)</sup></b>	F	F	NS	M
<b>(rac)-m-PPh<sub>3</sub>EHUCl<sub>2</sub>*</b>	10.9		<b>F<sup>(b)</sup></b>	F	F	NS	M
<b>(rac)-p-PPh<sub>3</sub>EHUCl<sub>2</sub>*</b>	10.9		<b>T<sup>(b)</sup></b>	T	T	<b>nd</b>	M
<b>(rac)-DMHUCl<sub>2</sub></b>	14.3		<b>T<sup>(b)</sup></b>	T	NS	nd	M
<b>(rac)-m-PPh<sub>3</sub>DMHUCl<sub>2</sub></b>	10.8		<b>T<sup>(b)</sup></b>	<b>T<sup>(b)</sup></b>	T	<b>T</b>	M
<b>(R,R)-PBEUCl<sub>2</sub></b>	13.2		<b>T<sup>(b)</sup></b>	<b>T/M</b>	NS	nd	F/M
<b>(rac)-m-PPh<sub>3</sub>EHUX</b>	11.6		<b>T<sup>(b)</sup></b>	T	T	NS	F
<b>(rac)-p-PPh<sub>3</sub>EHUX*<sup>(d)</sup></b>	12.4		<b>F<sup>(b)</sup>/T</b>	F/T	F/T	F/T	F/T
<b>(R,R)-PBEUX</b>	14.3		<b>T<sup>(b)</sup></b>	T	NS	nd	T
<b>(R)-m-PPh<sub>3</sub>PBEUX</b>	10.9		<b>T<sup>(b)</sup></b>	<b>T<sup>(b)</sup></b>	<b>T<sup>(b)</sup></b>	<b>T</b>	<b>F<sup>(b)</sup></b>
<b>(rac)-p-PPh<sub>3</sub>PBEUX*<sup>(d)</sup></b>	12.7		<b>F<sup>(b)</sup>/T</b>	F/T	F/T	F/T	F/T

M = monomer, F = filament, T = “thick structure” with two molecules in the cross-section, /M indicates the presence of a peak of free N-H in the FTIR, NS = not soluble, n.d. not determined, \* the bis-ureas contain an impurity. (a) concentration of FT-IR analyses: 10 mM (b) determined by SANS in the corresponding deuterated solvent. **(R,R)-PBEUT** was not analysed in this table as the SANS data were inexplotable (Table III-5).

For all newly synthesised bis-ureas at the exception of **(S,S)-PPheUT**, the shape of the FT-IR spectra and thus the structure of the self-assembly did not change in the three following solvents: toluene, CHCl<sub>3</sub> and DCM and for those soluble in DCE the same observation could also be made in this solvent. At the contrary shorter self-assemblies were observed for most bis-urea ligands in THF: filaments or monomers at the exception of **(R,R)-PBEUX**, **(rac)-p-PPh<sub>3</sub>EHUX** and **(rac)-p-PPh<sub>3</sub>PBEUX** that maintained their tube and filament form respectively. The results in Table III-8 also pointed out that the combination of PBE side chain and xylyl spacer were the most promising for chirality induction because enantiopure **PBE-NH<sub>2</sub>** was easily obtained but also the resulting bis-ureas formed the “thick structure” in three out of the four targeted solvents for catalysis.

#### 4. CD analyses

As the supramolecular structures observed for the newly synthesised bis-ureas were mostly “thick structures”, supramolecular chirality was expected for **(R,R)-PBEUT**, **(R,R)-PBEUCl<sub>2</sub>**, **(S,S)-PPheUT** and **(R)-m-PPh<sub>3</sub>PBEUX** (**(R,R)-PBEUX** was not investigated). CD analyses were recorded at 1 mM in order to limit signal saturation. Clear Cotton effects were observed for **(R,R)-PBEUT** and **(R,R)-PBEUCl<sub>2</sub>** that revealed the formation of chiral assemblies in cyclohexane solution (Figure III-7). On the other hand, **(S,S)-PPheUT** exhibited a weak CD signal pointing toward either the formation of non-chiral objects, weak association at this concentration or racemisation during the synthesis (as the enantiopurity of **(S,S)-PPheUT** has not been determined).

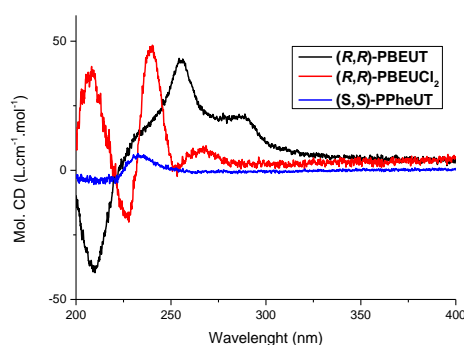


Figure III-7: CD spectra of the chiral bis-urea co-monomers (1 mM, cyclohexane).

The chiral nature of the assemblies formed by **(R)-m-PPh<sub>3</sub>PBEUX** was also probed by CD spectroscopy in several solvents. At this concentration, FT-IR analyses (Figure III-8, right) indicated that **(R)-m-PPh<sub>3</sub>PBEUX** was assembled in DCM and CHCl<sub>3</sub> but that the assemblies were short in both cases (presence of free N-H bonds). In THF, assemblies of **(R)-m-PPh<sub>3</sub>PBEUX** were significantly shorter than in these two solvents (free C=O bands are dominant). No CD signals were observed for **(R)-m-PPh<sub>3</sub>PBEUX** in these three solvents at room temperature. This is in agreement with the presence of short assemblies and/or of a filament structure since it has been shown that the filament structure formed by bis-ureas may not adopt a helical configuration.<sup>[5]</sup> Interestingly, a CD signal (maximum at  $\lambda \approx 250$  nm,  $\Delta\epsilon = 19$  L.mol<sup>-1</sup>.cm<sup>-1</sup>) was observed for solutions of **(R)-m-PPh<sub>3</sub>PBEUX** in chloroform and DCM at -10°C but still not in THF (Figure III-8, left). Cooling the DCM and CHCl<sub>3</sub> solutions likely allowed the transition between the CD inactive filament form and the CD active “thick structure”. It implied that chirality was expressed at the supramolecular level only for this latter structure. A shift of the maximum of CD spectra was observed for **(R)-m-PPh<sub>3</sub>PBEUX** when compared to the structurally related **(R,R)-EAUX** bis-urea (structure in the loose sheet). This might be due to the presence of an additional chromophore (the triarylphosphine) in the former bis-urea.

Intriguingly, the CD spectra of **(R)-m-PPh<sub>3</sub>PBEUX** in DCM and CHCl<sub>3</sub> at -10°C were mirror images. Two hypotheses can be made: i) the helicity of the supramolecular structure formed by **(R)-m-PPh<sub>3</sub>PBEUX** is inversed in DCM and CHCl<sub>3</sub> or ii) the chiral conformation of the

chromophores that absorb in the 250 nm region is inverted but the overall helicity of the supramolecular structure formed by **(R)-m-PPh<sub>3</sub>PBEUX** is the same in both solvents. One possible way to infirm one of these hypotheses is to make sergeants-and-soldiers experiments in both solvents and to observe whether the same helicity (or not) is induced to the resulting supramolecular structure. The other way is to check the influence of the solvent on the nature of the major enantiomer provided by **(R)-m-PPh<sub>3</sub>PBEUX** in catalytic experiments (see Annexes).

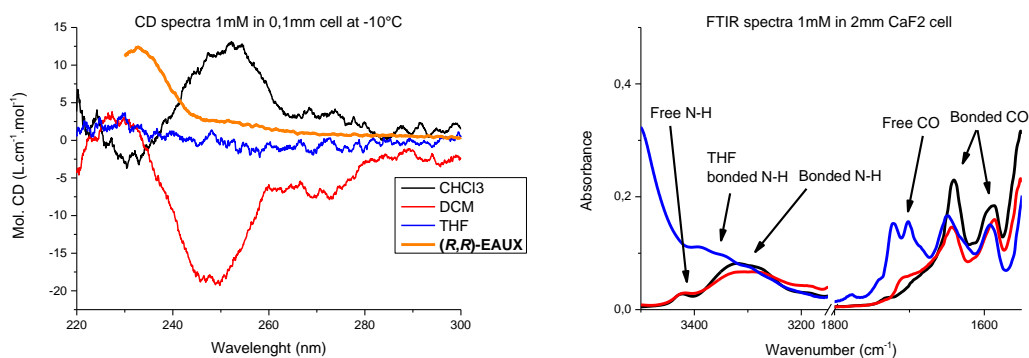


Figure III-8: Left: CD spectra (at  $-10^{\circ}\text{C}$ ) of 1 mM solutions of **(R)-m-PPh<sub>3</sub>PBEUX** in DCM (red),  $\text{CHCl}_3$  (black) and THF (blue) with the spectrum of the reference **(R,R)-EAUX** in DCM (orange).<sup>[7]</sup> Right: FT-IR spectra at room temperature of the corresponding solutions of **(R)-m-PPh<sub>3</sub>PBEUX**.

## D. Concluding remarks

6 bis-urea co-monomers and 11 bis-urea ligands were synthesised using different spacers or lateral chains. Most of them were obtained pure as confirmed by different analytical techniques but 4 of them, **(rac)-m-PPh<sub>3</sub>EHUCl<sub>2</sub>**, **(rac)-p-PPh<sub>3</sub>EHUCl<sub>2</sub>**, **(rac)-p-PPh<sub>3</sub>EHUX** and, **(rac)-p-PPh<sub>3</sub>PBEUX** were found to be contaminated with an impurity. Characterisation of their self-assembly properties was achieved using SANS and FT-IR analyses. For the co-monomers, the trend in the stability of the self-assemblies depended on the one previously observed for the bis-ureas of references (tolyl<1,3-dichloro<1,3-xylyl) and the side chains. The ligands, those with a single phosphine unit were able to self-assemble in toluene,  $\text{CHCl}_3$  and DCM at least in filament form. Self-association in more polar solvents such as THF was achieved using the 1,3-xylene spacer. Determination of the self-assembly structure in different solvents was achieved for the bis-urea ligands by combined analysis of SANS and FT-IR data. On uncertainty remained for the type of assembly formed by **(rac)-p-PPh<sub>3</sub>EHUCl<sub>2</sub>**, **(rac)-p-PPh<sub>3</sub>EHUX** and, **(rac)-p-PPh<sub>3</sub>PBEUX** that might arise from the impurity or gel syneresis. Five ligands were found to self-assemble into “thick structure” in the targeted catalysis solvents which was encouraging for the implementation of chirality amplification strategies.

Supramolecular chirality was assessed for the newly synthesised bis-ureas having an ether side chain. Unlike **(S,S)-PPheUT** which exhibited only a weak CD signal in cyclohexane, the two other soluble co-monomers (**(R,R)-PBEUT** and **(R,R)-PBEUCl<sub>2</sub>**) were CD active with Cotton effects at room temperature. The chiral ligand, **(R)-m-PPh<sub>3</sub>PBEUX**, also displayed CD signal in  $\text{CHCl}_3$  and DCM but



at lower temperature. These results were appealing for the use of these bis-urea assemblies in asymmetric catalysis.

## **E. Experimental part:**

*General procedures:* All chemicals were obtained from Acros, Alfa Aesar, Sigma-Aldrich, Strem chemicals or TCI suppliers and used as received.

Unless otherwise noted, chromatography-grade solvents were used as received. Dried solvents were obtained from an SPS solvent purification system (IT-Inc). Triethylamine was dried by storage over 4Å molecular sieves. *N,N*-Diisopropylethylamine was distilled over CaH<sub>2</sub> and stored under argon atmosphere in a Schlenk flask. All inert atmosphere reactions were carried out under an argon or nitrogen atmosphere with standard Schlenk-line techniques.

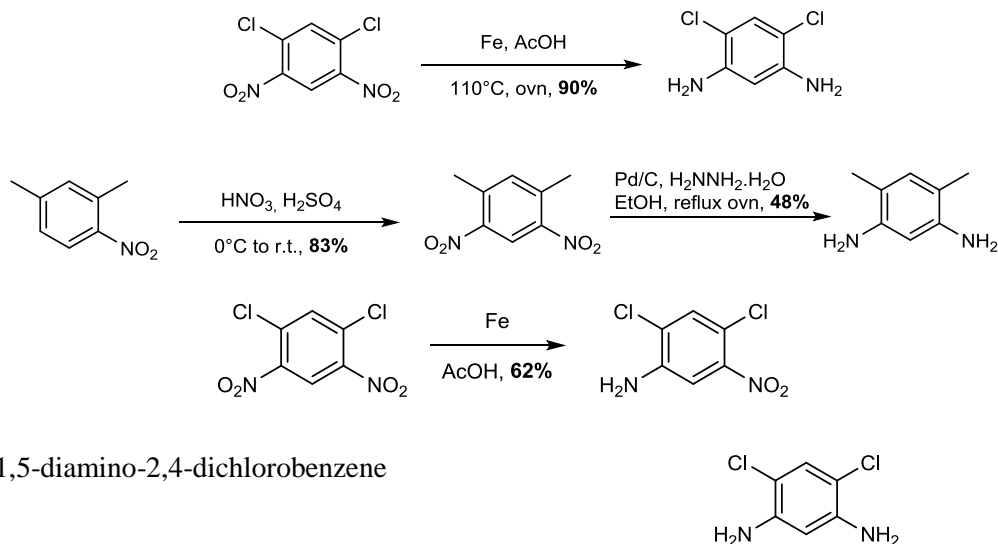
NMR spectra were recorded on a Bruker Advance 400, 300 or 200 spectrometer and calibrated to the residual solvent peak.<sup>[8]</sup> Peaks are reported with their corresponding multiplicity (s: singlet (br for broad); d: doublet, t: triplet; q: quartet; quint: quintuplet; hept: heptuplet; dd: doublet of doublets, dt: doublet of triplets; td: triplet of doublets) and integration, and respective J coupling constants are given in Hertz. Exact mass measurements (HRMS) were obtained on TQ R30-10 HRMS spectrometer by ESI+ ionisation and are reported in m/z for the major signal.

FT-IR measurements were performed on a Nicolet iS10 spectrometer in ATR (diamond probe). Solution spectra were measured in KBr or CaF<sub>2</sub> cells of various pathlength (0.5, 1 and 2 mm, according to the concentration) and are corrected for air, solvent and cell absorption.

Circular dichroism (CD) measurements were performed on a Jasco J-1500 spectrometer equipped with a Peltier thermostated cell holder and Xe laser, in 0.1 mm quartz cells. Data was recorded at 50 nm.min<sup>-1</sup> sweep rate, 2 nm bandwidth and 0.05 nm data pitch; spectra were corrected for solvent and cell contribution. Molar ellipticities and reported in L.mol<sup>-1</sup>.cm<sup>-1</sup> and are expressed as follows:  $\Delta\epsilon = \theta / (32980 \times l \times c)$  where  $\theta$  is the measured ellipticity (mdeg),  $l$  is the optical path length in cm and  $c$  is the concentration in mol.L<sup>-1</sup>. For all samples, linear dichroism (LD) contribution was negligible ( $\Delta LD < 0.005$  dOD). Small-angle neutron scattering measurements were made at the LLB (Saclay, France) on the Pace instrument or at ILL (Grenoble, France) on the D11 instrument, at two distance-wavelength combinations to cover the  $4 \times 10^{-3}$  to  $0.24 \text{ \AA}^{-1}$  q-range, where the scattering vector q is defined as usual, assuming elastic scattering ( $q = (4\pi/\lambda)\sin(\theta/2)$ , where  $\theta$  is the angle between incident and scattered beam). Data were corrected for the empty cell signal and the solute and solvent incoherent background. A light water standard was used to normalise the scattered intensities to cm<sup>-1</sup> units.

(*rac*)-PBEUT, (*rac*)-PBEUCl<sub>2</sub>, (*rac*)-PBEUX, (*rac*)-*m*-PPh<sub>3</sub>PBEUX were prepared in the purpose of determining the optical purity of (*R,R*)-PBEUT, (*R,R*)-PBEUCl<sub>2</sub>, (*R,R*)-PBEUX, and (*R*)-*m*-PPh<sub>3</sub>PBEUX respectively.

Synthesis of precursors:

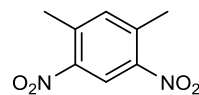


Adapted from literature.<sup>[2]</sup>

To a solution of 2,4-dichloro-1,5-dinitrobenzene (10 g, 42.2 mmol) in acetic acid (90 mL) and ethanol (55 mL) was added iron powder (37.7 g, 675.1 mmol). The resulting mixture was refluxed overnight, then filtrated on Celite and eluted with ethyl acetate. The organic phase was washed three times with NaOH (2 M), dried over MgSO<sub>4</sub> and evaporated under vacuum. The crude product was then sublimated (155°C, 10<sup>-2</sup> mbar) to get 1,5-diamino-2,4-dichlorobenzene as a white powder (6.7 g, 90%).

<sup>1</sup>H NMR (300 MHz, CDCl<sub>3</sub>): δ 7.12 (s, 1H), 6.18 (s, 1H), 3.91 (br s, 4H). The spectroscopic data are in agreement with the literature.<sup>[2]</sup>

1,5-dinitro-2,4-dimethylbenzene

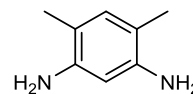


From literature.<sup>[9]</sup>

To a solution of 1-nitro-2,4-dimethylbenzene (20 mL, 148 mmol) in sulphuric acid (50 mL) was added nitric acid solution (70%, 10.3 mol) over 30 min at 0°C. After two hours, the resulting precipitate was washed with water. Then the crude product was recrystallised from methanol to yield 1,5-dinitro-2,4-dimethylbenzene as yellow needles (24.0 g, 83%).

$^1\text{H NMR}$  (200 MHz,  $\text{CDCl}_3$ ):  $\delta$  8.68 (s, 1H), 7.46–7.30 (m, 1H), 2.70–2.67 (m, 6H). The spectroscopic data are in agreement with the literature.<sup>[9]</sup>

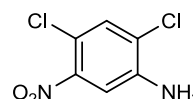
1,5-diamino-2,4-dimethylbenzene



To a solution of 1,5-dinitro-2,4-dimethylbenzene (6.0 g, 30 mmol) and Pd/C (1 g, hydrated 5% weight) in ethanol (200 mL) was added hydrazine monohydrate (44.3 mL, 910 mmol). The resulting solution was refluxed for 18 h, filtered over Celite, eluted with EtOAc. The organic phase was washed with brine (3x250 mL), dried over  $\text{MgSO}_4$  and evaporated under vacuum. The resulting solid was sublimed under  $10^{-3}$  mbar at  $90^\circ\text{C}$  to yield 1,5-diamino-2,4-dimethylbenzene as a white powder (2.0 g, 48%).

$^1\text{H NMR}$  (300 MHz,  $\text{CDCl}_3$ ):  $\delta$  6.73 (s, 1H), 6.13 (s, 1H), 3.35 (br s, 4H), 2.07 (s, 6H). The spectroscopic data are in agreement with the literature.<sup>[10]</sup>

2,4-dichloro-5-nitroaniline

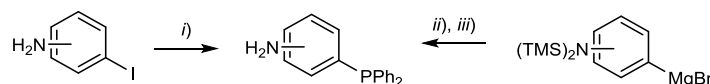


The procedure was adapted from a published procedure.<sup>[11]</sup>

To a solution of 1,5-dinitro-2,4-dichlorobenzene (6.0 g, 25.7 mmol) in acetic acid (200 mL) was added by portion iron powder (3.8 g, 69.4 mmol) over 1h while refluxing. The mixture was refluxed for two additional hours and quenched with saturated aqueous  $\text{K}_2\text{CO}_3$  solution. The resulting precipitate was filtrated and washed with  $\text{H}_2\text{O}$  to yield 2,4-dichloro-5-nitroaniline as a yellow solid (3.3 g, 62%).

$^1\text{H NMR}$  (300 MHz,  $\text{CDCl}_3$ ):  $\delta$  7.43 (s, 1H), 7.30 (s, 1H), 4.36 (s, 2H). The spectroscopic data are in agreement with the literature.<sup>[11]</sup>

*Synthesis of the diphenylphosphinoaniline:*



Synthesis of 3- and 4-diphenylphosphinoaniline: i)  $\text{CuI}$ , dimethylethylenediamine,  $\text{Cs}_2\text{CO}_3$ , diphenylphosphine, toluene, reflux, 2 days, 67% ii) THF,  $\text{PPh}_2\text{Cl}$ , iii) MeOH, reflux, overnight, 90% yield over steps ii) and iii). TMS = trimethylsilane

Buchwald coupling method:<sup>[12]</sup> i)

$\text{CuI}$  (5 mol%), dried and degassed toluene (0.4 M), diphenylphosphine (1.0 eq) and  $\text{N,N}'$ -dimethylethylenediamine (35 mol%) were added to an oven Schlenk flask under argon. The solution was stirred for 10 minutes at room temperature before addition of the iodoaniline (1.0 eq) and  $\text{Cs}_2\text{CO}_3$  (2.0 eq). The Schlenk tube was then closed under argon pressure with a greased glass stopper and

heated for 3 days at 110°C. The solution was then cooled down to room temperature and the solution was diluted with water and extracted with EtOAc (three times). The organic phases were combined and dried over MgSO<sub>4</sub>. The crude product was purified by flash chromatography on silica gel eluting with DCM.

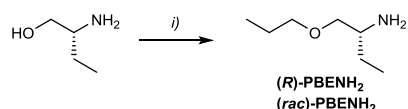
Grignard reagent method:<sup>[13]</sup> ii) and iii)

In a oven-dried Schlenk flask; a solution of Ph<sub>2</sub>PCL (1eq, 1.25 M) in THF was added to a stirred solution of [bis(trimethylsilyl)amino]phenylmagnesium (1 eq, *ca.* 0.5 M) chloride in THF at room temperature. The solution was stirred for 2 hours at room temperature before removal of the volatiles. The residue was then extracted under inert atmosphere in the flask through a canula with Et<sub>2</sub>O (same volume than THF). The volatiles were removed and the crude product was refluxed in MeOH (same volume than THF) overnight. The 4-(diphenylphosphino)aniline was purified by flash chromatography on silica gel whereas the 3-(diphenylphosphino)aniline precipitated from the MeOH solution and was filtered off.

4-(diphenylphosphino)aniline: yellowish oil. <sup>1</sup>H NMR (300 MHz, CDCl<sub>3</sub>): 7.26 (s, 10H), 7.15-7.08 (m, 2H), 6.67-6.60 (m, 2H), 3.78 (s (br), 2H). <sup>31</sup>P{<sup>1</sup>H} NMR (122 MHz, CDCl<sub>3</sub>): δ -7.3. The spectroscopic data are in agreement with the literature.<sup>[14]</sup>

3-(diphenylphosphino)aniline: white solid. <sup>1</sup>H NMR (300 MHz, CDCl<sub>3</sub>): δ 7.33 (d, *J* = 3.1 Hz, 10H), 7.15 (td, *J* = 7.7, 1.6 Hz, 1H), 6.80-6.65 (m, 3H), 4.08 (br s, 2H). <sup>31</sup>P{<sup>1</sup>H} NMR (122 MHz, CDCl<sub>3</sub>): δ -5.2. The spectroscopic data are in agreement with the literature.<sup>[13]</sup>

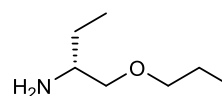
*Synthesis of the chiral amine*



i) NaH, 1-bromopropane, THF reflux, 53%,

(*R*)-1-propoxybutan-2-amine

(*R*)-PBENH<sub>2</sub>



The protocol was adapted from Meyers *et al.*<sup>[15]</sup>

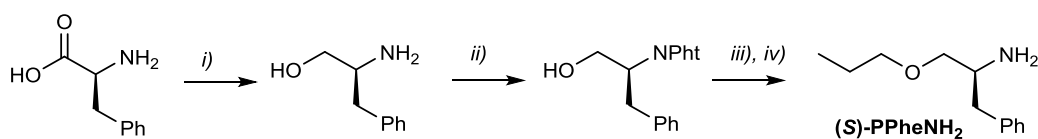
(*R*)-(-)-2-aminobutan-1-ol (4.7 mL, 50 mmol) was added dropwise to a suspension of NaH (2.5 g, 63 mmol, 60% in mineral oil) in dried THF (17.5 mL) and acetonitrile (3.8 mL) in an oven-dried Schlenk tube at room temperature. The resulting suspension was then refluxed until it formed a solid foam into the Schlenk tube. 1-bromopropane (6.8 mL, 75 mmol) was then added to the foam and the reaction was refluxed overnight. After cooling the reaction mixture to room temperature, Et<sub>2</sub>O (50 mL) was added and the organic phase was washed with 50 ml of water. The aqueous layer was extracted two times with 50 mL of Et<sub>2</sub>O and the organic phases were combined. The organic phase

was washed two times with 50 mL of brine, dried over  $K_2CO_3$ , and evaporated under vacuum. The residue was distilled under reduced pressure and the product was trapped with an ice bath yielding (*R*)-1-propoxybutan-2-amine ((*R*)-**PBENH**<sub>2</sub>) as a colourless oil (3.5 g, 53%). (*rac*)-**PBENH**<sub>2</sub> was prepared following the same synthetic protocol (1.7 g, 24%).

<sup>1</sup>H NMR (300 MHz, CDCl<sub>3</sub>): δ 3.47–3.32 (m, 4H), 3.19 (t, *J* = 9.2 Hz, 1H), 2.96–2.84 (m, 1H), 2.01 (s, 2H), 1.53–1.27 (m, 2H), 1.24 (t, *J* = 7.0 Hz, 1H), 0.93 (dt, *J* = 9.1, 7.4 Hz, 6H). <sup>13</sup>C NMR (75 MHz, CDCl<sub>3</sub>): δ 76.21, 73.07, 52.63, 27.26, 23.05, 10.74, 10.64. IR (ATR, cm<sup>-1</sup>): 3360 (br), 2961, 2935, 2876, 1463, 1381, 1114, 1053. HRMS: Calculated for C<sub>7</sub>H<sub>17</sub>NOH [M+H]<sup>+</sup>: 132.1382, found: 132.1382. The optical purity of (*R*)-1-propoxybutan-2-amine has not been measured. However, the amine obtained from this procedure was used in the synthesis of (*R,R*)-**PBEUT**, (*R,R*)-**PBEUCl**<sub>2</sub>, (*R,R*)-**PBEUX** and (*R*)-*m*-**PPh<sub>3</sub>PBEUX**, all obtained with e.e. > 99% indicating that no racemisation occurs during the synthesis.

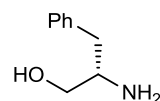
*Indirect route:*

Direct route was attempted without success and the indirect route allows the recuperation of the starting phthalimide during the purification of step *iii*).



Synthesis of (*S*)-**PPhNH**<sub>2</sub>: i) NaBH<sub>4</sub>, I<sub>2</sub>, THF, reflux 18h, 51%, ii) phthalic anhydride, AcOEt, reflux, 2 days, 87%, iii) NaH, NaI, 1-bromopropane, DMF, 50°C, 49%, iv) hydrazine monohydrate, THF, reflux, 4h, quantitative. Overall yield= 22%.

(*S*)-2-amino-3-phenylpropan-1-ol



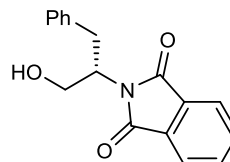
The product was synthesised accordingly to Meyers procedure.<sup>[16]</sup>

In an oven-dried three-necked round-bottom flask equipped with a reflux condenser and an addition funnel was suspended sodium borohydride (6.9 g, 183 mmol) in dried THF (200 mL) under inert atmosphere. (*L*)-Phenylalanine (12.6 g, 76 mmol) was added in one portion to the suspension and the remaining neck was sealed by a greased glass stopcock. The flask was cooled to 0°C and a solution of iodine (19.3 g 76 mmol) in dried THF (50 mL) was slowly added over 30 min resulting in a vigorous evolution of hydrogen gas. At the end of the addition the suspension was heated to reflux overnight and then cooled to room temperature. Methanol was added cautiously until the mixture became homogeneous. After 30 min of stirring, the solvents were removed under vacuum leaving a white paste which was dissolved into 150 mL of 20% aqueous KOH. The solution was stirred for 4 h before extraction with 3x150 mL of DCM. The combined organic phases were dried over Na<sub>2</sub>SO<sub>4</sub> and

evaporated under vacuum. The crude product was recrystallised from toluene to yield (*S*)-2-amino-3-phenylpropan-1-ol as a white solid (5.8 g, 51%).

$^1\text{H NMR}$  (300 MHz,  $\text{CDCl}_3$ ):  $\delta$  7.35–7.27 (m, 2H), 7.26–7.15 (m, 3H), 3.64 (dd,  $J = 10.6, 3.9$  Hz, 1H), 3.39 (dd,  $J = 10.6, 7.2$  Hz, 1H), 3.12 (m, 1H), 2.79 (dd,  $J = 13.5, 5.2$  Hz, 1H), 2.53 (dd,  $J = 13.5, 8.6$  Hz, 1H), 2.01 (s, 3H). The spectroscopic data are in agreement with the literature.<sup>[17]</sup>

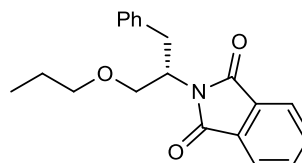
(*S*)-2-(1-hydroxy-3-phenylpropan-2-yl)isoindoline-1,3-dione



(*S*)-2-amino-3-phenylpropan-1-ol (4.5 g, 29.5 mmol) was added to a suspension of phthalic anhydride (4.4 g, 29.5 mmol) in EtOAc (35ml). The reaction mixture was refluxed overnight and then cooled to room temperature. The organic phase was dried two times with water then dried over  $\text{Na}_2\text{SO}_4$  and evaporated under vacuum to yield the product as a white solid (7.3 g, 87%).

$^1\text{H NMR}$  (300 MHz,  $\text{CDCl}_3$ ):  $\delta$  7.83–7.73 (m, 2H), 7.73–7.63 (m, 2H), 7.24–7.11 (m, 5H), 4.64 (tdd,  $J = 8.0, 7.1, 3.6$  Hz, 1H), 4.06 (broad t, 1H), 3.94 (dd,  $J = 11.8, 3.6$  Hz, 1H), 3.21 (d,  $J = 8.0$  Hz, 2H), 2.75 (s, 1H).  $^{13}\text{C}\{^1\text{H}\}$  NMR (75 MHz,  $\text{CDCl}_3$ ):  $\delta$  168.9, 137.4, 134.1, 131.7, 129.1, 128.5, 126.7, 123.3, 62.9, 55.3, 34.8. IR (ATR,  $\text{cm}^{-1}$ ): 2970, 2901, 1695, 1406, 1394, 1368, 1075, 1066, 1045, 1028, 1019. HRMS: Calculated for  $\text{C}_{17}\text{H}_{15}\text{NO}_3\text{Na}$   $[\text{M}+\text{Na}]^+$ : 304.09, found: 304.09.

(*S*)-2-(1-phenyl-3-propoxypropan-2-yl)isoindoline-1,3-dione



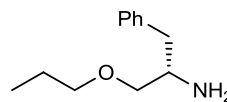
NaH (0.92 g, 23 mmol, 60% in mineral oil) was added to a solution of (*S*)-2-(1-phenyl-3-propoxypropan-2-yl)isoindoline-1,3-dione (5.0 g, 17.7 mmol) in dried DMF (20 mL) under inert atmosphere at  $0^\circ\text{C}$  in an ice bath. The resulting suspension was stirred at  $0^\circ\text{C}$  for 15 min, warmed to room temperature and stirred for 1 h. 1-bromopropane (9.6 mL, 106 mmol) was then added in one portion and the solution was stirred at  $50^\circ\text{C}$  overnight. After cooling to room temperature the reaction mixture was quenched with a saturated aqueous solution of  $\text{NH}_4\text{Cl}$  (20 mL) and the aqueous phase was extracted with DCM (3x50 mL). The combined organic phases were washed with water (2x20 mL), dried over  $\text{MgSO}_4$  and evaporated under vacuum. The crude product was purified using flash column chromatography on silica gel, eluting with petroleum ether/DCM (0 to 100%), yielding (*S*)-2-(1-phenyl-3-propoxypropan-2-yl)isoindoline-1,3-dione as a yellowish oil (2.8 g, 49%).

$^1\text{H NMR}$  (300 MHz,  $\text{CDCl}_3$ ):  $\delta$  7.77 (dt,  $J = 5.5, 2.8$  Hz, 2H), 7.67 (dd,  $J = 5.6, 3.0$  Hz, 2H), 7.25–7.12 (m, 5H), 4.79 (qd,  $J = 9.4, 5.8$  Hz, 1H), 4.05 (t,  $J = 9.6$  Hz, 1H), 3.78–3.66 (m, 1H), 3.46 (dt,  $J =$

9.2, 6.6 Hz, 1H), 3.32 (ddd,  $J = 14.5, 9.6, 7.3$  Hz, 2H), 3.15 (dd,  $J = 14.0, 6.1$  Hz, 1H), 1.50 (q,  $J = 7.1$  Hz, 2H), 0.80 (t,  $J = 7.4$  Hz, 3H).

(*S*)-1-phenyl-3-propoxypropan-2-amine,

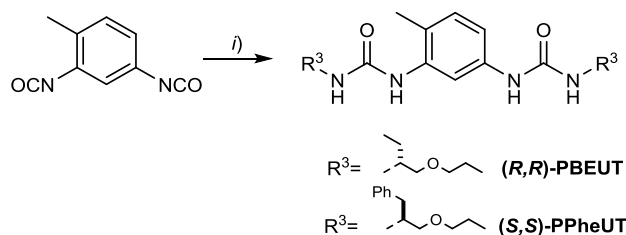
(*S*)-PPheNH<sub>2</sub>



To a solution of (*S*)-2-(1-phenyl-3-propoxypropan-2-yl)isoindoline-1,3-dione (2.8 g, 8.7 mmol) in THF (17 mL) was added hydrazine monohydrate (2 mL, 43 mmol). The resulting solution was refluxed until total consumption of the starting material as monitored by TLC. The resulting precipitate was filtered off and washed cautiously with THF. Evaporation of the filtrate under vacuum yields (*S*)-PPheNH<sub>2</sub> as a yellowish oil (1.8 g, quantitative).

<sup>1</sup>H NMR (200 MHz, CDCl<sub>3</sub>): δ 7.26 (s, 5H), 3.46–3.33 (m, 3H), 3.27 (m, 2H), 2.81 (dd,  $J = 13.4, 5.2$  Hz, 1H), 2.62 (dd,  $J = 13.3, 7.3$  Hz, 1H), 2.19 (br s, 2H), 1.71–1.46 (m, 2H), 0.93 (t,  $J = 7.4$  Hz, 3H). The optical purity of (*S*)-PPheNH<sub>2</sub> has not been measured.

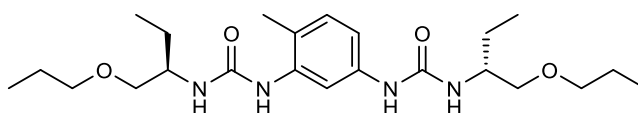
Synthesis of bis-urea co-monomers:



Synthesis of bis-urea co-monomers: i) R<sup>3</sup>NH<sub>2</sub>, 46% and 52% yield for (*R,R*)-PBEUT and (*S,S*)-PPheUT respectively

1,1'-(4-methyl-1,3-phenylene)bis(3-((*R*)-1-propoxybutan-2-yl)urea)

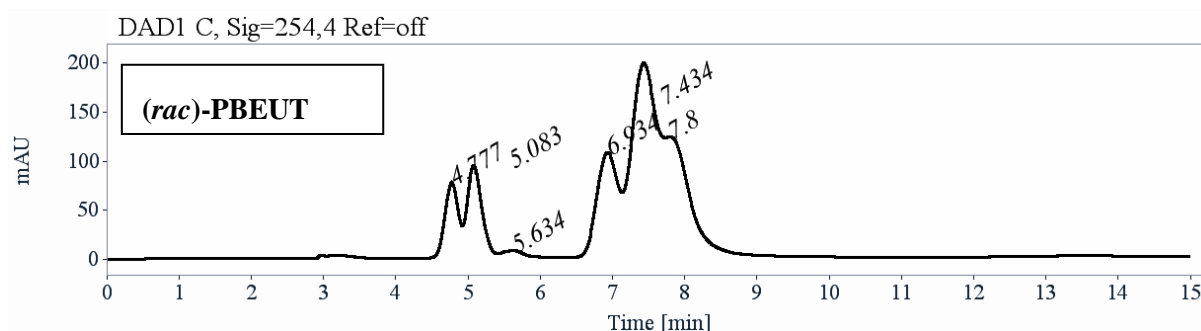
(*R,R*)-PBEUT



In an oven-dried Schlenk tube, (*R*)-PBENH<sub>2</sub> (2.3 mL, 13.9 mmol) was added dropwise to a solution of toluene 2,4-diisocyanate (1.2 mL, 7.3 mmol) in dried DCM (10 mL) at room temperature (the reaction is slightly exothermic). The reaction mixture was stirred overnight and then the solvents were evaporated under vacuum. The crude product was recrystallised from acetonitrile yielding (*R,R*)-PBEUT as a white powder (1.46 g, 46%). (*rac*)-PBEUT was prepared following the same synthetic protocol with (*rac*)-PBENH<sub>2</sub> (1.0 g, 35%).

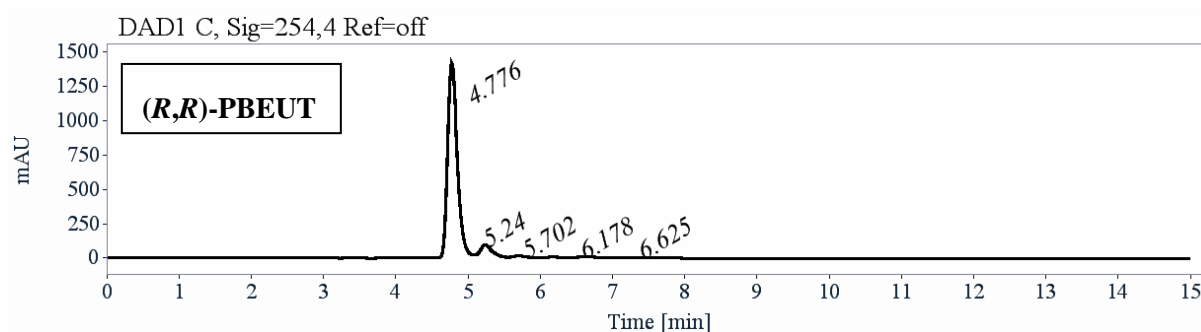
<sup>1</sup>H NMR (300 MHz, DMSO-*d*<sub>6</sub>): δ 8.31 (s, 1H), 7.75 (d,  $J = 2.2$  Hz, 1H), 7.55 (s, 1H), 7.09 (dd,  $J = 8.2, 2.2$  Hz, 1H), 6.92 (d,  $J = 8.5$  Hz, 1H), 6.43 (d,  $J = 8.4$  Hz, 1H), 5.85 (d,  $J = 8.5$  Hz, 1H), 3.73–3.57 (m, 2H), 3.44–3.22 (m, 8H), 2.08 (s, 3H), 1.65–1.25 (m, 8H), 0.93–0.81 (m, 12H). <sup>13</sup>C{<sup>1</sup>H} NMR (75 MHz, DMSO-*d*<sub>6</sub>): δ 155.0, 154.9, 138.5, 138.23, 129.9, 118.9, 111.3, 109.8, 72.0, 50.2, 50.0, 24.7,

22.4, 17.2, 10.5, 10.3. **IR** (ATR,  $\text{cm}^{-1}$ ): 3313, 2962, 2873, 166, 1562, 1505, 1464, 1292, 1274, 1235, 1135. **HRMS**: Calculated for  $\text{C}_{23}\text{H}_{40}\text{N}_4\text{O}_4\text{Na}$   $[\text{M}+\text{Na}]^+$ : 459.2942, found: 459.2939, e.e. >99%, d.e. = 80% (Lux-Cellulose-4, 25°C, Heptane/Ethanol (80/20), 1 mL/min).



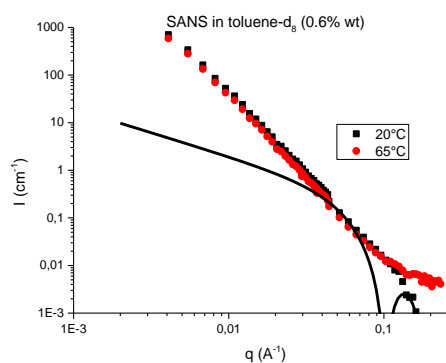
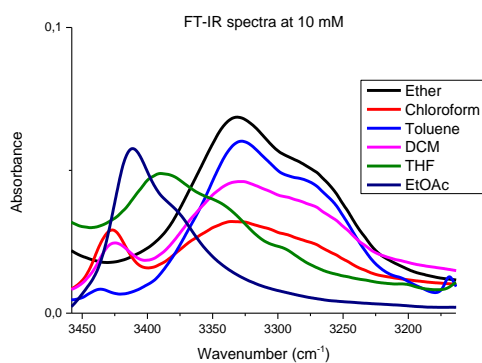
Signal: DAD1 C, Sig=254,4 Ref=off

RT [min]	Area	Area%
4.78	1002	7.91
5.08	1365	10.77
5.63	156	1.23
6.93	2152	16.98
7.43	5131	40.48
7.80	2868	22.63
Sum	12676	100.00



Signal: DAD1 C, Sig=254,4 Ref=off

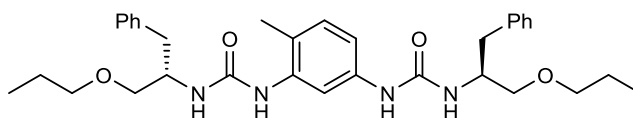
RT [min]	Area	Area%
4.78	13300	90.07
5.24	1046	7.08
5.70	134	0.91
6.18	84	0.57
6.63	202	1.37
Sum	14766	100.00





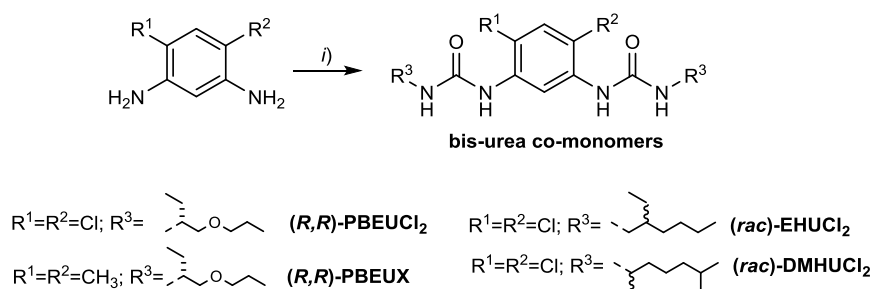
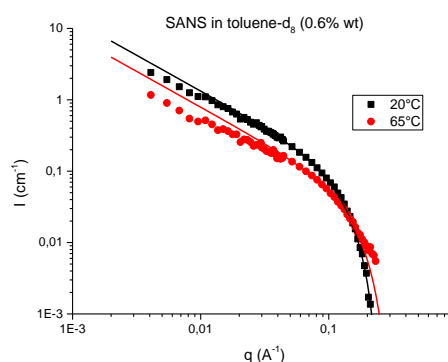
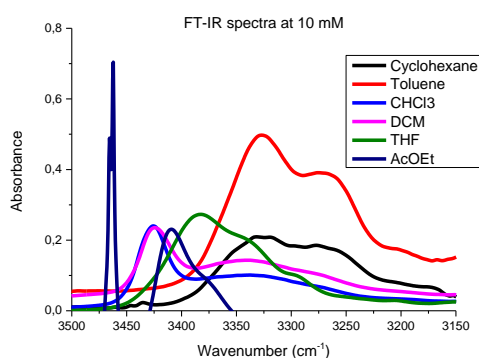
1,1'-(4-methyl-1,3-phenylene)bis(3-((*S*)-1-phenyl-3-propoxypropan-2-yl)urea)

**(*S,S*)-PPheUT**



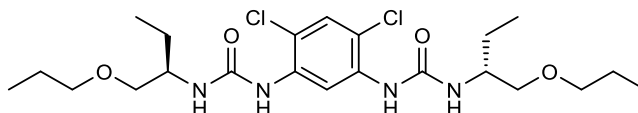
In an oven-dried Schlenk tube, toluene 2,4-diisocyanate (337  $\mu\text{L}$ , 2.3 mmol) was added to a solution of (*S*)-**PPheNH<sub>2</sub>** (1.0 g, 5.1 mmol) in dried DCM (10 mL) under inert atmosphere at room temperature. The reaction mixture was stirred overnight and acetonitrile (50 mL) was added. The resulting precipitate was filtered off and thoroughly washed with acetonitrile yielding (*S,S*)-**PPheUT** as a white powder (680 mg, 52%). The optical purity of (*S,S*)-**PPheUT** has not been measured.

**<sup>1</sup>H NMR** (300 MHz, DMSO-*d*<sub>6</sub>):  $\delta$  8.43 (s, 1H), 7.77 (d,  $J = 2.2$  Hz, 1H), 7.64 (s, 1H), 7.41-7.19 (m, 10H), 7.15 (dd,  $J = 8.2, 2.2$  Hz, 1H), 6.97 (d,  $J = 8.3$  Hz, 1H), 6.63 (d,  $J = 8.3$  Hz, 1H), 6.01 (d,  $J = 8.3$  Hz, 1H), 4.01 (tt,  $J = 8.0, 4.7$  Hz, 2H), 3.50-3.30 (m, 8H), 2.84 (m, 4H), 2.12 (s, 3H), 1.60 (ddt,  $J = 9.8, 6.9, 2.9$  Hz, 4H), 0.96 (td,  $J = 7.4, 1.4$  Hz, 6H). **<sup>13</sup>C{<sup>1</sup>H} NMR** (75 MHz, DMSO-*d*<sub>6</sub>):  $\delta$  155.2, 155.1, 139.3, 139.2, 138.9, 138.6, 130.4, 129.6, 128.7, 126.5, 72.6, 71.7, 51.0, 50.8, 38.1, 22.9, 17.7, 11.1. **IR** (ATR,  $\text{cm}^{-1}$ ): 3674, 3257, 2970, 2901, 1636, 1598, 1553, 1495, 1454, 1408, 1394, 1379, 1231, 1119, 1075, 1066, 1046. **HRMS**: Calculated for C<sub>33</sub>H<sub>44</sub>N<sub>4</sub>O<sub>4</sub>Na [M+Na]<sup>+</sup>: 583.3255, found: 583.3256.



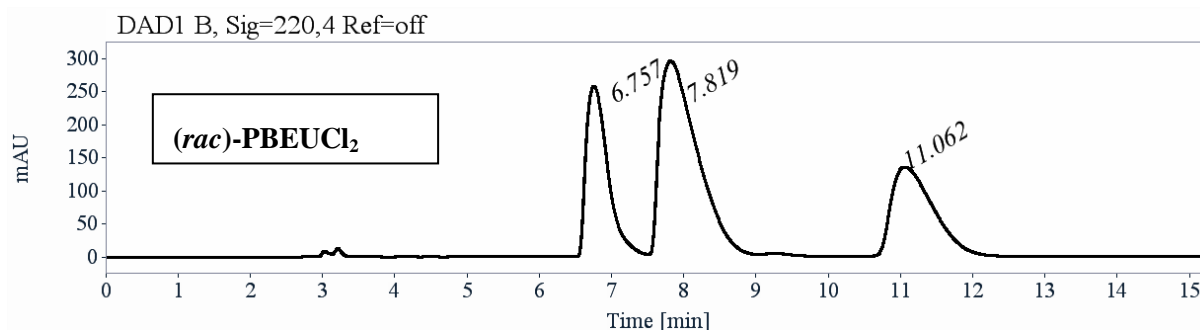
Synthesis of bis-urea co-monomers: i) R<sup>3</sup>NH<sub>2</sub>, triphosgene, DIEA (18%<yield<53%).

1,1'-(4,6-dichloro-1,3-phenylene)bis(3-(*R*)-  
1-propoxybutan-2-yl)urea  
**(*R,R*)-PBEUCl<sub>2</sub>**



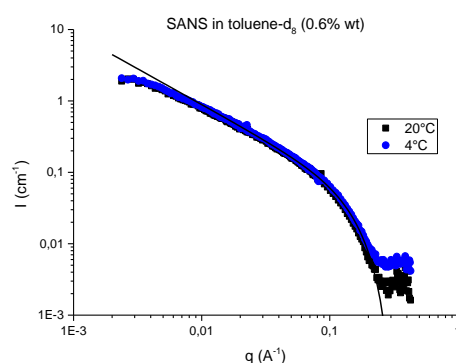
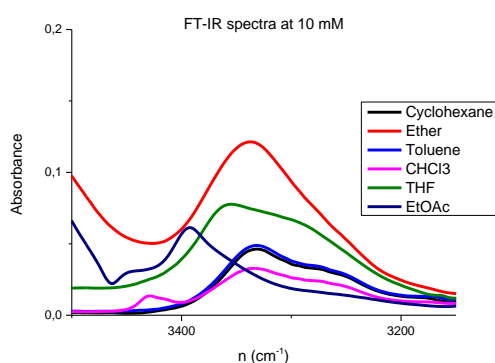
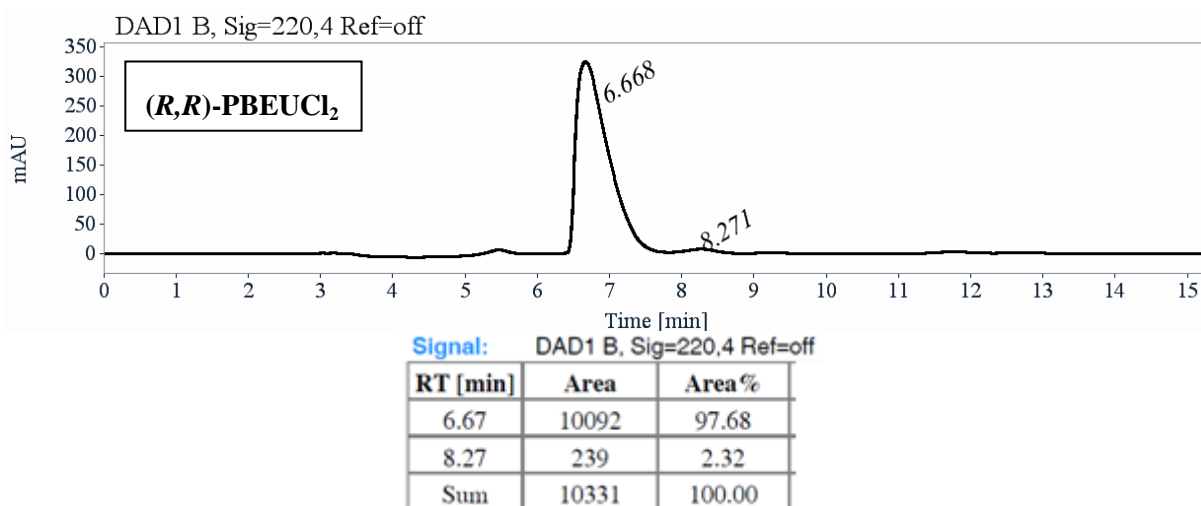
A solution of 1,5-diamino-2,4-dichlorobenzene (586 mg, 3.3 mmol) and DIEA (1.2 mL, 6.6 mmol) in dried DCM (50 mL) was slowly added using a syringe pump (2 mL/h) to an oven-dried Schlenk flask containing a solution of triphosgene (648 mg, 2.2 mmol) in dried DCM (30 mL) at room temperature. At the end of the addition, (*R*)-**PBENH<sub>2</sub>** (0.96 g, 6.1 mmol) and DIEA (1.2 mL, 6.6 mmol) were added to the suspension. The solution was stirred overnight and then the solvents were evaporated under vacuum. The crude product was recrystallised from acetonitrile yielding (*R,R*)-**PBEUCl<sub>2</sub>** as a white powder (0.3 g, 18%). (*rac*)-**PBEUCl<sub>2</sub>** was prepared following the same synthetic protocol with (*rac*)-**PBENH<sub>2</sub>** (622 mg, 49%).

<sup>1</sup>H NMR (200 MHz, DMSO-*d*<sub>6</sub>): δ 8.97 (s, 1H), 7.99 (s, 2H), 7.46 (s, 1H), 6.92 (d, *J* = 8.2 Hz, 2H), 3.65 (m, 2H), 3.47–3.22 (m, 8H), 1.68–1.30 (m, 6H), 1.20 (d, *J* = 11.8 Hz, 2H), 0.87 (td, *J* = 7.4, 2.5 Hz, 12H). <sup>13</sup>C{<sup>1</sup>H} NMR (75 MHz, DMSO-*d*<sub>6</sub>): δ 154.6, 136.3, 128.5, 114.3, 113.2, 72.5, 72.3, 50.8, 25.0, 22.9, 11.0, 10.8. IR (ATR, cm<sup>-1</sup>): 3328, 2965, 1644, 1591, 1554, 1461, 1412, 1391, 1241, 1084, 1052, 682. HRMS: Calculated for C<sub>22</sub>H<sub>36</sub>Cl<sub>2</sub>N<sub>4</sub>O<sub>4</sub>Na [M+Na]<sup>+</sup>: 513.2006, found: 513.2006. e.e. > 99%, d.e. = 95% (Chiralpak AD-H, 25°C, Heptane/isopropanol (90/10), 1 mL/min).



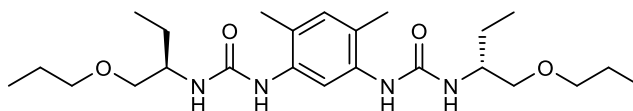
Signal: DAD1 B, Sig=220,4 Ref=off

RT [min]	Area	Area %
6.76	5408	25.21
7.82	10606	49.43
11.06	5443	25.37
Sum	21457	100.00



1,1'-(4,6-dimethyl-1,3-phenylene)bis(3-(*R*)-  
1-propoxybutan-2-yl)urea)

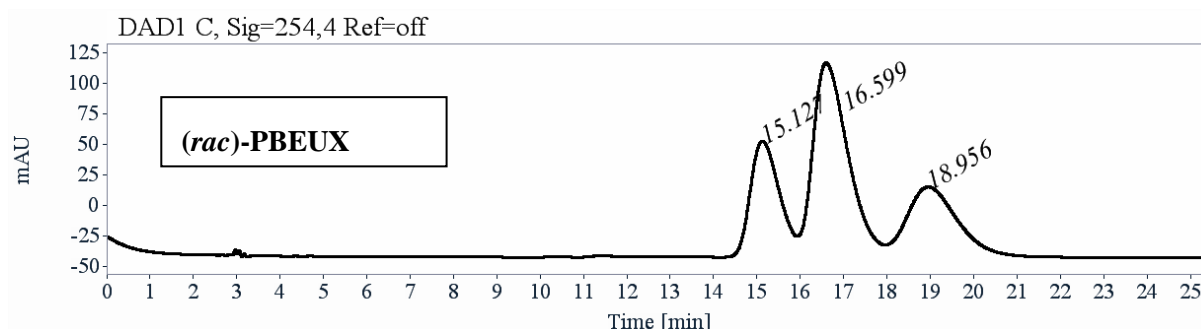
**(R,R)-PBEUX**



A solution of 1,5-diamino-2,4-methylbenzene (0.3 g, 2.2 mmol) and DIEA (750 μL, 4.4 mmol) in dried DCM (33 mL) was slowly added using a syringe pump (2 mL/h) to an oven-dried Schlenk flask containing a solution of triphosgene (430 mg, 1.4 mmol) in dried DCM (20 mL) at room temperature. At the end of the addition, (*R*)-**PBENH<sub>2</sub>** (637 mg, 4.8 mmol) and DIEA (750 μL, 4.4 mmol) were added to the suspension. The solution was stirred overnight and then the solvents were evaporated under vacuum. The crude product was recrystallised from acetonitrile yielding (*R,R*)-**PBEUX** as a white powder (365 mg, 37%). (*rac*)-**PBEUX** was prepared following the same synthetic protocol with (*rac*)-**PBENH<sub>2</sub>** (850 mg, 51%).

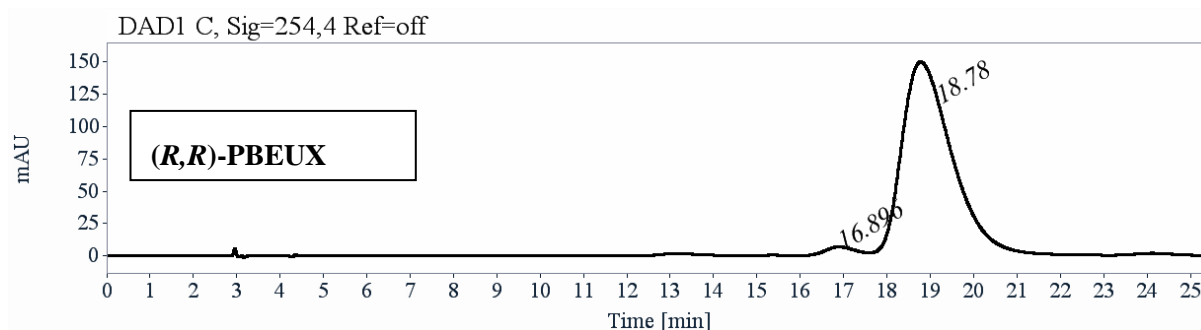
<sup>1</sup>H NMR (300 MHz, DMSO-*d*<sub>6</sub>): δ 8.01 (s, 1H), 7.51 (s, 2H), 6.84 (s, 1H), 6.21 (d, *J* = 8.4 Hz, 2H), 3.63 (m, 2H), 3.43–3.25 (m, 8H), 2.07 (s, 6H), 1.64–1.31 (m, 8H), 0.87 (td, *J* = 7.4, 3.1 Hz, 12H).  
<sup>13</sup>C{<sup>1</sup>H} NMR (75 MHz, DMSO-*d*<sub>6</sub>): δ 155.6, 136.2, 131.6, 122.3, 115.8, 72.6, 72.5, 50.7, 25.2, 22.9, 17.7, 11.0, 10.8. IR (ATR, cm<sup>-1</sup>): 3662, 3328, 2969, 2901, 1644, 1591, 1554, 1461, 1410, 1394, 1241,

1077, 1066, 1050, 1027. **HRMS**: Calculated for  $C_{24}H_{42}N_4O_4Na$   $[M+Na]^+$ : 473.3098, found: 473.3096.  
 e.e. > 99%, d.e. = 95% (Lux-Amylose-2, 25°C, Heptane/isopropanol (90/10), 1 mL/min).



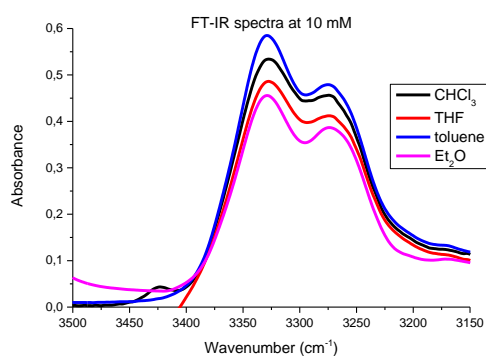
Signal: DAD1 C, Sig=254,4 Ref=off

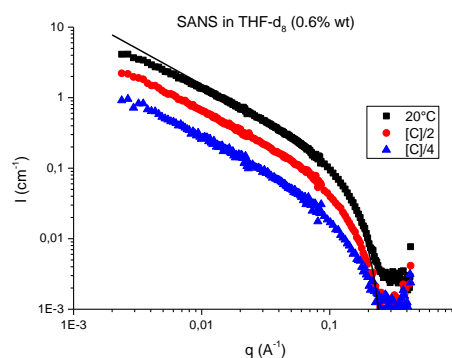
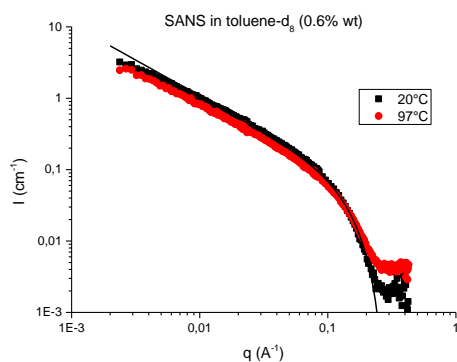
RT [min]	Area	Area %
15.13	4441	24.44
16.60	9036	49.73
18.96	4695	25.84
Sum	18172	100.00



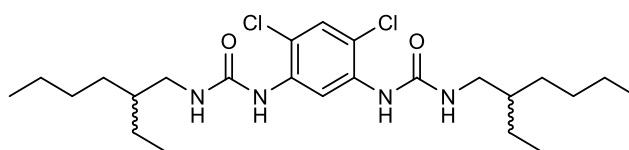
Signal: DAD1 C, Sig=254,4 Ref=off

RT [min]	Area	Area %
16.90	314	2.57
18.78	11914	97.43
Sum	12227	100.00



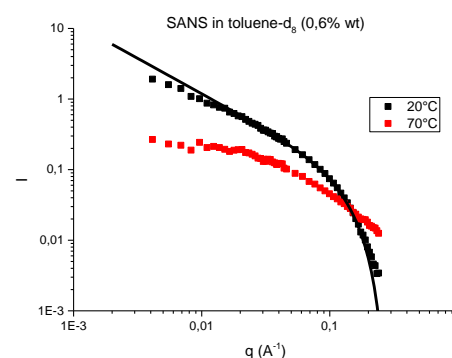
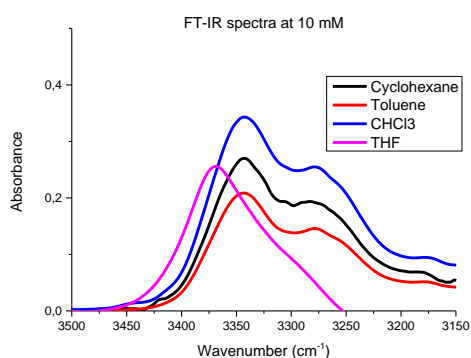


1,1'-(4,6-dichloro-1,3-phenylene)bis(3-(2-ethylhexyl)urea)  
**(rac)-EHUCl<sub>2</sub>**

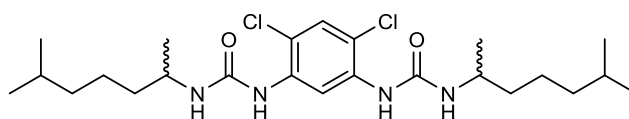


A solution of 1,5-diamino-2,4-dichlorobenzene (587 mg, 3.3 mmol) and DIEA (1.2 mL, 6.6 mmol) in dried DCM (47 mL) was slowly added using a syringe pump (3.5 mL/h) to an oven-dried Schlenk flask containing a solution of triphosgene (649 mg, 2.2 mmol) in dried DCM (37 mL) at room temperature. At the end of the addition, a solution of 2-ethylhexylamine (1.2 mL, 7.1 mmol) and of DIEA (1.2 mL, 6.6 mmol) in dried DCM (15 mL) was added. The solution was stirred overnight before cooling to  $-35^{\circ}\text{C}$  for 5h. The resulting precipitate was filtered off and washed with cold DCM (20 mL) yielding **(rac)-EHUCl<sub>2</sub>** as a white powder (790 mg, 49%).

<sup>1</sup>H NMR (300 MHz, DMSO-*d*<sub>6</sub>):  $\delta$  8.93 (s, 1H), 7.94 (s, 2H), 7.46 (s, 1H), 6.90 (s, 1H), 3.04 (q,  $J = 5.7$  Hz, 4H), 1.27 (m, 18H), 1.03–0.67 (m, 12H). The spectroscopic data are in agreement with the literature.<sup>[2]</sup>

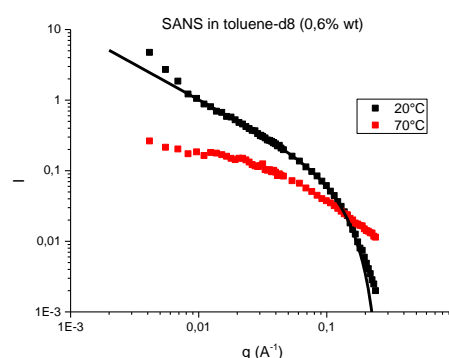
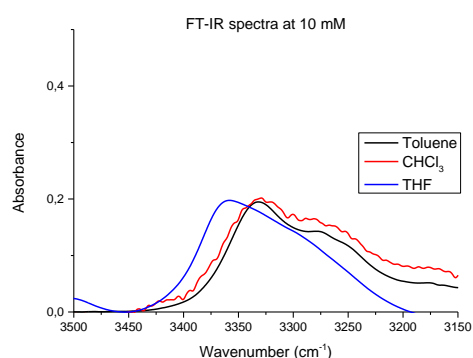


1,1'-(4,6-dichloro-1,3-phenylene)bis(3-(6-methylheptan-2-yl)urea)  
**(rac)-DMHUCl<sub>2</sub>**

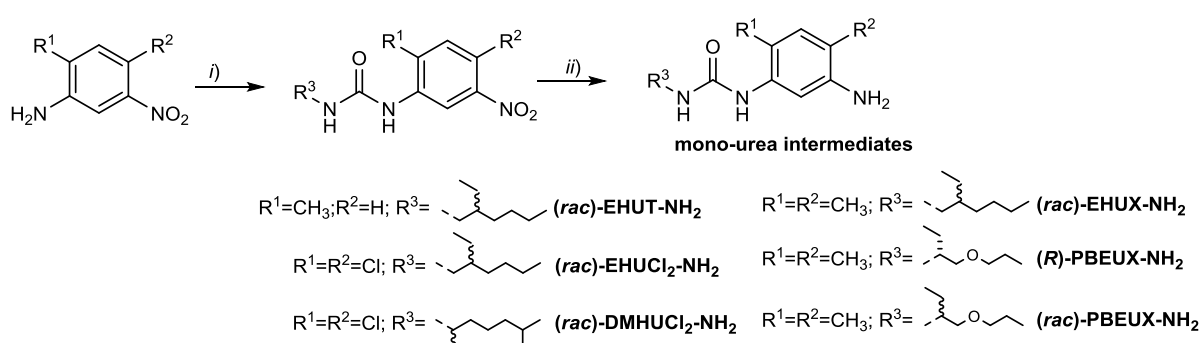


A solution of 1,5-diamino-2,4-dichlorobenzene (470 mg, 2.7 mmol) and DIEA (1.0 mL, 5.7 mmol) in dried DCM (30 mL) was slowly added using a syringe pump (2.5 mL/h) to an oven-dried Schlenk flask containing a solution of triphosgene (520 mg, 1.8 mmol) in dried DCM (21.5 mL) at room temperature. At the end of the addition, the solution was stirred for one hour and 2-Amino-6-methylheptane (960  $\mu$ L, 5.70 mmol) and DIEA (1.0 mL, 5.7 mmol) were added. The reaction mixture was refluxed for 4h and then the solvents were evaporated under vacuum. The crude product was recrystallised from acetonitrile yielding (*rac*)-DMHUCl<sub>2</sub> as a white powder (532 mg, 31%).

<sup>1</sup>H NMR (300 MHz, DMSO-*d*<sub>6</sub>):  $\delta$  8.94 (d, *J* = 1.5 Hz, 1H), 7.82 (s, 2H), 7.44 (s, 1H), 6.82 (d, *J* = 7.8 Hz, 2H), 3.62 (q, *J* = 6.9 Hz, 2H), 1.52 (dt, *J* = 13.2, 6.6 Hz, 2H), 1.43–1.10 (m, 12H), 1.07 (d, *J* = 6.5 Hz, 6H), 0.85 (d, *J* = 6.5 Hz, 12H). <sup>13</sup>C{<sup>1</sup>H} NMR (75 MHz, DMSO-*d*<sub>6</sub>):  $\delta$  154.2, 136.3, 128.4, 114.2, 113.0, 45.3, 38.8, 37.2, 27.8, 23.7, 23.0, 21.6. IR (ATR, cm<sup>-1</sup>): 3327, 2958, 2929, 1642, 1589, 1555, 1460, 1410, 1384, 1239, 1161, 1086. HRMS: Calculated for C<sub>24</sub>H<sub>40</sub>Cl<sub>2</sub>N<sub>4</sub>O<sub>2</sub>Na [M+Na]<sup>+</sup>: 509.2421, found: 509.2421.

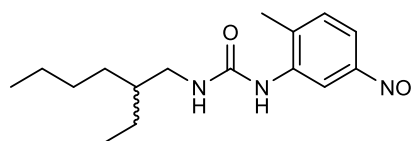


### Synthesis of mono-urea intermediates:



Synthesis of mono-urea intermediates: i) R<sup>3</sup>NCO (45% yield) or R<sup>3</sup>NH<sub>2</sub>, triphosgene, DIEA (57%<yield<95%), ii) Pd/C, hydrazine monohydrate (60%<yield< 80%) or Fe, AcOH (58%<yield<82%). 35%< overall yield <76%

### 1-(2-ethylhexyl)-3-(2-methyl-5-nitrophenyl)urea

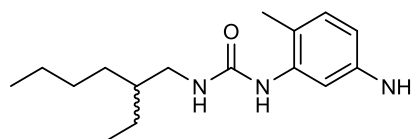


From literature.<sup>[18]</sup>

To an oven-dried flask, 2-methyl-5-nitroaniline (5.4 g, 35.2 mmol) was dissolved in toluene (100 mL) under inert atmosphere. 2-ethylhexylisocyanate (5.0 g, 32 mmol) was added in one portion at room temperature to the solution which was stirred at 70°C until consumption of the isocyanate (monitoring of the absorption band at 2270 cm<sup>-1</sup> by FT-IR). The volatiles were evaporated under vacuum. The crude product was purified using column chromatography on silica gel, eluting with petroleum ether/DCM, to yield 1-(2-ethylhexyl)-3-(2-methyl-5-nitrophenyl)urea as a yellowish solid (4.9 g, 45%).

<sup>1</sup>H NMR (200 MHz, CDCl<sub>3</sub>): δ 8.56 (d, *J* = 2.4 Hz, 1H), 7.87 (dd, *J* = 8.4, 2.4 Hz, 1H), 7.30 (d, *J* = 8.5 Hz, 1H), 5.19 (s, 1H), 3.22 (d, *J* = 5.8 Hz, 2H), 2.33 (s, 3H), 1.31 (d, *J* = 11.6 Hz, 9H), 0.97-0.83 (m, 6H). The spectroscopic data are in agreement with the literature.<sup>[18]</sup>

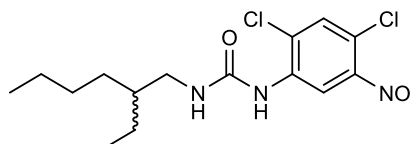
1-(5-amino-2-methylphenyl)-3-(2-ethylhexyl)urea  
*(rac)*-EHUT-NH<sub>2</sub>



1-(2-ethylhexyl)-3-(2-methyl-5-nitrophenyl)urea (3.5 g, 11.4 mmol) and Pd/C (100 mg, hydrated 5% weight) were suspended in EtOH (50 mL). Hydrazine monohydrate (9.8 mL, 201 mmol) was added in one portion and the suspension was refluxed overnight. The reaction was cooled to room temperature and the suspension was filtrated over a Celite® pad eluting with EtOAc until no product was present in the washings (checked by TLC). The resulting organic phase was washed two times with water, with brine, dried over MgSO<sub>4</sub> and the solvents were evaporated under vacuum. The crude product was dissolved in a small amount of DCM and precipitated by adding pentane. The solid was filtered off and thoroughly washed with pentane yielding *(rac)*-EHUT-NH<sub>2</sub> as a white solid (2.4 g, 78%). *(rac)*-EHUT-NH<sub>2</sub> was stored in a dessicator under vacuum in order to avoid degradation.

<sup>1</sup>H NMR (300 MHz, DMSO-*d*<sub>6</sub>): δ 7.33 (s, 1H), 7.19 (d, *J* = 2.3 Hz, 1H), 6.74 (d, *J* = 8.0 Hz, 1H), 6.41 (t, *J* = 5.8 Hz, 1H), 6.12 (dd, *J* = 8.0, 2.4 Hz, 1H), 4.77 (s, 2H), 3.05 (m, 2H), 2.03 (s, 3H), 1.39-1.19 (m, 9H), 0.89 (m, 6H). <sup>13</sup>C{<sup>1</sup>H} NMR (75 MHz, DMSO-*d*<sub>6</sub>): δ 155.9, 147.1, 139.0, 130.5, 108.5, 107.2, 42.0, 39.9, 31.0, 29.0, 24.2, 23.0, 17.6, 14.5, 11.3. IR (ATR, cm<sup>-1</sup>): 3311, 2988, 2969, 2900, 1635, 1567, 1407, 1394, 1380, 1249, 1076, 1066, 1045. HRMS: Calculated for C<sub>16</sub>H<sub>27</sub>N<sub>3</sub>ONa [M+Na]<sup>+</sup>: 278.2227, found: 278.2227.

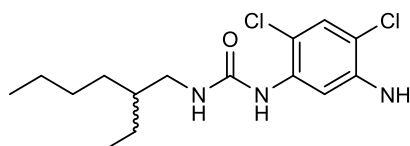
1-(2,4-dichloro-5-nitrophenyl)-3-(2-ethylhexyl)urea



In an oven-dried Schlenk flask at room temperature was added with a syringe pump (10 mL/h) a solution of 2,4-dichloro-5-nitroaniline (1.96 g, 9.47 mmol) and DIEA (1.8 mL, 10.42 mmol) in dried DCM (33 mL) to a solution of triphosgene (1.04 g, 3.50 mmol) in dried DCM (19 mL). The solution was stirred 5 additional minutes and 2-ethylhexylamine (1.6 mL, 9.47 mmol) and DIEA (1.8 mL, 10.42 mmol) was added to the solution. The reaction mixture was stirred overnight. The volatiles were evaporated under vacuum and the crude product was taken up in AcOEt and washed successively with an aqueous solution of  $\text{KHSO}_4$  (10%), an aqueous solution of  $\text{NaHCO}_3$  (5%) and brine. The organic phase was dried over  $\text{MgSO}_4$  and evaporated under vacuum to yield the crude product. The crude product was purified by flash column chromatography on silica gel using petroleum ether/DCM (1/1) as eluent yielding 1-(2,4-dichloro-5-nitrophenyl)-3-(2-ethylhexyl)urea as an orange solid (2.8g, 81%).

$^1\text{H NMR}$  (300 MHz,  $\text{CDCl}_3$ )  $\delta$  8.95 (d,  $J = 0.6$  Hz, 1H), 7.51 (d,  $J = 0.5$  Hz, 1H), 6.85 (s, 1H), 4.85 (s, 1H), 3.23 (td,  $J = 5.8, 2.4$  Hz, 1H), 1.50 (t,  $J = 5.9$  Hz, 1H), 1.43-1.21 (m, 9H), 0.99-0.83 (m, 6H).

1-(5-amino-2,4-dichlorophenyl)-3-(2-ethylhexyl)urea  
(*rac*)-EHUCl<sub>2</sub>-NH<sub>2</sub>

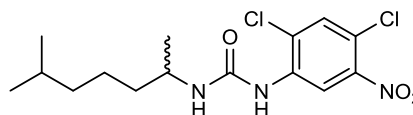


Iron (1.8 g, 32.2 mmol) was added to a solution of 1-(2,4-dichloro-5-nitrophenyl)-3-(2-ethylhexyl)urea (1.9 g, 5.4 mmol) in acetic acid (100 mL). The resulting suspension was refluxed overnight and cooled to room temperature. Brine was added and the aqueous phase was extracted three times with DCM. The combined organic phases were washed two times with  $\text{NaHCO}_{3(\text{sat})}$ , dried over  $\text{Na}_2\text{SO}_4$  and evaporated under vacuum. The resulting solid was dissolved in a minimum amount of DCM and precipitated by adding pentane. The solid was filtered off and thoroughly washed with pentane yielding (*rac*)-EHUCl<sub>2</sub>-NH<sub>2</sub> as a white solid (1.5 g, 82%).

$^1\text{H NMR}$  (300 MHz,  $\text{DMSO}-d_6$ ):  $\delta$  7.78 (s, 1H), 7.72 (s, 1H), 7.19 (s, 1H), 6.92 (t,  $J = 5.7$  Hz, 1H), 5.39 (s, 2H), 3.04 (q,  $J = 5.7$  Hz, 2H), 1.27 (m, 7H), 0.87 (m, 6H).  $^{13}\text{C NMR}$  (75 MHz, DMSO):  $\delta$  155.2, 144.4, 128.5, 118.9, 115.0, 110.2, 108.2, 98.8, 31.0, 29.0, 24.2, 23.0, 14.5, 11.3. **IR** (ATR,  $\text{cm}^{-1}$ ): 2988, 2970, 2901, 1640, 1406, 1394, 1381, 1250, 1076, 1066, 1042, 1028. **HRMS**: Calculated for  $\text{C}_{15}\text{H}_{23}\text{Cl}_2\text{N}_3\text{O}_2\text{Na}$   $[\text{M}+\text{Na}]^+$ : 354.1110, found: 354.1111.



1-(2,4-dichloro-5-nitrophenyl)-3-(6-methylheptan-2-yl)urea

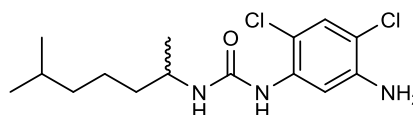


In an oven-dried Schlenk flask at room temperature was added with a syringe pump (10 mL/h) a solution of 2,4-dichloro-5-nitroaniline (1.03 g, 4.95 mmol) and DIEA (950  $\mu$ L, 5.45 mmol) in dried DCM (18 mL) to a solution of triphosgene (543 mg, 1.83 mmol) in dried DCM (10 mL). The solution was stirred 5 additional minutes and 2-amino-6-methylheptane (850  $\mu$ L, 4.95 mmol) and DIEA (950  $\mu$ L, 5.45 mmol) were added to the solution. The reaction mixture was stirred overnight. The volatiles were evaporated under vacuum and the crude product was taken up in AcOEt and washed successively with an aqueous solution of  $\text{KHSO}_4$  (10%), an aqueous solution of  $\text{NaHCO}_3$  (5%) and brine. The organic phase was dried over  $\text{MgSO}_4$  and evaporated under vacuum to yield the crude product. The crude product was purified by flash column chromatography on silica gel using petroleum ether/DCM (1:1) as eluent yielding 1-(2,4-dichloro-5-nitrophenyl)-3-(6-methylheptan-2-yl)urea as an orange solid (1.0 g, 61%).

$^1\text{H NMR}$  (300 MHz,  $\text{CDCl}_3$ ):  $\delta$  8.95 (s, 1H), 7.50 (s, 1H), 6.87 (s, 1H), 4.80 (d,  $J = 8.1$  Hz, 1H), 3.92-3.73 (m, 1H), 1.64-1.26 (m, 7H), 1.21 (d,  $J = 6.6$  Hz, 3H), 0.87 (d,  $J = 6.6$  Hz, 6H).  $^{13}\text{C NMR}$  (75 MHz,  $\text{CDCl}_3$ ):  $\delta$  153.0, 146.8, 135.7, 131.0, 125.0, 119.2, 116.5, 46.9, 38.8, 37.4, 27.9, 23.8, 22.6, 22.5, 21.2.

1-(5-amino-2,4-dichlorophenyl)-3-(6-methylheptan-2-yl)urea

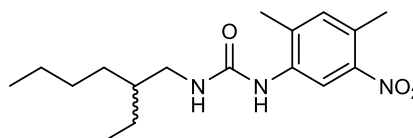
(*rac*)- $\text{DMHUCl}_2\text{-NH}_2$



Iron (1 g, 18 mmol) was added to a solution of 1-(2,4-dichloro-5-nitrophenyl)-3-(6-methylheptan-2-yl)urea (1.0 g, 3.0 mmol) in acetic acid (40 mL). The resulting suspension was refluxed overnight and cooled to room temperature. Brine was added and the aqueous phase was extracted three times with DCM. The combined organic phases were washed two times with  $\text{NaHCO}_{3(\text{sat})}$ , dried over  $\text{Na}_2\text{SO}_4$  and evaporated under vacuum. The resulting solid was dissolved in a minimum amount of DCM and precipitated by adding pentane. The solid was filtered off and thoroughly washed with pentane yielding (*rac*)- $\text{DMHUCl}_2\text{-NH}_2$  as a white solid (0.58 g, 58%).

$^1\text{H NMR}$  (200 MHz,  $\text{DMSO-}d_6$ ):  $\delta$  7.70 (s, 1H), 7.65 (s, 1H), 7.17 (s, 1H), 6.83 (d,  $J = 7.7$  Hz, 1H), 5.37 (s, 2H), 1.36-1.10 (m, 9H), 1.04 (d,  $J = 6.6$  Hz, 3H), 0.83 (d,  $J = 6.5$  Hz, 6H).

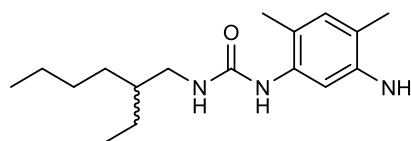
1-(5-nitro-2,4-dimethylphenyl)-3-(2-ethylhexyl)urea



In an oven-dried Schlenk flask at room temperature was added with a syringe pump (10 mL/h) a solution of 2,4-dimethyl-5-nitroaniline (1.94 g, 11.7 mmol) and DIEA (2.25 mL, 12.9 mmol) in dried DCM (40 mL) to a solution of triphosgene (1.28 g, 4.21 mmol) in dried DCM (10 mL). The solution was stirred 5 additional minutes and 2-ethyl-1-hexylamine (2.2 mL, 12.87 mmol) and DIEA (2.25 mL, 12.9 mmol) were added to the solution. The reaction mixture was stirred overnight. The volatiles were evaporated under vacuum and the crude product was taken up in AcOEt and washed successively with an aqueous solution of KHSO<sub>4</sub> (10%), an aqueous solution of NaHCO<sub>3</sub> (5%) and brine. The organic phase was dried over MgSO<sub>4</sub> and evaporated under vacuum to yield 1-(5-nitro-2,4-dimethylphenyl)-3-(2-ethylhexyl)urea as an orange solid (3.6 g, 95%). The product was engaged in the next step without further purification.

<sup>1</sup>H NMR (300 MHz, DMSO-*d*<sub>6</sub>): δ 8.76 (s, 1H), 7.89 (s, 1H), 7.25 (s, 1H), 6.72 (t, *J* = 5.7 Hz, 1H), 3.11 (q, *J* = 5.7 Hz, 2H), 2.54 (p, *J* = 1.9 Hz, 2H), 2.46 (s, 3H), 2.27 (s, 3H), 1.29 (m, 7H), 0.98-0.83 (m, 6H). <sup>13</sup>C NMR (75 MHz, DMSO): δ 155.1, 146.5, 137.3, 133.8, 131.8, 124.9, 114.1, 41.5, 30.5, 28.4, 23.7, 22.5, 19.2, 17.7, 13.9, 10.7. IR (ATR, cm<sup>-1</sup>): 2961, 2926, 1642, 1560, 1524, 1338, 1250, 1066, 1046. HRMS: Calculated for C<sub>17</sub>H<sub>27</sub>N<sub>3</sub>O<sub>3</sub>Na [M+Na]<sup>+</sup>: 344.1945, found: 344.1945.

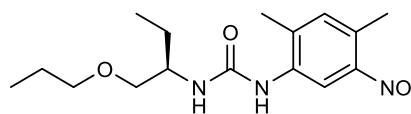
1-(5-amino-2,4-dimethylphenyl)-3-(2-ethylhexyl)urea  
(*rac*)-EHUX-NH<sub>2</sub>



1-(2-ethylhexyl)-3-(2-methyl-5-nitrophenyl)urea (1.8 g, 5.6 mmol) and Pd/C (150 mg, hydrated 5% weight) were suspended in EtOH (40 mL). Hydrazine monohydrate (4.1 mL, 83.6 mmol) was added in one portion to the suspension which was refluxed overnight. The reaction was cooled to room temperature and the suspension was filtrated over a Celite® pad eluting with EtOAc until no product was present in the washings (checked by TLC). The resulting organic phase was washed two times with brine, dried over MgSO<sub>4</sub> and the solvents were evaporated under vacuum. The crude product was dissolved in a small amount of DCM and precipitated by adding pentane. The solid was filtered off and thoroughly washed with pentane yielding (*rac*)-EHUCl<sub>2</sub>-NH<sub>2</sub> as an off-white solid (1.3 g, 80%). (*rac*)-EHUX-NH<sub>2</sub> is stored in a dessicator under vacuum in order to avoid degradation.

<sup>1</sup>H NMR (300 MHz, DMSO-*d*<sub>6</sub>): δ 7.30 (s, 1H), 7.14 (s, 1H), 6.64 (s, 1H), 6.31 (t, *J* = 5.8 Hz, 1H), 4.55 (s, 2H), 3.04 (q, *J* = 5.5 Hz, 2H), 2.01 (s, 3H), 1.97 (s, 3H), 1.29 (dd, *J* = 10.8, 4.9 Hz, 9H), 0.93-0.83 (m, 6H). <sup>13</sup>C NMR (75 MHz, DMSO): δ 155.6, 144.1, 136.3, 131.2, 115.2, 114.6, 107.7, 41.6, 30.6, 28.5, 23.7, 22.6, 16.9, 16.7, 14.0, 10.8. IR (ATR, cm<sup>-1</sup>): 3312, 2969, 2901, 1634, 1589, 1560, 1463, 1249, 1217, 1111, 1079, 1066, 1047. HRMS: Calculated for C<sub>17</sub>H<sub>29</sub>N<sub>3</sub>ONa [M+Na]<sup>+</sup>: 292.2383, found: 292.2383.

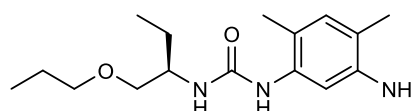
1-(5-nitro-2,4-dimethylphenyl)-3-(-(R)-1-propoxybutan-2-yl)urea



In an oven-dried Schlenk flask at room temperature was added with a syringe pump (10 mL/h) a solution of 2,4-dimethyl-5-nitroaniline (1.74 g, 10.4 mmol) and DIEA (2 mL, 11.4 mmol) in dried DCM (36 mL) to a solution of triphosgene (1.14 g, 3.85 mmol) in dried DCM (9 mL). The solution was stirred 5 additional minutes and the (*R*)-PBENH<sub>2</sub> (3g, 11.4 mmol) and DIEA (2 mL, 11.4 mmol) were added to the solution. The reaction mixture was stirred overnight. The volatiles were evaporated under vacuum and the crude product was taken up in AcOEt and washed successively with an aqueous solution of KHSO<sub>4</sub> (10%), an aqueous solution of NaHCO<sub>3</sub> (5%) and brine. The organic phase was dried over MgSO<sub>4</sub> and evaporated under vacuum to yield the crude product. The crude product was washed with hot heptane, filtered off and washed twice with pentane to yield 1-(5-nitro-2,4-dimethylphenyl)-3-(-(R)-1-propoxybutan-2-yl)urea as an off-white solid (1.9 g, 57%).

<sup>1</sup>H NMR (300 MHz, DMSO-*d*<sub>6</sub>): δ 8.75 (s, 1H), 7.95 (s, 1H), 7.26 (s, 1H), 6.71 (d, *J* = 8.4 Hz, 1H), 3.71 (td, *J* = 8.1, 4.1 Hz, 1H), 3.47-3.32 (m, 4H), 2.44 (s, 3H), 2.26 (s, 3H), 1.68-1.36 (m, 4H), 0.90 (td, *J* = 7.4, 5.2 Hz, 6H). <sup>13</sup>C NMR (75 MHz, DMSO): δ 154.7, 146.5, 137.3, 133.9, 131.9, 125.0, 114.1, 72.0, 71.8, 50.3, 24.6, 22.3, 19.2, 17.7, 10.4, 10.3. IR (ATR, cm<sup>-1</sup>): 3327, 2969, 2901, 1636, 1560, 1531, 1406, 1394, 1380, 1242, 1076, 1067, 1045. HRMS: Calculated for C<sub>16</sub>H<sub>25</sub>N<sub>3</sub>O<sub>4</sub>Na [M+Na]<sup>+</sup>: 346.1737, found: 346.1737.

1-(5-amino-2,4-dimethylphenyl)-3-(-(R)-1-propoxybutan-2-yl)urea  
(*R*)-PBEUX-NH<sub>2</sub>

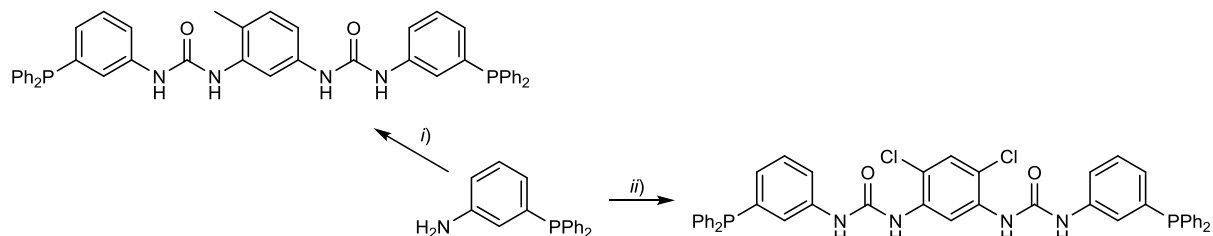


1-(5-nitro-2,4-dimethylphenyl)-3-(-(R)-1-propoxybutan-2-yl)urea (800 mg, 2.4 mmol) and Pd/C (25 mg, 5% weight) were suspended in EtOH (25 mL). Hydrazine monohydrate (1.7 mL, 36 mmol) was added in one portion to the suspension which was refluxed overnight. The reaction was cooled to room temperature and the suspension was filtrated over a Celite® pad eluting with EtOAc until no product was present in the washings (checked by TLC). The volatiles were evaporated under vacuum yielding (*R*)-PBEUX-NH<sub>2</sub> as an off-white solid (640 mg, 91%). (*rac*)-PBEUX-NH<sub>2</sub> was synthesised using the same reaction pathway (45% yield over two steps).

<sup>1</sup>H NMR (300 MHz, DMSO-*d*<sub>6</sub>): δ 7.34 (s, 1H), 7.10 (s, 1H), 6.63 (s, 1H), 6.22 (d, *J* = 8.4 Hz, 1H), 4.47 (s, 2H), 3.65 (m, 1H), 3.46-3.13 (m, 4H), 1.99 (s, 3H), 1.95 (s, 3H), 1.64-1.28 (m, 5H), 0.88 (td, *J*

= 7.4, 2.8 Hz, 6H).  $^{13}\text{C}$  NMR (75 MHz, DMSO):  $\delta$  155.2, 144.3, 136.1, 131.2, 115.2, 114.6, 107.6, 72.1, 72.0, 50.1, 24.7, 22.4, 16.9, 16.7, 10.5, 10.3. IR (ATR,  $\text{cm}^{-1}$ ): 3326, 2969, 2901, 1636, 1421, 1076, 1067, 1045. HRMS: Calculated for  $\text{C}_{17}\text{H}_{29}\text{N}_3\text{ONa}$   $[\text{M}+\text{Na}]^+$ : 294.2176, found: 294.2177.

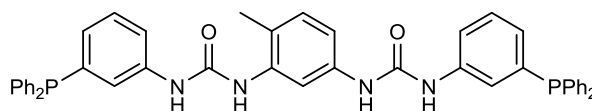
Synthesis of bis-urea ligands with two phosphine units:



i) 3-(diphenylphosphino)aniline, toluene-2,4-diisocyanate, DCM, r.t. (25% yield) ii) 3-(diphenylphosphino)aniline, triphosgene, 1,5-diamino-2,4-dichlorobenzene, DIEA, DCM, r.t. (32% yield).

1,1'-(4-methyl-1,3-phenylene)bis(3-(3-(diphenylphosphino)phenyl)urea)

***m*-(PPh<sub>3</sub>)<sub>2</sub>UT**

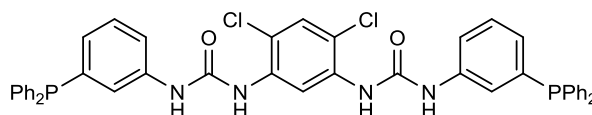


In an oven-dried Schlenk tube was added dropwise a solution of 3-(diphenylphosphino)aniline (427 mg, 1.54 mmol) in dried DCM (10 mL) to a solution of toluene 2,4-diisocyanate (120  $\mu\text{L}$ , 0.70 mmol) at room temperature. The reaction mixture was stirred overnight and then the resulting precipitate was filter off yielding ***m*-(PPh<sub>3</sub>)<sub>2</sub>UT** as a white powder (128 mg, 25%).

$^1\text{H}$  NMR (300 MHz, DMSO- $d_6$ ):  $\delta$  9.08 (s, 1H), 8.57 (d,  $J$  = 6.1 Hz, 2H), 7.85 (d,  $J$  = 2.9 Hz, 2H), 7.65-7.51 (m, 2H), 7.48-7.23 (m, 24H), 7.18 (dd,  $J$  = 8.2, 2.2 Hz, 1H), 7.03 (d,  $J$  = 8.3 Hz, 1H), 6.83 (q,  $J$  = 7.5 Hz, 2H), 2.15 (s, 3H).  $^{13}\text{C}\{^1\text{H}\}$  NMR (75 MHz, DMSO):  $\delta$  152.4, 152.3, 140.3, 140.2, 140.1, 140.1, 137.6, 137.4, 137.3, 137.1, 136.7, 136.6, 133.4, 133.1, 130.2, 129.3, 129.2, 129.1, 129.0, 128.9, 128.8, 128.7, 126.6, 126.4, 122.6, 122.4, 122.3, 122.1, 120.6, 118.6, 118.5, 112.7, 110.9, 17.2.  $^{31}\text{P}\{^1\text{H}\}$  NMR (122 MHz, DMSO)  $\delta$  -5.61, -5.82. IR (ATR,  $\text{cm}^{-1}$ ): 3322, 2988, 2970, 2900, 1654, 1552, 1480, 1297, 1226, 1076, 1066, 1045, 1028.

1,1'-(4,6-dichloro-1,3-phenylene)bis(3-(3-(diphenylphosphino)phenyl)urea)

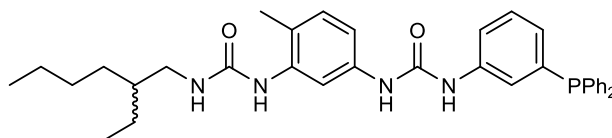
***m*-(PPh<sub>3</sub>)<sub>2</sub>UCl<sub>2</sub>**



In an oven-dried Schlenk flask at room temperature was added with a syringe pump (at 2.5 mL/h) was added a solution of 2,4-dichloro-1,5-diaminobenzene (556 mg, 3.14 mmol) and DIEA (1.1 mL, 6.28 mmol) in dried DCM (45 mL) to a solution of triphosgene (616 mg, 2.08 mmol) in dried DCM (35

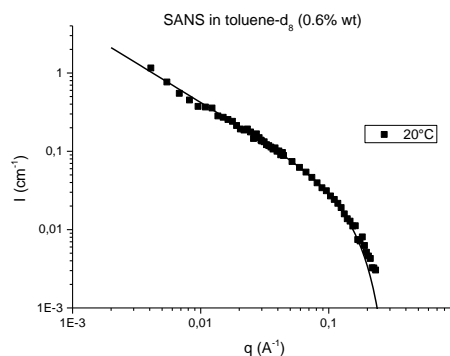
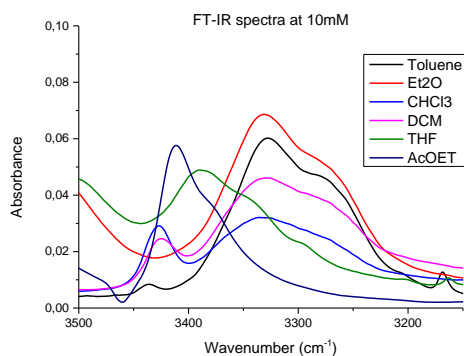


1-(5-(3-(3-(diphenylphosphino)phenyl)ureido)-  
2-methylphenyl)-3-(2-ethylhexyl)urea  
**(rac)-m-PPh<sub>3</sub>EHUT**

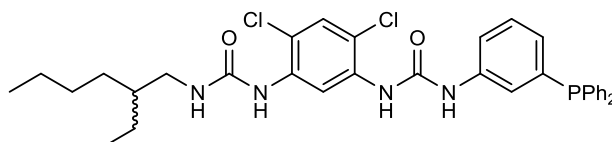


In an oven-dried Schlenk flask at room temperature, to a solution of triphosgene (131 mg, 0.44 mmol) in dry DCM (7 mL) was added with a syringe pump a solution of **(rac)-EHUTNH<sub>2</sub>** (332 mg, 1.2 mmol) and DIEA (230  $\mu$ L, 1.3 mmol) in dry DCM (17 mL). The solution was stirred 5 additional minutes and the 3-(diphenylphosphino)aniline (331 mg, 1.2 mmol) and DIEA (230  $\mu$ L, 1.3 mmol) in DCM was added to the solution. The reaction mixture was stirred overnight. The solvents were then evaporated under vacuum. The crude product was purified by flash column chromatography on silica gel using DCM/EtOAc (0% to 20% gradient) as eluent yielding **(rac)-m-PPh<sub>3</sub>EHUT** as a white solid (186 mg, 27%).

<sup>1</sup>H NMR (300 MHz, DMSO-*d*<sub>6</sub>):  $\delta$  8.51 (d, *J* = 6.0 Hz, 2H), 7.83 (d, *J* = 2.2 Hz, 1H), 7.57-7.50 (m, 2H), 7.45-7.37 (m, 6H), 7.27 (m, 6H), 7.11 (dd, *J* = 8.2, 2.2 Hz, 1H), 6.97 (d, *J* = 8.3 Hz, 1H), 6.83-6.75 (m, 1H), 6.49 (t, *J* = 5.7 Hz, 1H), 3.05 (q, *J* = 5.5 Hz, 2H), 2.10 (s, 3H), 1.40-1.16 (m, 9H), 0.88 (h, *J* = 3.6, 3.2 Hz, 6H). <sup>31</sup>P{<sup>1</sup>H} NMR (122 MHz, DMSO):  $\delta$  -6.29. IR (ATR, cm<sup>-1</sup>): 3200, 2988, 2969, 2921, 2901, 1635, 1407, 1394, 1379, 1250, 1076, 1066, 1045, 1028. HRMS: Calculated for C<sub>35</sub>H<sub>41</sub>N<sub>4</sub>O<sub>2</sub>PNa [M+Na]<sup>+</sup>: 603.2859, found: 603.28.



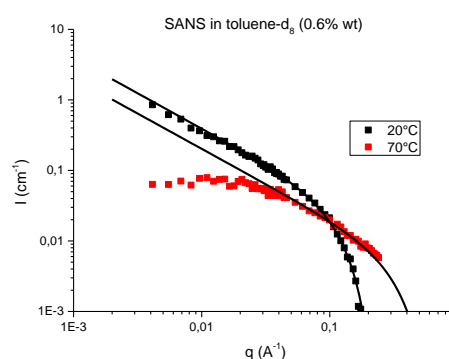
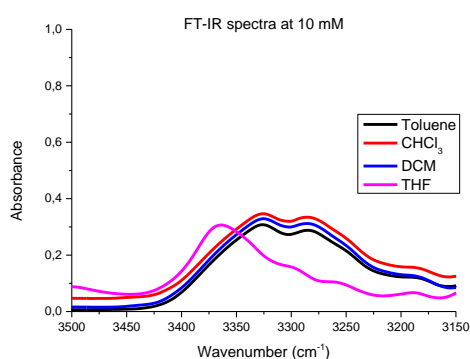
1-(2,4-dichloro-5-(3-(3-(  
(diphenylphosphino)phenyl)ureido)phenyl)-3-  
(2-ethylhexyl)urea  
**(rac)-m-PPh<sub>3</sub>EHUCl<sub>2</sub>**



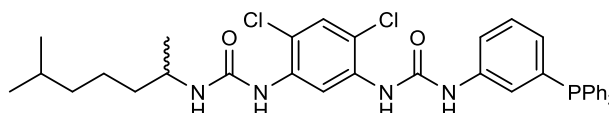
In an oven-dried Schlenk flask at room temperature, to a solution of triphosgene (208 mg, 0.70 mmol) in dry DCM (12 mL) was added with a syringe pump (at 2 mL/h) a solution of **(rac)-EHUCl<sub>2</sub>NH<sub>2</sub>** (705 mg, 2.12 mmol) and DIEA (395  $\mu$ L, 2.27 mmol) in dry DCM (30 mL). The solution was stirred 5 additional minutes and 3-(diphenylphosphino)aniline (588 mg, 2.12 mmol) and DIEA (395  $\mu$ L, 2.27

mmol) were added neat to the solution. The reaction mixture was stirred overnight. The solvents were then evaporated under vacuum. The crude product was recrystallised from acetonitrile to yield (*rac*)-*m*-PPh<sub>3</sub>EHUCl<sub>2</sub> as a white solid (0.9 g, 67%).

<sup>1</sup>H NMR (500 MHz, DMSO-*d*<sub>6</sub>): δ 9.37 (s, 1H), 8.95 (s, 1H), 8.19 (s, 1H), 8.01 (s, 1H), 7.63-7.59 (m, 1H), 7.52 (s, 1H), 7.44-7.37 (m, 6H), 7.33 (td, *J* = 7.9, 1.8 Hz, 1H), 7.27 (tt, *J* = 7.6, 2.2 Hz, 5H), 3.05 (m, 2H), 1.37 (p, *J* = 5.9 Hz, 1H), 1.32-1.20 (m, 10H), 0.90-0.84 (m, 6H). <sup>13</sup>C{<sup>1</sup>H} NMR (126 MHz, DMSO-*d*<sub>6</sub>): δ 154.9, 152.2, 140.2, 138.0, 137.1, 137.0, 136.5, 135.3, 133.9, 133.7, 129.8, 129.5, 129.3, 129.2, 128.7, 127.4, 127.3, 123.0, 122.8, 119.2, 115.2, 113.6, 42.0, 31.0, 28.9, 24.1, 23.0, 14.5, 11.3. <sup>31</sup>P{<sup>1</sup>H} NMR (202 MHz, DMSO-*d*<sub>6</sub>): δ -5.9. IR (ATR, cm<sup>-1</sup>): 3326 (br), 2958, 2923, 1650, 1589, 1534, 1499, 1434, 1413, 1315, 1279, 1217, 1184, 1089, 1046. HRMS: Calculated for C<sub>34</sub>H<sub>37</sub>Cl<sub>2</sub>N<sub>4</sub>O<sub>2</sub>PNa [M+Na]<sup>+</sup>: 657.1923, found: 657.1929.



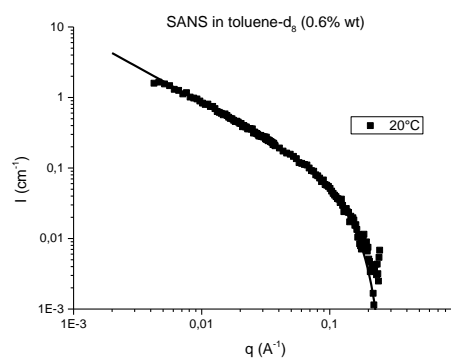
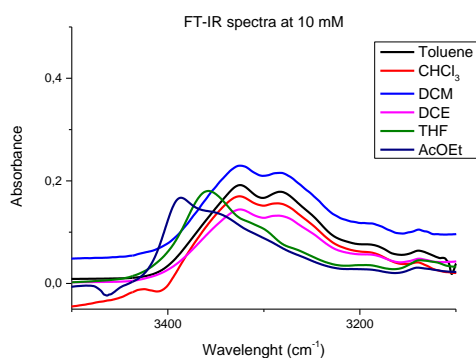
1-(2,4-dichloro-5-(3-(3-(diphenylphosphino)phenyl)ureido)phenyl)-3-(6-methylheptan-2-yl)urea  
(*rac*)-*m*-PPh<sub>3</sub>DMHUCl<sub>2</sub>



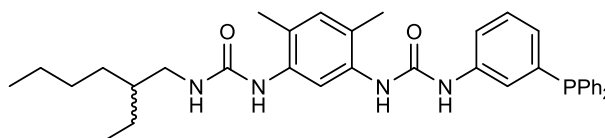
In an oven-dried Schlenk flask at room temperature, to a solution of triphosgene (160 mg, 0.54 mmol) in dried DCM (8 mL) was added with a syringe pump (at 2 mL/h) was added a solution of (*rac*)-**DMUCl<sub>2</sub>NH<sub>2</sub>** (544 mg, 1.64 mmol) and DIEA (300 μL, 1.75 mmol) in dried DCM (27 mL). The solution was stirred 5 additional minutes and the 3-(diphenylphosphino)aniline (455 mg, 1.64 mmol) and DIEA (300 μL, 1.75 mmol) were added neat to the solution. The reaction mixture was stirred overnight. The solvents were then evaporated under vacuum. The crude product was recrystallised from acetonitrile to yield (*rac*)-*m*-PPh<sub>3</sub>DMHUCl<sub>2</sub> as a white solid (568 mg, 55%).

<sup>1</sup>H NMR (400 MHz, DMSO-*d*<sub>6</sub>): δ 9.39 (s, 1H), 9.00 (s, 1H), 8.20 (s, 1H), 7.90 (s, 1H), 7.64 (dd, *J* = 8.1, 2.1 Hz, 1H), 7.49 (s, 1H), 7.43-7.24 (m, 12H), 6.91-6.82 (m, 2H), 3.67 (p, *J* = 6.7 Hz, 1H), 1.51 (m, 1H), 1.34 (m, 4H), 1.16 (m, 2H), 1.08 (d, *J* = 6.5 Hz, 3H), 0.84 (d, *J* = 6.6 Hz, 6H). <sup>13</sup>C NMR (101 MHz, DMSO): δ 153.8, 151.7, 139.8, 139.7, 137.5, 137.4, 136.6, 136.5, 136.1, 134.8, 133.4, 133.2,

129.3, 129.2, 129.0, 128.8, 128.7, 128.2, 126.9, 126.8, 122.6, 122.3, 118.7, 114.6, 114.6, 113.0, 44.1, 38.4, 36.8, 27.4, 23.3, 22.5, 21.1.  $^{31}\text{P}\{^1\text{H}\}$  NMR (202 MHz, DMSO- $d_6$ ):  $\delta$  -5.82. IR (ATR,  $\text{cm}^{-1}$ ): 2970, 2901, 1644, 1548, 1408, 1394, 1222, 1074, 1066, 1047, 1028. HRMS: Calculated for  $\text{C}_{34}\text{H}_{37}\text{Cl}_2\text{N}_4\text{O}_2\text{PNa}$   $[\text{M}+\text{Na}]^+$ : 657.1923, found: 657.1931.



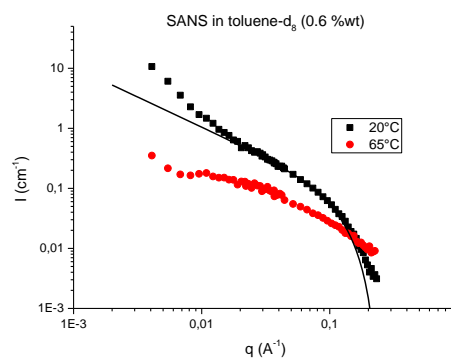
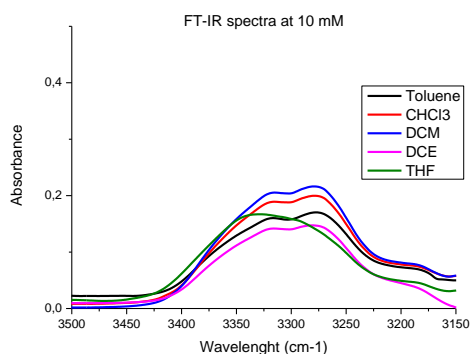
1-(5-(3-(3-(diphenylphosphino)phenyl)ureido)-  
2,4-dimethylphenyl)-3-(2-ethylhexyl)urea  
**(rac)-m-PPh<sub>3</sub>EHUX**



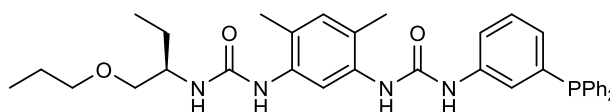
1,1'-Carbonyldiimidazole (CDI, 1.4 g, 8.58 mmol) was dissolved in dry acetonitrile (20 mL) in an oven-dried Schlenk flask under inert atmosphere. 3-(diphenylphosphino)aniline (951 mg, 3.43 mmol) in dry acetonitrile (30 mL) was added using a syringe pump (1.5 mL/h) to the CDI solution at 0°C. The solution was allowed to reach room temperature during the time of addition. At the end of the addition, water (1 mL/9 mmol of CDI) was added and the solution was stirred for two hours at room temperature. **(rac)-EHUX-NH<sub>2</sub>** (1.0 g, 3.43 mmol) is then added to the solution and stirred at room temperature for 3 days. The resulting precipitate was filtered off and washed with acetonitrile to give **(rac)-m-PPh<sub>3</sub>EHUX** as a white powder (1.0 g, 51%).

$^1\text{H}$  NMR (300 MHz, DMSO- $d_6$ ):  $\delta$  8.87 (s, 1H), 8.03 (s, 1H), 7.74 (s, 1H), 7.60 (dd,  $J$  = 8.0, 2.2 Hz, 1H), 7.49 (s, 1H), 7.44-7.37 (m, 6H), 7.28 (m, 6H), 6.89 (s, 1H), 6.85-6.77 (m, 1H), 6.31 (t,  $J$  = 5.7 Hz, 1H), 3.03 (q,  $J$  = 5.4 Hz, 2H), 2.09 (s, 6H), 1.27 (t,  $J$  = 5.3 Hz, 9H), 0.87 (h,  $J$  = 4.4, 3.9 Hz, 6H).  $^{13}\text{C}\{^1\text{H}\}$  NMR (75 MHz, DMSO):  $\delta$  155.4, 152.5, 140.5, 140.3, 136.7, 136.5, 136.0, 134.6, 133.4, 133.1, 131.2, 129.2, 128.9, 128.8, 128.7, 126.4, 126.2, 122.5, 122.4, 122.1, 118.5, 115.6, 41.7, 39.3, 30.5, 28.5, 23.7, 22.5, 17.2, 17.1, 13.9, 10.8.  $^{31}\text{P}\{^1\text{H}\}$  NMR (122 MHz, DMSO):  $\delta$  -5.7. IR (ATR,  $\text{cm}^{-1}$ ): 3320, 2970, 2900, 1640, 1584, 1549, 1409, 1226, 1066, 1046. HRMS: Calculated for  $\text{C}_{36}\text{H}_{43}\text{N}_4\text{O}_2\text{PNa}$   $[\text{M}+\text{Na}]^+$ : 617.3016, found: 617.3019.





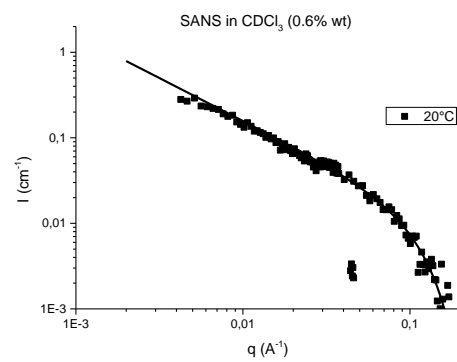
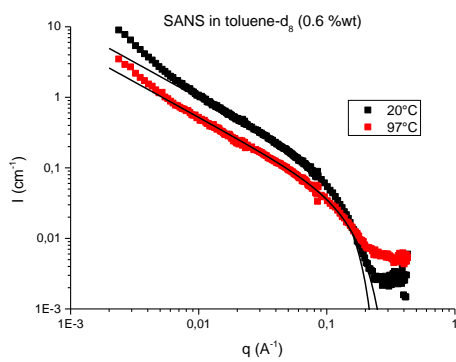
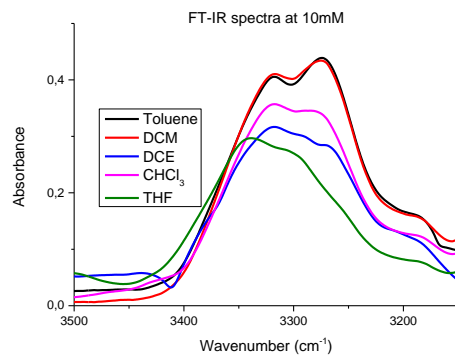
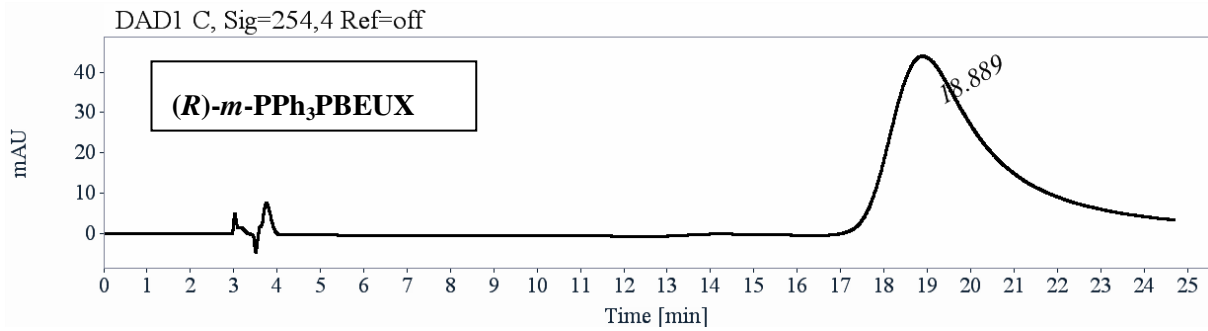
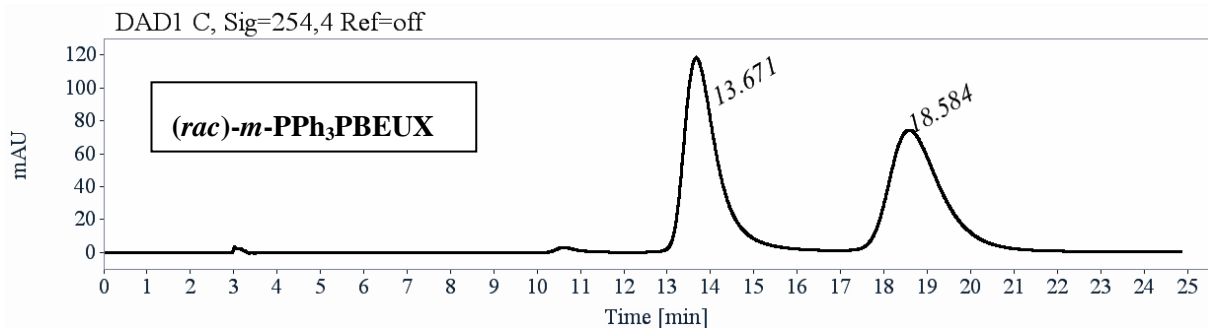
1-(5-(3-(3-(diphenylphosphino)phenyl)ureido)-  
2,4-dimethylphenyl)-3-(*R*)-1-propoxybutan-2-  
yl)urea

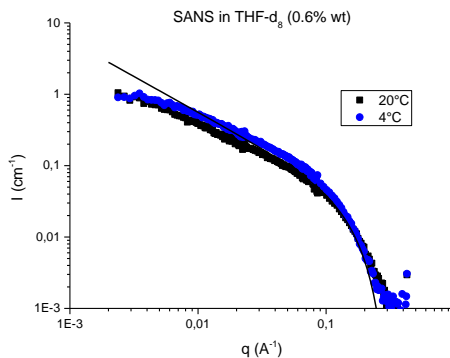
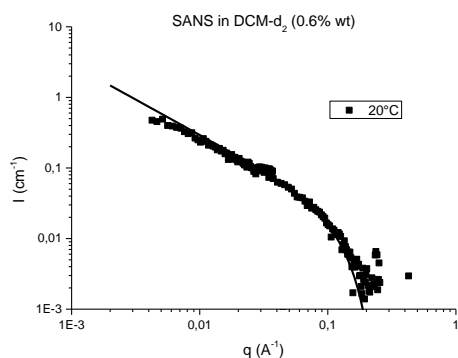


**(*R*)-*m*-PPh<sub>3</sub>PBEUX**

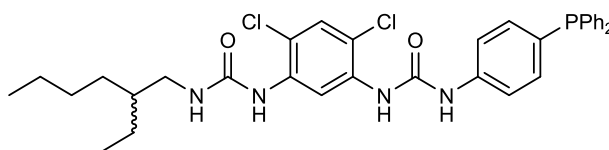
1,1'-Carbonyldiimidazole (691 mg, 4.26 mmol) was dissolved in dry acetonitrile (10 mL) in an oven-dried Schlenk flask under inert atmosphere. 3-(diphenylphosphino)aniline (473 mg, 1.70 mmol) in dry acetonitrile (15 mL) was added using a syringe pump (1.5 mL/h) to the CDI solution at 0°C. The solution was allowed to reach room temperature during the time of addition. At the end of the addition, water (0.5 mL) was added and the solution was stirred for two hours at room temperature. The mixture was then transferred to a flask containing (*R*)-EHUX-NH<sub>2</sub> (500 mg, 1.70 mmol) in acetonitrile (100 mL) and refluxed for 5 hours. The solution was allowed to reach room temperature. The resulting precipitate was filtered off and washed with acetonitrile to give (*R*)-*m*-PPh<sub>3</sub>PBEUX as a white powder (413 mg, 40%). (*rac*)-*m*-PPh<sub>3</sub>PBEUX was prepared following the same synthetic protocols with (*rac*)-EHUX-NH<sub>2</sub> (60 mg, 16%).

<sup>1</sup>H NMR (300 MHz, DMSO-*d*<sub>6</sub>): δ 8.88 (s, 1H), 8.06 (s, 1H), 7.74 (s, 1H), 7.66-7.53 (m, 2H), 7.-7.28 (m, 12H), 6.89 (s, 1H), 6.81 (t, *J* = 7.6 Hz, 1H), 6.29 (d, *J* = 8.4 Hz, 1H), 3.66 (dq, *J* = 8.3, 4.4 Hz, 1H), 3.45-3.23 (m, 4H), 2.10 (s, 6H), 1.48 (m, 4H), 0.88 (m, 6H). <sup>13</sup>C{<sup>1</sup>H} NMR (75 MHz, DMSO): δ 155.1, 152.5, 140.5, 140.3, 137.3, 137.1, 136.7, 136.6, 135.9, 134.7, 133.4, 133.1, 131.3, 129.2, 129.1, 128.9, 128.8, 128.7, 126.4, 126.2, 122.4, 122.4, 122.1, 118.5, 115.5, 72.0, 50.2, 24.7, 22.4, 17.2, 17.1, 10.5, 10.3. <sup>31</sup>P{<sup>1</sup>H} NMR (122 MHz, DMSO): δ -5.7. IR (ATR, cm<sup>-1</sup>): 3250 (br), 2988, 2970, 2901, 1640, 1546, 1406, 1934, 1381, 1250, 1228, 1076, 1066, 1045. HRMS: Calculated for C<sub>35</sub>H<sub>41</sub>N<sub>4</sub>O<sub>3</sub>PNa [M+Na]<sup>+</sup>: 620.2842, found: 620.2843. ee > 99% (Chiralpak IA, 25°C, Heptane/Ethanol (90/10), 1 mL/min).



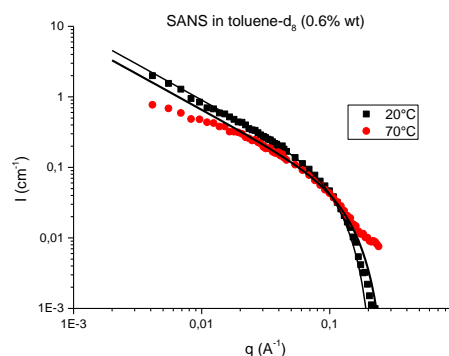
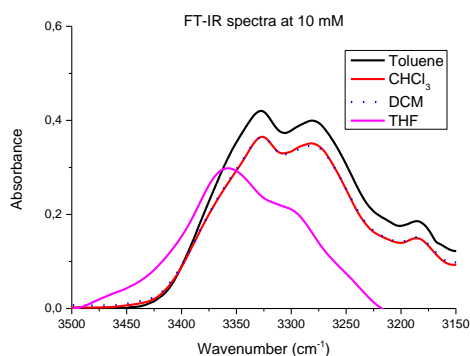


1-(2,4-dichloro-5-(3-(4-(diphenylphosphino)phenyl)ureido)phenyl)-3-(2-ethylhexyl)urea  
*(rac)-p*-PPh<sub>3</sub>EHUCl<sub>2</sub>



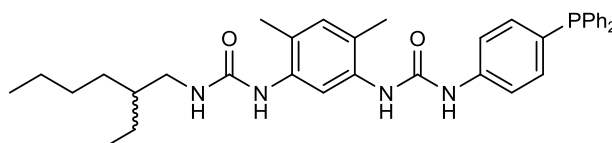
In an oven-dried Schlenk flask at room temperature, to a solution of triphosgene (224 mg, 0.75 mmol) in dried DCM (13 mL) was added with a syringe pump (2.5 mL/h) to a solution of *(rac)*-EHUCl<sub>2</sub>-NH<sub>2</sub> (759 mg, 2.28 mmol) and DIEA (425 μL, 1.25 mmol) in dried DCM (32 mL). The solution was stirred 5 additional minutes and the 4-(diphenylphosphino)aniline (697 mg, 2.51 mmol) and DIEA (425 μL, 1.25 mmol) in DCM (10 mL) was added to the solution. The reaction mixture was stirred overnight. The DCM phase was washed two times with water, dried over MgSO<sub>4</sub> and evaporated under vacuum. The crude product was recrystallised from EtOAc to yield *(rac)-p*-PPh<sub>3</sub>EHUCl<sub>2</sub> as a white solid (428 mg, 30%).

<sup>1</sup>H NMR (300 MHz, DMSO-*d*<sub>6</sub>): δ 9.54 (s, 1H), 9.05 (s, 1H), 8.32 (s, 1H), 8.03 (s, 1H), 7.69 – 7.45 (m, 5H), 7.37 (m, 5H), 7.29 – 7.17 (m, 5H), 6.96 (t, *J* = 5.7 Hz, 1H), 3.07 (q, *J* = 5.7 Hz, 2H), 1.27 (d, *J* = 10.7 Hz, 9H), 0.91 – 0.81 (m, 6H). <sup>13</sup>C{<sup>1</sup>H} NMR (75 MHz, DMSO): δ 154.5, 151.7, 140.5, 137.4, 137.2, 136.1, 134.7, 134.5, 134.3, 133.1, 132.9, 131.5, 131.4, 128.7, 128.6, 128.5, 128.2, 118.4, 118.3, 114.8, 114.7, 113.1, 41.6, 39.2, 30.5, 28.4, 23.7, 22.5, 13.9, 10.7. <sup>31</sup>P{<sup>1</sup>H} NMR (122 MHz, DMSO): δ -7.80. IR (ATR, cm<sup>-1</sup>): 3326 (br), 2958, 2923, 1650, 1589, 1534, 1499, 1434, 1413, 1315, 1279, 1217, 1184, 1089, 1046. HRMS: Calculated for C<sub>34</sub>H<sub>37</sub>Cl<sub>2</sub>N<sub>4</sub>O<sub>2</sub>PNa [M+Na]<sup>+</sup>: 657.1923, found: 657.1931.



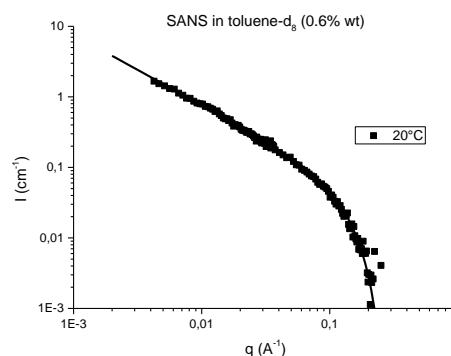
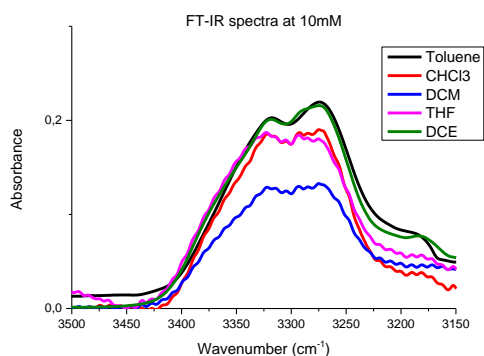
1-(5-(3-(4-(diphenylphosphino)phenyl)ureido)-  
2,4-dimethylphenyl)-3-(2-ethylhexyl)urea

**(rac)-p-PPh<sub>3</sub>EHUX**

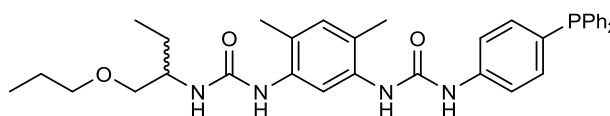


1,1'-Carbonyldiimidazole (CDI, 1.0 g, 6.125 mmol) was dissolved in dry acetonitrile (ca. for 3 mL) in an oven-dried Schlenk flask under inert atmosphere. 4-(diphenylphosphino)aniline (680 mg, 2.45 mmol) in dry acetonitrile (10 mL) was added using a syringe pump (1.5 mL/h) to the CDI solution at 0°C. The solution was allowed to reach room temperature during the time of addition. At the end of the addition, water (1 mL) was added and the solution was stirred for two hours at room temperature. The mixture was then transferred to a flask containing **(rac)-EHUX-NH<sub>2</sub>** (714 mg, 2.45 mmol) in acetonitrile (30 mL) and refluxed for 2 hours. The solution was allowed to reach room temperature. The resulting precipitate was filtered off and washed with acetonitrile to give **(rac)-p-PPh<sub>3</sub>EHUX** as a white solid (483 mg, 33%).

<sup>1</sup>H NMR (400 MHz, DMSO-*d*<sub>6</sub>): δ 9.01 (s, 1H), 8.09 (s, 1H), 7.86 (s, 1H), 7.58 – 7.47 (m, 3H), 7.38 (m, 6H), 7.27 – 7.13 (m, 6H), 6.90 (s, 1H), 6.34 (t, *J* = 5.7 Hz, 1H), 3.03 (h, *J* = 7.6 Hz, 2H), 2.13 (s, 3H), 2.13 (s, 3H), 1.41 – 1.19 (m, 9H), 0.86 (td, *J* = 6.9, 4.4 Hz, 6H). <sup>13</sup>C{<sup>1</sup>H} NMR (75 MHz, DMSO): δ 155.5, 152.5, 141.1, 137.5, 137.3, 136.0, 134.6, 134.5, 134.2, 133.1, 132.8, 131.3, 128.7, 128.6, 127.7, 127.6, 122.5, 122.5, 118.1, 118.0, 115.6, 41.7, 39.3, 30.5, 28.5, 23.7, 22.5, 17.2, 17.1, 13.9, 10.8. <sup>31</sup>P{<sup>1</sup>H} NMR (162 MHz, DMSO): δ -8.0. IR (ATR, cm<sup>-1</sup>): 3328, 2969, 2901, 1641, 1591, 1541, 1226, 1078, 1067, 1044. HRMS: Calculated for C<sub>36</sub>H<sub>43</sub>N<sub>4</sub>O<sub>2</sub>PNa [M+Na]<sup>+</sup>: 617.3016, found: 617.3019.



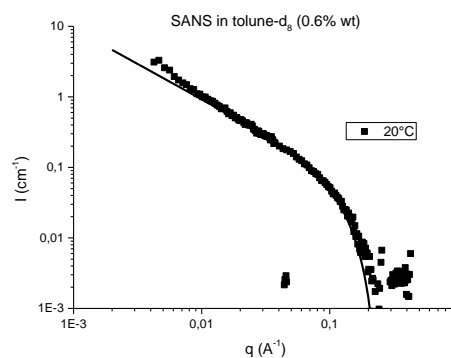
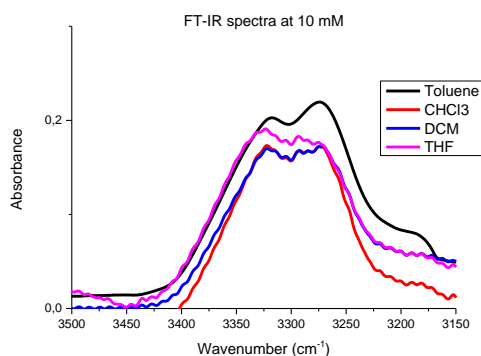
1-(5-(3-(4-(diphenylphosphino)phenyl)ureido)-  
2,4-dimethylphenyl)-3-((*R*)-1-propoxybutan-2-  
yl)urea



**(*rac*)-*p*-PPh<sub>3</sub>PBEUX**

1,1'-Carbonyldiimidazole (CDI, 1.0 g, 6.125 mmol) was dissolved in dry acetonitrile (ca. for 3 mL) in an oven-dried Schlenk flask under inert atmosphere. 4-(diphenylphosphino)aniline (680 mg, 2.45 mmol) in dry acetonitrile (10 mL) was added using a syringe pump (1.5 mL/h) to the CDI solution at 0°C. The solution was allowed to reach room temperature during the time of addition. At the end of the addition, water (1 mL) was added and the solution was stirred for two hours at room temperature. The mixture was then transferred to a flask containing (*rac*)-PBEUX-NH<sub>2</sub> (718 mg, 2.45 mmol) in acetonitrile (30 mL) and refluxed for 2 hours. The solution was allowed to reach room temperature. The resulting precipitate was filtered off and washed with acetonitrile to give (*rac*)-*p*-PPh<sub>3</sub>PBEUX as a white powder (637 mg, 44%).

<sup>1</sup>H NMR (300 MHz, DMSO-*d*<sub>6</sub>): δ 9.01 (s, 1H), 8.11 (s, 1H), 7.85 (s, 1H), 7.58 (s, 1H), 7.52 (d, *J* = 8.5 Hz, 2H), 7.38 (m, 6H), 7.29-7.14 (m, 6H), 6.90 (s, 1H), 6.30 (d, *J* = 8.4 Hz, 1H), 3.66 (td, *J* = 8.2, 5.0 Hz, 1H), 3.43-3.24 (m, 4H), 2.12 (d, *J* = 7.8 Hz, 6H), 1.64 – 1.31 (m, 4H), 0.88 (td, *J* = 7.4, 5.5 Hz, 6H). <sup>13</sup>C{<sup>1</sup>H} NMR (75 MHz, DMSO): δ 155.1, 152.5, 141.1, 137.5, 137.3, 136.0, 134.6, 134.5, 134.2, 133.1, 132.8, 131.3, 128.7, 128.6, 127.8, 127.6, 122.5, 122.4, 118.1, 118.0, 115.5, 72.0, 50.2, 24.7, 22.4, 17.2, 17.1, 10.5, 10.3. <sup>31</sup>P{<sup>1</sup>H} NMR (122 MHz, DMSO): δ -7.9. IR (ATR, cm<sup>-1</sup>): 3250 (br), 2988, 2969, 2901, 1641, 1541, 1407, 1394, 1380, 1228, 1078, 1067, 1045. HRMS: Calculated for C<sub>35</sub>H<sub>41</sub>N<sub>4</sub>O<sub>3</sub>PNa [M+Na]<sup>+</sup>: 619.2808, found: 619.2813.



## F. References

- [1] V. Simic, L. Bouteiller, M. Jalabert, *J. Am. Chem. Soc.* **2003**, *125*, 13148–13154.
- [2] I. Giannicchi, Synthesis of New Building Blocks for the Construction of Self-Assembled Molecular Architectures. Ph. D. Thesis, University La Sapienza, Roma, **2011**.
- [3] B. Isare, G. Pembouong, F. Boué, L. Bouteiller, *Langmuir* **2012**, *28*, 7535–7541.
- [4] K. J. Padiya, S. Gavade, B. Kardile, M. Tiwari, S. Bajare, M. Mane, V. Gaware, S. Varghese, D. Harel, S. Kurhade, *Org. Lett.* **2012**, *14*, 2814–2817.
- [5] B. Isare, M. Linares, L. Zargarian, S. Fermandjian, M. Miura, S. Motohashi, N. Vanthuyne, R. Lazzaroni, L. Bouteiller, *Chem. Eur. J.* **2010**, *16*, 173–177.
- [6] L. Bouteiller, O. Colombani, F. Lortie, P. Terech, *J. Am. Chem. Soc.* **2005**, *127*, 8893–8898.
- [7] J. Dubarle-Offner, J. Moussa, H. Amouri, B. Jouvelet, L. Bouteiller, M. Raynal, *Chem. Eur. J.* **2016**, *22*, 3985–3990.
- [8] G. R. Fulmer, A. J. M. Miller, N. H. Sherden, H. E. Gottlieb, A. Nudelman, B. M. Stoltz, J. E. Bercaw, K. I. Goldberg, *Organometallics* **2010**, *29*, 2176–2179.
- [9] A. Zhang, Y. Han, K. Yamato, X. C. Zeng, B. Gong, *Org. Lett.* **2006**, *8*, 803–806.
- [10] C. Fonteneau, S. Pensec, L. Bouteiller, *Polym. Chem.* **2014**, *5*, 2496–2505.
- [11] J. T. Manka, F. Guo, J. Huang, H. Yin, J. M. Farrar, M. Sienkowska, V. Benin, P. Kaszynski, *J. Org. Chem.* **2003**, *68*, 9574–9588.
- [12] D. Gelman, L. Jiang, S. L. Buchwald, *Org. Lett.* **2003**, *5*, 2315–2318.
- [13] D. Rivillo, H. Gulyás, J. Benet-Buchholz, E. C. Escudero-Adán, Z. Freixa, P. W. N. M. van Leeuwen, *Angew. Chem. Int. Ed.* **2007**, *46*, 7247–7250.
- [14] N. Soh, T. Ariyoshi, T. Fukaminato, H. Nakajima, K. Nakano, T. Imato, *Org. Biomol. Chem.* **2007**, *5*, 3762–3768.
- [15] A. I. Meyers, G. S. Poindexter, Z. Brich, *J. Org. Chem.* **1978**, *43*, 892–898.
- [16] M. J. McKennon, A. I. Meyers, K. Drauz, M. Schwarm, *J. Org. Chem.* **1993**, *58*, 3568–3571.
- [17] C. A. M. Cariou, B. M. Kariuki, J. S. Snaith, *Org. Biomol. Chem.* **2008**, *6*, 3337–3348.
- [18] M. Roman, C. Cannizzo, T. Pinault, B. Isare, B. Andrioletti, P. van der Schoot, L. Bouteiller, *J. Am. Chem. Soc.* **2010**, *132*, 16818–16824.

# IV. Asymmetric rhodium-catalysed hydrogenation of dimethylitaconate

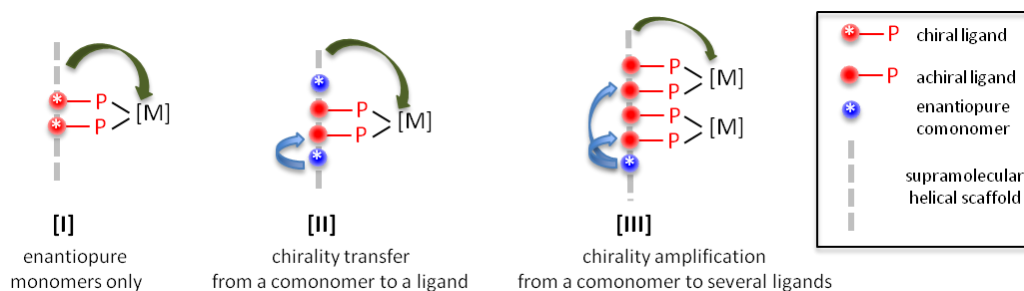
*Abstract:* For the first time, supramolecular helical rods composed of an achiral metal complex and a complementary enantiopure monomer provided good level of enantioinduction in asymmetric catalysis. Mixtures containing an achiral ligand monomer (**BTA**<sup>PPh<sub>2</sub></sup>, 2 mol%) and an enantiopure ligand-free co-monomer (ester BTA, 2.5 mol%), both possessing a complementary benzene-1,3,5-tricarboxamide (BTA) central unit, were investigated in combination with [Rh(cod)<sub>2</sub>]BAR<sub>F</sub> (1 mol%) in the asymmetric hydrogenation of dimethyl itaconate. Notably, efficient chirality transfer occurs within the hydrogen-bonded co-assemblies formed by **BTA** **Ie** and the intrinsically achiral catalytic rhodium catalyst, providing the hydrogenation product with up to 85% *ee*. The effect of the relative content of **BTA** **Ie** compared to the ligand was investigated. The amount of chiral co-monomer can be decreased down to one fourth of that of the ligand without deteriorating the enantioselectivity of the reaction while the enantioselectivity decreases for mixtures containing high amounts of **BTA** **Ie**. The non-linear relationship between the amount of chiral co-monomer and the enantioselectivity indicates that chirality amplification effects are at work in this catalytic system. The rhodium complex of **BTA**<sup>PPh<sub>2</sub></sup> and **BTA** **Ie** co-assemble under the form of right-handed helical rods as confirmed by various spectroscopic and scattering techniques. Remarkably, the major enantiomer and the selectivity of the catalytic reaction are related to the handedness and the net helicity of the co-assemblies, respectively. Further development of this class of catalysts built on chirally-amplified helical scaffolds should contribute to the design of asymmetric catalysts operating with low amounts of chiral entities. This work was published in *J. Am. Chem. Soc.*, 2016, **138**, 4908–4916, (DOI: 10.1021/jacs.6b01306) and was reported here as published with formatting to match with the rest of the thesis. In this chapter all the BTA ligands are derived from 3-(diphenylphosphino)aniline (**BTA**<sup>mPPh<sub>2</sub></sup>) and ester BTA without chirality mentioned are derived from the (*L*)-amino-acids. My participation for this publication involves the characterisation of the Rh-pre-catalytic species using FT-IR and CD analyses shown in the paper (Figures IV-2b and IV-3) and in the supporting information (Figures S2, S3, S4, S8 and S9; Table S4 and S5) as well as the synthesis and characterisation of **BTA** **Phg**.

## A. Introduction

Chirality amplification, the phenomenon by which a small asymmetric bias is translated into a large chiral preference, is a central topic of investigation mainly aiming at elucidating the origin of homochirality.<sup>[1]</sup> It also opens new avenues in the preparation of enantio-enriched molecules<sup>[2]</sup> and materials with promising perspectives of applications including the development of sensors,<sup>[3]</sup> stimuli-responsive gels,<sup>[4]</sup> liquid crystal displays,<sup>[5]</sup> stationary phases<sup>[6]</sup> and catalysts.<sup>[7]</sup>

Chirality amplification effects are particularly strong in dynamic molecular helices,<sup>[8]</sup> such as those formed by covalent<sup>[9]</sup> and supramolecular polymers,<sup>[10]</sup> and foldamers<sup>[8b,11]</sup> since a minimal energetic bias at the monomeric level is cooperatively transferred along the polymeric main chain. In particular, when a few enantiopure monomers (called "the sergeants") impose their handedness to a large number of achiral ones (called "the soldiers"), the macromolecular helicity obeys the sergeants-and-soldiers principle. Following the pioneering results of Green and co-workers on poly(isocyanates),<sup>[9a,12]</sup> this phenomenon has been observed experimentally in a great number of examples which in turn have been consistently modeled at the theoretical level.<sup>[13]</sup> Such an approach is particularly appealing for the construction of asymmetric catalysts since it might enable a good control of the asymmetric environment around the metal center with a limited amount of chiral inducers.

Surprisingly, only very recently chirality amplification in helical polymers was applied for the first time in the construction of efficient asymmetric catalysts.<sup>[14]</sup> Suginome and co-workers<sup>[7a,7c]</sup> demonstrated that *covalent* poly(quinoxaline-2,3-diyl)s terpolymers containing achiral phosphine monomers (0.4%), achiral phosphine-free monomers (82%)<sup>[15]</sup> and only 18% of enantiopure monomeric units formed purely one-handed helical structures that promoted palladium-catalyzed asymmetric hydrosilylation and Suzuki-Miyaura cross-coupling reactions with remarkably high enantioselectivity.<sup>[16]</sup>



Scheme IV-1: Possible strategies [I]-[III] for the construction of supramolecular helices supporting catalytic metal centers (the arrows illustrate the chirality transfers).

Helical *supramolecular* polymers also showed interesting features for catalysts development: i) they are stimuli-responsive,<sup>[17]</sup> ii) their supramolecular structure may enhance the activity and selectivity of catalytic centers arranged on their scaffold,<sup>[18]</sup> and iii) their composition can be tuned by simply mixing different types of complementary monomers.<sup>[17b,19]</sup> Despite these promising achievements, little is known about how the chirality of a supramolecular polymer can be transferred to intrinsically-



achiral metal centers located at its periphery,<sup>[20]</sup> which can in turn be used as catalytic metals for asymmetric reactions.<sup>[19,21]</sup> One can envisage three strategies for the construction of chiral supramolecular helices supporting catalytic metal centers: the use of enantiopure monomers only (**[I]**, Scheme IV-1), the use of a mixture of an achiral ligand monomer with a enantiopure ligand-free monomer in a nearly stoichiometric ratio (**[II]**, chirality transfer) and the use of an enantiopure monomer as the minor component (**[III]**, chirality amplification). While strategy **[I]** has already been successfully described,<sup>[19,21]</sup> strategies **[II]** and **[III]** remain to be implemented in an efficient way. The challenge in these cases is to obtain a good level of enantioinduction since any achiral metal catalysts that will not be located in a chiral environment will significantly decrease the selectivity of the reaction.<sup>[22]</sup> However, supramolecular co-polymers used as efficient scaffolds for asymmetric catalysis should possess unique features: i) they can be prepared by simply mixing the different monomers alleviating the synthetic efforts that are required for the preparation of covalent co-polymers and ii) chirality amplification effects that operate in these polymers can be used to decrease the amount of chiral inducers required to promote asymmetric catalysis.

Here, we demonstrate that supramolecular helical rods formed between an achiral rhodium complex of a benzene-1,3,5-tricarboxamide (BTA) ligand<sup>[23]</sup> and an enantiopure BTA co-monomer can indeed be used as efficient scaffolds for the asymmetric hydrogenation of dimethyl itaconate (up to 85% *ee*). Chirality amplification effects are at work in this catalytic system, which allows decreasing the amount of chiral co-monomer down to one fourth of that of the ligand monomer without deteriorating the enantioselectivity of the catalytic reaction. Moreover, we show that the selectivity of the catalytic reaction is related to the structure of the co-assemblies, and notably to their helicity (as measured by CD spectroscopy), which may facilitate further development of this unique class of catalysts.

## **B. Results and discussion**

The magnitude of chirality transfer and chirality amplification effects displayed by supramolecular assemblies between achiral and enantiopure monomers depend, amongst other factors, on the nature of the monomers.<sup>[10]</sup> Ester BTAs (Chart IV-1) were chosen as chiral co-monomers since they are derived from an important accessible chiral pool and can be prepared straightforwardly in two synthetic steps (see the Supporting Information).<sup>[24]</sup> When studied individually, ester BTAs exhibit unusual self-association properties in cyclohexane compared to classically-investigated alkyl BTAs<sup>[23]</sup> since the nature of the substituent at the stereogenic carbon and the concentration determine the nature of the dominant species in solution, *i.e.* stacks or dimers. Moreover, preliminary results indicated that co-assemblies formed between an achiral alkyl BTA and an ester BTA, used as the enantiopure co-monomer, display strong chirality amplification effects.<sup>[24c]</sup>

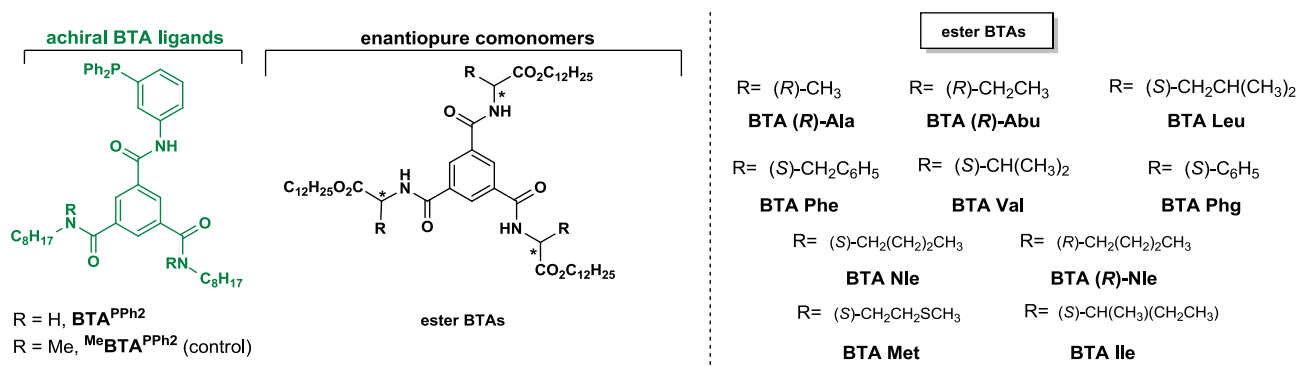
## 1. Catalytic experiments.

Mixtures composed of an achiral BTA ligand (**BTA**<sup>PPh<sub>2</sub></sup>, 2 mol%), the metal precursor ([Rh(cod)<sub>2</sub>]BAR<sub>F</sub>, 1 mol%) and an enantiopure co-monomer (ester BTA) were tested in the rhodium-catalyzed hydrogenation of dimethyl itaconate. Catalytic components were mixed in CH<sub>2</sub>Cl<sub>2</sub> in order to ensure the formation of the Rh complex between **BTA**<sup>PPh<sub>2</sub></sup> and [Rh(cod)<sub>2</sub>]BAR<sub>F</sub> then CH<sub>2</sub>Cl<sub>2</sub> was removed under vacuum and replaced by the solvent selected for catalysis. In the following, the molar ratio between the ester BTA and **BTA**<sup>PPh<sub>2</sub></sup> initially present in the catalytic mixtures will be designated as R<sup>0</sup><sub>esterBTA</sub>.

### a) Chirality transfer

The ease of preparation of the catalytic mixtures allowed us to test ten ester BTAs (R<sup>0</sup><sub>esterBTA</sub>=1.25) as potential enantiopure co-monomers for the catalytic reaction (Table IV-1). In hexane/CH<sub>2</sub>Cl<sub>2</sub> (10:1), the hydrogenation product of dimethyl itaconate was obtained with significant *ee* (enantiomeric excess) for all ester BTAs.

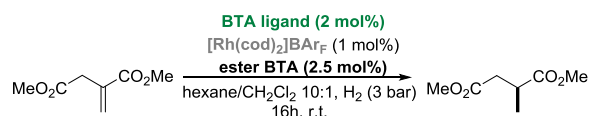
Chart IV-1: Structures of the BTA ligands and co-monomers used in the asymmetric hydrogenation reaction.



The selectivity of the catalytic reaction strongly depends on the nature of ester BTA (40% e.e. < selectivity < 85% e.e.) thus showing the importance of having a library of enantiopure co-monomers at one's disposition for catalytic screening. **BTA Ile** (Entry 10) and **BTA Val** (Entry 9) provided the (S) enantiomer of the hydrogenation product with the best selectivity (85% e.e.), a selectivity similar to the one obtained with chiral monomers ([I], Scheme IV-1).<sup>[19]</sup> By inverting the chirality of the co-monomer, we were able to access both enantiomers of the hydrogenation product with the same BTA ligand. For example, co-monomers **BTA (L)-Nle** and **BTA (D)-Nle** furnish opposite enantiomers with similar *ee* (74% and 72% e.e. respectively, entry 7 and 8). Control experiments (entries 11-12) confirmed that the selectivity of the reaction stems from the formation of hydrogen-bonded co-assemblies between the rhodium complex of **BTA**<sup>PPh<sub>2</sub></sup> and ester BTAs. Indeed, **Me****BTA**<sup>PPh<sub>2</sub></sup>, a BTA ligand in which the amide groups have been *N*-methylated (Chart IV-1),<sup>[19]</sup> shows no selectivity in presence of **BTA Ile** (entry 11). **BTA Ile** alone provided no e.e. either, demonstrating

that ester BTAs do not influence the stereochemical outcome of the catalytic reaction by fortuitous coordination to the Rh center (entry 12).

Table IV-1: Asymmetric hydrogenation of dimethyl itaconate with mixtures of BTA ligand,  $[\text{Rh}(\text{cod})_2]\text{BAR}_F$  and ester BTA: screening of various co-monomers.<sup>[a]</sup>



Entry	BTA ligand	Co-monomer	e.e. (%)
1	<b>BTA<sup>PPh2</sup></b>	<b>BTA Phe</b>	40 ( <i>S</i> )
2	<b>BTA<sup>PPh2</sup></b>	<b>BTA Ala</b>	-46 ( <i>R</i> )
3	<b>BTA<sup>PPh2</sup></b>	<b>BTA Met</b>	53 ( <i>S</i> )
4	<b>BTA<sup>PPh2</sup></b>	<b>BTA Leu</b>	54 ( <i>S</i> )
5	<b>BTA<sup>PPh2</sup></b>	<b>BTA Phg</b>	62 ( <i>S</i> )
6	<b>BTA<sup>PPh2</sup></b>	<b>BTA Abu</b>	-66 ( <i>R</i> )
7	<b>BTA<sup>PPh2</sup></b>	<b>BTA (<i>D</i>)-Nle</b>	-72 ( <i>R</i> )
8	<b>BTA<sup>PPh2</sup></b>	<b>BTA Nle</b>	74 ( <i>S</i> )
9	<b>BTA<sup>PPh2</sup></b>	<b>BTA Val</b>	85 ( <i>S</i> )
10	<b>BTA<sup>PPh2</sup></b>	<b>BTA Ile</b>	85±7 ( <i>S</i> ) <sup>(b)</sup>
11	<b>Me-BTA<sup>PPh2</sup></b>	<b>BTA Ile</b>	0
12	-	<b>BTA Ile</b>	0
13 <sup>[c]</sup>	<b>BTA<sup>PPh2</sup></b>	<b>BTA Ile</b>	<i>nd</i>

(a)  $R^0_{\text{esterBTA}}=1.25$ ,  $n^0_{\text{BTA}^{\text{PPh}_2}}=4.0$   $\mu\text{mole}$ ,  $[\text{dimethyl itaconate}]=0.4$  M. Full conversion except for entry 13. Each experiment was performed in triplicate (except for control experiments 11-13) and the indicated ee corresponds to the average value (standard deviation  $\leq 5\%$ ). Positive value of the ee corresponds to the (*S*) enantiomer.<sup>[25]</sup> See Chart IV-1 for the structures of the BTAs. See the SI for more details on the preparation of the catalytic mixtures. (b) **Based on repeatability tests (16 runs, Table S.1)**. (c) The catalytic mixture is filtered and catalysis is performed with the supernatant: no hydrogenation product was obtained. *nd* = not determined.

We performed additional catalytic experiments with mixtures composed of **BTA<sup>PPh2</sup>** and **BTA Ile** ( $R^0_{\text{BTAlle}}=1.25$ , Table IV-2 and S.2). For catalytic experiments conducted in a mixture of hexane/ $\text{CH}_2\text{Cl}_2$  10:1, the results were repeatable with a mean value of 85±7% e.e. based on 16 runs (Entry 1, Table IV-2 and Table S.1). The amount of  $\text{CH}_2\text{Cl}_2$  in this solvent mixture can be increased to 20% without altering the selectivity (entry 2). However, the selectivity significantly decreases in a more polar hexane/ $\text{CH}_2\text{Cl}_2$  2:1 mixture and in toluene and no selectivity is obtained in  $\text{CH}_2\text{Cl}_2$  (entries 3-5). This is related to the disruption of the hydrogen-bonded assemblies in these solvents.<sup>[19]</sup> In pure hexane, the selectivity appears to vary significantly from one run to another presumably because catalyst aggregates of variable size form under these conditions (Table S.2 and *vide infra*). Changing the nature of the alkane solvent does not significantly influence the selectivity outcome of the reaction (Table S.2).<sup>[26]</sup> While a lower concentration in substrate does not change the selectivity (entry 6), the *ee* significantly drops at higher substrate concentration perhaps as a result of competitive interactions between the substrate and the hydrogen-bonded assemblies (entry 7). Finally, lowering the temperature (-20 °C) leads to a decrease in the selectivity (entry 8 and Table S.2).

Table IV-2: Screening of the catalytic conditions with BTA Ile as the co-monomer ( $R^0_{\text{BTAIle}}=1.25$ )<sup>(a)</sup>

Entry	solvent	[dimethyl itaconate] (M)	e.e. (%)
1	hexane/DCM 10:1	0.4	85±7 (S) <sup>(b)</sup>
2	hexane/DCM 5:1	0.4	85 (S)
3	hexane/DCM 2:1	0.4	52 (S)
4	toluene	0.4	51 (S)
5	DCM	0.4	0
6	hexane/DCM 10:1	0.2	85 (S)
7	hexane/DCM 10:1	0.8	55 (S)
8	hexane/DCM 10:1	0.4	74 (S) <sup>(c)</sup>

(a)  $\text{BTA}^{\text{PPh}_2}$  (2 mol%),  $[\text{Rh}(\text{cod})_2]\text{BAR}_F$  (1 mol%), BTA (*L*)-Ile (2.5 mol%), room temperature unless otherwise stated. Full conversion. Each experiment was performed in duplicate and the indicated ee corresponds to the average value (standard deviation  $\leq 5\%$ ). See Table S.2 for additional screening experiments. (b) Based on repeatability tests (16 runs, Table S.1). (c) Catalytic experiment performed at  $-20^\circ\text{C}$ .

These screening experiments reveal that both the nature of the enantiopure co-monomer and the experimental conditions are crucial factors to obtain optimal selectivity for these catalytic systems. Taken all together, these results indicate that the supramolecular chirality displayed by co-assemblies formed between an achiral ligand monomer and an enantiopure co-monomer ( $R^0_{\text{esterBTA}}=1.25$ ) can be efficiently transferred to the peripheral rhodium centers which in turn promote the hydrogenation reaction with very good enantioselectivity (**[II]**, Scheme IV-1).

### b) Chirality amplification

Encouraged by our initial screening performed with  $R^0_{\text{esterBTA}}=1.25$ , we probed the influence of the amount of enantiopure co-monomer on the selectivity of the catalytic reaction. **BTA Ile**, one of the two most efficient ester BTAs, was selected and was mixed in variable amounts (0.1-8 mol%) to fixed quantities of  $\text{BTA}^{\text{PPh}_2}$  (2 mol%,  $n^0\text{BTA}^{\text{PPh}_2}=4.0 \mu\text{mole}$ ) and  $[\text{Rh}(\text{cod})_2]\text{BAR}_F$  (1 mol%).<sup>[27]</sup> The enantioselectivity of the hydrogenation reaction exhibits a strong dependence on  $R^0_{\text{BTAIle}}$  (Figure IV-1,  $R^0_{\text{BTAIle}}=n^0\text{BTA Ile}/n^0\text{BTA}^{\text{PPh}_2}$ ). In fact, 48% ee is observed for the mixture containing the lowest amount of **BTA Ile** ( $R^0_{\text{BTAIle}}=0.05$  i.e. 0.1 mol% loading in **BTA Ile**); then the ee increases up to a plateau at 78-85% ee for  $0.25 \leq R^0_{\text{BTAIle}} \leq 1.25$  and then decreases for  $R^0_{\text{BTAIle}} > 1.25$ . The non-linear increase of the selectivity of the catalytic reaction (see inset in Figure IV-1) as a function of  $R^0_{\text{BTAIle}}$  clearly reveals that chirality amplification effects are at work in this catalytic system (**[III]**, Scheme IV-1). As a result of these chirality amplification effects, the amount of enantiopure co-monomer can be decreased down to one fourth of that of the ligand without deteriorating the enantioselectivity of the catalytic reaction. Further characterisation is required to relate the chirality amplification effects displayed by this catalyst to the net helicity of the co-assemblies, i.e. to the bias between left and right-handed helical fragments. Also, these effects alone cannot explain the entire selectivity outcome of the catalytic reaction as the enantioselectivity decreases at higher  $R^0_{\text{BTAIle}}$  values ( $R^0_{\text{BTAIle}} \geq 1.5$ ). This suggests that the structure the catalyst evolves as a function of the composition of the co-assemblies (*vide infra*).<sup>[28]</sup>

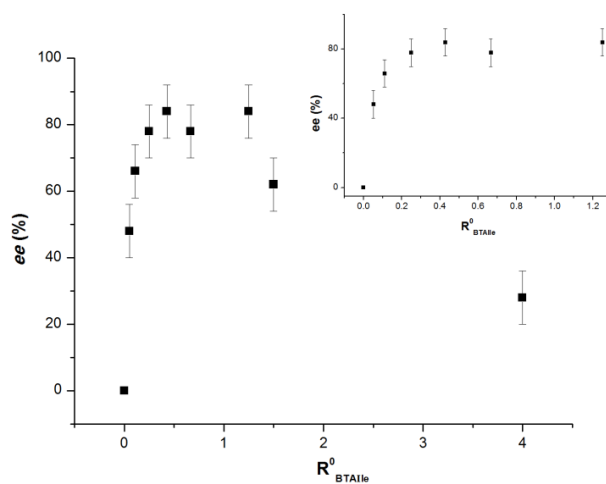


Figure IV-1: Enantioselectivity of the hydrogenation reaction as a function of  $R^0\text{BTAIle}$ .  $R^0\text{BTAIle} = n^{\circ}\text{BTA Ile}/n^{\circ}\text{BTA}^{\text{PPh}_2}$ . Inset: zoom on the region for values of  $R^0\text{BTAIle} < 1.5$ .

### c) Nature of the catalytically active co-assemblies.

In order to rationalise the catalytic results, it is important to gain information into the assembly process and on the solubility properties of the resulting co-assemblies. Firstly, the catalytic mixture ( $\text{BTA}^{\text{PPh}_2} + \text{BTA Ie} + [\text{Rh}(\text{cod})_2]\text{BAR}_F$ ) is prepared in  $\text{CH}_2\text{Cl}_2$ , a solvent in which no selectivity is observed suggesting that co-assembly between  $\text{BTA}^{\text{PPh}_2}$  coordinated to Rh and  $\text{BTA Ie}$  does not occur to a significant extent (Table IV-2). In fact, co-assembly likely occurs upon evaporation of  $\text{CH}_2\text{Cl}_2$  and the rhodium complex remains insoluble as we observed no significant dissolution of the resulting yellow solid upon addition of hexane/ $\text{CH}_2\text{Cl}_2$  10:1, the solvent mixture used in the catalytic experiments. However, this second solvent does have an influence on the size of the solid aggregates as we observed well-dispersed aggregates in hexane/ $\text{CH}_2\text{Cl}_2$  mixtures but not in pure hexane (Table S.2). We also found that the supernatant obtained after filtration of this yellow solid is not catalytically active (Table IV-1, entry 13). If we consider that the solubility of the co-assemblies does not evolve during the catalytic reaction, then this result suggests that the reaction is actually catalyzed by insoluble co-assemblies formed between the rhodium complex of  $\text{BTA}^{\text{PPh}_2}$  and  $\text{BTA Ie}$  after evaporation of  $\text{CH}_2\text{Cl}_2$ .

## 2. Characterisation of the assemblies.

With the objective of correlating the selectivity of the catalytic reaction with the structure of the BTA assemblies, we precisely probed the homo- and co-assembly properties of  $\text{BTA}^{\text{PPh}_2}$  and  $\text{BTA Ie}$ , in solution and in the solid-state, by means of Fourier Transform-Infrared (FT-IR) spectroscopy, UV absorption, Circular Dichroism (CD) and Small Angle Neutron Scattering (SANS) analyses. These analyses were performed both in presence and absence of Rh coordinated to  $\text{BTA}^{\text{PPh}_2}$ .

### a) Homo-assemblies.

When studied separately  $\text{BTA}^{\text{PPh}_2}$  and  $\text{BTA Ie}$  display different association properties in cyclohexane.<sup>[29]</sup>  $\text{BTA}^{\text{PPh}_2}$  forms long and rigid stacks (Figure S.1) as shown by: i) FT-IR bands at 3245

$\text{cm}^{-1}$  (NH bonded to amide CO),  $1634 \text{ cm}^{-1}$  and  $1549 \text{ cm}^{-1}$  (amide CO bonded to NH, amide I and II bands respectively) and, ii) the  $q^{-1}$  dependence of the SANS intensity at low  $q$  values characteristic of isolated cylindrical rigid rods ( $r=12.6 \text{ \AA}$ ,  $L>200 \text{ \AA}$ ). In striking contrast, **BTA IIe** only forms dimers in which the amide NH are linked to the ester carbonyl instead of the amide carbonyl. **BTA IIe** does not form stacks across the whole range of concentration investigated (0.05-50 mM). The dimers of **BTA IIe** possess the same spectroscopic and scattering signature as those previously characterised for **BTA Nle**<sup>[24c]</sup> (for a proposed molecular arrangement and analyses see Figure S.2). The assembly of **BTA IIe** into dimers in cyclohexane is in sharp contrast with its ability to form stacks in the solid-state (Figure S.3). The positive Cotton effect observed above 200 nm in CD analyses infers the preferential formation of right-handed helical stacks<sup>[30]</sup> of **BTA IIe** as previously found in the X-ray structure of a related ester BTA.<sup>[31]</sup>

Importantly, the rhodium complex formed by reacting **BTA**<sup>PPh2</sup> with  $[\text{Rh}(\text{cod})_2]\text{BAR}_F$ , in a 2:1 ratio, is soluble in  $\text{CH}_2\text{Cl}_2$  but not in cyclohexane. UV and FT-IR analyses of the thus obtained solid indicate that this rhodium complex assembles into stacks (Figure S.4b,c). As expected, given that **BTA**<sup>PPh2</sup> is achiral, these stacks show no helical preference (Figure S.4a).

## b) Composition and structure of the co-assemblies

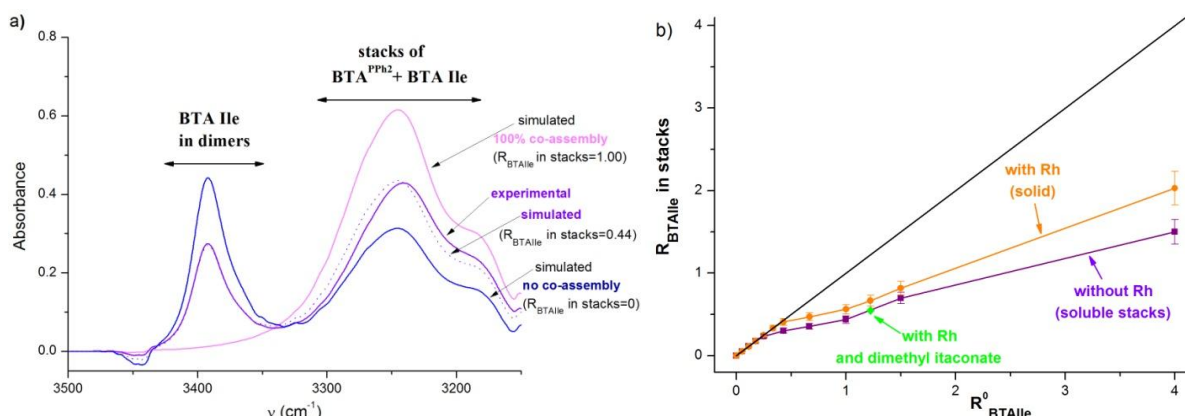


Figure IV-2: Quantification of the amount of **BTA IIe** present in the co-assemblies. Left: FT-IR spectrum (zoom on the NH region) of the mixture of **BTA**<sup>PPh2</sup> and **BTA IIe** ( $R_{\text{BTAIIe}}^0=1.00$ ,  $[\text{BTA}^{\text{PPh2}}]^0=8.0 \text{ mM}$ ) in cyclohexane. Simulated spectra for the extreme cases for which all or no **BTA IIe** is present in the co-assemblies.  $R_{\text{BTAIIe}}^{\text{in stacks}}$  (here 0.44) is deduced from the amount of **BTA IIe** in dimers. Right:  $R_{\text{BTAIIe}}^{\text{in stacks}}$  as a function of  $R_{\text{BTAIIe}}^0$  (with or without Rh coordinated to **BTA**<sup>PPh2</sup>). For the co-assemblies in presence of Rh, the amount of **BTA IIe** in the insoluble stacks is deduced from the amount of **BTA IIe** that remains as dimers in the cyclohexane phase. The black line ( $y=x$ ) helps to visualise mixtures for which **BTA IIe** is fully incorporated into stacks.  $R_{\text{BTAIIe}}^{\text{in stacks}}=n\text{BTA IIe in stacks}/n^0\text{BTA}^{\text{PPh2}}$ .

Upon mixing two complementary monomers, one can envisage: i) the formation of their homo-assemblies exclusively (narcissistic self-sorting), ii) the formation of co-assemblies exclusively (social self-sorting) and iii) an intermediate situation in which homo- and co-assemblies are concomitantly present. Determining whether the co-assembly process follows one of the above hypotheses (i-iii) is challenging particularly when the species have similar analytical signatures. In our case, stacks and dimers can be easily differentiated by means of spectroscopic and scattering analyses which allow us to precisely determine the composition and structure of the co-assemblies. Mixtures of **BTA**<sup>PPh2</sup> and

**BTA IIe**, with fixed amount of **BTA<sup>PPh2</sup>** and variable amount of **BTA IIe** ( $0.05 \leq R_{\text{BTAIIe}}^0 \leq 4.0$ ), proved to be fully soluble in cyclohexane. For mixtures with  $R_{\text{BTAIIe}}^0 \leq 0.18$ , FT-IR analyses show that all **BTA** monomers are in stacks inferring that all **BTA IIe** monomers are incorporated into the co-assemblies (case ii above). In contrast, for others mixtures, FT-IR analyses indicate both the presence of stacks and dimers suggesting that **BTA IIe** only partly co-assembles with **BTA<sup>PPh2</sup>** (case iii). In that case, the quantity of **BTA IIe** that is incorporated into the stacks is deduced from the amount of **BTA IIe** that remains as dimers as measured by FT-IR (Figure IV-2a and S.5) and SANS analyses (Figure S.6). Accordingly, co-assemblies are observed for all mixtures (Table S.3) and the ratio of **BTA IIe** that actually co-assembles with **BTA<sup>PPh2</sup>** is defined as  $R_{\text{BTAIIe in stacks}} = n_{\text{BTA IIe in stacks}} / n_{\text{BTA<sup>PPh2.</sup>$

The same approach can be applied to mixtures of **BTA<sup>PPh2</sup>**, **BTA IIe** and  $[\text{Rh}(\text{cod})_2]\text{BAR}_F$  in order to determine the composition of the co-assemblies between the rhodium complex of **BTA<sup>PPh2</sup>** and **BTA IIe**. Here, all mixtures form heterogeneous suspensions in cyclohexane and characterisation of the soluble part indicates that it only contains **BTA IIe** (in the form of dimers, Figure S.8), *i.e.* all Rh and all ligand is in the solid. For all mixtures, the amount of **BTA IIe** in the soluble phase is significantly lower than the quantity of **BTA IIe** initially introduced in the mixtures, which indicates (and allows us to quantify) the presence of **BTA IIe** in the solid (Table S.4). It is important to note that the presence of **BTA IIe** in the solid demonstrates its co-assembly with the Rh complex of **BTA<sup>PPh2</sup>** since **BTA IIe** is fully soluble in cyclohexane. Thus, in contrast to co-assemblies without Rh, the co-assemblies between **BTA IIe** and the rhodium complex of **BTA<sup>PPh2</sup>** are insoluble and can be isolated from non-incorporated dimers of **BTA IIe** by simple centrifugation.

$R_{\text{BTAIIe in stacks}}$  can be plotted as a function of  $R_{\text{BTAIIe}}^0$  (Figure IV-2b). For both types of co-assemblies (with and without Rh), the same trend is observed. **BTA IIe** is quantitatively incorporated into the co-assemblies for mixtures with  $R_{\text{BTAIIe}}^0 < 0.25$ . For higher **BTA IIe** contents, the incorporation of **BTA IIe** in the co-assemblies levels off (plateau value at  $R_{\text{BTAIIe in stacks}} \approx 0.3-0.5$ ) and then increases again for  $R_{\text{BTAIIe}}^0 \geq 1.0$ . This non-uniform trend can be explained by potentially different thermodynamic stabilities displayed by the co-assemblies depending on their content in **BTA IIe**. Interestingly, the ratio of **BTA IIe** present in both types of co-assemblies (with or without Rh) are virtually the same. It suggests that the coordination of the  $[\text{Rh}(\text{cod})]^+$  fragment to **BTA<sup>PPh2</sup>** does not significantly modify the composition of the co-assemblies.

The structure of the co-assemblies between **BTA IIe** and the Rh complex of **BTA<sup>PPh2</sup>** was then probed in the solid state by UV and FT-IR analyses (Figure S.9). Despite their different composition (Figure IV-2a), similar spectra with bands that are characteristic of the stack form were observed for all mixtures. Accordingly, the different selectivities displayed by the co-assemblies for the catalytic reaction cannot be related to a change in the association pattern of the central **BTA** units.

### c) Chirality of the co-assemblies

The chirality of the co-assemblies, with and without Rh, was then probed by CD spectroscopy. For mixtures of **BTA**<sup>PPh<sub>2</sub></sup> and **BTA** **IIe** (soluble co-assemblies), CD spectra must be interpreted carefully since dimers of **BTA** **IIe** may contribute to the overall CD signals. Importantly, for mixtures with  $R^0_{\text{BTAIIe}} \leq 0.25$ , a Cotton effect is observed, the shape of which is similar to that commonly found in CD spectra of BTA helical stacks exhibiting a preferred handedness in the solid state<sup>[32]</sup> and in solution<sup>[23,30]</sup> (Figure S.7). A similar positive Cotton effect is observed in the CD spectra of the mixtures with Rh (insoluble co-assemblies, Figure IV-3a and Figure S.9)<sup>33</sup> indicating that in both cases right-handed helical stacks are formed.<sup>30</sup> Clearly, **BTA** **IIe** imposes its preferred handedness (as observed for its helical stacks in the solid state, Figure S.3) to the achiral ligand monomers.

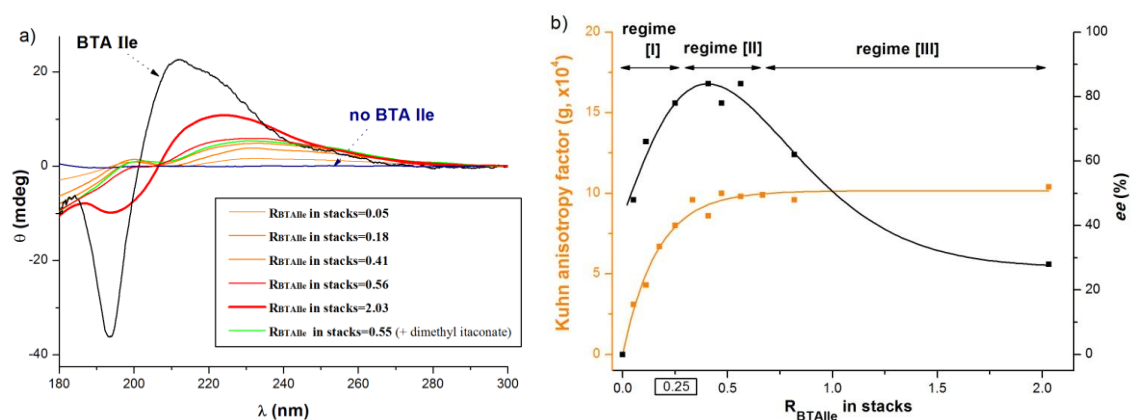


Figure IV-3: a) CD spectra of the co-assemblies formed between the rhodium complex of **BTA**<sup>PPh<sub>2</sub></sup> (8  $\mu\text{mole}$  in **BTA**<sup>PPh<sub>2</sub></sup> for all mixtures) and **BTA** **IIe**. For the CD spectra of all the mixtures see Figure S.9. b) Plots of the anisotropy factor ( $g$ ) of co-assemblies and of the enantioselectivity of the hydrogenation reaction as a function of  $R_{\text{BTAIIe}}$  in stacks. The lines are drawn to guide the eye.  $g$  values measured at  $\lambda=249.0$  nm.

Subsequently, the helicity of the co-assemblies between the Rh complex of **BTA**<sup>PPh<sub>2</sub></sup> and **BTA** **IIe** was measured for all the mixtures and expressed by the Kuhn anisotropy factor ( $g = \Delta\epsilon/\epsilon$  at  $\lambda=249.0$  nm). As expected for helical assemblies displaying chirality amplification properties, the helicity does not increase linearly as a function of the amount of enantiopure monomer in the co-assemblies (*i.e.* as a function of  $R_{\text{BTAIIe}}$  in stacks, Figure IV-3b). Maximum  $g$  values are reached for  $R_{\text{BTAIIe}}$  in stacks  $\geq 0.25$ , which coincides with the minimum content of chiral co-monomer ( $R^0_{\text{BTAIIe}}=0.25$ ) required to obtain the highest enantioselectivity for the hydrogenation reaction.

### 3. Rationalisation of the selectivity outcome

The selectivity observed in the catalytic hydrogenation of dimethyl itaconate (major enantiomer and enantioselectivity) can be related to the structure of the co-assemblies. Firstly, the handedness of the stacks dictates the nature of the major enantiomer. Indeed, the (*R*) hydrogenation product was obtained with our previously investigated chiral BTA ligand<sup>[19]</sup> that formed left-handed helical stacks whereas the (*S*) hydrogenation product is furnished by the rhodium catalyst supported by the right-handed helical co-assemblies of **BTA**<sup>mPPh<sub>2</sub></sup> and **BTA** (*L*)-**IIe**. Secondly, the net helicity of the co-assemblies



explains the first two regimes of the selectivity outcome of the catalytic reaction: stacks containing less than one **BTA (L)-Ile** monomer for four  ${}^H\text{BTA}^{\text{mPPh}_2}$  monomers (regime [I], Figure IV-3), do not (all) have the same handedness, so the catalytic selectivity is not optimal. For stacks containing between *ca.* one fourth and one half of **BTA (L)-Ile** relatively to  ${}^H\text{BTA}^{\text{mPPh}_2}$  (regime [II]), all the stacks have the same handedness (although the composition is evolving), so the catalytic selectivity is roughly constant. For regime [I] and [II], there is a direct correlation between the net helicity of the co-assemblies formed between the Rh complex of  ${}^H\text{BTA}^{\text{mPPh}_2}$  and **BTA (L)-Ile** and the selectivity outcome of the catalytic reaction. It is further corroborated by the fact that dimethyl itaconate, the substrate of the catalytic reaction, has no significant influence on the nature of the co-assemblies (Figure IV-2b and Figure IV-3a), at least at the concentration used in our optimised conditions (Table IV-2).

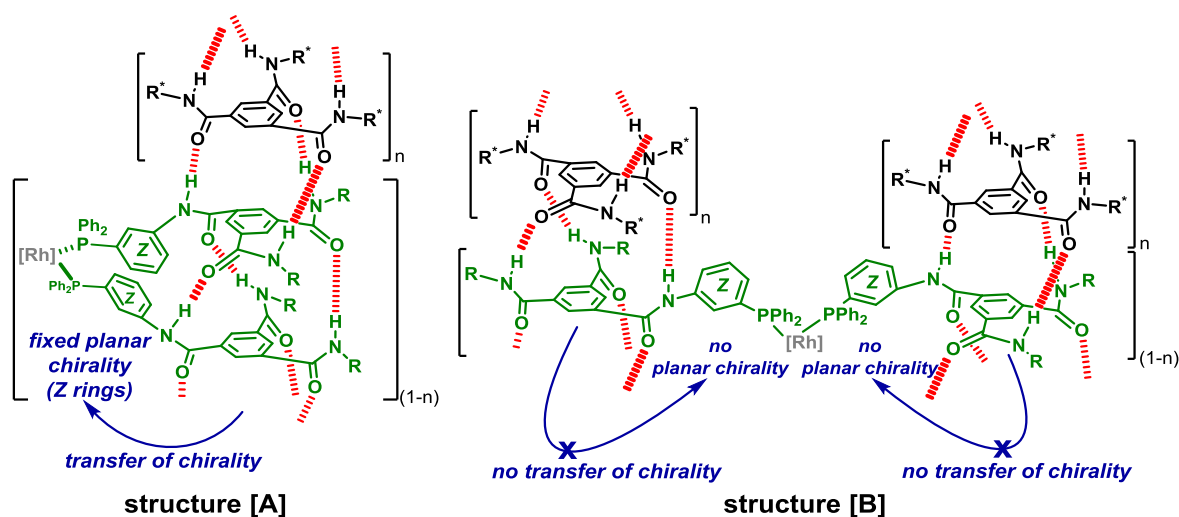


Figure IV-4: Proposed supramolecular **structures [A]** and **[B]** for the catalysts and postulated mechanism for the chirality transfer.

According to our experimental results, the decrease in selectivity observed for mixtures containing higher content of enantiopure co-monomer cannot be explained by a different structure or a lower net helicity of the stacks. To explain this decrease in selectivity (regime [III], Figure IV-3b), we propose that the binding mode of the  $\text{PPh}_2$  units to the Rh center evolves with the composition of the co-assembly (Figure IV-4). In **structure [A]**, two neighboring diphenylphosphino ( $\text{PPh}_2$ ) units maintained by the right-handed helical stacks<sup>[30]</sup> are well positioned to chelate one Rh center.<sup>[34]</sup> We hypothesise that within this structure, chirality transfer occurs from the right-handed helices of the polymeric scaffold to the connecting rings (labeled as *rings Z* in **structures [A]** and **[B]**) facing one another with their *Si,Si* (or *Re,Re*) faces<sup>[35]</sup> and from there to the peripheral  $\text{PPh}_2$  units which may adopt the well-known  $C_2$  quadrant configuration (regimes [I] and [II]). In contrast, increasing the amount of enantiopure co-monomers in the stacks reduces the probability of having two consecutive BTA ligands, which prevents the coordination of Rh by two  $\text{PPh}_2$  units belonging to the same stack. Accordingly, in the speculative **structure [B]**, Rh is acting as a bridge between two right-handed helical stacks and although these stacks exhibit the same handedness they cannot efficiently transfer

their helical chirality *via* a planar chiral rearrangement of the *rings Z* to the environment of the Rh catalytic center (regime [III]).

Based on **structures [A]** and **[B]**, a consistent rationale of the selectivity outcome of the catalytic reaction is obtained. In this specific catalytic system, CD experiments may be used to predict: i) the major enantiomer produced by the catalytic reaction and ii) the minimum amount of chiral co-monomer required to get the optimal selectivity.

## C. Conclusions

The above results clearly reveal the potential of supramolecular helical co-assemblies as efficient scaffolds for asymmetric reactions. Achiral rhodium complexes of BTA ligands, when combined with suitable enantiopure complementary co-monomers, are located within the chiral environment displayed by the co-assemblies and promote the hydrogenation of dimethyl itaconate with good level of enantioinduction. The selectivity of the catalytic reaction is correlated to the handedness, the helicity and the binding mode of the PPh<sub>2</sub> units to the catalytic rhodium center. The handedness and the helicity are dictated by the enantiopure co-monomer while the preferred binding mode of the phosphine ligands is related to their relative position in the helical stacks. Importantly, the helicity of co-assemblies is not proportional to the amount of enantiopure co-monomer. Benefiting from the chirality amplification properties displayed by the co-assemblies, optimal selectivity for the catalytic system can be obtained with the amount of chiral co-monomer being one fourth of that of the achiral ligand. Performing an asymmetric reaction with little or no help of chiral entities raises many fundamental questions with potentially important applications.<sup>[2c]</sup> To date, only very rare but fascinating examples of asymmetric auto-catalysts are able to promote asymmetric reactions by chirality amplification of a minute chiral imbalance.<sup>[2d,2h,36]</sup> To the best of our knowledge, the present asymmetric metal catalyst also constitutes the first example in which a sub-stoichiometric amount of a chiral inducer relative to the achiral ligand can be used without eroding the stereoselectivity of the catalytic reaction. Helped by our proposed rationale of the selectivity outcome of the catalytic reaction, we are currently selecting combinations of achiral and chiral monomers based on their chiroptical properties with the aim of further reducing the amount of chiral inducer needed to get optimal selectivity.

## D. Experimental section

**Materials Preparation.** All amino acids were purchased from Sigma-Aldrich or Alfa Aesar (99% *ee*) and used as received. Benzene-1,3,5-tricarbonyl chloride was purchased from Alfa Aesar, dimethyl itaconate, 1-dodecanol *p*-TsOH.H<sub>2</sub>O, carbonyldiimidazole and trimesic acid were acquired from Sigma Aldrich, and were used directly. The synthesis and characterisation of **BTA**<sup>PPh<sub>2</sub></sup>,<sup>[19]</sup> **MeBTA**<sup>PPh<sub>2</sub></sup>,<sup>[19]</sup> **[Rh(cod)<sub>2</sub>]BAr<sub>F</sub>**,<sup>[37]</sup> **BTA Met**,<sup>[24c]</sup> **BTA Phe**,<sup>[24c]</sup> **BTA Nle**<sup>[24c]</sup> and **BTA (R)-Nle**<sup>[24c]</sup> have been described previously. The experimental details for the synthesis and characterisation of the ester BTAs

are provided in the Supporting Information. Racemic ester BTAs, (*rac*)-BTAs, were prepared for the purpose of determining the optical purity of (*R*)-BTAs and BTAs (enantiomeric and diastereomeric excesses, see the Supporting Information for analytical details).

**Catalytic experiments.** Preparation of the catalytic system: Mother solutions of each component were prepared separately in dry CH<sub>2</sub>Cl<sub>2</sub> without any precaution to exclude air or moisture. This solvent readily dissolves each compound listed below. The following mother solutions are required: ester BTA: 50.0 mM; BTA ligand: 40.0 mM; [Rh(cod)<sub>2</sub>]BAR<sub>F</sub>: 20.0 mM; dimethyl itaconate: 1.0 M. For catalytic reactions performed with variable amounts of **BTA Ile**, a 10.0 mM mother solution of **BTA Ile** was used. The components are then mixed together in glass vials suitable for a 24-well pressurised reactor (CAT-24 reactor provided by HEL®) equipped with small magnetic stirring bars, in the following order: ester BTA (desired volume), BTA ligand (100 μL, 4 μmole), [Rh(cod)<sub>2</sub>]BAR<sub>F</sub> (100 μL, 2 μmole) and dimethyl itaconate (200 μL, 200 μmole). The vials are left open and stirred overnight in a well-ventilated fume-hood (900 m<sup>3</sup>.h<sup>-1</sup> flow) to evaporate the CH<sub>2</sub>Cl<sub>2</sub>. The next day, the vials are dried under a 10<sup>-3</sup> mbar vacuum for 1 hour to obtain a dry, gum-like solid (the dried reaction mixture). Catalysis: The aforementioned dried reaction system is taken up (desired volume) in the desired solvent, sonicated for a few seconds to obtain a bright yellow suspension, briefly heated to solvent reflux, and then transferred to the CAT-24 reactor, which is sealed and set on a magnetic stirrer at room temperature and at 1000 rpm for one hour. The reactor is then purged 3 times with hydrogen gas (3-5 bar) before pressurising it again at 3 bar of H<sub>2</sub>. The hydrogenation is performed at room temperature, 1000 rpm stirring, over 16 hours without compensating H<sub>2</sub> consumption. Determination of the conversion and the enantiomeric excess: The conversion was determined by <sup>1</sup>H NMR after evaporation of the catalytic solutions under vacuum. *Ee* was measured by chiral GC (Betadex 225, capillary 30.0mx250μmx0.25μm, flow = 1.5mL/min, P<sub>He</sub> = 17.6 psi, isotherm at 70°C (10 min) then 2°C/min until 95°C, tr(*R*)=27.5 min, tr(*S*)=27.8 min). For examples of GC spectra (one racemate and the result of the catalytic reaction performed with **BTA Ile** (R<sup>0</sup><sub>BTAIle</sub>=1.25), **BTA<sup>PPh2</sup>** and [Rh(cod)<sub>2</sub>]BAR<sub>F</sub>) see the Supporting Information. Assignment of enantiomers was made according to published data.<sup>25</sup> In Table 1, Table 2, Table S.1 and Table S.2, enantiomeric excesses in favor of the (*R*) enantiomer are set as negative values (those of the (*S*) enantiomer are positive).

**Preparation of <sup>H</sup>BTA<sup>PPh2</sup> and BTA Ile mixtures (without Rh) for spectroscopic analyses:** For FT-IR analyses: Solutions at different R<sup>0</sup><sub>BTAIle</sub> values were made using mother solutions of **BTA<sup>PPh2</sup>** (40.0 mM in CH<sub>2</sub>Cl<sub>2</sub>) and **BTA Ile** (40.0 mM in CH<sub>2</sub>Cl<sub>2</sub>). The components are then mixed together in glass vials equipped with small magnetic stirring bars, in the following order: **BTA Ile** (desired volume) and **BTA<sup>PPh2</sup>** (200 μL, 8 μmole). The vials are left open and stirred overnight in a fume-hood. The resulting solids were put under vacuum (10<sup>-3</sup> mbar) for 3 hours before the addition of 1.0 mL of cyclohexane and sonicated for a few seconds to obtain a solution ([**BTA<sup>PPh2</sup>**]=8.0 mM and 0.42<[**BTA Ile**]<32.0 mM). The solutions were briefly heated to reflux and cooled to r.t. before analyses. For CD

analyses: Solutions with a fixed concentration in **BTA**<sup>PPh<sub>2</sub></sup> (1.0 mM) and variable concentrations in **BTA IIe** (0.05-4.0 mM) were prepared in the same way than solutions for FT-IR analyses. For SANS analyses: Solutions with a fixed concentration in **BTA**<sup>PPh<sub>2</sub></sup> (3.5 g.dm<sup>-3</sup>, 5.1 mM) and variable concentrations in **BTA IIe** (2.2 and 24.5 mM) were prepared in C<sub>6</sub>D<sub>12</sub> in the same way than solutions for FT-IR and CD analyses.

**Preparation of the Rh complex of BTA**<sup>PPh<sub>2</sub></sup> **and BTA IIe mixtures for spectroscopic analyses:** Rh containing mixtures were prepared similarly to those used in the catalytic experiments (*vide supra*). Solutions at different R<sup>0</sup><sub>BTAIIe</sub> values were made using mother solutions of [Rh(cod)<sub>2</sub>]BAR<sub>F</sub> (40.0 mM in CH<sub>2</sub>Cl<sub>2</sub>), **BTA**<sup>PPh<sub>2</sub></sup> (40.0 mM in CH<sub>2</sub>Cl<sub>2</sub>) and **BTA IIe** (40.0 mM in CH<sub>2</sub>Cl<sub>2</sub>). The components are then mixed together in an Eppendorf tube® in the following order: **BTA IIe** (desired volume), **BTA**<sup>PPh<sub>2</sub></sup> (200 µL, 8 µmole) and [Rh(cod)<sub>2</sub>]BAR<sub>F</sub> (100 µL, 4 µmole). In one case (R<sup>0</sup><sub>BTAIIe</sub>=1.22) dimethyl itaconate (400 µmole) was also added to the catalytic mixtures. The resulting solutions were left to evaporate overnight in a fume hood. The resulting solids were put under vacuum (10<sup>-3</sup> mbar) for 3 hours before the addition of 1.0 mL of cyclohexane. The Eppendorf tubes® were sonicated for 1 min before centrifugation using a Gilson GmCLab® at 6000 rpm for 30 min. The resulting solids and supernatants were then separated. The solids were dried under vacuum (10<sup>-3</sup> mbar) for 3 hours.

**FT-IR measurements:** FT-IR measurements were performed on a Nicolet iS10 spectrometer. Solution spectra were measured in KBr or CaF<sub>2</sub> cells of 0.5 mm or 1.0 mm path length and are corrected for air, solvent and cell absorption. FT-IR spectra of the solids were recorded after evaporation of a CHCl<sub>3</sub> solution (8.85 g.L<sup>-1</sup>) of the sample over KBr pellets.

**Circular dichroism (CD):** CD measurements were performed on a Jasco J-1500 spectrometer equipped with a Peltier thermostated cell holder and Xe laser (lamp XBO 150W/4). Data was recorded at 20°C with the following parameters: 20 nm.min<sup>-1</sup> sweep rate, 0.05 nm data pitch and 1.0 nm bandwidth and between 350 and 180 nm. The obtained signals were processed as follow: solvent and cell contribution was subtracted and the signals were smoothed (Savitzky-Golay method). Spectra were corrected for solvent and cell contribution. Kuhn anisotropy factors (g) are dimensionless and expressed as follows:  $g = \Theta / (32980 \times \text{Abs})$ , where  $\Theta$  is the measured ellipticity (mdeg) and Abs the absorbance measured at the same wavelength. For CD measurements in solution, a 1 mm quartz cell (cyclohexane phase of catalytic mixtures) or a 0.1 mm dismountable quartz cell (mixtures of **BTA**<sup>PPh<sub>2</sub></sup> and **BTA IIe**) was used. Molar CD values are reported in L.mol<sup>-1</sup>.cm<sup>-1</sup> and are expressed as follows:  $\Delta\epsilon = \theta / (32980 \times l \times c)$  where  $\theta$  is the measured ellipticity (mdeg), l is the optical path length in cm and c is the total concentration ( $[\text{BTA}^{\text{PPh}_2}] + [\text{BTA IIe}]$ ) in mol.L<sup>-1</sup>. For all samples, LD contribution was negligible ( $\Delta\text{LD} < 0.005$  dOD). For CD measurements of solids, a CHCl<sub>3</sub> solution (8.85g.L<sup>-1</sup>) of the sample was spin coated over a quartz plate using a Laurell WS-650-23 Spin Coater (3000 rpm). For all the samples, no linear dichroism effects were present and the shape of the CD signal was independent of the orientation of the quartz slide.

**UV spectroscopy:** UV absorption spectra were extracted from CD analyses on each of the above samples and obtained after correction for air, solvent and cell absorption.

**Small-angle neutron scattering (SANS) analyses:** SANS measurements were made at the LLB (Saclay, France) on the Pace instrument, at two distance-wavelength combinations to cover the  $4 \times 10^3$  to  $0.24 \text{ \AA}^{-1}$   $q$ -range, where the scattering vector  $q$  is defined as usual, assuming elastic scattering, as  $q=(4\pi/\lambda)\sin(\theta/2)$ , where  $\theta$  is the angle between incident and scattered beam. Data were corrected for the empty cell signal and the solute and solvent incoherent background. A light water standard was used to normalise the scattered intensities to  $\text{cm}^{-1}$  units.

## Supplementary Tables: Catalytic experiments [Table S.1 to S.2]

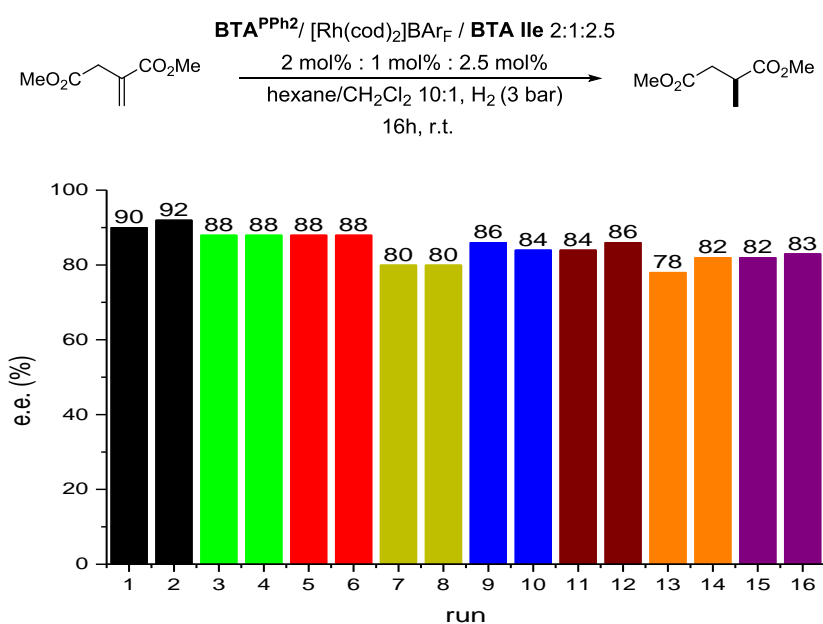
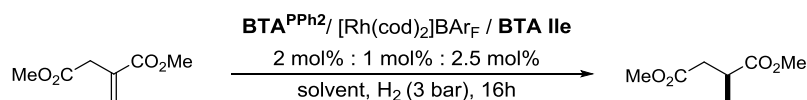


Table S.1 Repeatability of the catalytic experiments performed with BTA<sup>PPh2</sup> and enantiopure co-monomer BTA Ile.<sup>[a]</sup>

[a] The above table summarises 8 batches of duplicate reactions, *i.e.* every color refers to a different batch (reactor), and each column corresponds to a separate run (vial). Based on this repeatability assessment, a mean *ee* value of 85% is determined over the 16 runs. The standard deviation is  $s=4.0$  (4.7%) and the variance is  $s^2=15.7$ . Accordingly, an error bar of  $\pm \frac{1}{2}$  variance ( $\pm 7.8\%$  *ee*) was set to the *ee* values obtained with mixtures of BTA<sup>PPh2</sup> and BTA Ile (Table 1, Table 2 and Figure 1).



Entry	Solvent	Substrate Concentration	Temp. (°C)	ee (%)
1	Hexane	0.4 M	25	79 <sup>[b]</sup>
2	Pentane	0.4 M	25	79
3	Isooctane	0.4 M	25	75
4	Cyclohexane	0.4 M	25	76
5	Methylcyclohexane	0.4 M	25	79
6	Hexane/Toluene 4:1	0.4 M	25	77
7	Hexane/CH <sub>2</sub> Cl <sub>2</sub> 20:1	0.4 M	25	85
8	Methylcyclohexane	0.4 M	-20 <sup>[c]</sup>	74

Table S.2 Additional catalytic experiments performed with BTA<sup>PPh<sub>2</sub></sup> and enantiopure co-monomer BTA IIe.<sup>[a]</sup>

[a] Full conversion is observed in all cases. The (*S*) enantiomer is obtained in excess in all cases.<sup>1</sup> For preparation of the catalytic mixtures: see below. Each experiment was performed in duplicate and the indicated *ee* corresponds to the average value. [b] Repeatability issues were observed in hexane, giving wide variations in *ee* from one run to another. We hypothesised it was related to the formation of catalyst aggregates of variable size. Indeed, an orange gum was observed in this solvent which only partly formed colloidal suspensions even after prolonged sonication or heating. When alkane/CH<sub>2</sub>Cl<sub>2</sub> was used as the solvent mixture for the catalytic experiments, a fine yellow suspension was obtained and the enantioselectivity proved to be repeatable with acceptable standard deviation (see Table S.1). [c] Reactor was stirred 1h at -20°C prior to pressurising it at 3 bar H<sub>2</sub>. Reaction was run overnight at -20°C, then degassed before warming to r.t.

a) **Supplementary Figures: Homo-assemblies formed by BTA<sup>PPh<sub>2</sub></sup>, BTA<sup>Ile</sup> and the rhodium complex of BTA<sup>PPh<sub>2</sub></sup> [Figure S.1 to S.4]**

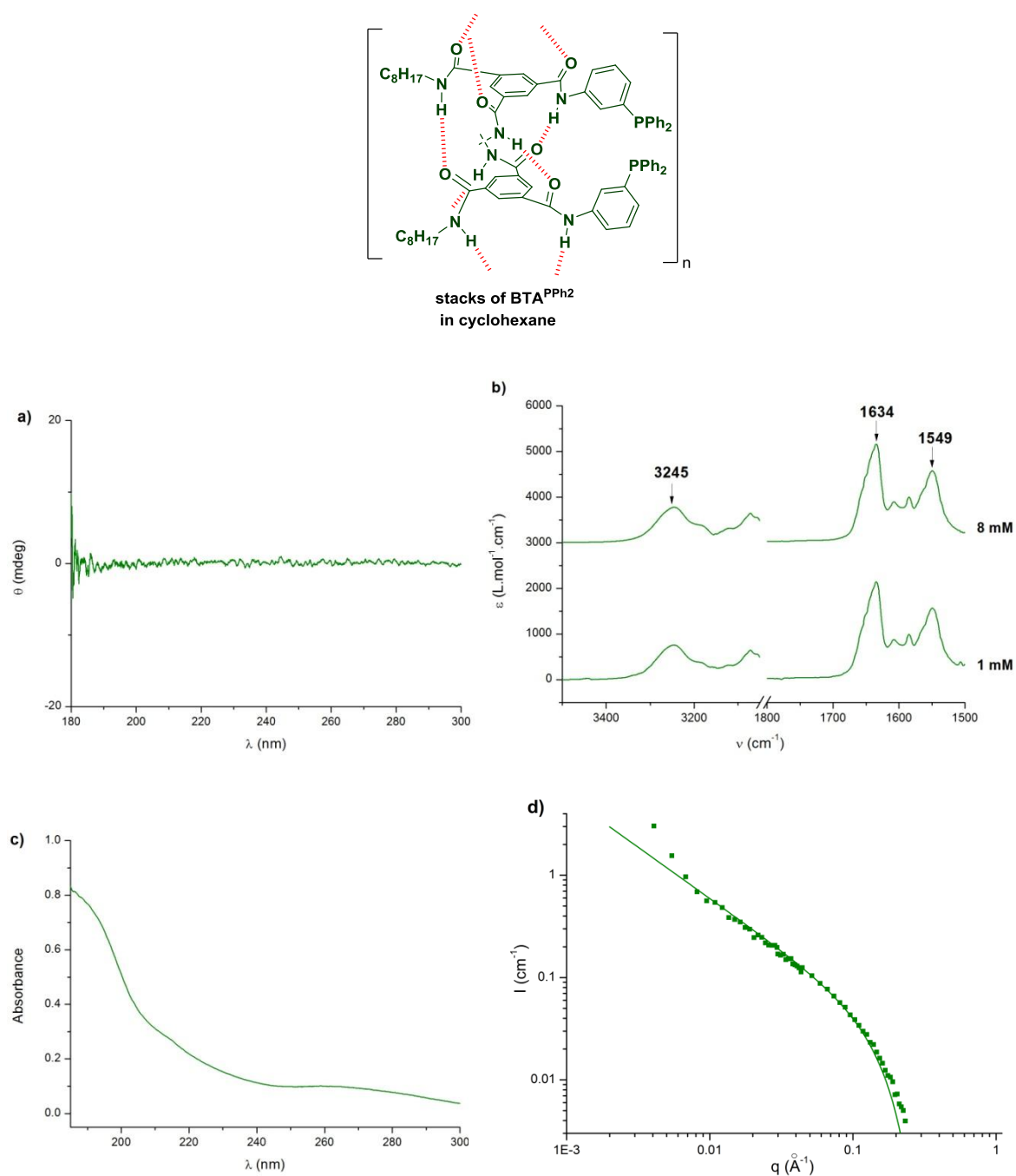


**Figure S.1** Racemic stacks formed by **BTA<sup>PPh<sub>2</sub></sup>** in cyclohexane as characterised by a) CD (0.01mM), b) FT-IR, c) UV (0.01mM) and d) SANS (5.1 mM) analyses.

FT-IR analyses show that the amide groups are hydrogen bonded (the 8 mM spectrum is shown with an offset of 3000 L.mol<sup>-1</sup>.cm<sup>-1</sup>). For SANS analysis (3.5 g.dm<sup>-3</sup>/5.1 mM in C<sub>6</sub>D<sub>12</sub>), the curve is fitted according to the form factor for rigid rods with a circular cross-section and a uniform scattering length density yielding a radius of 12.6 Å. The rods are longer than 200 Å.

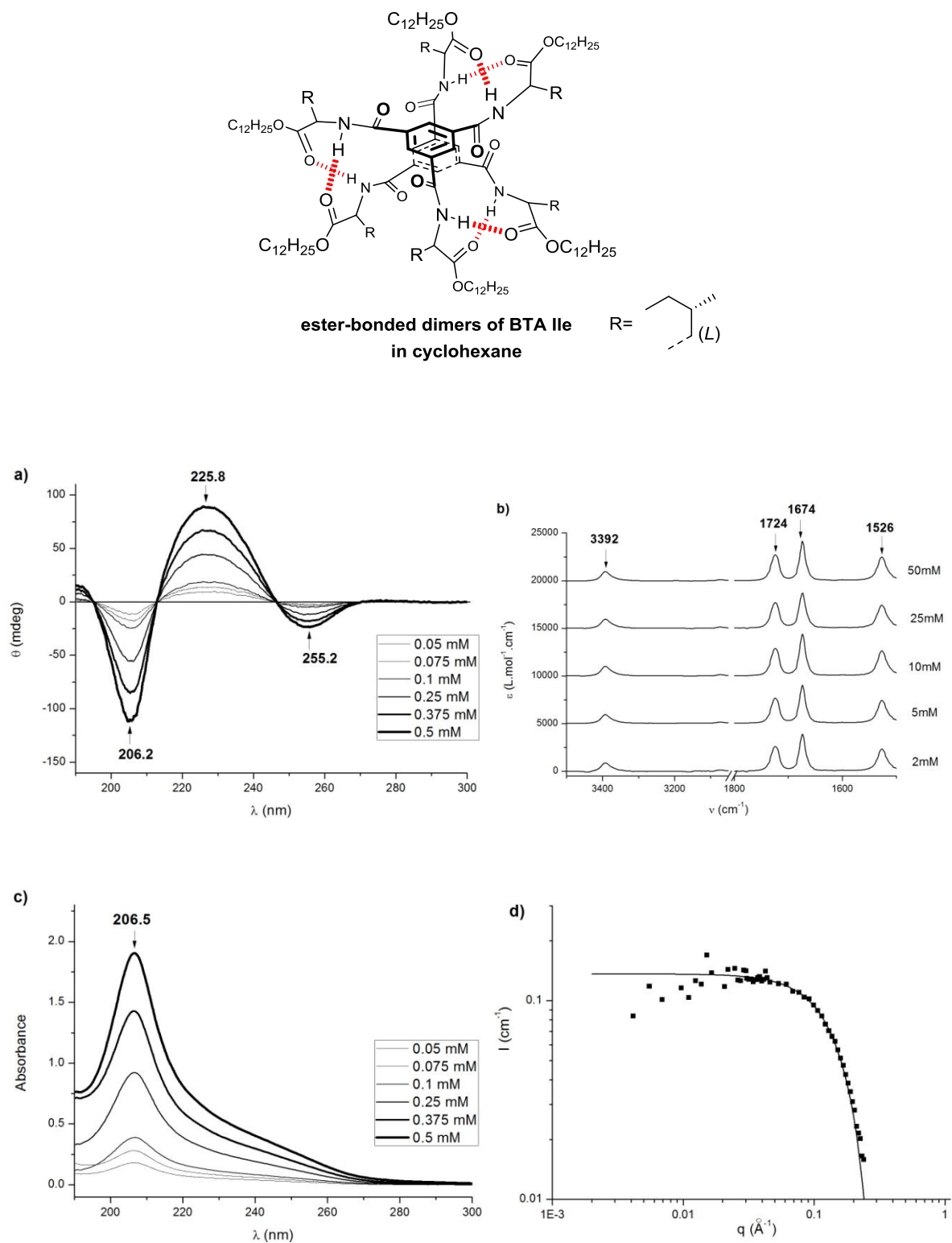


**Figure S.2** Ester-bonded dimers formed by the chiral co-monomer **BTA IIe** in cyclohexane as characterised by a) CD, b) FT-IR, c) UV and d) SANS analyses.

FTIR analyses show that the amide NH groups are hydrogen bonded to ester carbonyls (spectra are shown with an offset of  $5000 \text{ L.mol}^{-1}.\text{cm}^{-1}$ ).<sup>2</sup> For SANS analysis ( $10.6 \text{ g.dm}^{-3}/10.0 \text{ mM}$  in  $\text{C}_6\text{D}_{12}$ ), the curve is fitted according to the form factor for a sphere yielding a radius of  $13.5 \text{ \AA}$  and a mass of  $2000 \text{ g.mol}^{-1}$ . This value confirms that **BTA IIe** exists as a dimeric species ( $M_{\text{spherical object}}/M_{\text{monomer}}=1.9$ ).



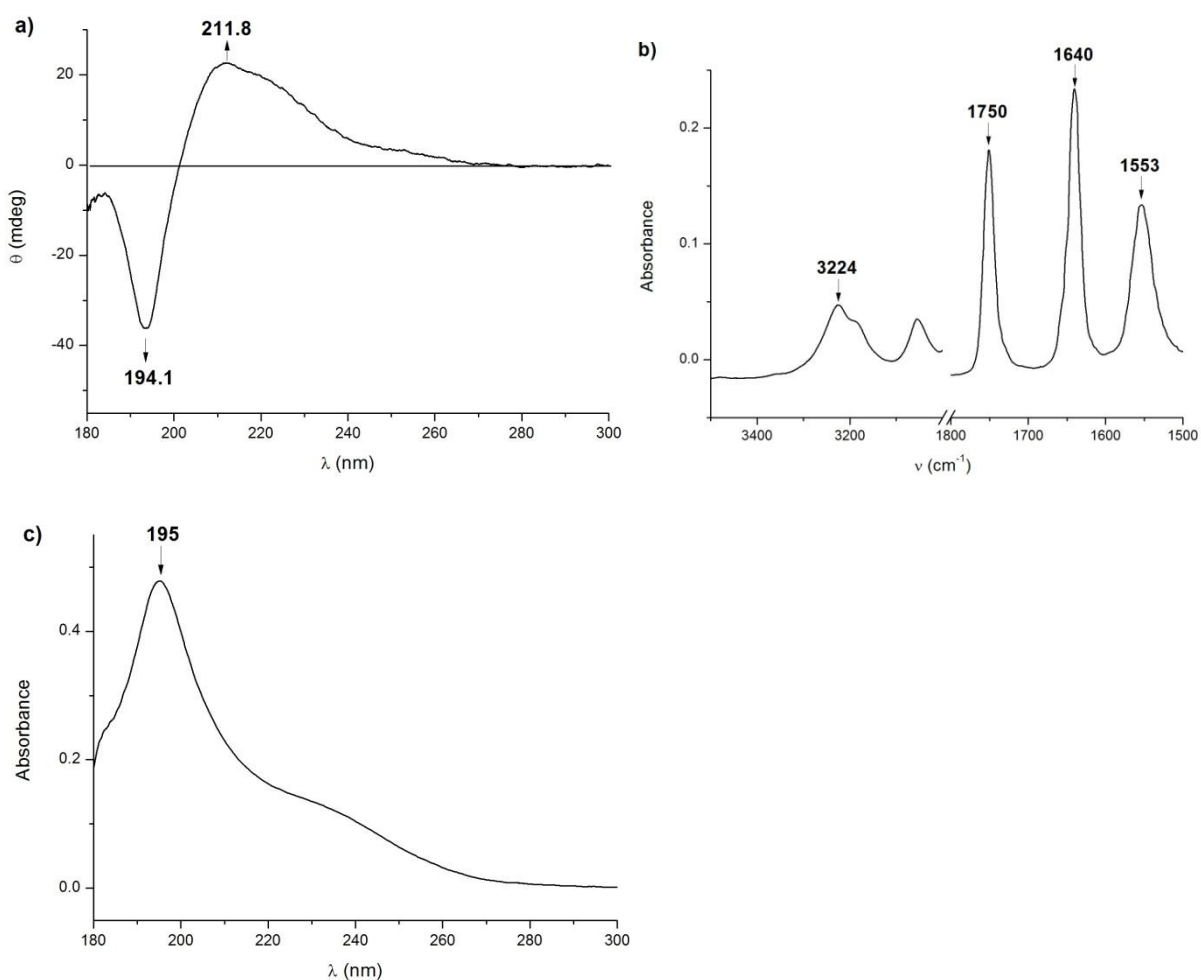
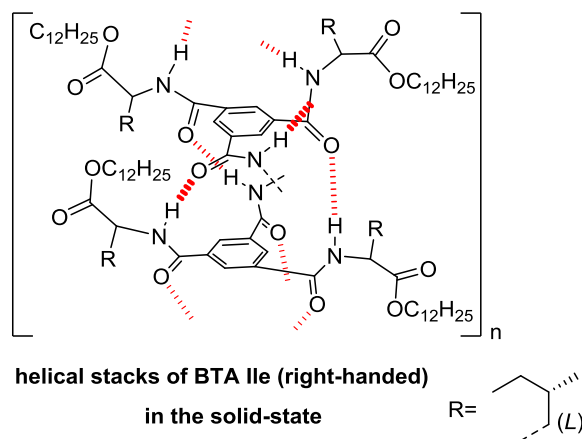


**Figure S.3** Chiral helical stacks formed by the chiral co-monomer **BTA IIe** in the solid-state as characterised by a) CD, b) FT-IR and c) UV.

The samples were prepared by evaporation of a  $\text{CHCl}_3$  solution ( $8.85 \text{ g}\cdot\text{L}^{-1}$ ).

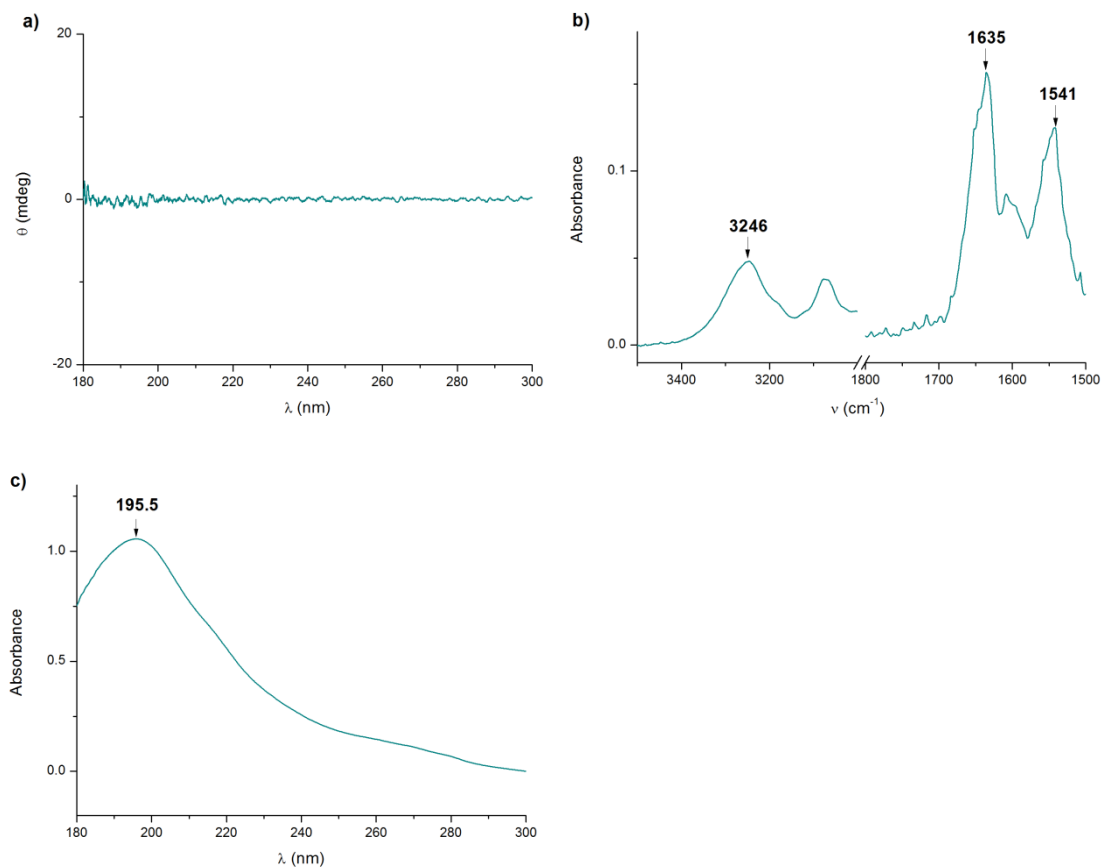
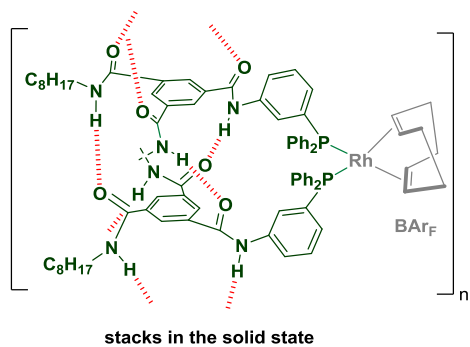


**Figure S.4** Stacks formed by the rhodium complex obtained by reacting **BTA**<sup>PPh<sub>2</sub></sup> with [Rh(cod)<sub>2</sub>]BAr<sub>F</sub> in 2:1 ratio as characterised in the solid-state by a) CD, b) FT-IR and c) UV.

**The samples were prepared by evaporation of a CHCl<sub>3</sub> solution (8.85 g.L<sup>-1</sup>).**

In the represented structure, the three amide groups are oriented in the same direction despite the fact that an "antiparallel" orientation of the amide groups is also plausible.<sup>[38]</sup>

b) **Supplementary Figures: Characterisation of the co-assemblies formed between  $\text{BTA}^{\text{PPh}_2}$  and  $\text{BTA Ile}$  [Figure S.5 to S.7, Table S.3]**

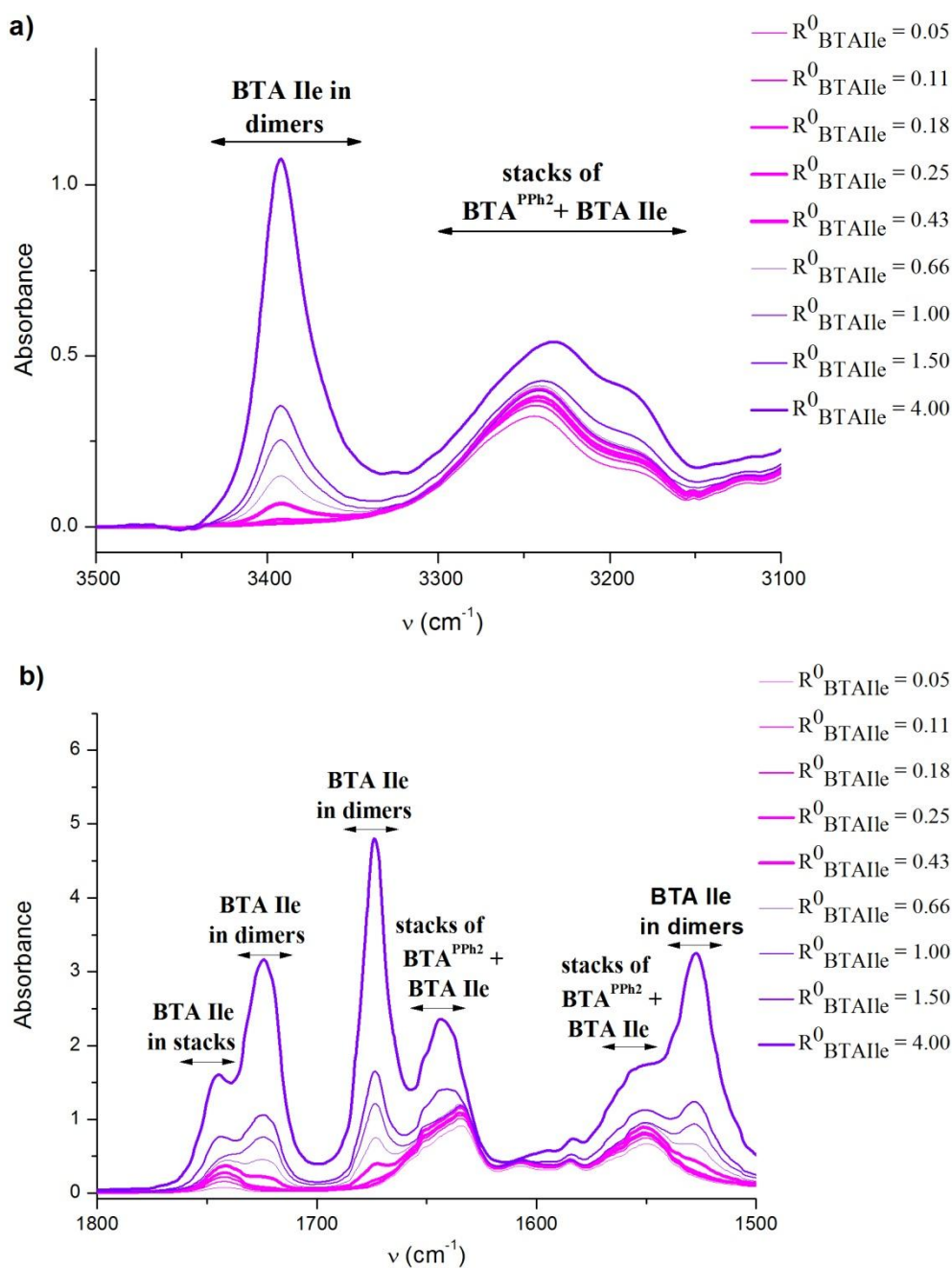


**Figure S.5** Characterisation by FT-IR spectroscopy of the co-assemblies formed between  $\text{BTA}^{\text{PPh}_2}$  and  $\text{BTA Ile}$  in cyclohexane for mixtures at different  $R^0_{\text{BTAIle}}$  values ( $[\text{BTA}^{\text{PPh}_2}]^0 = 8 \text{ mM}$  and  $0.42 < [\text{BTA Ile}]^0 < 32 \text{ mM}$ ). Zoom on a) the NH region and b) the CO region.

$$R^0_{\text{BTAIle}} = n^0 \text{BTA Ile} / n^0 \text{BTA}^{\text{PPh}_2}$$

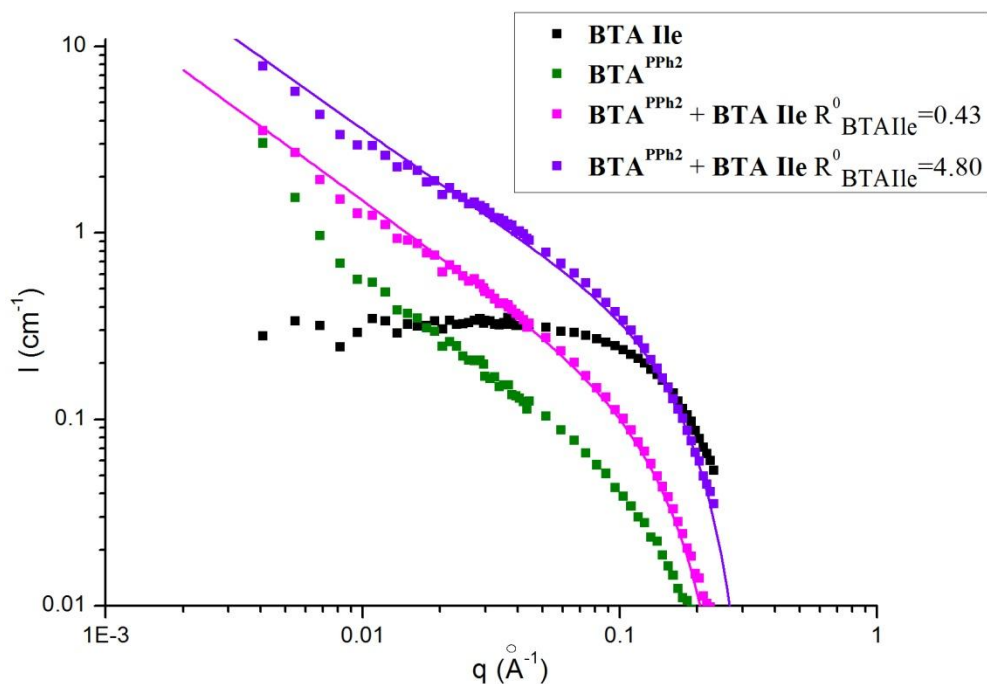


**Figure S.6** Characterisation by SANS analyses of the co-assemblies formed between **BTA<sup>PPh2</sup>** (3.5 g.dm<sup>-3</sup>) and **BTA Ile** in C<sub>6</sub>D<sub>12</sub> solution for mixtures at  $R_{\text{BTAIle}}^0=0.43$  and  $R_{\text{BTAIle}}^0=4.80$ .  $[\text{BTA}^{\text{PPh2}}]^0=5.1$  mM and  $[\text{BTA Ile}]^0=2.2$  mM or 24.5 mM for  $R_{\text{BTAIle}}^0=0.43$  or  $R_{\text{BTAIle}}^0=4.80$  respectively.

Curves for the mixtures at  $R_{\text{BTAIle}}^0=0.43$  and  $R_{\text{BTAIle}}^0=4.80$  are fitted according to the hypothesis that **BTA Ile** in part co-assembles with **BTA<sup>PPh2</sup>** and that the remaining **BTA Ile** exists as dimers. The hypothesis is confirmed by the quality of the fit and by FT-IR analyses presented above (Figure S.5). The fits give the following results:  $R_{\text{BTAIle}}$  in stacks=0.43 or 2.21 for the mixtures at  $R_{\text{BTAIle}}^0=0.43$  or  $R_{\text{BTAIle}}^0=4.80$  respectively. These values are in agreement with the FT-IR data (see Table S.3).

$R_{\text{BTAIle}}^0$	$n^0\text{BTA Ie}$ ( $\mu\text{mole}$ )	$n\text{BTA Ie}$ in dimers ( $\mu\text{mole}$ ) <sup>[a]</sup>	$n\text{BTA Ie}$ in stacks ( $\mu\text{mole}$ )	% of <b>BTA Ie</b> in dimers/stacks	$R_{\text{BTAIle}}$ in <b>stacks</b> <sup>[b],[c]</sup> (soluble stacks)
<b>0.05</b>	0.42	$\leq 0.02$	0.42	0/100	<b>0.05</b>
<b>0.11</b>	0.89	$\leq 0.02$	0.89	0/100	<b>0.11</b>
<b>0.18</b>	1.41	$\leq 0.02$	1.31	0/100	<b>0.18</b>
<b>0.25</b>	2.0	0.1	1.90	1/99	<b>0.24</b>
<b>0.43</b>	3.43	1.00	2.43	29/71	<b>0.30</b>
<b>0.66</b>	5.33	2.5	2.83	47/53	<b>0.35</b>
<b>1.00</b>	8.0	4.5	3.5	56/44	<b>0.44</b>
<b>1.50</b>	12	6.4	5.6	53/47	<b>0.70</b>
<b>4.00</b>	32	20.0	12.0	63/37	<b>1.50</b>

**Table S.3** Amount of **BTA Ie** assembled in dimers and in stacks for mixtures of **BTA<sup>PPh2</sup>** and **BTA Ie** at different  $R_{\text{BTAIle}}^0$  values (cyclohexane,  $n^0\text{BTA}^{\text{PPh2}}=8 \mu\text{mole}$ ). Determination of the fraction of **BTA Ie** present in stacks in absence of Rh ( $R_{\text{BTAIle}}$  in stacks, soluble stacks).

[a] Amount of **BTA Ie** assembled in dimers as determined by deconvolution of the NH bands corresponding to dimers and stacks in the FT-IR analyses (Figure S.3). Sensitivity $\approx 0.02$  mM. Error bar:  $\pm 10\%$ .

[b]  $R_{\text{BTAIle}}$  in stacks =  $n\text{BTA Ie}$  in stacks /  $n^0\text{BTA}^{\text{PPh2}}$

[c] Values in accordance with those deduced from the SANS analyses (Figure S.6). For  $R_{\text{BTAIle}}^0=0.43$ ,  $R_{\text{BTAIle}}$  in stacks = 0.43 and for  $R_{\text{BTAIle}}^0=4.80$ ,  $R_{\text{BTAIle}}$  in stacks = 2.21.

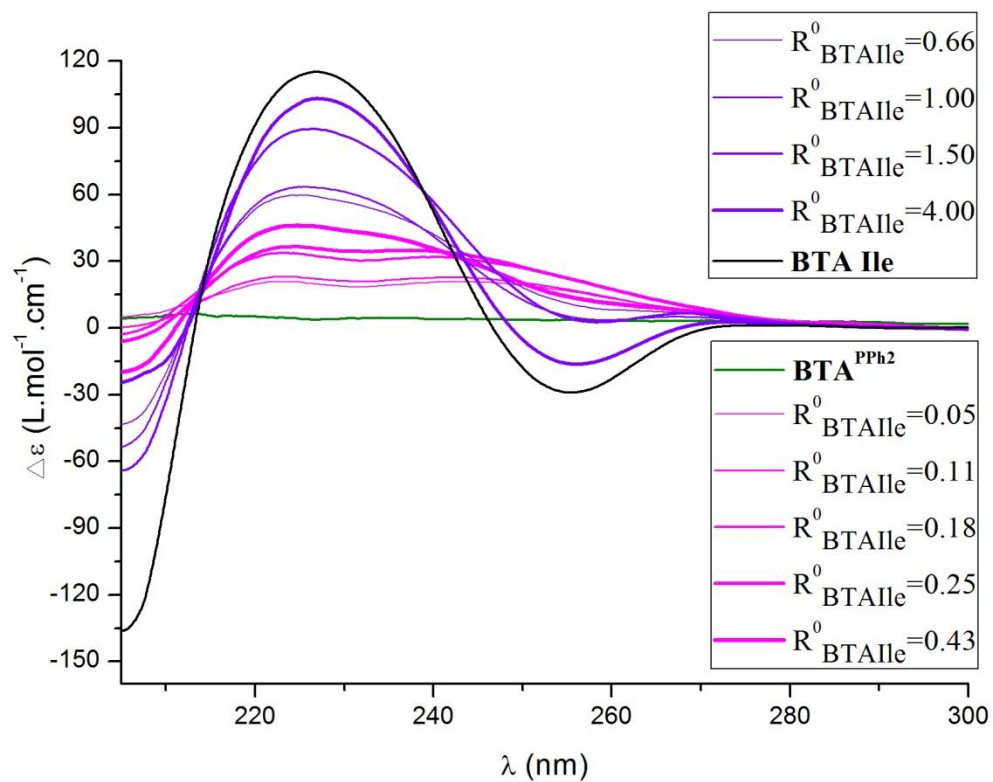


**Figure S.7** CD spectra of mixtures of **BTA<sup>PPh2</sup>** and **BTA Ile** at different  $R^0_{\text{BTAIle}}$  values (cyclohexane,  $[\text{BTA}^{\text{PPh2}}]^0 = 1.0 \text{ mM}$  and  $0 < [\text{BTA Ile}]^0 < 4.0 \text{ mM}$ ).

c) **Supplementary Figures: Characterisation of the co-assemblies formed between the rhodium complex of  $\text{BTA}^{\text{PPh}_2}$  and  $\text{BTA Ile}$  [Figure S.8 to S.9, Table S.3 to S.4]**

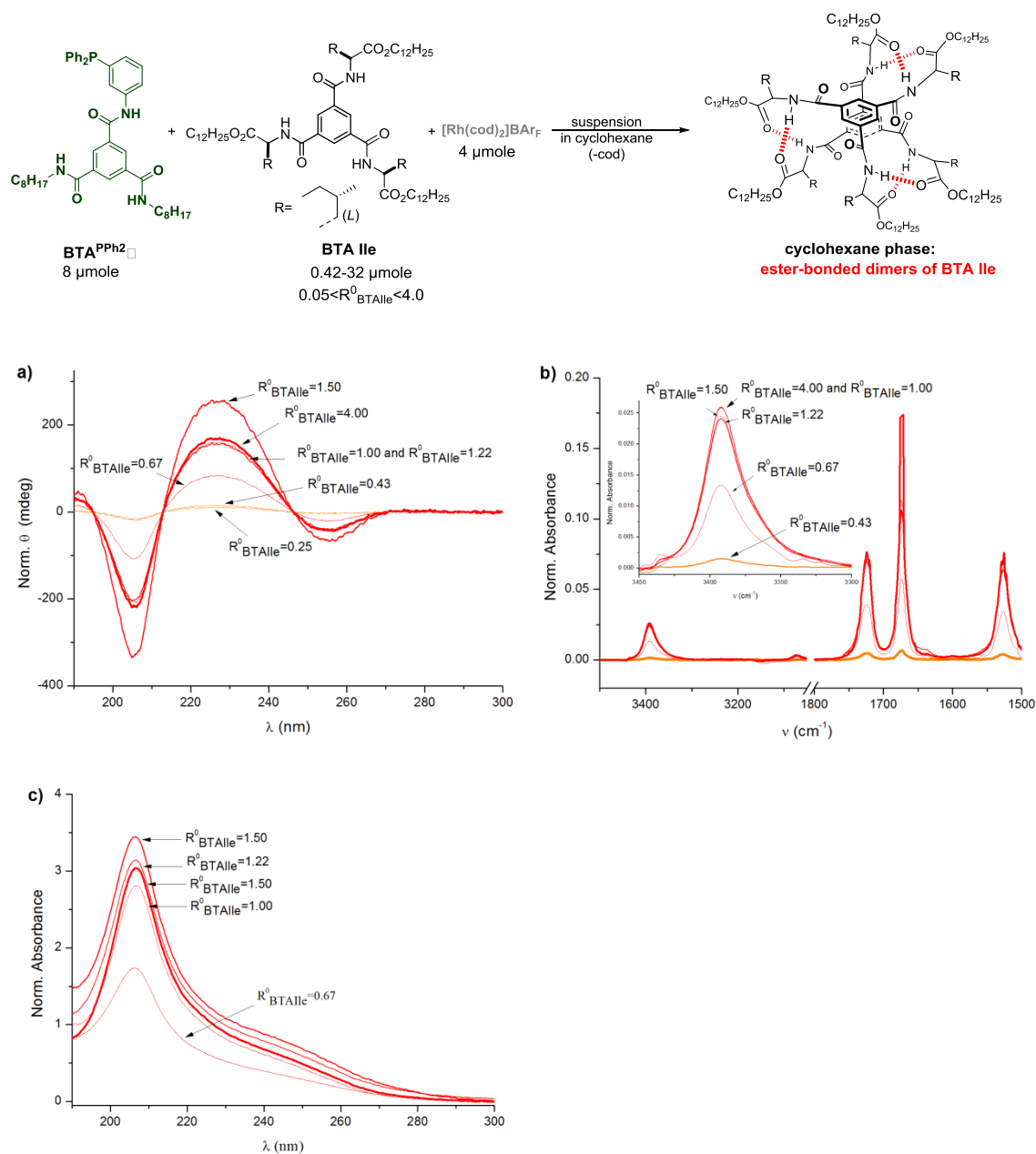


**Figure S.8** Characterisation of the cyclohexane phase (after centrifugation) for mixtures of  $\text{BTA}^{\text{PPh}_2}$  (8  $\mu\text{mole}$ ),  $[\text{Rh}(\text{cod})_2]\text{BAR}_F$  (4  $\mu\text{mole}$ ) and  $\text{BTA Ile}$  (0.42–32  $\mu\text{mole}$ ) at different  $R^0_{\text{BTAlle}}$  values. Only ester-bonded dimers of  $\text{BTA Ile}$  are present as characterised by a) CD, b) FT-IR and c) UV.

Spectra are normalised according to  $[\text{BTA Ile}]^0$  and dilution.

$R^0_{\text{BTAIle}}$	$n^0\text{BTA Ie}$ ( $\mu\text{mole}$ )	<b>BTA Ie</b> in the cyclohexane phase ( $\mu\text{mole}$ ) <sup>[a]</sup>	<b>BTA Ie</b> in the solid ( $\mu\text{mole}$ ) <sup>[d]</sup>	% of <b>BTA Ie</b> in cyclohexane/solid	$R_{\text{BTAIle}}$ <b>in stacks</b> (insoluble stacks)
<b>0.05</b>	0.42	$\leq 0.02$ <sup>[b]</sup>	0.42	0/100	<b>0.05</b>
<b>0.11</b>	0.89	$\leq 0.02$ <sup>[b]</sup>	0.89	0/100	<b>0.11</b>
<b>0.18</b>	1.41	$\leq 0.02$ <sup>[b]</sup>	1.41	0/100	<b>0.18</b>
<b>0.25</b>	2.00	$\leq 0.02$ <sup>[b]</sup>	2.00	0/100	<b>0.25</b>
<b>0.33</b>	2.67	$\leq 0.02$ <sup>[b]</sup>	2.67	0/100	<b>0.33</b>
<b>0.43</b>	3.43	0.1	3.33	3/97	<b>0.41</b>
<b>0.67</b>	5.33	1.6	3.73	30/70	<b>0.47</b>
<b>1.00</b>	8.00	3.5	4.5	44/56	<b>0.56</b>
<b>1.22</b>	9.78	4.5	5.28	46/54	<b>0.67</b>
<b>1.22</b> <sup>[c]</sup>	9.78	5.4	4.38	55/45	<b>0.55</b>
<b>1.50</b>	12.0	5.4	6.6	45/55	<b>0.82</b>
<b>4.00</b>	32.0	15.7	16.3	49/51	<b>2.03</b>

**Table S.4.** Amount of **BTA Ie** assembled into dimers (cyclohexane phase) and into stacks (solid phase) for mixtures of **BTA**<sup>PPH2</sup> (8  $\mu\text{mole}$ ),  $[\text{Rh}(\text{cod})_2]\text{BAR}_F$  (4  $\mu\text{mole}$ ) and **BTA Ie** (0.42-32  $\mu\text{mole}$ ) at different  $R^0_{\text{BTAIle}}$  values. Determination of the ratio of **BTA Ie** in the stacks in presence of Rh ( $R_{\text{BTAIle}}$  **in stacks**, insoluble stacks). [a] Determined by FT-IR analyses (dimers of **BTA Ie**, Figure S.8). Sensitivity $\approx 0.02$  mM. Error bar:  $\pm 10\%$  determined by duplicating the experiment at  $R^0_{\text{BTAIle}}=1.00$  (**BTA Ie** in the cyclohexane phase=3.9  $\mu\text{mol}$  for the duplicated experiment).[b] Below the detection threshold of FT-IR instrument. [c] Experiment performed in presence of dimethyl itaconate (400  $\mu\text{mole}$ ). [d] Obtained by subtracting the amount of **BTA Ie** present in cyclohexane from  $n^0\text{BTA Ie}$ . These values are in accordance with those deduced by weighing the solids: for  $R^0_{\text{BTAIle}}=1.22$ , mass of **BTA Ie**=5.5 mg (5.2  $\mu\text{mole}$ ) and for  $R^0_{\text{BTAIle}}=1.50$ , mass of **BTA Ie**=6.5 mg (6.2  $\mu\text{mole}$ ).



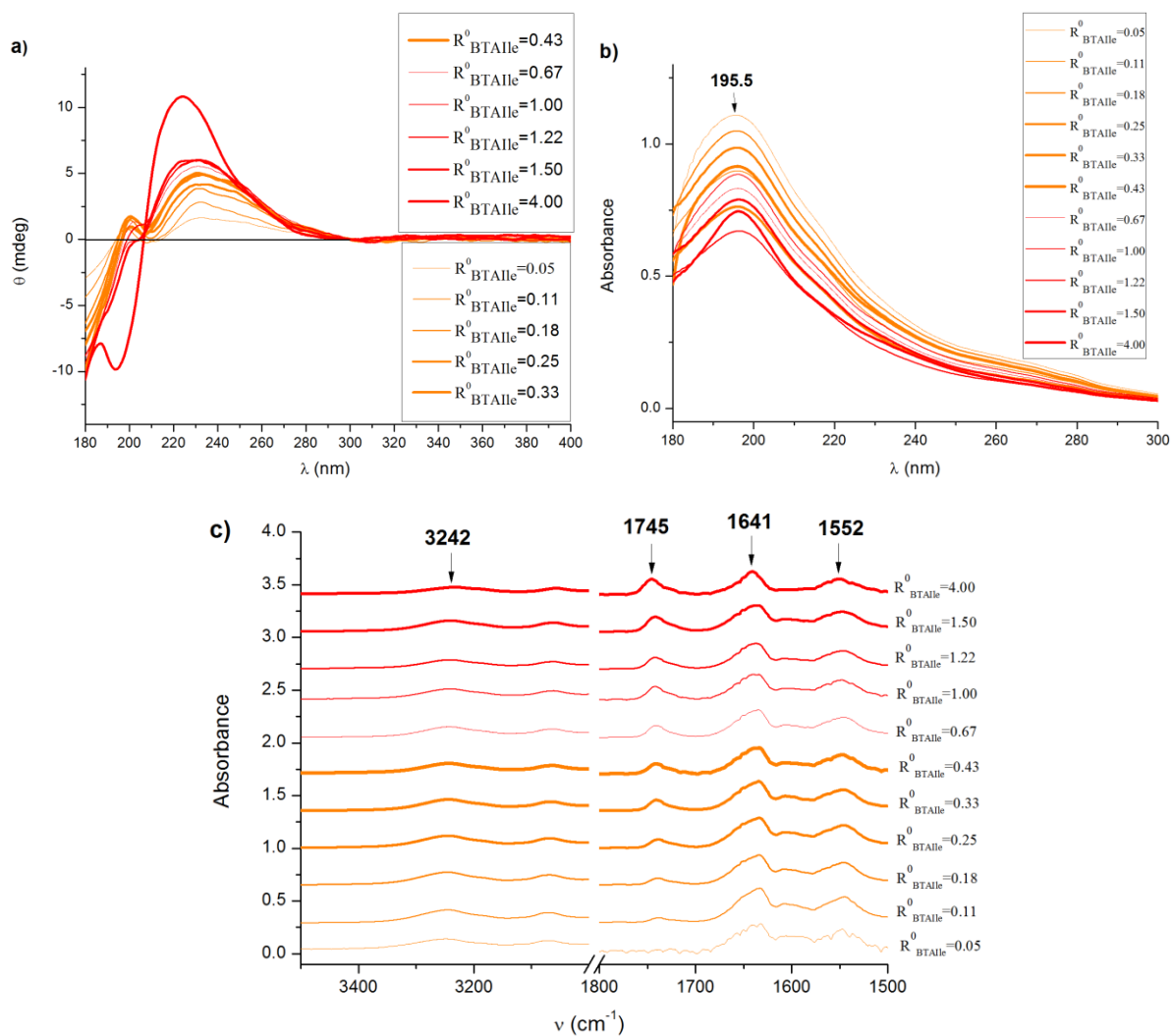
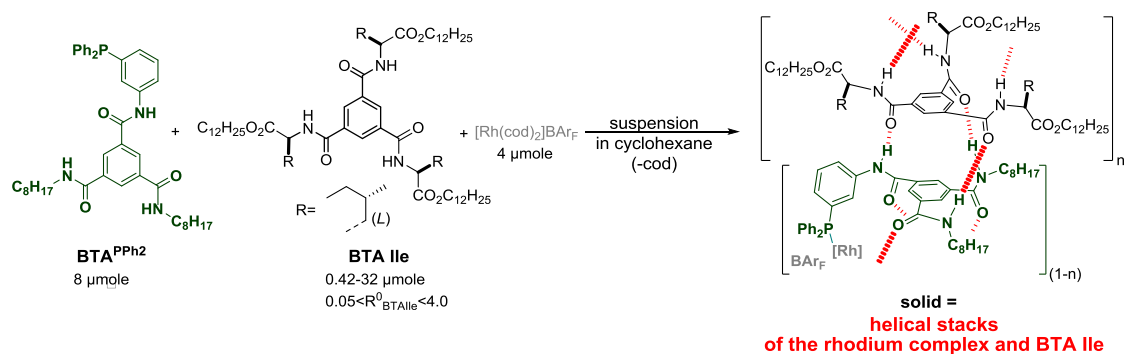


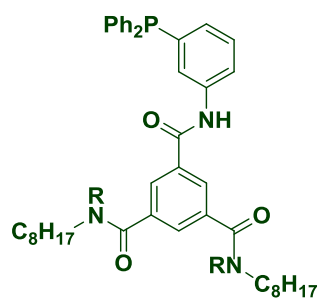
**Figure S.9** Characterisation by a) CD, b) UV and c) FT-IR spectroscopy of the solid obtained (after centrifugation) for mixtures of **BTA<sup>PPh<sub>2</sub></sup>** (8 μmole), **[Rh(cod)<sub>2</sub>]BAR<sub>F</sub>** (4 μmole) and **BTA IIe** (0.42-32 μmole) at different  $R^0_{\text{BTAlIe}}$  values.

The samples were prepared by centrifugation of the cyclohexane dispersion, dissolution of the solid in  $\text{CHCl}_3$ , and evaporation of the  $\text{CHCl}_3$  solution (8.85  $\text{g}\cdot\text{L}^{-1}$ ). CD spectra are normalised according to the UV absorbance at  $\lambda=249.0$  nm (see Table S.5).

$R_{\text{BTAlIe}}^0$	$R_{\text{BTAlIe}}$ in stacks (insoluble stacks)	$\theta$ (mdeg) <sup>[a]</sup>	Abs <sup>[c]</sup>	relative Abs at $\gamma=249.0$ nm	$g$ (anisotropy factor, $\times 10^4$ ) <sup>[d]</sup>
<b>0.05</b>	0.05	2.48	0.244	1.85	3.1
<b>0.11</b>	0.11	2.72	0.190	1.44	4.3
<b>0.18</b>	0.18	5.12	0.231	1.75	6.7
<b>0.25</b>	0.25	5.66	0.214	1.62	8.0
<b>0.33</b>	0.33	4.92	0.155	1.17	9.6
<b>0.43</b>	0.41	6.04	0.212	1.61	8.6
<b>0.67</b>	0.47	5.70	0.173	1.31	10.0
<b>1.00</b>	0.56	6.07	0.188	1.42	9.8
<b>1.22</b>	0.67	4.32	0.132	1.00	9.9
<b>1.22<sup>[b]</sup></b>	0.55	5.32	0.168	1.27	9.6
<b>1.50</b>	0.82	5.03	0.159	1.20	9.6
<b>4.00</b>	2.03	5.13	0.149	1.13	10.4

**Table S.5** Anisotropy factor values for the co-assemblies formed between the Rh complex of **BTA<sup>PPh2</sup>** and **BTA Ie** for mixtures at different  $R_{\text{BTAlIe}}^0$  and  $R_{\text{BTAlIe}}$  in stacks values. [a] Values of the ellipticity at  $\lambda=249.0$  nm. Error bar:  $\pm 5\%$  as determined by duplicating the experiment at  $R_{\text{BTAlIe}}^0=0.43$  (Anisotropy factor  $g=8.2$  for the duplicated experiment). [b] Experiment performed in presence of dimethyl itaconate (400  $\mu\text{mole}$ ). [c] Values of the absorbance at  $\lambda=249.0$  nm. [d]  $g=\theta/(32980\times\text{Abs})$ , measured at  $\lambda=249.0$  nm.

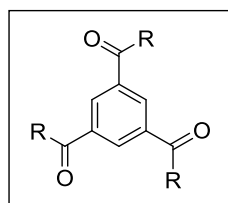
### achiral BTA ligands



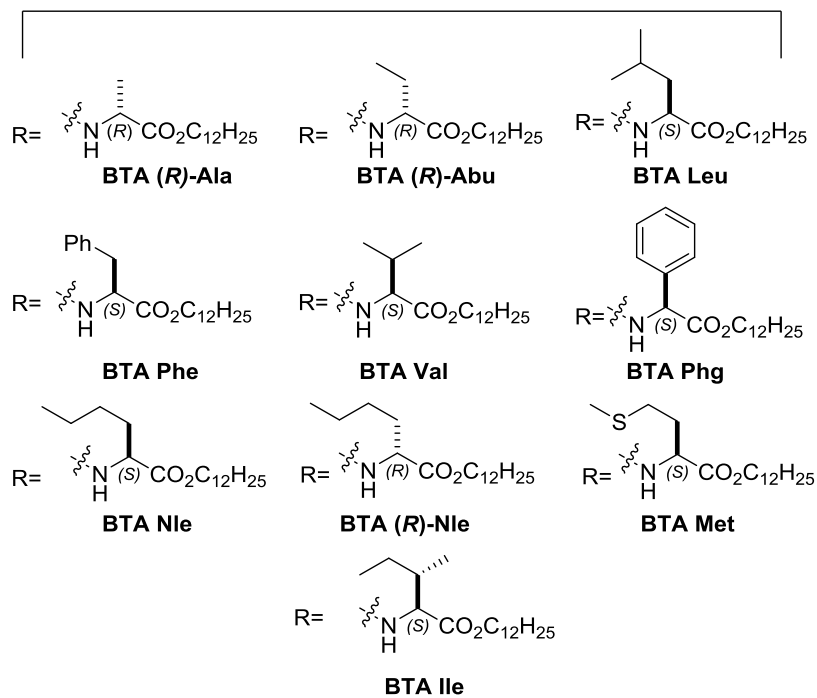
R = H, **BTA<sup>PPH2</sup>**

R = Me, **MeBTA<sup>PPH2</sup>** (control)

### enantiopure co-monomers = Ester BTAs



**Ester BTAs**



Structure of the achiral BTA ligands and of the ester BTAs used in the asymmetric hydrogenation reaction.

## Synthetic procedures.

All amino acids were purchased from Sigma-Aldrich or Alfa Aesar (99% *ee*) and used as received. Benzene-1,3,5-tricarbonyl chloride was purchased from Alfa Aesar, dimethyl itaconate, 1-dodecanol *p*-TsOH.H<sub>2</sub>O, carbonyldiimidazole and trimesic acid were acquired from Sigma Aldrich, and were used directly. The synthesis and characterization of **BTA**<sup>PPh<sub>2</sub></sup>,<sup>[19]</sup> **MeBTA**<sup>PPh<sub>2</sub></sup>,<sup>[19]</sup> [Rh(cod)<sub>2</sub>]BAr<sub>F</sub>,<sup>[37]</sup> **BTA Met**,<sup>[23c]</sup> **BTA Phe**,<sup>[23c]</sup> **BTA Nle**<sup>[23c]</sup> and **BTA (R)-Nle**<sup>[23c]</sup> have been described previously.

**Unless otherwise noted, chromatography-grade solvents were used as received. Dried solvents were obtained from an SPS solvent purification system (IT-Inc) and stored on 4Å molecular sieves. Triethylamine was dried by distillation over CaH<sub>2</sub> and stored over 4Å molecular sieves. All inert atmosphere reactions were carried out under an argon atmosphere with standard Schlenk-line techniques.**

NMR spectra were recorded on a Bruker Avance 300 spectrometer and calibrated to the residual solvent peak: DMSO-d<sub>6</sub> (<sup>1</sup>H: 2.50 ppm; <sup>13</sup>C: 39.52 ppm); Acetone-d<sub>6</sub> (<sup>1</sup>H: 2.05 ppm; <sup>13</sup>C: 29.84 ppm); CDCl<sub>3</sub> (<sup>1</sup>H: 7.26 ppm). Peaks are reported with their corresponding multiplicity (s: singlet; d: doublet, t: triplet; q: quartet; p: pentuplet; hept: heptuplet; dt: doublet of triplets; td: triplet of doublets) and integration, and respective *J* coupling constants are given in Hertz. Exact mass measurements (HRMS) were obtained on TQ R30-10 HRMS spectrometer by ESI+ ionization and are reported in *m/z* for the major signal. FT-IR analyses of the solids were performed on a Nicolet iS10 spectrometer in ATR (diamond probe) or in transmission between KBr disks.

Racemic ester BTAs, (*rac*)-BTAs, were prepared for the purpose of determining the optical purity of (*R*)-BTAs and BTAs (enantiomeric and diastereomeric excesses, see pages S22-S24 for analytical details).

### General Method A: Synthesis of dodecyl ester *p*-TsOH salts of amino-acids:

In a Dean-Stark apparatus-mounted two-neck flask, the amino acid (1 eq., 15.0 mmol) is suspended in toluene (0.1 M, 150 mL), and *p*-TsOH.H<sub>2</sub>O (1.2 eq., 18.0 mmol) is added at room temperature. Dodecanol (1.1 eq., 16.5 mmol) is then added, and the resulting slurry is stirred at reflux temperature overnight. After cooling the reaction mixture to room temperature, the crude reaction mixture is evaporated under reduced pressure to give a thick oil or a solid. This residue is taken up in ca. 70 mL of Et<sub>2</sub>O, gently heated to 35°C, and let cool in an ice bath. The resulting precipitate is filtered under vacuum and washed with ice-cold ether to remove residual reactants. The white solid is then dried under vacuum to yield the pure ammonium tosylate (63-97% yield).

When the ammonium tosylate is somewhat soluble in Et<sub>2</sub>O (*e.g.* **BTA Leu**), the crude reaction mixture is washed with heptane instead, and used as such for the next step.

### General Method B: Synthesis of ester BTAs:

In a flame-dried round-bottom flask under argon atmosphere, benzene-1,3,5-tricarbonyl chloride (1 eq., 3.0 mmol) is dissolved in dry CH<sub>2</sub>Cl<sub>2</sub> (100 mL) at room temperature. The ammonium tosylate (3.3 eq.; 9.9 mmol) is then added in one portion, and the resulting mixture is cooled to 0°C with an ice/water bath. Dry Et<sub>3</sub>N is then added dropwise, the reaction is let warm to room temperature and stirred for 36-42h. Brine is then added to the flask, and the crude mixture is extracted thrice with CH<sub>2</sub>Cl<sub>2</sub>. The combined organic phases are dried over MgSO<sub>4</sub>, filtered, and the solvent is evaporated under reduced pressure. The resulting solid is taken up as a slurry in a little CH<sub>2</sub>Cl<sub>2</sub>, and purified on a short column of silica gel (elution: CH<sub>2</sub>Cl<sub>2</sub>/EtOAc 6:1) to remove salts and impurities (R<sub>f</sub> ~ 0.85-0.9). The product is repurified by column chromatography on silica gel, eluting with petroleum ether/EtOAc 95:5 – 80:20 gradient (R<sub>f</sub> ~ 0.1–0.2). The pure BTA is isolated as a sticky white gum (53-87% yield).

#### **BTA (*R*)-Ala:**

Obtained from (*R*)-alanine using General Method A, then B, with an overall yield of 72%, as a white gum.

<sup>1</sup>H NMR (300 MHz, DMSO-d<sub>6</sub>) δ 9.03 (d, *J* = 6.9 Hz, 3H), 8.49 (s, 3H), 4.49 (p, *J* = 7.2 Hz, 3H), 4.12 – 4.00 (m, 6H), 1.56 (dt, *J* = 13.7, 6.8 Hz, 6H), 1.43 (d, *J* = 7.3 Hz, 9H), 1.27 – 1.21 (m, 54H), 0.85 (t, *J* = 6.7 Hz, 9H). <sup>13</sup>C{<sup>1</sup>H} (75 MHz, Acetone-d<sub>6</sub>): δ 173.7, 166.7, 136.1, 129.9, 65.9, 50.0, 32.9, 30.62, 30.61, 30.56, 30.5, 30.2, 29.7, 26.8, 23.6, 17.8, 14.6. **HRMS:** Calculated for C<sub>54</sub>H<sub>94</sub>N<sub>3</sub>O<sub>9</sub> [M+H]<sup>+</sup>: 928.6985, found: 928.6979. **IR** (solid, ATR diamond) see page S20-S21. *ee*>99%, *de*=94%.

#### **BTA (*R*)-Abu:**

Obtained from (*R*)-3-aminobutyric acid using General Method A, then B, with an overall yield of 87%, as a white gum.

<sup>1</sup>H NMR (300 MHz, DMSO-d<sub>6</sub>): δ 8.98 (d, *J* = 7.2 Hz, 3H), 8.49 (s, 3H), 4.36 (dd, *J* = 14.3, 7.3 Hz, 3H), 4.13 – 4.00 (m, 6H), 1.92 – 1.76 (m, 6H), 1.61 – 1.52 (m, 6H), 1.30 – 1.20 (m, 54H), 0.97 (t, *J* = 7.4 Hz, 9H), 0.85 (t, *J* = 6.7 Hz, 9H). <sup>13</sup>C{<sup>1</sup>H} NMR (75 MHz, Acetone-d<sub>6</sub>) δ 173.1, 167.0 166.9, 136.2, 130.1, 65.8, 55.8, 32.9, 30.62, 30.60, 30.5, 30.2, 29.7, 26.9, 25.9, 23.6, 14.6, 11.2. **HRMS:** Calculated for C<sub>57</sub>H<sub>100</sub>N<sub>3</sub>O<sub>9</sub> [M+H]<sup>+</sup>: 970.7454, found: 970.7451. **IR** (solid, ATR diamond) see page S20-S21. *ee*>99%, *de*=96%.

#### **BTA Val:**

Obtained from (*S*)-valine using General Method A, then B, with an overall yield of 56%, as an off-white gum.

<sup>1</sup>H NMR (300 MHz, CDCl<sub>3</sub>) δ 8.43 (s, 3H), 6.87 (d, *J* = 8.6 Hz, 3H), 4.78 (dd, *J* = 8.6, 5.0 Hz, 3H), 4.18 (td, *J* = 6.7, 2.3 Hz, 6H), 2.30 (dq, *J* = 13.6, 6.8 Hz, 3H), 1.68 (dd, *J* = 13.8, 7.2 Hz, 6H), 1.39 – 1.25 (m, 54H), 1.02 (dd, *J* = 6.7, 5.8 Hz, 18H), 0.88 (t, *J* = 6.7 Hz, 9H). <sup>13</sup>C{<sup>1</sup>H} NMR (75 MHz, Acetone-d<sub>6</sub>) δ 172.6, 167.2, 136.3, 130.3, 65.8, 59.8, 32.9, 31.8, 30.63, 30.57, 30.5, 30.2, 29.7, 26.9,

23.6, 19.9, 19.3, 14.6. **HRMS:** Calculated for C<sub>60</sub>H<sub>106</sub>N<sub>3</sub>O<sub>9</sub> [M+H]<sup>+</sup>: 1012.7924, found: 1012.7922. **IR** (solid, ATR diamond) see page S20-S21. *ee*>99%, *de*>99%.

#### **BTA Ile:**

Obtained from (*S*)-isoleucine using General Method A, then B, with an overall yield of 63%, as an off-white gum.

<sup>1</sup>H NMR (300 MHz, Acetone-d<sub>6</sub>) δ 8.43 – 8.40 (m, 3H), 8.05 – 7.99 (m, 3H), 4.65 (app. dt, *J* = 17.1, 8.5 Hz, 3H), 4.16 (app. pd, *J* = 10.8, 6.5 Hz, 6H), 1.72 – 1.57 (m, 9H), 1.43 – 1.29 (m, 60H), 1.04 – 0.84 (m, 27H).; <sup>13</sup>C{<sup>1</sup>H} NMR (75 MHz, Acetone-d<sub>6</sub>) δ 172.7, 167.0, 136.2, 130.2, 65.8, 58.8, 38.4, 32.9, 30.7, 30.66, 30.6, 30.56, 30.2, 29.7, 27.0, 26.7, 23.6, 16.4, 14.7, 12.0. **HRMS:** Calculated for C<sub>63</sub>H<sub>112</sub>N<sub>3</sub>O<sub>9</sub> [M+H]<sup>+</sup>: 1054.8393, found: 1054.8389. **IR** (solid ATR diamond) see page S20-S21. *ee*>99%, *de*>99%.

#### **BTA Leu:**

Obtained from (*S*)-leucine using General Method A, then B, with an overall yield of 53%, as an off-white gum.

<sup>1</sup>H NMR (300 MHz, Acetone-d<sub>6</sub>) δ 8.48 (s, 3H), 8.24 (d, *J* = 7.8 Hz, 3H), 4.73 (td, *J* = 9.7, 5.0 Hz, 3H), 4.13 (td, *J* = 6.6, 1.7 Hz, 6H), 1.90 – 1.80 (m, 6H), 1.77 – 1.60 (m, 9H), 1.42 – 1.28 (m, 54H), 0.98 (dd, *J* = 6.2, 1.6 Hz, 18H), 0.88 (t, *J* = 6.5 Hz, 9H); <sup>13</sup>C{<sup>1</sup>H} NMR (75 MHz, Acetone-d<sub>6</sub>) δ 172.4, 165.7, 135.0, 128.9, 64.7, 51.6, 40.4, 31.7, 29.5, 29.4, 29.3, 29.0, 28.5, 25.7, 24.8, 22.4, 22.4, 21.0, 13.4. **HRMS:** Calculated for C<sub>63</sub>H<sub>112</sub>N<sub>3</sub>O<sub>9</sub> [M+H]<sup>+</sup>: 1054.8393, found: 1054.8390. **IR** (solid, ATR diamond) see page S20-S21.

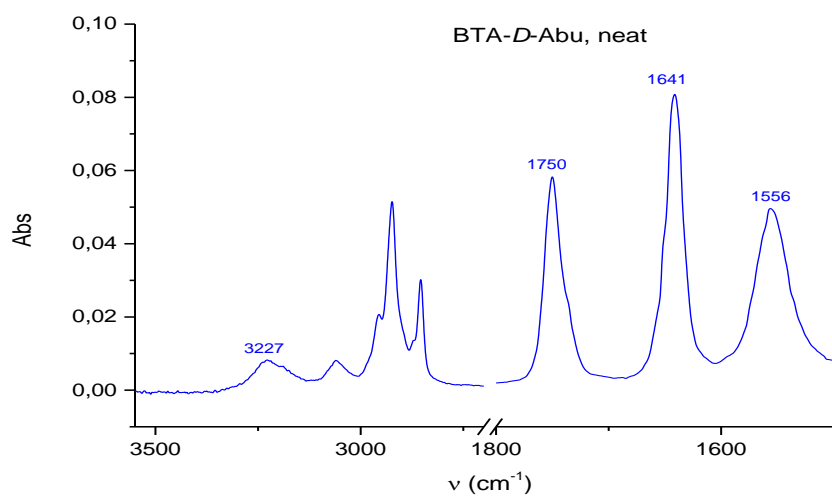
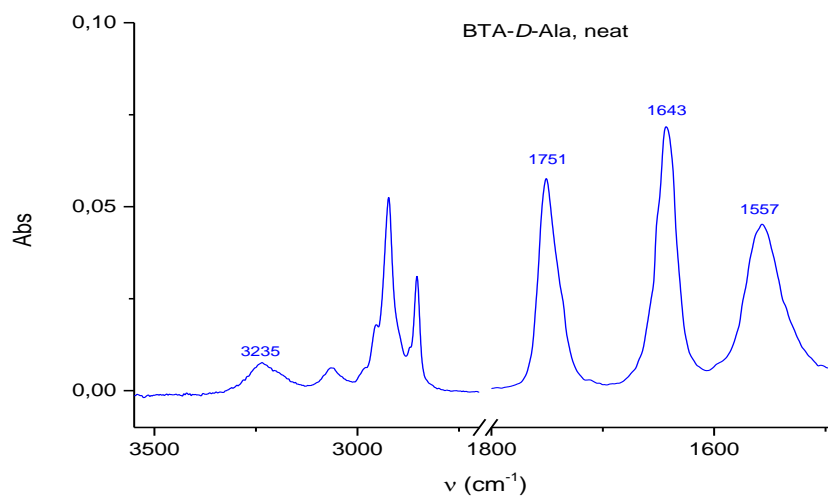
#### **Synthesis of BTA Phg:**

The dodecyl ester *p*-TsOH salt of (*S*)-phenylglycine was prepared according to General Method A.

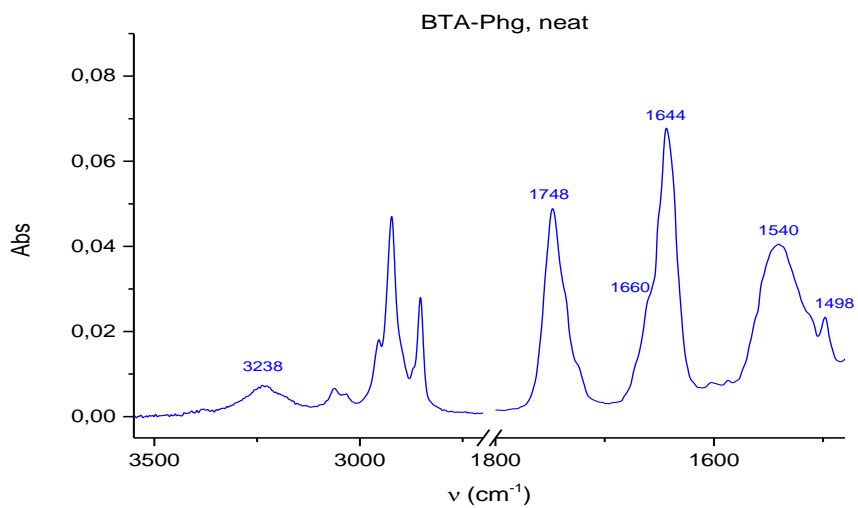
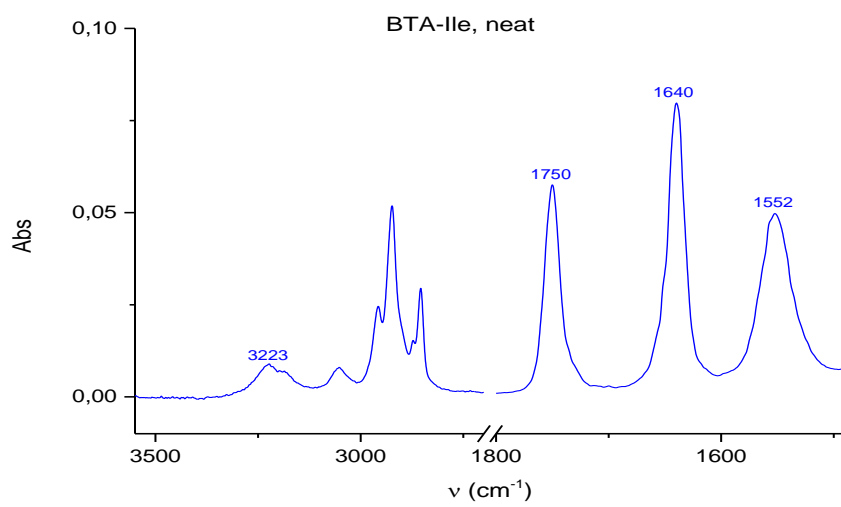
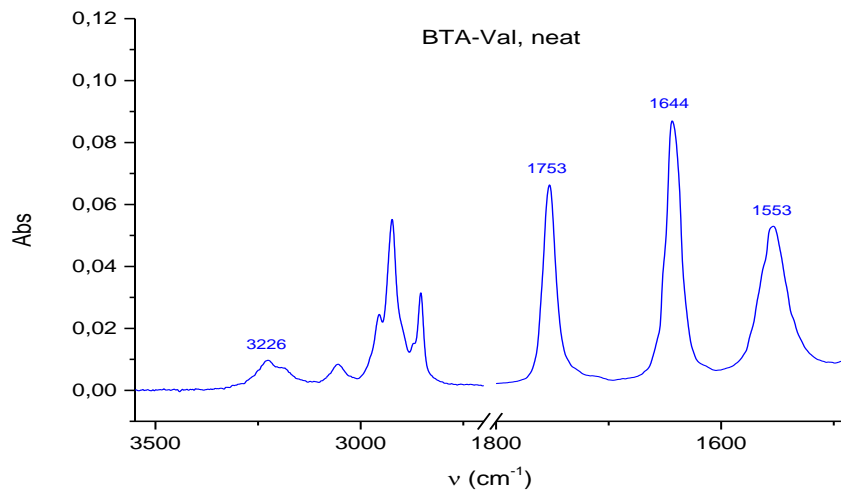
Then **BTA Phg** was prepared according to a published reference<sup>[39]</sup> in order to limit racemization: In a flame-dried round-bottom flask under argon atmosphere, carbonyldiimidazole (775 mg, 4.8 mmol) is dissolved in dry DMF (50 mL) at room temperature. Trimesic acid (313 mg; 1.5 mmol) dissolved in dry DMF (15 mL) is then added over 5min, and the resulting mixture is stirred for 90min. The dodecyl ester *p*-TsOH salt of (*S*)-phenylglycine (5.3 g, 10.8 mmol) is then added in one portion and the reaction is stirred for 5h. The reaction mixture is then poured into 0.1M HCl, extracted two times with Et<sub>2</sub>O. The combined organic phases are washed with brine and dried over MgSO<sub>4</sub>, filtered, and the solvent is evaporated under reduced pressure without heating over 30°C. The crude product is purified by flash chromatography (elution: CH<sub>2</sub>Cl<sub>2</sub>/EtOAc 100:0 to 90:10) to yield **BTA Phg** as a white solid (1.2 g, overall yield of 70% from (*S*)-phenylglycine).

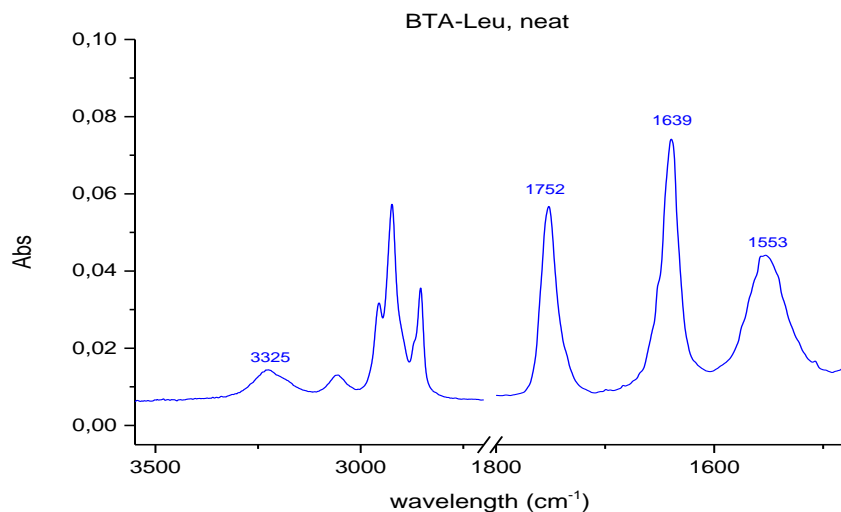
**<sup>1</sup>H NMR** (300 MHz, Acetone-d<sub>6</sub>) δ 8.57 – 8.51 (m, 5H), 7.52 (dd, *J* = 7.8, 1.6 Hz, 6H), 7.42 – 7.32 (m, 10H), 5.76 – 5.74 (m, 3H), 4.21 – 4.06 (m, 6H), 1.60 – 1.56 (m, 6H), 1.26 (m, 54H), 0.88 (t, *J* = 6.0 Hz, 9H); **<sup>13</sup>C{<sup>1</sup>H} NMR** (75 MHz, Acetone-d<sub>6</sub>) δ 171.5, 166.5, 137.9, 135.8, 130.6, 129.8, 129.4, 129.1, 128.3, 66.3, 58.7, 32.9, 30.5, 30.46, 26.7, 23.6, 14.6. **HRMS**: Calculated for C<sub>69</sub>H<sub>100</sub>N<sub>3</sub>O<sub>9</sub> [M+H]<sup>+</sup>: 1114.7454, found: 1114.7452. **IR** (solid, ATR diamond) see page S20-S21. *ee*>99%, *de*=80%.

## Neat IR spectra of ester BTAs (solid, ATR diamond).





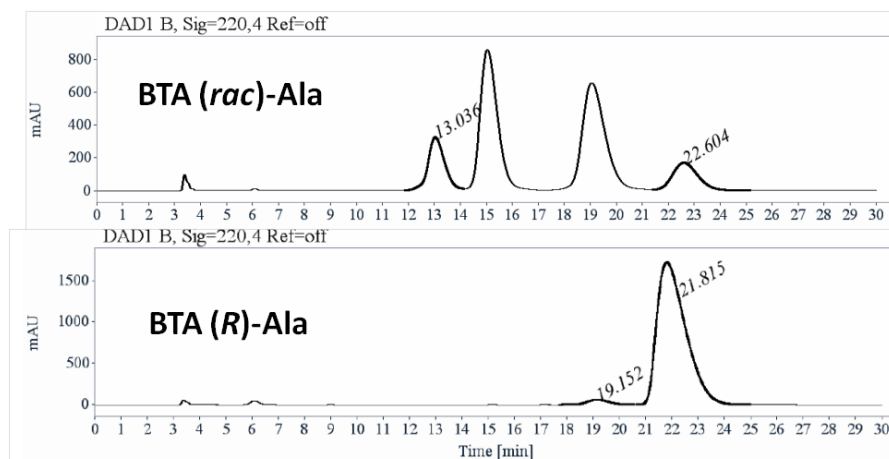




## Chiral HPLC

### Optical purity of BTA (*R*)-Ala

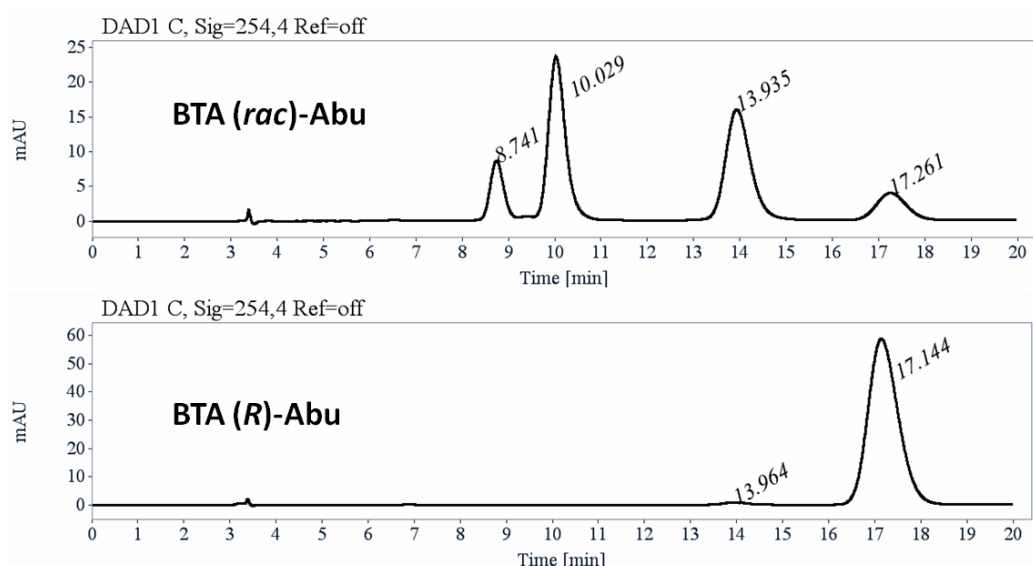
Method description: column=Chiralpak IC, heptane/ethanol 90/10, flow=1 mL/min, detection at 220 nm.



RT [min]	Area	Area%
19.16	598	2.48
21.82	23565	97.52

### Optical purity of BTA (*R*)-Abu

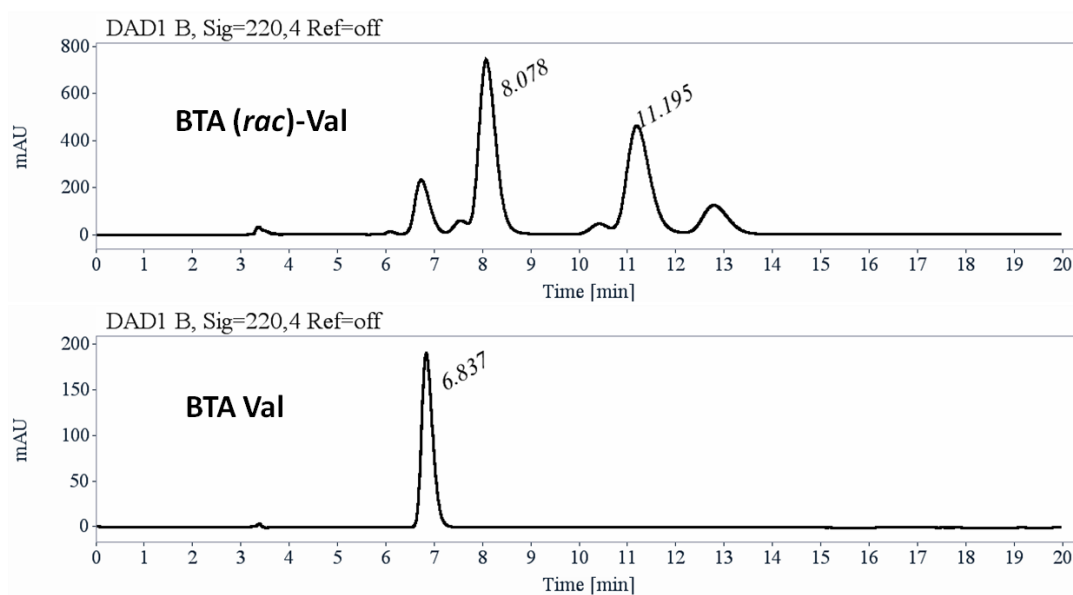
Method description: column=Chiralpak IC, heptane/ethanol 90/10, flow=1 mL/min, detection at 254 nm.



RT [min]	Area	Area%
13.96	32	1.19
17.14	2686	98.81

## Optical purity of BTA Val

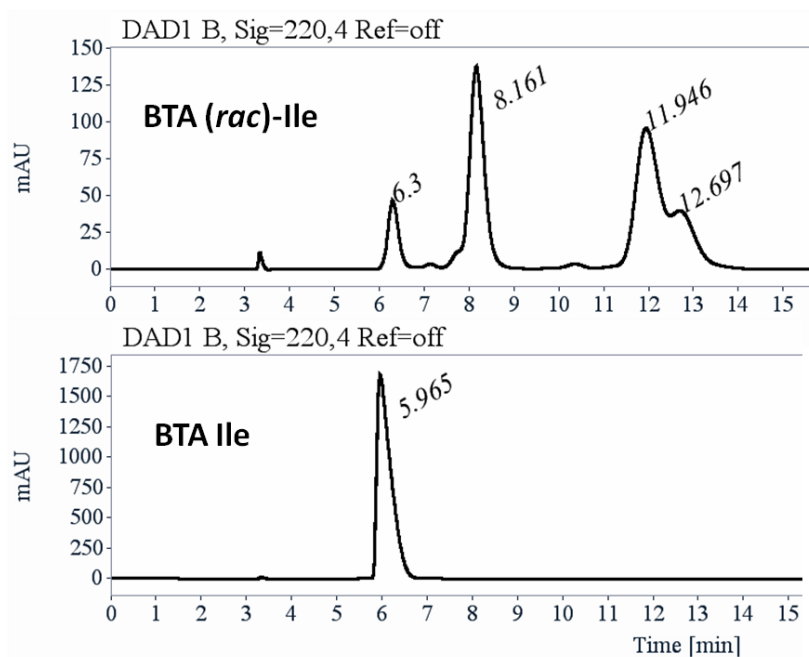
Method description: column=Chiralpak IC, heptane/ethanol 90/10, flow=1 mL/min, detection at 220 nm.



RT [min]	Area	Area%
6.84	3090	100.00

## Optical purity of BTA Ile

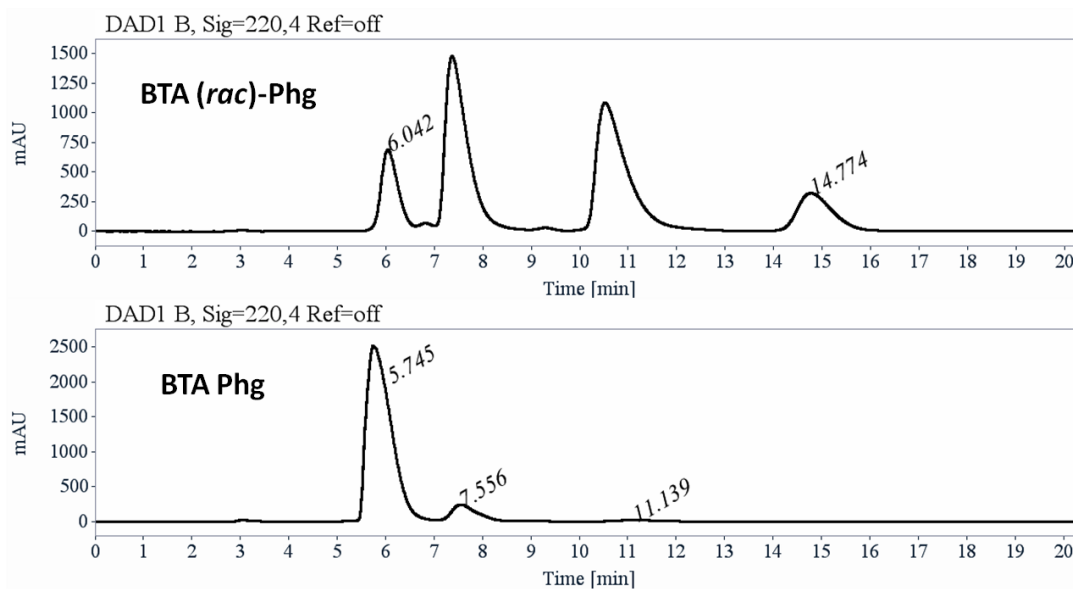
Method description: column=Chiralpak IC, heptane/ethanol 90/10, flow=1 mL/min, detection at 220 nm.



RT [min]	Area	Area%
5.97	36072	100.00

## Optical purity of BTA Phg

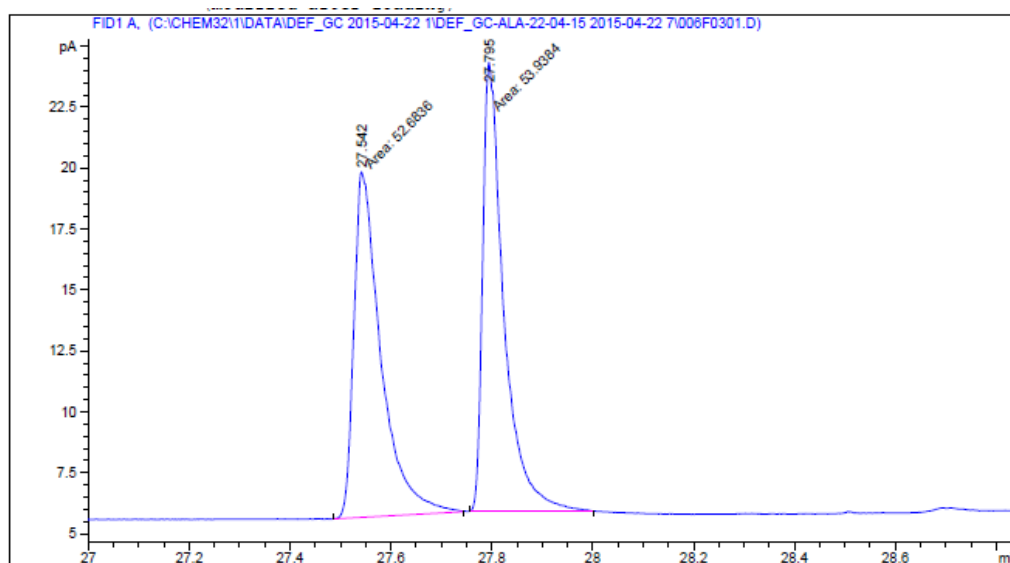
Method description: column=Lux-Cellulose-2, heptane/ethanol 90/10, flow=1 mL/min, detection at 220 nm.



RT [min]	Area	Area%
5.74	88326	90.22
7.56	8554	8.74
11.14	1019	1.04

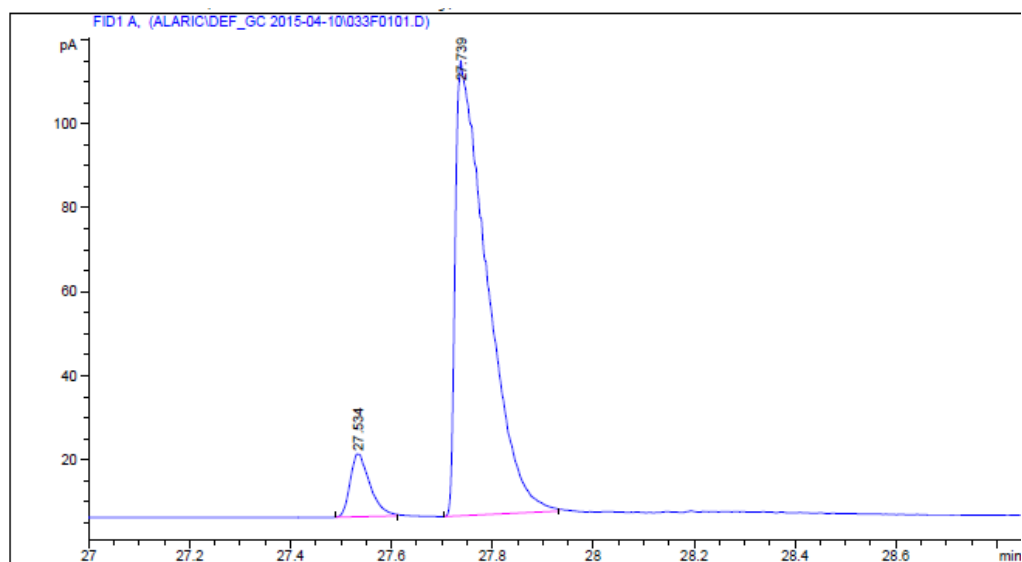
## Chiral GC.

Racemate:



Peak #	RetTime [min]	Type	Width [min]	Area [pA*s]	Height [pA]	Area %
1	27.542	MM	0.0619	52.68360	14.18007	49.41156
2	27.795	MM	0.0488	53.93842	18.42737	50.58844

Catalytic reaction, 84% *ee* (**BTA IIe** ( $R_{\text{BTAIle}}^0=1.25$ ), **BTA<sup>PPh2</sup>** and  $[\text{Rh}(\text{cod})_2]\text{BAr}_\text{F}$ ):



Peak #	RetTime [min]	Type	Width [min]	Area [pA*s]	Height [pA]	Area %
1	27.534	BB	0.0399	40.75589	14.88480	7.94570
2	27.739	BB	0.0573	472.17426	107.40559	92.05430

## E. References

- [1] (a) Siegel, J. S. *Chirality* **1998**, *10*, 24-27. (b) Bailey, J. *Origins Life Evol. B* **2001**, *31*, 167-183. (c) Cintas, P.; Viedma, C. *Chirality* **2012**, *24*, 894-908. (d) Hein, J. E.; Blackmond, D. G. *Acc. Chem. Res.* **2012**, *45*, 2045-2054.
- [2] (a) Noyori, R.; Kitamura, M. *Angew. Chem. Int. Ed. Engl.* **1991**, *30*, 49-69. (b) Soai, K.; Shibata, T.; Morioka, H.; Choji, K. *Nature* **1995**, *378*, 767-768. (c) Feringa, B. L.; van Delden, R. A. *Angew. Chem. Int. Ed.* **1999**, *38*, 3419-3438. (d) Todd, M. H. *Chem. Soc. Rev.* **2002**, *31*, 211-222. (e) Klussmann, M.; Iwamura, H.; Mathew, S. P.; Wells, D. H.; Pandya, U.; Armstrong, A.; Blackmond, D. G. *Nature* **2006**, *441*, 621-623. (f) Noorduyn, W. L.; Izumi, T.; Millemaggi, A.; Leeman, M.; Meeke, H.; Van Enckevort, W. J. P.; Kellogg, R. M.; Kaptein, B.; Vlieg, E.; Blackmond, D. G. *J. Am. Chem. Soc.* **2008**, *130*, 1158-1159. (g) Satyanarayana, T.; Abraham, S.; Kagan, H. B. *Angew. Chem. Int. Ed.* **2009**, *48*, 456-494. (h) Soai, K.; Kawasaki, T.; Matsumoto, A. *Acc. Chem. Res.* **2014**, *47*, 3643-3654. (i) Dijken, D. J.; Beierle, J. M.; Stuart, M. C. A.; Szymanski, W.; Browne, W. R.; Feringa, B. L. *Angew. Chem. Int. Ed.* **2014**, *53*, 5073-5077. (j) Kawasaki, T.; Araki, Y.; Hatase, K.; Suzuki, K.; Matsumoto, A.; Yokoi, T.; Kubota, Y.; Tatsumi, T.; Soai, K. *Chem. Commun.* **2015**, *51*, 8742-8744. (k) Bukhryakov, K. V.; Almahdali, S.; Rodionov, V. O. *Langmuir* **2015**, *31*, 2931-2935.
- [3] (a) Yashima, E.; Matsushima, T.; Okamoto, Y. *J. Am. Chem. Soc.* **1995**, *117*, 11596-11597. (b) Yashima, E.; Matsushima, T.; Okamoto, Y. *J. Am. Chem. Soc.* **1997**, *119*, 6345-6359.
- [4] (a) Aparicio, F.; Matesanz, E.; Sanchez, L. *Chem. Commun.* **2012**, *48*, 5757-5759. (b) Duan, P. F.; Cao, H.; Zhang, L.; Liu, M. H. *Soft Matter* **2014**, *10*, 5428-5448.
- [5] Eelkema, R.; Feringa, B. L. *Org. Biomol. Chem.* **2006**, *4*, 3729-3745.
- [6] Shimomura, K.; Ikai, T.; Kanoh, S.; Yashima, E.; Maeda, K. *Nat. Chem.* **2014**, *6*, 429-434.
- [7] (a) Yamamoto, T.; Adachi, T.; Suginome, M. *ACS Macro Lett.* **2013**, *2*, 790-793. (b) Ke, Y.-Z.; Nagata, Y.; Yamada, T.; Suginome, M. *Angew. Chem. Int. Ed.* **2015**, *54*, 9333-9337. (c) Nagata, Y.; Nishikawa, T.; Suginome, M. *J. Am. Chem. Soc.* **2015**, *137*, 4070-4073.
- [8] (a) Rowan, A. E.; Nolte, R. J. M. *Angew. Chem. Int. Ed.* **1998**, *37*, 63-68. (b) Pijper, D.; Feringa, B. L. *Soft Matter* **2008**, *4*, 1349-1372.
- [9] (a) Green, M. M.; Park, J. W.; Sato, T.; Teramoto, A.; Lifson, S.; Selinger, R. L. B.; Selinger, J. V. *Angew. Chem. Int. Ed.* **1999**, *38*, 3139-3154. (b) Maeda, K.; Yashima, E. *Top. Curr. Chem.* **2006**, *265*, 47-88. (c) Yashima, E.; Maeda, K.; Iida, H.; Furusho, Y.; Nagai, K. *Chem. Rev.* **2009**, *109*, 6102-6211.
- [10] (a) Palmans, A. R. A.; Meijer, E. W. *Angew. Chem. Int. Ed.* **2007**, *46*, 8948-8968. (b) Liu, M. H.; Zhang, L.; Wang, T. Y. *Chem. Rev.* **2015**, *115*, 7304-7397.
- [11] Lockman, J. W.; Paul, N. M.; Parquette, J. R. *Prog. Polym. Sci.* **2005**, *30*, 423-452.
- [12] (a) Green, M. M.; Reidy, M. P.; Johnson, R. J.; Darling, G.; O'Leary, D. J.; Willson, G. *J. Am. Chem. Soc.* **1989**, *111*, 6452-6454. (b) Green, M. M.; Garetz, B. A.; Munoz, B.; Chang, H. P.; Hoke, S.; Cooks, R. G. *J. Am. Chem. Soc.* **1995**, *117*, 4181-4182.
- [13] (a) Green, M. M.; Peterson, N. C.; Sato, T.; Teramoto, A.; Cook, R.; Lifson, S. *Science* **1995**, *268*, 1860-1866. (b) van Gestel, J.; van der Schoot, P.; Michels, M. A. J. *Macromolecules* **2003**, *36*, 6668-6673. (c) van Gestel, J. *Macromolecules* **2004**, *37*, 3894-3898. (d) van Gestel, J.; van der Schoot, P.; Michels, M. A. J. *J. Chem. Phys.* **2004**, *120*, 8253-8261. (e) Markvoort, A. J.; ten Eikelder, H. M. M.; Hilbers, P. A. J.; de Greef, T. F. A.; Meijer, E. W. *Nat. Commun.* **2011**, *2*, 509-517. (f) ten Eikelder, H. M. M.; Markvoort, A. J.; de Greef, T. F. A.; Hilbers, P. A. J. *J. Phys. Chem. B* **2012**, *116*, 5291-5301. (g) Jabbari-Farouji, S.; van der Schoot, P. *J. Chem. Phys.* **2012**, *137*, 064906; doi: 10.1063/1.4742192.
- [14] For a review on asymmetric catalysis with helical polymers see: Megens, R. P.; Roelfes, G. *Chem. Eur. J.* **2011**, *17*, 8514-8523.
- [15] The presence of a large amount of phosphine-free monomers, used in combination to the phosphine monomers and the chiral co-monomers, is a characteristic of this class of helical catalysts since phosphine-rich polymers were found to be less selective: Yamamoto, T.; Suginome, M. *Angew. Chem. Int. Ed.* **2009**, *48*, 539-542.
- [16] Poly(phenylacetylene) co-polymers composed of achiral imidazolidinone monomers and chiral co-monomers were also investigated but provided modest enantioselectivity in Diels-Alder reactions:

- Takata, L. M. S.; Iida, H.; Shimomura, K.; Hayashi, K.; dos Santos, A. A.; Yashima, E. *Macromol. Rapid. Commun.* **2015**, *36*, 2047-2054.
- [17] (a) Huerta, E.; van Genabeek, B.; Lamers, B. A. G.; Koenigs, M. M. E.; Meijer, E. W.; Palmans, A. R. A. *Chem. Eur. J.* **2015**, *21*, 3682-3690. (b) Neumann, L. N.; Baker, M. B.; Leenders, C. M. A.; Voets, I. K.; Lafleur, R. P. M.; Palmans, A. R. A.; Meijer, E. W. *Org. Biomol. Chem.* **2015**, *13*, 7711-7719.
- [18] de Torres, M.; van Hameren, R.; Nolte, R. J. M.; Rowan, A. E.; Elemans, J. A. A. W. *Chem. Commun.* **2013**, *49*, 10787-10789.
- [19] Raynal, M.; Portier, F.; van Leeuwen, P. W. N. M.; Bouteiller, L. *J. Am. Chem. Soc.* **2013**, *135*, 17687-17690.
- [20] (a) Tam, A. Y. Y.; Wong, K. M. C.; Yam, V. W. W. *Chem. Eur. J.* **2009**, *15*, 4775-4778. (b) Po, C.; Ke, Z. H.; Tam, A. Y. Y.; Chow, H. F.; Yam, V. W. W. *Chem. Eur. J.* **2013**, *19*, 15735-15744. (c) Zhu, L. L.; Li, X.; Wu, S. J.; Nguyen, K. T.; Yan, H.; Agren, H.; Zhao, Y. L. *J. Am. Chem. Soc.* **2013**, *135*, 9174-9180. (d) Jung, S. H.; Jeon, J.; Kim, H.; Jaworski, J.; Jung, J. H. *J. Am. Chem. Soc.* **2014**, *136*, 6446-6452. (e) Dubarle-Offner, J.; Moussa, J.; Amouri, H.; Jouvelet, B.; Bouteiller, L.; Raynal, M. *Chem. Eur. J.* **2016**, *22*, 3985-3990.
- [21] Jin, Q. X.; Zhang, L.; Cao, H.; Wang, T. Y.; Zhu, X. F.; Jiang, J.; Liu, M. H. *Langmuir* **2011**, *27*, 13847-13853.
- [22] For leading examples of asymmetric catalysis performed with a combination of an achiral or racemic metal complex and a chiral inducer see: (a) Faller, J. W.; Lavoie, A. R.; Parr, J. *Chem. Rev.* **2003**, *103*, 3345-3367. (b) Mikami, K.; Yamanaka, M. *Chem. Rev.* **2003**, *103*, 3369-3400. (c) Hamilton, G. L.; Kang, E. J.; Mba, M.; Toste, F. D. *Science* **2007**, *317*, 496-499. (d) Ding, K. L. *Chem. Commun.* **2008**, 909-921. (e) Nishioka, Y.; Yamaguchi, T.; Kawano, M.; Fujita, M. *J Am Chem Soc* **2008**, *130*, 8160-8161. (f) Boersma, A. J.; Megens, R. P.; Feringa, B. L.; Roelfes, G. *Chem. Soc. Rev.* **2010**, *39*, 2083-2092. (g) Park, S.; Sugiyama, H. *Angew. Chem. Int. Ed.* **2010**, *49*, 3870-3878. (h) Ward, T. R. *Acc. Chem. Res.* **2011**, *44*, 47-57. (i) Lo, C.; Ringenberg, M. R.; Gnanndt, D.; Wilson, Y.; Ward, T. R. *Chem. Commun.* **2011**, *47*, 12065-12067. (j) Dydio, P.; Rubay, C.; Gadzikwa, T.; Lutz, M.; Reek, J. N. H. *J. Am. Chem. Soc.* **2011**, *133*, 17176-17179. (k) van Leeuwen, P. W. N. M.; Rivillo, D.; Raynal, M.; Freixa, Z. *J. Am. Chem. Soc.* **2011**, *133*, 18562-18565. (l) Mahlau, M.; List, B. *Isr. J. Chem.* **2012**, *52*, 630-638. (m) Phipps, R. J.; Hamilton, G. L.; Toste, F. D. *Nat. Chem.* **2012**, *4*, 603-614. (n) Ohmatsu, K.; Ito, M.; Kunieda, T.; Ooi, T. *Nat. Chem.* **2012**, *4*, 473-477. (o) Ohmatsu, K.; Ito, M.; Kunieda, T.; Ooi, T. *J. Am. Chem. Soc.* **2013**, *135*, 590-593. (p) Wang, L. X.; Xiang, J. F.; Tang, Y. L. *Adv. Synth. Catal.* **2015**, *357*, 13-20.
- [23] For the chirality amplification properties of alkyl BTAs see: (a) Smulders, M. M. J.; Schenning, A. P. H. J.; Meijer, E. W. *J. Am. Chem. Soc.* **2008**, *130*, 606-611. (b) Smulders, M. M. J.; Filot, I. A. W.; Leenders, J. M. A.; Van der Schoot, P.; Palmans, A. R. A.; Schenning, A. P. H. J.; Meijer, E. W. *J. Am. Chem. Soc.* **2010**, *132*, 611-619. (c) Smulders, M. M. J.; Stals, P. J. M.; Mes, T.; Pfaffen, T. F. E.; Schenning, A. P. H. J.; Palmans, A. R. A.; Meijer, E. W. *J. Am. Chem. Soc.* **2010**, *132*, 620-626. (d) Stals, P. J. M.; Smulders, M. M. J.; Martín-Rapún, R.; Palmans, A. R. A.; Meijer, E. W. *Chem. Eur. J.* **2009**, *15*, 2071-2080.
- [24] (a) de Loos, M.; van Esch, J. H.; Kellogg, R. M.; Feringa, B. L. *Tetrahedron* **2007**, *63*, 7285-7301. (b) Veld, M. A. J.; Haveman, D.; Palmans, A. R. A.; Meijer, E. W. *Soft Matter* **2011**, *7*, 524-531. (c) Desmarchelier, A.; Raynal, M.; Brocorens, P.; Vanthuyne, N.; Bouteiller, L. *Chem. Commun.* **2015**, *51*, 7397-7400.
- [25] Fernandez-Perez, H.; Donald, S. M. A.; Munslow, I. J.; Benet-Buchholz, J.; Maseras, F.; Vidal-Ferran, A. *Chem. Eur. J.* **2010**, *16*, 6495-6508.
- [26] In contrast to this observation, the conformation of poly(quinoxaline-2,3-diyl)s polymers is strongly affected by the nature of the alkane solvent. It led to inversion of the major enantiomer obtained *e.g.* in *n*-octane and cyclooctane when these polymers were used as scaffolds for catalysis. See: Nagata, Y.; Nishikawa, T.; Suginome M. *J. Am. Chem. Soc.* **2014**, *136*, 15901-15904.
- [27] The effect of the amount of chiral co-monomer on the selectivity displayed by **BTA Val** was not probed. However, catalytic experiments performed with different amounts of **BTA Nle** and a fixed amount of **BTA<sup>PPh2</sup>** showed the same trend than the one observed for **BTA Ile**: 55% *ee* ( $R_{\text{BTANle}}^0=0.25$ ), 74% *ee* ( $R_{\text{BTANle}}^0=1.25$ ) and 35% *ee* ( $R_{\text{BTANle}}^0=4.0$ )

- [28] Suginome and co-workers reported on a decrease of the enantioselectivity for the palladium-catalyzed hydrosilylation of styrene catalyzed by poly(quinoxaline-2,3-diyl)s ligands incorporating more than 15% chiral units. It was attributed to higher disorder of the helical structure as a result of steric repulsion imposed by the bulky chiral groups. See reference 7a.
- [29] Cyclohexane has been used for spectroscopic characterisations, instead of hexane/CH<sub>2</sub>Cl<sub>2</sub> (10:1) in the case of catalytic experiments.
- [30] According to the assignment made by Meijer and co-workers: Nakano, Y.; Hirose, T.; Stals, P. J. M.; Meijer, E. W.; Palmans, A. R. A. *Chem. Sci.* **2012**, *3*, 148-151.
- [31] Jana, P.; Paikar, A.; Bera, S.; Maity, S. K.; Haldar, D. *Org. Lett.* **2014**, *16*, 38-41.
- [32] Roosma, J.; Mes, T.; Leclère, P.; Palmans, A. R. A.; Meijer, E. W. *J. Am. Chem. Soc.* **2008**, *130*, 1120-1121.
- [33] For all the solids, no linear dichroism effects were present and the shape of the CD signal was independent of the orientation of the quartz slide.
- [34] In these structures we arbitrary chose that the three amide groups are oriented in the same direction despite the fact that an "asymmetric" orientation of the amide groups is also plausible see: Bejagam, K. K.; Fiorin G.; Klein M. L.; Balasubramanian S. *J. Phys. Chem. B* **2014**, *118*, 5218-5228.
- [35] The relative *Re* or *Si* configuration of the *meta*-substituted aryl *Z* rings is not known. Chirality transfer from stacked aromatic rings to prochiral metals is known for disubstituted ferrocene peptides<sup>35a</sup> and has been postulated for supramolecular catalysts.<sup>22k,35b-f</sup> For one example of chirality transfer in covalent asymmetric catalysts see reference 35g. (a) Kirin S. I.; Kraatz, H. B.; Metzler-Nolte N. *Chem. Soc. Rev.* **2006**, *35*, 348-354. (b) Laungani, A. C.; Breit, B. *Chem. Commun.* **2008**, 844-846. (c) Laungani, A. C.; Slattery, J. M.; Krossing, I.; Breit, B. *Chem. Eur. J.* **2008**, *14*, 4488-4502. (d) Kokan Z.; Kirin S. I. *RSC Adv.* **2012**, *2*, 5729- 5737. (e) Kokan Z.; Kirin S. I. *Eur. J. Org. Chem.* **2013**, *2013*, 8154- 8161. (f) Kokan Z.; Glasovac Z.; Elenkov M. M.; Gredicak M.; Jeric I.; Kirin S. I. *Organometallics* **2014**, *33*, 4005-4015. (g) Yu J. F.; RajanBabu T. V.; Parquette J. R. *J. Am. Chem. Soc.* **2008**, *130*, 7845-7847.
- [36] Bissette, A. J.; Fletcher, S. P. *Angew. Chem. Int. Ed.* **2013**, *52*, 12800-12826.
- [37] Neumann, E.; Pfaltz, A. *Organometallics* **2005**, *24*, 2008-2011.
- [38] Bejagam, K. K.; Fiorin, G.; Klein, M. L.; Balasubramanian, S. *J. Phys. Chem. B* **2014**, *118*, 5218-5228.
- [39] Cantekin, S.; ten Eikelder, H. M. M.; Markvoort, A. J.; Veld, M. A. J.; Korevaar, P. A.; Green, M. M.; Palmans, A. R. A.; Meijer, E. W. *Angew. Chem. Int. Ed.* **2012**, *51*, 6426-6431.



# V. Asymmetric copper-catalysed hydrosilylation of acetophenone derivatives

*Abstract:* In this chirally amplified BTA supramolecular polymers will be used as scaffolds in the copper-catalysed hydrosilylation of acetophenone derivatives. Mixture of an achiral BTA ligand and an enantiopure BTA co-monomer provide a good selectivity for the copper-catalysed hydrosilylation of 4'-NO<sub>2</sub>-acetophenone (up to 80% e.e.). The supramolecular co-polymer catalyst was found to be soluble and exhibited strong chirality amplification properties. Indeed, a scalemic mixture of enantiopure co-monomers (33% e.e.) provided 90% of the optimal selectivity. These properties were used to switch the chirality of the catalyst during the course of the reaction and thus the nature of the major enantiomer. It constitutes the first step of a dynamic and chirality-switchable catalyst. Preliminary investigation of the structure of the Cu catalyst was also reported. A part of the experiments mentioned in section 1,2 and 3 have performed by J. Zimbron (ANR, supracatal, Chimie ParisTech).

## A. Introduction

Nature has always been an inspiration for the development of drugs, materials and catalysts. In the latter case, it led to the elaboration of highly selective and active synthetic catalysts.<sup>[1]</sup> Also, mimicking the allosteric regulation of enzymes, catalysts have been designed which can be switched into two or more catalytic states upon activation by a stimulus. Such catalysts have been studied for decades<sup>[2]</sup> and have been recently reviewed.<sup>[3]</sup> Most of those switchable catalysts are based on an on/off switch in order to control their activity which can be used for tackling synthetic challenges: i) the selected activation of two substrates from a substrate mixture<sup>[4]</sup> and ii) the design of temporally switchable polymerisation systems which allow for the preparation of a block copolymers starting from a mixture of L-lactide and  $\epsilon$ -caprolactone.<sup>[5]</sup> Of particular interest is the design of chirality-switchable catalysts since it allows the preparation of the two stereoisomers of a reaction from a single chiral entity. Chemical additives (anions,<sup>[6]</sup> redox agents<sup>[7,8]</sup>), temperature,<sup>[9,10]</sup> solvent,<sup>[11–14]</sup> light<sup>[15]</sup> or a combination of these stimuli<sup>[16–18]</sup> have been used to trigger chirality inversion of the catalytic centre. In most of these examples, the chirality switch occurs at the level of the ligand, the metal pre-catalyst or the organocatalyst prior to the catalytic reaction. In contrast, reversible inversion of the stereochemical outcome during the course of the catalytic reaction has been overlooked. To the best of our knowledge, only one example has been demonstrated by Melchiorre *et al.* who demonstrated that the diastereoselectivity exhibited by an ion-paired catalyst can be switched from *syn* to *anti* during the course of the reaction by changing the nature of the achiral Brønsted acid partner.<sup>[19]</sup> Clearly, the rational control of the stereoselectivity exhibited by a dynamic and chirality-switchable catalyst will constitute an important step towards the development of sophisticated adaptive chemical systems.

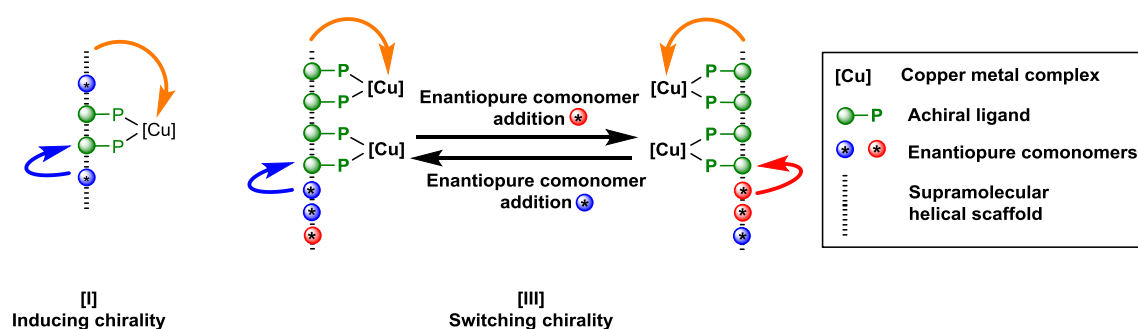


Figure V-1: Strategies envisaged in this chapter

Such a catalyst must be built on a dynamic scaffold whose chirality can be switched at will during the route of the catalytic process. The handedness of dynamic macromolecular or supramolecular helices can be switched reversibly upon activation by different stimuli.<sup>[20–22]</sup> Notably, chirality amplification effects have been particularly-well rationalised in such classes of molecules.<sup>[20]</sup> the handedness and net helicity of the polymer is imposed by the chiral enantiomer for mixtures of chiral and achiral monomers (“sergeants-and-soldiers” experiments) or by the major enantiomer for scalemic mixtures of monomers (“majority-rule” experiments). These properties have been exploited very recently for the

construction of efficient asymmetric catalysts exhibiting strong chirality-amplification properties.<sup>[23–25]</sup> Suginome *et al.* showed that poly(quinoxaline-2,3-diyl)s (PQXs) composed of a scalemic mixture of enantiopure monomers (30% e.e.) and an achiral phosphine monomer in a 19:1 ratio adopted a single-handed helical structure and served as ligands in asymmetric palladium-catalysed hydrosilylation and cross-coupling reactions (up to 94% e.e.).<sup>[24]</sup> However, several challenges appear upon envisaging a general strategy for controlling the stereoselectivity of metal catalysts during the course of the catalytic reaction: i) the lack of chirality amplification properties (which prevents full inversion of the stereoselectivity), ii) their insolubility and iii) the fact the overall configuration of the molecular catalyst is fixed upon complexation of the ligands by the catalytic metal. Based on our previous investigations of 1,3,5-benzene tricarboxamide (BTA) polymers as scaffolds for asymmetric catalysts,<sup>[23]</sup> we describe herein a dynamic copper catalyst whose selectivity can be fully inverted during the course of the catalytic reaction by changing the nature of the major enantiomer constituting its supramolecular helical structure (see a schematic representation in Figure V-1). The chirally-switchable nature of the catalyst is granted by the strong chirality-amplification effects displayed by the BTA supramolecular polymer scaffold.

## **B. Design rules and choice of the catalytic reaction**

In Chapter IV, we showed that sergeants-and-soldiers type BTA supramolecular polymers were highly efficient chirality amplification scaffolds for the rhodium-catalysed hydrogenation of dimethyl itaconate. Indeed, mixtures containing only one quarter of chiral BTA co-monomers compared to the achiral BTA ligand provided the optimal enantioselectivity for this system (85% e.e.). In order to design the metal catalyst schematised in Figure V-1, we sought to investigate the catalytic properties of supramolecular polymers combining an achiral ligand BTA or bis-urea monomer coordinated to the catalytic metal centre and a scalemic mixture of ligand-free enantiopure BTA or bis-urea co-monomers. Such polymers must have the following properties: i) chirality must be induced efficiently from the chiral supramolecular structure to the intrinsically achiral metal complexes, ii) they should exhibit strong chirality amplification properties (majority rule) and iii) they should be dynamic under the catalytic conditions. An implicit requirement of the last point is that the catalytic system should be soluble, which is in contrast to our previously-investigated rhodium catalysts. In that aim, we turned our attention to the asymmetric copper-catalysed hydrosilylation of aromatic ketones (Figure V-2).

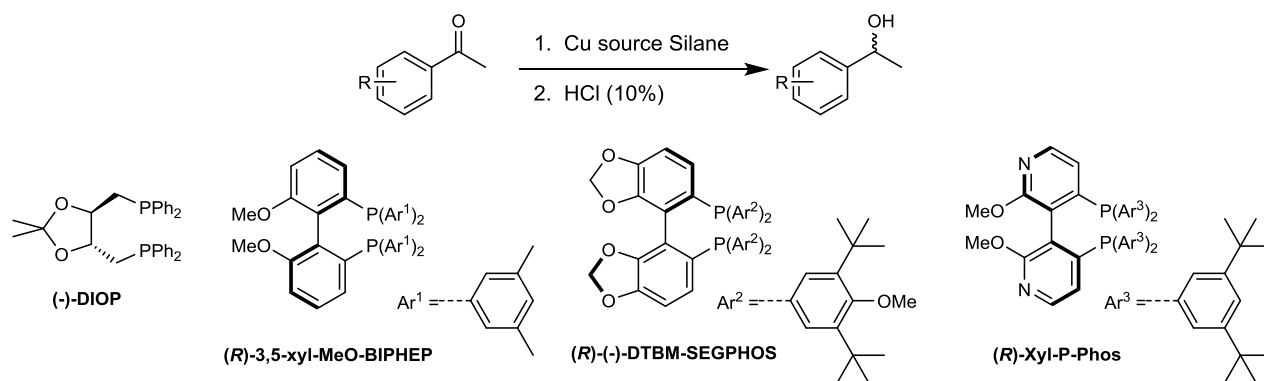


Figure V-2: Copper catalysed hydrosilylation of aromatic ketones and some of the various ligands used in the literature

The hydrosilylation of acetophenone derivatives has become an interesting source of chiral alcohols with high enantiopurity. Although several metals were described to catalyse this reaction (Rh<sup>[26–28]</sup> and Fe<sup>[29]</sup> amongst other metals), copper is attractive due to its low toxicity and price. The first asymmetric copper-catalysed hydrosilylation reaction has been reported in 1984 by Brunner *et al.* using **DIOP** ligand and diphenylsilane albeit with modest enantioselectivity (up to 39% e.e.).<sup>[30]</sup> This reaction was reinvestigated by several groups since 2001 following the report of a highly efficient asymmetric catalytic system by Lipschutz and co-workers using CuCl/NaOtBu with **(R)-3,5-xyl-MeO-BIPHEP**.<sup>[31]</sup> Since then, various enantiopure bidentate ligands and copper sources were tried which provided high enantioselectivity. Replacing the CuCl/NaOtBu precatalyst by air stable copper sources such as CuF<sub>2</sub><sup>[32]</sup> or Cu(OAc)<sub>2</sub>·H<sub>2</sub>O<sup>[33]</sup> did not hamper the selectivity. Interestingly, the Binap copper complex formed with CuF<sub>2</sub> provided an air stable catalyst with low moisture sensitivity however the origin of the increased robustness remains unclear.<sup>[32]</sup> High turnover numbers (TONs) were obtained as published by Lipschutz *et al.* with **DTBM-SEGPHOS** as ligand (TON = 1.10<sup>5</sup>)<sup>[34]</sup> or by Chan *et al.* with **(S)-Xyl-P-Phos** (TON = 2.10<sup>5</sup>).<sup>[35]</sup> The active species in all these systems is a phosphine copper hydride complex as demonstrated by: i) the fact that only copper sources which undergo transmetalation in the presence of silanes are efficient and ii) its observation by spectroscopic techniques.<sup>[36]</sup> However, the exact mode of activation of the ketone substrates by the copper hydride complex remained unclear. Importantly for our project, this copper hydride complex is neutral and is thus expected to be soluble in solvents compatible with the formation of BTA supramolecular polymers.

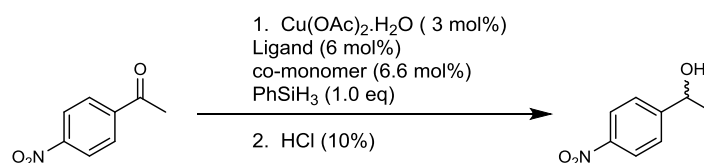
## C. Chirality induction and solubility

### 1. Screening of ligands and co-monomers

Preliminary screening studies were performed in order to determine whether BTA and bis-urea helical supramolecular polymers were able to transfer efficiently their chirality to copper catalytic centres. The hydrosilylation of 4'-NO<sub>2</sub>-acetophenone was chosen as the reaction of reference. Only a limited set of bis-urea were screened for this reaction (e.e. < 30%) are the best results presented in the appendix of this thesis. Two methods were used for the preparation of the copper complexes of the

BTA ligands: i) the BTA ligand and the copper source were directly mixed in the solvent used in catalysis (method A) and ii) the BTA ligand and the copper source were mixed in THF, a solvent in which BTAs are under the form of monomers, the THF solvent was removed and the solvent desired for catalysis was added (method B). Chiral BTA ligands alone ( $(S,S)$ - $^H$ BTA<sup>pPPh<sub>2</sub></sup> or  $(S,S)$ - $^H$ BTA<sup>mPPh<sub>2</sub></sup>) as well as mixtures between an achiral BTA ligand ( $^H$ BTA<sup>pPPh<sub>2</sub></sup> or  $^H$ BTA<sup>mPPh<sub>2</sub></sup>) and an enantiopure co-monomer in 1:1.1 ratio were evaluated (see loose sheet for the formulas). The synthesis and characterisation of the new BTA monomers are reported in the Experimental Section. The results of this catalytic screening are listed in Table V-1.

Table V-1: Screening of BTA ligands and BTA co-monomers for the hydrosilylation of 4'-NO<sub>2</sub>-acetophenone



Entry	Method	BTA ligand	BTA co-monomer	e.e. (%)
1	A	$(S,S)$ - $^H$ BTA <sup>pPPh<sub>2</sub></sup>	none	-48 ( <i>S</i> )
2	A	$(S,S)$ - $^H$ BTA <sup>mPPh<sub>2</sub></sup>	none	25 ( <i>R</i> )
4	A	$^H$ BTA <sup>pPPh<sub>2</sub></sup>	BTA ( <i>D</i> )-Phe	-13 ( <i>S</i> )
5	A	$^H$ BTA <sup>pPPh<sub>2</sub></sup>	( <i>S</i> )-BTA	-19 ( <i>S</i> )
6	A	$^H$ BTA <sup>pPPh<sub>2</sub></sup>	BTA ( <i>L</i> )-Ala	25 ( <i>R</i> )
7	A	$^H$ BTA <sup>pPPh<sub>2</sub></sup>	BTA ( <i>L</i> )-Phg	35 ( <i>R</i> )
8	A	$^H$ BTA <sup>pPPh<sub>2</sub></sup>	BTA ( <i>D</i> )-Nle	-38 ( <i>S</i> )
9	A	$^H$ BTA <sup>pPPh<sub>2</sub></sup>	BTA ( <i>L</i> )-Met	38 ( <i>R</i> )
10	A	$^H$ BTA <sup>pPPh<sub>2</sub></sup>	BTAL ( <i>L</i> )- <i>t</i> Leu	46 ( <i>R</i> )
11	A	$^H$ BTA <sup>pPPh<sub>2</sub></sup>	BTA ( <i>L</i> )-Val	49 ( <i>R</i> )
12	A	$^H$ BTA <sup>pPPh<sub>2</sub></sup>	BTA ( <i>D</i> )-Abu	-52 ( <i>S</i> )
13	A	$^H$ BTA <sup>pPPh<sub>2</sub></sup>	BTA ( <i>L</i> )-Leu	55 ( <i>R</i> )
14	A	$^H$ BTA <sup>pPPh<sub>2</sub></sup>	BTA ( <i>L</i> )-Ile	58 ( <i>R</i> )
15	A	$^H$ BTA <sup>pPPh<sub>2</sub></sup>	BTA ( <i>D</i> )-Cha	-59 ( <i>S</i> )
16	A	$^H$ BTA <sup>pPPh<sub>2</sub></sup>	BTA ( <i>L</i> )-Cha	60 ( <i>R</i> )
17	A	$^H$ BTA <sup>mPPh<sub>2</sub></sup>	BTA ( <i>D</i> )-Cha	-11 ( <i>S</i> )
18	A	$^H$ BTA <sup>pPPh<sub>2</sub></sup>	BTA ( <i>D</i> )-Cha	0 <sup>(a)</sup>
19	A	$^H$ BTA <sup>pPPh<sub>2</sub></sup>	BTA ( <i>D</i> )-Cha	-59 <sup>(b)</sup> ( <i>S</i> )
20	A	$^H$ BTA <sup>pPPh<sub>2</sub></sup>	BTA ( <i>D</i> )-Cha	-70 <sup>(c)</sup> ( <i>S</i> )
21	B	$^H$ BTA <sup>pPPh<sub>2</sub></sup>	BTA ( <i>D</i> )-Cha	-63 <sup>(c)</sup> ( <i>S</i> )
22	A	$^H$ BTA <sup>pPPh<sub>2</sub></sup>	BTA ( <i>D</i> )-Cha	-78 <sup>(d)</sup> ( <i>S</i> )

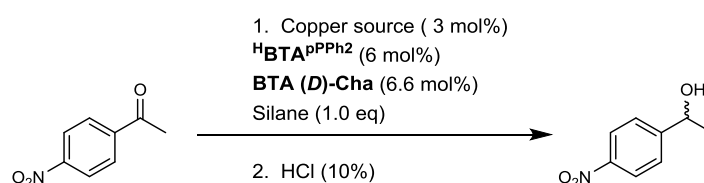
Reaction conditions: 4'-NO<sub>2</sub>-acetophenone (0.17 mmol, 0.3 M), Cu(OAc)<sub>2</sub>.H<sub>2</sub>O (3 mol%), **BTA ligand** (6 mol%), BTA co-monomer (6.6 mol% if present), PhSiH<sub>3</sub> (1.0 eq), toluene (570 μL), room temperature, 30 min. Full conversion in all cases. Conversion was monitored by TLC and <sup>1</sup>H NMR. e.e. was determined by chiral GC analysis and negative value of the e.e. corresponds to the (*S*) enantiomer.<sup>[37]</sup> All reactions were done in duplicate (a) reaction performed in THF (b) pre-catalytic mixture centrifuged and reaction performed with the supernatant (c) reaction performed at 0°C (d) reaction performed at -25°C

When comparing the selectivity displayed by the chiral ligands  $(S,S)$ - $^H$ BTA<sup>mPPh<sub>2</sub></sup> (25% e.e.) and  $(S,S)$ - $^H$ BTA<sup>pPPh<sub>2</sub></sup> (-42% e.e.), it clearly appeared that the position of the phosphine relative to the amide bond had a great influence on the selectivity of the catalytic reaction. The *para*-substituted PPh<sub>2</sub> ligand was also superior to the *meta*-substituted one in reactions conducted with a mixture of achiral BTA ligand and an enantiopure co-monomer (compare entries 16 and 17). We thus selected  $^H$ BTA<sup>pPPh<sub>2</sub></sup> (6 mol%) as the achiral BTA ligand for the screening of various chiral co-monomers (6.6

mol%, including alkyl and ester BTAs). Here, the aim was to select the best chiral co-monomer for the chirality amplification studies. As observed previously,<sup>[38]</sup> the nature of the chiral co-monomer had a large influence on the enantioselectivity of the reaction since the enantiomeric excess varies from 13% to 60%. In two cases (**BTA Cha** and **BTA Ile**), we even observed a better enantiomeric excess for the mixture of achiral ligand and ester BTA than for the chiral BTA ligand alone (compared entry 1, 14 and 15). The two enantiomers of the hydrosilylation product were obtained with the same selectivity by inverting the chirality of the co-monomers (entries 15 and 16). The best chirality induction was obtained with **BTA Cha** as the chiral co-monomer providing the (*S*) (or (*R*)) enantiomer of the hydrosilylation product with 59% e.e. at room temperature. A control experiment performed in THF confirmed that the selectivity arises from the formation of a supramolecular assembly (entry 18, 0% e.e.). Also, the selective copper catalyst was soluble under the reaction conditions as demonstrated by a positive control experiment in which only the supernatant of the centrifuged catalyst was engaged in the reaction (entry 19). Decreasing the temperature significantly increased the enantioselectivity as -70% e.e and -78% e.e. were obtained at 0°C and -25°C respectively for the mixture of <sup>H</sup>**BTA**<sup>PPPh<sub>2</sub></sup> and **BTA Cha** (entries 20 and 22). The method of preparation of the Cu catalyst had a weak but measurable influence on its selectivity (entries 20 and 21). Factors that might explain the effect of the method of preparation (A or B) of the catalyst will be discussed separately below. With our best combination of BTA monomers in hands, we checked whether we could further improve the selectivity by changing the copper source, the silane, the temperature or the solvent.

## 2. Optimisation of the reaction conditions for method A

Table V-2: Screening of various copper sources and silanes



Entry	Cu source	Silane	Temperature	e.e.
1	Cu(OAc) <sub>2</sub> ·H <sub>2</sub> O	PhSiH <sub>3</sub>	r.t.	-60% ( <i>S</i> )
2	CuF <sub>2</sub>	PhSiH <sub>3</sub>	r.t. <sup>(a)</sup>	-61% ( <i>S</i> )
3	CuCl + NaOt-Bu	PhSiH <sub>3</sub>	r.t. <sup>(a)</sup>	-60% ( <i>S</i> )
4	Cu(OAc) <sub>2</sub> ·H <sub>2</sub> O	PhSiH <sub>3</sub>	0°C	-70% ( <i>S</i> )
5	Cu(OAc) <sub>2</sub>	PhSiH <sub>3</sub>	0°C	-69% ( <i>S</i> )
6	Cu( <i>Oi</i> -butyrate)	PhSiH <sub>3</sub>	0°C	-67% ( <i>S</i> )
7	Cu(OAc) <sub>2</sub> ·H <sub>2</sub> O	Ph <sub>2</sub> SiH <sub>3</sub>	r.t. <sup>(a)</sup>	-62% ( <i>S</i> )
8	Cu(OAc) <sub>2</sub> ·H <sub>2</sub> O	PhMeSiH <sub>2</sub>	r.t. <sup>(a)</sup>	-60% ( <i>S</i> )
9	Cu(OAc) <sub>2</sub> ·H <sub>2</sub> O	( <i>t</i> Bu) <sub>2</sub> SiH <sub>2</sub>	r.t.	-
10	Cu(OAc) <sub>2</sub> ·H <sub>2</sub> O	Me(MeO) <sub>2</sub> SiH	r.t.	-
11	Cu(OAc) <sub>2</sub> ·H <sub>2</sub> O	PMHS	r.t.	-

Reaction conditions: 4'-NO<sub>2</sub>-acetophenone (0.17 mmol, 0.3 M), copper source (3 mol%), <sup>H</sup>**BTA**<sup>PPPh<sub>2</sub></sup> (6 mol%), **BTA (D)-Cha** (6.6 mol%), silane (1 eq), toluene (570 μL), Method of preparation: A. PMHS: Polymethylhydrosiloxane. Full conversion in all cases. Conversion was monitored by TLC and <sup>1</sup>H NMR and e.e. was determined by chiral GC analysis. – indicates that no conversion of the substrate was observed in that conditions (a) no reactivity was observed at 0°C.

Not surprisingly, all copper sources which may undergo transmetalation in the presence of a silane were active for the hydrosilylation reaction (Table V-2). It included hydrated and anhydrous  $\text{Cu}(\text{OAc})_2$ ,  $\text{CuF}_2$ ,  $\text{Cu}(\text{O}i\text{-butyrate})_2$  and  $\text{CuCl}+\text{NaO}t\text{-Bu}$ . However, all copper complexes provided the product with virtually the same selectivity. The use of diphenylsilane or phenyl(methyl)silane instead of phenylsilane did not improve the enantiomeric excess neither (entries 7 and 8) but the reaction was sluggish with these silanes as demonstrated by the absence of reaction at  $0^\circ\text{C}$ .  $(t\text{Bu})_2\text{SiH}_2$  and monohydride silane sources (including PMHS) did not allow any conversion (entries 9-11). The absence of enantioselectivity improvement observed when changing the copper and the silane sources led us to continue our catalyst optimisation studies with  $\text{Cu}(\text{OAc})_2\cdot\text{H}_2\text{O}$  and  $\text{PhSiH}_3$ .

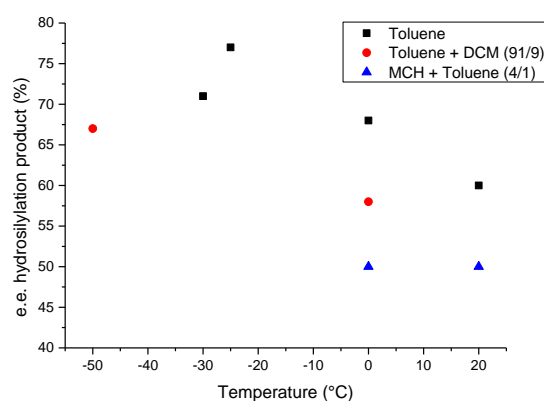


Figure V-3: Influence of the solvent and of the temperature on the enantioselectivity of the hydrosilylation of the 4'-NO<sub>2</sub>-acetophenone. Reaction conditions: 4'-NO<sub>2</sub>-acetophenone (0.17 mmol, 0.3 M),  $\text{Cu}(\text{OAc})_2\cdot\text{H}_2\text{O}$  (3 mol%),  $^{\text{H}}\text{BTA}^{\text{PPh}_2}$  (6 mol%), **BTA (D)-Cha** (6.6 mol%),  $\text{PhSiH}_3$  (1 eq), solvent (570  $\mu\text{L}$ ), Method of preparation: A.

As previously mentioned, when the reaction was conducted in toluene, decreasing the temperature from room temperature (60% e.e.) to  $0^\circ\text{C}$  (70% e.e.) and  $-25^\circ\text{C}$  (80% e.e.) increased the enantiomeric excess (black squares, Figure V-3). However, a further decrease of the temperature led to slurry reaction and unreliable results. This might arise from an increased viscosity of the reaction medium or precipitation of the supramolecular polymer catalyst. Switching to a slightly more polar solvent mixture (toluene/DCM 91/9) seemed to yield a more soluble catalyst since activity was observed down to  $-50^\circ\text{C}$ . However, the selectivity (67% e.e. at  $-50^\circ\text{C}$ ) was lowered in this solvent mixture presumably because the supramolecular assemblies were shorter in this solvent. The selectivity was also decreased when the catalytic experiment was conducted in methylcyclohexane (MCH)/toluene (4/1). This was more surprising considering that MCH was less polar than toluene. This screening of solvents revealed that a good balance between solvent polarity and solubility of the catalytic system was required to get an efficient supramolecular catalyst.

Next, we investigated whether the amount of chiral co-monomer relatively to that of the ligand had an influence on the selectivity outcome of the catalytic reaction. Sergeants and soldiers type experiments were conducted at three temperatures ( $20^\circ\text{C}$ ,  $0^\circ\text{C}$  and  $-25^\circ\text{C}$ ,  $R^0\text{Cha} = n^0\text{BTA Cha}/n^0\text{HBTA}^{\text{PPh}_2}$ ). For  $0 < R^0\text{Cha} < 1$ , the enantioselectivity was almost linearly related to the amount of chiral co-monomer for

the three temperatures which indicated no significant chirality amplification (Figure V-4). Also, a plateau was reached at  $R^0\text{Cha} \approx 1.1$  which corresponded to the optimal selectivity. In striking contrast with the selectivity outcome observed in the rhodium-catalysed hydrogenation of dimethyl itaconate (Figure IV-1), no erosion of enantioselectivity was observed for mixtures containing an excess of **BTA (D)-Cha** compared to the BTA ligand. It was a very interesting point considering our objective to switch the chirality of the chiral helices by consecutive addition of chiral co-monomers since it indicated that a large proportion of the co-monomers present in the assembly will not be detrimental for the selectivity.

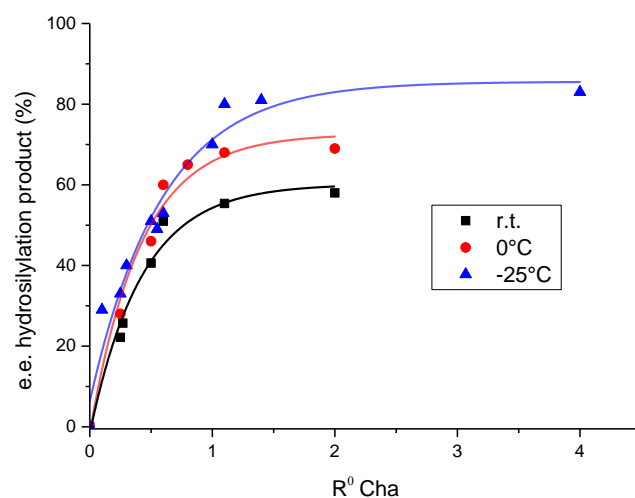


Figure V-4: Plot of the enantioselectivity of the hydrosilylation reaction as a function of  $R^0\text{Cha}$  at different temperatures. The lines are drawn to guide the eye.  $R^0\text{Cha} = n^0\text{BTA Cha}/n^0\text{H}^0\text{BTA}^{\text{pPh}_2}$ . Fixed amount in  $\text{H}^0\text{BTA}^{\text{pPh}_2}$  (6 mol%) and variable amount of **BTA (D)-Cha** (0-24 mol%), toluene. Method of preparation: A.

### 3. Influence of the method of preparation of the catalyst

For  $\text{H}^0\text{BTA}^{\text{pPh}_2}/\text{BTA Cha}/\text{Cu}(\text{OAc})_2\cdot\text{H}_2\text{O}$  catalytic mixtures prepared according to method A, *i.e.* mixing of all the components in toluene, a long induction period was observed for the hydrosilylation reactions conducted at 0°C and below. This induction period also varied significantly from one experiment to another (between 0.5 to 4 hours at 0°C for example). This variable induction period was hypothesised to arise from a slow coordination of copper by the ligand in toluene since the copper source ( $\text{Cu}(\text{OAc})_2\cdot\text{H}_2\text{O}$ ) was not soluble in this solvent. Centrifugation of pre-catalytic mixture composed of  $\text{H}^0\text{BTA}^{\text{pPh}_2}/\text{BTA Cha}/\text{Cu}(\text{OAc})_2\cdot\text{H}_2\text{O}$  indeed revealed the presence of a significant amount of copper acetate in the precipitate. To overcome this issue, we changed the method of preparation of the catalyst by mixing  $\text{Cu}(\text{OAc})_2\cdot\text{H}_2\text{O}$  with of  $\text{H}^0\text{BTA}^{\text{pPh}_2}$  in THF, a solvent in which  $\text{H}^0\text{BTA}^{\text{pPh}_2}$  was dissociated, to ensure full coordination of the copper by the BTA ligand (method B). The THF was then removed and the Cu complex dried under vacuum to eliminate the possible traces of THF that might interfere with the self-assembly. Toluene was then added to the thus formed Cu complex. Upon adding **BTA Cha**, a fully homogeneous catalyst was obtained as no suspension was present in toluene.



Catalytic experiments performed by using  $^H\text{BTA}^{\text{pPPH}_2}/\text{BTA Cha}/\text{Cu}(\text{OAc})_2\cdot\text{H}_2\text{O}$  mixtures prepared following method B proved to be repeatable: no induction period was observed at 0°C for the hydrosilylation of 4'-NO<sub>2</sub> acetophenone and the reaction was fast (less than 30 min). We were thus interested in comparing the performance of the Cu catalysts obtained by mixing  $^H\text{BTA}^{\text{pPPH}_2}$ , **BTA Cha** and Cu(OAc)<sub>2</sub>·H<sub>2</sub>O with the two methods A and B. For 4'-NO<sub>2</sub>-acetophenone, the catalyst prepared by method B was more active but less selective than the one prepared according to method A (compared entries 1 and 2, Table V-3).

Next, the substrate scope of these Cu catalysts was evaluated (Table V-3). The catalyst prepared by method A converted a variety of acetophenone derivatives having electron-withdrawing groups at the 2', 3' or 4' position of the aromatic ring. In all cases, the selectivity was lower than the one obtained with 4'-NO<sub>2</sub>-acetophenone ranging from 0% e.e. for 2'-NO<sub>2</sub>-acetophenone to 55% e.e. for 3'-NO<sub>2</sub>-acetophenone. The absence of selectivity observed for 2'-NO<sub>2</sub>-acetophenone was not surprising considering that enantioselectivity for this substrate was never describe with copper catalysed hydrosilylation. We then compared the performance of this catalyst depending on its method of preparation for three substrates: acetophenone, 4'-Me-acetophenone and 4'-Br-acetophenone. The difference of reactivity for acetophenone and 4'-Me-acetophenone was striking: whilst no activity was observed with catalyst prepared by method A, the one prepared by method B was active leading to 91% and 58% conversion for acetophenone and 4'-Br-acetophenone respectively. The effect was important: the catalyst prepared by method A did not convert acetophenone even upon reflux. The selectivity obtained for the hydrosilylation of acetophenone and 4'-Me-acetophenone was modest in both cases

Table V-3: Influence of the preparation method of the catalyst on the reactivity towards acetophenone derivatives

Entry	ketone	method	time	temperature	conversion	e.e.
1	R = 4'-NO <sub>2</sub>	A	1-7 h	0°C	100%	-68% (S)
2	R = 4'-NO <sub>2</sub>	B	20 min	0°C	100%	-63% (S)
3	R = H	A	12 h	r.t.	0% <sup>(a)</sup>	-
4	R = H	B	30 min	0°C	91%	-23% (S)
5	R = 4'-Me	A	12 h	r.t.	5%	-
6	R = 4'-Me	B	12 h	0°C	58%	-30% (S)
7	R = 4'-F	A	2 h	r.t.	38%	-29% (S)
8	R = 4'-Cl	A	12 h	r.t.	68%	-40% (S)
9	R = 4'-Br	A	12 h	r.t.	70%	-42% (S)
10	R = 4'-Br	B	15 min	0°C	100%	-50% (S)
11	R = 4'-CF <sub>3</sub>	A	12h	r.t.	100%	-39% (S)
12	R = 3'-NO <sub>2</sub>	A	12 h	r.t.	100%	-55% (S)
13	R = 2'-NO <sub>2</sub>	A	12 h	r.t.	70%	0%

Reaction conditions: acetophenone derivative (0.17 mmol, 0.3 M), Cu(OAc)<sub>2</sub>·H<sub>2</sub>O (3 mol%),  $^H\text{BTA}^{\text{pPPH}_2}$  (6 mol%), **BTA (D)-Cha** (6.6 mol%), PhSiH<sub>3</sub> (1 eq), toluene (570 μL). The conversion was estimated and the e.e. determined by chiral GC analysis. The most retained enantiomer (negative e.e. value on the chiral GC used is always the (S) for enantiomer.<sup>[37]</sup> (a) No conversion observed even upon reflux.

Whereas the enhanced reactivity displayed by the fully soluble catalyst (method B) is likely related to a higher proportion of copper atoms coordinated to the BTA polymers, the origin of the different selectivities displayed by the two methods in the case of 4'-NO<sub>2</sub>-acetophenone remained to elucidate. At this moment, several hypotheses can be made: i) traces of THF are still present which reduces the length of the BTA assemblies, ii) the nature of the copper complex is different and iii) the local environment of the Cu complex is different.

#### D. Chirality amplification: diluted majority rule experiments

Having selected the best BTA monomers and reaction conditions for the catalyst, we next envisaged testing its chirality amplification properties. Before testing our strategy to switch the selectivity of the catalytic reaction, we sought to determine the conditions in which the chirality amplification properties of the catalyst are optimal. As the chirally-switchable catalyst will be composed of a scalemic mixture of enantiopure co-monomers (**BTA Cha**) and achiral <sup>H</sup>**BTA**<sup>pph<sub>2</sub></sup> ligand, the chirality amplification properties will be governed by: i) the ability of the major enantiomer to impose its chirality to the minor enantiomer and ii) the transfer of chirality from the scalemic mixture to the achiral monomer. Such experiments, in which the enantiomeric monomers are mixed with achiral monomers, are called “diluted majority rule” experiments. Meijer *et al.* has shown previously that the temperature has a strong influence on the degree of chirality amplification exhibited by such systems.<sup>[39]</sup> Thus, diluted majority rule experiments were performed under several conditions (temperature, R<sup>0</sup>Cha, C<sup>ion</sup>) by using 25% enantiomeric excess of **BTA Cha**. The results are shown in Table V-4 in which the majority-rule factor (R<sub>ampl</sub>) represents the enantiomeric excess obtained experimentally divided by the enantiomeric excess that should be obtained in absence of chirality amplification. This factor quantifies the extent of chirality amplification exhibited by the Cu catalytic system.

Table V-4: Diluted majority rule experiments performed under different reaction conditions

Entry	Method	Temp	R <sup>0</sup> Cha	BTA Cion <sup>(a)</sup> (mM)	Majority-rule factor R <sub>ampl</sub>
1	A	-25°C	1.1	35.5	1.65
2	A	0°C	1.1	35.5	1.82
3	A	25°C	1.1	35.5	1.46
4	A	0°C	2.2	71	2.73
5	A	0°C	2.2	142	2.70
6	B	0°C	1.1	35.5	1.72
7	B	0°C	2.2	71	2.87

Conditions: 4'-NO<sub>2</sub>-acetophenone (0.17 mmol): Cu(OAc)<sub>2</sub>·H<sub>2</sub>O (3 mol%), <sup>H</sup>**BTA**<sup>pph<sub>2</sub></sup> (6 mol%), **BTA Cha** (25% e.e., 6.6 mol% (R<sup>o</sup> = 1.1) or 12.2 mol% (R<sup>o</sup> = 2.2)), PhSiH<sub>3</sub> (1 eq), solvent (570 μL or 285 μL for Cion = 142 mM), Majority rule factor = (e.e. product obtained with 25% e.e BTA Cha)/(e.e. obtained without MR effect *i.e.* 0.25\*optimal activity under these conditions). (a) Total BTA concentration = [<sup>H</sup>**BTA**<sup>pph<sub>2</sub></sup>] + [**BTA Cha**]

We were pleased to see that in all the conditions tested, the catalyst exhibited a significant degree of chirality amplification (R<sub>ampl</sub>>>1.0). The degree of chirality amplification did not vary monotonously with the temperature: the majority rule factor is higher at 0°C than at -25°C and 20°C (compared entries 1-3). We also found that R<sup>0</sup><sub>cha</sub> was an important parameter: doubling the amount of **BTA Cha**

compared to  $\text{H}^{\text{BTA}}\text{P}^{\text{PPh}_2}$  strongly increased the extent of chirality amplification ( $R_{\text{ampl}}$  from 1.82 to 2.73, entry 1 and 4). This increase in the degree of chirality amplification might be related to a higher total concentration in BTA inferring that longer supramolecular assemblies were present. However, an optimal length was probably reached in these conditions since doubling the total BTA concentration did not further increase the degree of chirality amplification (entry 5). The method of preparation of the catalyst did not modify significantly  $R_{\text{ampl}}$  (compare entries 1 and 6 and entries 4 and 7). The higher and more reliable reactivity of the fully soluble catalyst (method B) led us to rely on this method for the preparation of our dynamic and chirality-switchable catalyst.

Chirality amplification property of this catalyst was finely probed by measuring its selectivity as a function of the enantiomeric excess of the BTA Cha co-monomers (Figure V-5). This plot clearly demonstrated that the catalyst displays strong chirality amplification properties: 50% of enantiomeric excess in **BTA-Cha** already yielded the optimal selectivity (60% e.e.) for the catalytic reaction and 33% e.e. in **BTA Cha** provided the hydrosilylation product in 90% of the optimal selectivity (55% e.e.). As expected, the degree of chirality amplification was the same for the catalysts of inverse chirality.

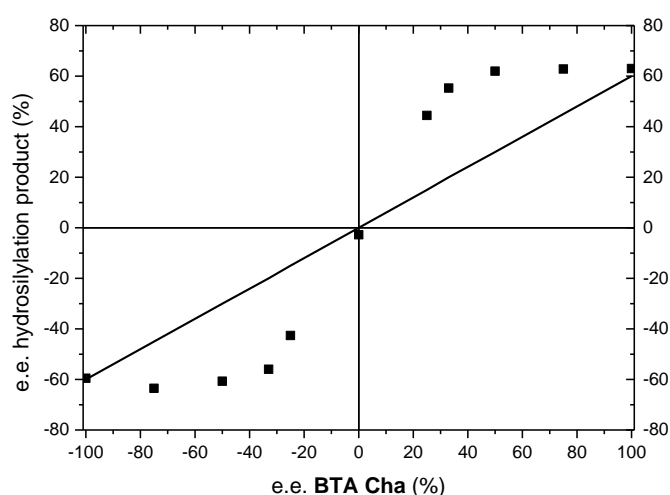


Figure V-5: Plot of the enantioselectivity of the hydrosilylation reaction as a function of the enantiomeric excess of the BTA co-monomer **BTA-Cha**. The black line represents the e.e. of the product obtained in absence of chirality amplification. Conditions:  $\text{Cu}(\text{OAc})_2 \cdot \text{H}_2\text{O}$  (3 mol%),  $\text{H}^{\text{BTA}}\text{P}^{\text{PPh}_2}$  (6 mol%), ester **BTA Cha** (12.2 mol%),  $\text{PhSiH}_3$  (1 eq), 4'-NO<sub>2</sub>-acetophenone, toluene, 0°C, 30 min. Method of preparation B.

#### a) Dynamic and chirality-switchable supramolecular catalyst

A preliminary experiment was conducted to test the dynamic behaviour of the Cu supramolecular catalytic system. **BTA (L)-Cha** was added during the course of the catalytic reaction after *ca.* 40% of conversion of 4'-NO<sub>2</sub>-acetophenone instead of prior to the catalytic experiment as above. Chiral GC analysis prior to the addition of **BTA (L)-Cha** confirms that the reaction was not selective. At the end of the catalytic reaction, the final product exhibits 40% of enantiomeric excess, which was close to the e.e. expected for conversion of 60% of the starting material with the optimal selectivity (60% e.e. at room temperature). This indicated that the **BTA (L)-Cha** was able to insert into the already formed Cu

supramolecular catalyst during the course of the reaction. This also ruled out any kinetic effects: (i) in the incorporation of newly introduced **BTA Cha** in the solution of the already formed stacks, and (ii) in the chirality amplification. Such rapid mixing of different BTA supramolecular structure with rapid chirality amplification is not unusual and was previously described by Meijer *et al.*<sup>[39]</sup>

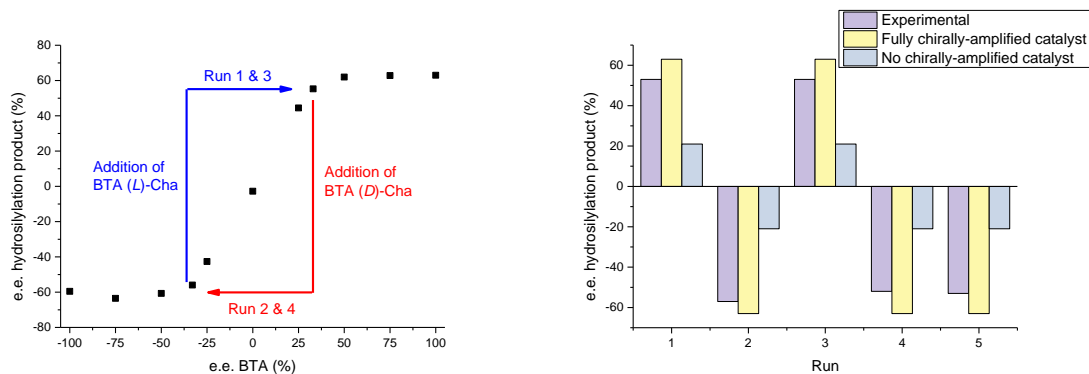


Figure V-6: In-situ probe of the chirality-switch of the supramolecular catalyst. Left: schematic representation of the proof-of-concept experiment. Right: experimental results: starting conditions: 4'-NO<sub>2</sub>-acetophenone (0.17 mmol), Cu(OAc)<sub>2</sub>·H<sub>2</sub>O (3 mol%), <sup>H</sup>BTA<sup>dppPh<sub>2</sub></sup> (6 mol%), **BTA (L)-Cha** (33% e.e., 13.2 mol%, PhSiH<sub>3</sub> (0.34), toluene (570 μL), method of preparation: B, 0°C. Complete experimental detail can be found in experimental part. For each run, the observed experimental e.e. for the product is compared with the optimal selectivity that would be obtained with a fully chirally-amplified catalyst and the selectivity obtained for a catalyst with no chirality amplification properties. During this experiment a TON of 267 is obtained. Calculation for the e.e. of each run can be found in Table V-S1

Finally, we probed the feasibility of our concept for the design of a dynamic and chirally-switchable catalyst. We started the first catalytic run in the optimised conditions mentioned above for the hydrosilylation of 4'-NO<sub>2</sub>-acetophenone with a scalemic mixture of **BTA Cha** (33% e.e. in favour of the (*L*)-enantiomer). After completion of the first run, 2 equivalents of **BTA (D)-Cha** relatively to **BTA (L)-Cha** was added to reverse the catalyst helicity (33% e.e. in favour of the (*D*)-enantiomer) and a new portion of substrate and silane was added (run 2). The same protocol was followed for runs 3 and 4 (see a schematic representation of the in-situ experiment with the maximal e.e. achievable for each run in Figure V-6, left). The e.e. of the hydrosilylation product was determined at the end of each run (Figure V-6, right). We were pleased to observe that the selectivity (absolute average value ≈ 54% e.e.) was: i) inverted for consecutive runs during the course of the reaction, ii) virtually identical (55% e.e.) to the maximum selectivity achievable considering the chirality amplification properties of the catalyst (see Figure V-5) and iii) close to the optimal selectivity (63% e.e.) that would be obtained with a fully chirally-amplified catalyst.

It is important to note that a dynamic catalyst with no chirality amplification properties would have performed the reaction with a far lower selectivity (<20% e.e.). This experiment was a clear proof-of-concept of the dynamic and chirally-switchable properties of the Cu supramolecular catalyst. Interestingly, the selectivity was maintained over a fifth run with addition of 4 equivalents of 4'-NO<sub>2</sub>-acetophenone that indicated a good stability of the Cu supramolecular catalyst.

## E. Characterisation of the Cu supramolecular catalyst

To definitively correlate the chirally-switchable properties of the supramolecular catalyst with the structure of the BTA polymers we performed several spectroscopic and scattering analyses.

### 1. FT-IR analyses:

The pre-catalysts obtained by mixing  ${}^H\text{BTA}^{\text{pPh}_2}$ , **BTA (L)-Cha** and  $\text{Cu}(\text{OAc})_2 \cdot \text{H}_2\text{O}$  according to methods A or B were characterised. Previously, we have shown that **BTA Cha** forms dimers in the solid state and in solution (II.C.1.b)).<sup>[40]</sup>

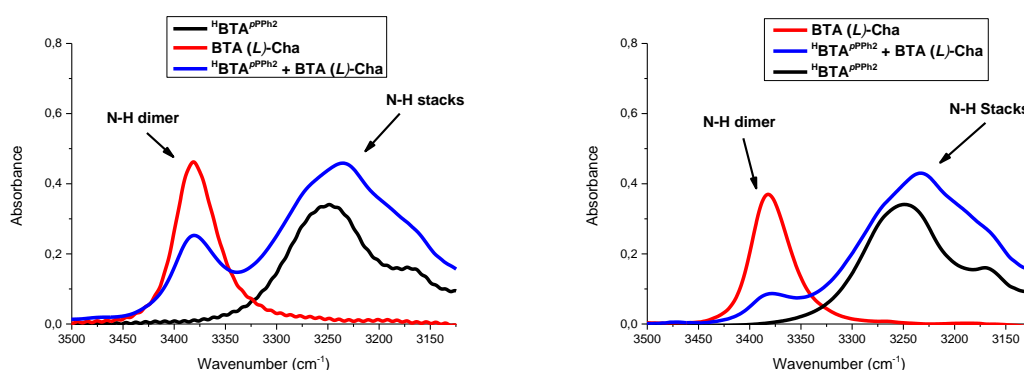


Figure V-7: FT-IR spectra of **BTA (L)-Cha** (red line, 18.6 mM),  ${}^H\text{BTA}^{\text{pPh}_2}$  (black line, 16.9 mM) and 1:1 mixture of **BTA Cha** and  ${}^H\text{BTA}^{\text{pPh}_2}$  (blue line, 16.9mM each). Left: toluene, right: MCH/toluene (4/1). MCH = methylcyclohexane. Zoom on the N-H region.

Firstly, we probed whether, similarly to **BTA IIe** (Figure IV-2), **BTA (L)-Cha** might incorporate into the stacks formed by  ${}^H\text{BTA}^{\text{pPh}_2}$  by means of FT-IR analyses. FT-IR analyses were performed in two different solvents (toluene and MCH/toluene 4/1). Analysis of a mixture of  ${}^H\text{BTA}^{\text{pPh}_2}$  and **BTA (L)-Cha** in toluene confirmed the partial incorporation of **BTA (L)-Cha** into the stacks of  ${}^H\text{BTA}^{\text{pPh}_2}$  (Figure V-7). Indeed, at equal concentration, the absorbance of the characteristic peak of the dimer of **BTA (L)-Cha** (red line,  $\nu = 3381 \text{ cm}^{-1}$ ) was lower in the mixture with  ${}^H\text{BTA}^{\text{pPh}_2}$  than in the pure sample. Also, the absorbance of the characteristic peak for the stacks was higher in the mixture (blue line compared to black line  $\nu = 3251 \text{ cm}^{-1}$ ). According to these FT-IR analyses,  $\approx 55\%$  of the **BTA (L)-Cha** in the toluene solution was incorporated into the stacks. Similar observation was drawn for the FT-IR of mixture of **BTA (L)-Cha** and  ${}^H\text{BTA}^{\text{pPh}_2}$  in MCH/toluene (4/1) albeit in that case  $\approx 77\%$  of **BTA (L)-Cha** was incorporated into the stacks. At that time, we have no explanation for the enhanced incorporation of **BTA (L)-Cha** in MCH/toluene compared to pure toluene.

We then probe the influence of the presence of copper coordinated to  ${}^H\text{BTA}^{\text{pPh}_2}$ . Results in Table V-5 indicate that in all steps of the catalyst preparation, copolymers are formed between **BTA (L)-Cha** and  ${}^H\text{BTA}^{\text{pPh}_2}$  (Figure V-8). The degree of incorporation of **BTA (L)-Cha** does not vary significantly as a function of the method of preparation of the catalyst, meaning that the different catalytic behaviour between the two catalysts likely arise from the number and nature of Cu coordination sites, not from the percentage of **BTA (L)-Cha** incorporated into the stacks.

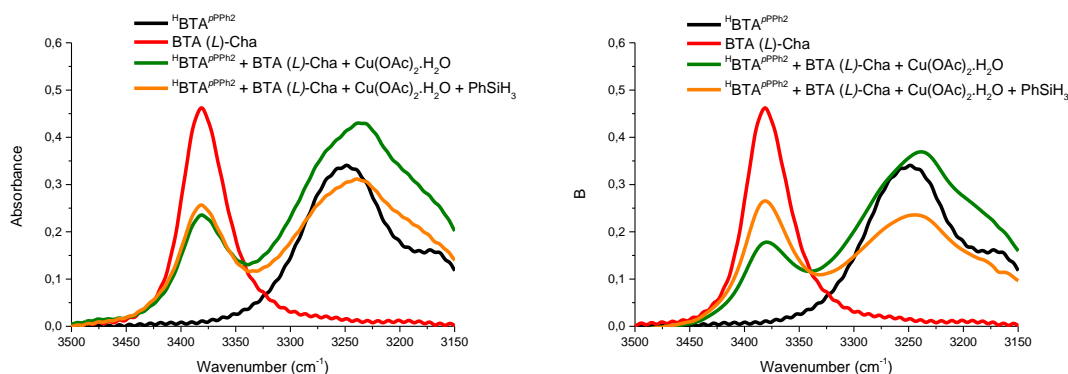


Figure V-8: FT-IR spectra in CaF<sub>2</sub> cell (0.5 mm) of **BTA (L)-Cha** (red line, 18.6 mM), <sup>H</sup>**BTA**<sup>pPPh<sub>2</sub></sup> (black line, 16.9 mM), **BTA (L)-Cha** (18.6 mM) + <sup>H</sup>**BTA**<sup>pPPh<sub>2</sub></sup> (16.9 mM) + Cu(OAc)<sub>2</sub>·H<sub>2</sub>O (8.45 mM) (green line) and **BTA (L)-Cha** (18.6 mM) + <sup>H</sup>**BTA**<sup>pPPh<sub>2</sub></sup> (16.9 mM) + Cu(OAc)<sub>2</sub>·H<sub>2</sub>O (8.45 mM) + PhSiH<sub>3</sub> (0.3 M) (orange line). Left: preparation method A. Right: preparation method B.

Table V-5: Determination by FT-IR spectroscopy of the amount of ester **BTA-(L)-Cha** incorporated into the supramolecular stacks of <sup>H</sup>**BTA**<sup>pPPh<sub>2</sub></sup>

Method	Composition <sup>(a)</sup>	% Cha <sup>(b)</sup>	R <sub>Cha</sub> in stacks <sup>(c)</sup>
No Cu	R <sup>0</sup> <sub>Cha</sub> = 1.1	55%	0.61
A	R <sup>0</sup> <sub>Cha</sub> = 1.1 + Cu	52%	0.57
	R <sup>0</sup> <sub>Cha</sub> = 1.1 + Cu + PhSiH <sub>3</sub>	47%	0.52
B	R <sup>0</sup> <sub>Cha</sub> = 1.1 + Cu	61%	0.67
	R <sup>0</sup> <sub>Cha</sub> = 1.1 + Cu + PhSiH <sub>3</sub>	42%	0.46

(a) Cu(OAc)<sub>2</sub>·H<sub>2</sub>O (4.95 μmol), <sup>H</sup>**BTA**<sup>pPPh<sub>2</sub></sup> (9.9 μmol), **BTA (L)-Cha** (R<sup>0</sup> equivalent compared to <sup>H</sup>**BTA**<sup>pPPh<sub>2</sub></sup>), toluene (570 μL). (b) %Cha = % Cha incorporated into stacks = A<sub>BTA-Cha</sub> mixture / A<sub>BTA-Cha</sub> pure at the same concentration. (c) R<sub>Cha</sub> in stacks = n**BTA (L)-Cha** incorporated / (n<sup>H</sup>**BTA**<sup>pPPh<sub>2</sub></sup>)

## 2. SANS analyses:

The nature and composition of the co-polymers formed by mixing <sup>H</sup>**BTA**<sup>pPPh<sub>2</sub></sup>, coordinated or not to Cu, and **BTA (L)-Cha** were also probed by SANS analyses performed in toluene-d<sub>8</sub> (Figure V-9, left). Fitting the SANS data according to a form factor for spherical objects confirmed that **BTA (L)-Cha** alone formed small objects at the concentration used in catalysis ( $r = 12.0 \text{ \AA}$ ,  $M_{\text{spherical object}}/M_{\text{monomer}} = 1.5$ ). The formation of dimers was ascertained by the FT-IR analyses mentioned above (Figure V-7). <sup>H</sup>**BTA**<sup>pPPh<sub>2</sub></sup> alone formed cylindrical objects longer than  $230 \text{ \AA}$  with a radius ( $r = 10.5 \text{ \AA}$ ) consistent with the presence of a single molecule of BTA monomer in the cross-section. The SANS analysis of the mixture between <sup>H</sup>**BTA**<sup>pPPh<sub>2</sub></sup> and **BTA (L)-Cha** ( $\text{BTA (L)-Cha}/\text{BTA}^{\text{pPPh}_2} = 1.1$ , 18.6 and 16.9 mM respectively, *i.e.* the catalysis concentration of Table V-1) confirmed the incorporation of the dimers of **BTA (L)-Cha** into the stacks of the ligand. Indeed, the scattering intensity of the SANS signal obtained for the mixture was superior to the signal of <sup>H</sup>**BTA**<sup>pPPh<sub>2</sub></sup> which corroborated the incorporation of **BTA (L)-Cha** into the stacks. Then the signal was fitted making the hypothesis that **BTA (L)-Cha** partly inserts into the stacks and that the remaining **BTA (L)-Cha** forms dimers. A very good fit was indeed obtained confirming the validity of the hypothesis. The fit indicated that 67% of the **BTA (L)-Cha** was inserted into the stacks at these concentrations. This

result was in the same order than that independently obtained from FT-IR measurements (55% of **BTA (L)-Cha** incorporated). SANS analyses therefore corroborated the results obtained by FT-IR.

The analysis of the scattering curves obtained for mixtures containing copper was far more complex and must be interpreted carefully (Figure V-9). Copper pre-catalysts prepared according to method B have not been analysed.

Firstly, a mixture of  ${}^{\text{H}}\text{BTA}^{\text{pPPh}_2}$ , **BTA (L)-Cha** and  $\text{Cu}(\text{OAc})_2 \cdot \text{H}_2\text{O}$  prepared in toluene- $d_8$  similarly to method A mentioned above yielded a yellowish solution after removal of the precipitate (expected to be mainly  $\text{Cu}(\text{OAc})_2 \cdot \text{H}_2\text{O}$ ). This sample was measured after a few days and a new (colourless) precipitate had appeared at that time. The SANS intensity (Figure V-9, right green square) was lower for this mixture than for **BTA (L)-Cha**/ ${}^{\text{H}}\text{BTA}^{\text{pPPh}_2}$  mixture mentioned above confirming the partial precipitation of the BTA monomers. The SANS mixture was used for the hydrosilylation of 4'- $\text{NO}_2$ -acetophenone: it proved to be active but not selective (0% e.e.). Clearly, this  ${}^{\text{H}}\text{BTA}^{\text{pPPh}_2}$ , **BTA (L)-Cha** and  $\text{Cu}(\text{OAc})_2 \cdot \text{H}_2\text{O}$  mixture analysed by SANS was different from the active and selective Cu pre-catalyst obtained in the classical conditions.

Secondly, a mixture of  ${}^{\text{H}}\text{BTA}^{\text{pPPh}_2}$  and  $\text{Cu}(\text{OAc})_2 \cdot \text{H}_2\text{O}$  was prepared in toluene- $d_8$  without **BTA (L)-Cha**. After removing the insoluble part (expected to be non-coordinated  $\text{Cu}(\text{OAc})_2 \cdot \text{H}_2\text{O}$ ) by centrifugation, a colourless solution was obtained. No precipitate formed prior to SANS analysis. Surprisingly, a higher scattering intensity was found for the “mixture” of  ${}^{\text{H}}\text{BTA}^{\text{pPPh}_2}$  and copper than for pure  ${}^{\text{H}}\text{BTA}^{\text{pPPh}_2}$  (Figure V-9, right magenta square). Results of the fit suggested the formation of long cylindrical objects with two BTA molecules in the cross-section. This could indicated the aggregation of several stacks by means of copper atoms serving as bridges between the assemblies. However further investigation is required to ascertain the structure of the assemblies formed by mixing  ${}^{\text{H}}\text{BTA}^{\text{pPPh}_2}$  and  $\text{Cu}(\text{OAc})_2 \cdot \text{H}_2\text{O}$ .

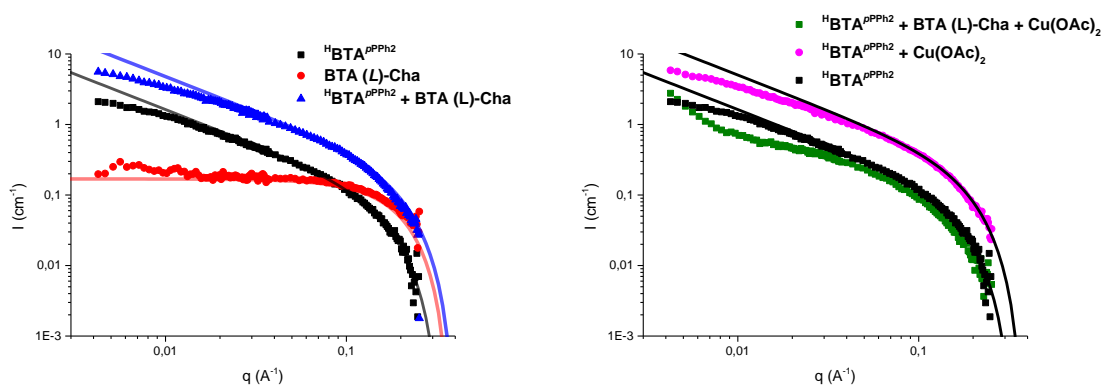


Figure V-9: SANS analyses in toluene- $d_8$ , the black line represents the fit for long rod-shape objects and the red one the fit for spherical objects. Left: **BTA (L)-Cha** (red circle, 18.6 mM),  ${}^{\text{H}}\text{BTA}^{\text{p-Ph}_2}$  (black square, 16.9 mM) and the mixture of both (blue triangle). Right: **BTA (L)-Cha** (18.6 mM) +  ${}^{\text{H}}\text{BTA}^{\text{p-Ph}_2}$  (16.9 mM) +  $\text{Cu}(\text{OAc})_2 \cdot \text{H}_2\text{O}$  (8.45 mM) (green square) and  ${}^{\text{H}}\text{BTA}^{\text{pPPh}_2}$  (16.9 mM) +  $\text{Cu}(\text{OAc})_2 \cdot \text{H}_2\text{O}$  (8.45 mM) (magenta square). For the Cu complexes: method of preparation A and the suspensions were centrifuged to discard the insoluble part.

### 3. $^{31}\text{P}\{^1\text{H}\}$ NMR analyses

Having established the formation of copolymers between **BTA Cha** and  $^{\text{H}}\text{BTA}^{\text{PPh}_2}$ , coordinated or not to Cu, we next attempted to gain information into the nature of the copper complex formed between the BTA ligand and  $\text{Cu}(\text{OAc})_2 \cdot \text{H}_2\text{O}$ .  $^{31}\text{P}\{^1\text{H}\}$  NMR analyses were prepared in toluene- $\text{d}_8$  for each step of the preparation of the Cu supramolecular catalyst for both methods of preparation (Figure V-10). It is important to remind that NMR analyses of copper complexes prepared with methods A and B are hard to interpret for the following reasons: i) mixing a copper(II) precursor with phosphine ligands may lead to phosphine copper complexes at oxidation states I and/or II, ii) Cu(II) complexes are paramagnetic, iii) triphenylphosphine complexes of copper exist under different forms in equilibrium in solution,<sup>[41,42]</sup> and iv) Cu quadrupolar interactions complicate the splitting of the phosphorus resonances.<sup>[43]</sup>

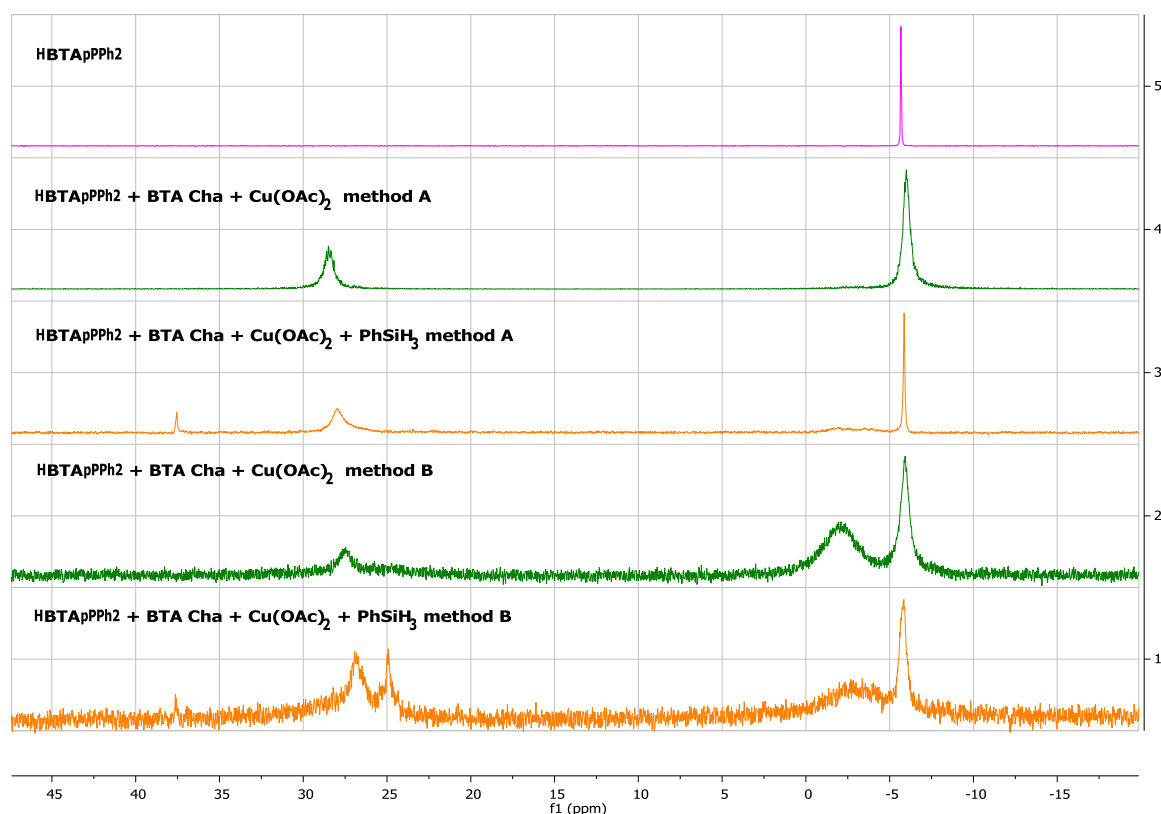


Figure V-10:  $^{31}\text{P}\{^1\text{H}\}$  NMR spectra for each step of the preparation of the copper catalyst in toluene- $\text{d}_8$ . Method A:  $\text{Cu}(\text{OAc})_2 \cdot \text{H}_2\text{O}$  (4.95  $\mu\text{mol}$ ),  $^{\text{H}}\text{BTA}^{\text{P-Ph}_2}$  (9.9  $\mu\text{mol}$ ), **BTA (L)-Cha** (10.9  $\mu\text{mol}$ ), toluene- $\text{d}_8$  (570  $\mu\text{L}$ ). Method B:  $\text{Cu}(\text{OAc})_2 \cdot \text{H}_2\text{O}$  (4.95  $\mu\text{mol}$ ),  $^{\text{H}}\text{BTA}^{\text{P-Ph}_2}$  (9.9  $\mu\text{mol}$ ) in THF (500  $\mu\text{L}$ ) then removal of the THF and addition of **BTA (L)-Cha** (10.9  $\mu\text{mol}$ ), toluene- $\text{d}_8$  (570  $\mu\text{L}$ ). Note: The complex of  $^{\text{H}}\text{BTA}^{\text{P-Ph}_2}$  and  $[\text{Cu}(\text{OAc})_2]$  prepared with method B, *i.e.* without **BTA (L)-Cha**, is not soluble in toluene- $\text{d}_8$  and therefore not analysed.

The copper complex between  $^{\text{H}}\text{BTA}^{\text{PPh}_2}$  and  $\text{Cu}(\text{OAc})_2 \cdot \text{H}_2\text{O}$  prepared according to method A showed a broad signal that appeared at *ca.* 28 ppm concomitantly to a broadening of the resonance corresponding to the BTA ligand ( $\delta$  at -6 ppm). Similar signals were observed for the Cu complex obtained by means of method B but a major broad signal was also present at *ca.* -2 ppm. Addition of  $\text{PhSiH}_3$  to these mixtures induced some changes in the ratio of these signals and a new peak appears at



ca. 25 ppm in case of Cu complex prepared by method B. These  $^{31}\text{P}\{^1\text{H}\}$  NMR analyses confirmed the coordination of Cu centres to the phosphine ligand and that several Cu species were formed which were in slow exchange (on the NMR timescale) with the free phosphine ligands. However, the exact nature of these Cu species and their role in the catalytic process are still under investigation.

#### 4. CD analyses

Finally, we probed the chiroptical properties of the copolymers. CD analyses were performed at the same concentrations ( $C_{\text{BTA}}$  total= 35.5 mM) than those used in the proof-of-concept of the chirality-switchable ability of our catalyst (Figure V-11). Analyses were conducted in cyclohexane/toluene (4/1) instead of pure toluene in order to limit the solvent absorption (Figure V-11). Indeed, CD analyses, in pure toluene, of the mixture between  $^{\text{H}}\text{BTA}^{\text{pPPh}_2}$ , **BTA Cha** and  $\text{Cu}(\text{OAc})_2 \cdot \text{H}_2\text{O}$  prepared with method B gave a low intensity CD signal at  $\lambda=330$  nm that limits the possible interpretation (see Figure V-S1 in the experimental part).

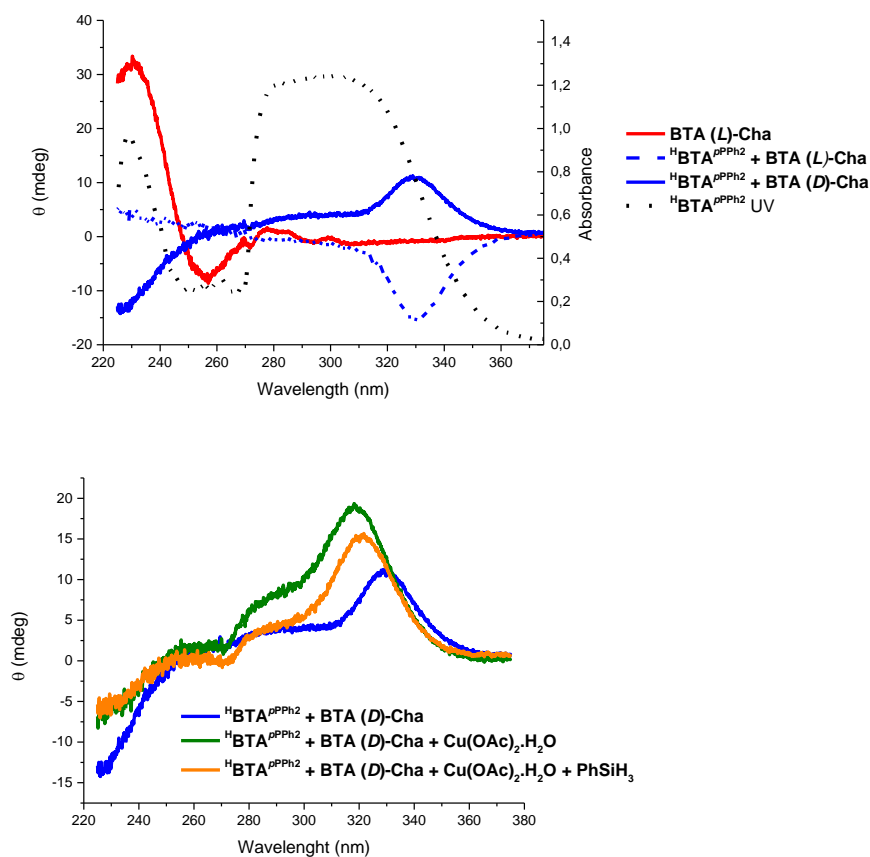


Figure V-11: CD analyses of the copolymers in MCH/toluene 4/1, top: **BTA (D)-Cha** (18.6 mM, red line),  $^{\text{H}}\text{BTA}^{\text{pPPh}_2}$  + **BTA (D)-Cha** (16.9 mM and 18.6 mM respectively blue line),  $^{\text{H}}\text{BTA}^{\text{pPPh}_2}$  + **BTA (L)-Cha** (16.9 mM and 18.6 mM respectively blue dot); UV spectrum of  $^{\text{H}}\text{BTA}^{\text{pPPh}_2}$  (black dotted line). bottom:  $^{\text{H}}\text{BTA}^{\text{pPPh}_2}$  + **BTA (D)-Cha** (16.9 mM and 18.6 mM respectively blue),  $^{\text{H}}\text{BTA}^{\text{pPPh}_2}$  + **BTA (D)-Cha** +  $\text{Cu}(\text{OAc})_2 \cdot \text{H}_2\text{O}$  (16.9 mM, 18.6 mM, 8mM respectively green),  $^{\text{H}}\text{BTA}^{\text{pPPh}_2}$  + **BTA (D)-Cha** +  $\text{Cu}(\text{OAc})_2 \cdot \text{H}_2\text{O}$  +  $\text{PhSiH}_3$  (16.9 mM, 18.6 mM, 8mM and 280 mM respectively orange). Cu complexes were prepared according to method A except that MCH/toluene 4/1 is used instead of pure toluene.

In MCH/toluene, the copolymer formed between **BTA (D)-Cha** and  $^{\text{H}}\text{BTA}^{\text{pPPh}_2}$  (1.1 ratio) exhibits, a CD signal ca. 330 nm, a region in which only the ligand absorbs (see the UV trace of the ligand in

black dotted line, Figure V-11, top spectra, black dot). This indicates that the intrinsically achiral BTA ligand is located within the chiral environment of the supramolecular copolymer. Coordination of copper to the BTA ligand gave a similar CD spectrum (Figure V-11, bottom spectra, green line) with a shoulder in the 280-300 nm region. Addition of PhSiH<sub>3</sub> to the Cu complex led to a similar spectrum but with decreased intensity for the CD signal that might indicate a modification of the stacks. As expected, the induced CD signal is inverted when **BTA (L)-Cha** is used instead of **BTA (D)-Cha** as the enantiopure co-monomer. This clearly demonstrates that the chiral environment around the copper centre is induced by the chiral co-monomer and that the handedness of the BTA supramolecular copolymer is controlled by the co-monomer.

## F. Conclusion

Chiral BTA ligands and mixtures between an intrinsically-achiral BTA ligand and an enantiopure ester BTA co-monomer provided good selectivity in the copper-catalysed hydrosilylation of 4'-NO<sub>2</sub>-acetophenone. Screening of various BTA co-monomers showed that **BTA Cha** was the best chirality inducer. Control experiments clearly demonstrated that the selectivity arose from the formation of a supramolecular helical copolymer and that this supramolecular catalyst was soluble under the reaction conditions. The following optimised conditions allowed to reach 80% e.e. for the reaction conducted at -25°C in toluene: Cu(OAc)<sub>2</sub>·H<sub>2</sub>O as the copper source, <sup>H</sup>**BTA**<sup>pPh<sub>2</sub></sup> as the ligand, **BTA Cha** as the co-monomer and PhSiH<sub>3</sub> as the silane source. An equimolar amount of **BTA Cha** relatively to <sup>H</sup>**BTA**<sup>pPh<sub>2</sub></sup> was required in order to get the optimal selectivity.

The supramolecular Cu catalyst exhibited a strong chirality amplification effect as demonstrated by the investigation of several scalemic mixtures of **BTA Cha** and <sup>H</sup>**BTA**<sup>pPh<sub>2</sub></sup> which provided the same selectivity as mixtures with enantiopure **BTA Cha** monomers. This chirality amplification effect was optimised: a scalemic mixture of **BTA Cha** (33% e.e.) with the achiral ligand was able to induce up to 90% of the optimal enantioselectivity. The solubility of the Cu supramolecular catalyst and its strong chirality amplification properties allowed us to reversibly inverse the chirality of the Cu catalytic species during the course of the reaction upon successive addition of **BTA Cha** monomers. The chirality-switchable nature of the catalyst was demonstrated by inverting four times the major enantiomer obtained in the hydrosilylation of 4'-NO<sub>2</sub>-acetophenone. The selectivity was close to the one expected for a fully chirally-amplified catalytic system and far higher than those expected for a catalyst lacking chirality amplification properties.

The supramolecular Cu complex was characterised by means of FT-IR, SANS, NMR and CD analyses. These analyses confirm the formation of a supramolecular copolymer between **BTA Cha** and <sup>H</sup>**BTA**<sup>pPh<sub>2</sub></sup>, coordinated or not to Cu. The exact nature of the Cu complex was not determined. CD analyses revealed that the copper metal was located in a chiral environment within the co-assemblies and that the handedness of the co-assemblies was controlled by the nature of the enantiopure co-

monomer. Together with the catalytic results, these analyses confirmed that the chirality-switchable nature of the catalyst was predictable since related to the supramolecular structure of the BTA co-assemblies. Such a dynamic and chirality-switchable catalyst could be useful in cascade catalysis in which the enantioselectivity of each reaction could be tuned. Also in the case of a single substrate with multiple reacting sites, one can envisage to control the sense of diastereoiduction in order to access all possible stereoisomers with a single chiral catalyst.<sup>[44]</sup>

Further studies are in due course which concern: i) CD analyses and more precisely diluted majority experiments in order to correlate the chirality amplification properties of the catalyst with that of the supramolecular BTA copolymer and, ii) a further understanding of the origin of the different catalytic performance exhibited by the Cu catalysts depending on their mode of preparation.

## G. Experimental part:

General Procedures: CD, SANS, FT-IR and NMR see chapter III.

### 1. Supplementary Figures:

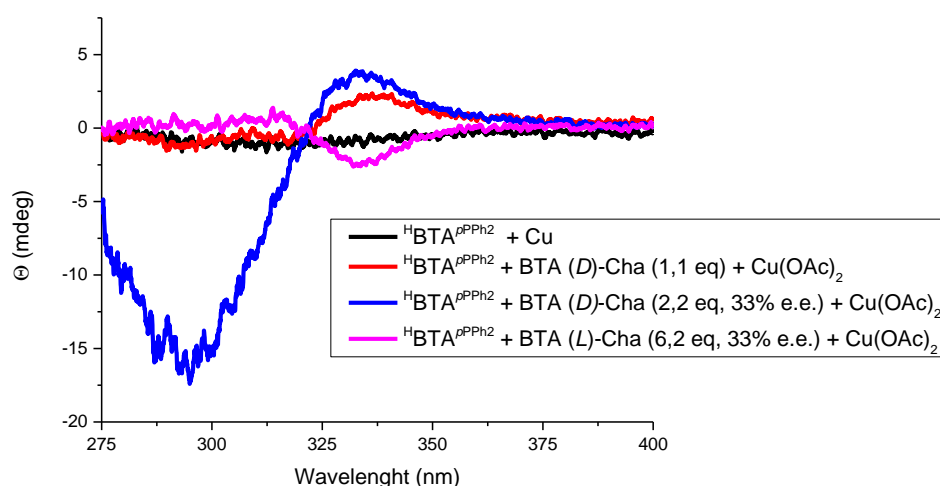
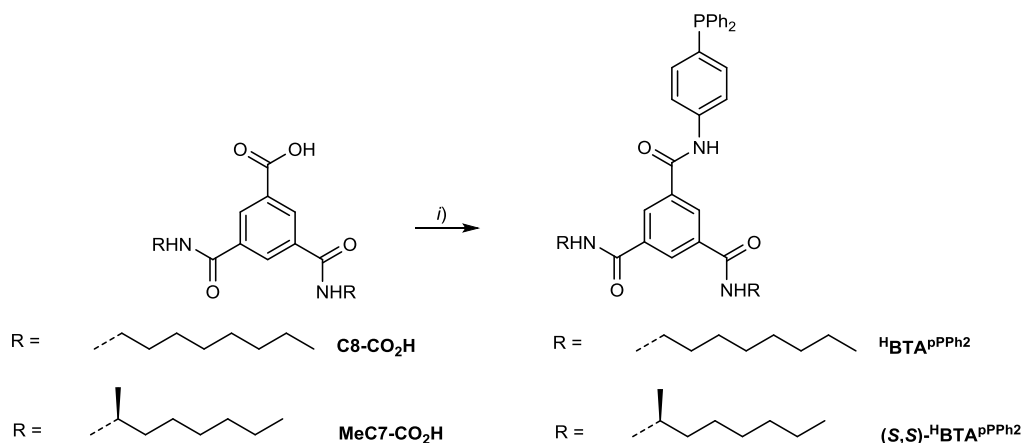


Figure V-S1: CD analyses of the co-polymers in toluene.  $\text{H-BTA}^{\text{pPPh}_2} + \text{Cu}(\text{OAc})_2 \cdot \text{H}_2\text{O}$  (16.9 mM and 8 mM respectively),  $R_{\text{Cha}}^{\circ} = 1.1$  at 100% e.e (18.6 mM). (red line),  $R_{\text{Cha}}^{\circ} = 2.2$  and at 33% e.e in favour of the (*D*) enantiomer (37.2 mM) (blue line) and  $R_{\text{Cha}}^{\circ} = 6.2$  at 33% e.e. in favour of the (*L*) enantiomer (115.3 mM) (purple line). Cu complexes were prepared according to method B.

### 2. Synthesis

The synthesis of the ester BTAs<sup>[40,45]</sup> and the preparation of (*S,S*)- $\text{H-BTA}^{\text{mPPh}_2}$ ,<sup>[23]</sup>  $\text{H-BTA}^{\text{mPPh}_2}$ <sup>[23]</sup> and  $\text{C8-CO}_2\text{H}$ <sup>[46]</sup> were described previously.



**(S,S)-MeC7-CO<sub>2</sub>H**: An oven-dried Schlenk flask under argon was loaded with 1-methyl ester-1,3,5-benzenetricarboxylic acid (3.0 g, 13.3 mmol) and dry THF (80 mL). Then N,N-dimethylaminopyridine (5.6 g, 45.5 mmol), Et<sub>3</sub>N-(3-dimethylaminopropyl)-N'-ethylcarbodiimide hydrochloride (8.7 g, 45.5 mmol) and (S)-2-aminooctane (4.0 mL, 39.9 mmol) were added. The suspension was refluxed for 2 days before evaporation under reduced pressure. The crude product was purified by column chromatography on silica gel eluting with DCM/EtOAc (92/8) to yield **(S,S)-MeC7-CO<sub>2</sub>Me** as a colourless solid which was engaged in the next step without further purification. **(S,S)-MeC7-CO<sub>2</sub>Me** (1.61 g, 3.6 mmol) and LiOH (138 mg, 5.76 mmol) were dissolved in MeOH (150 mL) and water (3 mL) was added. The resulting solution was heated to 55°C overnight. Then 500 mL of water were added and the product was precipitated by addition of HCl 1N. The precipitate was filtered off, washed with water and dried over P<sub>2</sub>O<sub>5</sub> to give **MeC7-CO<sub>2</sub>H** as a white powder (1.56 g, 27% yield over two steps).

**<sup>1</sup>H NMR** (300 MHz, DMSO-*d*<sub>6</sub>) δ 13.33 (s, 1H), 8.49 (m, 5H), 4.02 (m, 2H), 1.51 (m, 4H), 1.26 (m, 16H), 1.15 (d, *J* = 6.6 Hz, 6H), 0.89-0.75 (m, 6H). **<sup>13</sup>C{<sup>1</sup>H} NMR** (75 MHz, DMSO-*d*<sub>6</sub>) δ 166.6, 164.5, 135.5, 131.0, 130.5, 130.1, 45.1, 35.8, 31.2, 28.6, 25.8, 22.0, 20.7, 13.9.

Synthesis of **HBTAP<sup>PPH<sub>2</sub></sup>**: **C8-CO<sub>2</sub>H** (1.5 g, 3.5 mmol), dry THF (100 mL) are mixed in an oven-dried Schlenk flask under argon, then the N,N-dimethylaminopyridine (721 mg, 5.9 mmol), the N-(3-Dimethylaminopropyl)-N'-ethylcarbodiimide hydrochloride (1.13 g, 5.9 mmol) and the 4-diphenylphosphinoaniline (1.44 g, 5.2 mmol) were added as solids. The suspension was refluxed for 2 days before concentration under reduced pressure. The crude product was purified by column chromatography on silica gel eluting with DCM/EtOAc (95/5 to 7/1) to yield **HBTAP<sup>PPH<sub>2</sub></sup>** as a white solid (1.9 g, 79%). **<sup>1</sup>H NMR** (300 MHz, DMSO-*d*<sub>6</sub>) δ 10.62 (s, 1H), 8.68 (t, *J* = 5.6 Hz, 2H), 8.45 (dd, *J* = 7.7, 1.6 Hz, 3H), 7.84 (d, *J* = 8.1 Hz, 2H), 7.46-7.37 (m, 6H), 7.31-7.21 (m, 6H), 3.29-3.22 (m, 4H), 1.61-1.47 (m, 4H), 1.36-1.11 (m, 20H), 0.90-0.79 (m, 6H). **<sup>31</sup>P{<sup>1</sup>H} NMR** (122 MHz, DMSO-*d*<sub>6</sub>) δ -7.7. **HRMS**: Calculated for C<sub>43</sub>H<sub>55</sub>N<sub>3</sub>O<sub>3</sub>PH [M+H]<sup>+</sup>: 692.3976, found: 692.3973.

Synthesis of (*S,S*)-<sup>H</sup>BTA<sup>pPh<sub>2</sub></sup>: MeC7-CO<sub>2</sub>H (1.5 g, 3.5 mmol), dry THF (100 mL) were mixed in an oven-dried Schlenk flask under argon. Then the N,N-dimethylaminopyridine (727 mg, 5.95 mmol), the N-(3-Dimethylaminopropyl)-N'-ethylcarbodiimide hydrochloride (1.14 g, 5.95 mmol) and the 4-diphenylphosphinoaniline (1.46 g, 5.25 mmol) were added as solid. The suspension was refluxed for 2 days before evaporation under reduced pressure. The crude product was purified by column chromatography on silica gel eluting with DCM/EtOAc (100/0 to 90/10) to yield (*S,S*)-<sup>H</sup>BTA<sup>pPh<sub>2</sub></sup> as a white solid (1.9 g, 79%).

<sup>1</sup>H NMR (300 MHz, DMSO-*d*<sub>6</sub>) δ 10.61 (s, 1H), 8.49-8.37 (m, 5H), 7.84 (dd, *J* = 8.6, 1.3 Hz, 2H), 7.45-7.37 (m, 6H), 7.27 (m, 6H), 4.04 (p, *J* = 7.3 Hz, 2H), 1.63-1.37 (m, 4H), 1.36-1.23 (m, 16H), 1.16 (d, *J* = 6.6 Hz, 6H), 0.85 (q, *J* = 5.4, 4.2 Hz, 6H). <sup>13</sup>C{<sup>1</sup>H} NMR (75 MHz, DMSO-*d*<sub>6</sub>) δ 165.1, 164.7, 139.8, 137.0, 135.3, 135.1, 134.1, 133.8, 133.1, 132.9, 128.8, 128.7, 128.6, 120.4, 120.3, 45.1, 35.8, 31.1, 28.5, 25.7, 21.9, 20.6, 13.8. <sup>31</sup>P{<sup>1</sup>H} NMR (122 MHz, Acetone-*d*<sub>6</sub>) δ -6.5. HRMS: Calculated for C<sub>43</sub>H<sub>55</sub>N<sub>3</sub>O<sub>3</sub>PH [M+H]<sup>+</sup>: 692.3976, found: 692.3972.

### 3. Catalytic experiments (screening)

Typical experimental procedures for the BTA screening and for determination of the optimal conditions.

#### Method A

An oven-dried test tube was loaded with Cu(OAc)<sub>2</sub>·H<sub>2</sub>O (1 mg, 3 mol%) and the substrate (27.5 mg, 0.165 mmol) and flushed with argon for 10 seconds. Then the ligand (6.9 mg, 6 mol% in 300 μL of dry toluene) and the ester-BTA (12.9 mg in 200 μL of dry toluene) and dry toluene (ca. for volume of 570 μL) were added. The mixture was stirred 15 min before at room temperature before being cooled to the reaction temperature and further stirred for 15 min. The reaction was started by the addition of PhSiH<sub>3</sub> (21 μL, 0.165 mmol) and conversion was monitored by TLC. When reaction was completed, HCl (10%, 400 μL) was added and the mixture was stirred 30 min (until the solution becomes translucent). Then, the products were extracted with Et<sub>2</sub>O (3x1 mL) and once with EtOAc (1 mL). The solvent were removed by rotatory evaporation and the residue was taken up in DCM and passed through a silica plug eluting with DCM. The solvents were evaporated and the resulting product was analyzed <sup>1</sup>H NMR and GC.

#### Method B

An oven-dried test tube was loaded with Cu(OAc)<sub>2</sub>·H<sub>2</sub>O (1 mg, 3 mol%) and <sup>H</sup>BTA<sup>pPh<sub>2</sub></sup> ligand (6.9 mg, 6 mol% in dry THF (500 μL). The solvent was removed by rotatory evaporation and the test tube was put under vacuum (1.10<sup>-3</sup> mbar) for 1 hour. Then the substrate (27.5 mg, 0.165 mmol) was added before flushing the tube with argon for 10 seconds. The ester-BTA (12.9 mg in 200 μL of dry toluene) and dry toluene (ca. for volume of 570 μL) in then added and the mixture was stirred 15 min at room

temperature before being cooled to the reaction temperature and further stirred for 15 min. The reaction was started by the addition of PhSiH<sub>3</sub> (21 μL, 0.165 mmol) and conversion was monitored by TLC. When reaction was completed, HCl (10%, 400 μL) was added and the mixture was stirred 30 min (until the solution becomes translucent). Then, the products were extracted with Et<sub>2</sub>O (3x1 mL) and once with EtOAc (1 mL). The solvent were removed by rotatory evaporation and the residue was taken up in DCM and passed through a silica plug eluting with DCM. The solvents were evaporated and the resulting product was analyzed <sup>1</sup>H NMR and GC.

#### 4. Catalytic procedures for the chirality amplification experiments:

Proof-of-concept of the chirality-switchable nature of the Cu supramolecular catalyst:

Experimental procedure

An oven-dried test tube was loaded with Cu(OAc)<sub>2</sub>·H<sub>2</sub>O (1 mg, 3 mol%) and <sup>H</sup>BTA<sup>pph2</sup> ligand (6.9 mg, 6 mol% in) in dry THF (500 μL). The solvent was removed by rotatory evaporation and the test tube was put under vacuum (1.10<sup>-3</sup> mbar) for 1 hour. Then the substrate (27.5 mg, 0.165 mmol) was added before flushing the tube with argon for 10 seconds. **BTA Cha** (25.8 mg in 80μL of dry toluene and 33% e.e. in favour of the (*L*)-enantiomer) and dry toluene (*ca.* for volume of 570μL) was then added and the mixture was stirred 15 min before at room temperature before being cooled to 0°C and further stirred for 15 min. The reaction was started by the addition of PhSiH<sub>3</sub> (42 μL, 0.33 mmol) and conversion was monitored by TLC. When reaction was completed, an aliquot was taken out and quenched with HCl (10%, 1 mL) for analysis. Then BTA (*D*)-Cha (25.4 mg) was added to the reaction mixture which was stirred 30 min before substrate addition (27.5 mg) and PhSiH<sub>3</sub> (21 μL). The conversion was monitored by TLC. When reaction was completed, an aliquot is taken out and quenched with HCl (10%, 1 mL) for analysis. Then BTA (*L*)-Cha (50.7 mg) was added to the reaction mixture which was stirred 30 min before substrate addition (27.5 mg) and PhSiH<sub>3</sub> (21 μL). The conversion was monitored by TLC. When reaction was completed, an aliquot was taken out and quenched with HCl (10%, 1 mL) for analysis. Then BTA (*D*)-Cha (100 mg) was added to the reaction mixture which was stirred 30 min before substrate addition (27.5 mg) and PhSiH<sub>3</sub> (21 μL). The conversion was monitored by TLC. When reaction was completed, an aliquot was taken out and quenched with HCl (10%, 1 mL) for analysis. Then substrate was added (110 mg) and PhSiH<sub>3</sub> (84 μL). The conversion was monitored by TLC. When reaction was completed, HCl (10%, 1.6 mL) was added and the mixture was stirred 30 min (until the solution becomes translucent). Then, the products were extracted with Et<sub>2</sub>O (3x2 mL) and once with AcOEt (2 mL). The solvent were removed by rotatory evaporation and the residue was taken up in DCM and passed through a silica plug eluting with DCM. The solvents were evaporated and the resulting product was analyzed <sup>1</sup>H NMR and GC.

Table V-S1: total enantiomeric excess measured for each run and the e.e. of the run calculated

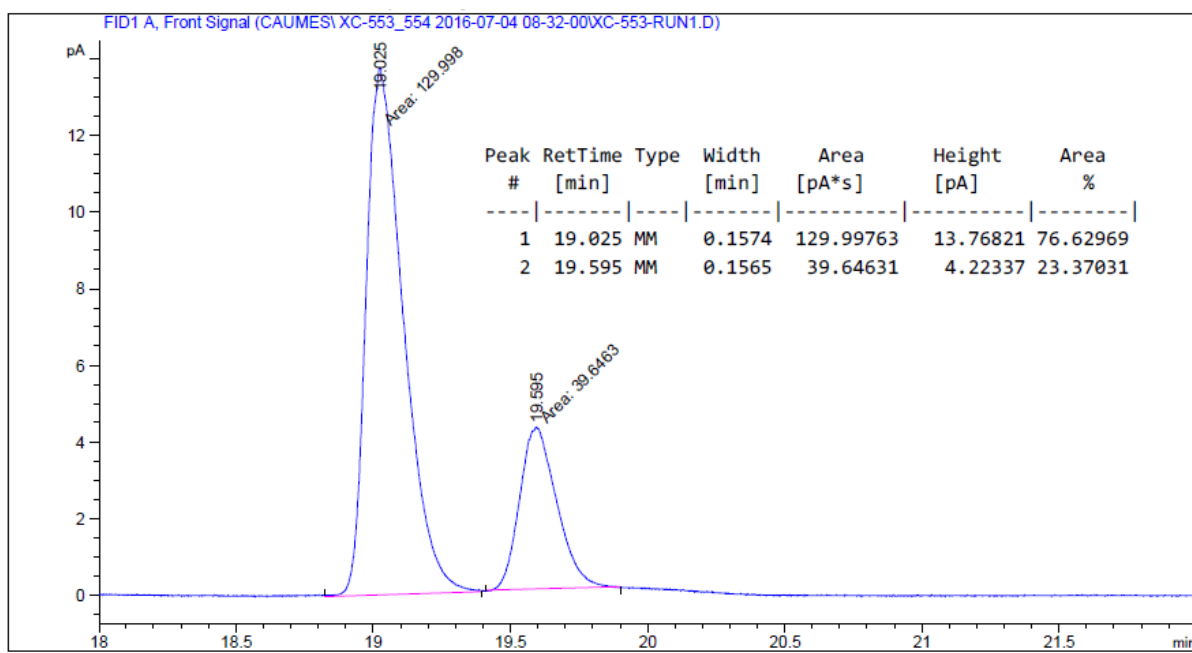
run	eq. substrat	e.e.(a)	total ( <i>R</i> )/( <i>S</i> ) ratio(b)	ratio run (c)	e.e. run
1	1	53%	76.5/23.5	-	53%
2	1	-1,60%	98.4/101.6	22/78	-56%
3	1	16,70%	175/125	77/23	53%
4	1	-0,40%	199/201	24/76	-52%
5	4	-26,60%	294/506	95/305	-53%

(a) e.e. of the aliquot taken after each run (b) determined from the GC and the number of substrate equivalent (c) determined by subtraction of the previous run ratio.

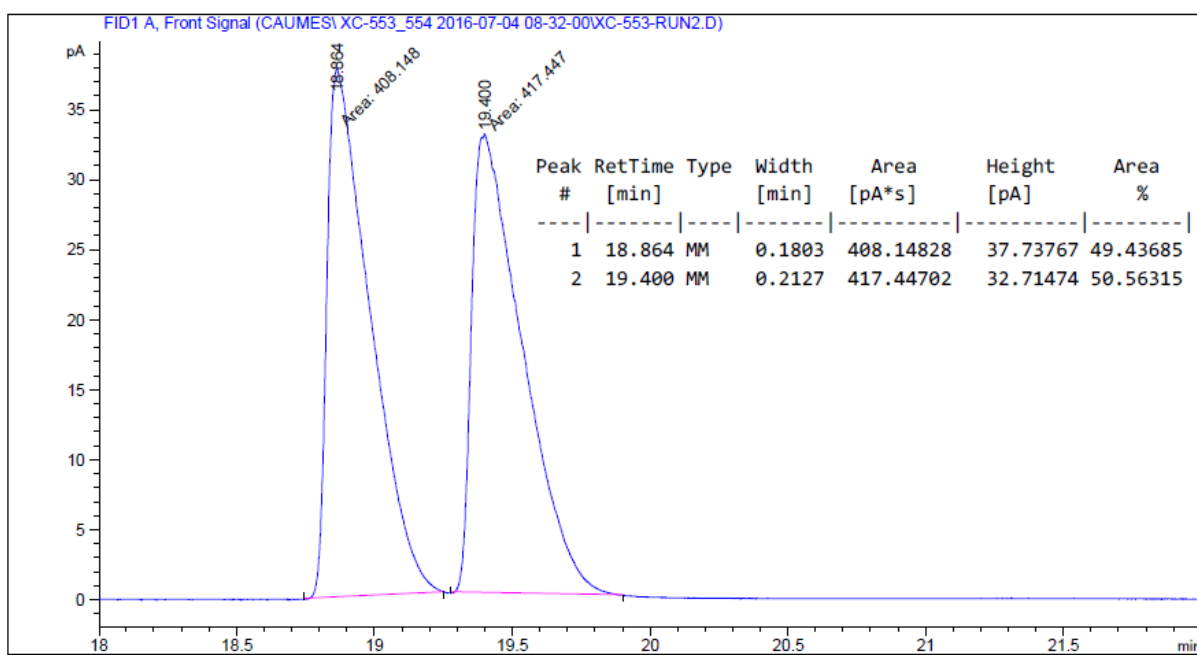
## 5. GC analyses

GC analysis of the aliquots of the proof of concept (for each run no starting material was detectable the chromatogram)

Run 1:

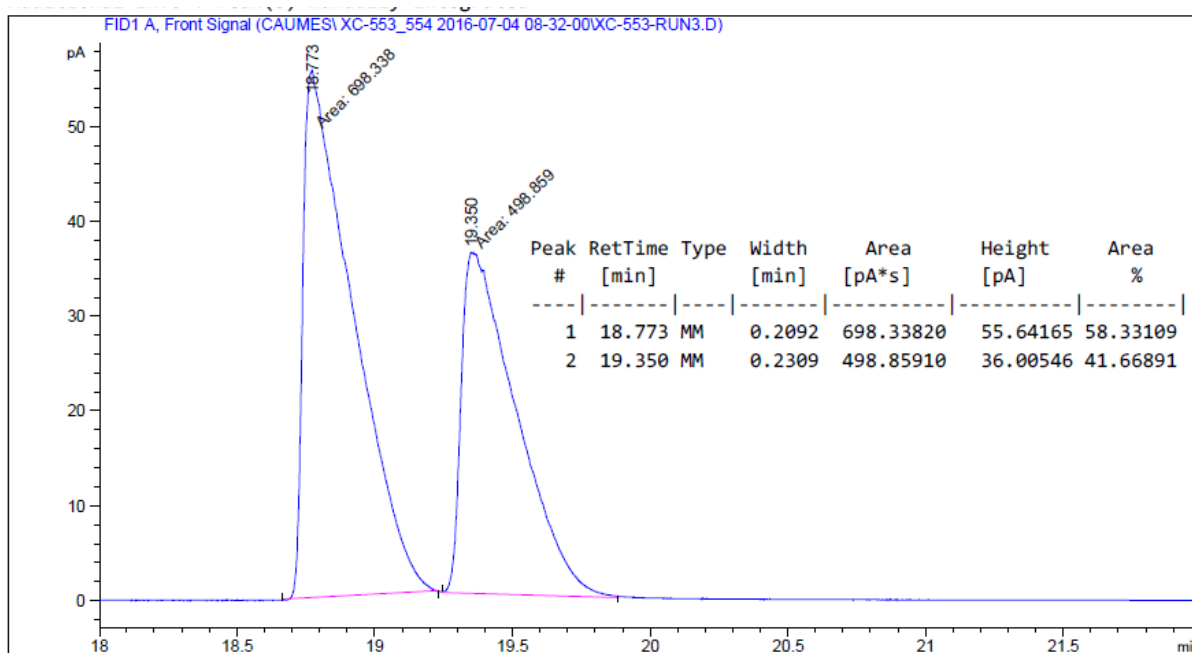


Run 2:

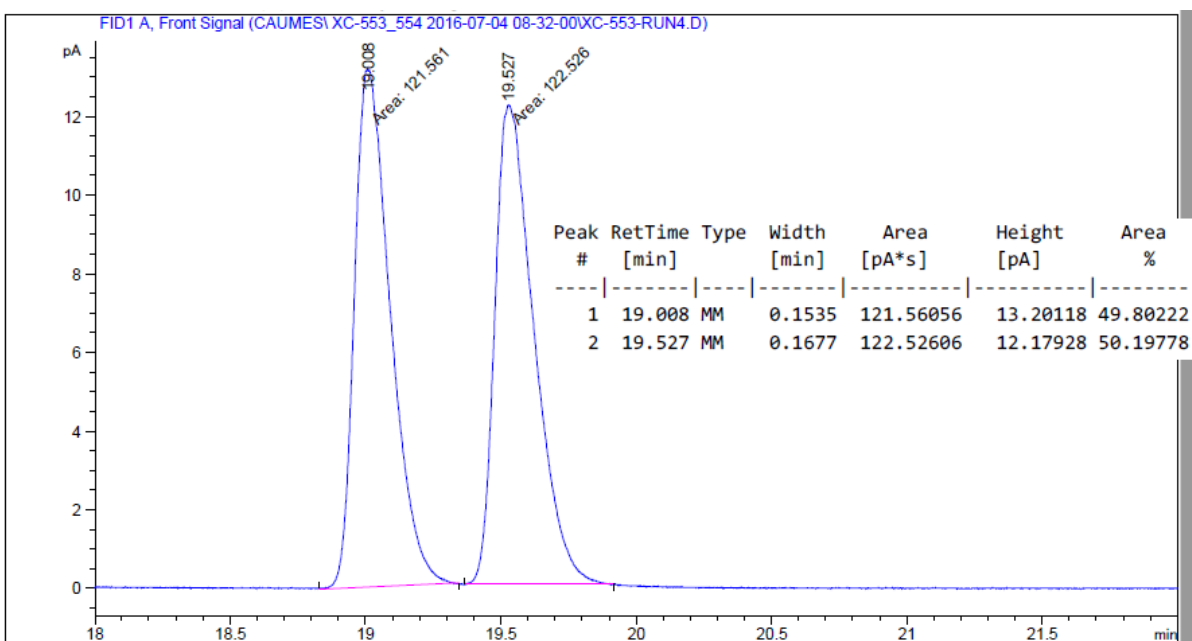




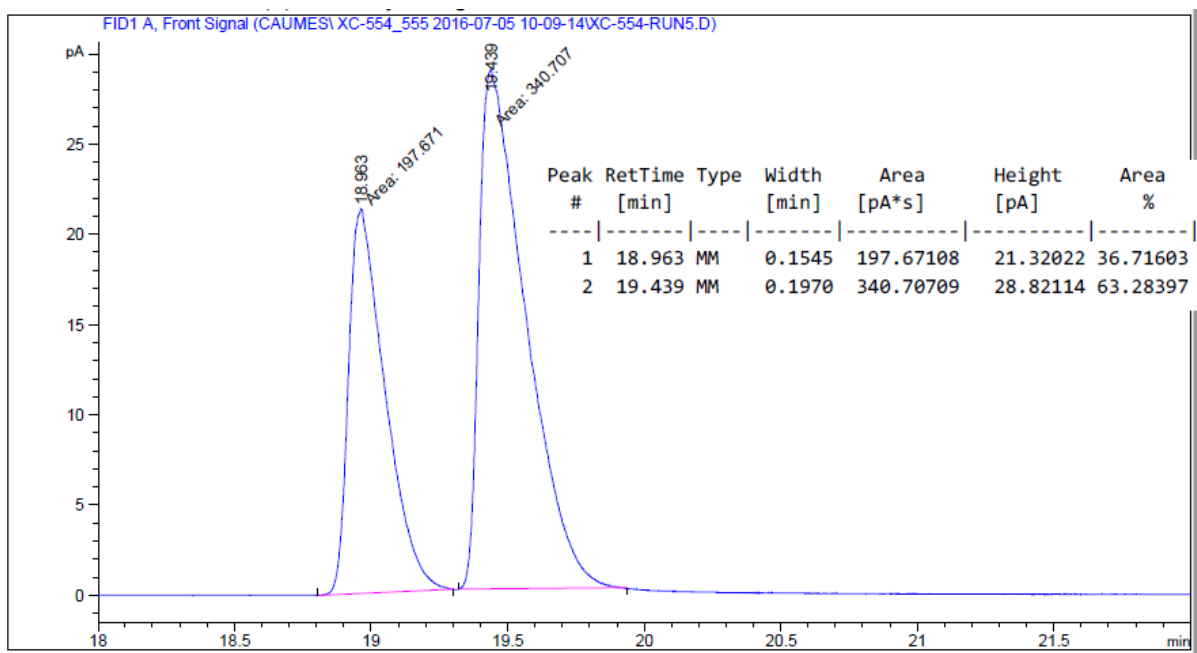
Run 3:



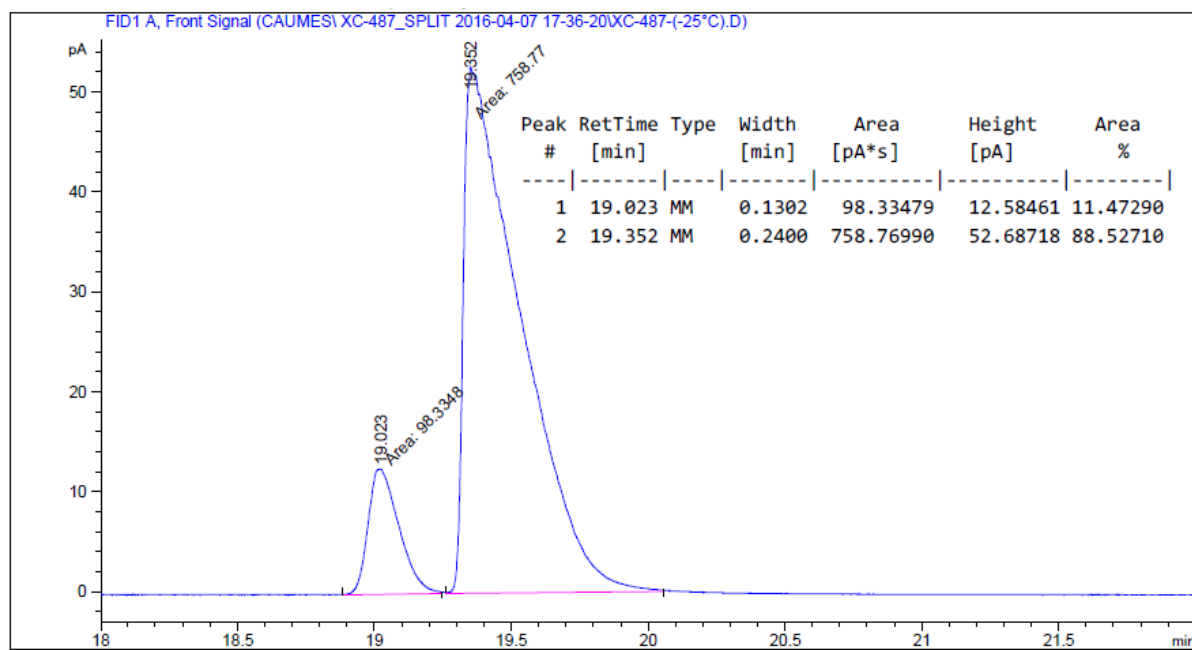
Run 4:



Run 5:



GC analysis of the reaction performed with the optimal conditions (-77% e.e.) with **H**BTA<sup>pPh<sub>2</sub></sup> and **BTA (D)-Cha** at -25°C preparation method A (entry 22 Table V-1).



NMR and GC data of the substrate and products

1-phenylethanol, 1-(4-methylphenyl)ethanol, 1-(4-chlorophenyl)ethanol, 1-(4-bromophenyl)ethanol, 1-(4-trifluoromethylphenyl)ethanol, 1-(4-fluorophenyl)ethanol, 1-(3-nitrophenyl)ethanol and 1-(2-nitrophenyl)ethanol were described previously.<sup>[47–49]</sup>

GC parameters: Chiral Cyclosil-B column, 30 m × 250 μm × 0.25 μm, inlet pressure = 12.6 psi.

#### 1-phenylethanol:

<sup>1</sup>H NMR (300 MHz, CDCl<sub>3</sub>) δ 7.46 – 7.21 (m, 6H), 4.91 (q, *J* = 6.4 Hz, 1H), 1.77 (s, 1H), 1.51 (d, *J* = 6.3 Hz, 3H). **GC**: injection temperature = 250°C; detector temperature = 250°C, column temperature = 115°C. Retention time: 6.2 min (starting material), 11.0 min ((*R*)-enantiomer) and 11.7 min ((*S*)-enantiomer).

#### 1-(4-methylphenyl)ethanol:

**GC** injection temperature = 250°C; detector temperature = 250°C, column temperature = 115°C. Retention time: 9.2 min (starting material), 12.6 min ((*R*)-enantiomer) and 13.6 min ((*S*)-enantiomer).

#### 1-(4-fluorophenyl)ethanol:

<sup>1</sup>H NMR (400 MHz, CDCl<sub>3</sub>) δ 7.38 – 7.31 (m, 2H), 7.06 – 6.99 (m, 2H), 4.90 (q, *J* = 6.5 Hz, 1H), 1.71 (s, 1H), 1.48 (d, *J* = 6.4 Hz, 3H). <sup>19</sup>F{<sup>1</sup>H} NMR (376 MHz, CDCl<sub>3</sub>) δ -115.35. **GC**: injection temperature = 250°C; detector temperature = 250°C, column temperature = 115°C. Retention time: 10.4 min ((*R*)-enantiomer) and 10.9 min ((*S*)-enantiomer).

#### 1-(4-chlorophenyl)ethanol:

**<sup>1</sup>H NMR** (300 MHz, CDCl<sub>3</sub>) δ 7.32 (s, 4H), 4.89 (q, *J* = 6.4 Hz, 1H), 1.70 (s, 1H), 1.48 (d, *J* = 6.5 Hz, 3H). **GC**: injection temperature = 250°C; detector temperature = 250°C, column temperature = 120°C for 10 min then 1°C/min to 140°C. retention time: 6.2 min (starting material), 16.3 min ((*R*)-enantiomer) and 16.7 min ((*S*)-enantiomer).

**1-(4-bromophenyl)ethanol:**

**<sup>1</sup>H NMR** (400 MHz, CDCl<sub>3</sub>) δ 7.50-7.44 (m, 2H), 7.26 (m, 2H), 4.87 (q, *J* = 6.5 Hz, 1H), 1.67 (d, *J* = 26.1 Hz, 2H), 1.48 (d, *J* = 6.5 Hz, 3H). **GC**: injection temperature = 250°C; detector temperature = 250°C, column temperature = 150°C for 10 min then 0.5°C/min to 160°C hold for 10 min. Retention time: 6.2 min (starting material), 10.3 min ((*R*)-enantiomer) and 10.5 min ((*S*)-enantiomer).

**1-(4-trifluoromethylphenyl)ethanol:**

**<sup>1</sup>H NMR** (300 MHz, CDCl<sub>3</sub>) δ 7.61 (d, *J* = 8.2 Hz, 2H), 7.56 – 7.44 (m, 2H), 4.98 (q, *J* = 6.5 Hz, 1H), 1.77 (d, *J* = 31.6 Hz, 1H), 1.51 (d, *J* = 6.5 Hz, 3H). **GC**: injection temperature = 250°C; detector temperature = 250°C, column temperature = 115°C. Retention time: 16.4 min ((*R*)-enantiomer) and 17.8 min ((*S*)-enantiomer).

**1-(2-nitrophenyl)ethanol:**

**<sup>1</sup>H NMR** (300 MHz, CDCl<sub>3</sub>) δ 7.87 (m, 2H), 7.65 (m, 1H), 7.42 (td, *J* = 8.4, 7.9, 1.5 Hz, 1H), 5.43 (q, *J* = 6.4 Hz, 1H), 2.21 (s, 1H), 1.59 (d, *J* = 6.4 Hz, 3H). **GC**: injection temperature = 250°C; detector temperature = 250°C, column temperature = 160°C. Retention time: 11.7 min ((*R*)-enantiomer) and 16.0 min ((*S*)-enantiomer).

**1-(3-nitrophenyl)ethanol:**

**<sup>1</sup>H NMR** (400 MHz, CDCl<sub>3</sub>) δ 8.26 (t, *J* = 2.2 Hz, 1H), 8.13 (ddd, *J* = 8.1, 2.3, 1.1 Hz, 1H), 7.72 (dt, *J* = 7.7, 1.7 Hz, 1H), 7.53 (t, *J* = 7.9 Hz, 1H), 5.03 (q, *J* = 6.5 Hz, 1H), 1.89 (s, 1H), 1.55 (d, *J* = 6.5 Hz, 3H). **GC**: injection temperature = 250°C; detector temperature = 250°C, column temperature = 155°C for 10 min then 1°C/min to 165°C. Retention time: 15.6 min ((*R*)-enantiomer) and 15.7 min ((*S*)-enantiomer).

**1-(4-nitrophenyl)ethanol:**

**<sup>1</sup>H NMR** (300 MHz, CDCl<sub>3</sub>) δ 8.31-8.13 (m, 2H), 7.63-7.46 (m, 2H), 5.03 (q, *J* = 6.5 Hz, 1H), 1.92 (s, 1H), 1.53 (d, *J* = 6.5 Hz, 3H). **GC**: injection temperature = 220°C; detector temperature = 300°C; column temperature = 165°C. Retention time: 8.6 min (starting material) 18.9 min ((*R*)-enantiomer) and 19.3 min ((*S*)-enantiomer).

## H. References

- [1] T. P. Yoon, E. N. Jacobsen, *Science* **2003**, *299*, 1691–1693.
- [2] L. Kovbasyuk, R. Krämer, *Chem. Rev.* **2004**, *104*, 3161–3188.
- [3] V. Blanco, D. A. Leigh, V. Marcos, *Chem. Soc. Rev.* **2015**, *44*, 5341–5370.
- [4] J. Beswick, V. Blanco, G. De Bo, D. A. Leigh, U. Lewandowska, B. Lewandowski, K. Mishiro, *Chem. Sci.* **2015**, *6*, 140–143.
- [5] X. Wang, A. Thevenon, J. L. Brosmer, I. Yu, S. I. Khan, P. Mehrkhodavandi, P. L. Diaconescu, *J. Am. Chem. Soc.* **2014**, *136*, 11264–11267.
- [6] S. Schoumacker, O. Hamelin, J. Pécaut, M. Fontecave, *Inorg. Chem.* **2003**, *42*, 8110–8116.
- [7] S. Mortezaei, N. R. Catarineu, J. W. Canary, *J. Am. Chem. Soc.* **2012**, *134*, 8054–8057.
- [8] S. Mortezaei, N. R. Catarineu, X. Duan, C. Hu, J. W. Canary, *Chem. Sci.* **2015**, *6*, 5904–5912.
- [9] G. Storch, O. Trapp, *Angew. Chem. Int. Ed.* **2015**, *54*, 3580–3586.
- [10] P. Oczipka, D. Müller, W. Leitner, G. Franciò, *Chem. Sci.* **2016**, *7*, 678–683.
- [11] Y. Sohtome, S. Tanaka, K. Takada, T. Yamaguchi, K. Nagasawa, *Angew. Chem. Int. Ed.* **2010**, *49*, 9254–9257.
- [12] M. Messerer, H. Wennemers, *Synlett* **2011**, *2011*, 499–502.
- [13] T. Yamada, Y. Nagata, M. Suginome, *Chem. Commun.* **2010**, *46*, 4914.
- [14] Y. Nagata, T. Nishikawa, M. Suginome, *J. Am. Chem. Soc.* **2014**, *136*, 15901–15904.
- [15] B. A. F. Le Bailly, L. Byrne, J. Clayden, *Angew. Chem. Int. Ed.* **2016**, *55*, 2132–2136.
- [16] M. Vlatković, L. Bernardi, E. Otten, B. L. Feringa, *Chem. Commun.* **2014**, *50*, 7773.
- [17] J. Wang, B. L. Feringa, *Science* **2011**, *331*, 1429–1432.
- [18] D. Zhao, T. M. Neubauer, B. L. Feringa, *Nat. Commun.* **2015**, *6*, 6652.
- [19] X. Tian, C. Cassani, Y. Liu, A. Moran, A. Urakawa, P. Galzerano, E. Arceo, P. Melchiorre, *J. Am. Chem. Soc.* **2011**, *133*, 17934–17941.
- [20] A. R. A. Palmans, E. W. Meijer, *Angew. Chem. Int. Ed.* **2007**, *46*, 8948–8968.
- [21] E. Yashima, K. Maeda, H. Iida, Y. Furusho, K. Nagai, *Chem. Rev.* **2009**, *109*, 6102–6211.
- [22] M. Liu, L. Zhang, T. Wang, *Chem. Rev.* **2015**, *115*, 7304–7397.
- [23] M. Raynal, F. Portier, P. W. N. M. van Leeuwen, L. Bouteiller, *J. Am. Chem. Soc.* **2013**, *135*, 17687–17690.
- [24] Y.-Z. Ke, Y. Nagata, T. Yamada, M. Suginome, *Angew. Chem. Int. Ed.* **2015**, *54*, 9333–9337.
- [25] Y. Nagata, T. Nishikawa, M. Suginome, *J. Am. Chem. Soc.* **2015**, *137*, 4070–4073.
- [26] M. Sawamura, R. Kuwano, Y. Ito, *Angew. Chem. Int. Ed.* **1994**, *33*, 111–113.
- [27] C. Reyes, A. Prock, W. P. Giering, *Organometallics* **2002**, *21*, 546–554.
- [28] C. Reyes, A. Prock, W. P. Giering, *J. Organomet. Chem.* **2003**, *671*, 13–26.
- [29] N. S. Shaikh, S. Enthaler, K. Junge, M. Beller, *Angew. Chem. Int. Ed.* **2008**, *47*, 2497–2501.
- [30] H. Brunner, W. Miehl, *J. Organomet. Chem.* **1984**, *275*, c17–c21.
- [31] B. H. Lipshutz, K. Noson, W. Chrisman, *J. Am. Chem. Soc.* **2001**, *123*, 12917–12918.
- [32] S. Sirol, J. Courmarcel, N. Mostefai, O. Riant, *Org. Lett.* **2001**, *3*, 4111–4113.
- [33] D. Lee, J. Yun, *Tetrahedron Lett.* **2004**, *45*, 5415–5417.
- [34] B. H. Lipshutz, K. Noson, W. Chrisman, A. Lower, *J. Am. Chem. Soc.* **2003**, *125*, 8779–8789.
- [35] J. Wu, J.-X. Ji, A. S. C. Chan, *Proc. Natl. Acad. Sci.* **2005**, *102*, 3570–3575.
- [36] B. H. Lipshutz, B. A. Frieman, *Angew. Chem. Int. Ed.* **2005**, *44*, 6345–6348.
- [37] G. Uray, W. Stampfer, W. M. F. Fabian, *J. Chromatogr. A* **2003**, *992*, 151–157.
- [38] A. Desmarchelier, X. Caumes, M. Raynal, A. Vidal-Ferran, P. W. N. M. van Leeuwen, L. Bouteiller, *J. Am. Chem. Soc.* **2016**, *138*, 4908–4916.
- [39] M. M. J. Smulders, I. A. W. Pilot, J. M. A. Leenders, P. van der Schoot, A. R. A. Palmans, A. P. H. J. Schenning, E. W. Meijer, *J. Am. Chem. Soc.* **2010**, *132*, 611–619.
- [40] A. Desmarchelier, B. G. Alvarenga, X. Caumes, L. Dubreucq, C. Troufflard, M. Tessier, N. Vanthuyne, J. Idé, T. Maistriaux, D. Beljonne, et al., *Soft Matter* **2016**, *12*, 7824–7838.
- [41] S. Espinoza, P. Arce, E. San-Martín, L. Lemus, J. Costamagna, L. Farías, M. Rossi, F. Caruso, J. Guerrero, *Polyhedron* **2015**, *85*, 405–411.
- [42] G. V. Goeden, J. C. Huffman, K. G. Caulton, *Inorg. Chem.* **1986**, *25*, 2484–2485.
- [43] J. W. Diesveld, E. M. Menger, H. T. Edzes, W. S. Veeman, *J. Am. Chem. Soc.* **1980**, *102*,

7935–7936.

- [44] S.-L. Shi, Z. L. Wong, S. L. Buchwald, *Nature* **2016**, 532, 353–356.
- [45] A. Desmarchelier, M. Raynal, P. Brocorens, N. Vanthuyne, L. Bouteiller, *Chem. Commun.* **2015**, 51, 7397–7400.
- [46] M. A. J. Veld, D. Haveman, A. R. A. Palmans, E. W. Meijer, *Soft Matter* **2011**, 7, 524–531.
- [47] M. Vasiloiu, P. Gaertner, R. Zirbs, K. Bica, *Eur. J. Org. Chem.* **2015**, 2015, 2374–2381.
- [48] Y. Li, S. Yu, X. Wu, J. Xiao, W. Shen, Z. Dong, J. Gao, *J. Am. Chem. Soc.* **2014**, 136, 4031–9.
- [49] R. Hodgkinson, V. Jurčík, A. Zanotti-Gerosa, H. G. Nedden, A. Blackaby, G. J. Clarkson, M. Wills, *Organometallics* **2014**, 33, 5517–5524.

# **VI. Gold(I) complexes supported on supramolecular scaffolds: characterisation and use in catalysis**

*Abstract:* In this chapter, the synthesis, characterisation and self-assembly properties of a series of neutral gold chloride complexes supported on BTA or bis-urea supramolecular scaffolds will be described. In some cases, the phosphine gold bis-urea monomers assemble into long aggregates in DCM as evidenced by spectroscopic and scattering analyses. Important efforts have been devoted towards the generation of catalytically-active gold species under mild conditions starting from these phosphine gold chloride complexes. Preliminary investigation of the catalytic properties of gold complexes of BTA or bis-urea ligands in the cycloisomerisation of 1,6-enynes substrates and in the Conia-ene reaction will also be reported.

## A. Introduction

### 1. Gold(I) catalysis

Gold was considered for a long time as only a shiny inert metal before gold catalysis emerged as a hot topic at the changing of the millenary. Gold(I) catalysis especially has drawn a lot of interest due to its peculiar reactivity. Unsaturated gold(I) complexes usually act as strong Lewis acids, have the ability to stabilise cationic intermediates and are tolerant to moisture and oxygen. This singular reactivity arises from relativistic effects which induce contraction of the 6s orbital for the gold atom (Figure VI-1a) and are at the origin of the relatively strong ligand-gold interactions, the high ionisation potential of Au<sup>0</sup> (Figure VI-1b), the aurophilic character of Au<sup>I</sup> (Au-Au bond) and the preferred linear coordination geometry of Au(I) complexes.<sup>[1]</sup>

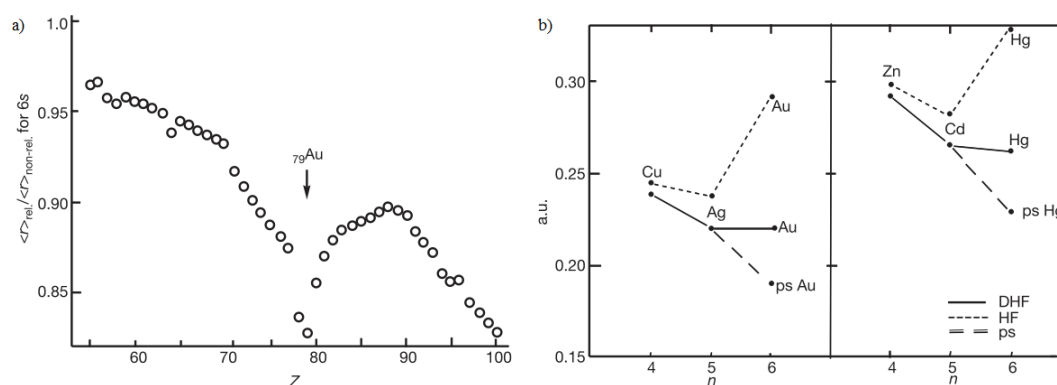


Figure VI-1: a) Calculated relativistic contraction of the 6s orbital. The relativistic and non-relativistic 6s orbital radii were determined computationally. b) Calculated ionisation potentials for the Group 11 and Group 12 transition metals. Three different methods are compared: Dirac–Hartree–Fock (DHF) (relativistic), Hartree–Fock (HF) (non-relativistic), and pseudopotential (ps) (without regard for f electrons). The difference between the HF and ps calculations results from accounting for the lanthanide contraction; the difference between DHF and HF results from accounting for relativistic effects. The experimental ionisation potentials closely match those given by DHF. From reference<sup>[1]</sup>

The reactivity of gold complexes differs according to the oxidation state of the gold metal<sup>[2]</sup> and to the nature of the ligands used.<sup>[3]</sup> In most cases, neutral gold catalyst precursors exhibit a relatively strong Au-X bond and abstraction of X is needed in order to generate a catalytically active cationic gold complex. Neutral Au(I) complex of anionic ligands can also be active.<sup>[4]</sup> In only a limited number of examples, neutral gold chloride complexes have been used directly in catalysis with no need of an apparent activator. These examples are limited to catalysis in polar media or confined environment and the involvement of gold nanoparticles as the active species in those cases cannot be discarded.<sup>[5–8]</sup>

Abstraction of the halide in gold(I) complexes with a silver salt results in the precipitation of the resulting AgX. The thus generated cationic gold(I) complex is usually not isolated. Accordingly, the exact molecular structure of these gold complexes is hard to establish unequivocally. Moreover, remaining silver salts in solution may play a role in the catalytic process. Shi *et al.* investigated the effect of the exceeding silver on the reactivity of gold complexes.<sup>[9]</sup> Remaining Ag<sup>+</sup> and AgX were separated from [PPh<sub>3</sub>Au]<sup>+</sup> complexes by filtration over Celite®. Differences in <sup>31</sup>P{<sup>1</sup>H} NMR shifts



between filtrated and non-filtrated samples for different equivalents of AgOTf relatively to PPh<sub>3</sub>AuCl are displayed in Table VI-1.

Table VI-1: <sup>31</sup>P{<sup>1</sup>H} NMR changes before and after filtration of PPh<sub>3</sub>AuCl complexes activated by AgOTf (50 mM in CDCl<sub>3</sub>) from reference<sup>[9]</sup>

AgOTf eq	<sup>31</sup> P{ <sup>1</sup> H} NMR chemical shift (ppm)	
	Before filtration	After filtration
0	33.8	
0.5	31.5	30.5
0.75	30.2	29.3
0.9	29.2	28.7
1.5	28.1	27.1
2	28.1	27.1

It clearly appeared from the results in Table VI-1 that the presence of remaining silver salts in solution affects the nature of the [PPh<sub>3</sub>Au]<sup>+</sup> complex since the <sup>31</sup>P{<sup>1</sup>H} chemical shifts were markedly different between the filtrated and non-filtrated samples. Interestingly, addition of silver triflate on silver-free (*i.e.* filtrated) [PPh<sub>3</sub>Au]<sup>+</sup>OTf<sup>-</sup> complex gave a chemical shift from 27.1 ppm back to 28.1 ppm, *i.e.* the chemical shift of the silver-containing [PPh<sub>3</sub>Au]<sup>+</sup>OTf<sup>-</sup> complex. In contrast, adding AgCl had no influence on the chemical shift of the silver-free [PPh<sub>3</sub>Au]<sup>+</sup>OTf<sup>-</sup> complex. It clearly suggested the influence of the silver salts arose from the presence of remaining AgOTf in solution not AgCl. These observations led the authors to classify the gold-catalysed reactions into three categories: i) genuine gold catalysis (LAu<sup>+</sup> complex possesses similar or higher reactivity than silver-containing gold(I) complex, ii) bimetallic catalysis (only the silver-containing gold(I) complex is active) and iii) silver-assisted catalysis (both LAu<sup>+</sup> and the silver-containing gold(I) complexes are active). However, for a given ligand, the nature of the anion can change the reaction pathway and thus shift the reaction from one of the above categories to another.<sup>[10]</sup> For example, isolated complex PPh<sub>3</sub>·AuNTf<sub>2</sub> was found to promote most reactions in which the silver-free complex [PPh<sub>3</sub>Au]<sup>+</sup>OTf<sup>-</sup> gave no conversion.

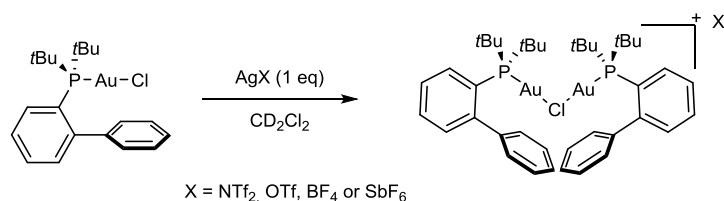


Figure VI-2: Formation of the digold chloride-bridge complex by treatment of **JohnPhosAuCl** with different silver salts (AgX). Adapted from reference<sup>[11]</sup>

Further investigation on the influence of silver on the active gold complex formation was done by Echavarren *et al.*<sup>[11]</sup> Upon treatment of **JohnPhosAuCl** with AgSbF<sub>6</sub>, the authors isolated an unexpected monocationic digold chloride-bridge complex (Figure VI-2). They also observed that a large excess of silver salts was required to fully convert the **JohnPhosAuCl** into cationic [JohnPhosAu]<sup>+</sup> complex. Increasing the coordination ability of the anion led to a decrease in the proportion of the **JohnPhosAuCl** relatively to [JohnPhosAu]<sup>+</sup>. The ideal preparation protocol for the

generation of the catalytically-active gold complex was set as sonication of the LAuCl and AgX mixture followed by centrifugation.<sup>[12]</sup> Such procedure was meant to limit the amount of silver salts remaining in solution. Sonication was found more efficient than stirring for the chloride abstraction and centrifugation avoids the use of Celite® that was found to poison the gold catalyst in some cases.<sup>[13]</sup> It should also be noted that the nature of the counterion has a huge effect on the regio/chemo/stereoselectivity of the gold(I) catalyst.<sup>[10]</sup> The basicity of the counterion has notably a strong influence on the reactions whose pathway involves a hydrogen shift.<sup>[14]</sup>

Not surprisingly, new protocols have emerged for the preparation of catalytically-active gold(I) complexes which were well-defined and could be easily handled. It included the isolation of gold complexes for which the vacant coordination site was stabilised by: i) strongly coordinating anions (*e.g.* acetate, trifluoroacetate, benzoate,<sup>[15]</sup> bis(trifluoromethanesulfonyl)imideate {NTf<sub>2</sub>}<sup>[16]</sup>), ii) neutral donor ligands such acetonitrile,<sup>[17]</sup> benzonitrile,<sup>[18]</sup> η<sup>2</sup>-coordinated toluene molecule<sup>[19]</sup> or a benzotriazole ligand.<sup>[9]</sup> In parallel, suitable alternative procedures to the use of silver salts for the generation of the cationic gold(I) species from the neutral gold chloride complexes were developed: i) the use of the alkali salt of poorly coordinating anions (NaBARF,<sup>[18,20]</sup> KBARF,<sup>[21]</sup> and Na[Me<sub>3</sub>NB<sub>12</sub>Cl<sub>11</sub>])<sup>[22]</sup> and ii) the activation with [Cu(OTf)<sub>2</sub>].<sup>[23]</sup> These strategies are particularly appealing in the framework of our project considering that mild conditions for the generation of the active species are required in order to maintain the hydrogen-bonded network.

## 2. Emerging strategies to control the selectivity of gold catalysis

As described above, the selectivity in gold catalysis can be tuned by the right choice of the ligand, the nature of counterion and the solvent. On the other hand, reaching a good level of enantioselectivity in gold catalysis remains challenging due to the linear coordination geometry preferentially adopted by Au(I) complexes that put the chirality of the ligand in a remote position from the substrate.<sup>[24,25]</sup> A significant degree of chiral induction were achieved with atropisomeric ligands (*e.g.* Binam-P and Segphos derivatives) or phosphoramidite ligands<sup>[25]</sup> and chiral anions.<sup>[26]</sup> Innovative strategies were also currently developed which rely on the use of tripodal ligands,<sup>[27]</sup> or ligands supported by inherently chiral helicene<sup>[28]</sup> or cyclodextrin backbones.<sup>[29]</sup>

The role of aurophilic interactions in enantioselective gold catalysis remains unclear.<sup>[25]</sup> However, Gade *et al.* investigated the influence of such interactions by comparing the selectivity of C<sub>2</sub>-symmetric or C<sub>3</sub>-symmetric phosphalane ligands (Figure VI-3).<sup>[27]</sup> In the solid-state, **C<sub>3</sub>Me•AuCl** complex exhibited intermolecular aurophilic interactions (Au-Au 3.432 Å) whereas **C<sub>3</sub>Ph•AuCl** showed shorter intramolecular aurophilic interaction (Au–Au 2.978 Å).

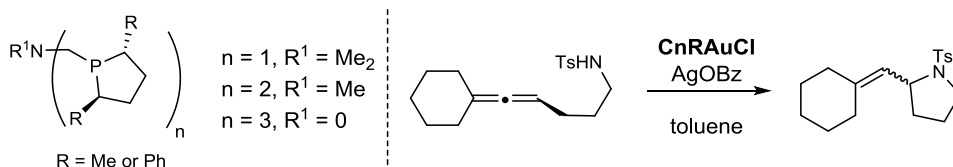


Figure VI-3: Phosphalane·AuCl-catalysed intramolecular hydroamination of an allene substrate. Adapted from reference<sup>[27]</sup>

**C<sub>3</sub>PhAuCl** was found to be an active catalyst, in presence of AgOBz, for intramolecular hydroamination of N-protected  $\gamma$ -allenyl sulphonamides. Surprisingly, a correlation with the number of gold atoms bound to the catalyst and the enantioselectivity was observed (**C<sub>1</sub>Ph·AuCl**: *rac*, **C<sub>2</sub>Ph·AuCl**: 36% e.e. and **C<sub>3</sub>Ph·AuCl**: 95% e.e.). The authors hypothesised the importance of aurophilic interactions in this result.

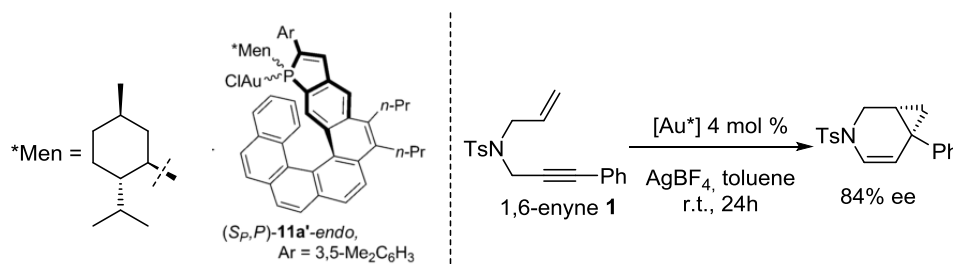


Figure VI-4: Chiral helicenes as ligands in asymmetric gold-catalysed cycloisomerisation of 1,6-enyne **1**. Adapted from reference<sup>[28]</sup>

Marinetti, Voituriez *et al.* developed a series of chiral phosphole ligands appended to a helicenic skeleton and probed their selectivity in the cycloisomerisation of 1,6-enyne substrates (Figure VI-4).<sup>[28]</sup> Clearly, the overall selectivity was dictated by the local chirality of the phosphole ligands, the helicity of the helicenic skeleton and the orientation of the gold complex relative to the helicene (*endo/exo*). The selectivity outcome was rationalised using the classically-employed quadrant method: three quadrants of the gold complex were sterically hindered by the phenyl and the menthyl substituents of the phosphole moiety but also by the helicenic skeleton itself.

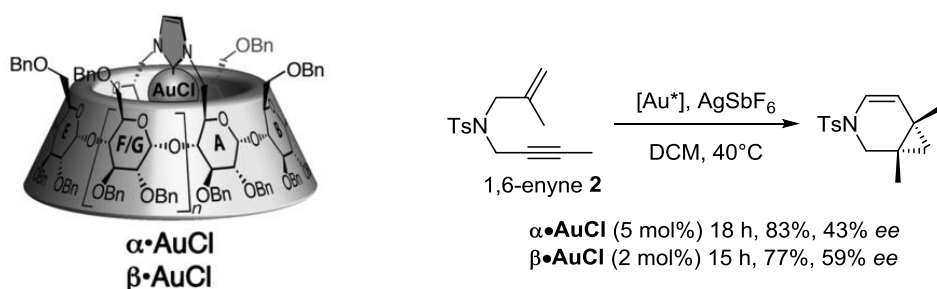


Figure VI-5: Cyclodextrins as inherently chiral skeletons for the asymmetric gold-catalysed cycloisomerisation of 1,6-enyne **2**. Adapted from reference<sup>[29]</sup>

Sollogoub *et al.* used modified  $\alpha$ - and  $\beta$ -cyclodextrins with a bridging NHC ligand (Figure VI-5).<sup>[29]</sup> The respective copper chloride complexes of these ligands were isolated confirming that the metal was buried deep inside the cavity.  $\alpha\text{-AuCl}$  and  $\beta\text{-AuCl}$  were evaluated in presence of AgSbF<sub>6</sub> in the context of the asymmetric cycloisomerisation of 1,6-enyne **2**. The inherent chirality of the cyclodextrin was

transferred to the gold centre which in turn provides modest enantiomeric excess for the catalytic reaction (43% e.e. and 59% e.e. for  $\alpha$ -AuCl and  $\beta$ -AuCl respectively).

These examples pointed out different strategies developed to induce chirality to gold catalysts. Some of these concepts are quite interesting in the frame of the use of supramolecular polymers as scaffolds in gold catalysis. Indeed, the example of Gade emphasised the possible importance of aurophilic interactions in enantioselective gold catalysis. These interactions might occur in the case of supramolecular polymers decorated with a large number of gold complexes. Such proximity between gold complexes is conceivable in BTA or bis-urea scaffolds in which the lateral chains are close to each other. The others two examples point out that the inherent chirality of the structure surrounding the ligand can be induced to the gold catalyst. A similar behaviour can be expected with our supramolecular scaffolds as described in the Chapters IV and V in the context of rhodium and copper catalysis.

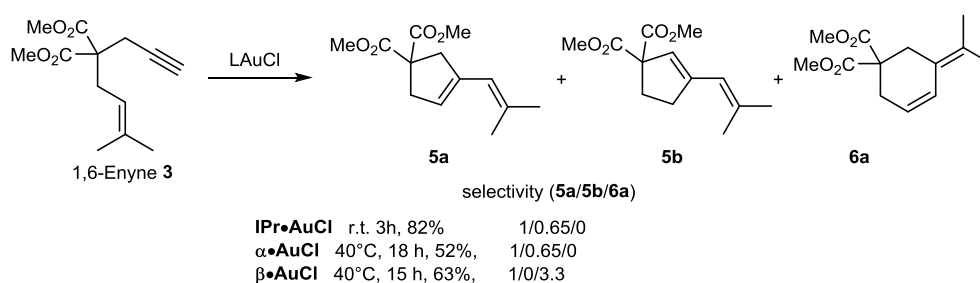


Figure VI-6: Regioselective cycloisomerisation of 1,6-enyne **3** with ligands supported by a cyclodextrin scaffold. Adapted from reference<sup>[29]</sup>

Not only the enantioselectivity but also the regioselectivity of gold-catalysed reactions can be modulated by carefully designing the nature of the ligands. For example,  $\beta$ -AuCl complex was found to display different regioselectivity for the cycloisomerisation of enyne **3** when compared to a non-encapsulated complex **IPr•AuCl** (Figure VI-6). Also, the cycloisomerisation of 1,7-enynes substrates, which was very slow with usual ligands, was strongly accelerated in the presence of bulky phosphine ligands: alkynyl substituted phosphine ligand with hindered silyl groups (Figure VI-7).<sup>[30]</sup> These ligands created a cavity around the gold atom and helped the prefolding of the substrate thus increasing the kinetics of the reaction. These ligands were also successfully employed for the Conia-ene reaction of challenging substrates<sup>[31]</sup> and for other 7-*exo*-dig cyclisation reactions.<sup>[32,33]</sup>

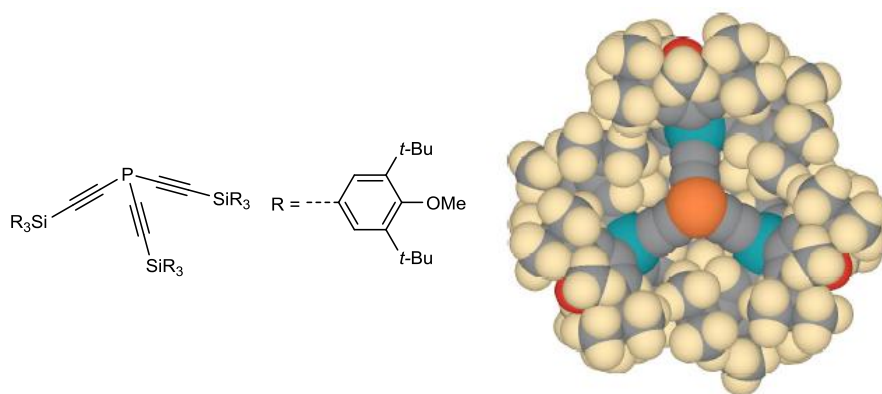


Figure VI-7: Holey phosphine ligand developed by Sawamura *et al.* From reference<sup>[30]</sup>

Another approach to improve the selectivity of gold-catalysed reactions was developed by Goldup *et al.* by developing a gold rotaxane catalyst (Figure VI-8).<sup>[34]</sup> As such, their catalyst exhibited poor reactivity as the bipyridine located in the rotaxane scaffold was found to coordinate the gold cationic centre and thus prevents its reactivity. Addition of one equivalent of TfOH, [Cu(MeCN)<sub>4</sub>]PF<sub>6</sub>, Zn(OTf)<sub>2</sub> or Cd(OTf)<sub>2</sub> led to an increased reactivity of the gold complex. This effect of the additive was related to the coordination or protonation of the bipyridine ligand by the additive. Compared to control experiments with non-interlocked catalysts, the rotaxane catalyst provided higher diastereoselectivity for the reaction between a propargylic ester and styrene. This was related to an increased steric hindrance around the metal centre provided by the rotaxane skeleton. Also, the diastereoselectivity was tuned by changing the nature of the additive since higher selectivity was obtained with copper compared to zinc additive. This more subtle effect was attributed to a change in the conformation between the macrocycle and the thread which in turn rigidified the catalyst framework and modified the space around the catalytic site.

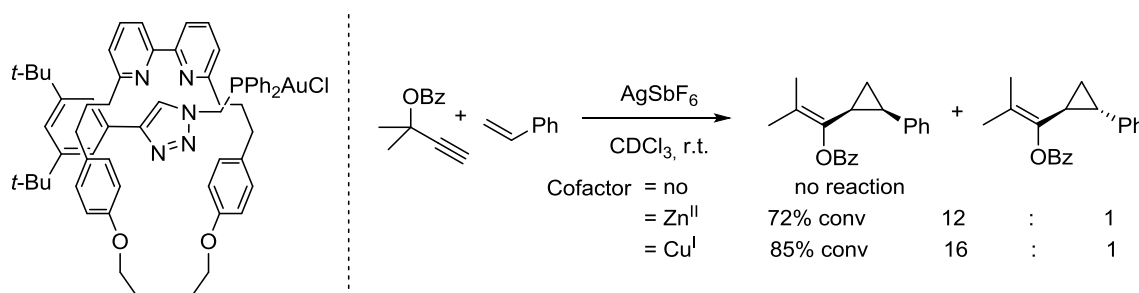


Figure VI-8: Diastereoselective gold-catalysed cyclopropanation of styrene using a rotaxane catalyst. Adapted from reference<sup>[34]</sup>

Such examples of pre-folding of the substrate or increased diastereoselectivity due to steric hindrance around the gold centre are interesting in the frame of our supramolecular scaffolds. Indeed, the presence of alkyl chains or bulky peripheral substituents around the gold catalyst is expected to give similar effects.

### 3. Interest of gold catalysts supported by supramolecular scaffolds

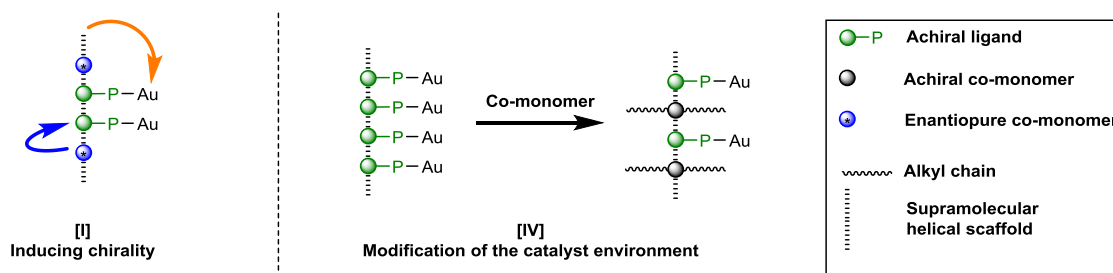


Figure VI-9: Strategies envisaged in this chapter for gold catalysts supported by supramolecular helical scaffolds.

We can envisage several strategies to tune the selectivity of gold catalysts supported by a supramolecular scaffold (Figure VI-9). Firstly, we aim to transfer the supramolecular chirality to the intrinsically achiral gold centre located at the periphery of bis-urea or BTA supramolecular polymers (strategy [I]). Accordingly, either chiral ligands alone or mixtures of an achiral ligand and a chiral co-monomer will be screened. Also, the supramolecular scaffold may influence the regioselectivity or diastereoselectivity outcome of the catalytic reaction as this scaffold can bring some steric hindrance and maybe help the folding of the substrate (strategy [IV]). Here, mixtures between a ligand and a co-monomer (not necessarily chiral) will be tested in the context of reactions which may operate through different catalytic pathways.

Firstly, we will describe the synthesis, characterisation and self-assembly properties of a series of neutral chloride gold complexes of bis-urea or BTA ligands. We will bring particular attention to the generation of catalytically-active gold catalysts under mild conditions from these gold chloride complexes which is not a trivial task (*vide supra*). Preliminary results of the use of gold complexes of bis-urea or BTA ligands as catalysts for the cycloisomerisation of 1,6-enynes substrates and for the Conia-ene reaction will be described.

## B. Synthesis, characterisation and self-assembly properties of neutral gold chloride complexes containing a bis-urea or a BTA moiety

### 1. Synthesis and characterisation

The synthesis of gold chloride complexes took place under mild conditions starting with  $[\text{AuCl}(\text{SMe}_2)]$  as the gold precursor. Simple mixing of the ligand and  $[\text{AuCl}(\text{SMe}_2)]$  at room temperature for 30 minutes in a suitable solvent (*i.e.* in which the ligand is poorly self-associated) gave complete coordination as monitored by  $^{31}\text{P}\{^1\text{H}\}$  NMR. The phosphine gold chloride complexes were isolated by precipitation in pentane followed by simple filtration. The precipitation was required to avoid traces of adsorbed  $\text{SMe}_2$  and non-reacted  $[\text{AuCl}(\text{SMe}_2)]$  which otherwise led to the formation of gold nanoparticles (NPs) over time. However, in some cases, despite following this cautious protocol, slightly purple-coloured complexes were obtained which indicated the presence of Au NPs. It was even the case for some batches of normally colourless  $\text{PPh}_3\text{AuCl}$  complexes which meant that the

presence of Au NPs was not necessarily related to side reactions involving the assembly units. The content of Au NPs in our phosphine gold chloride complexes was presumed to be low since only one peak in  $^{31}\text{P}\{^1\text{H}\}$  NMR was observed. Several phosphine gold chloride complexes were synthesised and the yields,  $^{31}\text{P}\{^1\text{H}\}$  NMR shifts and the aspects of the samples are listed in Table VI-2.

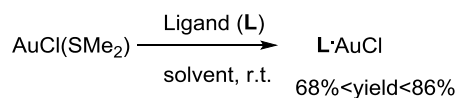


Table VI-2: BTA and bis-urea phosphine gold chloride complexes.

	Ligand L	$^{31}\text{P}\{^1\text{H}\}$ L <sup>(a)</sup>	$^{31}\text{P}\{^1\text{H}\}$ L·AuCl <sup>(a)</sup>	yield	aspect	Solubility <sup>(b)</sup>
references	<b>PPh<sub>3</sub></b>	-5.8	32.7 <sup>(c)</sup>	75%	white	toluene
	<b>P(<i>o</i>-Tol)<sub>3</sub></b>	-27.8	8.1 <sup>(c)</sup>	86%	white	toluene
	<b>PCy<sub>3</sub></b>	10.8	53.5 <sup>(c)</sup>	69%	white	toluene
	<b>PMes<sub>3</sub></b>	-36.8	-5.7	68%	white	toluene
BTA ligands	<b><sup>H</sup>BTA<sup>mPPh2</sup></b>	-4.4	33.0	70%	white	CHCl <sub>3</sub> /DCM
	<b>(<i>S,S</i>)-<sup>H</sup>BTA<sup>mPPh2</sup></b>	-1.6	33.0	69%	white	CHCl <sub>3</sub> /DCM
	<b><sup>H</sup>BTA<sup>pPPh2</sup></b>	-5.7	31.7	80%	white	CHCl <sub>3</sub> /DCM
	<b>(<i>S,S</i>)-<sup>H</sup>BTA<sup>pPPh2</sup></b>	-8.1	31.4	nd	white	CHCl <sub>3</sub> /DCM
Bis-urea ligands	<b>(<i>rac</i>)-<i>m</i>-PPh<sub>3</sub>EHUCl<sub>2</sub>*</b>	-6.4	33.3	86%	slightly purple	CHCl <sub>3</sub> /DCM
	<b>(<i>rac</i>)-<i>m</i>-PPh<sub>3</sub>EHUX</b>	-6.1	33.4	79%	white	CHCl <sub>3</sub> /DCM
	<b>(<i>R</i>)-<i>m</i>-PPh<sub>3</sub>PBEUX</b>	-6.2	33.5	79%	white	CHCl <sub>3</sub> /DCM
	<b>(<i>rac</i>)-<i>p</i>-PPh<sub>3</sub>PBEUX*</b>	-8.1	31.3	73%	white	CHCl <sub>3</sub> /DCM

Conditions: for references, BTA ligands and (*rac*)-*m*-PPh<sub>3</sub>EHUCl<sub>2</sub>: ligand (1 eq), AuCl(SMe)<sub>2</sub> (1.0 eq) and dry DCM (0.12 M). For (*rac*)-*m*-PPh<sub>3</sub>EHUX, (*R*)-*m*-PPh<sub>3</sub>PBEUX and (*rac*)-*p*-PPh<sub>3</sub>PBEUX: ligand (1 eq), AuCl(SMe)<sub>2</sub> (1.0 eq) and mixture of DCM/THF/MeOH to assure the solubility of the ligand. nd= not-determined. \* These bis-urea contain an impurity (a) All NMR analyses were performed in CDCl<sub>3</sub> except for bis-urea ligands for which analyses have been done in DMSO-*d*<sub>6</sub> in order to disrupt the hydrogen-bonded network. (b) The least polar solvents in which L·AuCl is soluble (c) These values are in agreement with literature data.  $^{31}\text{P}\{^1\text{H}\}$  spectra have not been acquired on the same NMR apparatus, thus slight differences in the absolute values of the chemical shifts must be interpreted cautiously.

The downfield shift observed in phosphorus NMR on going from the ligands to the gold chloride complexes was consistent with the formation of phosphine gold chloride complexes. No traces of side products was detected upon characterisation of these phosphine gold complexes by  $^1\text{H}$  NMR,  $^{31}\text{P}\{^1\text{H}\}$  NMR, FT-IR and mass spectrometry analyses, even in the cases for which the presence of Au NPs was presumed.

The phosphine gold chloride complexes containing BTA or bis-urea assembly units were not soluble in toluene and alkanes. However, all these complexes remained soluble in DCM (without any apparent viscosity) and accordingly their self-assembly was probed in this solvent.

## 2. SANS analyses

The nature of the self-assemblies formed by phosphine gold chloride complexes (*R*)-*m*-PPh<sub>3</sub>PBEUX·AuCl and (*rac*)-*m*-PPh<sub>3</sub>EHUCl<sub>2</sub>·AuCl was probed by SANS analysis in CD<sub>2</sub>Cl<sub>2</sub>

(0.4 and 0.8 % wt, 3.4 mM and 7.3 mM respectively). SANS analyses are shown in Figure VI-10 and the results of the fits are compiled in Table VI-3.

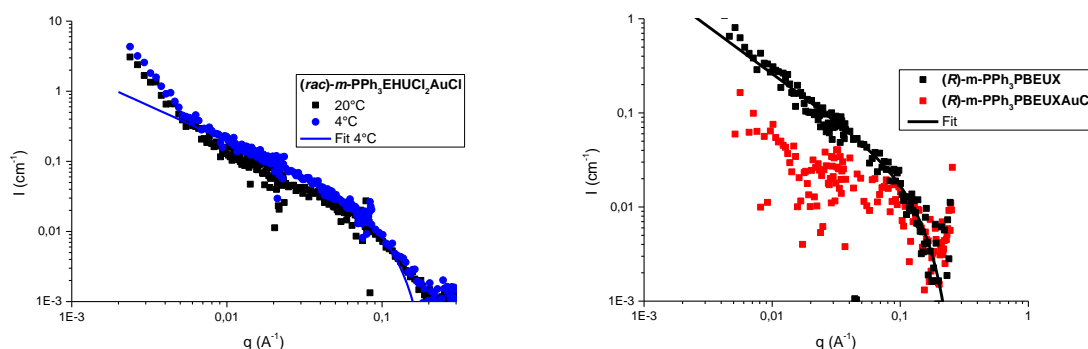


Figure VI-10: SANS data. Left: *m*-PPh<sub>3</sub>EHUCl<sub>2</sub>·AuCl at 0.8% wt in CD<sub>2</sub>Cl<sub>2</sub>. Right: (*R*)-*m*-PPh<sub>3</sub>PBEUX and (*R*)-*m*-PPh<sub>3</sub>PBEUX·AuCl at 0.4% wt in CD<sub>2</sub>Cl<sub>2</sub>. The lines correspond to the best fit with the form factor for long and rigid rods of circular cross-section and uniform contrast.

In both cases, the SANS signals were noisy: it was related to the low concentration in gold complex and the low contrast inherent to the use of CD<sub>2</sub>Cl<sub>2</sub>. A precipitate was observed for (*rac*)-*m*-PPh<sub>3</sub>EHUCl<sub>2</sub>·AuCl which might arise from the presence of Au NPs that would have precipitated during the time between the preparation of the sample and the analysis (more than a week). Therefore, the SANS analyses were interpreted only in a qualitative way. For (*rac*)-*m*-PPh<sub>3</sub>EHUCl<sub>2</sub>·AuCl complexes, the  $q^{-1}$  dependence of the scattered intensity at intermediate  $q$  values was consistent with the presence of cylindrical objects. Moreover, the length of the assemblies clearly increased upon decreasing the temperature. At 4°C, the objects were long and the result of the fit was consistent with a supramolecular polymer with a filament structure (*i.e.* with a single bis-urea monomer in the cross-section). At this temperature, the objects were longer than 250 Å. For the (*R*)-*m*-PPh<sub>3</sub>PBEUX·AuCl complex, the less than  $q^{-1}$  dependence at low  $q$  compared to the ligand, meant that the bis-ureas are still assembled into rod-like objects, but they are shorter than in the absence of gold chloride coordinated to the phosphine.

Table VI-3: Number of bis-urea molecules ( $n$ ) in the cross-section of the cylindrical objects and linear density ( $n_L$ ) as function of the temperature, deduced from the fits of the SANS Data.

	Sample	Con	aspect	$n$	$n_L$	T
complex	( <i>rac</i> )- <i>m</i> -PPh <sub>3</sub> EHUCl <sub>2</sub> ·AuCl	7.3 mM	fluid <sup>(a)</sup>	0.6 <sup>(b)</sup>	0.14	22°C
	( <i>rac</i> )- <i>m</i> -PPh <sub>3</sub> EHUCl <sub>2</sub> ·AuCl	7.3 mM	fluid <sup>(a)</sup>	0.9 <sup>(b)</sup>	0.20	4°C
ligand	( <i>rac</i> )- <i>m</i> -PPh <sub>3</sub> EHUCl <sub>2</sub>	-	-	1 <sup>(c)</sup>		20°C
complex	( <i>R</i> )- <i>m</i> -PPh <sub>3</sub> PBEUX·AuCl	3.4 mM	fluid	1.3 <sup>(b)</sup>	0.28	20°C
ligand	( <i>R</i> )- <i>m</i> -PPh <sub>3</sub> PBEUX	5.9 mM	go	2.1	0.44	20°C

(a) A black precipitate was observed in this sample. (b) The values of the fits are not precise given that SANS signal is noisy (c) determined in chapter III



### 3. FT-IR analyses

*In the bulk:* FT-IR analyses of the phosphine gold chloride complexes containing a BTA or a bis-urea assembly unit indicated that the monomers were fully assembled in the bulk (diagnostic frequencies for bonded N-H at *ca.* 3250 cm<sup>-1</sup> and 3340 cm<sup>-1</sup> region for BTA and bis-urea respectively and for bonded C=O at *ca.* 1640 cm<sup>-1</sup>, see experimental section).

*In DCM solution:* The self-assembly behaviour of the whole series of phosphine gold chloride complexes in DCM was probed by means of FT-IR analyses performed at various concentrations.

The phosphine gold chloride complexes containing a BTA assembly unit were not fully associated in DCM at 20 mM concentration (see all the FT-IR spectra in the experimental section Figure VI-S1). At this concentration, (S,S)-<sup>H</sup>BTA<sup>pPPh<sub>2</sub></sup>·AuCl was the most associated BTA monomer of the series, yet its self-assemblies were short as evidenced by the presence of free N-H bonds ( $\nu = 3430$  cm<sup>-1</sup>, Figure VI-11). (S,S)-<sup>H</sup>BTA<sup>pPPh<sub>2</sub></sup> and (S,S)-<sup>H</sup>BTA<sup>pPPh<sub>2</sub></sup>·AuCl displayed similar FT-IR spectra at this concentration indicating that the presence of the peripheral gold chloride moiety did not significantly influence the self-assembly behaviour of this BTA monomer. On the other hand, (S,S)-<sup>H</sup>BTA<sup>mPPh<sub>2</sub></sup>·AuCl gold complex was less associated than its ligand (S,S)-<sup>H</sup>BTA<sup>mPPh<sub>2</sub></sup> inferring that in that case the closer proximity between the gold chloride moiety and the BTA hydrogen bonding units prevented significantly the assembly of the gold chloride complex.

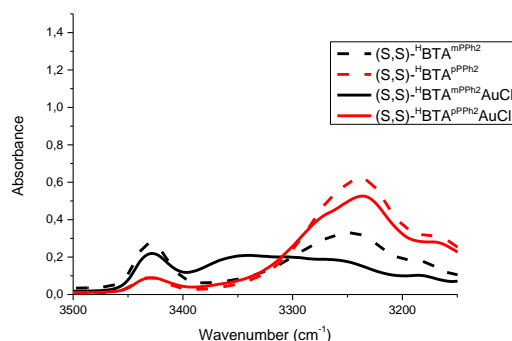


Figure VI-11: FT-IR spectra at 20 mM of BTA ligands (dashed line) and BTA gold chloride complexes (plain line) in DCM.

The assembly of bis-urea gold chloride complexes in DCM were compared (Figure VI-12a). At 10 mM, the FT-IR spectra of (*rac*)-*m*-PPh<sub>3</sub>EHUCl<sub>2</sub>·AuCl, (*rac*)-*m*-PPh<sub>3</sub>EHUX·AuCl and (*rac*)-*p*-PPh<sub>3</sub>PBEUX·AuCl indicated that these bis-urea monomers were fully associated. Only slight differences were present in the shape of the N-H absorption bands when comparing the gold chloride complexes to their respective ligands. It might infer that the polymeric assemblies formed by the gold chloride complexes and the ligands had the same structure (filament or other) at this concentration in DCM, but additional experiments were needed to fully confirm these hypotheses. The cases of (*rac*)-*m*-PPh<sub>3</sub>EHUCl<sub>2</sub>·AuCl and (*R*)-*m*-PPh<sub>3</sub>PBEUX·AuCl deserved further comments since the structure of the assemblies formed by these two monomers were probed by SANS analyses (*vide supra*). FT-IR analyses performed at the same concentration than that of SANS analyses (*ca.* 5 mM, Figure VI-12b)

showed that **(R)-m-PPh<sub>3</sub>PBEUX·AuCl** was associated although the assemblies are short as indicated by the presence of free N-H in the spectra. These observations are in agreement with our SANS data. Taken together, the SANS and FT-IR analyses confirm that **(R)-m-PPh<sub>3</sub>PBEUX·AuCl** and **(rac)-m-PPh<sub>3</sub>EHUCl<sub>2</sub>·AuCl** formed assemblies in DCM solution and that these assemblies likely adopted a filament structure (a single molecule in the cross-section). The ability of these bis-urea monomers to form a thicker structure in DCM (*i.e.* a structure with two or more bis-urea monomers in the cross-section) was not investigated but some hint will be gained by means of CD analyses.

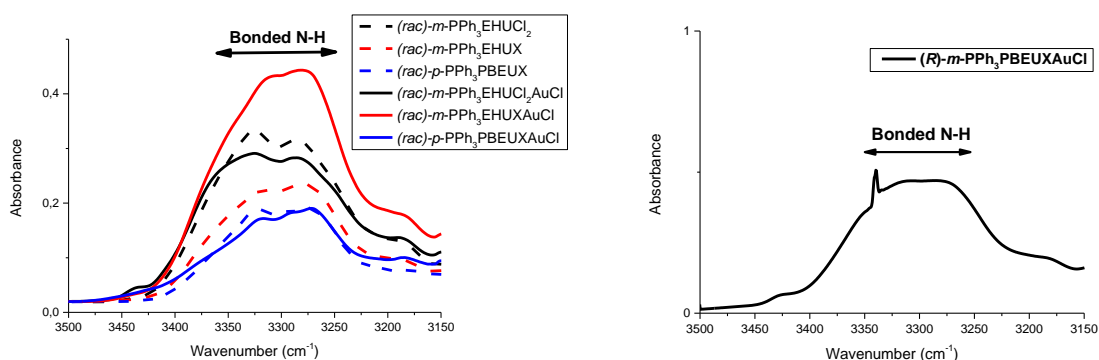


Figure VI-12: FT-IR spectra of bis-urea ligands and gold chloride complexes in DCM, left: comparison of the spectra of bis-urea ligand and their gold chloride at 10 mM. Right: spectra of the SANS solution for **(R)-m-PPh<sub>3</sub>PBEUX·AuCl** at 5.9 mM (the artefact at  $\nu = 3339 \text{ cm}^{-1}$  results from the high absorption of CD<sub>2</sub>Cl<sub>2</sub> in this region)

Preliminary FT-IR analyses of **(rac)-m-PPh<sub>3</sub>EHUX·AuCl** in other solvents indicated that this bis-urea was mostly associated in CHCl<sub>3</sub> and associated to some extent in THF (Figure VI-S2).

#### 4. CD analyses

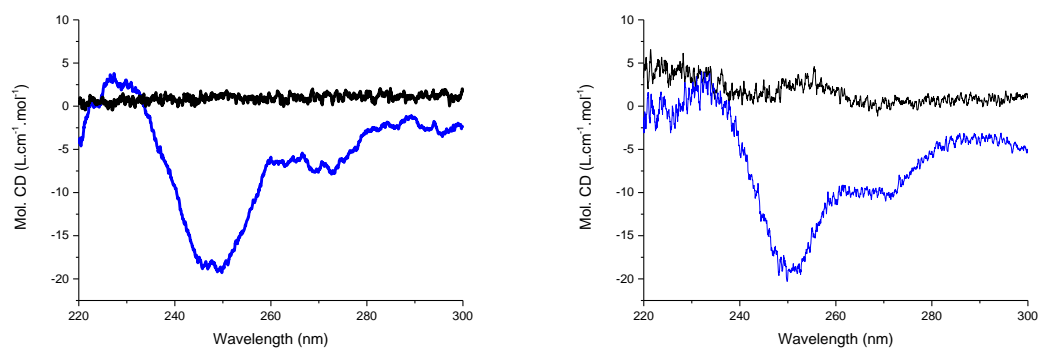


Figure VI-13: Left: CD spectra of **(R)-m-PPh<sub>3</sub>PBEUX** and right: CD spectra of **(R)-m-PPh<sub>3</sub>PBEUX·AuCl** in DCM (1 mM) at 20°C (black line) and -10°C (blue line).

The ability of **(R)-m-PPh<sub>3</sub>PBEUX·AuCl** to form chiral supramolecular assemblies was particularly important considering its application in asymmetric catalysis. CD analyses of **(R)-m-PPh<sub>3</sub>PBEUX·AuCl** were performed at 1 mM in DCM. At this concentration, the assemblies formed by **(R)-m-PPh<sub>3</sub>PBEUX·AuCl** were short as demonstrated by FT-IR analyses (experimental part, Figure VI-S3). It infers that at this concentration and temperature, **(R)-m-PPh<sub>3</sub>PBEUX·AuCl** formed short filaments or a mixture of filaments and monomers. Not surprisingly, no CD signal was

observed for 1 mM DCM solution of (*R*)-*m*-PPh<sub>3</sub>PBEUX·AuCl at 20°C (Figure VI-13). Like the ligand in the same conditions, cooling the solution to -10°C led to the appearance of a strong CD signal. The CD signal obtained was quasi-identical to the one of the ligand and thus transfer of chirality to the gold chloride moiety could not be confirmed.

This result suggested that a sharp transition occurred for (*R*)-*m*-PPh<sub>3</sub>PBEUX·AuCl between a CD inactive filament form and a CD active “thick structure”. It is of the highest importance for the application of (*R*)-*m*-PPh<sub>3</sub>PBEUX·AuCl as a precursor in asymmetric reactions.

### C. Synthesis, characterisation and self-assembly properties of NTf<sub>2</sub> gold complexes containing a bis-urea or a BTA moiety

Having established that BTA gold chloride complexes and, to a greater extent, bis-urea gold chloride complexes were able to form assemblies in DCM, we next want to find mild conditions for the generation of the catalytically-active gold species from these phosphine gold chloride complexes. We anticipated that the presence of remaining Ag salts in solution or of strong coordinating anions will be detrimental for maintaining of the hydrogen bond network. Gold complexes stabilised by a NTf<sub>2</sub> anion combine the advantages of being relatively stable in the solid state which allows their isolation and of being active in catalysis with no need of an additional activator.<sup>[16]</sup> We thus attempted to isolate (*rac*)-*m*-PPh<sub>3</sub>EHUCl<sub>2</sub>·AuNTf<sub>2</sub> and (*rac*)-*m*-PPh<sub>3</sub>EHUX·AuNTf<sub>2</sub> from the corresponding gold chloride complexes.

Table VI-4: Synthesis of bis-urea phosphine gold NTf<sub>2</sub> complexes.

Gold chloride complexes	<sup>31</sup> P{ <sup>1</sup> H} (a) L·AuCl	<sup>31</sup> P{ <sup>1</sup> H} (a) L·AuNTf <sub>2</sub>	yield	aspect	Solubility <sup>(b)</sup>
PPh <sub>3</sub> ·AuCl	32.7	30.1	n.d.	deep purple	Toluene
( <i>rac</i> )- <i>m</i> -PPh <sub>3</sub> EHUCl <sub>2</sub> ·AuCl	35.4	31.3	92%	deep purple	CHCl <sub>3</sub> /DCM
( <i>rac</i> )- <i>m</i> -PPh <sub>3</sub> EHUX·AuCl	33.4	n.d.	n.d.	slightly purple	CHCl <sub>3</sub> /DCM

(a) NMR analyses were performed in CDCl<sub>3</sub> for PPh<sub>3</sub> and in DMSO-*d*<sub>6</sub> for bis-urea ligands in order to disrupt the hydrogen-bonded network. (b) Least polar solvents for which the L·AuNTf<sub>2</sub> is soluble. n.d. not determined.

(*rac*)-*m*-PPh<sub>3</sub>EHUCl<sub>2</sub>·AuNTf<sub>2</sub> and (*rac*)-*m*-PPh<sub>3</sub>EHUX·AuNTf<sub>2</sub> were prepared by reacting the corresponding bis-urea·AuCl complexes with AgNTf<sub>2</sub> (1.0 equiv.) in DCM for (*rac*)-*m*-PPh<sub>3</sub>EHUCl<sub>2</sub>·AuCl and in THF for (*rac*)-*m*-PPh<sub>3</sub>EHUX·AuCl. The complexes were isolated after filtration over Celite® and purple coloured solids were obtained. This colour suggested the presence of Au NPs. Surprisingly, PPh<sub>3</sub>·AuNTf<sub>2</sub> in our hands is also a deeply coloured solid. However, the upfield shift of the <sup>31</sup>P{<sup>1</sup>H} NMR signal for the gold chloride to gold NTf<sub>2</sub> complexes was consistent with the formation of the gold NTf<sub>2</sub> complexes of PPh<sub>3</sub> and (*rac*)-*m*-PPh<sub>3</sub>EHUCl<sub>2</sub>. However, no chemical

shift was observed for *(rac)*-*m*-PPh<sub>3</sub>EHUX·AuNTf<sub>2</sub>. Mass spectrometry analysis revealed that the chloride abstraction did not occur in this case (see experimental part).

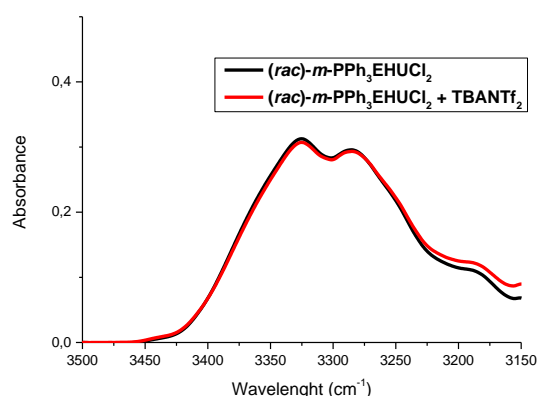


Figure VI-14: Influence of the NTf<sub>2</sub> anion (1 equivalent) on the self-assembly of *(rac)*-*m*-PPh<sub>3</sub>EHUCl<sub>2</sub> in DCM at 10 mM monitored by FT-IR. Zoom on the N-H region

Before investigating the self-assembly properties of these NTf<sub>2</sub> complexes by FT-IR analyses, we aimed to probe whether the NTf<sub>2</sub> anion was a hydrogen-bond competitor for the assembly of the bis-urea monomers. We thus compared the FT-IR spectra of *(rac)*-*m*-PPh<sub>3</sub>EHUCl<sub>2</sub> in absence and presence of 1.0 equiv. of TBANTf<sub>2</sub> (TBA = tetrabutylammonium) (Figure VI-14). Both FT-IR spectra were virtually identical which clearly pointed out that the poor hydrogen-bond competitor ability, if any, of the NTf<sub>2</sub> anion towards the hydrogen bond network formed by *(rac)*-*m*-PPh<sub>3</sub>EHUCl<sub>2</sub>. For the influence of a series of anion and cation on the self-assembly of *(rac)*-EHUCl<sub>2</sub> see Figure VI-S4.

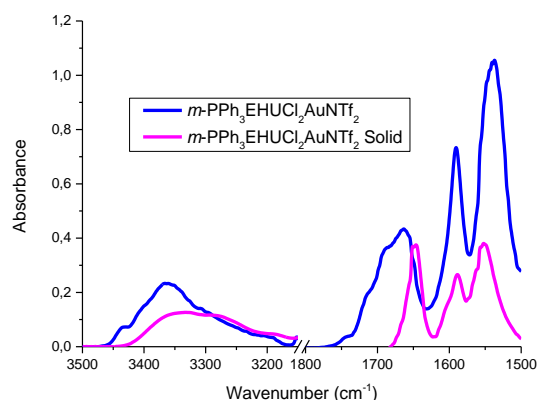


Figure VI-15: FT-IR spectra of *(rac)*-*m*-PPh<sub>3</sub>EHUCl<sub>2</sub>·AuNTf<sub>2</sub> in DCM (10 mM) and in the solid state.

FT-IR analysis in solid state of *(rac)*-*m*-PPh<sub>3</sub>EHUCl<sub>2</sub>·AuNTf<sub>2</sub> displayed the expected bonded N-H at *ca.* 3320 and 3280 cm<sup>-1</sup> (Figure VI-15) as well as a small shoulder around 3360 cm<sup>-1</sup>. It is indicated that *(rac)*-*m*-PPh<sub>3</sub>EHUCl<sub>2</sub>·AuNTf<sub>2</sub> was mostly associated in the bulk. On the other hand, FT-IR analysis of *(rac)*-*m*-PPh<sub>3</sub>EHUCl<sub>2</sub>·AuNTf<sub>2</sub> at 10 mM in DCM showed the presence of a small amount of free N-H bond ( $\nu=3430$  cm<sup>-1</sup>) along a broad peak at *ca.* 3380 cm<sup>-1</sup> which clearly demonstrated that the

hydrogen bonds were partially disrupted. Interestingly the carbonyl peak was also affected: the well resolved C=O bond at  $1640\text{ cm}^{-1}$  was replaced by a broad peak at *ca.*  $1680\text{ cm}^{-1}$ .

To interpret this result, it was important to remind that: i) this bis-urea  $\text{NTf}_2$  gold complex was mostly associated in the solid-state and ii) that the  $\text{NTf}_2$  anion was a poor hydrogen-bond competitor for the assemblies formed by *(rac)-m-PPh<sub>3</sub>EHUCl<sub>2</sub>*. Consequently, several hypotheses were made for the disruption of hydrogen-bonded assemblies in DCM for *(rac)-m-PPh<sub>3</sub>EHUCl<sub>2</sub>·AuNTf<sub>2</sub>*: i) the  $\text{Au}^+ \text{NTf}_2^-$  ion pair was loose in solution and thus the carbonyl functions are coordinated to the gold atom (such interactions were for thiourea)<sup>[35]</sup> and ii) Au NPs or other impurities generated during the formation of the  $\text{AuNTf}_2$  complex competed with the hydrogen-bond network. Similar spectra in solution was obtained for *(S,S)-<sup>H</sup>BTA<sup>pPPh<sub>2</sub></sup>·AuNTf<sub>2</sub>* (See experimental part, Figure VI-S5).

Synthesis of *(R)-m-PPh<sub>3</sub>PBEUX·AuNTf<sub>2</sub>* would have been interesting to investigate the possible effect of the 1,3-xylyl spacer of the self-assembly of a bis-urea· $\text{AuNTf}_2$ . However synthesis issues still need to be addressed as the attempt of the formation of *(rac)-m-PPh<sub>3</sub>EHUX·AuNTf<sub>2</sub>* was unsuccessful. It is likely due to the strong association of the bis-ureas with 1,3-xylyl spacer which prevents the chloride abstraction.

## D. Gold-catalysed reactions

Considering the above-mentioned self-assembly studies, one can envisage the following approaches to maintain the hydrogen-bond network upon activation of the gold chloride bond: i) using *(rac)-m-PPh<sub>3</sub>EHUX·AuCl* and *(R)-m-PPh<sub>3</sub>PBEUX·AuCl* as precursors since the assemblies formed by these complexes are expected to be particularly stable, ii) performing catalysis in conditions in which the gold complexes are poorly soluble since the assemblies are maintained in the solid state, and iii) finding alternatives to silver salts for the abstraction of the chloride in order to avoid the side reactions observed during the preparation of our  $\text{NTf}_2$  gold complexes. Unfortunately, only the last two approaches were investigated in the next examples since complexes *(rac)-m-PPh<sub>3</sub>PBEUX·AuCl* and *(R)-m-PPh<sub>3</sub>PBEUX·AuCl* were obtained too late to be tested in the timeframe of this Ph.D. project.

### 1. Generation of catalytically-active phosphine gold species under mild conditions

The cycloisomerisation of 1,6-enyne **1** was chosen as benchmark reaction for the survey of a variety of chloride abstractors using  $\text{PPh}_3\cdot\text{AuCl}$  as the model of the gold chloride complex. In the context of applying our supramolecular systems to gold catalysis, this substrate presented the following advantages; i) the enantioselective version of this reaction was described<sup>[28,36]</sup> and ii) the substrate was anticipated to be a poor hydrogen-bond competitor.

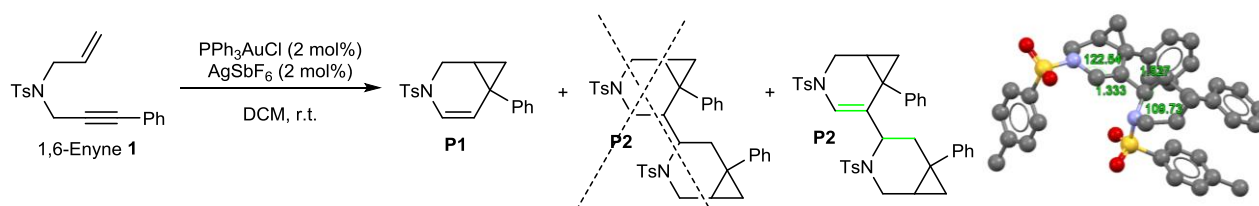


Figure VI-16: Gold-catalysed cycloisomerisation of 1,6-enyne **1**. Adapted from reference<sup>[37]</sup>

In the original publication, the authors isolated the cycloisomerisation product **P1** by reaction of **1** in presence of a mixture of **PPh<sub>3</sub>·AuCl** and AgSbF<sub>6</sub> (no filtration mentioned to remove silver salts). Despite full conversion, **P1** was isolated with a good but not excellent 74% yield owing to the concomitant formation of the side-product **P2**, assigned according to its X-ray structure. However, we re-interpreted the X-ray data and found out that the dimer structure described in the publication<sup>[37]</sup> was not the reductive dimerised product but the results of the intermolecular alkene addition on another alkene. It is clearly stated by the length of the carbon–carbon bonds (1.333 Å and 1.527 Å) and the values of the dihedral angles of 122.54° and 109.73° containing the two green bonds in **P2** which are characteristic of a Csp<sup>2</sup>–Csp<sup>2</sup> and Csp<sup>3</sup>–Csp<sup>3</sup> bond respectively (Figure VI-16). Anyway, we investigated the cycloisomerisation of the 1,6-enyne **1** using either silver salts or silver-free chloride abstractors and the results are listed in Table VI-5.

Table VI-5: Screening of silver-salt and silver-free chloride abstractors for the cycloisomerisation of **1**

Entry	Chloride Abstractor	Conversion (time)	<sup>31</sup> P{ <sup>1</sup> H} NMR (secondary peak), ppm <sup>(a)</sup>
1	AgSbF <sub>6</sub>	71% (30 min)	30.1 (44.7)
2	AgNTf <sub>2</sub>	12% (45 min)	30.1
3	AgBF <sub>4</sub>	55% (30 min)	30.4 (44.6)
4	Na[Me <sub>3</sub> NB <sub>12</sub> C <sub>11</sub> ]	100% (4 days)	32.7
5	NaBArF	0%	44.7 (40.4)
6	KBArF <sub>20</sub>	53% (4 days)	32.0
7	CsBArF	0%	31.9

Reaction conditions: 1,6-enyne **1** (1.0 eq, 40 mM), PPh<sub>3</sub>AuCl (5 mol%), chloride abstractor (7 mol%), DCM, r.t.. No filtration of the *in situ* formed silver or alkali salts. (a) <sup>31</sup>P{<sup>1</sup>H} in CDCl<sub>3</sub> for PPh<sub>3</sub>AuCl = 32.7 ppm

We reproduced successfully the reaction mentioned in the publication and **P2** was also observed as a side product of **P1** (*ca.* 22% of dimer after 2 h of reaction). Surprisingly, only AgSbF<sub>6</sub> led to a fast conversion of the substrate (entry 1) whereas other silver salts provided lower completion (entries 2 and 3). The low activity of the mixture of **PPh<sub>3</sub>·AuCl** and AgNTf<sub>2</sub> was particularly intriguing given the fact that this is usually a high-performing combination in gold catalysis.<sup>[16]</sup> Silver-free carborane (Na[Me<sub>3</sub>NB<sub>12</sub>Cl<sub>11</sub>]) previously employed by Kirsh *et al.* in other types of cycloisomerisation reactions<sup>[22]</sup> and potassium tetrakis(pentafluorophenyl)borate (BArF<sub>20</sub>) gave respectively full and 53% conversion but after prolonged reaction times (entries 4 and 6). Interestingly no dimer formation was observed with these salts even though the reaction was performed during four days. On the other hand

sodium and cesium tetrakis(3,5-bis(trifluoromethyl)phenyl)borate (BArF) gave no conversion (entries 5 and 7).

Independently, the resulting gold cationic complexes were prepared in absence of the substrate and analysed by  $^{31}\text{P}\{^1\text{H}\}$  NMR. For all chloride abstractors no signal corresponding to the unreacted  $\text{PPh}_3\cdot\text{AuCl}$  was observed after 15 min. This indicated a rapid chloride abstraction even in the absence of silver. Compared to  $\text{PPh}_3\cdot\text{AuCl}$ , an upfield shift was observed in all cases (except for NaBArF) which was consistent with the formation of the  $\text{PPh}_3\cdot\text{Au}^+$  species. In addition, a second peak was present at *ca.* 44.6 ppm for  $\text{AgSbF}_6$  and  $\text{AgBF}_4$  which corresponded to  $[(\text{PPh}_3)_2\text{Au}]\text{X}$  species.<sup>[38]</sup> The formation of this species was likely accompanied by the generation of Au NPs.<sup>[8]</sup> Interestingly, a clean monoligated gold complex was formed in the cases of  $\text{AgNTf}_2$ ,  $\text{Na}[\text{Me}_3\text{NB}_{12}\text{Cl}_{11}]$ ,  $\text{KBArF}_{20}$  and  $\text{CsBArF}$ . In contrast, NaBArF failed to generate a monoligated gold complex and mainly formed  $[(\text{PPh}_3)_2\text{Au}]^+\text{BArF}^-$  and a non-identified species. This was likely due to the poor stability of  $\text{PPh}_3\text{Au}^+\text{BArF}^-$  complex which immediately degrades in the absence of substrate. However the absence of conversion in the presence of  $\text{CsBArF}$  was quite surprising as chloride abstraction seemed to occur.

Considering the low stability and low reactivity of gold cationic complexes with poorly-coordinating anions, we wondered whether these properties might be improved by increasing the steric hindrance around the gold atom. Several complexes were synthesised using phosphine ligands with higher cone angles than  $\text{PPh}_3$  and their catalytic ability for the cycloisomerisation of **1** was probed (Table VI-6).

Table VI-6: Correlation between the cone angle of selected phosphine ligands and their reactivity in the cycloisomerisation of 1,6-enyne **1**

Complex		$\text{PPh}_3\cdot\text{AuCl}$	$\text{PCy}_3\cdot\text{AuCl}$	$\text{P}(o\text{-tolyl})_3\cdot\text{AuCl}$	$\text{P}(\text{Mes})_3\cdot\text{AuCl}$
Cone Angle		145°	170°	194°	212°
Conversion after	$\text{LiBArF}_{20}$	14%	14%	30%	31%
	$\text{KBArF}_{20}$	35%	61%	51%	92%
2 days	$\text{NaBArF}$	0%	0%	0%	48%

Reaction conditions: 1,6-enyne **1** (1 eq, 50 mM),  $\text{LAuX}$  (10 mol%), salt (13 mol%), DCM. No filtration of the in situ formed alkali salts. Mes = mesitylene (1,3,5-trimethylbenzene)

Increasing the cone angle of the phosphine ligand improved the conversion in substrate for all the borate alkali salts.  $\text{P}(\text{Mes})_3\cdot\text{AuCl}$  was the only complex active after addition of NaBArF which provided 48% conversion after 2 days of reaction. Higher steric hindrance around the gold atom could: i) enhance the rate of the metathesis reaction and thus the rate of formation of the cationic gold complex, ii) stabilise the highly reactive cationic complex and iii) prevent the generation of the inactive bisligated gold complexes.

These results point out that carborane or borate alkali salts can be used instead of silver salts for the cycloisomerisation of **1** with  $\text{PPh}_3\cdot\text{AuCl}$  but at the cost of a lower catalytic rate. These salts will be far

more useful for the activation of hindered phosphine ligands which is an important element for the design of future bis-urea and BTA ligands.

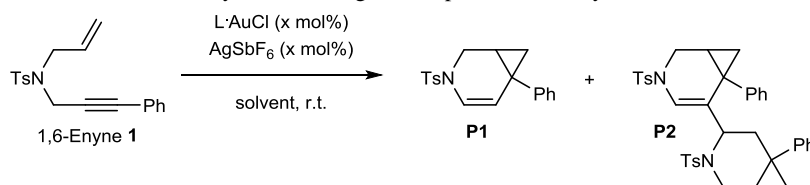
## 2. Gold-catalysed reactions with gold complexes containing a BTA or bis-urea moiety

### a) 1,6-enyne cycloisomerisation

We probed the catalytic properties of: i) mixtures composed of a gold chloride complex of a BTA or a bis-urea ligand and of a chloride abstractor and ii) isolated NTF<sub>2</sub> gold complexes. Only selected results obtained with BTA gold complexes will be described since bis-urea gold complexes proved to be active but no enantiopure ligands or co-monomers were probed (see the experimental part, Table VI-S1). Based on the above-mentioned results, the catalytic experiments were performed in conditions in which the gold complexes are poorly soluble, *i.e.* apolar solvents, since it was expected that the BTA assemblies supporting the catalytically-active cationic gold centres were maintained in the solid state.

BTA gold chloride complexes were evaluated in the gold-catalysed cycloisomerisation of enyne **1** with AgSbF<sub>6</sub> as chloride abstractor and the results are listed in Table VI-7.

Table VI-7: Reactivity of the BTA gold complexes for the cycloisomerisation of **1**



Entry	Catalyst	Solvent	Time	conversion	<b>P2</b> <sup>(a)</sup>	e.e. <sup>(b)</sup>
	<b>PPh<sub>3</sub>·AuCl</b>	DCM	30 min	71%	43%	-
1	<b>PPh<sub>3</sub>·AuCl + BTA C8</b>	DCM	30 min	63%	0%	-
2	<b><sup>H</sup>BTA<sup>pPPh<sub>2</sub></sup>·AuCl</b>	DCM	12 h	85%	60%	-
3	<b>PPh<sub>3</sub>·AuCl</b>	cyclohexane	10 days	92%	10%	-
4	<b><sup>H</sup>BTA<sup>pPPh<sub>2</sub></sup>·AuCl</b>	pentane	3 days	51%	65%	-
5	<b><sup>H</sup>BTA<sup>pPPh<sub>2</sub></sup>·AuCl</b>	cyclohexane	2 days	93%	0%	-
6	<b>(S,S)-<sup>H</sup>BTA<sup>pPPh<sub>2</sub></sup>·AuCl</b>	cyclohexane	3 days	89%	0%	0%
7	<b>(S,S)-<sup>H</sup>BTA<sup>pPPh<sub>2</sub></sup>·AuCl + BTA (S)</b>	cyclohexane	3 days	95%	0%	0%
8	<b>(S,S)-<sup>H</sup>BTA<sup>mPPh<sub>2</sub></sup>·AuCl</b>	cyclohexane	3 days	34%	0%	0%
9	<b>(S,S)-<sup>H</sup>BTA<sup>mPPh<sub>2</sub></sup>·AuCl + BTA (S)</b>	cyclohexane	3 days	77%	0%	0%

Reaction conditions: **1**, **L·AuCl** (10 mol%) except for **<sup>H</sup>BTA<sup>pPPh<sub>2</sub></sup>·AuCl** (14 mol%), AgSbF<sub>6</sub> (14 mol%), co-monomer (1 eq. toward **L·AuCl** if present), solvent (*ca.* 0.4M). No filtration of the in situ formed silver salts. (a) after at least 5 hours of reaction. (b) Determined by chiral HPLC.

We first probed the influence of a BTA co-monomer, **BTA C8**, on the fate of the reaction catalysed by [PPh<sub>3</sub>·Au]SbF<sub>6</sub>. We observed: i) similar reaction rate and ii) no dimer formation (**P2**) after a long reaction time. The exact role of **BTA C8** in preventing the formation of the dimer is not known. Nevertheless, the absence of dimer could be related to the coordination of the amide C=O functions of the BTA to the gold catalytic centre. A higher competition would then exist between the **BTA C8** and



**P1** than between **BTA C8** and the 1,6-enyne **1** that could explain the inhibition of the dimer formation. A mixture of  ${}^{\text{H}}\text{BTA}^{\text{pPPh}_2}\cdot\text{AuCl}$  and  $\text{AgSbF}_6$  was found to be active for the cycloisomerisation reaction in DCM but the reaction rate was significantly lower than for  $\text{PPh}_3\cdot\text{AuCl}$ . It might be due to a reversible coordination of the amide C=O functions to the gold catalytic centre. However the difference of behaviour of **BTA C8** and of  ${}^{\text{H}}\text{BTA}^{\text{pPPh}_2}\cdot\text{AuCl}$  remained unclear and might arise from the proximity of the gold with the amide in  ${}^{\text{H}}\text{BTA}^{\text{pPPh}_2}\cdot\text{AuCl}$ . Interestingly, the combination of  $\text{L}\cdot\text{AuCl}$  and  $\text{AgSbF}_6$  was also active in alkanes despite the poor solubility of the catalyst, the substrate and the products (entries 3 and 5). The dimers formation was strongly reduced with  $\text{PPh}_3\cdot\text{AuCl}$  and absent on the time scale of the reaction with the  $\text{BTA}\cdot\text{AuCl}$  complexes. This inhibition of the dimer formation could be related to the poor solubility of **P1** in cyclohexane.

We next engaged either enantiopure ligands alone or a mixture of an enantiopure ligand and an enantiopure co-monomer in the same reaction in cyclohexane. A lower reactivity was observed for  $(S,S)\text{-}{}^{\text{H}}\text{BTA}^{\text{mPPh}_2}\cdot\text{AuCl}$  when compared with  $(S,S)\text{-}{}^{\text{H}}\text{BTA}^{\text{pPPh}_2}\cdot\text{AuCl}$  (entries 5 and 7). Interestingly an increase in reactivity was observed when the reaction was performed in the presence of the chiral co-monomer **BTA (S)** (compare entries 5 and 6 & entries 7 and 8). Unfortunately, the product was obtained as a racemic mixture in all cases.

No chirality induction to the catalytic gold centre was observed using chiral BTA ligand monomers under conditions in which they are self-assembled (solid-state). Several hypotheses might explain the absence of selectivity in the above experiments: a) the substrate bound to the gold atom was too far to be influenced by the chirality of the self-assemblies; b) the supramolecular chirality of the BTA ligand was lost upon coordination of the gold centre; c) the catalysis is performed by Au NPs and d) the self-assembly, albeit in the solid state, was disrupted during the catalytic process.

## b) Conia-ene reaction

The reactivity of our gold complexes was also investigated in the Conia-ene reaction (Figure VI-17). The gold version of this old reaction<sup>[39]</sup> was recently reported and offers an easy access to substituted cyclopentane.<sup>[40]</sup> Interestingly this reaction was described by Shi *et al.* as a Au/Ag bimetallic reaction<sup>[9]</sup> however isolated  $\text{PPh}_3\cdot\text{AuNTf}_2$  complex proved to also be active.<sup>[16]</sup>

Dissociated BTAs slow down the rate of the Conia-ene reaction of substrate **4**. Adding **BTA C8** to highly active  $\text{PPh}_3\cdot\text{AuNTf}_2$  in DCM almost completely inhibits the reaction. A long induction time was observed which can be due to the dissociation between the **BTA C8** and  $\text{PPh}_3\cdot\text{AuNTf}_2$ . Interestingly, the  $\text{NTf}_2$  complex of benzamide- $\text{PPh}_2$ , a ligand with a single amide function, was as active as  $\text{PPh}_3\cdot\text{AuNTf}_2$ . It inferred that the inhibition (or slow down) of the reaction in presence of BTAs was due to the coordination of the *alkyl* amide functions, not the aryl one, to the gold atom. Accordingly to these observations, it is not surprising to observed that the activity of  ${}^{\text{H}}\text{BTA}^{\text{mPPh}_2}\cdot\text{AuNTf}_2$  and  ${}^{\text{H}}\text{BTA}^{\text{pPPh}_2}\cdot\text{AuNTf}_2$  and  $(rac)\text{-}m\text{-PPh}_3\text{EHUCl}_2\cdot\text{AuNTf}_2$  was significantly

lower than that of  $\text{PPh}_3\cdot\text{AuNTf}_2$ ,  ${}^{\text{H}}\text{BTA}^{\text{mPPh}_2}\cdot\text{AuNTf}_2$  and  ${}^{\text{H}}\text{BTA}^{\text{PPh}_2}\cdot\text{AuNTf}_2$  were active in cyclohexane but no asymmetric version of the reaction has been attempted (see Table VI-S2 in the experimental part).

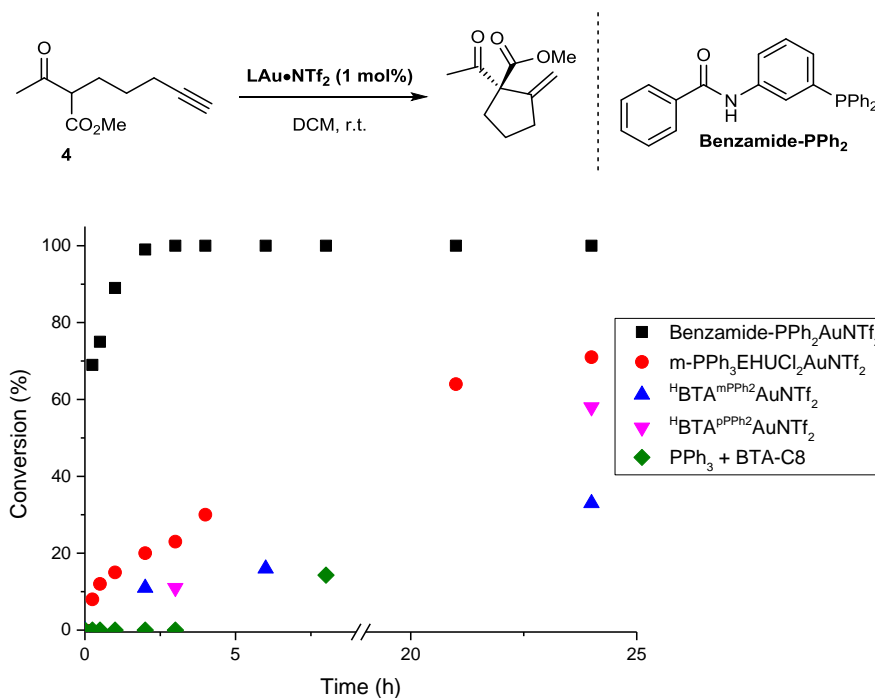


Figure VI-17: Conversion of **S1** as a function of time for different catalysts. Reaction conditions: **S1** (0.44 M), **L·AuNTf<sub>2</sub>** (1 mol%), DCM. Note: **benzamide-PPh<sub>2</sub>·AuNTf<sub>2</sub>** displays similar reactivity as **PPh<sub>3</sub>·AuNTf<sub>2</sub>**.<sup>[16]</sup>

## E. Conclusion

In this chapter, the synthesis of several gold complexes based on supramolecular scaffolds was described. Characterisation of their self-assembly properties using FT-IR and SANS analyses gave some interesting highlights. Concerning the bis-ureas gold chloride complexes the association is confirmed in DCM. However, upon chloride abstraction a competition seemed to exist for the carbonyl binding between the N-H and the cationic gold atoms and not surprisingly the ureas remained more associated than BTAs. Moreover a CD signal for (*R*)-*m*-PPh<sub>3</sub>PBEUX·AuCl is observed which is of good promise for chirality induction that will in the context of asymmetric catalysis.

For the catalysis, the lower kinetics observed with the supramolecular scaffolds compared to PPh<sub>3</sub> were in accordance with competition between the urea or the amide and the substrate for the gold coordination. The influence of the counterion was probed and it seemed that a fine tuning between the coordination ability of the anion and the type of reaction was needed. Indeed, poorly coordinating anions always gave no conversion and degradation of the gold catalyst in our supramolecular scaffolds. However the choice of the anion is constrained by the reaction as it also has a great influence on the reactivity.

Use of our supramolecular scaffolds for strategies [I] and [IV] in gold catalysis was not successful so far however the chiral (*R*)-*m*-PPh<sub>3</sub>PBEUXAuCl has yet to be tested. Other more coordinating anions could be interesting to maintain the assembly of supramolecular scaffolds.

## F. Experimental Part

All chemicals were purchased from Acros, Alfa Aesar, Sigma-Aldrich, Strem chemicals or TCI. [AuClSMe<sub>2</sub>] was purchase from TCI chemicals, AgNTf<sub>2</sub> was purchased from Acros and AgNTf<sub>2</sub>·MeCN was purchased from Strem. The carborane (Na[Me<sub>3</sub>NB<sub>12</sub>Cl<sub>11</sub>]) was graciously offered by Stefan F. Kirsh.

General procedures for solvents, NMR, FT-IR, CD and SANS are the same as in chapter III.

The catalysis products have been characterised using a Waters HPLC after filtration of the sample over Teflon 20 µm.

### 1. Complementary figures

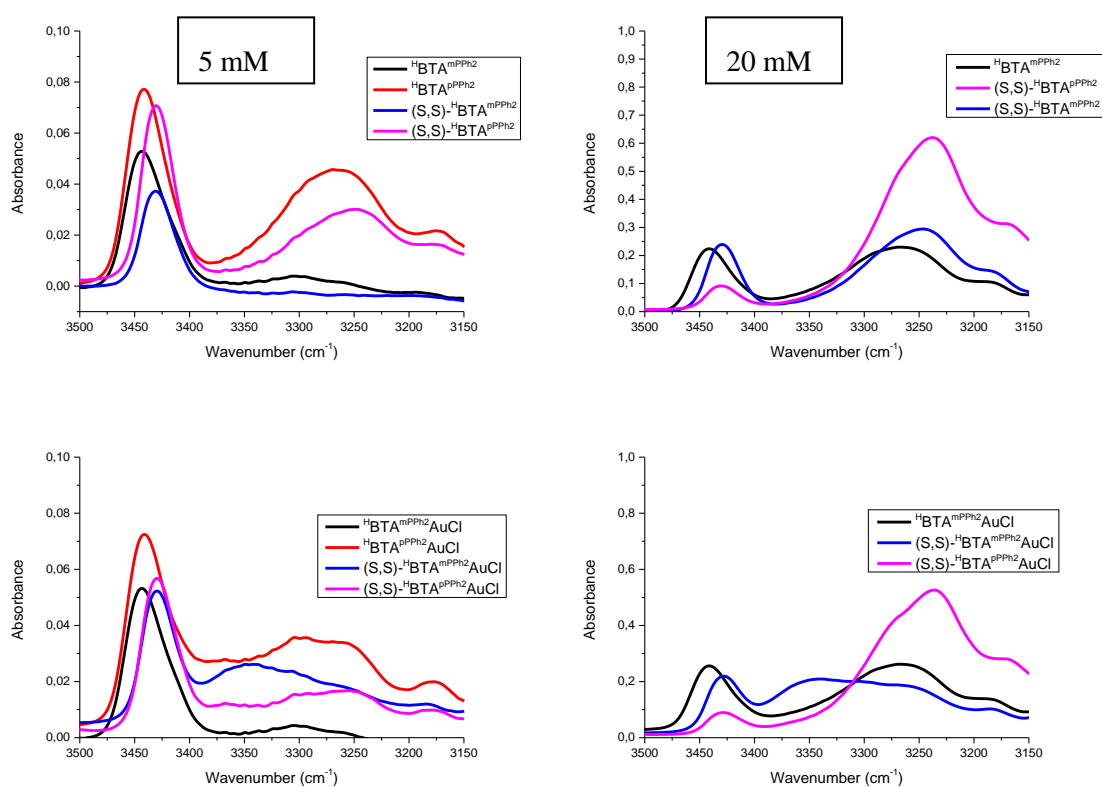


Figure VI-S1: FTIR spectra of BTA ligand (top) and BTA·AuCl complexes (bottom) in DCM at 5 mM (left) and 20 mM (right).

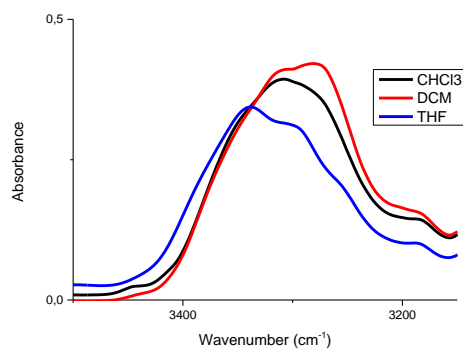


Figure VI-S2: FTIR spectra of *(rac)*-*m*-PPh<sub>3</sub>EHUX·AuCl at 10 mM in different solvents

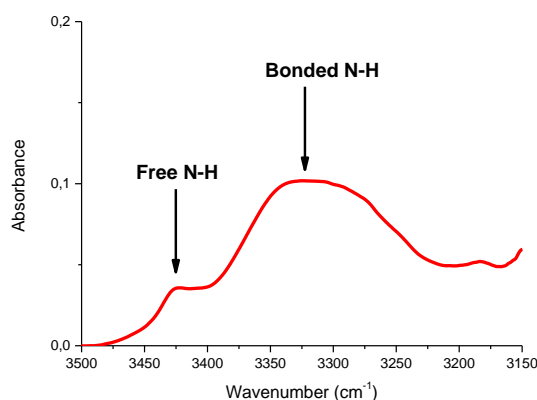


Figure VI-S3: FTIR spectra of *(R)*-*m*-PPh<sub>3</sub>PBEUX·AuCl at 1 mM

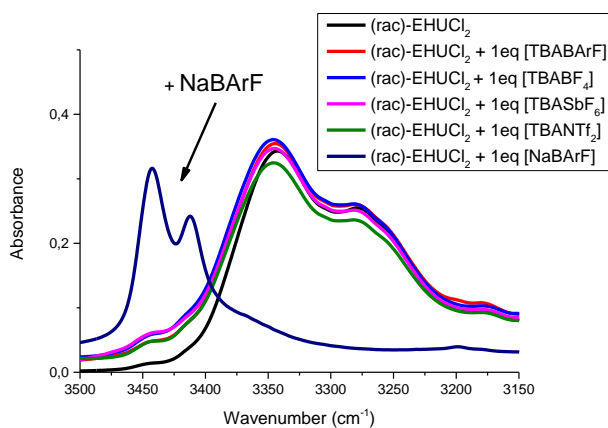


Figure VI-S4: FT-IR spectra in chloroform (10 mM) of *(rac)*-EHUCl<sub>2</sub> were recorded with BArF, BF<sub>4</sub>, SbF<sub>6</sub>, NTf<sub>2</sub> as tetrabutylammonium (TBA) salts. For all those anions no effect on the self-assembly of *(rac)*-EHUCl<sub>2</sub> was observed as the shape of the spectra is quasi identical. On the other hand addition of sodium (NaBARF) in the solution led to a dramatic change in the FT-IR spectra as no more association was observed (only signals in the free N-H region were observed at 3425 to 3460 cm<sup>-1</sup>).

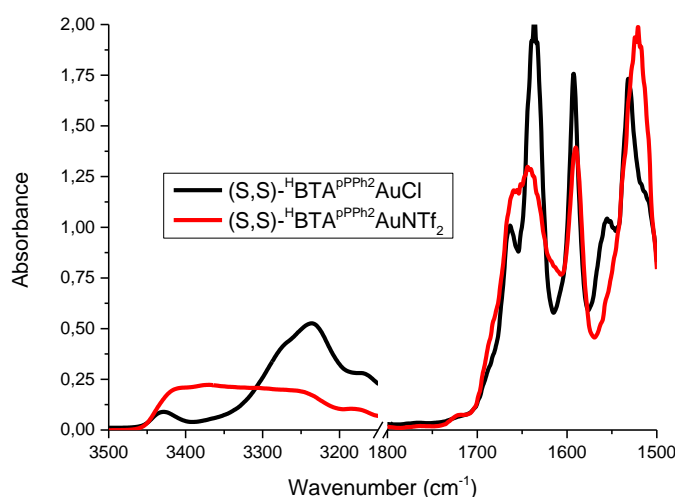


Figure VI-S5: FT-IR spectra of  $(S,S)\text{-}^H\text{-BTA}^{p\text{PPH}_2}\cdot\text{AuCl}$  and  $(S,S)\text{-}^H\text{-BTA}^{p\text{PPH}_2}\cdot\text{AuNTf}_2$  complexes in DCM (20 mM). For this BTA complex, in addition to the free N-H bonds already present in the parent gold chloride complex, one can observe an extremely broad band from 3450 to 3200  $\text{cm}^{-1}$ . The origin of this band is not established but it clearly reveals that a third species is present in addition to monomers and stacks. Similarly to the bis-urea the carbonyl is also affected and a broadening of the carbonyl band is observed.

## 2. Synthesis of the gold complexes:

$\text{PPh}_3\cdot\text{AuCl}$ ,  $\text{PPh}_3\cdot\text{AuNTf}_2$ ,  $(o\text{-Tol})_3\cdot\text{AuCl}$  and  $\text{P}(\text{Cy})_3\cdot\text{AuCl}$  have been already described in the literature.<sup>[41]</sup>

Benzamide- $\text{PPh}_2$  synthesis:

In an oven-dried Schlenk flask, 3-diphenylphosphinoaniline (300 mg, 1.08 mmol) was dissolved in dry DCM (20 mL) under  $\text{N}_2$ . Then dry  $\text{Et}_3\text{N}$  (1.51 mL, 1.08 mmol) was added to the solution followed by the dropwise addition of benzoyl chloride (182 mg, 1.21 mmol). The reaction turned pale yellow and was left to stir for overnight. The volatiles were removed by rotatory evaporation and the product was purified via column chromatography on silica gel (4:1 DCM:ETOAc) to form a white solid (281.9 mg, 68.2% yield).

$^1\text{H NMR}$  (300 MHz,  $\text{CDCl}_3$ )  $\delta$  7.96 (d,  $J = 8.1$  Hz, 1H), 7.87 – 7.76 (m, 2H), 7.67 – 7.29 (m, 16H), 7.14 – 7.06 (m, 1H).  $^{31}\text{P}\{^1\text{H}\}$  NMR (122 MHz,  $\text{CDCl}_3$ )  $\delta$  -5.4.

**L·AuCl** complexes:

To a solution of ligand (1.0 equivalent) dissolved in dry DCM (ca. for 0.12 M) was added chloro(dimethylsulfide)gold(I) (1.0 equivalent) in one portion. The reaction can be monitored by  $^{31}\text{P}\{^1\text{H}\}$  NMR and was usually complete within 30 min. Then the resulting **L·AuCl** complex was precipitated by addition of pentane to the reaction medium and filtrated.

### **Benzamide-PPh<sub>2</sub>·AuCl**

Off-white powder, 170 mg (90%).

<sup>1</sup>H NMR (400 MHz, CDCl<sub>3</sub>): δ 8.14 (d, *J* = 8.1 Hz, 1H), 7.95 (s, 1H), 7.90-7.85 (m, 2H), 7.68 (dt, *J* = 14.6, 1.9 Hz, 1H), 7.61-7.43 (m, 14H), 7.25-7.18 (m, 1H). <sup>13</sup>C{<sup>1</sup>H} NMR (101 MHz, CDCl<sub>3</sub>): δ 134.4, 134.3, 132.4, 132.3, 129.5, 129.4, 129.1, 127.3, 125.6, 115.2. <sup>31</sup>P{<sup>1</sup>H} NMR (162 MHz, CDCl<sub>3</sub>) δ 33.8. IR (ATR, cm<sup>-1</sup>): 3676, 2972, 2901, 1407, 1394, 1250, 1076, 1066, 1048, 1028. HRMS: Calculated for C<sub>25</sub>H<sub>20</sub>NOPAuClNa [M+Na]<sup>+</sup>: 636.0529, found: 636.0534.

### **P(Mes)<sub>3</sub>·AuCl**

White powder, 108.5 mg (68%).

<sup>1</sup>H NMR (300 MHz, CDCl<sub>3</sub>): δ 6.87 (s, 6H), 2.30 (s, 9H), 2.30 (br s, 18H). <sup>13</sup>C{<sup>1</sup>H} NMR (75 MHz, CDCl<sub>3</sub>) δ 141.33, 141.29, 131.92, 131.79, 125.97, 125.25, 21.03, 21.02. <sup>31</sup>P{<sup>1</sup>H} NMR (122 MHz, CDCl<sub>3</sub>): δ -5.3. IR (ATR, cm<sup>-1</sup>): 2969, 1603, 1558, 1445, 1399, 1379, 1289, 1503, 1032, 1017. HRMS: Calculated for C<sub>27</sub>H<sub>33</sub>PAuClNa [M+Na]<sup>+</sup>: 634.1566, found: 634.1574.

### **<sup>H</sup>BTA<sup>pPh<sub>2</sub></sup>·AuCl**

White powder, 106 mg (80%).

<sup>1</sup>H NMR (400 MHz, DMSO-*d*<sub>6</sub>) δ 10.88 (s, 1H), 8.72 (t, *J* = 5.6 Hz, 2H), 8.48 (dd, *J* = 14.2, 1.6 Hz, 3H), 8.10-7.97 (m, 2H), 7.70-7.48 (m, 12H), 3.31 (m, 2H), 1.60-1.50 (m, 4H), 1.36-1.18 (m, 22H), 0.89-0.82 (m, 6H). <sup>31</sup>P{<sup>1</sup>H} NMR (162 MHz, DMSO-*d*<sub>6</sub>) δ 31.6. HRMS: Calculated for C<sub>43</sub>H<sub>54</sub>N<sub>3</sub>O<sub>3</sub>PAuClNa [M+Na]<sup>+</sup>: 946.3149, found: 946.3171.

### **<sup>H</sup>BTA<sup>mPh<sub>2</sub></sup>·AuCl**

White powder, 93 mg (70%).

<sup>1</sup>H NMR (400 MHz, DMSO-*d*<sub>6</sub>) δ 10.78 (s, 1H), 8.69 (t, *J* = 5.6 Hz, 2H), 8.46 (dd, *J* = 7.6, 1.7 Hz, 3H), 8.19-8.00 (m, 2H), 7.72-7.51 (m, 10H), 7.24 (dd, *J* = 12.9, 7.6 Hz, 1H), 3.31-3.24 (m, 4H), 1.54 (t, *J* = 7.0 Hz, 4H), 1.37-1.13 (m, 22H), 0.89-0.81 (m, 6H). <sup>31</sup>P{<sup>1</sup>H} NMR (162 MHz, DMSO-*d*<sub>6</sub>) δ 33.6. <sup>13</sup>C{<sup>1</sup>H} NMR (101 MHz, DMSO-*d*<sub>6</sub>) δ 165.1, 135.2, 134.8, 133.9, 133.7, 132.4, 129.7, 129.6, 128.8, 128.5, 127.8, 40.2, 31.2, 29.0, 28.7, 28.6, 26.5, 22.17, 13.9. IR (ATR, cm<sup>-1</sup>): 3254, 2955, 2923, 1636, 1535, 1482, 1415, 1294, 1255, 1102.

### **(S,S)-<sup>H</sup>BTA<sup>pPh<sub>2</sub></sup>·AuCl**

White powder, 106 mg (80%).

<sup>1</sup>H NMR (400 MHz, DMSO-*d*<sub>6</sub>) δ 10.88 (s, 1H), 8.49-8.41 (m, 5H), 8.04 (dd, *J* = 8.8, 2.2 Hz, 2H), 7.697.50 (m, 10H), 4.10-3.97 (m, 2H), 1.61-1.40 (m, 4H), 1.37 – 1.21 (m, 18H), 1.16 (d, *J* = 6.5 Hz, 6H), 0.88 – 0.79 (m, 6H). IR (ATR, cm<sup>-1</sup>): 3253, 2969, 2928, 1637, 1591, 1526, 1103, 1067, 1049.

$^{31}\text{P}\{^1\text{H}\}$  NMR (162 MHz, DMSO- $d_6$ )  $\delta$  31.6. **HRMS**: Calculated for  $\text{C}_{43}\text{H}_{54}\text{N}_3\text{O}_3\text{PAuClNa}$   $[\text{M}+\text{Na}]^+$ : 946.3149, found: 946.3171.

### **(S,S)- $^{\text{H}}$ -BTA $^{\text{mPPh}_2}$ ·AuCl**

White powder, 92 mg (69%).

$^1\text{H}$  NMR (400 MHz, DMSO- $d_6$ )  $\delta$  10.79 (s, 1H), 8.51-8.37 (m, 5H), 8.19-8.01 (m, 2H), 7.73-7.47 (m, 10H), 7.24 (dd,  $J = 12.9, 7.6$  Hz, 1H), 4.03 (p,  $J = 7.1$  Hz, 2H), 1.64-1.39 (m, 4H), 1.27 (d,  $J = 14.8$  Hz, 18H), 1.15 (d,  $J = 6.6$  Hz, 6H), 0.88-0.81 (m, 6H).  $^{31}\text{P}\{^1\text{H}\}$  NMR (162 MHz, DMSO- $d_6$ )  $\delta$  33.4. **IR** (ATR,  $\text{cm}^{-1}$ ): 3230, 2968, 2927, 1635, 1544, 1481, 1436, 1308, 1102. **HRMS**: Calculated for  $\text{C}_{43}\text{H}_{54}\text{N}_3\text{O}_3\text{PAuClNa}$   $[\text{M}+\text{Na}]^+$ : 946.3149, found: 946.3172.

### **Bis-urea AuCl complexes:**

#### **(rac)- $m$ -PPh $_3$ EHUCl $_2$ ·AuCl**

To a solution of **(rac)- $m$ -PPh $_3$ EHUCl $_2$**  (104 mg, 0.16 mmol) in dry DCM (2 mL) and MeOH (2 mL) was added chloro(dimethylsulfide)gold(I) (48.1 mg, 0.16 mmol). The solution was stirred at room temperature for 1 hour before addition of pentane (10 mL). The resulting precipitate was filtered-off to gave **(rac)- $m$ -PPh $_3$ EHUCl $_2$ ·AuCl** as a slightly purple powder, 122 mg (86%).

$^1\text{H}$  NMR (400 MHz, DMSO- $d_6$ )  $\delta$  9.61 (s, 1H), 8.90 (s, 1H), 8.26 (s, 1H), 8.02 (s, 1H), 7.85 (d,  $J = 8.2$  Hz, 1H), 7.69-7.48 (m, 13H), 7.13-7.05 (m, 1H), 6.95 (t,  $J = 5.7$  Hz, 1H), 3.06 (m, 2H), 1.44-1.12 (m, 9H), 0.87 (m, 6H).  $^{13}\text{C}\{^1\text{H}\}$  NMR (75 MHz, DMSO- $d_6$ )  $\delta$  154.5, 151.7, 136.1, 134.6, 134.0, 133.8, 132.5, 129.7, 129.6, 128.7, 128.3, 117.3, 115.0, 41.6, 30.5, 28.4, 23.7, 22.5, 13.9, 10.8.  $^{31}\text{P}\{^1\text{H}\}$  NMR (162 MHz, DMSO- $d_6$ )  $\delta$  33.3. **IR** (ATR,  $\text{cm}^{-1}$ ): 3280, 2955, 2925, 1645, 1588, 1550, 1481, 1463, 1436, 1411, 1238, 1219. **HRMS**: Calculated for  $\text{C}_{34}\text{H}_{37}\text{N}_4\text{O}_2\text{PAuCl}_3\text{Na}$   $[\text{M}+\text{Na}]^+$ : 889.1277, found: 889.1296.

#### **(rac)- $m$ -PPh $_3$ EHUX·AuCl**

To a suspension of **(rac)- $m$ -PPh $_3$ EHUX** (168 mg, 0.28 mmol) in dry DCM (3 mL) and MeOH (3 mL) was added chloro(dimethylsulfide)gold(I) (85.3 mg, 0.28 mmol). The suspension disappeared after the addition of the chloro(dimethylsulfide)gold(I). The solution was stirred at room temperature for 3 hours before concentration by rotatory evaporation and precipitation with pentane (25 mL). The resulting precipitate was filtered-off to gave **(rac)- $m$ -PPh $_3$ EHUX·AuCl** as a white powder, 186 mg (79%).

$^1\text{H}$  NMR (300 MHz, DMSO- $d_6$ ):  $\delta$  9.12 (s, 1H), 7.99 (s, 1H), 7.80 (d,  $J = 10.4$  Hz, 2H), 7.75-7.45 (m, 13H), 7.04 (dd,  $J = 13.1, 7.6$  Hz, 1H), 6.90 (s, 1H), 6.32 (t,  $J = 5.7$  Hz, 1H), 3.03 (q,  $J = 5.4$  Hz, 2H), 2.10 (s, 6H), 1.47-1.12 (m, 9H), 0.87 (m, 6H).  $^{13}\text{C}\{^1\text{H}\}$  NMR (75 MHz, DMSO- $d_6$ ):  $\delta$  155.4, 152.5, 141.2, 141.0, 136.0, 134.4, 133.9, 133.7, 132.3, 131.3, 130.3, 130.1, 129.7, 129.5, 129.0, 128.6, 128.2, 127.8, 122.9, 122.8, 122.2, 121.4, 115.9, 41.6, 30.5, 28.4, 23.7, 22.5, 17.3, 17.1, 14.0, 10.8.  $^{31}\text{P}\{^1\text{H}\}$

**NMR** (122 MHz, DMSO- $d_6$ ):  $\delta$  33.5. **IR** (ATR,  $\text{cm}^{-1}$ ): 3343, 2972, 2901, 1640, 1550, 1407, 1394, 1381, 1242, 1228, 1076, 1066, 1049, 1028. **HRMS**: Calculated for  $\text{C}_{36}\text{H}_{43}\text{N}_4\text{O}_2\text{PAuClNa}$   $[\text{M}+\text{Na}]^+$ : 849.2370, found: 849.2383.

#### **(rac)-p-PPh<sub>3</sub>PBEUX·AuCl**

**(rac)-p-PPh<sub>3</sub>PBEUX** (108 mg, 0.18 mmol) was suspended in dry DCM (5 mL) before addition of chloro(dimethylsulfide)gold(I) (53.5 mg, 0.18 mmol). The addition of chloro(dimethylsulfide)gold(I) did not improve the solubility and led to the gelation of the solution. THF (5 mL) was added and the suspension was stirred at room temperature for 1 hour before precipitation with pentane (10 mL). The resulting precipitate was filtered-off to give **(rac)-p-PPh<sub>3</sub>PBEUX·AuCl** as a white powder, 109 mg (73%).

**<sup>1</sup>H NMR** (400 MHz, DMSO- $d_6$ ):  $\delta$  9.33 (s, 1H), 8.10 (s, 1H), 7.96 (s, 1H), 7.77-7.40 (m, 15H), 6.92 (s, 1H), 6.31 (d,  $J = 8.4$  Hz, 1H), 3.64 (m, 1H), 3.42-3.28 (m, 4H), 2.11 (d,  $J = 10.1$  Hz, 6H), 1.63-1.30 (m, 4H), 0.87 (m, 6H). **<sup>13</sup>C{<sup>1</sup>H} NMR** (101 MHz, DMSO- $d_6$ ):  $\delta$  155.1, 152.3, 144.0, 136.0, 135.1, 134.9, 134.4, 133.6, 133.5, 132.1, 131.3, 129.6, 129.5, 129.3, 128.6, 122.6, 118.3, 118.2, 115.5, 72.0, 50.1, 24.7, 22.4, 17.3, 17.1, 10.5, 10.3. **<sup>31</sup>P{<sup>1</sup>H} NMR** (162 MHz, DMSO- $d_6$ ):  $\delta$  31.5. **IR** (ATR,  $\text{cm}^{-1}$ ): 3343, 2972, 2901, 1641, 1541, 1394, 1225, 1103, 1076, 1066, 1046. **HRMS**: Calculated  $\text{C}_{36}\text{H}_{43}\text{N}_4\text{O}_2\text{PAuClNa}$   $[\text{M}+\text{Na}]^+$ : 849.2370, found: 849.2383.

#### **(R)-m-PPh<sub>3</sub>PBEUX·AuCl**

To a solution of **(R)-m-PPh<sub>3</sub>PBEUX** (96.8 mg, 0.16 mmol) dissolved in dry THF (4 mL) was added chloro(dimethylsulfide)gold(I) (47.8 mg, 0.16 mmol). The solution was stirred at room temperature for 1 hour before addition of pentane (10 mL). The resulting precipitate was filtered-off to give **(R)-m-PPh<sub>3</sub>PBEUX·AuCl** as a white powder, 106 mg (79%).

**<sup>1</sup>H NMR** (400 MHz, DMSO- $d_6$ ):  $\delta$  9.15 (s, 1H), 8.01 (s, 1H), 7.84 (s, 1H), 7.79 (d,  $J = 8.3$  Hz, 1H), 7.70 – 7.52 (m, 12H), 7.49 (td,  $J = 7.9, 3.3$  Hz, 1H), 7.04 (dd,  $J = 13.0, 7.6$  Hz, 1H), 6.90 (s, 1H), 6.29 (d,  $J = 8.4$  Hz, 1H), 3.65 (m, 1H), 3.40-3.26 (m, 4H), 2.10 (s, 6H), 1.61-1.44 (m, 3H), 1.43-1.31 (m, 1H), 0.87 (td,  $J = 7.4, 5.4$  Hz, 6H). **<sup>13</sup>C{<sup>1</sup>H} NMR** (101 MHz, DMSO- $d_6$ ):  $\delta$  155.1, 152.5, 135.6, 134.4, 133.8, 133.7, 132.3, 131.3, 130.3, 130.1, 129.7, 129.6, 128.5, 127.9, 122.8, 122.7, 122.4, 122.3, 121.4, 115.8, 114.5, 72.0, 50.1, 24.7, 22.4, 17.3, 17.1, 10.5, 10.3. **<sup>31</sup>P{<sup>1</sup>H} NMR** (162 MHz, DMSO- $d_6$ ):  $\delta$  33.5. **IR** (ATR,  $\text{cm}^{-1}$ ): 3328, 2967, 2900, 1641, 1546, 1482, 1437, 1409, 1226, 1103, 1078, 1066, 1044. **HRMS**: Calculated for  $\text{C}_{35}\text{H}_{41}\text{N}_4\text{O}_3\text{PAuClNa}$   $[\text{M}+\text{Na}]^+$ : 851.2163, found: 851.2176.

LAuNTf<sub>2</sub> complexes:

#### **(rac)-m-PPh<sub>3</sub>EHUCl<sub>2</sub>·AuNTf<sub>2</sub>**

To a solution of **(rac)-m-PPh<sub>3</sub>EHUCl<sub>2</sub>** (127 mg, 0.2 mmol) dissolved in dry DCM (5 mL) was added chloro(dimethylsulfide)gold(I) (58.9 mg, 0.2 mmol). The solution was stirred at room temperature for



50 minutes. The coordination of the phosphine was confirmed by  $^{31}\text{P}\{^1\text{H}\}$  NMR. Then silver bis(trifluoromethanesulfonyl)imide (77.6 mg, 0.2 mmol) was added in one portion. The solution was stirred and turned to a brownish/red colour. Then the resulting **(rac)-m-PPh<sub>3</sub>EHUCl<sub>2</sub>·AuNTf<sub>2</sub>** complex was filtered through a short celite® pad and eluted with dry DCM (twice the volume of the reaction). Then the solvent was removed by rotatory evaporation giving **(rac)-m-PPh<sub>3</sub>EHUCl<sub>2</sub>·AuNTf<sub>2</sub>** as a brownish/red solid (204 mg, 92%).

$^1\text{H}$  NMR (300 MHz, DMSO-*d*<sub>6</sub>):  $\delta$  9.62 (s, 1H), 8.93 (s, 1H), 8.27 (s, 1H), 8.02 (s, 1H), 7.82 (d, *J* = 15.5 Hz, 1H), 7.75-7.49 (m, 13H), 7.13 (dd, *J* = 13.1, 7.5 Hz, 1H), 6.97 (m, 1H), 3.05 (m, 2H), 1.28 (m, 9H), 0.86 (m, 6H).  $^{13}\text{C}\{^1\text{H}\}$  NMR (75 MHz, DMSO-*d*<sub>6</sub>):  $\delta$  154.56, 151.7, 136.1, 134.6, 134.0, 133.8, 132.5, 129.7, 129.6, 128.3, 117.3, 115.0, 114.5, 41.6, 39.1, 30.5, 28.4, 23.7, 22.5, 13.9, 10.8.  $^{31}\text{P}\{^1\text{H}\}$  NMR (122 MHz, DMSO-*d*<sub>6</sub>):  $\delta$  30.2. IR (ATR, cm<sup>-1</sup>): 3333, 2959, 2928, 1646, 1589, 1552, 1483, 1438, 1403, 1351, 1331, 1197, 1136, 1058. HRMS: Calculated for C<sub>34</sub>H<sub>37</sub>N<sub>4</sub>O<sub>2</sub>PAuCl<sub>2</sub>Na [M+Na]<sup>+</sup>: 854.1589, found: 854.1511.

#### **(rac)-m-PPh<sub>3</sub>EHUX·AuNTf<sub>2</sub>**

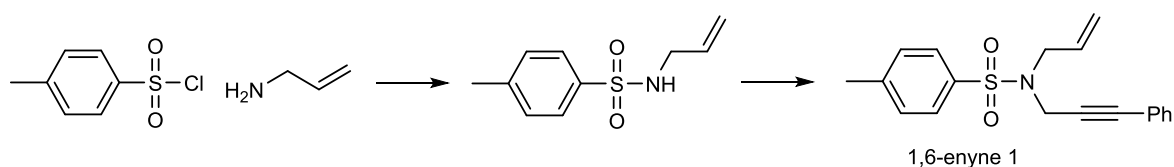
**(rac)-m-PPh<sub>3</sub>EHUXAuCl** (101 mg, 0.12 mmol) was completely dissolved in dry THF (12 mL) and silver bis(trifluoromethanesulfonyl)imide·acetonitrile (47.5 mg, 0.12 mmol) was added and a precipitate was immediately formed. Then MeOH (10 mL) was added to help the solubilisation and the solution was filtered through a short celite® pad and eluted with MeOH. The volatiles were removed and the crude product was recrystallised from acetonitrile to give a slightly purple solid obtained that correspond to the starting material:  $^{31}\text{P}\{^1\text{H}\}$  NMR (122 MHz, DMSO-*d*<sub>6</sub>)  $\delta$  33.5. HRMS: main peak 849.24 ligand:  $^{31}\text{P}\{^1\text{H}\}$  NMR (122 MHz, DMSO-*d*<sub>6</sub>):  $\delta$  33.5. HRMS: Calculated for C<sub>36</sub>H<sub>43</sub>N<sub>4</sub>O<sub>2</sub>PAuClNa [M+Na]<sup>+</sup>: 849.2370, found: 849.2383.

### 3. Catalysis:

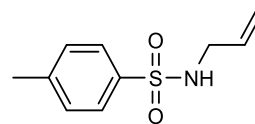
Typical experimental procedure:

#### a) 1,6-enyne 1 cycloisomerisation (Table VI-7):

##### Synthesis of 1



*N*-Allyl-4-methylbenzenesulfonamide

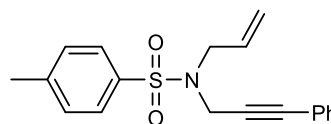


To a solution of *para*-toluenesulfonyl chloride (9.5 g, 45.5 mmol) and triethylamine (7 mL, 45.5 mmol) in DCM (250 mL) was cautiously added the allylamine (3.75 mL, 50 mmol). The solution was then refluxed for 2 hours before the organic phase was washed with water, dried over MgSO<sub>4</sub>. Removal of the solvents gave the pure product as a colourless solid (10g, quantitative).

<sup>1</sup>H NMR (200 MHz, Chloroform-*d*) δ 7.76 (d, *J* = 8.0 Hz, 2H), 7.30 (d, *J* = 8.1 Hz, 2H), 5.71 (m, 1H), 5.25-4.99 (m, 2H), 4.92 (t, *J* = 6.5 Hz, 1H), 3.57 (t, *J* = 5.4 Hz, 2H), 2.73 (s, 3H). The spectroscopic data are in agreement with the literature.<sup>[43]</sup>

*N*-(1-Methyl-2-propenyl)-*N*-(3-phenyl-2-propynyl)-4-methylphenylsulfonamide

**1**



To an oven-dried round bottom flask 3-phenyl-2-propyn-2-ol (800 μL, 6.4 mmol) was added to a solution of *N*-Allyl-4-methylbenzenesulfonamide (1.35 g, 6.4 mmol) and triphenylphosphine (1.68 g, 6.4 mmol) in dry THF (75 mL). Then diethylazodicarboxylate (1 mL, 6.4 mmol) was added to the solution and the yellow solution was stirred overnight at room temperature. The solvents were removed by rotatory evaporation and the crude product was directly purified by column chromatography on silica gel (EP/DCM 50% to 100%) yielding an off-white solid (675 mg, 32%).

<sup>1</sup>H NMR (300 MHz, CDCl<sub>3</sub>) δ 7.78 (d, *J* = 8.3 Hz, 2H), 7.26 (m, 5H), 7.14-7.02 (m, 2H), 5.81 (m, 1H), 5.39-5.21 (m, 2H), 4.31 (s, 2H), 3.89 (dt, *J* = 6.5, 1.3 Hz, 2H), 2.34 (s, 3H). The spectroscopic data are in agreement with the literature.<sup>[44]</sup>

### Catalytic experiments

With PPh<sub>3</sub>·AuCl:

An oven-dried test tube was loaded with PPh<sub>3</sub>AuCl (5 mol%) and the substrate (1 eq) in dry DCM (*ca.* 40 mM). The mixture was stirred until complete dissolution before addition of the silver salt (7 mol%). The silver salt was added after the substrate to avoid the degradation of the catalyst that can occur without substrate stabilisation of the cationic gold.<sup>[11]</sup> The reaction was monitored by <sup>1</sup>H NMR by taking a small aliquot filtrated through short silica pad. Similarly the reaction was stopped by filtration over a short silica pad to remove all gold and silver species and then the crude product was analysed by <sup>1</sup>H NMR to determine the conversion.

With **L·AuCl** with salts as chloride abstractor:

An oven-dried test tube was loaded with  $\text{PPh}_3 \cdot \text{AuCl}$  (10 mol%), the co-monomer if present (10 mol%) and the substrate (1 eq) in dry DCM (*ca.* 50 mM). The mixture was stirred until complete dissolution before addition of the silver salt (14 mol%). The reaction was monitored by  $^1\text{H}$  NMR by taking a small aliquot filtrated through short silica pad. Similarly the reaction was stopped by filtration over a short silica pad to remove all gold and silver species and then the crude product was analysed by  $^1\text{H}$  NMR to determine the conversion.

With  $^{\text{H}}\text{BTA}^{\text{PPh}_2} \cdot \text{AuCl}$ :

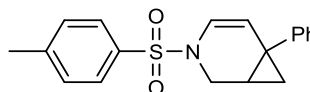
An oven-dried test tube was loaded with  $^{\text{H}}\text{BTA}^{\text{PPh}_2} \cdot \text{AuCl}$  (14 mol%) and the substrate (1 eq) in solvent (pentane or cyclohexane *ca.* 50 mM). The reaction was started by the addition of the  $\text{AgSbF}_6$  (14 mol%). The reaction was monitored by  $^1\text{H}$  NMR by taking a small aliquot filtrated through short silica pad. Similarly the reaction was stopped by filtration over a short silica pad to remove all gold and silver species and then the crude product was analysed by  $^1\text{H}$  NMR to determine the conversion.

With the other BTA complexes:

An oven-dried test tube was loaded with  $\text{BTA} \cdot \text{AuCl}$  (10 mol%), the co-monomer if present (10 mol%) and the substrate (1 eq) in cyclohexane (*ca.* 50 mM). The reaction was started by the addition of the  $\text{AgSbF}_6$  (14 mol%). The reaction was monitored by  $^1\text{H}$  NMR by taking a small aliquot filtrated through short silica pad. Similarly the reaction was stopped by filtration over a short silica pad to remove all gold and silver species and then the crude product was analysed by  $^1\text{H}$  NMR to determine the conversion.

6-Phenyl-3-(toluene-4-sulfonyl)-3-aza-  
bicyclo[4.1.0]hept-4-ene

**P1**



$^1\text{H}$  NMR (200 MHz,  $\text{CDCl}_3$ )  $\delta$  7.69 (d,  $J = 8.1$  Hz, 2H), 7.33 (d,  $J = 7.8$  Hz, 2H), 7.25-7.10 (m, 3H), 6.46 (d,  $J = 8.2$  Hz, 1H), 5.50 (d,  $J = 8.2$  Hz, 1H), 3.99 (d,  $J = 11.6$  Hz, 1H), 3.21-3.06 (m, 1H), 2.44 (s, 3H), 1.71 (m, 1H), 1.41-1.22 (m, 1H), 0.89 (t,  $J = 5.5$  Hz, 1H). The spectroscopic data are in agreement with the literature.<sup>[42]</sup> Dimer formation of **P2** can be monitored by NMR with the apparition of the characteristic peak of the dimer at  $\delta$  0.63 ppm

**HPLC analysis:** Daicel Chiralcel®-OD-H, hexane/isopropanol 99/1, retention times: 31.1 min and 34.6 min.

Table VI-S1: 1,6-enyne **1** cycloisomerisation using bis-urea gold complexes

Catalyst	Solvent	Chloride abstractor	Time	conversion
<i>(rac)</i> - <i>p</i> -PPh <sub>3</sub> EHUCl <sub>2</sub> ·AuCl (5 mol%)	DCM	AgSbF <sub>6</sub> 7 mol%	3h	90%
<i>(rac)</i> - <i>p</i> -PPh <sub>3</sub> EHUCl <sub>2</sub> ·AuCl (5 mol%)	CDCl <sub>3</sub>	AgSbF <sub>6</sub> 7 mol%	4.7h	90%
<i>(rac)</i> - <i>p</i> -PPh <sub>3</sub> EHUCl <sub>2</sub> ·AuCl (5 mol%) + <i>(rac)</i> -PBEUT (5 mol%)	CDCl <sub>3</sub>	AgSbF <sub>6</sub> 5 mol%	12h	41%
<i>(rac)</i> - <i>p</i> -PPh <sub>3</sub> EHUCl <sub>2</sub> ·AuNTf <sub>2</sub> (10 mol%)	cyclohexane	---	48h	100%

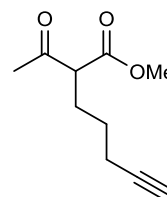
Reaction conditions: **Substrate** (0.4 M), solvent. The catalysts were prepared in the reaction solvent.

## b) Conia-ene

### Substrate 4 synthesis

2-acetyl-methyl-hept-6-ynoate

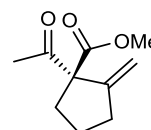
**4**



To an oven-dried Schlenk-flask under nitrogen, NaI (580 mg, 3.85 mmol), NaH (340 mg, 8.74 mmol, 60% dispersion in oil) were mixed in a 1/1 mixture THF/DMF (16 ml). Methyl acetoacetate (1 ml, 9.25 mmol) was added dropwise to this suspension and after 10 min of stirring, 5-chloropent-1-yne (817  $\mu$ L, 7.7 mmol) was added in one portion and the mixture was refluxed for 1 day. The mixture was cooled to room temperature and Et<sub>2</sub>O was added. The organic phase was washed with HCl (3%, twice), brine and dried over MgSO<sub>4</sub>. The crude product was purified by flash chromatography on silica gel eluting with EP/DCM (50% to 100%) yielding a yellowish oil (946 mg, 67%).

<sup>1</sup>H NMR (200 MHz, CDCl<sub>3</sub>)  $\delta$  3.74 (s, 3H), 3.46 (t,  $J$  = 7.4 Hz, 1H), 2.23 (s, 3H), 2.26-2.18 (m, 2H), 2.14 (s, 1H), 2.04-1.90 (m, 2H), 1.61-1.23 (m, 2H). The spectroscopic data are in agreement with the literature.<sup>[45]</sup>

**P4**



<sup>1</sup>H NMR (300 MHz, CDCl<sub>3</sub>)  $\delta$  5.29 (t,  $J$  = 2.3 Hz, 1H), 5.22 (t,  $J$  = 2.3 Hz, 1H), 3.75 (s, 3H), 2.50-2.33 (m, 3H), 2.22 (s, 3H), 2.18 (m, 1H), 1.83-1.65 (m, 2H). The spectroscopic data are in agreement with the literature.<sup>[40]</sup>

### Catalytic experiments

To an oven-dried test tube loaded was added L·AuNTf<sub>2</sub> (1 mol%) and dry DCM (ca. 0.44 M). The mixture was stirred until complete dissolution of the gold complex before addition of the 2-acetyl-methyl-hept-6-ynoate (1.0 eq). The reaction was stirred at room temperature until stopped by filtration

over a short silica pad to remove all gold species and then the crude product was analysed by  $^1\text{H}$  NMR to determine the conversion.

Table VI-S2: Conia-ene reaction using BTA goldNTf<sub>2</sub> complexes

Entry	Catalyst	Co-monomer	Solvent	Temperature	Time	Conversion
1	$^{\text{H}}\text{BTA}^{\text{pPh}_2}\cdot\text{AuNTf}_2$	no	DCM	25	24h	58%
2	$^{\text{H}}\text{BTA}^{\text{pPh}_2}\cdot\text{AuNTf}_2$	no	cyclohexane	25	24h	34%
3	$^{\text{H}}\text{BTA}^{\text{pPh}_2}\cdot\text{AuNTf}_2$	no	cyclohexane	50	24h	100%
4	$^{\text{H}}\text{BTA}^{\text{pPh}_2}\cdot\text{AuNTf}_2$	<b>BTA C8</b>	cyclohexane	50	24h	17%
5	$^{\text{H}}\text{BTA}^{\text{mPh}_2}\cdot\text{AuNTf}_2$	no	cyclohexane	25	3h	14%
6	$^{\text{H}}\text{BTA}^{\text{mPh}_2}\cdot\text{AuNTf}_2$	<b>BTA C8</b>	cyclohexane	25	24h	9%
7	$^{\text{H}}\text{BTA}^{\text{mPh}_2}\cdot\text{AuNTf}_2$	no	cyclohexane	50	3h	34%
8	$^{\text{H}}\text{BTA}^{\text{mPh}_2}\cdot\text{AuNTf}_2$	<b>BTA C8</b>	cyclohexane	50	3h	12%
9	$^{\text{H}}\text{BTA}^{\text{mPh}_2}\cdot\text{AuNTf}_2$	no	decaline	25	24h	50%
10	$^{\text{H}}\text{BTA}^{\text{mPh}_2}\cdot\text{AuNTf}_2$	no	decaline	50	24h	93%

Reaction conditions: **4** (0.4 M),  $^{\text{H}}\text{BTA}^{\text{pPh}_2}\text{AuNTf}_2$  (1 mol%), **BTA C8** (if present 1 mol%), solvent.

## G. References

- [1] D. J. Gorin, F. D. Toste, *Nature* **2007**, *446*, 395–403.
- [2] B. Ranieri, I. Escofet, A. M. Echavarren, *Org. Biomol. Chem.* **2015**, *13*, 7103–7118.
- [3] D. J. Gorin, B. D. Sherry, F. D. Toste, *Chem. Rev.* **2008**, *108*, 3351–3378.
- [4] S. Kronig, E. Theuergarten, C. G. Daniliuc, P. G. Jones, M. Tamm, *Angew. Chem. Int. Ed.* **2012**, *51*, 3240–3244.
- [5] R. Gramage-Doria, J. Hessels, S. H. A. M. Leenders, O. Tröppner, M. Dürr, I. Ivanović-Burmazović, J. N. H. Reek, *Angew. Chem. Int. Ed.* **2014**, *53*, 13380–13384.
- [6] F. Li, N. Wang, L. Lu, G. Zhu, *J. Org. Chem.* **2015**, *80*, 3538–3546.
- [7] K. Belger, N. Krause, *Eur. J. Org. Chem.* **2015**, *2015*, 220–225.
- [8] J. Oliver-Meseguer, J. R. Cabrero-Antonino, I. Dominguez, A. Leyva-Perez, A. Corma, *Science* **2012**, *338*, 1452–1455.
- [9] D. Wang, R. Cai, S. Sharma, J. Jirak, S. K. Thummanapelli, N. G. Akhmedov, H. Zhang, X. Liu, J. L. Petersen, X. Shi, *J. Am. Chem. Soc.* **2012**, *134*, 9012–9019.
- [10] M. Jia, M. Bandini, *ACS Catal.* **2015**, *5*, 1638–1652.
- [11] A. Homs, I. Escofet, A. M. Echavarren, *Org. Lett.* **2013**, *15*, 5782–5785.
- [12] Z. Lu, J. Han, G. B. Hammond, B. Xu, *Org. Lett.* **2015**, *17*, 4534–4537.
- [13] M. Kumar, G. B. Hammond, B. Xu, *Org. Lett.* **2014**, *9–12*.
- [14] C. Obradors, A. M. Echavarren, *Chem. Commun.* **2014**, *50*, 16–28.
- [15] D. Weber, T. D. Jones, L. L. Adduci, M. R. Gagné, *Angew. Chem. Int. Ed.* **2012**, *51*, 2452–2456.
- [16] N. Mézailles, L. Ricard, F. Gagosz, *Org. Lett.* **2005**, *7*, 4133–4136.
- [17] P. Pérez-Galán, N. Delpont, E. Herrero-Gómez, F. Maseras, A. M. Echavarren, *Chem. Eur. J.* **2010**, *16*, 5324–5332.
- [18] A. Homs, C. Obradors, D. Lebcœuf, A. M. Echavarren, *Adv. Synth. Catal.* **2014**, *356*, 221–228.
- [19] E. Herrero-Gómez, C. Nieto-Oberhuber, S. López, J. Benet-Buchholz, A. M. Echavarren, *Angew. Chem. Int. Ed.* **2006**, *45*, 5455–5459.
- [20] F. Kleinbeck, F. D. Toste, *J. Am. Chem. Soc.* **2009**, *131*, 9178–9179.
- [21] M. J. López-Gómez, D. Martin, G. Bertrand, *Chem. Commun.* **2013**, *49*, 4483.
- [22] M. Wegener, F. Huber, C. Bolli, C. Jenne, S. F. Kirsch, *Chem. Eur. J.* **2015**, *21*, 1328–1336.
- [23] W. Fang, M. Presset, A. Guérinot, C. Bour, S. Bezzenine-Lafollée, V. Gandon, *Chem. Eur. J.*

- 2014**, *20*, 5439–5446.
- [24] Y. Wang, A. D. Lackner, F. D. Toste, *Acc. Chem. Res.* **2014**, *47*, 889–901.
- [25] W. Zi, F. Dean Toste, *Chem. Soc. Rev.* **2016**, *45*, 4567–4589.
- [26] G. L. Hamilton, E. J. Kang, M. Mba, F. D. Toste, *Science* **2007**, *317*, 496–499.
- [27] L.-I. Rodríguez, T. Roth, J. Lloret Fillol, H. Wadepohl, L. H. Gade, *Chem. Eur. J.* **2012**, *18*, 3721–3728.
- [28] K. Yavari, P. Aillard, Y. Zhang, F. Nuter, P. Retailleau, A. Voituriez, A. Marinetti, *Angew. Chem. Int. Ed.* **2014**, *53*, 861–865.
- [29] M. Guitet, P. Zhang, F. Marcelo, C. Tugny, J. Jiménez-Barbero, O. Buriez, C. Amatore, V. Mourières-Mansuy, J.-P. Goddard, L. Fensterbank, *et al.*, *Angew. Chem. Int. Ed.* **2013**, *52*, 7213–7218.
- [30] A. Ochida, H. Ito, M. Sawamura, *J. Am. Chem. Soc.* **2006**, *128*, 16486–16487.
- [31] H. Ito, Y. Makida, A. Ochida, H. Ohmiya, M. Sawamura, *Org. Lett.* **2008**, *10*, 5051–5054.
- [32] H. Ito, T. Harada, H. Ohmiya, M. Sawamura, *Beilstein J. Org. Chem.* **2011**, *7*, 951–959.
- [33] H. Ito, H. Ohmiya, M. Sawamura, *Org. Lett.* **2010**, *12*, 4380–4383.
- [34] M. Galli, J. E. M. Lewis, S. M. Goldup, *Angew. Chem. Int. Ed.* **2015**, *54*, 13545–13549.
- [35] J.-H. Pan, M. Yang, Q. Gao, N.-Y. Zhu, D. Yang, *Synthesis* **2007**, *2007*, 2539–2544.
- [36] Z. Wu, K. Isaac, P. Retailleau, J.-F. Betzer, A. Voituriez, A. Marinetti, *Chem. Eur. J.* **2016**, *22*, 3278–3281.
- [37] S. I. Lee, S. M. Kim, M. R. Choi, S. Y. Kim, Y. K. Chung, W.-S. Han, S. O. Kang, *J. Org. Chem.* **2006**, *71*, 9366–9372.
- [38] A. Zhdanko, M. Ströbele, M. E. Maier, *Chem. Eur. J.* **2012**, *18*, 14732–14744.
- [39] J. M. Conia, P. Le Perchec, *Synthesis* **1975**, *1975*, 1–19.
- [40] J. J. Kennedy-Smith, S. T. Staben, F. D. Toste, *J. Am. Chem. Soc.* **2004**, *126*, 4526–4527.
- [41] C. Nieto-Oberhuber, M. P. Muñoz, S. López, E. Jiménez-Núñez, C. Nevado, E. Herrero-Gómez, M. Raducan, A. M. Echavarren, *Chem. Eur. J.* **2006**, *12*, 1677–1693.
- [42] A. Fürstner, H. Szillat, F. Stelzer, *J. Am. Chem. Soc.* **2000**, *122*, 6785–6786.
- [43] B. Schmidt, S. Krehl, E. Jablowski, *Org. Biomol. Chem.* **2012**, *10*, 5119–5130.
- [44] B. L. Pagenkopf, T. Livinghouse, *J. Am. Chem. Soc.* **1996**, *118*, 2285–2286.
- [45] G. Fournet, G. Balme, J. Gore, *Tetrahedron* **1991**, *47*, 6293–6304.

# **VII. Use of salts additives to tune the structures of urea-based supramolecular polymers: *towards switchable hydrogen- bonded organocatalysts***

*Abstract:* In this chapter, we probed the influence of salts on the association properties in toluene of (*rac*)-EHUT and of a mixed urea-thiourea monomer. The length of the assemblies in toluene is shortened in presence of NaBARF or CsBARF and then restored by consecutive addition of tetrabutylammonium iodide (TBAI). This effect is due to the metathesis reaction that generates TBABArF which does not compete with the hydrogen-bond network and NaI or CsI which are not soluble. Thus, the length of the bis-urea assemblies can be modulated reversibly at ambient temperature. We envisaged to implement this strategy in order to control reversibly the activity of a urea-thiourea mixed monomer in organocatalytic reactions (Michael addition and Friedel-Craft reaction). However, in the case of the Michael addition, the urea-thiourea is active in both its associated and dissociated states. Also, NaBARF, our envisaged triggering agent, is active on its own for both catalytic reactions.

## A. Introduction

Organocatalysis has emerged as a promising tool for organic synthesis with numerous advantages compared to transition metal catalysis. Most organic catalysts are air and moisture stable, the modification of their chemical structures is quite straightforward and small organic molecules often present lower toxicity compared to transition metals.<sup>[1]</sup> Among the large variety of organocatalysts<sup>[2]</sup> we decided to focus on hydrogen bond donors (HBD)<sup>[3]</sup> and notably (thio)urea derivatives<sup>[4]</sup> as they should possess both good assembly and catalytic properties.

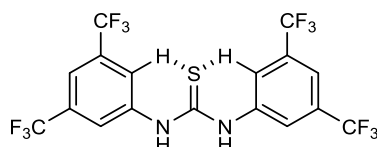


Figure VII-1: Schreiner thiourea catalyst exhibits hydrogen bond interactions between the sulfur atom and aromatic hydrogen atoms which block the *trans/trans* conformation of the thiourea moiety. Adapted from reference<sup>[5]</sup>

Reactions catalysed by (thio)ureas require relatively acidic hydrogen bonds and thus aryl substituent with electron withdrawing groups are usually employed. Tuning the nature of this group allows to modulate the activity of the (thio)urea moiety.<sup>[6]</sup> Trifluoromethyl is the preferred electron withdrawing group given its higher stability compared to nitro group and also for its conformational effect on the thiourea moiety.<sup>[4]</sup> Indeed, contrarily to *N,N'*-disubstituted ureas that are in a *trans/trans* conformation, thioureas are more sensitive to their substituents: their *cis* and *trans* conformations are in equilibrium in solution.<sup>[7-10]</sup> Trifluoromethyl substituent on aryl thiourea was found to favour the *trans/trans* conformation. This is due to the presence of hydrogen bond interactions between the sulfur atom and the aromatic hydrogen atoms (rendered relatively acidic by means of the inductive effects exerted by the CF<sub>3</sub> groups) which in turn block the rotation of the N-C<sub>Ar</sub> bond (Figure VII-1).<sup>[11]</sup>

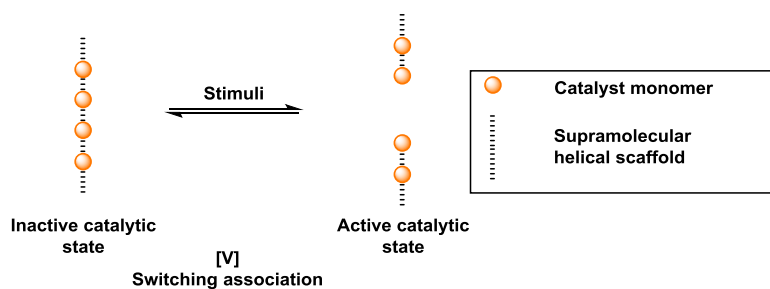


Figure VII-2: Strategy envisioned in this chapter

We were interested in designing a dynamic self-assembled (thio)urea catalyst whose activity can be controlled by changing its degree of association (strategy [V], Figure VII-2). A similar strategy in which the number of free, and thus active, HBD was controlled by assembly was previously described by Mirkin and co-workers.<sup>[12-14]</sup> Their strategy was based on a “weak link approach” in which modification of the coordinating nature of the ligands of a platinum complex modulates the accessibility of the catalytic centre (Figure VII-3). In the closed complex, the hydrogen bond donors could not interact with each other and were thus available for the activation of the substrate. Addition



of chloride anion to this “**closed complex**” led to a ligand exchange on the platinum centre between the sulfur ligand supporting the HBD donor and Cl. In this resulting “**open complex**”, the HBD donors could interact with each other and cannot activate the substrate.

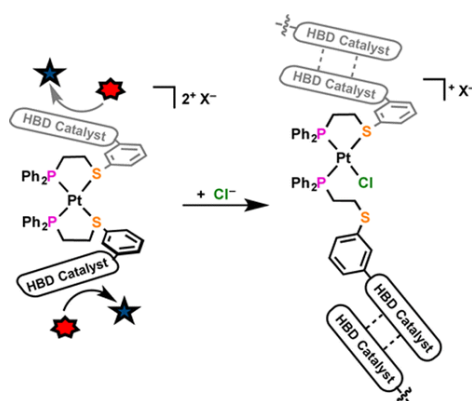


Figure VII-3: Weak link approach to modulate the reactivity of an HBD organocatalyst. HBD= hydrogen-bond donor. From reference<sup>[14]</sup>

The chemical structures of such catalysts were complex. Also, we surmised that the different distances between of the HBD and the metal centre in the two states could be the true source of catalytic activation/deactivation.<sup>[15]</sup> We thus propose an alternative approach based on a much simpler chemical structure: (*rac*)-EHUT-ThioPh(CF<sub>3</sub>)<sub>2</sub> (Figure VII-4). This mixed urea-thiourea was designed following structural guidelines: i) the 3,5-substituted trifluoromethyl aryl group was expected to impart the thiourea moiety with a suitable conformation for substrate activation (*vide supra*), ii) the thiourea moiety was chosen for substrate activation (free state) and deactivation (associated state) and iii) the urea moiety is added to strengthen the assembly of the monomer. We can thus expect that by right choice of the stimulus, the length of the assemblies formed by (*rac*)-EHUT-ThioPh(CF<sub>3</sub>)<sub>2</sub> can be modulated and so will be the catalytic activity of the thiourea moiety (Figure VII-4).

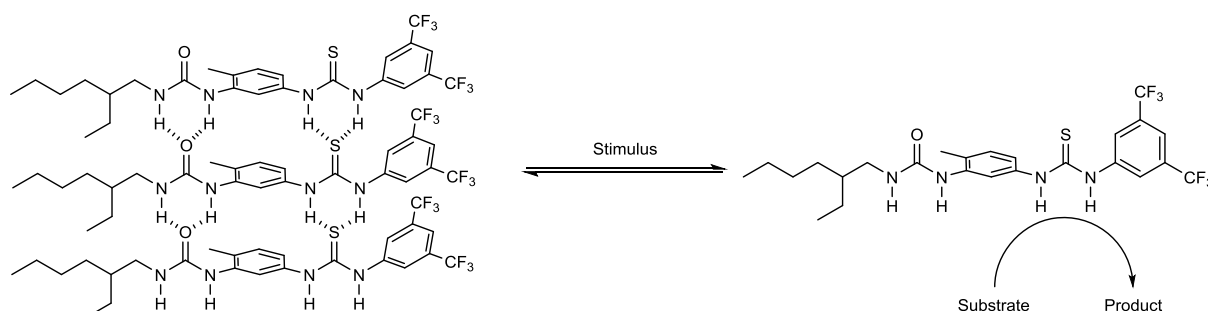


Figure VII-4: expected self-assembly and reversible regulation of the catalytic activity of (*rac*)-EHUT-ThioPh(CF<sub>3</sub>)<sub>2</sub> triggered by a stimulus

Reversible modulation of the self-association of bis-urea monomers was previously described in our group based on temperature or the use of a chain stopper resulting in a reduced viscosity.<sup>[16–18]</sup> Temperature might not be a suitable stimulus in our case as temperature for the transition between assemblies and monomers could be quite high and removing the direct effect of temperature on the kinetics of a catalytic reaction is not always easy. We decided to focus on the chain stopper effect as stimulus for the modulation of the association. In order to achieve switchable catalysis we needed a

chain stopper that can be removed reversibly. Unfortunately the ones based on organic molecules lacked this important property. Alternatively, anions were shown to be good chain stoppers of bisurea assemblies.<sup>[19]</sup>

However anions were not appropriate in our case since they will bind to the hydrogen bond donor and thus will not be able to switch “on” the catalytic activity. We thus decided to focus on the use of cations to trigger the catalytic activity of (*rac*)-EHUT-ThioPh(CF<sub>3</sub>)<sub>2</sub> (Figure VII-5). A cation will act as chain stopper by binding the carbonyl group of the urea or thiourea moiety. Two strategies were envisaged to remove the cation and thus restore the assembly: i) the use of a crown ether and ii) a metathesis reaction. The latter strategy will be studied here since many metathesis reactions between salts exist which are easy to handle. We will first investigate our strategy on (*rac*)-EHUT as a model monomer and then on (*rac*)-EHUT-ThioPh(CF<sub>3</sub>)<sub>2</sub>. The length of the assemblies formed by both monomers can be controlled at room temperature. Catalytic properties of (*rac*)-EHUT-ThioPh(CF<sub>3</sub>)<sub>2</sub> in two reactions (Michael addition and Friedel-Craft reaction) are reported.

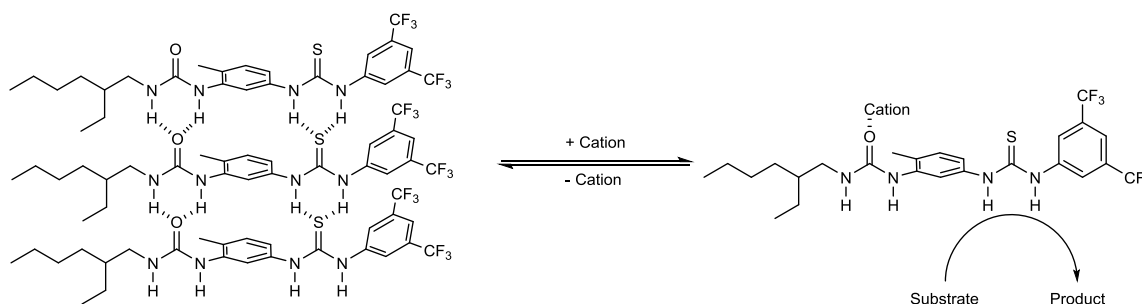


Figure VII-5: expected self-assembly and reversible regulation of the catalytic activity of (*rac*)-EHUT-ThioPh(CF<sub>3</sub>)<sub>2</sub> using a cation as stimulus.

## B. Salt influence on the structure of (*rac*)-EHUT self-assemblies

We first studied the influence of 10 mol% of NaBARf and 10 mol% of TBAI (tetrabutylammonium iodide) on the assembly properties of (*rac*)-EHUT (10 mM) in toluene. We chose these two salts for the following reasons: i) their metathesis reaction is fast and complete, and ii) their metathesis reaction generates TBABArF which does not compete with the H-bond network (Figure VI-S4) and NaI which is not soluble in toluene.

Firstly, we noted a strong influence on the viscosity of the solutions. Whilst (*rac*)-EHUT formed a strong gel in toluene, the presence of 10 mol% of NaBARf led to a viscous solution. A totally fluid solution was obtained with 10% mol of TBAI. A viscous solution was recovered if both TBAI and NaBARf were present.

### 1. FT-IR analyses

We next probed the nature of the assemblies present in these mixtures by FT-IR spectroscopy. FT-IR analysis of (*rac*)-EHUT with 10 mol% of NaBARf displayed a peak at 3420 cm<sup>-1</sup> which was characteristic of free N-H functions (Figure VII-6). The appearance of a small peak at 1684 cm<sup>-1</sup> in the

carbonyl region also corroborated this hypothesis. This was a very important point since it indicated that by adding 10 mol% of NaBArF to a fully associated bis-ureas, free N-H groups were generated which can in turn potentially activate an electrophile. A different FT-IR spectrum was obtained for the mixture with 10 mol% of TBAI: no signal characteristic of free N-H bonds was detected. However, we found out by investigating the association behaviour of (*rac*)-EHUT with incremental amount of TBAI (see Figure VII-S1 in the experimental part) that the frequency of a N-H bonded to iodide was  $\approx 3300\text{ cm}^{-1}$ , *i.e.* below the frequencies of urea-bonded N-H functions. Therefore, in the (*rac*)-EHUT/TBAI mixture, short assemblies were likely present which were stopped by iodide anions.

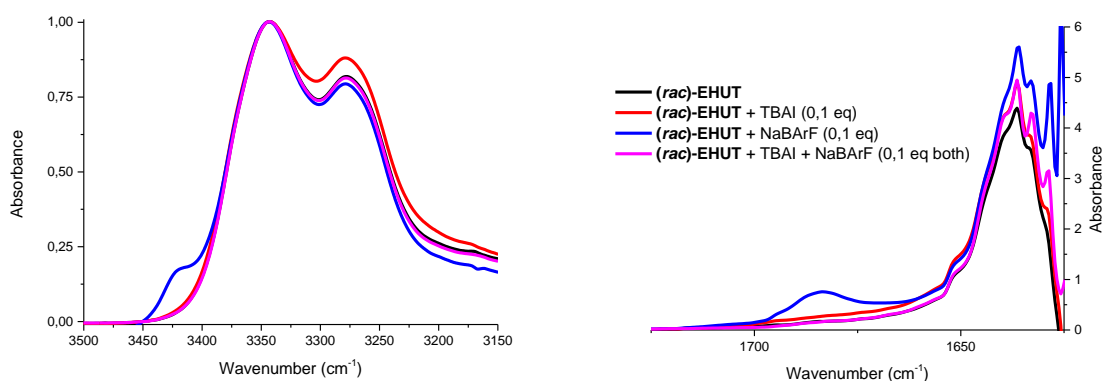


Figure VII-6: Normalised FT-IR spectra of (*rac*)-EHUT pure (black line) with 0.1 equivalent of the following salts: TBAI (red line), NaBArF (blue line) and mixture TBAI:NaBArF (1:1, magenta line) in toluene. Zoom on the N-H and C=O regions. [(*rac*)-EHUT] = 10 mM.

We next investigated the (*rac*)-EHUT/NaBArF/TBAI three-component mixture prepared by mixing the two solutions mentioned above in 1:1 ratio. FT-IR analysis of the three-component mixture was very similar to that of (*rac*)-EHUT indicating that only very long objects were present in solution. We could therefore conclude that thanks to the metathesis reaction the short assemblies present in the (*rac*)-EHUT/NaBArF or (*rac*)-EHUT/TBAI mixtures were replaced by long assemblies in the (*rac*)-EHUT/NaBArF/TBAI three-component mixture.

We next probed the stability of the assemblies by performing FT-IR analyses between 25°C and 110°C for (*rac*)-EHUT and the different mixtures. For (*rac*)-EHUT, the temperature of the transition between the tubular and filament assemblies ( $T^{**}$ ) was precisely probed by plotting the ratio of the absorbance at  $\nu = 3342\text{ cm}^{-1}$  and  $\nu = 3300\text{ cm}^{-1}$  as a function of the temperature (Figure VII-7, left). The value obtained for the transition temperature ( $T^{**} = 47.5^\circ\text{C}$ ) was in agreement with that reported in the literature.<sup>[16]</sup> For the (*rac*)-EHUT/NaBArF/TBAI three-component mixture, the same transition temperature than for pure (*rac*)-EHUT was obtained which corroborates the fact that the same, or very similar, assemblies were present in both solutions. For the (*rac*)-EHUT/NaBArF mixture, the transition temperature was slightly lower ( $T^{**} = 40^\circ\text{C}$ ) and the only differences in the FT-IR spectra was the presence of free N-H bonds above the transition. This was in agreement with the (*rac*)-EHUT being associated under the form of tubular assemblies in the (*rac*)-EHUT/NaBArF mixture. Finally, assemblies present in the (*rac*)-EHUT/TBAI mixture were far less stable and only the elongation

temperature can be measured ( $T_e = 40^\circ\text{C}$ ).<sup>[20]</sup> After the transition ( $75^\circ\text{C}$ ), the shape of the N-H bands was very similar for *(rac)*-EHUT and all the mixtures which indicated that the *(rac)*-EHUT monomers were assembled under the form of filaments in all cases (Figure VII-7, right).

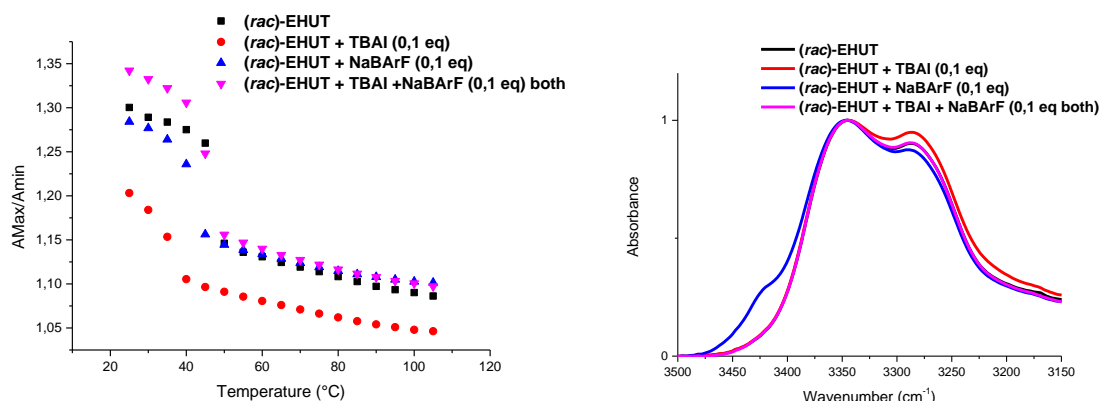


Figure VII-7: Left: ratio  $A_{\text{max}}/A_{\text{min}}$  versus temperature for solutions (10 mM toluene) of *(rac)*-EHUT pure (black square) with 0.1 equivalent of the following salts: TBAI (red disk), NaBArF (blue triangle) and the mixture TBAI:NaBArF (magenta inverted triangle). Right: corresponding FT-IR spectra of the solutions at  $70^\circ\text{C}$ .

## 2. SANS analysis

*(rac)*-EHUT and the three mixtures were analysed by SANS (0.6 wt%, 15 mM) in toluene- $d_8$  at  $20^\circ\text{C}$  (Figure VII-8). In all cases, the  $q^{-1}$  dependence of the scattering intensity confirmed the formation of long cylindrical objects. All these objects were longer than  $200 \text{ \AA}$  since the  $q^{-1}$  dependence was maintained down to the lowest  $q$  values measured. The deviation at low  $q$  values for the *(rac)*-EHUT/NaBArF/TBAI three-component mixture was due to presence of large aggregates, likely insoluble NaI particles. Fitting of the SANS data gave similar values for the radius and number of molecules in the cross-section for *(rac)*-EHUT and *(rac)*-EHUT/NaBArF/TBAI further confirming the presence of long tubular assemblies in the three-component mixture. For *(rac)*-EHUT/NaBArF and *(rac)*-EHUT/ TBAI mixtures the fit gives  $n=2.1$ . The lower intensity (20%) compared to *(rac)*-EHUT confirmed that much smaller objects were present due to the effect of the salts.

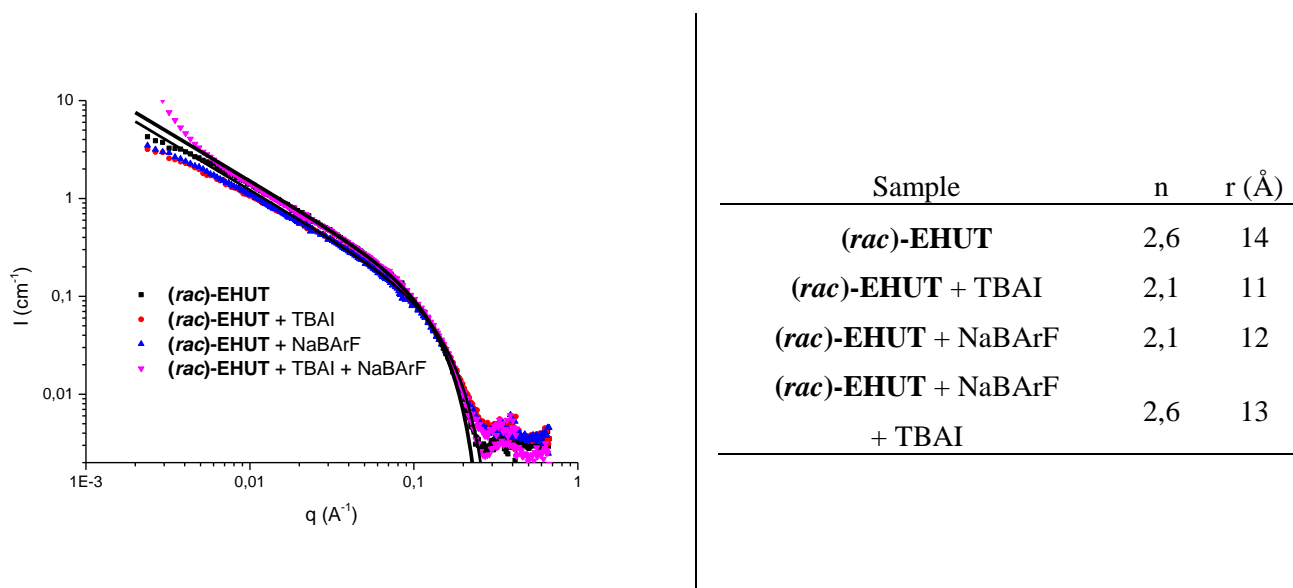


Figure VII-8: Left: SANS spectra with the corresponding fit for solution in toluene- $d_8$  of (*rac*)-EHUT pure (black square) with 0.1 equivalent of the following salts: TBAI (red disc), NaBArF (blue triangle) and mixture TBAI:NaBArF (magenta reverse triangle). Right: data deduced from the fit, n: number of molecule in the cross-section and r: geometrical radius.

The previous results showed the reversible interaction of salts with the tubular self-assemblies formed by (*rac*)-EHUT. Indeed, even though the viscosity of the three-component mixture (*rac*)-EHUT/NaBArF/TBAI was lower than (*rac*)-EHUT, the recovery of the tubular self-assembly, as proved by FT-IR and SANS analyses, was promising towards the formation of a switchable catalyst. The following step was thus the synthesis and *characterisation* of the assembly properties of (*rac*)-EHUT-ThioPh(CF<sub>3</sub>)<sub>2</sub>

## C. Salt influence on the structure of thiourea assemblies

### 1. Synthesis of the monomers

We decided to synthesise two monomers, the already-mentioned mixed urea-thiourea monomer ((*rac*)-EHUT-ThioPh(CF<sub>3</sub>)<sub>2</sub>) and a bis-thiourea monomer which served as a control since the association properties of this monomer were expected to be low.<sup>[18]</sup> The two monomers were synthesised in one step: i) from commercially available 2,4-diaminotoluene and 3,5-bis(trifluoromethyl)phenylisothiocyanate in the case of Ph(CF<sub>3</sub>)<sub>2</sub>ThioUT or ii) from synthesised 1-(5-amino-2-methylphenyl)-3-(2-ethylhexyl)urea and 3,5-bis(trifluoromethyl)phenylisothiocyanate in the case of (*rac*)-EHUT-ThioPh(CF<sub>3</sub>)<sub>2</sub>. Both reactions provided the pure products after purification by column chromatography on silica gel (Figure VII-9).



thiourea functions were free. Surprisingly, (*rac*)-EHUT-ThioPh(CF<sub>3</sub>)<sub>2</sub> was only slightly less associated in CHCl<sub>3</sub> (presence of free urea NH at 3440 cm<sup>-1</sup>) and more importantly the extent of free thiourea functions seemed to be virtually the same in both solvents. In DCM, (*rac*)-EHUT-ThioPh(CF<sub>3</sub>)<sub>2</sub> was less associated than in toluene and CHCl<sub>3</sub> as indicated by the presence of an increased amount of free thiourea and urea moieties.

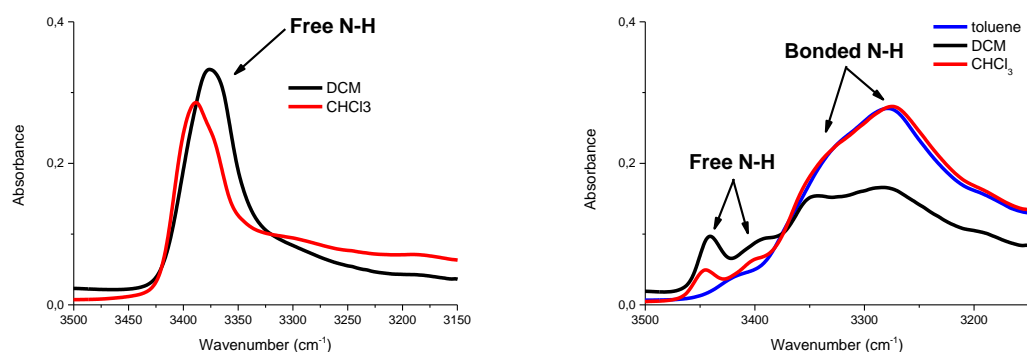


Figure VII-10: FT-IR spectra of Ph(CF<sub>3</sub>)<sub>2</sub>ThioUT (left) and (*rac*)-EHUT-ThioPh(CF<sub>3</sub>)<sub>2</sub> (right) at 10 mM in toluene (blue line), DCM (black) and CHCl<sub>3</sub> (red). Zoom on the N-H region.

## b) SANS analysis

The SANS analysis of (*rac*)-EHUT-ThioPh(CF<sub>3</sub>)<sub>2</sub> in toluene-*d*<sub>8</sub> (14 mM) confirmed the formation of cylindrical objects in solution (Figure VII-11). The  $q^{-1}$  dependence was lost at intermediate  $q$  values suggesting that the objects were short. This was in agreement with the observation of free thiourea groups in FT-IR analysis.

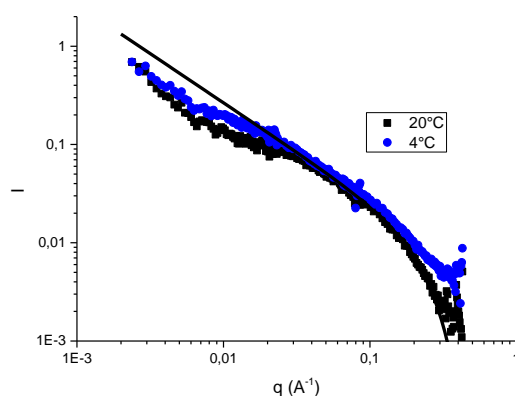


Figure VII-11: SANS analysis of (*rac*)-EHUT-ThioPh(CF<sub>3</sub>)<sub>2</sub> in toluene-*d*<sub>8</sub> (0.6 wt%, 14 mM) at 20°C and 4°C.

## c) Switchable association

We next investigated whether the length of the assemblies formed by (*rac*)-EHUT-ThioPh(CF<sub>3</sub>)<sub>2</sub> could be modulated in toluene. CsBArF was chosen instead of NaBArF as the chain stopper. Its solubility in toluene was low and thus it was added as a concentrated solution in THF. FT-IR analysis of a solution of (*rac*)-EHUT-ThioPh(CF<sub>3</sub>)<sub>2</sub> in a mixture of toluene/THF (95/5) was made to check the influence of the small amount of THF in the thiourea assembly. Clearly the proportion of free N-H

groups is higher in toluene/THF 95:5 than in pure toluene but most of the N-H functions remained associated (Figure VII-12). Addition of one equivalent of CsBarF to *(rac)*-EHUT-ThioPh(CF<sub>3</sub>)<sub>2</sub> led to a dramatic change in the spectral signature: the main absorption band in the N-H region was shifted toward *ca.* 3450 cm<sup>-1</sup> pointing out the disruption of the H-bond network. However, the self-assembly was recovered after addition of one equivalent of TBAI as indicated by the FT-IR spectrum of the *(rac)*-EHUT-ThioPh(CF<sub>3</sub>)<sub>2</sub>/CsBarF/TBAI three-component mixture which was very similar to the one of pure *(rac)*-EHUT-ThioPh(CF<sub>3</sub>)<sub>2</sub> in toluene/THF 95:5. These FT-IR analyses clearly revealed that the degree of association of our designed hydrogen-donor catalyst was reversibly controlled by consecutive addition of CsBarF and TBAI

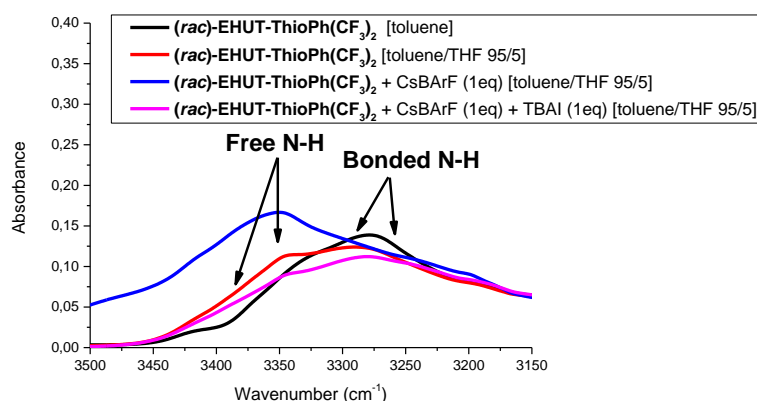


Figure VII-12: FT-IR spectra of *(rac)*-EHUT-ThioPh(CF<sub>3</sub>)<sub>2</sub> at 10 mM in toluene and in toluene/THF 95:5 and of *(rac)*-EHUT-ThioPh(CF<sub>3</sub>)<sub>2</sub> in toluene/THF 95:5 in the presence of CsBarF (100 mol%) and CsBarF/TBAI (1:1, 100 mol%).

## D. Organocatalytic reactions

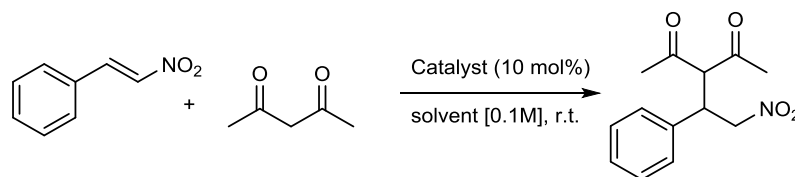
### 1. Michael addition

The Michael addition of acetylacetone (acac) on *trans*- $\beta$ -nitrostyrene was investigated in the presence of our two thiourea monomers and the results are listed in Table VII-2. Firstly, the reactions were conducted in CHCl<sub>3</sub>, a solvent in which Ph(CF<sub>3</sub>)<sub>2</sub>ThioUT was monomeric and *(rac)*-EHUT-ThioPh(CF<sub>3</sub>)<sub>2</sub> was moderately associated. The reaction required a catalytic amount of base (entries 1 and 2). With potassium carbonate, as used by Meijer *et al.* in this reaction,<sup>[21]</sup> the reaction appeared to be quite fast in our hands without need of catalyst (entry 3). Replacement of K<sub>2</sub>CO<sub>3</sub> by Et<sub>3</sub>N slowed down the reaction, even though this background conversion was far to be negligible (29% in 24 h entry 4). We were pleased to see that the reaction rate was significantly increased in presence of the thiourea monomers: 100% and 60% conversion for Ph(CF<sub>3</sub>)<sub>2</sub>ThioUT (entry 5) and *(rac)*-EHUT-ThioPh(CF<sub>3</sub>)<sub>2</sub> (entry 6) respectively. In order to implement our strategy, we had to perform the catalytic reaction at 10 mM in toluene, *i.e.* reactions conditions in which *(rac)*-EHUT-ThioPh(CF<sub>3</sub>)<sub>2</sub> was mostly associated. However, *(rac)*-EHUT-ThioPh(CF<sub>3</sub>)<sub>2</sub> proved to be as active in toluene as in CHCl<sub>3</sub> (entries 6 and 8). Albeit it can be regarded as a surprising result at first sight, it was in



agreement with the FT-IR data mentioned above (Figure VII-10, right) which indicated that the extent of free thiourea functions were about the same in toluene and in  $\text{CHCl}_3$ .

Table VII-2: Michael addition reaction tested



Entry	catalyst	solvent	base	time	Conversion <sup>(a)</sup>
1	<b>Ph(CF<sub>3</sub>)<sub>2</sub>ThioUT</b>	CHCl <sub>3</sub>	no	24 h	0%
2	<b>(rac)-EHUT-ThioPh(CF<sub>3</sub>)<sub>2</sub></b>	CHCl <sub>3</sub>	no	24 h	0%
3	no	CHCl <sub>3</sub>	K <sub>2</sub> CO <sub>3</sub>	7 h	100%
4	no	CHCl <sub>3</sub>	Et <sub>3</sub> N	24 h	29%
5	<b>Ph(CF<sub>3</sub>)<sub>2</sub>ThioUT</b>	CHCl <sub>3</sub>	Et <sub>3</sub> N	24 h	100%
6	<b>(rac)-EHUT-ThioPh(CF<sub>3</sub>)<sub>2</sub></b>	CHCl <sub>3</sub>	Et <sub>3</sub> N	24 h	60%
7	no	toluene	Et <sub>3</sub> N	24 h	6%
8	<b>(rac)-EHUT-ThioPh(CF<sub>3</sub>)<sub>2</sub></b>	toluene	Et <sub>3</sub> N	24 h	65%
9	<b>(rac)-EHUT-ThioPh(CF<sub>3</sub>)<sub>2</sub></b>	toluene/THF 95:5	Et <sub>3</sub> N	13 h	10% <sup>(b)</sup>
10	<b>(rac)-EHUT-ThioPh(CF<sub>3</sub>)<sub>2</sub>+CsBArF</b>	toluene/THF 95:5	Et <sub>3</sub> N	1 h	100% <sup>(b)</sup>
11	<b>CsBArF</b>	toluene	Et <sub>3</sub> N	2 h	100%

Reaction conditions: trans-β-nitrostyrene (0.1 M), acac (0.2 M), catalyst (10 mol%), base (10 mol%), solvent, r.t. (a) The conversion was determined by <sup>1</sup>H NMR (b) reaction performed in a NMR tube (see Figure VII-S3 in the experimental part).

Despite this significant background activity of **(rac)-EHUT-ThioPh(CF<sub>3</sub>)<sub>2</sub>** we investigated the possibility of increasing its catalytic rate by adding CsBArF. We followed the conversion by <sup>1</sup>H NMR. In that conditions, the activity of **(rac)-EHUT-ThioPh(CF<sub>3</sub>)<sub>2</sub>** appeared to be lowered (10% conversion after 13 h entry 9). It can be due to: i) the presence of THF which competes with the substrate for the coordination of the thiourea or ii) the lower diffusion rate in the NMR tube compared to the vigorously-stirred reactions performed in the test tubes. Anyway, the reaction was strikingly accelerated in presence of CsBArF (100% conversion in less than 1 h, entry 10).

To prove that the acceleration of the reaction arose from the disruption of the assemblies formed by **(rac)-EHUT-ThioPh(CF<sub>3</sub>)<sub>2</sub>**, we performed the control experiment with CsBArF alone. Surprisingly, CsBArF proved to be highly active on its own (entry 11). Although poorly acidic salts such as Bi(NO<sub>3</sub>)<sub>3</sub> are known to catalyse a wide scope of Michael and Friedel-Craft reactions,<sup>[22]</sup> the catalytic activity of alkali metals on their own in Michael addition reactions is, to the best of our knowledge, unprecedented.

To evaluate the generality of this finding we compared the inherent activity of several alkali metal and TBABArF (10 mol%) towards the Michael addition of acac on trans-β-nitrostyrene in toluene. The results are listed in the figure below (Figure VII-13). Intriguingly, most of the salts that we probed accelerated the reaction when combined with Et<sub>3</sub>N (10 mol%) at the exception of CsBAr, KSbF<sub>6</sub> and

KBar(*p-t*-Bu). For example, sodium iodide (pale blue bar) was found to be catalytically active even if not soluble in toluene. In the borate salt series, the more electron poor and the more soluble anions (BarF and BarF<sub>20</sub>) provided the best accelerations. With NaBARF and CsBARF the reaction was complete in less than two hours. Influence of the cation seemed also quite important in BAr anion series as lithium and caesium gave poorer conversions than potassium (respectively 15%, 20% and 40% conversion) whereas the sodium salt gave nearly full conversion (95%) after 16 hours of reaction. TBABArF, which is a non-alkali metal cation, also gave honourable conversion (53%). Quaternary ammonium salts are commonly used in phase-transfer catalysis as they form strong ion pairs with anionic intermediates. Here, the TBA cation was likely involved in the ion pair with the deprotonated acac. All those results underlined the difficulty to unravel the role of cations in these catalytic experiments. One possible explanation is that the salts accelerate the deprotonation of acac by generating an insoluble Et<sub>3</sub>NH<sup>+</sup>X<sup>-</sup> ion pair. However, this hypothesis can be discarded since the BarF<sup>-</sup> salt of Et<sub>3</sub>NH<sup>+</sup> is expected to be soluble in toluene. The conversion observed with sodium iodide also excluded the involvement of acidic boron impurities that might be present in borate salts. Another possibility might be that the reaction rate is enhanced by traces of different acids (*e.g.* metal salts) contaminating the salts.

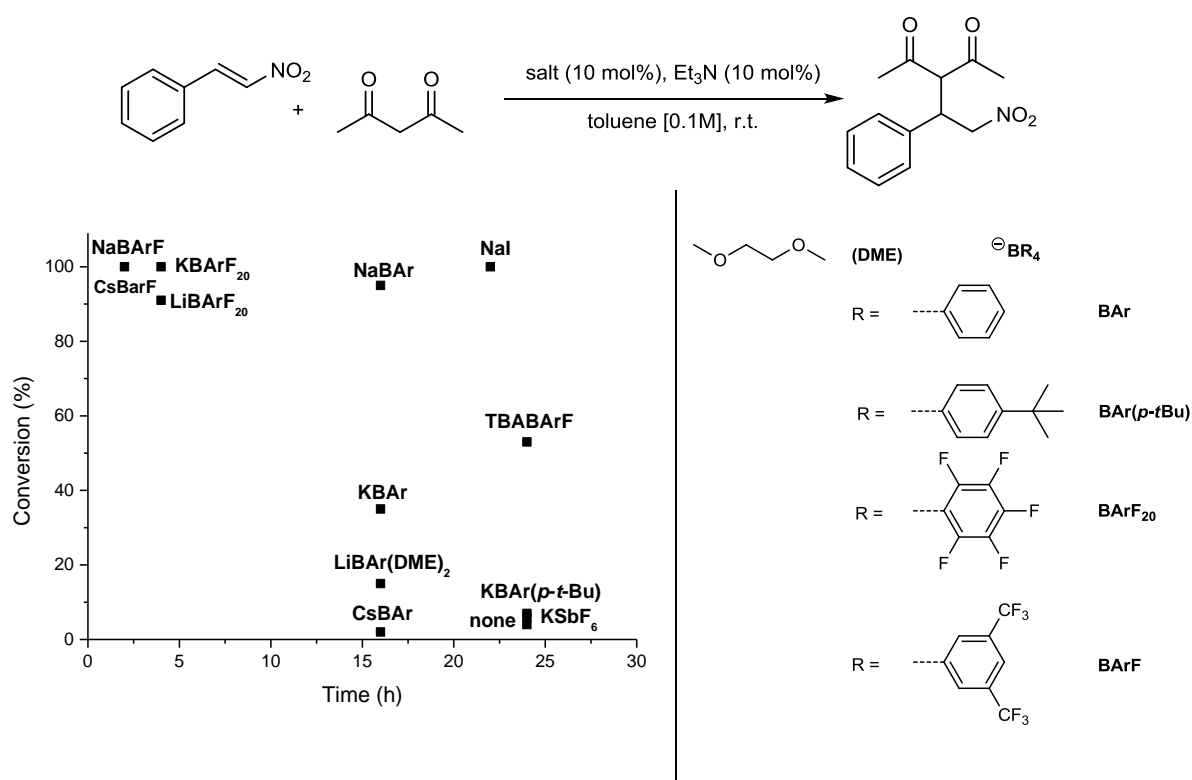


Figure VII-13: Left: Michael addition catalysed by different salts. Reaction conditions: trans-β-nitrostyrene (0.1 M), acac (0.2 M), salt (10 mol%), Et<sub>3</sub>N (10 mol%), toluene, r.t. Conversion determined by <sup>1</sup>H NMR. Right: Structure and nomenclature of the different borate anions.

If we discard this last hypothesis, we can hypothesise two pathways to explain the role of the cation in this reaction: i) the coordination of the cation to acac increases its acidity (Figure VII-14, “A”) and ii)

the coordination of the cation to the *trans*- $\beta$ -nitrostyrene increases its electrophilicity (Figure VII-14, “B”). Ultimately a combination of both pathways cannot be excluded.

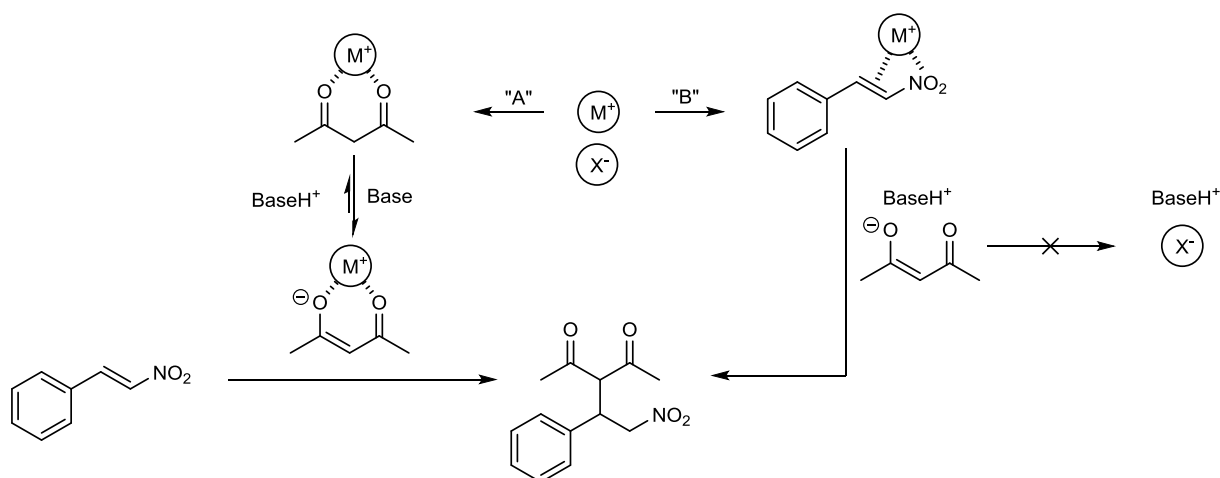


Figure VII-14: Proposed mechanistic pathways for the role of cations in the Michael addition reaction of acac on *trans*- $\beta$ -nitrostyrene.

In order to gain more information on these two possible reaction pathways, we performed the same reaction with quinine (used with other cinchona alkaloids as chiral blocks for organocatalyst)<sup>[3]</sup> instead of  $NEt_3$  in the presence or absence of NaBARF (Figure VII-15). The reaction was found to be faster with NaBARF than without similarly to what was observed previously with  $Et_3N$ . However, in presence of NaBARF the e.e. decreased from 21% to 8%. The strong erosion of the enantiomeric excess points towards mechanism “A” (Figure VII-14) as with an ion pair formed between  $Na^+$  and  $acac^-$ , the chiral base should not be present in the vicinity of the *trans*- $\beta$ -nitrostyrene and thus no chiral induction would be observed.

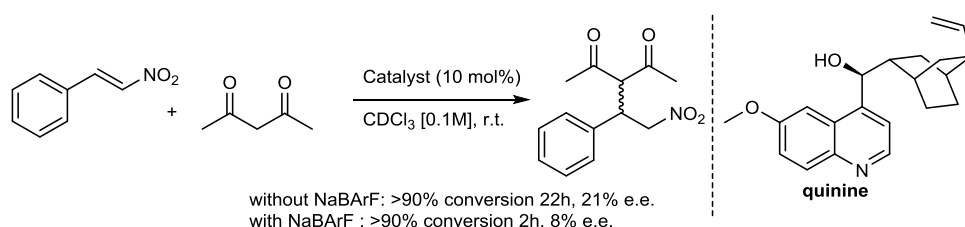
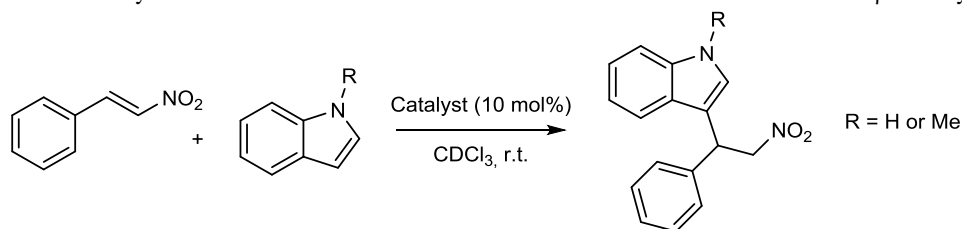


Figure VII-15: Michael addition reaction of acac on *trans*- $\beta$ -nitrostyrene catalysed by quinine in presence or absence of NaBARF

## 2. Friedel-Craft reactions

Whatever the precise reason for the effect of cations, the previous reaction did not appear to be suitable to implement our concept of dynamic self-assembled (thio)urea catalyst. These results led us to investigate an alternative reaction that would not be catalysed by the salts. Friedel-Craft reaction between indole derivatives and *trans*- $\beta$ -nitrostyrene was chosen because a base was not required for this reaction and also because the nucleophilicity of the indole derivatives is much lower than that of the acac anion.<sup>[23]</sup> The absence of an anionic intermediate in this reaction should avoid interference of the salts in the reaction kinetics (Table VII-3).

Table VII-3: Catalytic results for Friedel-Craft reactions between indoles derivatives and *trans*- $\beta$ -nitrostyrene

Entry	Nucleophile	Catalyst	Additive	Conversion
1	indole	<b>(rac)-EHUT-ThioPh(CF<sub>3</sub>)<sub>2</sub></b>	no	0% <sup>(a)</sup>
2	indole	<b>Ph(CF<sub>3</sub>)<sub>2</sub>ThioUT</b>	no	0%
3	indole	<b>no</b>	NaI	0%
4	indole	<b>no</b>	KSbF <sub>6</sub>	0%
5	indole	<b>no</b>	NaBAr	0%
6	indole	<b>no</b>	KBAr	0%
7	indole	<b>no</b>	NaBArF	29%
8	indole	<b>no</b>	CsBArF	13%
9	N-methylindole	<b>(rac)-EHUT-ThioPh(CF<sub>3</sub>)<sub>2</sub></b>	no	6%
10	N-methylindole	<b>no</b>	NaBArF	71%
11	N-methylindole	<b>(rac)-EHUT-ThioPh(CF<sub>3</sub>)<sub>2</sub></b>	NaI	0%
12	N-methylindole	<b>(rac)-EHUT-ThioPh(CF<sub>3</sub>)<sub>2</sub></b>	NaBAr	0%
13	N-methylindole	<b>(rac)-EHUT-ThioPh(CF<sub>3</sub>)<sub>2</sub></b>	KBAr	0%
14	N-methylindole	<b>(rac)-EHUT-ThioPh(CF<sub>3</sub>)<sub>2</sub></b>	KSbF <sub>6</sub>	0%

Reaction conditions: *trans*- $\beta$ -nitrostyrene (0.1 M), indole derivatives (2 eq), catalyst (10 mol%), additive (10 mol%) CDCl<sub>3</sub>, r.t., 40 h. (a) 24 h. The conversion was determined by <sup>1</sup>H NMR.

The Friedel-Craft reaction between *trans*- $\beta$ -nitrostyrene and indole was slow due to the relatively low nucleophilicity of the indole. Only a limited number of HBD donors, were found to catalyse the reaction<sup>[24–27]</sup> and Schreiner's thiourea was not reported to catalyse this reaction.<sup>[28]</sup> Accordingly, it was not surprising to find no reactivity for **(rac)-EHUT-ThioPh(CF<sub>3</sub>)<sub>2</sub>** and **Ph(CF<sub>3</sub>)<sub>2</sub>ThioUT** in CDCl<sub>3</sub> (entries 1 and 2) as well as for various salts of sodium and potassium salts (entry 3 and 8). Again NaBArF and CsBArF proved to be active on their own for this reaction yielding 29% and 13% conversion respectively after 40 h (entries 7 and 8).

We changed indole to N-methylindole, a better nucleophile. **(rac)-EHUT-ThioPh(CF<sub>3</sub>)<sub>2</sub>** was poorly active (6% conversion, entry 9) whereas NaBArF provided honourable conversion (entry 10, 71%). Attempts to switch “on” the reaction by addition of salts to **(rac)-EHUT-ThioPh(CF<sub>3</sub>)<sub>2</sub>** did not lead to any conversion for any salts tested (entries 11–14).

The Friedel-Craft reactions between *trans*- $\beta$ -nitrostyrene and indole or N-methylindole cannot be implemented in the context of our project since: i) **(rac)-EHUT-ThioPh(CF<sub>3</sub>)<sub>2</sub>**, in its moderately associated state, is poorly or not active for the reactions, ii) NaBArF is active on its own. We note

again the significant activity of NaBArF for these reactions. In that case, one can postulate an activation of *trans*- $\beta$ -nitrostyrene by the “naked” Na cation (see mechanism “B”, Figure VII-14).

## E. Conclusion

Cations and anions were used to tune the length and nature of the assemblies formed by (*rac*)-EHUT and a mixed urea/thiourea monomer, (*rac*)-EHUT-ThioPh(CF<sub>3</sub>)<sub>2</sub> in organic solvents. Both NaBArF and TBAI (10 mol%) act as chain stoppers for (*rac*)-EHUT polymers. *In-situ* metathesis reaction between NaBArF and TBAI restored the pristine (*rac*)-EHUT assemblies with no obvious change, according to FT-IR and SANS analyses, in the length and nature of the assemblies. However, the solution of three-component mixture (*rac*)-EHUT/NaBArF/TBAI was less viscous than that of pure (*rac*)-EHUT which surmised that the objects in the former case are shorter. An analogous protocol can be used to tune the length of the assemblies (filament structure) formed by (*rac*)-EHUT-ThioPh(CF<sub>3</sub>)<sub>2</sub> in toluene/THF 95:5: addition of CsBArF (100 mol%) disrupts the H-bond network which was restored by consecutive addition of TBAI (100 mol%). We noted that in the pure solvents, toluene and CHCl<sub>3</sub>, (*rac*)-EHUT-ThioPh(CF<sub>3</sub>)<sub>2</sub> was mostly associated but that a similar amount of free thiourea functions were present in both cases. We evaluated the catalytic properties of (*rac*)-EHUT-ThioPh(CF<sub>3</sub>)<sub>2</sub> with the aim of switching its activity reversibly by consecutive addition of NaBArF (or CsBArF) and TBAI. Unfortunately, in its expected associated state, (*rac*)-EHUT-ThioPh(CF<sub>3</sub>)<sub>2</sub> proved to be active for the Michael addition of acac on *trans*- $\beta$ -nitrostyrene. Enhancing its activity by adding NaBArF or other salts was hampered by the fact that these salts are moderately to highly active on their own for this reaction. In its moderately associated state, (*rac*)-EHUT-ThioPh(CF<sub>3</sub>)<sub>2</sub> was not or poorly active for the Friedel-Craft reactions between *trans*- $\beta$ -nitrostyrene and indole or N-methylindole. For the reaction with N-methylindole, the reaction could not be switched “on” in presence of NaBArF since NaBArF proved again to be quite active on its own for this reaction. The ability of salts like NaBArF and CsBArF to catalyse such Friedel-Craft reactions, and notably the usually slow reaction between *trans*- $\beta$ -nitrostyrene and indole, was quite unexpected and surmised the possibility of the activation of organic substrates by the use “naked” alkali metals.

## F. Experimental part

General procedures: (see Chapter III)

3,5-bis(trifluoromethyl)phenylisothiocyanate, *trans*- $\beta$ -nitrostyrene, acetylacetone, indole and N-methylindole, NaBArF, KBArF<sub>20</sub>, LiBArF<sub>20</sub>, NaBAr, KBAr, LiBAr(DME)<sub>2</sub>, CsBAr, NaI, KSbF<sub>6</sub> and KBAr(*p-t*-Bu) were purchased from Maybridge *via* Alfa Aesar, TCI chemicals and Sigma and used as received. The synthesis of 1-(5-amino-2-methylphenyl)-3-(2-ethylhexyl)urea ((*rac*)-EHUTNH<sub>2</sub>) was described in chapter III.

## 1. Supplementary figures

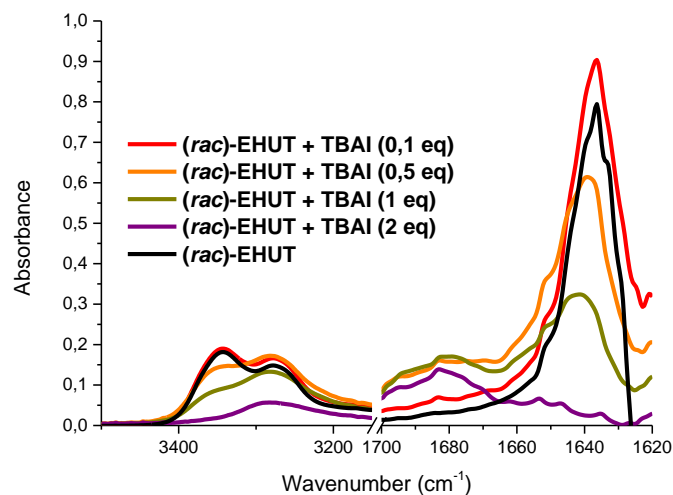


Figure VII-S1: FT-IR spectra of (*rac*)-EHUT (10mM in toluene) with increasing equivalents of TBAI: 0.0 eq (black line), 0.10 eq (red line), 0.5 eq (orange line), 1.0 eq (olive line) and 2.0 eq (purple line).

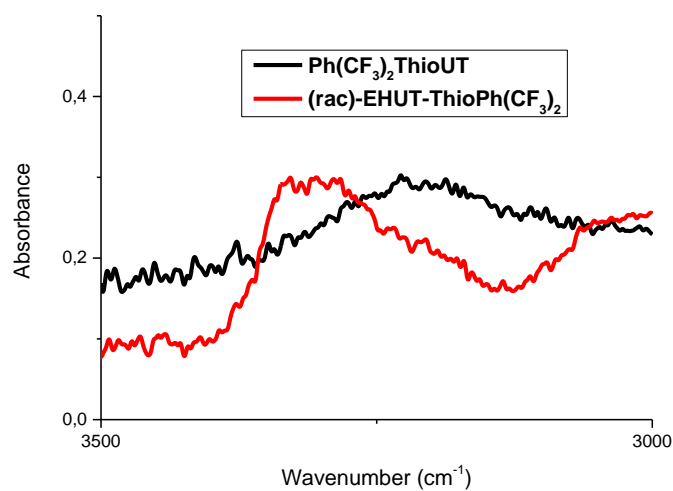


Figure VII-S2: Solid FT-IR spectra of EHUT-ThioPh(CF<sub>3</sub>)<sub>2</sub> and Ph(CF<sub>3</sub>)<sub>2</sub>ThioUT in the solid state. Zoom on the N-H region

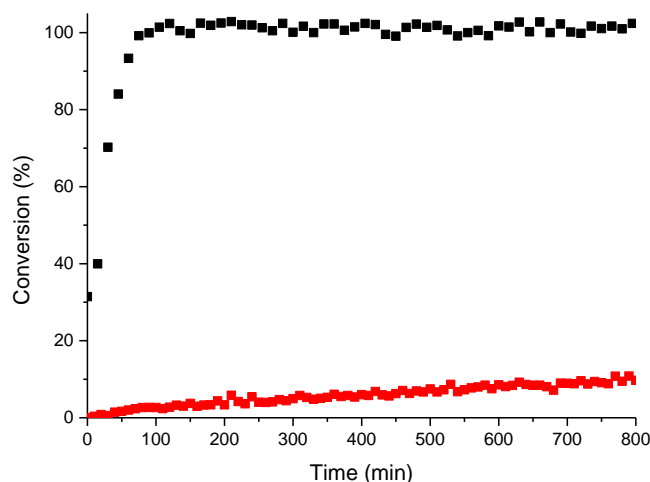
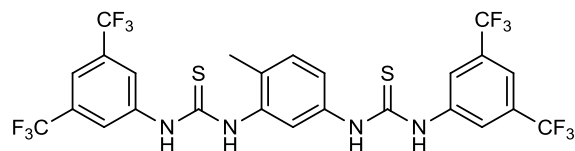


Figure VII-S3: Michael addition reaction between trans- $\beta$ -nitrostyrene (0.1 mM) and acac (0.2 mM) with (*rac*)-**EHUT-ThioPh(CF<sub>3</sub>)<sub>2</sub>** (10 mol%), Et<sub>3</sub>N (10 mol%) in toluene-*d*<sub>8</sub>/THF-*d*<sub>8</sub> (95/5), r.t. with CsBARF (10 mol%) (black square) and without (red square).

## 2. Synthesis of the thiourea monomers

1,1'-(4-methyl-1,3-phenylene)bis(3-(3,5-bis(trifluoromethyl)phenyl)thiourea)

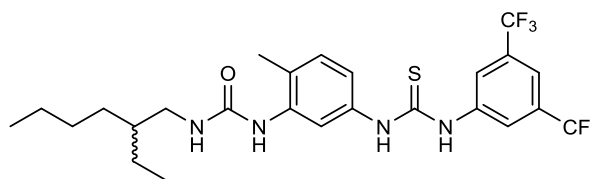
**Ph(CF<sub>3</sub>)<sub>2</sub>ThioUT**



In an oven-dried Schlenk flask 2,4-diaminotoluene (185 mg, 1.51 mmol) was dissolved in dry DCM (4 ml) under inert atmosphere. Then, 3,5-bis(trifluoromethyl)phenylisothiocyanate (610  $\mu$ L, 3.33 mmol) was added to the solution and the reaction mixture was stirred overnight. A precipitate was formed and THF (5 ml) was added to the suspension to allow the reaction to reach completion (followed by TLC). At the end of the reaction, the solvents were removed by rotatory evaporation and the crude product was purified by flash chromatography on silica gel eluting with DCM/MeOH (from 100/0 to 95/5) yielding **Ph(CF<sub>3</sub>)<sub>2</sub>ThioUT** as a white powder (1.0 g, 99%). The product took a yellowish colouration over time.

<sup>1</sup>H NMR (300 MHz, DMSO-*d*<sub>6</sub>)  $\delta$  10.34 (s, 1H), 9.99 (s, 1H), 9.92 (s, 1H), 9.84 (s, 1H), 8.13 (d, *J* = 5.6 Hz, 4H), 7.68 (s, 2H), 7.57 (d, *J* = 2.1 Hz, 1H), 7.34 (d, *J* = 8.2 Hz, 1H), 7.26 (dd, *J* = 8.2, 2.2 Hz, 1H), 2.28 (s, 3H). <sup>13</sup>C{<sup>1</sup>H} NMR (75 MHz, DMSO-*d*<sub>6</sub>)  $\delta$  180.5, 179.8, 141.8, 141.7, 137.0, 136.7, 131.6, 131.1, 130.5, 130.0, 129.6, 129.1, 128.6, 125.0, 124.3, 124.0, 123.5, 122.6, 121.4, 117.7, 116.9, 17.3. <sup>19</sup>F{<sup>1</sup>H} NMR (282 MHz, DMSO-*d*<sub>6</sub>)  $\delta$  -61.8 (d, *J* = 3.0 Hz). IR (ATR, cm<sup>-1</sup>): 3228, 1529, 1472, 1380, 1276, 1175, 1130, 1109. HRMS: Calculated for C<sub>25</sub>H<sub>16</sub>F<sub>12</sub>N<sub>4</sub>S<sub>2</sub>Na [M+Na]<sup>+</sup>: 687.0517, found: 687.0527.

1-(5-(3-(3,5-  
bis(trifluoromethyl)phenyl)thioureido)-2-  
methylphenyl)-3-(2-ethylhexyl)urea  
**(rac)-EHUT-ThioPh(CF<sub>3</sub>)<sub>2</sub>**



In an oven-dried Schlenk flask, 1-(5-amino-2-methylphenyl)-3-(2-ethylhexyl)urea (258 mg, 0.93 mmol) was dissolved in dry DCM (10 ml) under inert atmosphere. Then, 3,5-bis(trifluoromethyl)-phenylisothiocyanate (170  $\mu$ L, 0.93 mmol) was added to the solution which was stirred overnight. A precipitate was formed and the solvent was removed by rotatory evaporation. The crude product was purified by flash chromatography on silica gel eluting with DCM/MeOH (from 0 to 5%) yielding **(rac)-EHUT-ThioPh(CF<sub>3</sub>)<sub>2</sub>** as a white powder (0.3 g, 67%).

**<sup>1</sup>H NMR** (300 MHz, DMSO-*d*<sub>6</sub>)  $\delta$  10.20 (s, 1H), 9.99 (s, 1H), 8.30 (s, 2H), 7.94 (d, *J* = 2.2 Hz, 1H), 7.75 (s, 1H), 7.65 (s, 1H), 7.11 (d, *J* = 8.2 Hz, 1H), 7.00 (dd, *J* = 8.0, 2.2 Hz, 1H), 6.55 (t, *J* = 5.7 Hz, 1H), 3.05 (q, *J* = 5.5 Hz, 2H), 2.17 (s, 3H), 1.42 – 1.15 (m, 9H), 0.86 (h, *J* = 3.9, 3.4 Hz, 6H). **<sup>13</sup>C{<sup>1</sup>H} NMR** (75 MHz, DMSO)  $\delta$  179.4, 155.3, 141.9, 138.7, 136.3, 130.1, 129.6, 129.2, 125.0, 123.4, 123.2, 121.4, 117.5, 116.6, 115.6, 41.5, 39.3, 30.5, 28.4, 23.7, 22.5, 17.5, 13.9, 10.8. **<sup>19</sup>F{<sup>1</sup>H} NMR** (282 MHz, DMSO)  $\delta$  -61.6. **IR** (ATR, cm<sup>-1</sup>): 3328, 2968, 1717, 1659, 1469, 1382, 1340, 1276, 1219, 1173, 1133, 1106. **HRMS**: Calculated for C<sub>25</sub>H<sub>30</sub>F<sub>6</sub>N<sub>4</sub>OSNa [M+Na]<sup>+</sup>: 571.1937, found: 571.1938.

### 3. Catalytic experiments

#### a) General set-up for the Michael addition reaction

In the following, Et<sub>3</sub>N was added to toluene, toluene-*d*<sub>8</sub> or CDCl<sub>3</sub> and the mixture (10 mM) was used as stock solution.

An oven-dried test tube was loaded with the salts (10 mol%), acetylacetone (21  $\mu$ L, 0.2 mmol) and the thiourea monomer (10 mol%, 500  $\mu$ L of the stock solution, 20 mM). The test tube was rinsed with 250  $\mu$ L of the stock solution and stirred for 15 min before addition of *trans*- $\beta$ -nitrostyrene (14.9 mg, 0.1 mmol) dissolved in 250  $\mu$ L of the stock solution. The reaction was monitored quantitatively by <sup>1</sup>H NMR when the solvent is CDCl<sub>3</sub> or qualitatively, by scrutinising the disappearance of the yellow coloration indicating that the conversion is above 90% under these experimental conditions. The reaction mixture was then filtered over a short silica pad (eluted with DCM), concentrated under reduced pressure and analysed by <sup>1</sup>H NMR.

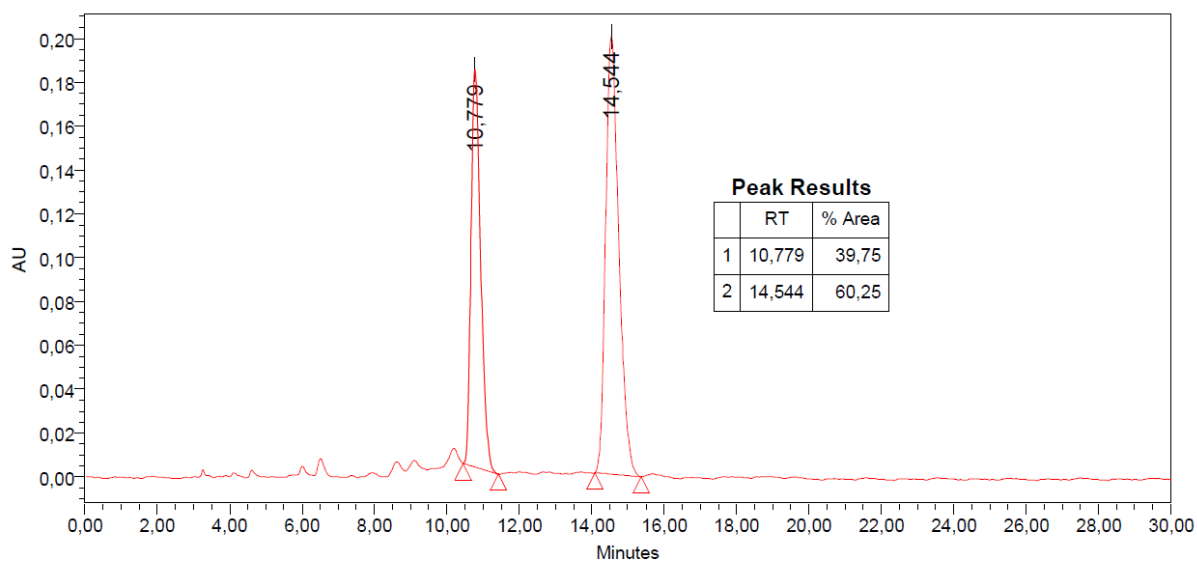
Characterisation of the Michael adduct: **<sup>1</sup>H NMR** (300 MHz, CDCl<sub>3</sub>)  $\delta$  7.36-7.27 (m, 3H), 7.21-7.14 (m, 2H), 4.65-4.60 (m, 2H), 4.36 (d, *J* = 10.7 Hz, 1H), 4.23 (m, 1H), 2.23 (s, 3H), 1.93 (s, 3H). The spectroscopic data are in agreement with the literature.<sup>[29]</sup>



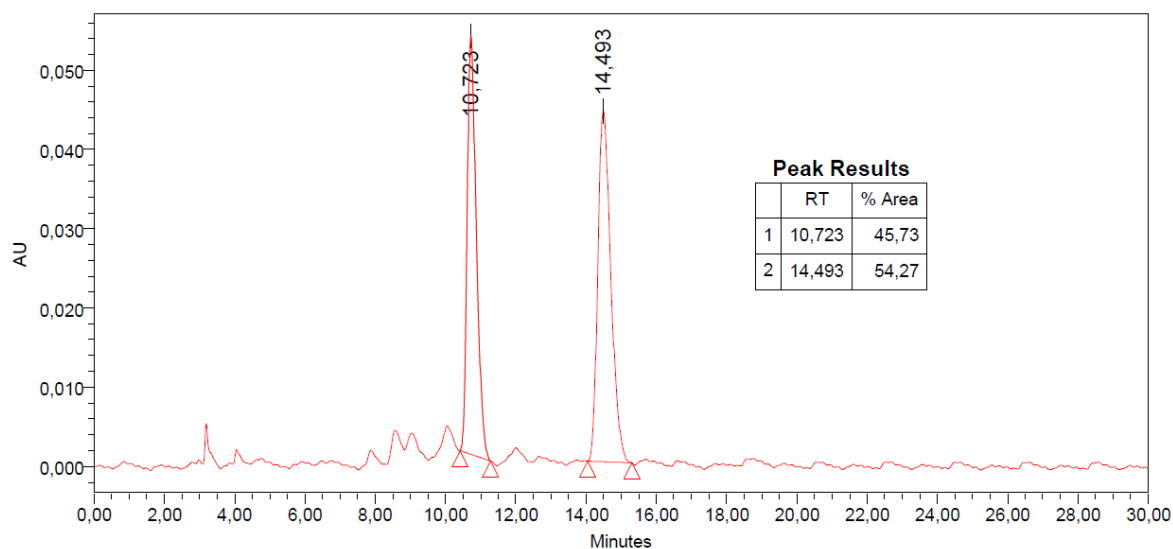
With quinine as base:

An oven-dried test tube is loaded with the *trans*- $\beta$ -nitrostyrene (14.9 mg, 0.1 mmol), quinine (3.23 mg, 10 mol%) and NaBARF (8.86 mg, 10 mol%). The reaction was started by the addition of acetylacetone (21  $\mu$ L, 0.2 mmol) and the solution was stirred for 24 h. The solution was filtered through a short silica pad and eluted with DCM. The product was then analysed by  $^1\text{H}$  NMR (conversion) and by chiral HPLC: AD-H heptane/isopropanol 90/10, 1 mL/min.

Quinine alone:



Quinine + NaBARF:



For the Michael addition reaction followed by  $^1\text{H}$  NMR :

With only (*rac*)-EHUT-ThioPh(CF<sub>3</sub>)<sub>2</sub>:

A 0.5 mm NMR tube was loaded with *trans*- $\beta$ -nitrostyrene (7.5 mg, 0.05 mmol) in 100  $\mu$ L of toluene- $d_8$ , a solution of (*rac*)-EHUT-ThioPh(CF<sub>3</sub>)<sub>2</sub> (10 mol% in 300  $\mu$ L) and THF-d<sub>8</sub> (40  $\mu$ L). Then, the NMR tube was introduced in the spectrometer, shimmed and the first spectrum was recorded. Addition of acetylacetone (10 mg in 75  $\mu$ L toluene-d<sub>8</sub>) marked t = 0.

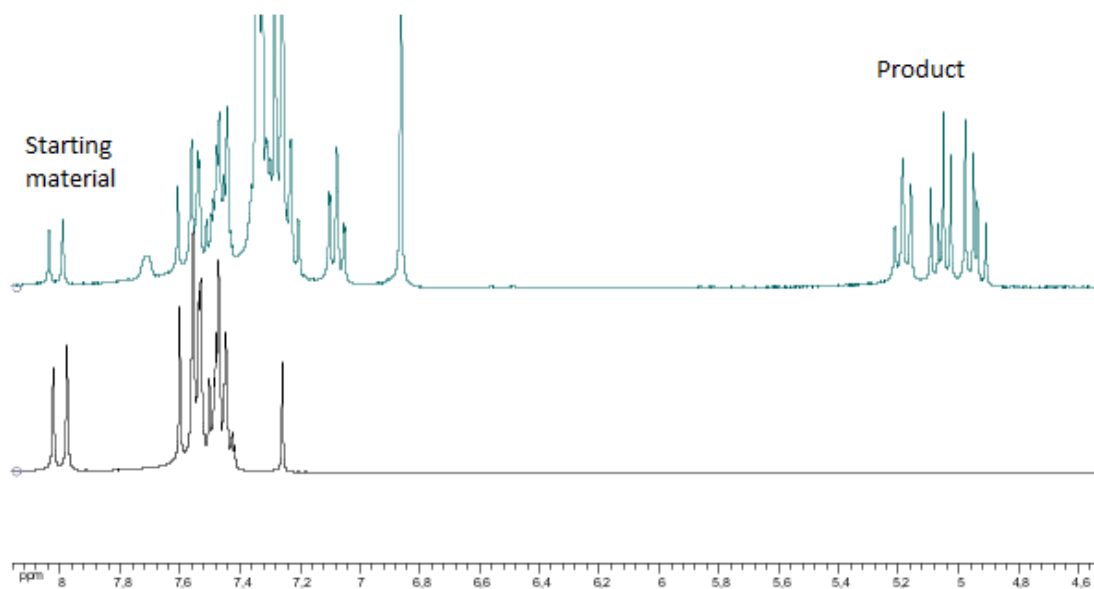
With (*rac*)-EHUT-ThioPh(CF<sub>3</sub>)<sub>2</sub> and CsBARF:

A 0.5 mm NMR tube was loaded with the *trans*- $\beta$ -nitrostyrene (7.5 mg, 0.05 mmol) in 100  $\mu$ L of toluene-d<sub>8</sub>, a solution of (*rac*)-EHUT-ThioPh(CF<sub>3</sub>)<sub>2</sub> (10 mol% in 300  $\mu$ L) and CsBARF (4.98 mg, 10 mol% in THF-d<sub>8</sub> 40  $\mu$ L). Then the NMR spectrometer was shimmed with the tube in place and the first spectrum was recorded. Addition of acetylacetone (10 mg in 75  $\mu$ L toluene-d<sub>8</sub>) marked t = 0.

### b) General set-up for the Friedel-Craft reaction

An oven-dried test tube was loaded with *trans*- $\beta$ -nitrostyrene (14.9 mg, 0.1 mmol), the thiourea monomer (10 mol%) and the salt (10 mol%) in CDCl<sub>3</sub> (1 mL). The reaction was started by the addition of indole or N-methylindole (0.2 mmol) and the solution was stirred at room temperature. The reaction was monitored by <sup>1</sup>H NMR

The reaction is monitored by <sup>1</sup>H NMR in CDCl<sub>3</sub> by measuring the intensity of the signal at  $\delta$  8.00 ppm (d, 1H, *trans*- $\beta$ -nitrostyrene) relatively to the peaks at  $\delta$  5.19 (t, *J* = 7.9 Hz, 1H), 5.06 (dd, *J* = 12.4, 7.4 Hz, 1H) and 4.94 (dd, *J* = 12.4, 8.5 Hz, 1H) which belong to the Friedel-Craft product (see figure below).



NMR spectra in CDCl<sub>3</sub> of a reaction mixture (top) and of the starting *trans*- $\beta$ -nitrostyrene (bottom)

## G. References

- [1] D. W. C. MacMillan, *Nature* **2008**, *455*, 304–308.
- [2] M. T. Reetz, B. List, S. Jaroch, H. Weinmann, Eds., *Organocatalysis*, Springer Berlin Heidelberg, **2008**.
- [3] A. G. Doyle, E. N. Jacobsen, *Chem. Rev.* **2007**, *107*, 5713–5743.
- [4] S. J. Connon, *Chem. Eur. J.* **2006**, *12*, 5418–5427.
- [5] A. Wittkopp, P. R. Schreiner, *Chem. Eur. J.* **2003**, *9*, 407–414.
- [6] G. Jakab, C. Tancon, Z. Zhang, K. M. Lippert, P. R. Schreiner, *Org. Lett.* **2012**, *14*, 1724–1727.
- [7] G. Vassilev, V. Koleva, M. Ilieva, B. Galabov, *J. Mol. Struct.* **1982**, *82*, 35–41.
- [8] L. V. Sudha, D. N. Sathyanarayana, *Spectrochim. Acta Part A Mol. Spectrosc.* **1984**, *40*, 751–755.
- [9] B. Galabov, G. Vassilev, N. Neykova, A. Galabov, *J. Mol. Struct.* **1978**, *44*, 15–21.
- [10] C. Lozanova, B. Galabov, M. Ilieva, G. Vassilev, *J. Mol. Struct.* **1984**, *115*, 427–430.
- [11] T. Okino, Y. Hoashi, Y. Takemoto, *J. Am. Chem. Soc.* **2003**, *125*, 12672–12673.
- [12] C. M. McGuirk, J. Mendez-Arroyo, A. I. D’Aquino, C. L. Stern, Y. Liu, C. A. Mirkin, *Chem. Sci.* **2016**, *7*, 6674–6683.
- [13] C. M. McGuirk, J. Mendez-Arroyo, A. M. Lifschitz, C. A. Mirkin, *J. Am. Chem. Soc.* **2014**, *136*, 16594–16601.
- [14] C. M. McGuirk, C. L. Stern, C. A. Mirkin, *J. Am. Chem. Soc.* **2014**, *136*, 4689–4696.
- [15] Activation of the HBD catalyst by interaction with the metal could not be discarded as such HBD (urea particularly) are known to display low reactivity
- [16] L. Bouteiller, O. Colombani, F. Lortie, P. Terech, *J. Am. Chem. Soc.* **2005**, *127*, 8893–8898.
- [17] F. Lortie, S. Boileau, L. Bouteiller, C. Chassenieux, F. Lauprêtre, *Macromolecules* **2005**, *38*, 5283–5287.
- [18] T. Pinault, B. Andrioletti, L. Bouteiller, *Beilstein J. Org. Chem.* **2010**, *6*, 869–875.
- [19] T. Pinault, C. Cannizzo, B. Andrioletti, G. Ducouret, F. Lequeux, L. Bouteiller, *Langmuir* **2009**, *25*, 8404–8407.
- [20] M. M. J. Smulders, A. P. H. J. Schenning, E. W. Meijer, *J. Am. Chem. Soc.* **2008**, *130*, 606–611.
- [21] F. Rodríguez-Llansola, E. W. Meijer, *J. Am. Chem. Soc.* **2013**, *135*, 6549–6553.
- [22] N. Srivastava, B. K. Banik, *J. Org. Chem.* **2003**, *68*, 2109–2114.
- [23] H. Mayr, “Mayr’s Database Of Reactivity Parameters,” can be found under <http://www.cup.lmu.de/oc/mayr/reaktionsdatenbank/>, **2012**.
- [24] R. P. Herrera, V. Sgarzani, L. Bernardi, A. Ricci, *Angew. Chem. Int. Ed.* **2005**, *44*, 6576–6579.
- [25] S. S. So, J. A. Burkett, A. E. Mattson, *Org. Lett.* **2011**, *13*, 716–719.
- [26] A. K. Chittoory, G. Kumari, S. Mohapatra, P. P. Kundu, T. K. Maji, C. Narayana, S. Rajaram, *Tetrahedron* **2014**, *70*, 3459–3465.
- [27] C. M. McGuirk, M. J. Katz, C. L. Stern, A. A. Sarjeant, J. T. Hupp, O. K. Farha, C. A. Mirkin, *J. Am. Chem. Soc.* **2015**, *137*, 919–925.
- [28] E. M. Fleming, T. McCabe, S. J. Connon, *Tetrahedron Lett.* **2006**, *47*, 7037–7042.
- [29] H. Y. Bae, S. Some, J. S. Oh, Y. S. Lee, C. E. Song, *Chem. Commun.* **2011**, *47*, 9621.



# General conclusion

The aim of this thesis was the development of scaffolds based on hydrogen-bonded supramolecular polymers for catalysis. Two scaffolds (BTA and bis-urea) in particular were taken into consideration as their key features for catalysis (*e.g.* self-association, chirality amplification) were previously known.

For BTAs as their use in catalysis was already reported in our group, chapter II relates the characterisation of the chiral co-monomer (ester BTA) developed within the frame of this thesis. Indeed ester BTA was found to self-assemble either into stacks or dimers according to the substituent on the  $\alpha$ -carbon and the concentration. The relation between structure and association was characterised using several analytical techniques such as FT-IR, SANS, CD of ester BTA in bulk or in solution. Concerning the dimer, its exact structure was unravelled using the unique properties of BTA Cha that self-assembles into dimers even in bulk. Synthesis of BTA Cha with the appropriate ester chain allowed the growth of suitable crystals for X-ray diffraction and thus structure determination.

In chapter III the synthesis and characterisation of bis-urea co-monomers and ligands was described. Modulation of the spacer and the lateral chain of the bis-urea urea offers efficient variation of their gelation properties. Their self-assemblies were monitored by FT-IR, SANS and CD spectroscopy and reveals that the newly synthesised bis-ureas are all associated in classical catalysis solvent such as toluene and chloroform and even for a few of them in dichloromethane or tetrahydrofuran.

Applications of the supramolecular scaffolds in this thesis have been divided upon IV strategies: [I] chirality induction, [II] chirality amplification via “sergeant and soldiers” effect, [III] chirality amplification via “majority rule” effect and modulation of the reactivity the composition [IV] or the association of the supramolecular polymer. The supramolecular nature of our scaffolds allowed fast screening of the best condition especially for the chirality induction experiments.

Strategy [I] and [III] was successfully applied with BTA to the rhodium-catalysed hydrogenation of dimethylitaconate in chapter IV. Chirality induction was observed in a mixture of  $^H\text{BTA}^{\text{mPPh}_2}$  and **BTA IIe** as the mixture of the two in presence of rhodium gave good enantioselectivity (85% e.e.). Strong chirality amplification (“sergeant and soldiers” effect) was observed as only five percent of the chiral co-monomer was needed to obtain some enantioselectivity while twenty-five percent gave the highest enantioselectivity. The structure of the precatalyst was probed by FT-IR, SANS and CD spectroscopy to correlate the composition of the precatalyst and its enantioselectivity. This study also pointed toward the possible origin of the erosion of the enantioselectivity at high percentages of **BTA IIe** in the mixture.

Similarly in the chapter V, BTAs were successfully used for strategy [I] and [III] in the copper-catalysed hydrosilylation of acetophenone derivatives. Chirality induction was observed in a mixture of  $^H\text{BTA}^{\text{pPPh}_2}$  and **BTA Cha** as the mixture of the two in presence of copper gave good enantioselectivity (80% e.e.). However the reactivity of the catalyst was found to be highly sensitive to the preparation method and pre-coordination of the copper to  $^H\text{BTA}^{\text{pPPh}_2}$  in the monomeric form was required to reach high reactivity. Chirality amplification (“majority rules” (MR) effect) was observed as a scalemic mixture of **BTA Cha** (33% e.e.) was found sufficient to give the same enantiomeric excess of the product than pure **BTA Cha**. Application of the MR effect to obtain chirality switchable catalyst was successfully applied to the copper-catalysed hydrosilylation of acetophenone derivatives. During these experiments the chirality of the product was changed three times and the catalyst showed high stability and TON. Characterisation of the precatalytic specie was made using FT-IR, NMR, CD spectroscopy and SANS.

In chapter VI the use of both scaffolds was described for the application of strategy [I] in gold catalysis. Gold complexes were synthesised and characterised for both scaffolds but only the bis-urea remained strongly self-assembled upon gold chloride coordination. Gold cationic complexes were also investigated but strong erosion of the self-assembly for most complexes were observed. Strategy [I] in the frame of 1,6-enyne cycloisomerisation was not successful even though chiral bis-ureas were not tested yet. However a better understanding of the chloride abstractor influence on the stability and reactivity of gold complexes was obtained.

The influence of salts on the self-assembly of bis-ureas was further investigated and the viscosity of an EHUT solution in toluene could be switched “on/off”. Application of this switchable association (strategy [V]) was probed on newly synthesised urea-thiourea hydrogen-bond donor catalysts. The urea-thiourea was found to be sensitive to the salt switch but unfortunately its use in catalysis was unsuccessful. Indeed the various salts used in catalysis were found to directly catalyse the Michael addition and Friedel-Craft reaction. If the exact mechanism of the catalysis by the salts remains unclear, certain hypotheses were drawn.

Along the chapters of this thesis certain points need to be emphasised which are a) the preparation method of the catalyst/precatalyst; and b) the influence of salts. Indeed strong variations appeared for BTA scaffold in the case of Cu hydrosilylation according to the preparation methods. A huge impact of the preparation method on reactivity was observed whereas the influence of the selectivity was more subtle.

The presence of salts can be detrimental to the self-assembly whether it is the anion (as described in literature in chapter II) or the cation as described in different parts of this thesis. The strong erosion of the association in presence of alkali metals (chapter VII) or transition metals (chapter VI) warned us on the possible deleterious effect that could be observed in catalysis. In the case of the gold

competition for the carbonyl binding, the spacer of the bis-urea ligand was found to be decisive to maintain self-assembly. Indeed a bis-urea with xylyl spacer was found to be self-assembled even in presence of gold cationic complexes giving encouraging results for future experiments.

Among the possible outlook for this thesis, three possibilities can be particularly underlined. The first is the investigation of the chirality induction of the ester bis-ureas because, like ester BTAs they provide a cheap and readily accessible source of chirality, but they also form more robust assemblies. The second possibility is the modulation of the ligand structure. Indeed the synthesis of both scaffolds is now optimised and modification of the ligand moiety could be sufficient to improve the enantioselectivity previously observed or lead to other reactivities. The third possibility is the exploration of other catalytic reactions that work in mild conditions and that could give a better frame for all the strategies previously proposed.

# Appendix: Asymmetric catalysts supported on hydrogen-bonded scaffolds: other potential systems and reactions

## A. Introduction

The successful application of the BTA supramolecular scaffold in rhodium-catalysed hydrogenation and copper-catalysed hydrosilylation led us to investigate other catalytic systems. As previously observed the chosen catalytic system should be performed in non-competing and low polarity solvent but also under mild conditions to maintain the self-assembly. Herein we describe the application of our supramolecular scaffolds in such catalyses namely rhodium-catalysed hydroboration and palladium-catalysed hydrosilylation of styrene and [3+2] phosphine catalysed cycloaddition. The application of bis-urea scaffold for the copper-catalyzed hydrosilylation of 4'-NO<sub>2</sub> acetophenone will also be reported.

## B. Copper-catalyzed hydrosilylation of 4'-NO<sub>2</sub> acetophenone

A small set of bis-urea ligands and conditions was screened concomitantly to BTA ligands (Chapter V) for the copper-catalyzed hydrosilylation of 4'-NO<sub>2</sub>-acetophenone. Two strategies were investigated; the first one was the chirality induction from an enantiopure chiral bis-urea monomer to a racemic bis-urea ligand similarly to BTA experiments described in Chapter V. The second one was to probe whether the nature of the major enantiomer yielded by the copper catalyst of (*R*)-*m*-PPh<sub>3</sub>PBEUX can be changed according to the nature of the solvent. This is related to the observation of mirror CD spectra for (*R*)-*m*-PPh<sub>3</sub>PBEUX in DCM and CHCl<sub>3</sub> (Figure A1, see Chapter III for more details)

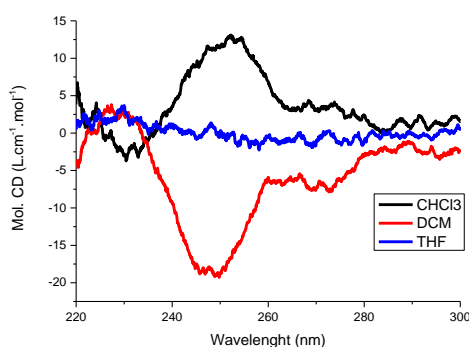


Figure A1: CD spectra of (*R*)-*m*-PPh<sub>3</sub>PBEUX at 1 mM

### 1. Chirality induction

All bis-urea copper catalysts were prepared by heating a toluene solution of Cu(OAc)<sub>2</sub>·H<sub>2</sub>O, the bis-urea ligand and the co-monomer at the reflux of the solvent for 1 min. Only racemic bis-urea ligands with the 1,3-dichlorobenzene spacer were investigated (Table A1). For all combinations of ligand and



co-monomer investigated, the reactions were fast (full conversion in less than 30 min). Using (*rac*)-*m*-**PPh<sub>3</sub>EHUCl<sub>2</sub>** with three different chiral co-monomers provided enantioselectivity for (*R,R*)-**EAUX** and (*S,S*)-**PPheUT** (14% and 20 % e.e. respectively entry 1 and 3) but not for (*R,R*)-**PBEUT** (entry 2). The position of the phosphine did not influence the extent of the enantioselectivity compared to what was observed with BTA monomers (Chapter V). However, it had a strong influence on the nature of the major enantiomer obtained as inversed chirality for the hydrosilylation product was observed with the same co-monomer (entry 3 and 4). It surmised that a different coordination copper complex is formed depending on the location of the PPh<sub>2</sub> group in the assemblies. Also, the peripheral alkyl chain of the bis-urea ligand influenced the selectivity as the replacement of the 2-ethylhexyl chain by a 1,5-dimethylhexyl chain led to the formation of the opposite enantiomer (entry 3 and 5). In that case it could be related to the fact the chiral co-monomer had to impose its chirality to two enantiomers (present in 1:1 mixture in the racemic ligand) and that the diastereoselection process might be inverted depending on the nature of the side-chain. Unfortunately, only modest enantioselectivity was obtained in all cases. It should be mentioned that inducing chirality to racemic ligands is expected to be more difficult than for achiral ones since the former possess an intrinsic chirality preference.

Table A1: Chirality induction with combinations of a racemic ligand and a chiral bis-urea commoner

Entry	Ligand	Co-monomer	time	Conversion	e.e.
1	( <i>rac</i> )- <i>m</i> - <b>PPh<sub>3</sub>EHUCl<sub>2</sub></b>	( <i>R,R</i> )- <b>EAUX</b>	10 min	89	14% ( <i>R</i> )
2	( <i>rac</i> )- <i>m</i> - <b>PPh<sub>3</sub>EHUCl<sub>2</sub></b>	( <i>R,R</i> )- <b>PBEUT</b>	5 min	100	0%
3	( <i>rac</i> )- <i>m</i> - <b>PPh<sub>3</sub>EHUCl<sub>2</sub></b>	( <i>S,S</i> )- <b>PPheUT</b>	10 min	100	20% ( <i>R</i> )
4	( <i>rac</i> )- <i>p</i> - <b>PPh<sub>3</sub>EHUCl<sub>2</sub></b>	( <i>S,S</i> )- <b>PPheUT</b>	10 min	100	-20% ( <i>S</i> )
5	( <i>rac</i> )- <i>m</i> - <b>PPh<sub>3</sub>DMHUCl<sub>2</sub></b>	( <i>S,S</i> )- <b>PPheUT</b>	5 min <sup>(a)</sup>	100	-10% ( <i>S</i> )

Reaction conditions: 4'-NO<sub>2</sub>-acetophenone (0.17 mmol, 0.3 M), Cu(OAc)<sub>2</sub>·H<sub>2</sub>O (3 mol%), bis-urea **Ligand** (6 mol%), bis-urea co-monomer (6 mol%), PhSiH<sub>3</sub> (1.0 eq), toluene (570 μL), 0°C. (a) reaction done at room temperature

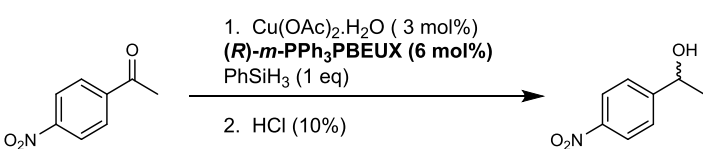
## 2. Chirality switch

Experiments were performed using the chiral ligand ((*R*)-*m*-**PPh<sub>3</sub>PBEUX**). The reaction was conducted in toluene, CHCl<sub>3</sub> and DCM with the aim of switching the chirality for the product of the hydrosilylation reaction between CHCl<sub>3</sub> and DCM (Table A2).

Enantioselectivity was obtained in the three solvents albeit a lower reaction temperature was required to obtain selectivity in the cases of CHCl<sub>3</sub> and DCM compared to toluene. The conversion was not complete in CHCl<sub>3</sub> even though the e.e. obtained was higher than in DCM. Unfortunately, no switch in the nature of the major enantiomer was observed between those two solvents as the selectivity was in favour of the (*S*)-enantiomer in both cases. This result was not in agreement with the mirror CD

spectra obtained for ((*R*)-**m-PPh<sub>3</sub>PBEUX** in DCM and CHCl<sub>3</sub> in the 240-260 nm region. It could be explained by: i) a different conformation adopted by a chromophore in the 240-260 nm region whilst the helicity of the supramolecular structure adopted by (*R*)-**m-PPh<sub>3</sub>PBEUX** is the same in both solvents or ii) a change in the helicity or in the supramolecular structure of (*R*)-**m-PPh<sub>3</sub>PBEUX** upon coordination of the copper atom. CD analysis of the copper complex of (*R*)-**m-PPh<sub>3</sub>PBEUX** might help to favour one of these hypotheses. To conclude, enantioinduction was obtained for mixtures of a racemic bis-urea ligand and an enantiopure co-monomer or for a chiral ligand alone. However, the enantiomeric excess remained modest in all cases (up to 22% e.e.). Improvement of the selectivity of the catalytic reaction could be expected by changing the chemical structures of the ligand, by evaluating other enantiopure co-monomers or by changing the reaction conditions.

Table A2: Hydrosilylation of 4'-nitroacetophenone with (*R*)-**m-PPh<sub>3</sub>PBEUX**



Solvent	Temperature	Time	Conversion	e.e.
Toluene	r.t.	1h	100%	-22% (S)
CHCl <sub>3</sub>	-25°C	12h	50%	-18% (S)
DCM	-25°C	12h	100%	-12% (S)

Reaction conditions: 4'-NO<sub>2</sub>-acetophenone (0.17 mmol), Cu(OAc)<sub>2</sub>·H<sub>2</sub>O (3 mol%), (*R*)-**m-PPh<sub>3</sub>PBEUX** (6 mol%), PhSiH<sub>3</sub> (1.0 eq) in toluene (0.3 M), CHCl<sub>3</sub> (0.15 M) or DCM (0.15 M).

### 3. Experimental section

General set-up for the catalytic reaction:

An oven-dried test tube was loaded with Cu(OAc)<sub>2</sub>·H<sub>2</sub>O (1 mg, 3 mol%) the ligand (6 mol%), the co-monomer (6 mol%) and 4'-NO<sub>2</sub>-acetophenone (27.5 mg, 0.165 mmol). The test tube was then flushed with argon for 10 seconds before addition of the dry solvent (ca. for volume of 570 μL or 1 mL according to the final concentration). The mixture was heated to the reflux during 1 min of the solvent to get complete dissolution of the ligand and then stirred while cooling down to room temperature. The solution was then put at the reaction temperature and further stirred for 15 min. The reaction was started by the addition of PhSiH<sub>3</sub> (21 μL, 0.165 mmol) and conversion was monitored by TLC. When reaction is completed, HCl (10%, 400 μL) was added and the mixture was stirred 30 min (until the solution becomes transparent). Then, the products were extracted with Et<sub>2</sub>O (3x1 mL) and AcOEt (1x1 mL). The solvents were removed under vacuum and the residue was taken up in DCM and passed through a silica plug eluting with DCM. The solvents were evaporated and the resulting product was analyzed <sup>1</sup>H NMR and chiral GC.

## C. Rhodium-catalysed hydroboration of styrene

### 1. Introduction

Hydroboration is the reaction between a borane and an alkene which was firstly described by Brown in 1961 in a non catalytic fashion.<sup>[1]</sup> The product itself is used as precursor for the preparation of other chemicals as depicted in Figure A2.<sup>[2]</sup>

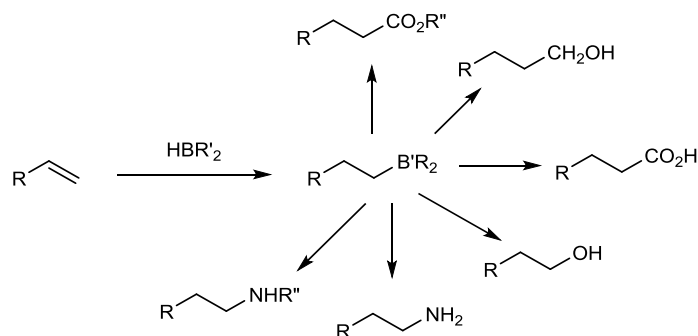


Figure A2: Hydroboration reaction and examples of possible functionalisation of the borane product adapted from reference<sup>[2]</sup>

Catalytic hydroboration has been developed over the last forty years and rhodium is mostly used among other metals (Ir, Ti, Sm and Cu). The seminal report of rhodium-catalysed hydroboration reaction was published by Nöth and Männig in 1983 with the use of Wilkinson's catalyst and catecholborane for the hydroboration of 5-hexen-2-one. The rhodium-catalysed reaction is fully chemoselective towards the hydroboration of alkene function instead of ketone in absence of rhodium.<sup>[3]</sup> Only catecholborane (CatBH) was found to be reactive whereas alkyl boranes remained inactive. The authors postulated that the acidity of the proton in CatBH was required for the oxidative addition step.

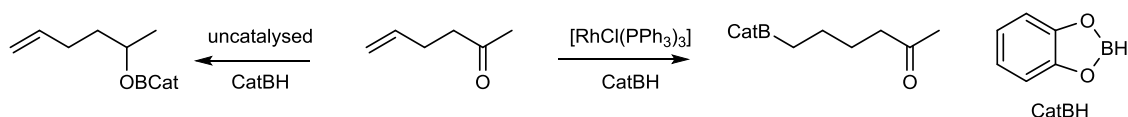


Figure A3: Chemoselectivity of the rhodium-catalysed hydroboration of 5-hexen-2-one adapted from reference<sup>[3]</sup>

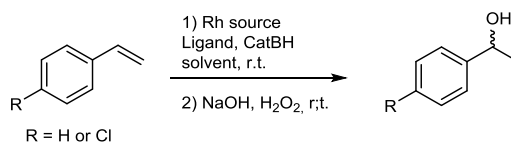
Investigations were conducted experimentally<sup>[4]</sup> and in silico<sup>[5]</sup> in order to determine the reaction mechanism. The branched product is favoured in the case of styrene derivatives arising from the formation of the stable rhodium  $\pi$ -benzyl complex intermediate. Initially, cationic rhodium complexes were thought to be necessary to obtain high branched/linear (b/l) ratio of the product<sup>[6]</sup> and phosphine ligands coordinated to Rh also enhance the selectivity of the reaction. Extensive study from Evans *et al.* led to the observation that decreased b/l ratio for neutral rhodium complexes was in fact related to ligand loss during the catalytic reaction.<sup>[4]</sup> Asymmetric hydroboration of styrene was explored with either cationic or neutral rhodium complexes however the highest regioselectivities were obtained with cationic complexes. A large variety of chiral ligands provided high enantioselectivity for the reaction such as Binap derivatives<sup>[7-9]</sup>, ferrocenyl P,N<sup>[10]</sup> and phosphoramidite ligands.<sup>[11,12]</sup> Only coordinating

solvent such as THF and dimethoxyethane (DME) have been reported in these reactions so far. For the binap ligand, high enantioselectivity was only obtained at low temperature whereas other chiral ligands were able to reach high e.e. at 0°C or even room temperature.

## 2. Catalytic results

Preliminary catalytic experiments using benchmark phosphine ligands (PPh<sub>3</sub> and binap) were run to investigate the influence of the solvent and the nature of the ligand (monodentate vs bidentate) on the regioselectivity (Table A3). It appeared that [Rh(COD)Cl]<sub>2</sub> provided lower b/l ratio in THF with than in toluene (entry 1 and 2) whereas the opposite trend was observed with cationic rhodium precursors ([Rh(COD)<sub>2</sub>]BArF and [Rh(COD)<sub>2</sub>]BF<sub>4</sub>). Binap provided higher b/l ratio than PPh<sub>3</sub> which might arise from a ability to chelate the rhodium centre (entry 3 and 5). Surprisingly, replacement of the BArF anion by BF<sub>4</sub> in the cationic rhodium precursor increased the ratio up to 95/5 for both ligands (entry 6 and 7). The trend in selectivity according to the solvent was also followed by (*rac*)-*m*-PPh<sub>3</sub>EHUCl<sub>2</sub> as lower b/l ratio was found in toluene than THF. Unfortunately for both solvent the ratio was lower for (*rac*)-*m*-PPh<sub>3</sub>EHUCl<sub>2</sub> than for PPh<sub>3</sub>. Changing the substrate from styrene to *p*-chlorostyrene also led to an increase of the b/l ratio from 86/14 to 94/6 for PPh<sub>3</sub> (entry 3 and 10) and for (*rac*)-*m*-PPh<sub>3</sub>EHUCl<sub>2</sub> (entry 11 and 12). We thus selected this substrate to further probe the reactivity of our supramolecular scaffolds.

Table A3: Screening of catalytic conditions for the hydroboration of styrene and *p*-Cl-styrene

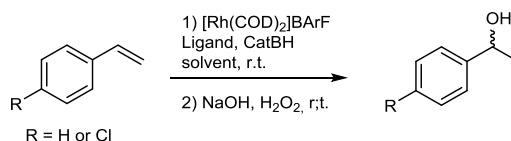


Entry	Substrate	Rhodium source	Ligand	Solvent	b/l ratio <sup>a</sup>
1	styrene	[Rh(COD)Cl] <sub>2</sub>	PPh <sub>3</sub>	THF	53/47
2	styrene	[Rh(COD)Cl] <sub>2</sub>	PPh <sub>3</sub>	toluene	66/34
3	styrene	[Rh(COD) <sub>2</sub> ]BArF	PPh <sub>3</sub>	THF	86/14
4	styrene	[Rh(COD) <sub>2</sub> ]BArF	PPh <sub>3</sub>	toluene	83/17
5	styrene	[Rh(COD) <sub>2</sub> ]BArF	( <i>rac</i> )-Binap	THF	93/7
6	styrene	[Rh(COD) <sub>2</sub> ]BF <sub>4</sub>	( <i>rac</i> )-Binap	THF	95/5
7	styrene	[Rh(COD) <sub>2</sub> ]BF <sub>4</sub>	PPh <sub>3</sub>	THF	95/5
8	styrene	[Rh(COD) <sub>2</sub> ]BF <sub>4</sub>	( <i>rac</i> )- <i>m</i> -PPh <sub>3</sub> EHUCl <sub>2</sub>	THF	81/19
9	styrene	[Rh(COD) <sub>2</sub> ]BF <sub>4</sub>	( <i>rac</i> )- <i>m</i> -PPh <sub>3</sub> EHUCl <sub>2</sub>	toluene	70/30
10	<i>p</i> -Cl-styrene	[Rh(COD) <sub>2</sub> ]BArF	PPh <sub>3</sub>	THF	94/6
11	<i>p</i> -Cl-styrene	[Rh(COD) <sub>2</sub> ]BArF	( <i>rac</i> )- <i>m</i> -PPh <sub>3</sub> EHUCl <sub>2</sub>	THF	85/15
12	<i>p</i> -Cl-styrene	[Rh(COD) <sub>2</sub> ]BArF	( <i>rac</i> )- <i>m</i> -PPh <sub>3</sub> EHUCl <sub>2</sub>	toluene	60/40

Reaction conditions: styrene derivative (1.0 mmol, 1.0 M), CatBH (1.1 mmol), Rh source (1 mol%), ligand (2 mol%), solvent at room temperature, 12h. For all reaction the catalyst has been prepared in the reaction solvent

After gaining more insight in the ideal conditions for the reaction, the potential of bis-urea and BTA ligands in catalysing the hydroboration of *p*-chlorostyrene was assessed into more details (Table A4). As previously observed, the b/l ratio decreased when the reaction was done in toluene compared to THF for (*rac*)-*m*-PPh<sub>3</sub>EHUCl<sub>2</sub> alone (entry 1 and 2). However, a lower b/l ratio was observed in presence of (*rac*)-PBEUX in THF (entry 3). The mode of preparation of the catalyst was found to significantly influence the selectivity of the reaction. When the rhodium precursor and the ligand were mixed in THF and thereafter taken up in toluene the b/l ratio of the reaction significantly increased compared to the catalyst prepared in toluene (entry 2 and 4). By using this method of preparation, a correlation between the self-association properties of the additives and the b/l ratio provided by the resulting bis-urea co-polymers was observed (entry 5-7). Indeed, the association strength increased in the following order **PBEUX**>**PBEUT**>**PPheUT** and the same order was followed for the selectivity obtained by mixing these co-monomers with (*rac*)-*m*-PPh<sub>3</sub>EHUCl<sub>2</sub>. Enantioselective version of the hydroboration reaction was attempted with the chiral bis-urea ligands (**R**)-*m*-PPh<sub>3</sub>PBEUX or the chiral BTA ligand (**S,S**)-<sup>H</sup>BTA<sup>mPPh2</sup>. The rhodium complex of (**S,S**)-<sup>H</sup>BTA<sup>mPPh2</sup> exhibited almost no regioselectivity for the reaction. Also for both chiral ligands, the branched product obtained was racemic.

Table A4: Catalytic performance of bisurea and BTA ligands in of the hydroboration of 4-chlorostyrene



Entry	Ligand	Co-monomers	Solvent	b/l ratio
1	( <i>rac</i> )- <i>m</i> -PPh <sub>3</sub> EHUCl <sub>2</sub>	no	THF	85/15
2	( <i>rac</i> )- <i>m</i> -PPh <sub>3</sub> EHUCl <sub>2</sub>	no	toluene	60/40
3	( <i>rac</i> )- <i>m</i> -PPh <sub>3</sub> EHUCl <sub>2</sub>	( <i>rac</i> )-PBEUX (1% mol)	THF	74/26
4	( <i>rac</i> )- <i>m</i> -PPh <sub>3</sub> EHUCl <sub>2</sub>	no	toluene <sup>(b)</sup>	83/17
5	( <i>rac</i> )- <i>m</i> -PPh <sub>3</sub> EHUCl <sub>2</sub>	( <i>rac</i> )-PBEUX (1% mol)	toluene <sup>(b)</sup>	88/12
6	( <i>rac</i> )- <i>m</i> -PPh <sub>3</sub> EHUCl <sub>2</sub>	( <b>R,R</b> )-PBEUT (1% mol)	toluene <sup>(b)</sup>	80/20(e)
7	( <i>rac</i> )- <i>m</i> -PPh <sub>3</sub> EHUCl <sub>2</sub>	( <b>S,S</b> )-PPheUT (1% mol)	toluene <sup>(b)</sup>	76/24(e)
8	( <b>R</b> )- <i>m</i> -PPh <sub>3</sub> PBEUX	no	THF	83/17 <sup>(d)</sup>
9	( <b>S,S</b> )- <sup>H</sup> BTA <sup>mPPh2</sup>	no	cyclohexane <sup>(c)</sup>	55/45 <sup>(d)</sup>

Reaction conditions: *p*-chlorostyrene (1.0 mmol, 1.0 M), CatBH (1.1 mmol), [Rh(COD)<sub>2</sub>]BARf (1 mol%), ligand (2 mol%), solvent room temperature, 12h. Selectivity determined by <sup>1</sup>H NMR. Unless otherwise stated the catalyst has been prepared in the solvent used in catalysis. (b) preparation of the catalyst in THF, (c) preparation of the catalyst in DCM, (d) for the branched product, no enantioselectivity was observed. (e) enantioselectivity of the branched product not determined

Only a few catalytic experiments were performed and no enantioinduction was observed. However, further experiments will be needed in order to estimate if enantioinduction was feasible with these catalytic systems. On the other hand, the lower b/l ratio observed and the absence of enantioselectivity for (**S,S**)-<sup>H</sup>BTA<sup>mPPh2</sup> in presence of [Rh(COD)<sub>2</sub>]BARf are not encouraging.

### 3. Experimental part

Typical set-up for the catalytic reaction:

Formation of the precatalyst and reaction in the same solvent:

An oven-dried Schlenk tube was loaded with Rh precursor (2 mol%), ligand (2 equivalent phosphine/Rh) and dry solvent (ca. 80 mM). To the solution was added styrene or 4-Cl styrene (1 eq) and after 5 minutes catecholborane (1.125 eq). The solution was stirred at room temperature overnight before starting the following work up: addition of EtOH (0.5 mL/mmol of styrene), NaOH (3 M aqueous solution, 1.4 mL/ mmol of styrene) and 30% H<sub>2</sub>O<sub>2</sub> in water (0.7 mL/mmol of styrene). The mixture was stirred for 2 hours before extraction three times with Et<sub>2</sub>O. The combined organic phases were dried over MgSO<sub>4</sub> and concentrated under vacuum. The resulting alcohol was analysed by <sup>1</sup>H NMR and if relevant by chiral GC.

Formation of the precatalyst in THF and catalytic reaction in toluene:

An oven-dried Schlenk tube was charged with [Rh(COD)<sub>2</sub>]BARF (1 mol%), ligand (2 mol%) and the additive if present (2 mol%). THF was added (ca. 15 mM) and the solution was stirred until complete dissolution. The volatiles were removed under vacuum and the resulting solid was taken up in toluene (ca. 15 mM). Then 4-Cl-styrene (1eq) was added and the solution was stirred for 10 minutes before addition of catecholborane (1.125 eq). The solution was stirred at room temperature overnight before the oxidative quench by addition of EtOH (0.5 mL/mmol of styrene), NaOH (3 M, 1.4 mL/ mmol of styrene) and 30% H<sub>2</sub>O<sub>2</sub> (0.7 mL/mmol of styrene). The mixture was stirred for 2 hours before extraction three times with Et<sub>2</sub>O. The combined organic phases were dried over MgSO<sub>4</sub> and concentrated under vacuum. The resulting alcohol was analysed by <sup>1</sup>H NMR and if relevant by chiral GC.

Formation of the precatalyst in DCM and catalytic reaction in cyclohexane:

An oven-dried Schlenk tube was charged with [Rh(COD)<sub>2</sub>]BARF (4.73 mg, 1 mol%), (*S,S*)-<sup>H</sup>BTA<sup>mPPh2</sup> (11.1 mg, 2 mol%). DCM was added (700 μL) and the solution was stirred until complete dissolution, then the volatiles were removed under vacuum and the solid was dried for 1 hour at 1 mBar. Then the solid was taken up with cyclohexane (700 μL) and sonicated for 15 minutes. 4-Cl-styrene (48μL, 0.8 mmol) was added and the solution was stirred for 10 minutes before addition of catecholborane (48μL, 0.9 mmol). The solution was stirred at room temperature overnight before the oxidative quench by addition of EtOH (0.5 mL/mmol of styrene), NaOH (3 M, 1.4 mL/ mmol of styrene) and 30% H<sub>2</sub>O<sub>2</sub> (0.7 mL/mmol of styrene). The mixture was stirred for 2 hours before extraction three times with Et<sub>2</sub>O. The combined organic phases were dried over MgSO<sub>4</sub> and concentrated under vacuum. The resulting alcohol was analysed by <sup>1</sup>H NMR and by chiral GC.

The enantiomeric excess was determined by chiral GC: Chiral Cyclosil-B column, 30 m × 250 μm × 0.25 μm, inlet pressure = 12.6 psi. Injection temperature = 250°C; detector temperature = 250°C, column temperature = 120°C for 10 min then 1°C/min to 140°C. retention time: 16.3 min (*R*)-enantiomer and 16.7 min (*S*)-enantiomer.

## D. Palladium-catalysed hydrosilylation of styrene

### 1. Introduction

Hydrosilylation of alkene was firstly developed for the functionalisation of silicone rubber using Speier, Lukevics or Karstedt platinum catalyst that gives the linear product selectively.<sup>[13]</sup> However palladium catalysts were found to preferentially give the branched products which can be converted into the corresponding alcohols after Tamao-Flemming oxidation and thus provided a rapid access to enantio-enriched alcohols.<sup>[14]</sup> This particular reaction requires non-chelating phosphine ligand and thus its development was initiated with the chiral monophosphine (**MOP**), synthesised by Hayashi in the 1980's (Figure A4).<sup>[15]</sup> High enantiomeric excess was obtained using **MOP-OMe** for the hydrosilylation of 1-octene whereas in the case of styrene the enantiomeric excess drops significantly.<sup>[16]</sup> Removal of the methoxy group on the ligand led to high enantiomeric excess for the hydrosilylation of styrene (**MOP-H**)<sup>[17]</sup>. Tuning the electronic properties of the aryl group on the phosphine ligand increased the enantiomeric excess up to 97%.<sup>[18]</sup>

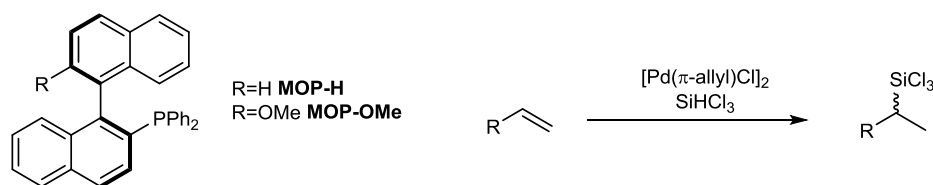


Figure A4: MOP ligands developed for the palladium-catalysed hydrosilylation of alkenes

A catalytic cycle was initially proposed by Chalk and Harrod<sup>[19]</sup> but further investigation using deuterium-substituted styrene at  $\alpha$  and  $\beta$ -position gave more information on the catalytic cycle. Hydrosilylation with  $\alpha$ -deuterated styrene gave the product without loss of deuterium which indicated that the carbopalladation was only possible at the benzylic position.<sup>[18]</sup> On the other hand, deuteration at the  $\beta$ -position gave products with deuterium scrambling which revealed that all the steps of the mechanism were reversible at the exception of the reductive elimination.

Apart MOP ligands, phosphoramidite ligands<sup>[20–22]</sup> also proved to be efficient ligands for the palladium-catalysed asymmetric hydrosilylation of styrene. Suginome *et al.* developed MOP type ligands supported on a polymer backbone.<sup>[23]</sup>

## 2. Catalytic results

Table A5: Catalytic results for the palladium-catalysed hydrosilylation of styrene

Entry	Ligand	L/Pd	Additives (mol%)	Time	Conversion	e.e.
1	PPh <sub>3</sub>	1	no	3d	87%	/
2	PPh <sub>3</sub>	2	no	5d	85%	/
3	<i>(rac)</i> - <i>m</i> -PPh <sub>3</sub> EHUCl <sub>2</sub> <sup>(a)</sup>	2	no	5d	85%	/
4	<i>(rac)</i> - <i>m</i> -PPh <sub>3</sub> EHUCl <sub>2</sub> <sup>(a)</sup>	1	no	5d	38%	/
5	<i>(rac)</i> - <i>m</i> -PPh <sub>3</sub> EHUCl <sub>2</sub>	2	no	5d	37% <sup>(a)</sup>	/
6	<i>(rac)</i> - <i>m</i> -PPh <sub>3</sub> EHUCl <sub>2</sub> <sup>(a)</sup>	1.2	(R,R)-PBEUT (0.22)	3d	81%	0%
7	<i>(rac)</i> - <i>m</i> -PPh <sub>3</sub> EHUCl <sub>2</sub> <sup>(a)</sup>	1.2	(S,S)-PPheUT (0.22)	3d	78%	0%
8	( <i>S,S</i> )- <sup>H</sup> BTA <sup>mPPh2</sup>	1.2	no additive	3d	89%	0%
9	( <i>S,S</i> )- <sup>H</sup> BTA <sup>pPPh2</sup>	1.2	no additive	3d	75%	0%

Reaction conditions: styrene (neat)/HSiCl<sub>3</sub>/[Pd(μ-Cl)(η<sup>3</sup>-C<sub>3</sub>H<sub>5</sub>)<sub>2</sub>] (1/1.1/0.001) and ligand, room temperature. Unless otherwise stated the catalyst has been prepared in the solvent used. Only the branched product was observed. The conversion was determined by <sup>1</sup>H NMR and enantiomeric excess determined by chiral HPLC or GC analysis after Tamao-Flemming oxidation of the silane intermediate. (a) Catalyst prepared in THF (b) reaction performed in CDCl<sub>3</sub> (catalyst concentration 10.4 mM).

The reaction was conducted in neat styrene since phosphine palladium catalysts used in the literature were found to be soluble in this solvent. Triphenylphosphine was used as a benchmark ligand and strong influence of the PPh<sub>3</sub>/palladium ratio on the activity of the reaction was found. Indeed, the reaction was faster with a ligand: Pd ratio of 1 compared to a ratio of 2 (entries 1 and 2). However, the opposite trend was found with the bis-urea ligand *(rac)*-*m*-PPh<sub>3</sub>EHUCl<sub>2</sub> for which 2 equivalents of ligand compared to palladium led to a faster reaction (entries 3 and 4). Running the reaction in chloroform instead of in neat styrene also reduced the reaction rate (entry 5). Investigation of chirality induction from an enantiopure bis-urea co-monomer to a racemic bis-urea ligand was tried and surprisingly higher conversion was observed in presence of the additive with a ligand: Pd ratio of 1.2 compared to the reaction without additives. However, no enantioselectivity was observed for the silane product (entries 6 and 7). Reactions using (*S,S*)-<sup>H</sup>BTA<sup>pPPh2</sup> (both regioisomers) were also performed but no enantioinduction was observed. The absence of chirality induction in conditions for which the BTA supramolecular catalysts were not soluble and thus expected to be associated suggests that i) the self-assembly are disrupted during the catalytic reaction, ii) no chirality transfer occurs from the supramolecular polymer to the catalytic palladium centres and iii) racemisation of the silane occurs during the isolation process.

## 3. Experimental part

Typical set-up for the catalytic reaction:

With bis-urea ligand and co-monomer:

In an oven-dried Schlenk under argon was added 2 mL of a stock solution of [Pd(μ-Cl)(η<sup>3</sup>-C<sub>3</sub>H<sub>5</sub>)<sub>2</sub>] (1.59 mg, 0.1 mol%) and *(rac)*-*m*-PPh<sub>3</sub>EHUCl<sub>2</sub> (6.08 mg, 0.22 mol%) in THF. The resulting solution



was stirred at room temperature for 15 minutes before addition of the co-monomer (0.22 mol%) and was further stirred until complete dissolution. The volatiles were removed under vacuum and the styrene (500  $\mu\text{L}$ , 4.35 mmol) was added. The resulting suspension was stirred at 0°C for 30 minutes before addition of  $\text{SiHCl}_3$  (440  $\mu\text{L}$ , 4.35 mmol). The reaction was then allowed to reach room temperature and stirred for 3 days. The conversion was analysed by  $^1\text{H}$  NMR and the silane was isolated pure by bulb to bulb distillation (170 °C,  $5.10^{-2}$  mbar) and converted to the corresponding alcohol using Tamao-Flemming procedure (vide infra).

The enantiomeric excess was determined by chiral HPLC: Daicel Chiralcel®-OD-H, hexane/isopropanol 95/5, 1 ml/min. Retention time: 14.4 min and 16.4 min.

With chiral BTA ligand:

In an oven-dried Schlenk under argon 500  $\mu\text{L}$  of a stock solution of  $[\text{Pd}(\mu\text{-Cl})(\eta^3\text{-C}_3\text{H}_5)]_2$  (1.59 mg, 0.1 mol%) in styrene was added to (*S,S*)- $^{\text{H}}\text{BTA}^{\text{PPh}_2}$  (6.1 mg, 0.22 mol%). The resulting solution was stirred at 0°C for 10 minutes before addition of  $\text{SiHCl}_3$  (880  $\mu\text{L}$ , 8.70 mmol). The reaction was then allowed to reach room temperature and stirred for 3 days. The conversion was analysed by  $^1\text{H}$  NMR and the pure product was isolated by bulb to bulb distillation (170 °C,  $5.10^{-2}$  mbar) and converted to the corresponding alcohol using Tamao-Flemming procedure.

The enantiomeric excess was determined by chiral GC: Chiral Cyclosil-B column, 30 m  $\times$  250  $\mu\text{m}$   $\times$  0.25  $\mu\text{m}$ , inlet pressure = 12.6 psi. inject temperature = 250°C; detector temperature = 250°C, column temperature = 115°C. Retention time: 11.0 ((*R*)-enantiomer min) and 11.7 min ((*S*)-enantiomer).

Tamao-Flemming procedure, Adapted from references:<sup>[24]</sup>

1-phenyl-1-(trichlorosilyl)ethane (190  $\mu\text{L}$ , 1 mmol) and 0.9 mL of 30%  $\text{H}_2\text{O}_2$  at room temperature were added to a suspension of KF (350 mg, 6.0 mmol) and  $\text{KHCO}_3$  (901 mg, 9.0 mmol) in a 1/1 mixture of THF/MeOH. The suspension was vigorously stirred overnight before addition of 3.3 mL of a saturated aqueous solution of  $\text{Na}_2\text{S}_2\text{O}_3$  and extracted three times with  $\text{Et}_2\text{O}$ . The combined organic phases were dried over  $\text{MgSO}_4$  and concentrated under vacuum. The resulting product was then analysed to determine its enantiomeric excess.

## E. Phosphine-catalysed 3+2 cycloaddition reactions

### 1. Introduction

Organocatalysis is commonly used in chemistry for long time as far as it concerns Brønsted/Lewis acid or base catalysis. However, development of asymmetric organocatalysis is quite recent. It has drawn a lot of interest due to its lower waste toxicity (as no transition metal is employed) and its simple tunability. One current limit is that the catalyst loading remains high (up to 10-20% in some cases). Amongst all the organocatalysts described, very simple chemical structures have been

developed; (thio)urea<sup>[25]</sup>, Proline<sup>[26]</sup> and phosphine<sup>[27]</sup> derivatives. As we possess a small library of bisurea and BTA ligands and that their association properties are well understood (see Chapter 2 and 3), phosphines-organocatalysed reactions particularly drawn our attention (some of these reactions are listed in the figure below).

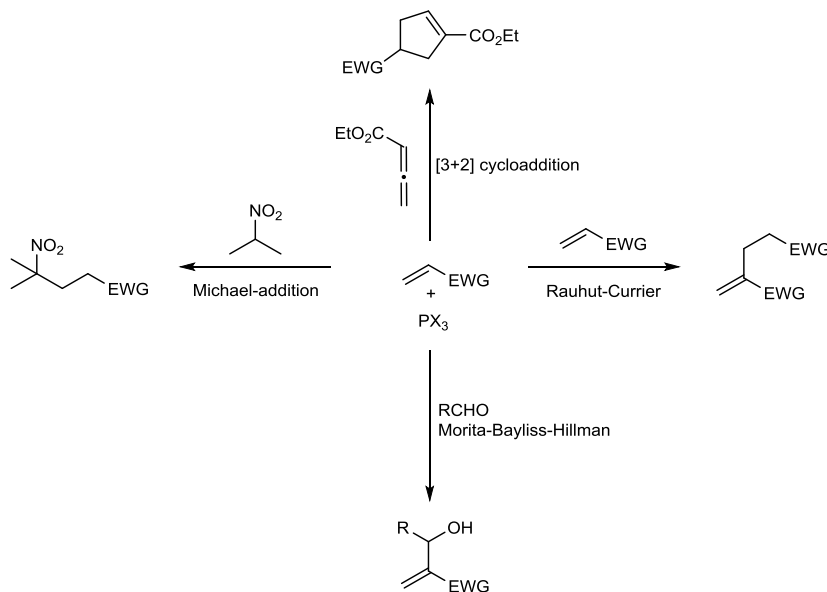


Figure A5: Examples of phosphine-organocatalysed reactions.

We decided to focus on the phosphine-catalysed [3+2] cycloaddition reaction between benzyl 2,3-butadienoate and various electrophiles. Those reactions (Figure A6) were performed by Maxime Gicquel at the Institut de Chimie des substances naturelles, (Université Paris-Saclay) under the supervision of Arnaud Voituriez and the results are listed below.

## 2. Catalytic results

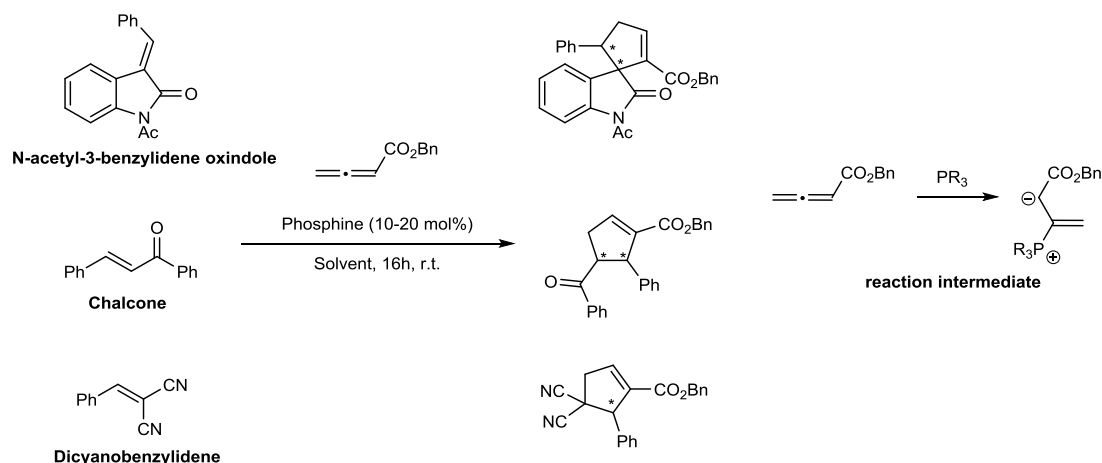


Figure A6: Substrates tested with our bis-urea and BTA ligands

Our chiral bis-urea and BTA ligands (10 mol%) promoted the [3+2] cycloaddition reaction between N-acetyl-3-benzylidene oxindole and benzyl 2,3-butadienoate with modest yields (from 40% to 65%, Table A6). The product was racemic in all cases ( $ee < 5\%$ ). The bis-urea and BTA ligand solutions were viscous and orange/reddish colour appears upon the addition of the allene which was

characteristic of the formation of the zwitterions. During the course of the reaction the solution was no longer viscous and a deposit was observed on the wall of the glassware.

Table A6: Catalytic results for the phosphine-catalysed [3+2] cycloaddition reaction between N-acetyl-3-benzylidene oxindole and benzyl 2,3-butadienoate

Ligand	Solvent	Conversion <sup>(a)</sup>	e.e. <sup>(b)</sup>
( <i>S,S</i> )- <sup>H</sup> BTA <sup>m-PPh2</sup>	toluene (10 mM)	40%	0%
( <i>S,S</i> )- <sup>H</sup> BTA <sup>p-PPh2</sup>	toluene (10 mM)	50%	5%
( <i>R</i> )-PPh <sub>3</sub> PBEUX	toluene/DCM (10/1) (3,3 mM)	65%	5%
( <i>R</i> )-PPh <sub>3</sub> PBEUX	DCM (2,5 mM)	50%	2%
( <i>R</i> )-PPh <sub>3</sub> PBEUX	THF (5 mM)	50%	2%

Reaction conditions: N-acetyl-3-benzylidene oxindole (0.15 mmol), benzyl 2,3butadienoate (0.3 mmol), and the phosphine (10 mol%) were stirred at room temperature in the corresponding solvent for 16 h. (a) Conversion determined by <sup>1</sup>H NMR (b) Enantiomeric excesses were measured by chiral HPLC.

When the reaction was performed using chalcone rather than the oxindole, no significant conversion was observed despite the use of a higher catalyst loading (20% instead of 10%). Clearly the reactivity of the chalcone was lowered compared to the oxindole.

Table A7: Catalytic results for the phosphine-catalysed [3+2] cycloaddition between chalcone and benzyl 2,3-butadienoate

Phosphine	Solvent [Concentration]	Conversion <sup>(a)</sup>
( <i>S,S</i> )- <sup>H</sup> BTA <sup>m-PPh2</sup>	toluene (10mM)	<10%
( <i>S,S</i> )- <sup>H</sup> BTA <sup>m-PPh2</sup>	toluene (10mM)	<10%
( <i>R</i> )-PPh <sub>3</sub> PBEUX	toluene/DCM (10/1) (3,3mM)	<10%

Reaction condition: chalcone (0.15 mmol), benzyl 2,3butadienoate (0.3 mmol), and the phosphine (20 mol%) were stirred at room temperature in corresponding solvent for 16 h. (a) Conversion determined by <sup>1</sup>H NMR

The last substrate tried was dicyanobenzylidene. Conversion was observed with BTA ligands but not with the bis-urea ligands. Decreasing the solvent polarity (from toluene to cyclohexane/DCM 10/1) led to a strong erosion of the conversion (from 55-60% to 20%). In both solvents, no enantioselectivity was observed.

Table A8: Catalytic results for the phosphine-catalysed [3+2] cycloaddition reaction between dicyanobenzylidene and benzyl 2,3-butadienoate

Phosphine	Solvent [Concentration]	Conversion <sup>(a)</sup>	e.e. <sup>(b)</sup>
( <i>S,S</i> )- <sup>H</sup> BTA <sup>m-PPh2</sup>	toluene [10mM]	55%	3%
( <i>S,S</i> )- <sup>H</sup> BTA <sup>m-PPh2</sup>	toluene [10mM]	60%	4%
( <i>S,S</i> )- <sup>H</sup> BTA <sup>m-PPh2</sup>	cyclohexane/DCM (10/1) [2 MM]	20%	2%
( <i>S,S</i> )- <sup>H</sup> BTA <sup>m-PPh2</sup>	cyclohexane/DCM (10/1) [2 MM]	20%	2%
( <i>R</i> )-PPh <sub>3</sub> PBEUX	toluene/DCM (10/1) [3,3mM]	<10%	-

Reaction condition: dicyanobenzylidene (0.15 mmol), benzyl 2,3butadienoate (0.18 mmol), and the phosphine (20 mol%) were stirred at room temperature in corresponding solvent for 24 h. (a) Conversion determined by <sup>1</sup>H NMR (b) Enantiomeric excesses have been measured by chiral HPLC on a Chiralpak IA column.

The disruption of the self-assembly clearly occurred during the reaction, as evidenced by the decreased viscosity and the absence of selectivity. The zwitterionic intermediate (Figure A6) formed upon addition of the phosphine to the allene might compete with the hydrogen bond network. The modest

conversion was also problematic as for the dicyanobenzylidene the TON did not exceed 1 or 2 in worst cases. All those data led to us to conclude that none of our phosphine ligand was stable enough to promote the [3+2] cycloaddition reaction with significant enantioselectivity.

### 3. Experimental part

Typical set up for the catalytic reaction between N-acetyl-3-benzylidene oxindole and chalcone The BTA or bis-urea phosphine ligand was dissolved in the reaction solvent (ca. for 2 to 10 mM) until the solution or gel was homogeneous and the electrophile (0.15 mmol) and the allene (0.30 mmol) were added. The reaction mixture was stirred at room temperature for 16h before evaporation of the solvents. The crude product was then analysed by  $^1\text{H}$  NMR for the conversion and purified by flash chromatography on silica gel before chiral HPLC to determine the e.e.

Typical experiment with the dicyanobenzylidene

The phosphine was dissolved in the reaction solvent (ca. for 2 to 10 mM) and when the solution was homogeneous the electrophile (0.15 mmol) followed by the allene (0.18 mmol). The reaction was stirred at room temperature for 16h before evaporation of the solvents. The crude product was then analysed by  $^1\text{H}$  NMR for the conversion and purified by flash chromatography on silica gel before chiral HPLC to determine the e.e.

## F. Conclusion

Application of our bis-urea and BTA ligands in a set of selected asymmetric reactions, showed mitigated success compared to their use in rhodium-catalysed hydrogenation (chapter IV) and copper-catalysed hydrosilylation (chapter V) reactions. However, preliminary experiments with a small set of bis-urea ligands and co-monomers indicated that chirality induction in the copper-catalysed hydrosilylation of 4'-NO<sub>2</sub> acetophenone was feasible with these systems. In the case of rhodium-catalysed hydroboration of styrene, modest regioselectivity was observed and no enantioselectivity could be obtained with both BTA and bis-urea ligands. However, a significant influence of the preparation method of the bis-urea precatalyst on the selectivity was observed. The absence of enantioselectivity could arise from perturbation of the self-assembly caused by the relatively acidic catecholborane. Chirality induction was also probed in the palladium-catalysed hydrosilylation of styrene but without success. This was more unexpected given that the reactants are poor hydrogen bond competitors and the conditions were mild. Phosphine organocatalysis with our supramolecular scaffolds displayed some incompatibility. The low conversion and enantioselectivity observed for these reactions pointed toward the destruction of the self-assembly during the reaction. Search for reaction with milder conditions compatible with our supramolecular scaffolds is thus still ongoing.

## G. References

- [1] H. C. Brown, *Tetrahedron* **1961**, *12*, 117–138.
- [2] C. M. Crudden, D. Edwards, *Eur. J. Org. Chem.* **2003**, *2003*, 4695–4712.
- [3] D. Männig, H. Nöth, *Angew. Chem. Int. Ed.* **1985**, *24*, 878–879.
- [4] D. A. Evans, G. C. Fu, B. A. Anderson, *J. Am. Chem. Soc.* **1992**, *114*, 6679–6685.
- [5] C. Widauer, H. Grützmacher, T. Ziegler, *Organometallics* **2000**, *19*, 2097–2107.
- [6] Y. Matsumoto, T. Hayashi, *Tetrahedron Lett.* **1991**, *32*, 3387–3390.
- [7] T. Hayashi, Y. Matsumoto, Y. Ito, *J. Am. Chem. Soc.* **1989**, *111*, 3426–3428.
- [8] T. Hayashi, Y. Matsumoto, Y. Ito, *Tetrahedron: Asymmetry* **1991**, *2*, 601–612.
- [9] J. M. Brown, D. Hulmes, T. P. Layzell, *Chem. Commun.* **1993**, 1673–1674.
- [10] A. Schnyder, L. Hintermann, A. Togni, *Angew. Chem. Int. Ed.* **1995**, *34*, 931–933.
- [11] S. A. Moteki, D. Wu, K. L. Chandra, D. S. Reddy, J. M. Takacs, *Org. Lett.* **2006**, *8*, 3097–3100.
- [12] S. M. Smith, J. M. Takacs, *Org. Lett.* **2010**, *12*, 4612–4615.
- [13] P. W. N. M. van Leeuwen, *Homogeneous Catalysis*, Springer Netherlands, Dordrecht, **2004**.
- [14] K. Tamao, N. Ishida, T. Tanaka, M. Kumada, *Organometallics* **1983**, *2*, 1694–1696.
- [15] Y. Uozumi, T. Hayashi, *J. Am. Chem. Soc.* **1991**, *113*, 9887–9888.
- [16] Y. Uozumi, K. Kitayama, T. Hayashi, *Tetrahedron: Asymmetry* **1993**, *4*, 2419–2422.
- [17] K. Kitayama, Y. Uozumi, T. Hayashi, *Chem. Commun.* **1995**, *1*, 1533.
- [18] T. Hayashi, S. Hirate, K. Kitayama, H. Tsuji, A. Torii, Y. Uozumi, *J. Org. Chem.* **2001**, *66*, 1441–1449.
- [19] A. J. Chalk, J. F. Harrod, *J. Am. Chem. Soc.* **1965**, *87*, 16–21.
- [20] J. F. Jensen, B. Y. Svendsen, T. V. la Cour, H. L. Pedersen, M. Johannsen, *J. Am. Chem. Soc.* **2002**, *124*, 4558–4559.
- [21] X.-X. Guo, J.-H. Xie, G.-H. Hou, W.-J. Shi, L.-X. Wang, Q.-L. Zhou, *Tetrahedron: Asymmetry* **2004**, *15*, 2231–2234.
- [22] K. Junge, B. Wendt, S. Enthaler, M. Beller, *ChemCatChem* **2010**, *2*, 453–458.
- [23] T. Yamamoto, T. Yamada, Y. Nagata, M. Suginome, *J. Am. Chem. Soc.* **2010**, *132*, 7899–7901.
- [24] Y. Uozumi, H. Tsuji, T. Hayashi, *J. Org. Chem.* **1998**, *63*, 6137–6140.
- [25] S. J. Cannon, *Chem. Eur. J.* **2006**, *12*, 5418–5427.
- [26] B. List, *Tetrahedron* **2002**, *58*, 5573–5590.
- [27] J. L. Methot, W. R. Roush, *Adv. Synth. Catal.* **2004**, *346*, 1035–1050.